For more information, please contact:

World Meteorological Organization

Research Department

Atmospheric Research and Environment Branch

7 bis, avenue de la Paix – P.O. Box 2300 – CH 1211 Geneva 2 – Switzerland

Tel.: +41 (0) 22 730 83 14 – Fax: +41 (0) 22 730 80 27

E-mail: cpa@wmo.int – Website: http://www.wmo.int/pages/prog/arep/index_en.html

World Meteorological Organization

Weather • Climate • Water

WWRP 2012 - 2

Proceedings of the 10th WMO Scientific Conference on Weather Modification

(Bali, Indonesia, 4-7 October 2011)

WWRP WORLD WEATHER RESEARCH PROGRAMME

WORLD METEOROLOGICAL ORGANIZATION

WORLD WEATHER RESEARCH PROGRAMME

WWRP 2012 - 2

PROCEEDINGS OF THE

10TH WMO SCIENTIFIC CONFERENCE

ON WEATHER MODIFICATION

World Meteorological Organization
Weather • Climate • Water

WWRP WORLD WEATHER RESEARCH PROGRAMME

April 2012

10th WMO Scientific Conference on Weather Modification
(Bali, Indonesia, 4-7 October 2011)

Conference Program

Tuesday 4 October 2011

09:00 – 10:30 MEETING OPENING
Chairman: Host representative

World Meteorological Organisation Representative: Weather modification research – WMO prospective

Minister of Research and Technology or Chairman of the BPPT: Welcome speech

Permanent Representative of Indonesia with WMO: Welcome speech

Chairman of BBPT: Welcome speech

Chair of the WMO Weather Modification Expert Team: Weather Modification in the Century of Weather, Water and Climate Challenges

Local Organizing Committee Representative: Logistic information

10:30 – 11:00 TEA/COFFEE BREAK

11:00- 12:00 INVITED TALKS
Chairman: M. Murakami

11:00 – 11:20
G. Vali: The race for ice

11:20 – 11:40
R. List: Invigorating and elevating weather modification

11:40 – 12:00
Z. Levin: Lessons learned from 50 years of cloud seeding in Israel

12:00-13:30 LUNCH

ORAL PRESENTATIONS

13:30 – 15:30 OBSERVATIONAL AND LABORATORY STUDIES
Chairman: S. Tessendorf

Ma XinCheng, Huang MengYu, Jin Hua, Zhang Lei, Zhang Qiang: Aircraft Measurements of Aerosols, Clouds and Precipitation Over Beijing

Daniel Martínez, Carlos A. Pérez, Guillermo Puente, Félix Gamboa, Sadiel Novo, Ibis Rivero, Graciela Angulo, Ismael Pomares, Alexei Gamboa, Elsa Velazco, Michel Rodríguez and Ernesto Chang: Artificial rainfall enhancement program in Cuba by convective cloud seeding. Achievements and shortcomings in the period 2005-2010.

Masataka Murakami and JCSEPA research group: Japanese Cloud Seeding Experiments for Precipitation Augmentation (JCSEPA) --- New Approaches and Some Results from Wintertime and Summertime Weather Modification Programs

P. A. Nesmeyanov, V. P. Korneev, M. S. Reznikov, V. N. Yemel'yanov and V. O. Sapozhnikov: Russian Technology for Regulation of the Processes of Atmospheric Precipitation Formation, Prevention of Formation and Fall of Hailstones and Fogs Dispersion

Thara V. Prabha, A. Khain, R. S. Maheshkumar, G. Pandithurai, J. R. Kulkarni, and B. N. Goswami: Microphysical signatures of aerosol-cloud interaction in the monsoon environment during CAIPEEX

Jiangping Pu, Wenhua Zeng, Zhanyu Yao, Wei Zhang and Yongyi Li: Compared Radar Reflectivity with Heavy Rain Droplet Size Distribution

Findy Renggono, Erwin Mulyana, Tri Handoko Seto, Budi Harsoyo, Djazim Syaifullah: Lake and Land Breezes on Lake Towuti and Their Effect on Convection in Larona Catchment Area, Sulawesi, Indonesia

Abdoulaye Sarr: New Development in the Senegalese Rain Enhancement Program "BAWAAN": Investigating key components in support to operations.

15:30 – 16:00 TEA/COFFEE BREAK

16:00 – 17:45 OBSERVATIONAL AND LABORATORY STUDIES

Chairman: Abdoulaye Sarr

Tri Handoko Seto, Samsul Bahri, Halda Aditya, Moch. Muchlis, Mahally Kudsy, Moh. Husni, Yusef Tiansyah, Rino B. Yahya, Heru Widodo, Mimin Karmini and Andi Suntoro: Weather Modification Program using Flare Technique at South Sulawesi,Indonesia – A Technology Transfer

Lijuan Su, Dabuxilatu, Shiqing Lu, Xiaodong Deng and Bing Yan: A Study of the Characteristics of Atmospheric Water Vapor and Its Relationship with Precipitation Using GPS Data

Hongping Sun, Peiren Li and Shiming Yan: A Study of Micro-physical Characteristics and Seedability of Cold Stratiform Clouds in North China

Sarah A. Tessendorf, Courtney E. Weeks, Roelof T. Bruintjes and Duncan Axisa: Cloud base aerosol characteristics and implications for microphysics from the Queensland Cloud Seeding Research Program

Xilatu Dabu, Shiqing Lu, Lijuan Su, Chengcai Li and Bin Yan: Monitoring Atmospheric Precipitable Water Using MODIS Satellite

Xueliang Guo and Danhong Fu: Effects of Giant-Particle Seeding on Cloud Microphysics and Precipitation Derived from Mesoscale Cloud-resolving Numerical Simulation

A.S. Drofa, V.G. Eran'kov, V.N. Ivanov, A.G. Shilin, G.F. Yaskevich: Experimental studies of salt powder efficiency at convective cloud modification for precipitation enhancement

Wednesday 5 October 2011

08:30 – 10:30 OBSERVATIONAL AND LABORATORY STUDIES
Chairman: G. Vali

U. Haryanto, R. D. Goenawan and D. Harsanti: The Development of Hygroscopic Cloud Seeding Flare In Indonesia: Evaluation and Measurement of Distribution Particles

B.P. Koloskov, V.P. Korneev, G.P. Beryulev, B.G. Danelyan, V.N. Stasenko: Twenty-five years of cloud seeding activity to modify weather conditions in cities

J. R. Kulkarni, R. S. Maheshkumar, S. B. Morwal, B. Padma Kumari, Mahen Konwar, C. G. Deshpande, R R. Joshi, R. V. Bhalwankar, G. Pandithurai, P.D. Safai, S. G. Narkhedkar, K. K. Dani, A. Nath, Sathy Nair., V. V. Sapre, P. V. Puranik, S. Kandalgaonkar, V. R. Mujumdar, R. M. Khaladkar, R. Vijayakumar, V. P. Thara and B. N. Goswami: Overview of CAIPEEX – Cloud-aerosol interaction experiment over Indian region

Lei Ji, Jianli Ma, Hongyu Li, Wei Zhou, Qiang Zhang, Jianzhong Liu: Analysis of Radar and Airborne Data for Artificial Seeding Effects

Andre A. Sinkevich, Terrence W. Krauss and Ayman S. Ghulam: Radar Investigation of AgI Seeding Efficiency in the Kingdom of Saudi Arabia

Samsul Bahri, Halda Aditya, F. Heru Widodo, Tri Handoko Seto: Weather Modification Activities in Indonesia

Terrence W. Krauss, Duncan Axisa, and Roelof Burger: Observations of Hygroscopic Flare Particles at Various Relative Humidity

Jun Zhou, Hengchi Lei, Hongbin Chen, Yanfei Wang, Zhen Zhao and Lei Ji: Retrieval of Cloud Liquid Water Content Distribution at Vertical Section for Microwave Radiometer Using 2D Tomography

10:30 – 11:00 TEA/COFFEE BREAK

11:00 – 12:45 OBSERVATIONAL AND LABORATORY STUDIES
Chairman: Tri Handoko Seto

Duncan Axisa, Lulin Xue, Roelof Burger, Don Collins, Evelyn Freney, Paul Kucera, Roelof Bruintjes and Peter Buseck: Evolution of boundary layer thermodynamics, aerosol and cloud microphysics during the weather modification assesment program in the southwest region of Saudi Arabia

Hayat Khan Azmat: Qualitative Assessment of the Effectiveness of Summertime Cloud Seeding Experiments in South-eastern Sindh-Pakistan

Siriluk Chumchean and Walairat Bunthai: Testing Efficacy of Rainmaking Activities in the Northeast of Thailand

Ying Duan, Jing Duan, Liling Ju: The Study of Distribution Character on Aerosols, Cloud Droplet and CCN over North China Useing Aircraft Observational Data

Jianli Ma: X-band dual linear polarimetric radar wave attenuation impact on hail identification

Yanwei Li and Niu Shengjie: Initial part discussion of cloud merger

Bart Geerts, Qun Miao, Dan Breed, Roy Rasmussen: Airborne radar and lidar studies of ground-based glaciogenic seeding of orographic clouds: preliminary findings and upcoming field campaign plans in Wyoming

12:45-14:15 LUNCH

14:15- 16:15 MODELLING STUDIES

Chairman: Theodore Karacostas

Mahally Kudsy, Ridwan, Findy Renggono and Faisal Sunarto: The Use of WRF Model To Support Cloud Seeding Operation: A Study in the Citarum Catchments Area

Rabia Merrouchi, Abdalah Mokssit, Jacques Piazzola and Mohamed Chagdali: Impact of natural production of coastal marine aerosols on convective clouds as simulated using cloud model with detailed microphysics: Comparison to cloud seeding with hygroscopic flares

Peiren Li, Junxia Li, Lijun Jin, Dongdong Shen and Gang Ren: A Numerical Study of Macro and Micro Structures of Stratus Precipitation Cloud in Spring of Shanxi Province

Yueqin Shi: Numerical Seeding Experiments on Stratiform Clouds in Spring in North China

Vlado Spiridonov, Zoran Dimitrovski and Mladjen Curic: Strategy of seeding using the results of a modelled hailstorm splitting

Yilin Wang and Zhanyu Yao: The improvement of cannon precipitation enhancement operations

Zhanshan Ma and Qijun Liu: Comparisons of Cloud Microphysical Characters between Mesoscale Model for Artificial Precipitation Enhancement and Satellite Observations

Daniel Breed, Lulin Xue and Roy Rasmussen: Numerical modelling studies in support of the Wyoming Weather Modification Pilot Program

16:15 – 16:45 TEA/COFFEE BREAK

16:45 – 17:45 MODELLING STUDIES

Chairman: Junxia Li

Joseph H. Golden, Daniel Rosenfeld, William R. Cotton, William L. Woodley, Isaac Ginis, Alexander Khain: Assessing A New Approach to Tropical Cyclone Modification by Hygroscopic Smoke

Xiaomin Chen: Numerical Simulation Studies with New Double-moment Explicit Microphysical Scheme in GRAPES

B. Sh. Kadyrov and V.P. Kurbatkin: Methods of modelling in controlling the processes in clouds

Theodore Karacostas, Vlado Spiridonov, Dimitrios Bampzelis and Ioannis Pytharoulis: A three-dimensional numerical simulation of supercell hailstorm seeding over Greece using a cloud model

Thursday 6 October 2011

09:00 – 11:00 MODELLING STUDIES
Chairman: B.P. Koloskov

Vlado Spiridonov and Mladjen Curic: Modeling of rainfall enhancement by seeding tropical convective clouds

Kien Truong Ba: Study, choose microphics and cumulus convection schemes in WRF Model to forecast heavy rain in Vietnam

Steven T. Siems and Michael J. Manton: Recent Progress in Glaciogenic Cloud Seeding over Southeast Australia and Tasmania

Sohaila Javanmard, Mahla Karimpirhayati, Javad BodaghJamali, Yusefali Abedini: Application of numerical cloud model in hail suppression of cold clouds

Xiaofeng Lou, Guanfang He, Zhijin Hu, Xing Zhang: Development of salt-seeding scheme in 3-D convective cloud model and seeding simulations

XiaoLi Liu and ShengJie Niu: Numerical simulation of macro- and micro-structures of intense convective clouds with a spectral bin microphysics model

Hongbin Li, Yuke He, Fansheng Zhao, Wenyao Pu: Applications of Doppler Radar Characteristic Parameters in Artificial Hail Suppression Decision Making

Junxia Li, Peiren Li, Yue Tao, Lijun Jin, Gang Ren: Contrast and Analysis of Numerical Simulation Results with the Airborne Detection Data of Precipitation Clouds

11:00 – 11:30 TEA/COFFEE BREAK

11:30 – 13:00 SEEDING MATERIAL AND METHODS OF DELIVERY
Chairman: V. Stasenko

Sutrisno, Tri Handoko Seto, Samsul Bahri, Tukiyat, Heru Widodo, Sunu Tikno, Budi Harsoyo, Djazim Syaifullah, Halda Aditya, Mimin Karmini and Krisna Aditya, Dini Harsanti: Weather Modification Program using Powder at West Java, Indonesia

Sarah A. Tessendorf, Roelof Bruintjes, Courtney Weeks, James W. Wilson, Charles A. Knight, Rita D. Roberts, Michael Dixon, Matt Pocernich, Peter R. Buseck, Evelyn Freney, and Duncan Axisa: A synthesis of physical and statistical analyses from the Queensland Cloud Seeding Research Program

M.T. Abshaev, A.M. Abshaev, B.K. Kuznecov, A.F. Kotelevich, T.H. Guzoev, N. Balakova, H.H. Chochaev B.V. Yakushkin, R.N. Ponomarenko, V.S. Trifonov: New advances in automation of anti-hail rocket technology

Mladjen Ćurić and Dejan Janc: Estimation of the deposited silver-iodide in the Hail Suppression Project in Serbia

Viktor Makitov: Integral radar parameters of hailstorms used on hail suppression projects.

Prapaporn Srisathidtham and Wassana Wongrat: Cloud Seeding Techniques in Eastern Region of Thailand

13:00-14:30 LUNCH

14:30 – 15:30 DATA ANALYSIS AND STATISTICAL METHODS
Chairman: D. Breed

Kianoush Keshavarzian: Assessment of cloud seeding projects using a combination of 'MAX' and 'SRI' radar images

Vlado Spiridonov and Mladjen Curic: A sensitivity study of the hailstorm seeding

M.T. Abshaev, A.M. Abshaev and A.M. Malkarova: Estimation of antihail projects efficiency considering the tendency of hail climatology change

Ružica Đurić: Efficiency of hail suppression based on radar data analysis

15:30 – 16:00 TEA/COFFEE BREAK

16:00 – 17:00 DATA ANALYSIS AND STATISTICAL METHODS
Chairman: D. Rosenfeld

S.G. Filippov: Estimation of orographic precipitation in the zone of spreading of the river flow in Uzbekistan

Daniel Breed: Design and preliminary results of the Wyoming Weather Modification Pilot Program Randomized Seeding Experiment

Zhanyu Yao, Ling Hou: Weekly Circulation Characteristics of Aerosol and Precipitation and the Possible Influencing Mechanism Analysis in Beijing and Surrounding Areas

Niu Shu-Zhen, Bao Xiang-Dong, Xi Shi-Ping, Yang Min: Analysis Application of Satellite Nephogram and CINRADAR Products in the Precipitation Enhancement Processes

EVENING AFTER DINNER: SESSION ON GEOENGINEERING ISSUES

Chairman: R. Bruntjes

Forum on "GEO-ENGINEERING AND CLIMATE CHANGE".

Friday 7 October 2011

08:00 – 10:00 WEATHER MODIFICATION AND THE PHYSICAL AND SOCIO-ECONOMIC ENVIRONMENT
Chairman: R. Bruntjes

Jean-Pierre Chalon: A short review on Geo-engineering proposals to fight against climate change

Roland List: 'Do no harm' geoengineering of climate and hurricanes

Zawiah Mohd Taib: Weather modification in Malaysia

M.V. Belyaeva, A.S. Drofa, V.N. Ivanov: Efficiency of Precipitation Enhancement from Convective Clouds at Salt Powder Modification

Budi Harsoyo, Nora H.Pandjaitan, Dwi Putro Tejo Baskoro: Analysis of Water Balance and Aridity Index to Detect the Effect of Global Warming in Catchment and Irrigation Area of Jatiluhur Dam

Ruijun Jin, Wan Wang, Wei Song, Zhaoyu Wang: Tianjin Precipitation Feature and Analysis of Weather Modification Influence

B.Sh. Kadyrov, V.P. Kurbatkin, V.F. Ushintseva: Demands of users in additional precipitation in Uzbekistan in the limits of their possible supply

Daniel Rosenfeld, Xing Yu, Guihua Liu, Xiaohong Xu, Yannian Zhu, Zhiguo Yue, Jin Dai, Zipeng Dong, Yan Dong, Yan Peng: Glaciation activity of desert dust, air pollution and smoke from forest fires in convective clouds

10:00 – 10:30 TEA/COFFEE BREAK

10:30 – 11:00 WEATHER MODIFICATION AND THE PHYSICAL AND SOCIO-ECONOMIC ENVIRONMENT

Chairman: J-P Chalon

Tri Handoko Seto, Samsul Bahri, Heru Widodo, Erwin Mulyana, Budi Harsoyo and Mimin Karmini: Weather Modification for Rain Reduction - A Conceptual Design

Stephen Beare, Ray Chambers, Scott Peak: Uncertainty and the Economic Implications of Weather Modification – Integrating Hypothesis Testing into Benefit-Cost Analysis

POSTER PRESENTATIONS

Qian Gao, Guanghe Wang, Yueqin Shi: Numerical Simulation and Seeding Tests on the Stratiform Precipitation in North China

B.P. Koloskov, V.P. Korneev, A.V. Kleimenova, B.N. Sergeev, A.V. Shapovalov: Numerical simulation of seeding material dispersion by ground-based AgI generators in mountainous terrain

Lixin Shi, Xiaobo Dong, Feng Lu and Xiangfeng Hu: Observations of Haze Aerosols over North China During Autumn 2009

Yuwen Sun, Wei Liu, Zhijun Zhao, Anying Shi, Yan Jiang: Hail types and Distribution of Related Factors

Dianli Gong and Shijun Liu: The Numerical Analysis About Water Vapor Budget and Precipitation Efficiency During July-October, 2003 in Shandong Province in China

M.V. Belyaeva, A.S. Drofa, V.N. Ivanov, Ridwan, M. Kudsy, U. Haryanto and R.D. Goenawan: Efficiency of Precipitation Enhancement from Convective Clouds at Salt Powder Modification

Rifeng Sheng, Zhanshan Ma, Jun Wang, Hongsheng Zhang and Peng Jiang: An analysis of a heavy snow occurred in Shandong Province of China in 2009

Zhen Zhao and Heng-Chi Lei: Numerical Simulation of Seeding Extra-Area Effects of Precipitation Using MM5

O.I. Drivotin, A.S. Drofa, A.V. Savchenko, A.G. Shilin, V.A. Shilin: Numerical Simulation of Heteorogeneous Pyrotechnic Compounds Combustion Processes

Sohaila Javanmard, Samane Golestani, Javad BodaghJamali, Yusef A. Abedini: Investigating on Microphysical Clouds Parameters Using Satellite TRMM-TMI

ESTIMATION OF ANTIHAIL PROJECTS EFFICIENCY CONSIDERING THE TENDENCY OF HAIL CLIMATOLOGY CHANGE

Abshaev M.T., Abshaev A.M., Malkarova A.M.
High Mountain Geophysical Institute, 360030, Lenin av. 2, Nalchik, Russia, abshaev@mail.ru

Abstract

Research results of global climate changes influence on hail climatology and evaluation of antihail projects are considered. It is shown that during last 50 years losses from hail and powerful hailstorms frequency in the North Caucasus mountain regions were reduced on the average in 2 times and was increased in adjacent foothill and plain areas by 20 - 30%. Therefore evaluation of hail suppression (HS) projects is recommended to be done with taking into account of tendency of hail hazard changes in each region.

1. About climate change tendencies

The estimation of HS projects efficiency is usually carried out in the assumption of hail climatology invariance [Guideline document, 2010]. At the same time, global climate warming on the North Caucasus over last 50 years has resulted to increases of air temperature by 0.36°C on average (fig. 1), air relative humidity by 6%, annual precipitation amount by 4 – 16% depending on regional orography (fig. 2) and also to change of hailstorms frequency both intensity and to high hail danger areas displacement [Abshaev, etc., 2003b, 2003c].

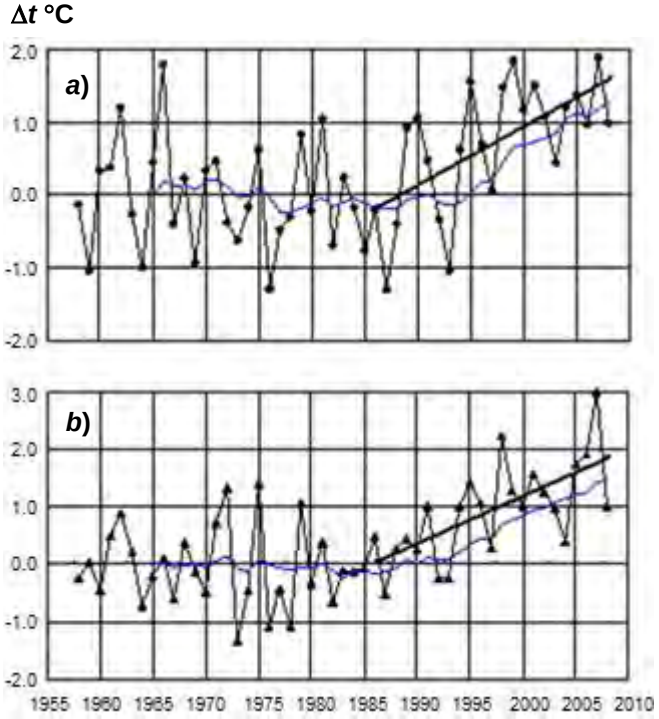


Fig. 1. Changes of air temperature on the North Caucasus averaged on 172 meteorological stations data:
a) mid-annual; ***b)*** in warm period of year.

Ignoring of these changes at estimation of hail suppression and precipitation enhancement (PE) efficiency can lead to overestimation of PE projects efficiency and also to biased efficiency estimation of HS projects.

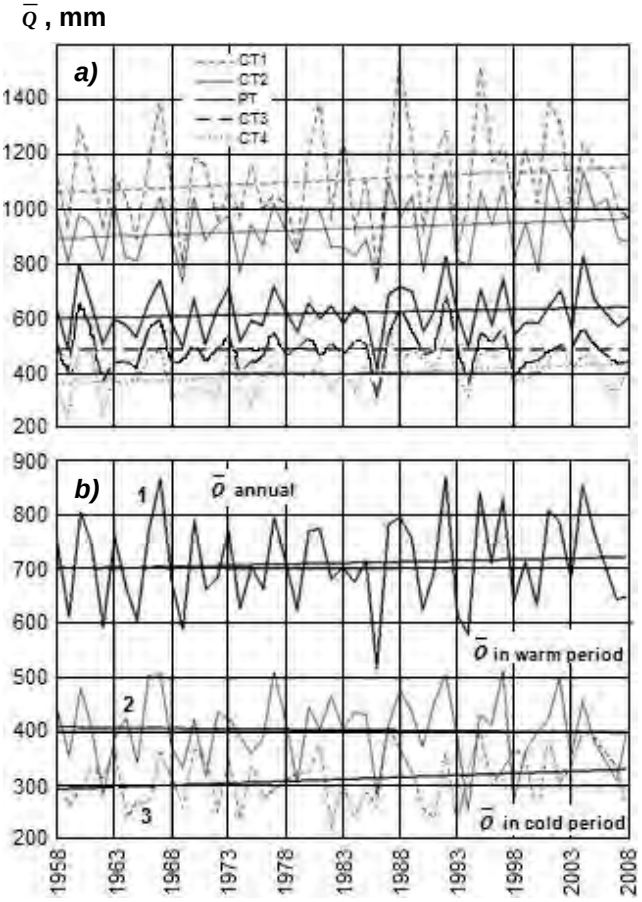


Fig. 2. Trend of precipitation amount $\bar{Q}$ (mm) in period 1958 – 2008 averaged on data of all meteorological stations in region: ***a)*** 4 control territories (CT_1, CT_2, CT_3, CT_4) and protected territory (PT); ***b)*** All territory of North Caucasus: 1 – annual sum $\bar{Q}$; 2 – warm period; 3 – cold period of year.

2. Tendency of hail danger change

Research of frequency of hail days on protected territory (PT), on 4 control territories (CT_1 - CT_4) and on all region of North Caucasus (fig. 3) has shown that the maximum number of hail days is fixed by mountainous meteorological stations (CT_2) and varies from 1.0 to 3.5 (average value is about 2.0) days in the year. High frequency of days with hail is marked also on PT: 1 - 3 days in year

(average value 1.5). Much less are on Black sea coast (CT_1), in steppe (CT_3) and plain areas (CT_4).

The average number of hail days in the North Caucasus in period 1960 - 1970 was raised and then some recession till 1990 is observed. After that, it remains approximately at one level. Essential reduction of averaged annual number of hail days is marked in mountainous areas (CT_2) and PT (possible this recession of hail activity on PT is connected with influence of HS).

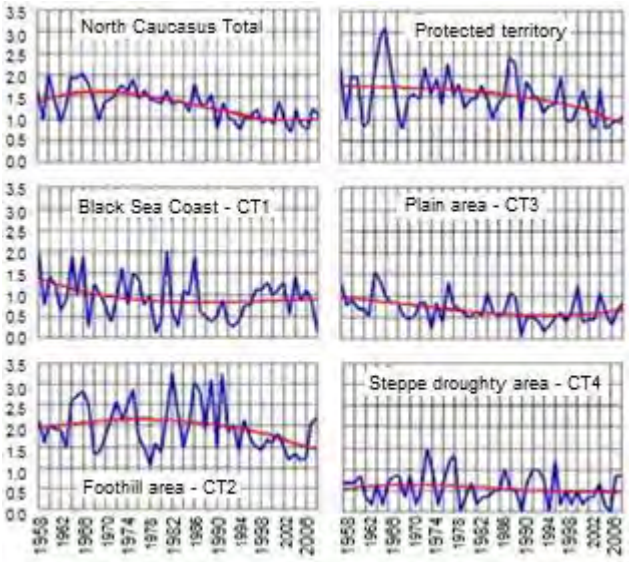


Fig. 3. Time course of averaged annual number of days with hail on CT_1, CT_2, PT, CT_3, CT_4 and the North Caucasus as a whole in 1958 - 2008.

Analysis of hail hazard according to meteorological stations of the North Caucasus in 1980 – 2008 has shown that highest change of hail days number $\overline{F}$ is observed in mountains and foothill areas.

In mountainous and foothill areas of North Caucasus were used data of 10 meteorological stations; in flat areas of Stavropol District - 4 meteorological stations and in foothill and plain areas of Krasnodar District were used data of 8 meteorological stations.

On fig. 4a the changes of number of days with hail during the warm period of year averaged on the specified groups of the meteorological stations located in mountainous and foothill areas of the North Caucasus, Krasnodar and Stavropol Districts is shown. From fig. 4a follows that those numbers of hail days have quasi periodic (with cycle 2 - 4 years) synchronous fluctuations on years of maxima and minima for all territory. It apparently is caused by that the majority of hail processes has frontal origin covering all region of the North Caucasus.

According to fig. 4a in period 1980 - 2008 the steady trend of reduction of hail frequency on mountainous and foothill areas of the North Caucasus and Krasnodar territory and some increase of frequency of days with hail in flat areas of Stavropol territory is marked.

In the beginning of the period of supervisions in mountains and foothills of the North Caucasus value of $\overline{F}_1$ was in 2,5 times higher than $\overline{F}_2$ of flat areas of Stavropol territory. In the time course $\overline{F}$ of all North Caucasus it is leveled and varies from $\overline{F}$ = 0.9 up to 1.1 hail days in counting on 1 meteorological station.

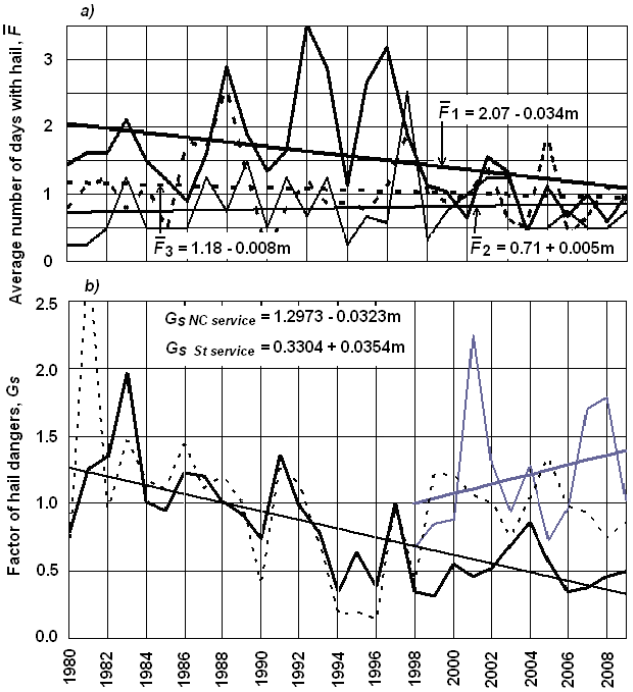


Fig. 4. Annual course: ***a)*** average numbers of days with hail according to meteorological network data: $\overline{F}_1$ - in mountainous and foothill areas of North Caucasus; $\overline{F}_2$ - in flat areas of Stavropol District; $\overline{F}_3$ - in mountain, foothill and flat areas of Krasnodar District. ***b)*** - coefficient of hail hazard G_S on PT of North Caucasian Service (dark continuous lines) and Stavropol (light continuous lines) and Krasnodar Service (dashed lines).

It testifies that value $\overline{F}_1$ in mountains and foothills in period 1980 - 2008 have fall tendency, and $\overline{F}_2$ in flat parts of the North Caucasus - an increase tendency: frequency of hail days in this period has decreased in 1.9 times. In Krasnodar District has decreased approximately on 20% (at the expense of its mountain and foothill parts), and in flat areas of Stavropol District has raised on 20%.

These changes of frequency of days with hail in different areas of the North Caucasus prove to be true changes of coefficient of hail hazard (G_S) on protected areas of three above-stated Antihail Services and also serious change of number of seeded hailstorms (see fig. 4b).

On PT of North Caucasian Service where hail suppression mainly covers mountain and foothill areas value of G_S in period 1993 – 1998 considerably decreased. On PT of Stavropol Service where protecting flats areas coefficient G_S increased by 40 % and on PT of Krasnodar Service (protecting mountain, foothill and flat areas) G_S first has decreased and since 1998 increased again.

3. Estimation of hail suppression efficiency

The estimation of efficiency of the Russian automated HS rocket technology is making according to the following equation:

$$E_f = \left(1 - \frac{N_S}{\overline{N}_C}\right) \cdot 100, \quad (1)$$

Where N_S and $\overline{N}_C$ – percent of agricultural products losses on PT in years with protection and their average long-term losses value before protection, counted in percents (%) under equations:

$$N_S = \frac{S_{100}}{S_\kappa} \cdot 100, \quad (2)$$

$$\overline{N}_C = \frac{1}{m} \sum_{i=1}^{m} \frac{S_{100_i}}{S_{\kappa_i}} \cdot 100, \quad (3)$$

Where S_{100} – area of hail damage recalculated on 100%; S_K – cultivated area on PT; m – number of years with observation.

However it is necessary to keep in mind that estimation of HS efficiency is essentially influenced by big variability of hail precipitation characteristics and hail hazards trend mentioned above. It can lead to underestimation of E_f value in years with raised hail danger and to overestimation of E_f in years with lowered hail danger.

To exclude such influence the estimation of physical efficiency of HS is recommended to be done in two different ways:

- By account coefficient of hail hazard of concrete year G_S (or the period of protection), in comparison with the previous period;
- By account frequency trend of hail days number established on long-term supervision.

To account coefficient of hail hazard in concrete year or the period with protection in comparison with the previous period the following equation is offered:

$$E_f = \left(1 - \frac{G_C N_S}{G_S \overline{N}_C}\right) \cdot 100, \quad (4)$$

Where S_{100} – area damaged from hail recalculated on 100%; G_C – coefficient of hail hazard before protection; G_S – coefficient of hail hazard in year with protection.

a) In years before protection G_C:

$$G_c = N_{c_i} / \overline{N}_c, \quad (5)$$

b) In year with protection G_S maybe calculated on the basis of seeding objects (SO) level, seeded in the year of protection to their mean annual number:

$$G_S = \sum_{i=1}^{4} A_i n_i / \sum_{i=1}^{4} A_i \overline{n}_i, \quad (6)$$

where N_{c_i} and $\overline{N}_c$ – losses of agricultural products from hail before protection in *i*-year and the average for all period of supervision in %; *Ai* – weight factors for SO of *i*-category; n_i – number of SO of *i*-category, seeded in year with protection; $\overline{n}_i$ – average long-term quantity of SO of *i*-category according to applied HS technology [Abshaev, 2010a] share on 4 categories: SO of I category – hail potentially clouds; SO of II category – hail dangerous clouds; SO of III category – hailstorms; SO of IV category – super-power hailstorms.

Values of factors *Ai* are defined with taking into account degree of hail danger of SO of various categories. For SO of III category value A_{III} = 1 is conditionally accepted and value A_{IV} is calculated under the relation of average values S_{100} from SO of IV and III category found on experimental data under the equation:

$$A_{IV} = \frac{n_{III}}{n_{IV}} \frac{\sum_{i=1}^{n_{IV}} S_{100IV}}{\sum_{i=1}^{n_{III}} S_{100III}}, \quad (7)$$

Thus, for the North Caucasus values *Ai* are accepted as following: A_I = 0.1; A_{II} = 0.3; A_{III} = 1.0; A_{IV} = 5.0. In province of Mendoza of Argentina A_{IV} = 5.59 [Abshaev, Malkarova, 1999].

On fig. 5 the annual distribution of HS efficiency E_f for each of 3 Russian Antihail Services, and on the total area of HS in Russia is presented:

- without G_S;
- with taking into account G_S;
- with taking into account the trend of hail days number $\overline{F}$.

From fig. 5 follows that the estimation of HS efficiency without G_S results to:

- Underestimation of E_f values in years of raised hail danger (for example, in 1983 on North Caucasus with abnormal high hail danger, value E_f was underestimated on 28%);
- Overestimation of E_f values in years with lowered hail danger (for example, in 1990 value E_f was overestimated on 11%).

Besides, on fig. 5 it is possible to see that at high efficiency of HS (with very small level of losses from hail on protected area) value E_f depends a little from estimation method with or without taking into account of hail hazard coefficient and its trend.

However, such estimation demands data about SO number of different categories in previous years. In the absence of such data (for example, in case of preparation of new HS project) estimation of project efficiency is offered to be done by the data of trend of hail days number.

Conclusion

1. On the basis of time course research of hail days frequency according to meteorological stations data of the North Caucasus the steady tendency of hailfalls frequency reduction in mountainous and foothill areas and its increase in flat areas is established for the last 30 years (1980 - 2008). Apparently it is caused by global climate warming and changes of atmospheric fronts intrusion directions.

2. With a purpose of increase objectivity and accuracy of estimation antihail projects efficiency the account of hail danger coefficient changes in years with protection or the trend of hail days number established on the basis of statistical investigation is offered. It allows excluding overestimation of HS projects efficiency in years of lowered hail danger and underestimation in years of raised hail danger.

3. Presence of steady trends of increase in an amount of precipitation in the North Caucasus testifies that the estimation of efficiency of precipitation enhancement projects also is carry out taking into account this trends.

References

Abshaev M.T., 2003a: Automated rocket technology of hail suppression. 8th WMO Sci. Conf. on Weather Modif. Casablanca, Morocco, 335-338.

——, Malkarova A.M., Borisova N.V., 2003b: Tendency of climate change on Northern Caucasus. Abstracts of World Climate Change Conf. Moscow, 323-324.

——, Malkarova A.M., 2003c: Efficiency of Russian hail suppression technology in different regions. Meeting of Experts on Hail Suppression. (WMO in Collaboration with Roshydromet), Nalchik, Russian Federation. 27 September – 2 October 2003, 99-115.

——, Malkarova A.M., 1999: Results of hail suppression Project in Argentina. 7th WMO Sci. Conf. On Weather Modif. Chiang Mai, Thailand. Vol. 2, 391-394.

Guideline document No 52.37.732-2010. Methods of estimation of efficiency of active influence on градовые processes. Nalchik, Publishing house. Elbrus, 2010, 48 pp.



Fig. 5. The time course of the HS efficiency:
a) North Caucasian Service, ***b)*** Krasnodar Service, ***c)*** Stavropol Service, ***d)*** All Services of the Russian Federation (1997 was out of protection).

DESIGN AND PRELIMINARY RESULTS OF THE WYOMING WEATHER MODIFICATION PILOT PROGRAM RANDOMIZED SEEDING EXPERIMENT

*Daniel Breed**

Research Applications Laboratory, National Center for Atmospheric Research, Boulder, CO 80307 USA

1. INTRODUCTION

The Wyoming Weather Modification Pilot Program (WWMPP) is funded by the State of Wyoming through the Wyoming Water Development Commission (WWDC), and is unique among state-sponsored programs in the USA in that it includes a substantial evaluation component. The main purposes of the WWMPP are to establish an orographic cloud seeding program in three target areas (the Medicine Bow Range, Sierra Madre Range and Wind River Range) and evaluate the feasibility and effectiveness of the cloud seeding. The logistics, infrastructure, and operations of the program are covered under a contract with Weather Modification Inc. (WMI), while the evaluation activities fall under a separate contract with the Research Applications Laboratory (RAL) of the National Center for Atmospheric Research (NCAR).



Figure 1. *Map of Wyoming with coarse representation of topography and land use. Red outlined areas denote the three mountain ranges selected for cloud seeding operations: Medicine Bow, Sierra Madre, and Wind River. The randomized seeding experiment involves only the two southern ranges, the Medicine Bows and Sierra Madres.*

Attempts to increase snowpack by seeding clouds have been carried out for well over fifty years. Average increases of 10 to 15% have been reported in some experiments, but the topic remains controversial and many operational programs and scientific experiments have ended without conclusive results. Because of the large natural variability of precipitation and the relatively small seeding effect expected, it is generally believed that no single analysis can be convincing regarding the effect of seeding. Rather, it is necessary to build multiple layers of evidence, both statistical and physical, to provide a consistent picture of the effect of cloud seeding. This paper addresses the statistical approach – the design of the randomized seeding experiment.

2. OVERVIEW OF THE DESIGN ELEMENTS

Resources used for carrying out the experimental design include 16 ground-based seeding generators (8 in each range), 21 precipitation gauges at 8 sites (with redundancy at each site and some experimental gauges), 12 weather stations (at each gauge site and four at generator sites), two microwave radiometers for detecting SLW, a radiosonde unit ("weather balloon" for measuring temperature and winds at cloud heights), and a numerical forecast model cycling every three hours with updated observations. The seeding generators, radiosonde unit, and one radiometer are operated by WMI, and the precipitation gauge network, one radiometer, and forecast model are operated by RAL/NCAR. Figure 2 shows all of the resources deployed in the southern mountain ranges. (The precipitation gauge sites of 5502E, Douglas Creek, and Rob Roy are no longer active.)

The following list highlights some details of the design elements of the randomized seeding experiment. These were established in 2007 and subsequent studies have modified some of the estimates, such as correlations, sample size, and annual number of cases, which are discussed in Section 3.

- Target areas have been identified near the crests of the Medicine Bows and the Sierra Madres, encompassing the existing SNOTEL sites at Brooklyn Lake and Old Battle (shown in Fig. 2). The SNOTEL data indicated that these target areas receive significant snowpack during a season [15 November – 15 April].
- Seeding generator sites have been chosen to affect the target areas under predominant wind directions (roughly from the southwest, west, and northwest directions). Their location on Forest Service lands required long permitting lead time and acceptable forest clearings. The spacing of generators was roughly determined from results of past studies, taking into account practical siting considerations, and was further characterized with plume modeling.

*Author address: NCAR/RAL, P.O.Box 3000, Boulder, CO 80307-3000, USA. Email: breed@ucar.edu

- Seeding generator sites have been chosen to affect the target areas under predominant wind directions (roughly from the southwest, west, and northwest directions). Their location on Forest Service lands required long permitting lead time and acceptable forest clearings. The spacing of generators was roughly determined from results of past studies, taking into account practical siting considerations, and was further characterized with plume modeling.
- A majority of the storms in this region affect both ranges. This is evident from the relatively high correlations of ~0.5 for daily snowfall between the ranges using SNOTEL data from sites in or near the target areas within each range.
- A cross-over design is planned, in which one range is randomly determined to be seeded while the other becomes the control. This results in paired cases.
- The seeding treatment period will be kept short (4-hr) to strive for homogeneous conditions as well as to obtain a greater number of cases. A buffer time period of 4-hr will be used between consecutive treatment periods to clear the area of seeding material.
- High-resolution precipitation measurements will be made using gauges (resolution 0.1 mm, recorded in 5-min periods) at both target and control sites in each range.
- Two closely-spaced (~2 km apart) sites will be used in each target area in the respective ranges and averaged to decrease the variance in the precipitation measurement at each site.
- Two control sites, one largely upwind and one largely cross-wind, will also be used in each range and treated independently in the statistical evaluation. The control sites will be used to help describe the natural variability in precipitation between targets and between events.
- Case selection requires: temperatures that are cold enough for efficient AgI IN activation; wind direction that is appropriate for some AgI generators to impact the target; and the presence of SLW. These criteria should be satisfied in both target ranges simultaneously.
- The primary statistical test will be based on ratios – summation of 4-hr accumulated precipitation at target gauges for seeded versus unseeded events, scaled by the ratio of 4-hr accumulated precipitation during seed/no-seed events at control gauges.
- The ratio test will be used to evaluate the null hypothesis that the ratio of the total measured precipitation for seeded versus unseeded conditions is equal to 1. A ratio significantly greater than one would suggest evidence for the effectiveness of the seeding method (see Gabriel, 1999).
- An estimate of the number of paired cases to be expected in an average season is about 60-70 with a sample size of the order of 165 to 360 to detect a 15% to 10% precipitation increase.

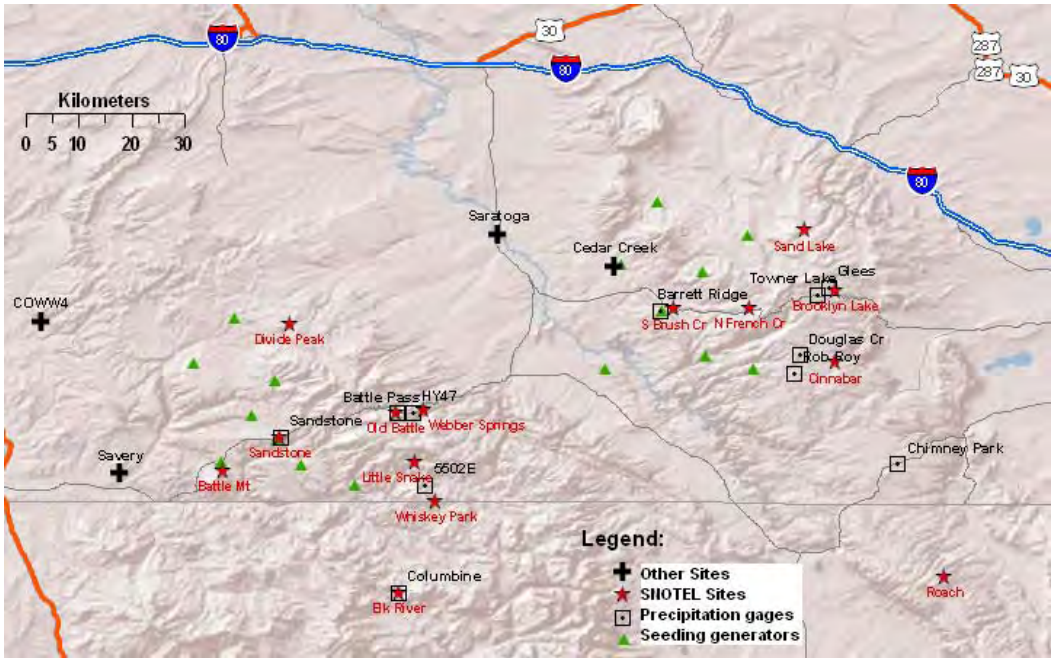


Figure 2. *Instrument sites and operational networks in the southern mountains of Wyoming (Medicine Bows to the east, Sierra Madres to the WSW). The precipitation gauge sites are indicated by a square; SNOTEL sites are indicated by red stars; AgI generator sites are indicated by green triangles; and other sites are indicated with bold crosses. Savery and Cedar Creek are radiometer sites, and the Saratoga site is where soundings are released. (COWW4 is the Cow Creek Remote Automated Weather Station site.)*

3. ESTIMATES OF SAMPLES NEEDED AND EXPECTED

The number of samples needed for statistical significance depends on several factors, as shown in the equation below (Gabriel, 1999; Eqn 6).

$$n_{RRR} = 2\sigma^2 (1-\tau)\left(1-\left(\frac{\kappa-\gamma}{1-\tau}\right)^2\right)\left[\frac{Z_\alpha + Z_\beta}{\ln(1+\delta)}\right]^2$$

The first term, σ^2, refers to the relative variance of the precipitation amounts; the second term takes into account the correlation (r) between the two target ranges; the third term includes correlations between control sites and the target ranges; and the fourth term contains variables dependent on the significance level, power, and the (assumed) effect or increase in precipitation. A range of significance levels and power of the statistical test (variables in the fourth term) were investigated using past experiments, and were used in the equation to determine sensitivity to various but appropriate values. The final design settled on a significance level of 0.95 (representing a guard against false positives) and a power of 0.80 (representing a guard against false negatives). Various levels of effects or precipitation increases (δ) can be assumed and used in sensitivity trials.

While the initial studies relied on historic data (e.g., from SNOTEL sites) to estimate the number of cases likely to be gathered in a season and the total number of cases needed for statistical significance (given some assumptions), data collected during actual cases have begun to refine those original estimates. Two key variables that directly affect the number of cases needed for the experiment are measurement variance (i.e., the variations of snow amounts that fell during cases) and correlation between ranges (i.e., how closely snowfall amounts in each range track each other for the cases).

Following two seasons of precipitation data and case selections, a re-examination of the number of cases expected and updates on correlations and variances was done. This re-examination was performed only to validate or demonstrate variability in the initial estimates and was not used to alter the experimental design in any way.

First, the actual number of cases selected in a season (35-40 per season) was about half of what was expected. This is largely due to case selection criteria, particularly temperature at 700 mb, not considered in the initial estimate, as well as a variety of other factors (e.g., ending the season early due to high snowpack, a larger buffer period in the experiment than was used in the initial estimates, etc.).

Second, correlations and precipitation variance were calculated from cases during two seasons. The number of cases is still quite small, so there is the possibility for high variability in these values. The correlations are not much different than the initial estimates. The overall correlation of the two seasons was ~0.6, which is basically the same as was initially assumer (0.6). The same was true for the control-target correlations. The precipitation variance is lower than initially estimated: ~0.61 versus 1.12. That value has been steady from season to season, which might be expected given that winter orographic precipitation at the 4-hr time period is not highly variable (unlike convective precipitation). The initial estimate used coarse-resolution data over longer time periods, both of which contributed to a higher variance.

Using the more representative data to estimate variance and correlations, the number of samples needed to detect a 10% effect was calculated to be 209 (with a range of 77-282). This updated estimate is less than initially calculated, mostly due to the change in the precipitation variance. This suggests that the lower number of cases per season currently being experienced will not be as limiting as first thought. However, this exercise points out the necessity of collecting appropriate data prior to an experiment in developing a final experimental design. A recent example of this is the seeding experiment designed for the Snowy Mountains in Australia (Manton et al., 2011).

4. COMMENTS

Elements for the cross-over design of a randomized seeding experiment of winter orographic storms for two southern mountain ranges in Wyoming have been described. A number of issues remain, particularly regarding effective targeting and potential contamination between ranges, which need to be assessed within the framework of the experimental design. The second path of the evaluation approach – exploratory studies – is addressing some of the issues as opportunities arise.

ACKNOWLEDGEMENTS

The Wyoming Water Development Commission (WWDC) of the State of Wyoming is the sponsor of the WWMPP and Barry Lawrence, the program manager representing WWDC, has been extremely helpful in carrying out this work. We also acknowledge the support and efforts of many RAL staff members, the crew at WMI, researchers at the University of Wyoming, and collaborators at the South Dakota School of Mines and Technology and the U.S. Forest Service. NCAR is sponsored by the National Science Foundation.

REFERENCES

Gabriel, K. R., 1999: Ratio statistics for randomized experiments in precipitation stimulation. *J. Appl. Meteor.*, **38**, 290-301.

Manton, M., L. Warren, S. Kenyon, A. Peace, S. Bilish and K. Kemsley, 2011: A cloud seeding project in the Snowy Mountains of Australia – Part 1: Experimental design and observed data. *J. Appl. Meteor. Climatol.*, in press.

Numerical Simulation of Heteorogeneous Pyrotechnic Compounds Combustion Processes

Drivotin O.I.[(1)], Drofa A.S.[(2)], Savchenko A.V.[(2)], Shilin A.G.[(2)], Shilin V.A.[(1)]
[1] *State University, 7, University naberezhnaya, Sanct-Peterburg, 199034, Russia, e-mail:valentine@metal-profi.ru.*
[2]*RPA "Typhoon",4, Pobedy st., Obninsk, Kaluga Region, 249038, Russia,e-mail: drofa@typhoon.obninsk.ru*

Knowledge of a yield of useful active aerosol particles in the products of pyrotechnic compounds combustion is needed for assessing the ice-forming efficiency of pyrotechnic flares developed for super cooled cloud modification activities aimed at precipitation monitoring or hail protection (Zimin, 1992). As far as the majority of cloud modification agents decompose to one or another degree during combustion of pyrotechnic compounds, the efficiency of the aerosol formed to a certain extent depends on the regimes of pyrotechnic mixture combustion and agent evaporation. A theoretical estimate of active ice-forming particles yield is usually made on the basis of thermodynamic calculations of combustion of a pyrotechnic mixture with a preset composition (Cruise, 1991). In this case it is assumed that during combustion the phase and chemical equilibrium states are conserved. It is also assumed that a pyrotechnic mixture is homogeneous in structure and combustion proceeds in flat-parallel layers, that does not occur in real conditions. Because of the nonhomogeneous structure of the substance the process of fragmented burning of separate granules of the mixture takes place.

Combustion fragmentation may be caused by granularity of the mixture or its components, local disturbances from the composition, the presence of defects or zones with increased mechanical stress in the pyrotechnic compound. Because of these reasons a heterogeneous temperature field – maximum in the zone of intense burning of the granules of the burning substance and a sharp decrease of temperature at a distance from them – is formed. A wide range of active substance evaporation at the destructive combustion is realized depending on the existing actual temperature field and the geometry of the combustion front. The destructive combustion regime of pyrotechnic compounds in the heterogeneous temperature field is likely to determine the dispersion properties and chemical composition of the aerosol formed. An extremal example of the pyrotechnic compounds fragmentation combustion may be a blow-out of unburned particles of the active substance outside the combustion zone.

The data of experimental measurements of yields of aerosol particles generated by pyrotechnic substances with different dispersion properties performed at the SI RPA "Typhoon" are shown in Figure 1. The same Figure gives the measurement results for the number of active crystallization nuclei obtained at combustion of the ice-forming pyrotechnic compound AD-1 used in Russia in anti-hail activities. The components of this compound were grounded in a ball mill. Depending on the time of grinding different dispersion properties of the pyrotechnic mixture was obtained – with increasing time of grinding the sizes of pyrotechnic compound particles become smaller. The composition obtained is pressed into tablets and then burned in a closed aerosol chamber. The samples of aerosol particles are taken and placed into the climatic chamber with supercooled fog at a temperature of – 10°C. Ice-forming activity of the compound was determined by counting the number of crystals formed. As is seen from Figure 1, the activity of one and the same compound depends on the degree of grinding of the pyrotechnic mixture. There exists a certain degree at which the activity of the compound is the highest.

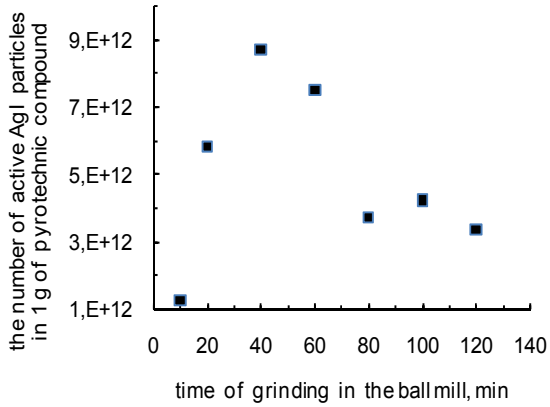


Figure 1. Dependence of AgI active particles yield on the time of pyrotechnic compound grinding

A theoretical estimate of ice-forming particles for the given AD-1 composition made on the basis of thermodynamic calculations gives the value of $1.26 \cdot 10^{13}$ of active AgI particles in combustion products of 1 g of pyrotechnic mixture. It is assumed that burning of AD-1 takes place in an equilibrium regime at a temperature of 1496^0K. As is seen from Figure 1, the number of active particles measured is considerably less than the theoretical value. A high degree of grinding the pyrotechnic mixture components is not optimal for obtaining the maximum activity of the aerosol formed. The results presented do not make it possible to interpret unambiguously depending on particle sizes of the pyrotechnic mixture as the

grinding of different components of the mixture in the ball mill depends on mechanical properties of separate components. But the experimental data show that the heterogeneous structure of distribution of separate components in the pyrotechnic compound influences significantly the yield of active particles generated. This effect should be considered at choosing the combustion regime of pyrotechnic compounds.

At present, the theory of combustion of pyrotechnic compounds generation aerosol with preset characteristics is at the stage of formation. In the present paper, the combustion processes of pyrotechnic compounds containing an active substance for aerosol particles generation were numerically simulated. The goal of the simulation is the investigation of a dependence of active aerosol particle yield on the thermodynamic characteristics of the pyrotechnic compound components and on their disperse composition.

When constructing the 3-D numerical model it is assumed that the pyrotechnic compound consists of two components – a burning substance realizing the process of combustion and an active substance evaporating in the temperature field formed within the substance. These substances are in the form of spherical granules of different diameters. The distribution of the granules is taken to be normal with preset modal diameters and dispersion of distributions. The granules of both types are located in the cylindrical part of the space randomly at the condition of minimizing a free space among the granules. Modeling of granules allocation in the cylinder is made with the help of a genetic algorithm (Lakhmi, 1998). The space among the granules is filled with a binder, the heat of combustion of which is neglected as compared to the heat of combustion of a burning substance. Purposeful numerical simulations are made for a pyrotechnic compound in which the ballistite is used as a burning agent. AgI is an active substance. The physical, chemical and thermodynamic characteristics of these substances are known.

Modeling of the processes of combustion, heat transfer in the medium and evaporation of the components of the compound is made on the basis of a numerical solution of the equation of changing heat within the pyrotechnic compound space:

$$\frac{\partial Q(x,y,z,t,T)}{\partial t} = \alpha_i \left(\frac{\partial^2 T}{\partial x^2} + \frac{\partial^2 T}{\partial y^2} + \frac{\partial^2 T}{\partial z^2} \right) + \quad (1)$$

$$+ Q_1(x,y,z,t,T) + Q_2(x,y,z,t,T)$$

Where:

t – actual time;

T – temperature of the medium at the point with coordinates x,y,z;

$Q_1(x,y,z,t,T)$ – amount of heat released in the region of burning substance combustion;

$Q_2(x,y,z,t,T)$ – amount of heat absorbed in the region of burning substance evaporation;

α_i – heat conductivity coefficient of the medium in corresponding regions.

The ignition of the burning substance is simulated by a contact of a granule with the hot surface. A heat outflow induced by the chemical combustion reaction from the surface of the granule takes place with the intensity calculated with the use of the heat conductivity equation for non-stationary exothermic reaction. Combustion of burning granules is calculated under the assumption that at the temperatures of the granule surface lower than the critical T_c heat absorption occurs, and when the temperature of the granule becomes higher than this, the process of combustion takes place with heat emission at a constant mass velocity.

To calculate the sublimation of the active substance in a heterogeneous temperature field the calculated dependence of the degree of destruction of the active substance on temperature was used. It was found with the use of programs for the calculations of the thermodynamic equilibrium. The calculations were made for the pyrotechnic compound AD-1 containing 8% of active AgI. Changes of the temperature of the compound combustion were modeled by the addition of the Mg-MgO substance (up to 20% in mass). As the calculations have shown, the composition of combustion products changed insignificantly, and the combustion temperature changed by more than 500^0K. The calculation results for the yield of non-destructed AgI are shown in Figure 2. The dashed line shows the calculation data approximated by the polynomial of degree:

$$P(T)=6.619E\text{-}7\cdot T^3\text{-}0.004015\cdot T^2+7.76\cdot T\text{-}4765 \quad (2)$$

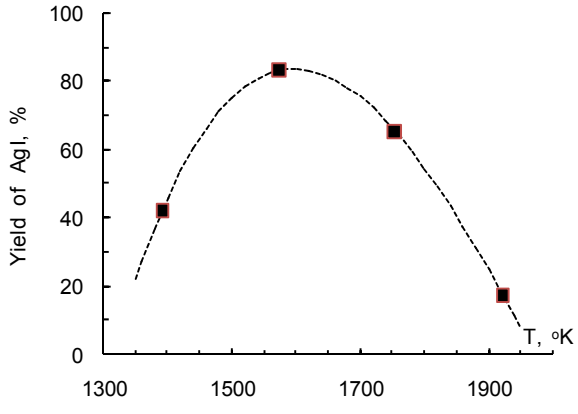


Figure 2. Dependence of AgI destruction degree on temperature.

Formula 2 was used in numerical simulation at calculations of AgI sublimation from the surface of the granule of the pyrotechnic compound active substance. It is assumed that after sublimation the

vapor phase of AgI leaves the combustion zone and does not destruct under high temperatures.

For numerical solution of the boundary-value problem (1) with corresponding initial and boundary conditions a non-uniform three-dimensional grid of space decomposition is applied. At calculations in the regions inside the granules a 1/10 of a granule diameter step was used. In the range between the granules the step equal to 1/10 of minimal diameter of the granules of the pyrotechnic compound was used. At transition from one integration range to another the decomposition step changes and the recalculation of the nodal values is made by the linear interpolation method.

The results of numerical simulation of a yield of non-destructed AgI in the vapor phase at the combustion of pyrotechnic compounds with different dispersion properties are given in the Table. The calculations are carried out for pyrotechnic compounds containing 8% of the active substance (AgI) at granules different sizes of the burning and active substances. As is seen from the Table, a non-monotonous dependence of non-destructed AgI is observed at varying initial sizes of pyrotechnic compound particles. When determining the grinding degree of the pyrotechnic compound components, maximum yield of AgI into the vapor phase without destruction is observed. The same character of changing active particles yield is also observed in the experimental data on the activity of ice-forming aerosol in the AD-1 pyrotechnic compound presented above.

Table. Results of modeling AgI transition into the vapor phase at different diameters of burning and active substances.

Burning substance, Diameter of granules, μm	Active substance, diameter of granules, μm	% of AgI that passed into the vapor phase without destruction
250	30	35 %
150	20	50 %
100	10	61 %
50	8	73 %
25	4	82 %
12	2	72 %
6	1	64 %

Thus, the results of numerical simulation show that the processes of fragmentary combustion of pyrotechnic compounds can significantly affect the efficiency of pyrotechnic generators operation. This effect must be taken into consideration at the development of such generators.

References

Zimin B. I. The active modification of clouds and fogs. Gidrometeoizdat, Moskow, 1992 [in Russian].

Cruise D. R., Theoretical Computations of Equilibrium Composition, Thermodynamic Properties, and Performance Characteristics of Propellant Systems. *NWC TP 6037*, Naval Weapons Center, China Lake, CA 93555-6001, 1991.

Lakhmi C. Jain; Martin N. M., Fusion of Neural Networks, Fuzzy Systems and Genetic Algorithms: Industrial Applications. CRC Press LLC, 1998.

EFFICIENCY OF HAIL SUPRESSION BASED ON RADAR DATA ANALYSIS

Ružica Đurić
Department of Meteorology, University of Belgrade
11000 Belgrade, Serbia
xmgrace@gmail.com

1. Introduction

In Serbia, hail suppression has been developed using radar datasets from 1967 till now. The hail suppression system covers approximately eight million hectares; four million hectares are agricultural and have eighteen hundred hail suppression stations.

Important aspects of the whole hail suppression activities is the collection of data needed for a further analyses. Two different types of data are collected: radar data and data from firing stations[1]. Observers on these stations have reported days when hail occurred at station, hail intensity, duration and size of hailstones (ranged in nine classes).

Radar data give us a large number of info-rmation such as: the radar cloud top heights, the heights of maximum reflectivity zone, the rate of maximum reflectivity, RHI and PPI pictures, CAPPI volumes etc.

The evaluation of the efficiency of hail suppression in Serbia has been based on two sources of data, which have been obtained independently of the hail control system (Radinović, 1988). These are: 1) the size of the hail-swept agricultural area and percentage of the damaged crops; 2) frequency of hail occurrences observed at the regular network of meteorological stations. Several statistical tests have been applied and they showed the significant efficiency (the hail swept area decreases for about 70%).

The effects of cloud seeding, which is associated with changes at the cloud top height, height of maximum radar reflectivity, height of increased radar reflectivity zone[2] and the maximum radar reflectivity, are researched and analysed.

2. Project design

In this study the same method of analysis as in the project Ćurić, (1989), applied to another, more recent data, is being used exactly. The method is based on analysis of the radar parameters which are observed in so called hail suppression field during summer months (15th April till 15th October) of 2009. Each field is approximately 30 km of radius with radar located at the centre of the field.

When the cloud reaches a given criteria (usually based on radar reflectivity values when they exceed 45 dBz), the cloud was seeded. The firing stations are on distance of about 5 km. Each m^3 of seeded zone contained the 10^5 – 10^6 artificial crystallizing nuclei.

3. Data

A large amount of ground measurements and observations, standard meteorological information and radar data are collected during the operational project.

The changes of multiple radar parameters are noted for every single cell in short periods of time. Some of them are: an indicator of variable in cell movement (its azimuth and distance), the cloud top height, height of maximum radar reflectivity, height of increased radar reflectivity zone and the maximum radar reflectivity.

The previous mentioned radar data are available every two or three minutes (and more often as needed), so we are able to follow the clouds evolution.

The report also contains the most important operational parameters, such as the number and type of rockets fired in the clouds and time of firing.

4. Method of evaluation

Assumption that seeding increases the concentration of the ice particles in the cloud; imply the question, what does this do to the previously mentioned radar parameters of cloud? Expected changes of radar parameters reflect dynamics and processes that are happening in the cloud. Some of possible effects are: change in cloud microphysics (glaciations); change in cloud dynamics (intensification of the updraft, shortening and lengthening of cell lifetime, etc (Foote et al., 1979; Federer and Waldvogel, 1978).

Radar parameters of 80 hail cells have been analysed and investigated. Those cells, which seeded and unseeded duration of periods were 20 minutes respectively, are selected. Obviously, long-lasting cells are considered. Within seeded period may be some unseeded sub periods if its duration is shorter than 5 minutes. In general, total unseeded period is sum of pre-seeded and post-seeded periods.

Between two successive measurements the linear change of data is assumed.

The following expression is used for calculation of the coefficient k as a measure of the tendency change for considered radar parameter Y

[1] substations manned by trained volunteer observers
[2] 45 dBz - intensity of isoline top

$$k_{iY} = \frac{1}{2}\frac{\left(Y(i+1)-Y(i)\right)^2}{\left(Y(i)-Y_{sr}\right)^2}$$

where *i is* the time interval, *Ysr* the average value of the considered radar parameter over the all time period (in our case this period is 20 minutes) . Since we considered time interval of 2 minutes for one cell, 10 values of coefficient *k* are calculated for seeded and 10 values for unseeded period. This coefficient is considered as predictor for the previously mentioned radar parameters.

seeded periods (the smaller slope of the curve). Spontaneous formation of hailstones leads to their higher growth so, their falling speed have higher values.

In unseeded periods which contains pre-seeded and post-seeded period, there are higher frequencies of occurrences coefficient k just after seeding, as we expected. After that there is dissipation of values as shown by the low frequency of this size (Radinović and Ćurić, 2008).

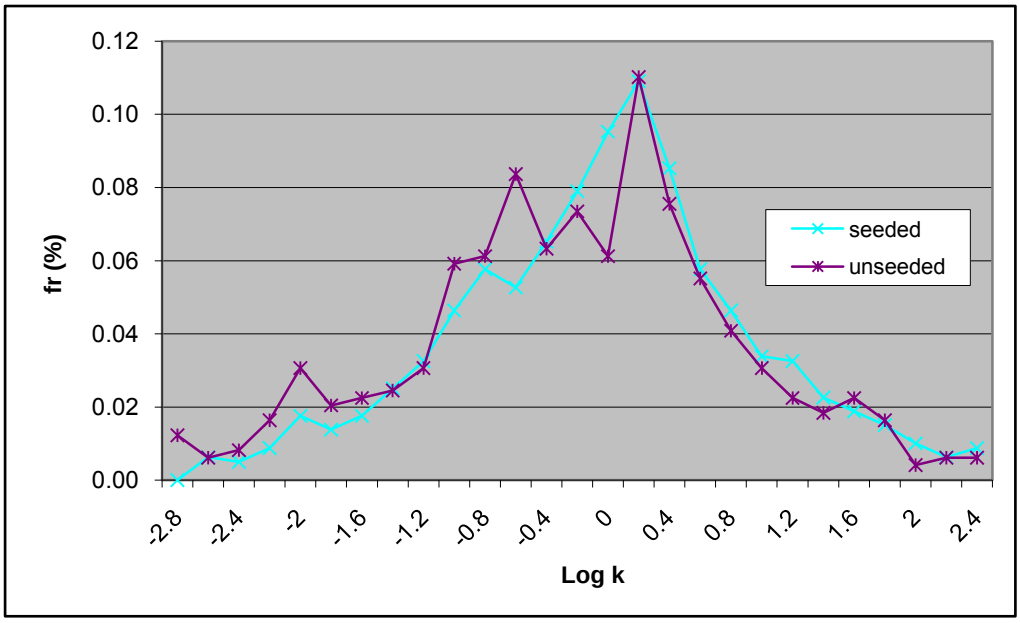


Fig. 1. Frequencies of the maximum reflectivity height as function of Log k for all cells.

5. Preliminary descriptions of the predictors

The purpose of this section is to find one quantity that predicts the behaviour of considered radar parameters in seeded and unseeded periods for all 80 cells. The difference between these quantities must have information about seeding effects on clouds. The frequency distribution of the considered radar parameters for all cells as a function of coefficient k is analysed, where frequency is given in percentage.

5. 1 The height of the maximum reflectivity

The frequency of maximum reflectivity heights of all cells as a function of log k is shown in Fig. 1.

For unseeded period two maximum frequencies of occurrence of values k are indicated, and even for seeded period (blue line) it is indicated one maximum which coincides with maximum of unseeded period with higher values of coefficient *k*. Second maximum of unseeded periods is moved toward the lower values of *k* and is significantly above the curve of seeded periods.

As well, there is slower decrease of frequencies in seeded periods than in pre-seeded and post-

5. 2 The height of increased radar reflectivity zone

The frequency of heights of increased radar reflectivity zone as a function of log k is shown on Fig. 2. These curves have similar behaviour as those for previously analysed radar parameters. The maximum frequencies are moved toward the smaller values of *k*. It is obvious for seeded cases that the increase of frequencies with higher values of coefficient k than for unseeded cases exist.

The increases of these heights in seeded period is greater than in pre-seeded and post-seeded periods because the resulting updraft is stronger due to the formation of new ice particles in cloud.

5. 3 The cloud top height

Seeding of convective clouds can modify cloud top height through microphysical and dynamical effects. This increase in cloud height is induced by artificial glaciations of super-cooled cloud water as noted by many authors (Simpson and Dennis, 1974; Dennis et al. , 1975; etc.) .

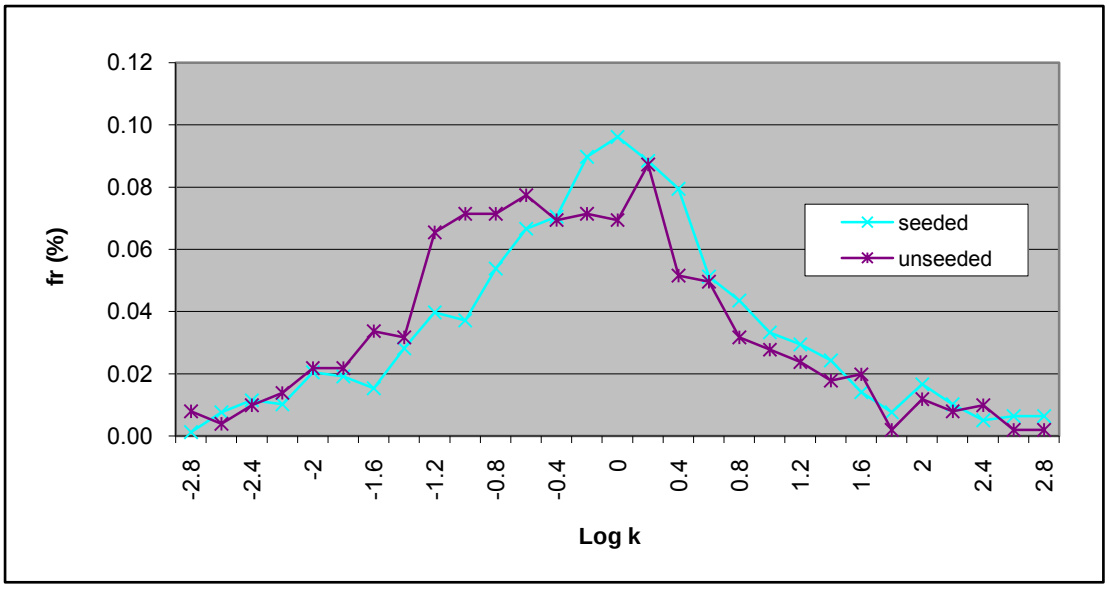


Fig. 2. Frequencies of increased radar reflectivity zone height as function of Log k for all cells

The frequency of cloud top heights as function of log k is shown in Fig. 3. The behaviour of this distribution is similar to the two previously analyzed heights. The main features which emerge from curves behaviour is expressed by increase of frequencies for higher values of *k* for seeded period (the large peak).

For unseeded periods, the maximum frequencies of values k are expressed, which is contrary to previously analysed cases.
This is explained by the fact that physical processes, on which seeding is based, are more important only after firing several rockets into the clouds (Ćurić and Janc, 1991).

5. 4 The maximum radar reflectivity

The frequency of maximum radar reflectivity as function of log k is shown in Fig. 4.

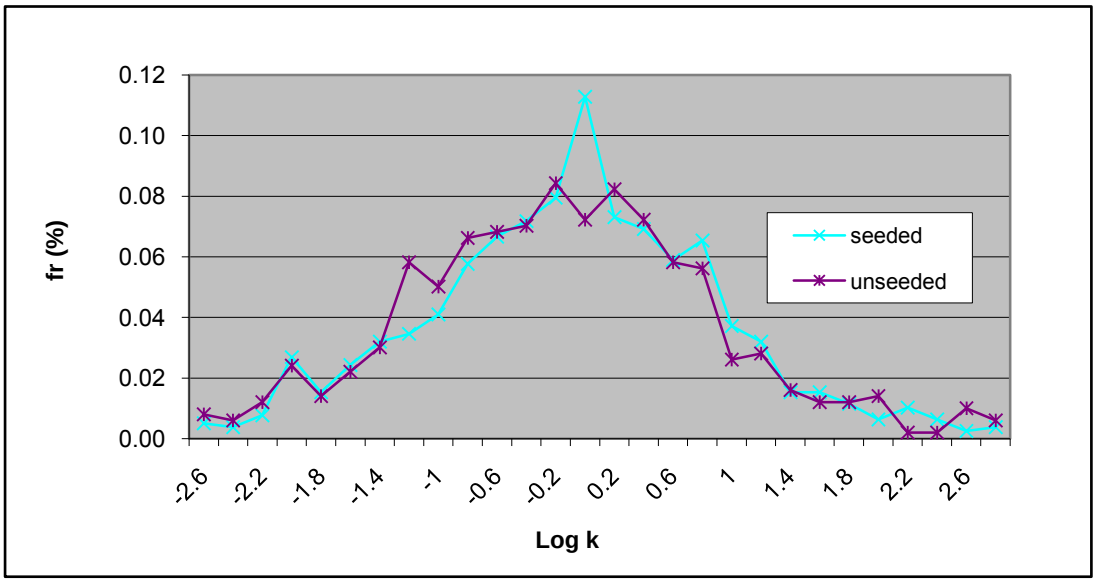


Fig. 3. Frequencies cloud top height as function of Log k for all cells

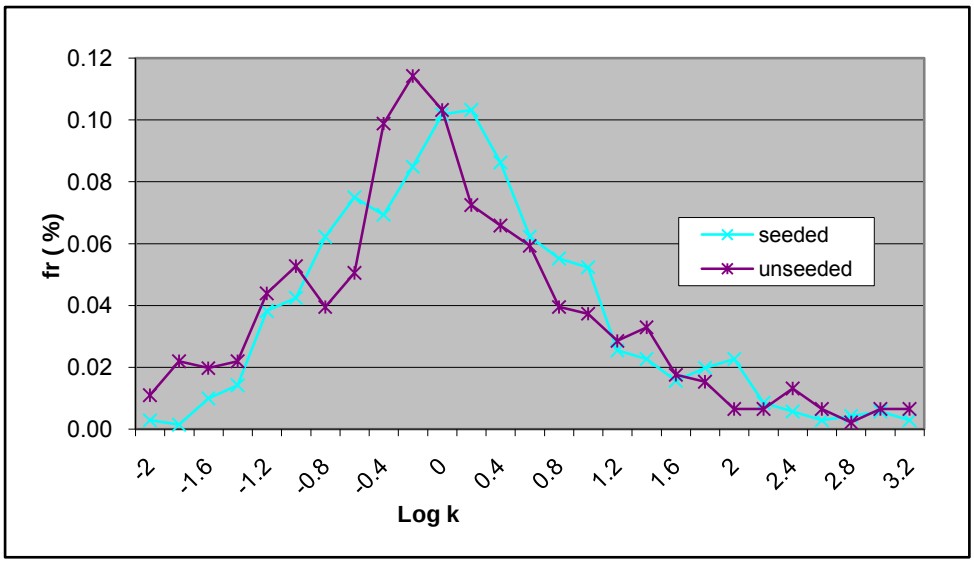


Fig. 4. Frequencies of the maximum radar reflectivity as function of Log k for all cells.

6. Conclusion

In this paper, the effects of hail suppression as one indicator of the seeding are analysed and the results include the following:

1) seeding has clearly expressed influence on frequencies distribution change (increase in number of cases with higher values of coefficient k for considered three radar parameters except for the maximum radar reflectivity where this increase is greater for unseeded periods);

2) changes of analyzed radar parameters are different in case without seeding, seeding with one rocket, two, etc.

This is confirmed by what is obtained with earlier radar data.

Acknowledgements

The author gratefully acknowledge to Republic Hydrometeorological Service of Serbia for providing the radar data used for this study and special thanks to Prof. Dr. Mladjen Ćurić and Julijana Nadj. Discussions with them were insightful and very helpful.

References

Ćurić , M., Efficiency of hail suppression derived from radar data analysis, *J. Wea. Modif*, 18, 601-604, 1989.

Ćurić , M. and D. Janc, Dependence of radar parameter changes from amount of reagent in seeding Cb clouds, *J. Wea. Modif*. 66 , 59-67, 1991.

Dennis, A. S. , et al. , Analysis of radar observations of a randomized cloud seeding experiment . *J. Appl. Meteor*. , 14, 897-908, 1975.

Federer, B. , and A. Waldvogel, Time resolved hailstone analysis and radar structure of Swiss hailstorms. *Quart. J. Roy. Meteor. Soc*. , 104 , 69-90, 1978.

Foote , G. B. , et al. , Results of a randomized hail suppression experiment in Northeast Colorado, part IV: Analysis of radar data for seeding effect and correlation with hailfall. *J. Appl. Meteor*. 18, 1569-1582, 1979.

Radinović, Đ. , Effectiveness of hail control in Serbia. *J. Wea. Modif*., 22, 70-75, 1988.

Radinović, Đ., and M. Ćurić, A specific evidence of hail suppression effectiveness in Serbia. *J.Wea.Mod.*39, 75-84, 2008.

Estimation of orographic precipitation in the zone of spreading of the river flow in Uzbekistan

Filippov S.G, NIGMI, Uzbekistan

Temperature increase caused by the change of the global climate and decrease of atmospheric precipitation can cause the decrease of water supply and increase of demand for water. The demand for water increases very sharply. At present 70 – 80% of fresh water is needed fore irrigation, 20% is required for the industrial needs, about 6% is necessary for domestic needs. The stability of production of food and industrial development will be dependent more and more on the rational and efficient use of water resources, elaboration of new technologies including weather modification for producing the additional precipitation in the areas of the irrigated and dry-farming lands. The problem is to develop and introduce water-saving technologies, new methods of precipitation management and getting the additional one in the regions where it is needed.

The reasonability of precipitation enhancement for the Central Asian region is determined by the availability of cloud resources, by the big territory occupied with mountains about 490.000 km^2 where about 470 mm of precipitation (the part of which the orographic ones are) falls. It is not easy to simulate the orographic precipitation as many factors should be taken into account: elevation of air flow, condensation and fallout of the condensed moisture. For the actual relief the vertical flow component which is perpendicular to the barrier is defined by following equation

$$w_{op} = u\frac{\partial h}{\partial x} + v\frac{\partial h}{\partial y},$$

where $\frac{\partial h}{\partial y}$ and $\frac{\partial h}{\partial x}$ - are the quantities of spatial mountain slopes. Regardless the simple structure of formula, it is very difficult to calculate the value of w_{op} which is very close to the actual value needed for calculation of different weather element. For this the digital map of the location recalculated to the steps of regular grid is needed. Such digital surface model (DSM) was created with GIS-technologies. The vertical currents linked with orography by Zalyznyak method [1]. These calculations were made with the digital elevation model and for the direction of air flows which make the main contribution to the precipitation share on the territory of Uzbekistan. Calculations showed that for different areas the vertical velocity related to orography can reach 5 – 6 cm/s (Fig.1). It was estimated that elevation of mechanical uplifting of air particle on which the kinetic energy of air flow raised from the earth was ~ 750 m with the account of friction.

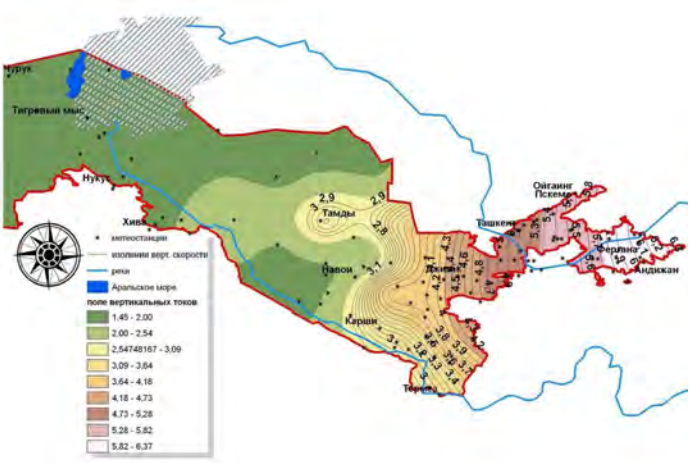


Fig.1. Vertical currents with the western directions of the air flows.

The drop growth in this layer is calculated by the formula $r_m = \sqrt{2\varepsilon D t}$, where D-coefficient of the water vapor in the air, time of drop life in the cloud. Assuming that the velocity $w_в$ of updraft is constant, then the time of water drop existence in the cloud layer can be estimated as: $t = \frac{H}{w_в - w_к}$ and then we derive formula for the growth of drops of r_m radius with elevation where

$r_m = \sqrt{2\frac{\varepsilon}{w}DH}$, ε - absolute supersaturation.

The value of r_m for not very thick cloud which was taken for calculations does depend on the updraft velocity. That is why $\varepsilon = \frac{D}{w} \approx \lambda$, λ - constant value and by estimation of N.S.Shishkin [2] it equals $\lambda \approx 10^{-11}$cm.

$r_m = \sqrt{2\lambda H} \approx 1{,}2 \cdot 10^{-3}$ cm =12 μ. For precipitation it is not sufficient but with the methods of weather modification this moisture reserve can be produced as precipitation. The results of our calculations coincides with the drop sizes experimentally assessed by Zaitsev V.A.[3] in 1948 and Mazin and Khrgian [4]

Increase of the radius of drops which determines the maximum water content of summer clouds with height according to Zaitsev V.A.

Height over the cloud base, m	100	200	400	600	800	1000
r_m, μ	5,5	9,0	9,5	9,5	11,5	14,5

Let's calculate the value of the absolute supersaturation for the considered conditions. By formula of Magnus the absolute moisture of saturating air is:

$$q = \frac{q_0}{1+\alpha_p T} e^{\frac{17.2T}{235+T}},$$

where α_p - coefficient of extension;

T-air temperature in °C. After time differentiation we get:

$$\frac{dq}{dt} = \frac{dq}{dt}\frac{dT}{dz}\frac{dz}{dt} = -\frac{(16.3-0.07T)}{235} q\gamma w,$$

γ – vertical temperature gradient inside cloud; *w* - updraft velocity. We use this value for calculation of the absolute supersaturation. The final result can be written as:

$$\varepsilon \approx \frac{(16{,}3-0{,}07T)}{235}\frac{4qr_m^2\gamma w}{15D\omega} + \varepsilon_0(r_m)$$

The second term does not depend on w. With T~3°C, as it was presumed above, D=0.22cm^2/s q=6.2·10^{-6}g/cm^3; γ=6·10^{-2} °/m; w≈10cm/s; $r_m \approx 10^{-3}$cm; $\omega \approx$10-6g/cm^3; supersaturation будет равно $\varepsilon \approx 8 \cdot 10^{-10}$

For approximate assessment calculations the supersaturation in the cloud can be considered as dependent only from the vertical flow velocity presented on Fig.2.

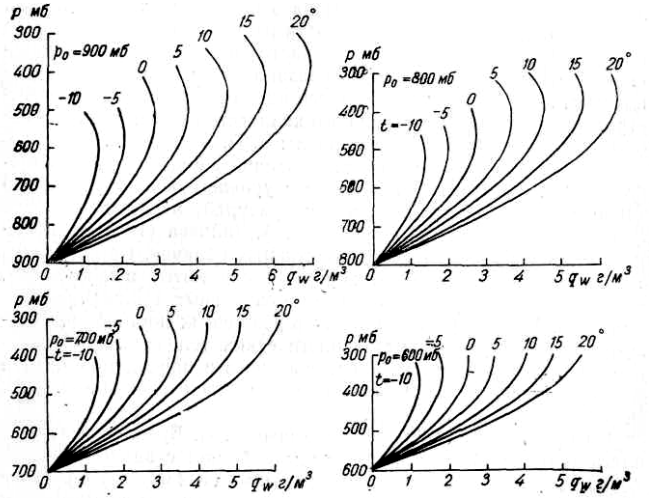


Fig.2. Change of adiabatic water content in the cloud base of which is at p_0 - level while the air temperature at this level is t_a [2] with height.

Basing on this it is possible to estimate water content of the clouds assuming that their relative air humidity is 100%, and the whole excessive moisture is condensed with the uplifting of cloud mass. This corresponds to the maximum possible cloud water content.

Results of calculations are given on Fig. 3. With w = 0,1 m/sec сек. из облака может выпасть 0,4 mm of precipitation can fall from the cloud, with w=1 m/sec - 3,7 mm, with w = 5 m/sec.- 11,3 mm.

The share of condensed moisture falling out as precipitation varies from 0,7 for the cloud with vertical flows with velocity about w = 0,5 m/sec. up to 6 for cloud with c *w = 3* m/sec.

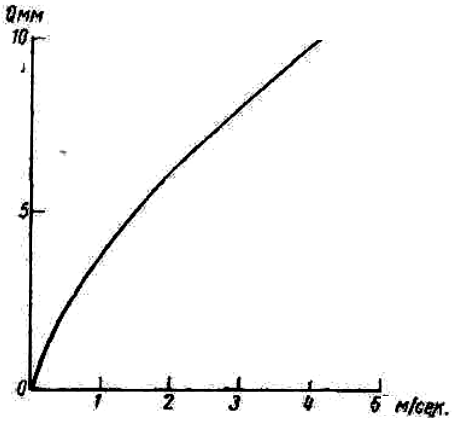


Fig. 3. Relationship between precipitation amount and updraft velocity in clouds for the case when the updraft is ceased after the beginning of rain [2].

Total precipitation regardless their intensity for the clouds with small intensity development can keep more then 1,5 hour.

The obtained results were compared with climatic data of precipitation on Fig. 5. For the comparison the long-term data for winter months, spring ones as the most humid and summer months were taken for comparison.

This schematic map shows that the field of vertical flows calculated for directions most often recorded for Central Asia region and making the biggest contribution to precipitation of this region has good correlation with field of precipitation. In this case the winter month was taken. The highest precipitation amount is recorded in alpine areas while here the maximum values of vertical flows are recorded.

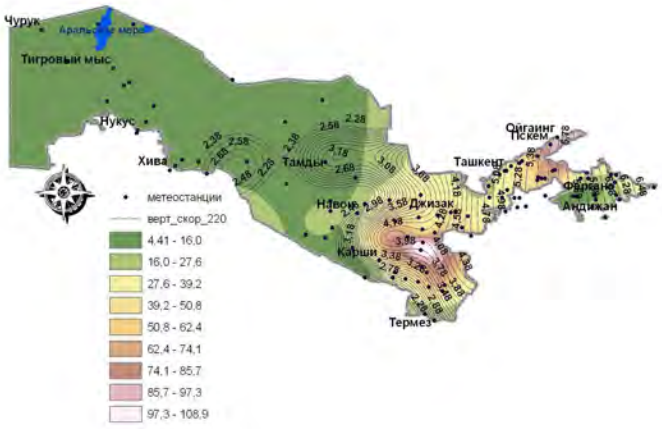


Fig.5 Field of precipitation and of vertical flows for 220° directions.

We consider that these calculations show the main characteristics of orographic precipitation in proper way. Basing on made calculations and shown graphs we estimated that the share of orographic precipitation comprises one tenth of the total precipitation amount, and this can serve as substantial contribution to addition of the moisture reserve of the region.

References:

1. Zalyznyak E.L. Calculation of the orographic air flows in the central and southern regions of Krasnoyarsk area//Proc. of Hydrometeorological Centre. -1972. - Vol.91.- p.110-115.
2. Shishkin N.S. Clouds, precipitation and thunderstorm electricity // Hydrometeorological publishing house. - Leningrad. - 1964. – 400pp.
3. Zaitsev V.A. Sizes and distribution of drops in the cumulus clouds // Proc. of GGO. - Vol.13.-1948.
4. Clouds and cloud atmosphere // Reference book. Edited by Dr. of Phys. & Math. Sc. Mazin I.P. and Dr. of Geogr. Khrgian A.Kh.

ASSESSMENT OF CLOUD SEEDING PROJECTS USING A COMBINATION OF 'MAX' AND 'SRI' RADAR IMAGES

Keshavarzian K.[a],
[a]*WRI, National Cloud Seeding Research Centre,*
Mojtame Edarat, Standard st., Daneshjoo blvd.,
Yazd, Iran, P.O. Box: 89195/611, Postal Code: 8916188115,
E-mail: kshvzn@gmail.com

1. Introduction

The effectiveness of cloud seeding projects is an important question that should be answered truly. Although the effect of seeding agents on precipitation enhancement could be investigated in cloud chambers, but in situ observation and measurement of the precipitation that occur after a cloud seeding project and a comparison to the estimated one, would provide a large amount of data about background ice nuclei and how they act in nature, the optimum injecting rate and method, the performance of a project and so on. In this work, a new method for evaluating the seeding projects is introduced and tested for three flights over Tehran (as a polluted area) on 13-Dec-2010. On that day, Tehran had distanced about three months without any rain or snow and the pollution had reached to its peak (at least near the earth). Then, this city was covered by stratiform clouds whose base was situated mostly at the height of 1500 meters. Three flights had been carried out with the aim of enhancement of the rain. Since the existing statistical evaluation is being used for long term projects (usually monthly or annual), a radar-based method is introduced for assessment of the three Tehran projects and could be used along with other useful methods (Larsen 2003, Novák 2009 and Woodley 2004).

This method is based on a comparison between MAX (maximum reflectivity of a vertical column in cloud) and SRI (rain intensity) products of radar. In this work, these products belong to a Gematronik dual polarized C-band radar. Because other radars in Iran are not dual polarized and I was seeking a method which could be used for any projects over Iran, its dual polarized products (differential reflectivity, correlation coefficient, linear depolarization ratio and specific differential phase) have not been used. In addition, we does not need the numerical value of rain intensity measured by radar until the last step (calculating of increased volume of rainfall) and only the reflectivity from precipitation level (1 km above the earth) is important. Also, in the central plateau of Iran, the rain intensity rarely exceeds *6 mm/hour* and in this interval, as reported in Ryzhkov 2003, the ordinary ZR relationship is reliable. Nevertheless, we are using the dual polarized products in further researches.

2. Basic Structure

The reflectivity measured by weather radars, Z, is directly proportional to the sum of backscattering cross sections of particles (rain drops and snow flake (SRI) or cloud droplets and ice crystals (MAX)) which is:

$$(1)\quad \sum \sigma = \frac{\pi^5}{\lambda^4}|K|^2 \sum D^6 ,$$

where λ is the wavelength, D is the effective radius of the particles in backscattering process and:

$$(2)\quad K = \frac{m^2 - 1}{m^2 + 2} ,$$

where m is the refraction index of the particles for wavelength of λ. This parameter is measured for water as $|K|^2=0.93$ and for ice as $|K|^2=0.21$. As a result, when we deliver ice nuclei in clouds and cause supercooled water to convert to ice (through Bergeron process) in fact, we cause $|K|^2$ to decrease about 4.4 times (provided that all of supercooled waters convert to ice crystals). On the other hand, due to the following reasons, D is increasing:

1. The volume of particles is increasing (due to the freezing process of water).
2. Ice crystals are sticking together to form snow flake such a way that their effective backscattering cross section is becoming greater than the sum of their individual cross sections.

This effect is visible in vertical profiles of radar images as the bright band (provided that the zero isotherm place above the cloud base). The reflectivity of the above and the below of the bright band is almost the same (Doviak 1993). Therefore, when artificial IN are active, the ratio of the reflectivity of cloud to that of precipitation level should vary, because the numerator remains almost constant and the denominator changes.

3. Statistical Calculations

In this method, the control and the target area situate in the same geographical co-ordination but different times. The boundaries of the target area could be determined using the latitude and longitude of the shooting points (injection places), speed and direction of the wind and the long life of the injected particles. The control areas locate at the same place but before the injection or after the time that IN had inactivated. Although there are many scripts that had reported different longevities for AgI to be active in clouds, I supposed the most common one *i.e.* 2 hours. Fig.1 shows the target (and the control) areas on sample pictures for three flights. It should be mentioned that because of the forbidden zone flights

over the capital city of Iran, we had many restrictions to choose the suitable flight routs.

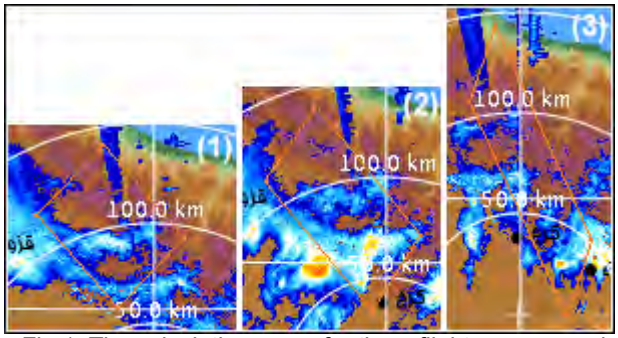


Fig.1: The calculation areas for three flights on a sample (SRI) radar picture. The pictures are chronologically sorted from left to right.

The time of the flights plus the duration of the activity AgI aerosols are:

1) Flight (1) from 03:32 to 07:02 GMT
2) Flight (2) from 09:32 to 12:17 GMT
3) Flight (3) from 15:02 to 17:32 GMT

We have three control zones for every flight:

1) Before the first flight (control A),
2) Between the first two flights (control B),
3) Between the last two flights (control C),

which they had the same diagram and position as target areas. As is discussed in the section 4, we can choose the best control pictures between A, B and C. It is important to choose a radar cloud picture which makes a reliable correlation with rain intensity. I found that MAX pictures acceptably satisfy this condition. Fig.2 illustrates the variation of spatial average of the MAX and SRI dBz for red quadrilateral shown in Fig.1, third flight.

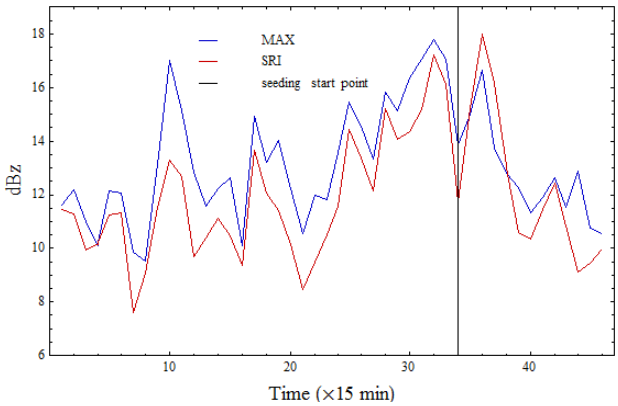


Fig.2: The dBz variation of MAX and SRI for the region shown in Fig.1, third flight.

The equivalent graphs also exist for the first and second flights (Figs.4 and 5). The ratio of the MAX over SRI for this flight is shown in Fig.3. Note that the scales of the vertical axes in these two figures have been assimilated in order that the comparison becomes more convenient. It is obvious from Fig.3 that the variations of 'MAX over SRI' are small and this relation remains near *1*. This issue bodes the good correlation between MAX and SRI pictures. In addition, we see a significant change after the moment that seeding is started. Such a sudden change also occurs in graphs of the first and second flights as is shown in Figs.4 and 5 and implies that this change should be the result of cloud seeding (some MAX pictures lost and the corresponding SRI pictures eliminated).

It should be mentioned that the height of zero isotherm was *1800 m* from the earth which is higher than the minimum of the height of the MAX images (*2000 m*). The *correlation* of the MAX and SRI for Fig.2 is *0.877*, for Fig.4 is *0.824* and for Fig.5 is *0.565* which shows, except for the second flight, we can use the MAX images to estimate the SRI values.

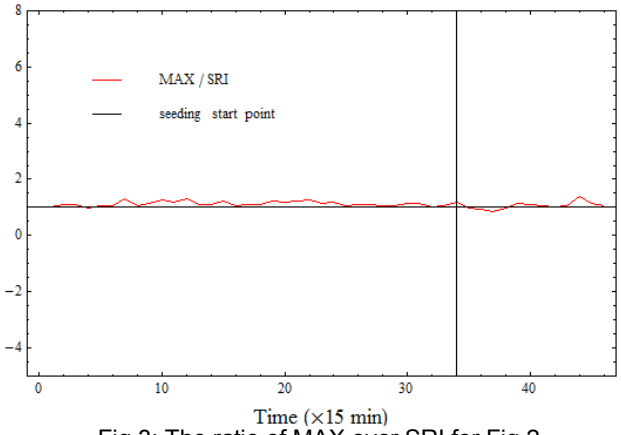


Fig.3: The ratio of MAX over SRI for Fig.2

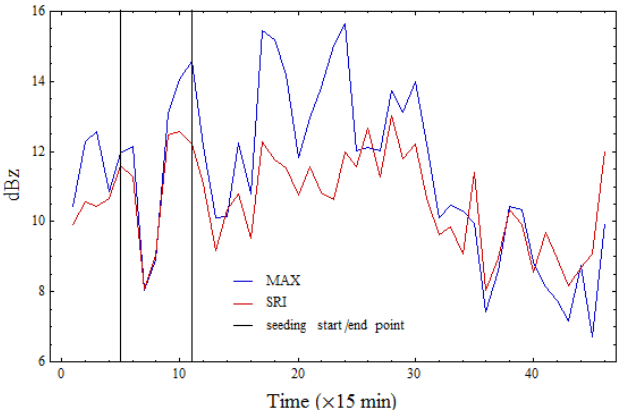


Fig.4: The dBz variation of MAX and SRI for the region shown in Fig.1, first flight.

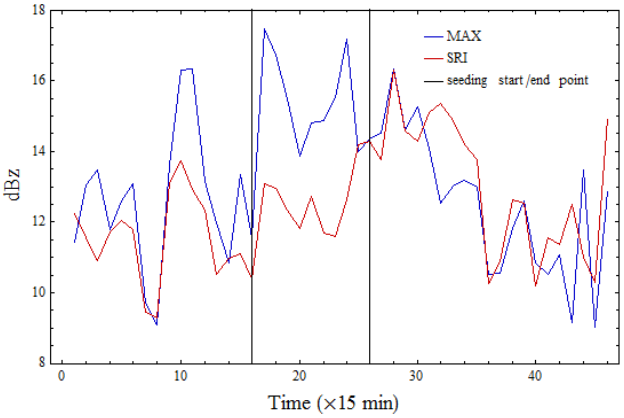


Fig.5: The dBz variation of MAX and SRI for the region shown in Fig.1, second flight.

To verify that if the MAX/SRI ratio lies inside the interval of natural variations or not, we have used

the *standard deviation* of this ratio for target and control pictures. When we deliver artificial aerosols in clouds inhomogenously, we would disturb the natural values of the ratio and as a result, the possibility of the values to occur far from the average would increase. The standard deviation should get back to the natural value when the aerosols had been distributed homogenously. It means that the standard deviation of the target pictures should be larger than that of control pictures.

4. Discussion and Results

The standard deviation of MAX/SRI and the correlation between MAX and SRI of the target and its three control pictures have been shown in table 1 for every flight. The results have been discussed in below:

Table 1: The information we need to choose the best control zone

		Standard Deviation	Correlation
Flight 1	Target	0.0737	0.968
	Control A	0.0879	0.510
	Control B	0.0621	0.796
	Control C	0.0876	0.768
Flight 2	Target	0.118	0.0935
	Control A	0.133	-0.901
	Control B	0.0796	0.598
	Control C	0.0792	0.336
Flight 3	Target	0.145	0.868
	Control A	0.0520	0.800
	Control B	0.103	0.479
	Control C	0.0575	0.903

Flight 1: The standard deviation of the target zone is larger than control B (so MAX/SRI variations lies outside of the natural variations of this control zone) and the correlation of this control zone is reliable (larger than 0.75). Also the correlation of the target zone is near 1. Knowing the MAX/SRI for control B we are able to calculate the expected SRI for target and compare it to its real value.

Flight 2: The standard deviation of the target zone is larger than all the three control zones but none of the zones have a reliable correlation value. As it is shown in Fig.1, the spatial expansion of the first and the second flight are very close to each other and the time interval between them was only 2 hours! Probably, the clouds had still been influenced by the aerosols of the first flight. In addition, because of the failure connection between the radar and the server, we missed 6 MAX pictures for this flight, which would increase the statistical error of the computations. Also it is likely that there exist convective clouds at the altitude that radar measures the rain intensity. In this case, the correlation between MAX and SRI will be decreased extremely. Fortunately, the dual polarized radars are able to distinguish between rain drops and cloud droplets with the aid of the algorithms that calculate the ratio of the two diameters of falling drops (Ryzhkov 2003). It is the issue of the further researches. Because of the mentioned reasons I excluded this flight from evaluation.

Flight 3: The standard deviation of the target is larger than all three controls, but the correlation of the control C is larger than that of others. In addition, the control C is instantly before the time of the third flight. The real and expected SRI variations of this flight are illustrated in Fig.6.

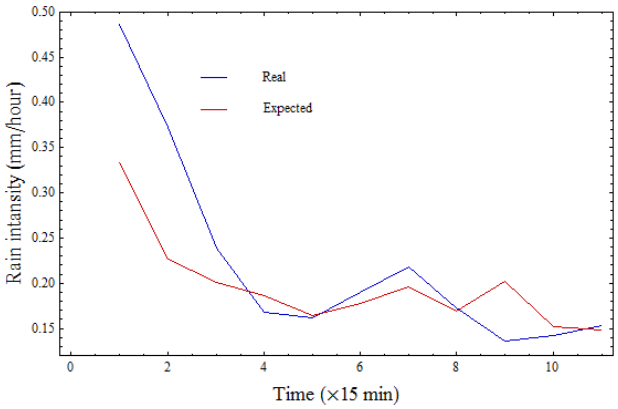


Fig.6: The real and expected SRI variations for third flight

The enhanced volume of water and the rain enhancement percentage is listed in table 2.

Table 2: The results of three projects

	Increased Volume (m^3)	Percentage
Flight 1	-6100.38	-2.1
Flight 2	Could not be determined	Could not be determined
Flight 3	83758.6	17.5

It is obvious from Fig.3 that the rain intensity during the first flight was not suitable for seeding. The dBz of rainfall varies only from 8 to slightly more than 12, whereas, Tehran is a big city and the air pollution usually exceeds the allowable limits during the day. It is highly probable that clouds had been over-seeded after this flight.

Also, Fig.2 shows that the rainfall dBz changes between 9 and 18 during the third flight. In addition the previous precipitations had decreased the aerosols concentration and as a result, the LWC of the clouds had been increased.

It should be mentioned that the increase in D in Eq.(1) may not compensate the decrease in $|K|^2$ and hence, the MAX pictures would change slightly due to seeding. To enhance the reliability of this model, we should take into account even these small variations. These calculations need the airborne cloud physics laboratory to investigate the relation between the concentration of AgI aerosols and the

concentration and size of ice crystals and water droplets in winter clouds.

5. Conclusion

The comparative models are not uncommon in assessing the cloud seeding projects. The comparison could be made between separate cumuliform clouds (Woodley 2004) or separate parts of a stratiform cloud. Usually the terrain has been neglected by most of these models. In this work, the target and control zones have the same spatial expansion and only differ in time. The vicinity (with respect to time) of the control and target zones could maximise their similarities and enhance the reliability of the predictions.

In this model, the good correlation between MAX and SRI variations shows that we can use one to estimate the other. To calculate the rain enhancement percentage, the calibration of the SRI pictures of radar is not important, because we need only the dBz of the SRI pictures. This calibration becomes significant only in calculation of the rainfall's volume which could be done by either radar or any other instrument (like rain guage).

Finally, it is feasible to use the nowcasting models to estimate the precipitation for the target region, but we should be careful because the radar-based ones usually use the extrapolation methods that have some uncertainties for the (extremely variable) precipitation process. Some reliable and good articles are listed in references (Anagnostou 2009 and Larsen 2003)

Acknowledgements

I acknowledge the director of the National Cloud Seeding Research Centre, Mr. Javadianzadeh for the financial support, and also the experts of this center, especially, Mr. Golkar, Mrs. Khatibi and Mrs. Moradian, who provided the radar pictures and radiosonde data for me. I am also thankful to the *Sharif University of Technology* for their scientific and executive support in the 'First Conference of Radar Technology'.

References

Anagnostou M.N., J. Kalogiros, E.N. Anagnostou, A. Papadopoulos; Experimental results on rainfall estimation in complex terrain with a mobile X-band polarimetric weather radar. J. *Atmos. Res.,* **94**, 579-595, 2009.

Barillec R. and D. Cornford; Data assimilation for precipitation nowcasting using Bayesian inference. J. *Adv. Wat. Res.,* **32**, 1050-1065, 2009.

Doviak, R.J., D.S. Zrnic; Doppler Radar and Weather Observations (Second ed.). *San Diego California: Academic Press.* ISBN 012221420X, 1993.

Larsen H.R. and W.R. Gray; Assessment of a radar-based nowcasting model for the Auckland region. J. *Hydrology (NZ),* **42(2)**, 101-112, 2003.

Marzano F.S., D. Cimini, M. Montopoli; Investigating precipitation microphysics using ground-based microwave remote sensors and disdrometer data. J. *Atmos. Res.,* **97**, 583-600, 2010.

Michaelides Sar., V. Levizzani, E. Anagnostou, P. Bauer, T. Kasparis, J.E. Lane; Precipitation: Measurement, remote sensing, climatology and modeling. J. *Atmos. Res.,* **94**, 512-533, 2009.

Novák P., L. Březková, P. Frolík; Quantitative precipitation forecast using radar echo extrapolation. J. *Atmos. Res.,* **93**, 328-334, 2009.

Ryzhkov A.; Rainfall measurements with the polarimetric WSR-88D radar (Report). *National Severe Storms Laboratory (Oklahoma)*, 2003.

Woodley W.L. and D. Rosenfeld; The development and testing of a new method to evaluate the operational cloud seeding programs in Texas. J. *Appl. Meteor.*, **43,** 249-263, 2004.

Analysis Application of Satellite Nephogram and CINRADAR Products in the Precipitation Enhancement Processes

NIU SHU-Zhen[1] BAO XIANG-Dong[2] XI SHI-Ping[1] YANG MIN[2]
（1 Henan Meteorological Observatory, Henan Zhengzhou 450003;
2 Henan Weather Modification Center, Henan Zhengzhou 450003)

Abstract

By using cloud cluster evolvement and TBB of FY-2C satellite nephogram and base reflectivity, Doppler velocity and vertical integrated liquid of Zhengzhou CINRADAR products combined with hour-by-hour precipitation rainfall of Henan auto station we analyze the precipitation enhancement task process that had used high cannon, rocket and plane in Henan Province on March 2-3, 2007. We not only researched the short-time condition forecast and optimal task opportunity and position of the precipitation enhancement task, but also discussed precipitation enhancement effect embodiment in the radar products' characters. These can provide scientific gist for better used FY-2C satellite nephogram and CINRADAR products to direct precipitation enhancement task to make use of high cannon, rocket and plane in Henan.

Keywords: TBB; base reflectivity; vertical integrated liquid; precipitation enhancement effect

1 Introduction

Weather modification is a complex systematic engineering. Many research proof that it's impossible to increasing rainfall in natural conditions unfavorable. Therefore, a good work to find weather condition and predict assignments region is the key to success and the primary condition of weather modification.

The weather radar plays an important role in the usual work on the weather modification as it has a real-time detection about horizontal distribution, intensity and vertical structure of the precipitation cloud. In the period of 'ninth five-year', we analyzed and summarized the characteristics of the conventional weather radar echo in Henan province when the plane precipitation enhancement task was being done in spring [1]. The main study is that: we investigated 31 plane processes on precipitation enhancement, the radar echo characteristics were analyzed and the basis on the perfect task region and height on plane precipitation enhancement in spring and autumn. What we had done played an important role in the command on aero artificial precipitation enhancement.

CINRADAR does better than conventional radar on whose higher resolution ratio and wider bound detection, it not only has ability of what the convention ones can do but also can gains the wind structure of the rainfall. Functional terminal display platform is another detection means on rainfall and severe convection warning and prediction and furthermore a fundamental tool on the artificial precipitation enhancement commands. In recent years, as CINRADAR networks have been completed, there are some researches on the prediction of precipitation and severe

convection and high cannon, rocket and artificial precipitation enhancement. The CINRADAR products have been used in Hebei and Tianjin province to investigate the convective cloud artificial precipitation enhancement [5-6]. Since the CINRADAR networks have been operating in Henan province from 2007, it has been playing an important role not only in monitoring and early warning of severe convective weather but also in artificial weather modification. In the process of March 2-3, 2007 in Henan, plane, rocket and high cannon have been carried out to fulfill the artificial rainfall enhancement operation where CINRADAR played an irreplaceable role and achieved remarkable results and good economic and social benefits.

We analyses the FY-2C satellite nephogram, the characterize of Zhengzhou CINRADAR products in this process and sums up the criteria, provides scientific basis on weather modification in Henan Province using high cannon, rockets and aircraft precipitation enhancement in the future and increases the effect of precipitation enhancement.

2 The precipitation process and overview of precipitation enhancement

2.1 **Analysis of the process**

By hollow trough moving eastward, shear line in low-level and the southwest stream affected, there was heavy rain in our province on March 2-4, the rainfall mainly concentrated in 17:00 on March 2nd to 17:00 on March 3rd. All parts of the province were more than 25mm in the process but Sanmenxia was 15-25mm. There were 93 stations with 25.0-49.9mm rainfall and 22 stations with 50.0-99.9mm, the precipitation center was in Changge and Xuchang, whose rainfall was 61mm and 60mm respectively. The precipitation amount in the area of aircraft precipitation enhancement operation and its downwind area was 44-61mm; the near center of precipitation, see Fig1b. It's rare in history on early March that the amount is so much in our province according to statistics what contains the effect of artificial precipitation enhancement.

2.2 **Situation of precipitation enhancement operations**

The aircraft precipitation enhancement was operated at 12:00-14:00 on March 3rd and the specific operating line was in the area of the triangle shown in Fig1a.

High cannon and rocket operations is shown in Fig1, the sites in the circle are high cannon and rocket operating point, Luanchuan in Luoyang high cannon operations at18:00-18:03 on 2nd; Anyang and Linzhou at 22:15-22:30, Anyang and Tangyin at 23:05-23:20 on 2nd and 01:10-01:30 on 3rd, 5 counties carried on high cannon and rocket operations, the operating height was 5000 meters, fired 450 rounds and 4 rockets; Gongyi of Zhengzhou high cannon operations at 00:00-01:00 on 3rd; Huixian of Xinxiang at 20:25-20:30, Huojia at 20:25-20:30 , Fengqiu and Yanjin at 21:05-21:50 high cannon operations respectively, the operating height was 5000 meters; Wangwu, Xiaye, Shaoyuan and Jiyuan 4 locals operated at 21:30-21:50, fired

3 rockets and 30 rounds; Mengzhou, Wuzhi, Xiuwu and Qinyang of Jiaozuo carried on rocket operations, fire 3 rockets; Puyang, Qingfeng and Nanle operated at 16:25-16:30 on 3rd, with 7 rockets and 17 rounds fired, the operating height was 5000 meters; Wuyang high cannon operations at 12:02-12:12 on March 3rd.

We can see that the precipitation enhancement operations in our province mainly operated by high cannon and rockets on March 2nd, and by aircraft, high cannon and rockets in city sites on March 3rd. Henan Weather Modification Center and city sites seized the opportunity to carried out the high cannon, rockets and aircraft precipitation enhancement effectively and comprehensively made the process significantly whose amount reached the criterion of regional storm, this eased the drought in our province and ensure the soil moisture.

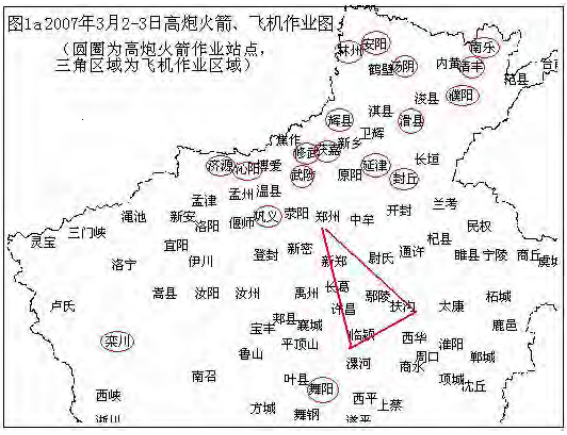


Fig 1a High cannon rockets and aircraft
precipitation enhancement plans on March 2-3, 2007
(circle area is high cannon rockets operation sites, triangle area is aircraft operation)

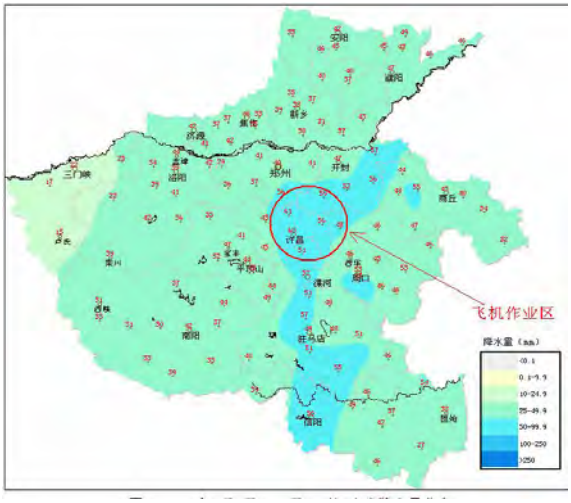


Fig 1b The precipitation distribution in Henan Province from 17:00 on March 2nd to 17:00 on 3rd, 2007

3 Analysis of FY-2C satellite nephogram

The precipitation process of the evolution of cloud systems is analyzed by FY-2C IR nephogram TBB data and hourly rainfall stations in Henan automatically. The clouds which has a center of the low value of -22℃ appears at 08:00 on March 2nd in Zaoyang and Suizhou in Hubei, that correspond to the north-intensive areas along the contour and weak rainfall below 5mm appears at 08:00-09:00 in Zhumadian, Nanyang, Xinyang in our province. With the cloud area A(Fig 2a) flows northward, the rainfall

area begins to move northward, and the bright white clouds B in western part of Hubei begins moving northeast, that gradually affects the southwest of Henan province, the TBB low center of -33℃ occurred near Xichuan in Nanyang at 12:00. Cloud A and B moves to the northeast at the same time, the boundary of them mergers in the process. Cloud A moves out of our province at 13:00 while cloud B is moving to strengthen and become the main impact cloud in the process (Fig 2b).

Cloud B continues moving northeast, and clouds later ads in to enhance the main one while the front of the cloud split and weakens. At 17:00(Fig 2c) in the main cloud region, TBB near Baofeng in Pingdingshan formats a low center of -38℃ and the direction in movement of the center in Nanyang is -27℃, which corresponds to 5mm in Baofeng and 6mm in Nanyang at 17:00-18:00.

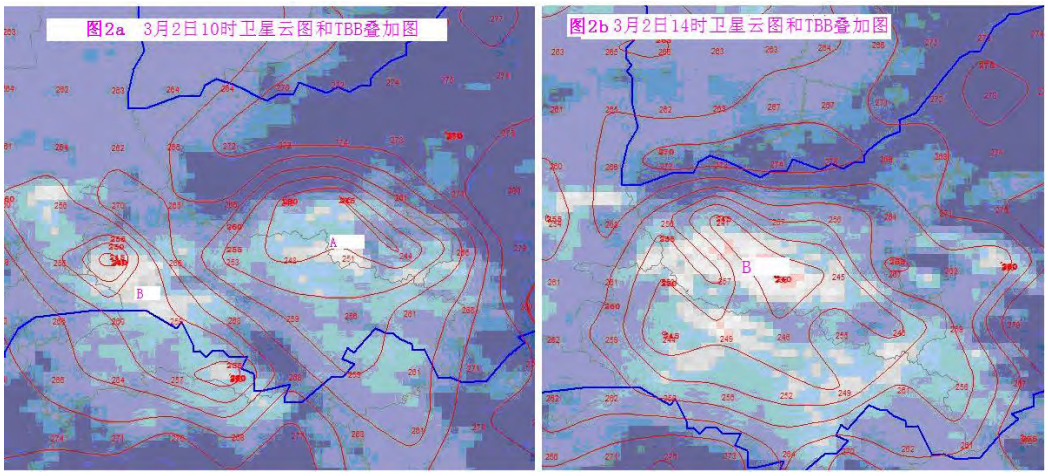


Fig 2 FY-2C satellite nephogram and TBB map at 10:00(a) and 14:00(b) on March 2nd, 2007

In the weather map at 20:00 on 2nd, the low-level southerly airstream affects our province which brings a steady stream of water vapor for the rainfall and provides sufficient moisture. In the 850hPa wind field, the province is in the central region of the curved top of the cyclone, the northern area is at the south of the convergence line which provides favorable environment conditions for the emergence and development of rainfall. Corresponding to the satellite nephogram at 21:00 on 2nd(Fig 2d) , the cloud strengthens in the north and central parts, where the low center -47℃ in Taikang and -39℃ in Songxian appears respectively, corresponding to the TBB contours of concentration side in two areas, a 3-8mm of strong precipitation appears at 21:00-22:00. Until the clouds moves to Hebei and Shandong Province at 07:00 on 3rd, the precipitation in our province was able to end.

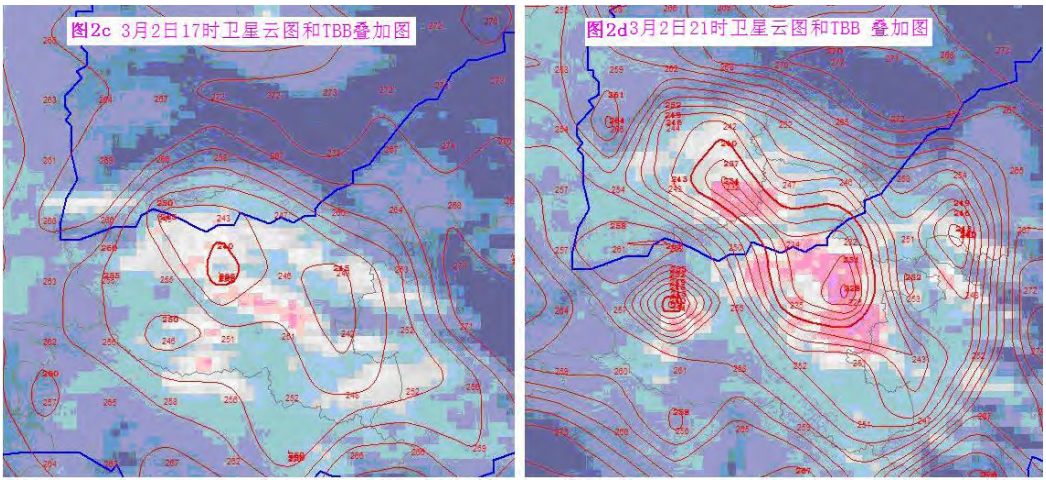


Fig 3 FY-2C satellite nephogram and TBB map at 17:00(c) and 21:00(d) on March 2nd, 2007

Cloud C begins to affect the western part of the province at 4:00 on the 3rd and moves quickly to the northeast, it formed a low center of -46℃ in the west at 05:00, after that the cloud area expands rapidly during the movement, TBB low center also moves northeast. Till 07:00 on 3rd, western part has been covered basically by cloud C (fig.2e), low center of -51℃ was in Songxian and Xinan area, what indicates that cloud develops strongly that is good to precipitation generation. Corresponds to 07:00-08:00, 3-9mm precipitation occurs in the contour dense area near the TBB low center.

Cloud C continues to develop during the movement to the northeast, as there are cloud moving into whose right front, making whose area increase gradually and it covers the province till 10:00(Fig 2f), the low center is in Taihang Mountains and the northwestern Shanxi, while in the surrounding contours dense band, precipitation amount in most areas of our province is 3-7mm, local 12-14mm.

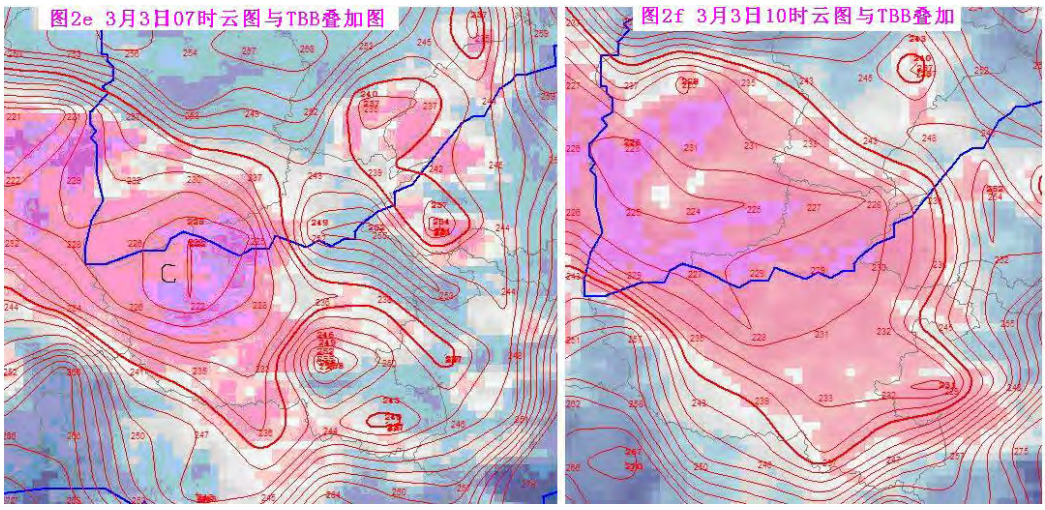


Fig 4 FY-2C satellite nephogram and TBB map at 07:00(e) and 10:00(f) on March 3rd, 2007

Then cloud C continues moving northeast, into whom there are cumulus clouds

develop and quickly incorporates, what makes the intensity strengthen and clouds develop. The main body of the cloud moves out of the province till 23:00 on 3rd, ending a strong precipitation.

The above analysis shows that there are mainly three clouds that affect the rainfall and are all moving to the northeast, there are stratus or cumulus clouds involving into their right front in the process of moving, promoting the development and growth; strong rainfall doesn't generate in the low center of TBB, but in the area of the dense contours band. Because when TBB is lowest, the highest cloud, when cloud is often the most productive stage of development, not the strongest of precipitation, the precipitation are strongest while the top of the cloud declines. So we should pay attention to select the TBB intensive areas, not to blindly choose the largest central area of TBB when choosing the area of artificial precipitation enhancement.

4 Analysis of radar product characteristics and precipitation enhancement effects

There are not only three basic products provided by CINRADAR: base reflectivity, Doppler velocity and spectral width, but also a set of secondary products calculated from the basic data, such as liquid water content, vertical wind profile, storm relative radial velocity, echo top, 1hour accumulated precipitation, mesoscale cyclone, etc. These are not only extremely useful for early warning of severe convective but also for aspects of the artificial precipitation enhancement timing, the best select area and its effect judgment , etc.

4.1 Base reflectivity(R) and Doppler velocity (V)

The evolution of base reflectivity shows echo at first appeared in Nanyang and Zhumadian and then moved to north-northeast, the echo is from 25 to 35dBz and the center of echo is from 35 to 48dBz. Since the low-level southerly jet moves to the north and the transmission of water vapor, the echo continues moving to northeast from Nanyang and Zhumadian. It forms a "train effect". Although the precipitation intensity isn't intensive, the process sustains and forms a heavy rain. The corresponding Doppler velocity shows the zero line presents a typical S-bend what illustrates that there is warm advection in the lower and this benefit in resulting rainfall.

Fig 5a and b is base reflectivity and velocity field at 20:10 on March 2nd, the echo moved northward to Zhengzhou and Xinxiang area, while there are large area of echoes appeared in Nanyang and Zhumadian, moves to the north, whose center intensity is 53dBz located at Xiping and Suiping. The corresponding Doppler velocity map shows the zero line corresponding to strong echo center forms a typical S-bend, the amount of rainfall is 6mm and 8mm in Xiping and Suiping of Zhumadian from 20:00 to 21:00.

Fig6 is the base reflectivity map during and after the aircraft task, we can see the

echo inside the area and leeward is strengthening obviously after task, from 25-30dBz original to 38-43dBz after aircraft operations, the area whose echo is more than 33dBz expands significantly. The precipitation in the operations area is 16-19mm from12:00 to 14:00. As the echo moving northeast, it should be weakened in the operation area and downwind area. However, precipitation enhancement makes the echo moves from southwest is strengthened in the operation area, and this makes the precipitation sustained. The AWS precipitation in the operation area still maintains more than 5mm/h after 2 hours, it means the rainfall sustains 11-14mm within 2 hours, 17-20mm within 4 hours, what shows an obviously operation effect.

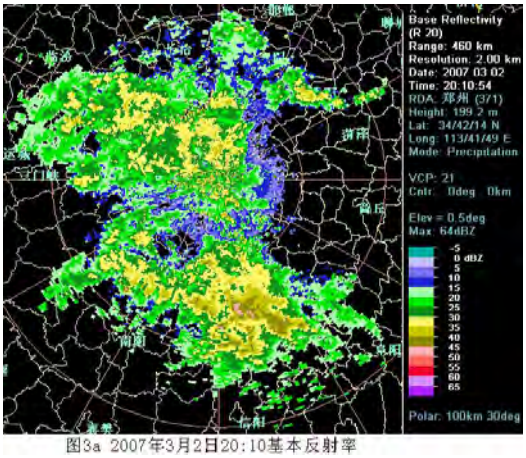


图3a 2007年3月2日20:10基本反射率

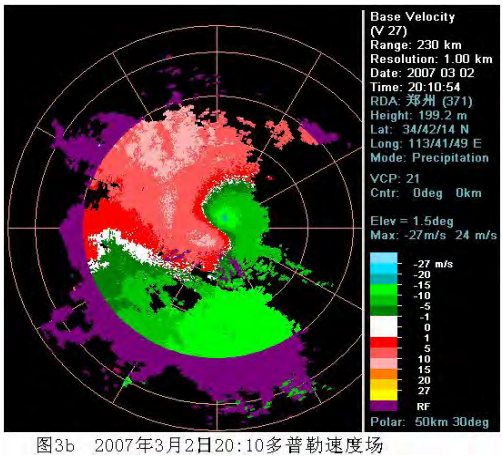


图3b 2007年3月2日20:10多普勒速度场

Fig 5 Base reflectivity (a) and radial velocity(b) at 20:10 on March 2nd, 2007

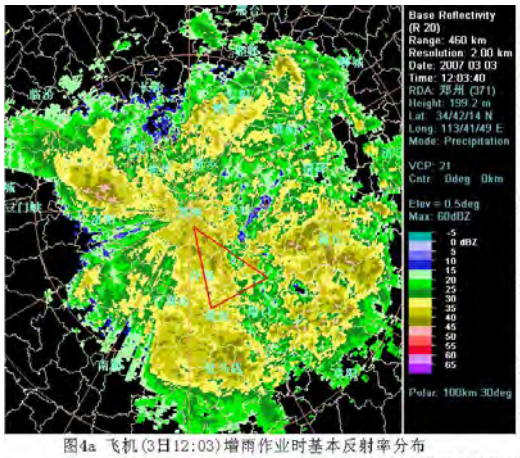


图4a 飞机(3日12:03)增雨作业时基本反射率分布

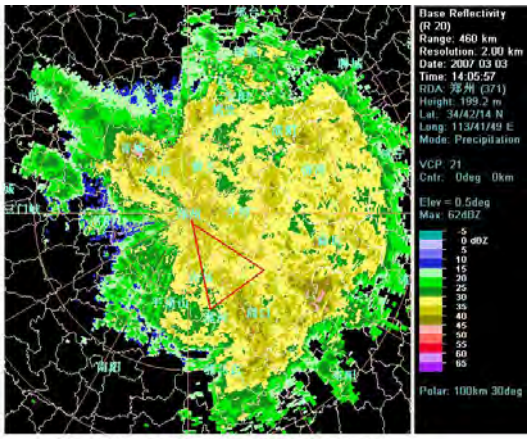


图4b 飞机增雨作业后(14:05)基本反射率分布

(图中黄色三角区为飞机增雨作业区域)

Fig 6 Base reflectivity during(a) and after(b) the aircraft precipitation enhancement on March 2nd, 2007 (The red triangle area is the aircraft operation area)

The base reflectivity distribution, from areas before and after the high cannon rocket operation, shows that (Table 1): The echo in the period of development stage enhances 5-20dBZ after 1 hour to what the work operates. the echo in the mature stage, when the precipitation enhancement operate, can maintain 1-3 hours after that; While the echo in the dispersed phase weakened after the operations. Be sure to select the area where the echo is in the development phase and work effect is obvious.

Table 1 The base reflectivity (0.5°) of the precipitation echo evolution before and after the high cannon rocket precipitation enhancement operation

Operation Time/Location	Echo Before Operations	Echo After Operations
2nd 20:05-20:30/Fengqiu	28dBz（Develop）	33dBz(5minutes after operation)、38dBz(23 minutes after operation)
2nd 20:05-20:30/Yanjin	28dBz（Develop）	33dBz(maintained 41 minutes and weakened after that)
2nd 20:25-20:30/Huixian	38dBz（Develop）	43dBz(after 30 minutes)
2nd 20:25-20:30/Huojia	38dBz（Mature）	33dBz(maintained 41 minutes and weakened to 28 dBz after that)
2nd 21:05-21:50/Kaifeng	38dBz（Develop）	38dBz(maintained 50 minutes and heightened to 43 dBz and maintained 2 hours after that)
2nd 21:05-21:50/Changyuan	—	8 dBz when the end, after 27 minutes, heightened to 28dBz and maintained 21 minutes, heightened to 33dBz, after 67 minutes, heightened to 38dBz(maintained 1hour)
3rd 07:25-07:40/Mengzhou	33-38dBz(Disperse)	28dBz(weakened after 26 minutes)
3rd 07:25-07:40/Wuzhi	33-43dBz(Disperse)	33-38dBz, maintained 27 minutes and weakened to 18dBz after that
3rd 07:25-07:40/Xiuwu	33-43dBz（Mature）	Weakened to 28dBz after 27 minutes
3rd 07:25-07:40/Qinyang	28-33dBz（Mature）	Weakened to 28dBz after 28 minutes
3rd 16:25-16:30/Puyang	38-43dBz(Develop)	Heightened to 48dBz after 13 minutes, maintained to 38dBz for 2 hours and 10 minutes after 20 minutes
3rd 16:25-16:30/Qingfeng	38dBz(Develop)	38-43dBz(maintained 3 hours after operation)

4.2 Combination Reflectivity

In a volume combination reflectivity (CR) is product that is found in the maximum reflectivity on the grid in azimuth scan angle of elevation and is projected onto the Cartesian. It is useful for analyzing the effect of precipitation enhancement.

Analysis of reflectivity before and after the CR of precipitation enhancement operation shows that the echo in the development stage increases 5-10dBz after the operation done 1 hour later, of whom effect is obvious; the echo in weakening phase will also be reduced after the operation, no effect of precipitation enhancement. Fig 7 is the CR distribution before and after the high cannon and rocket operations in Gongyi of Zhengzhou at 00:00-01:00 on 3rd, from 43-48dBz when operating, to 53-58dBz 50 minutes after the operations, the CR increased 10dBz, and the area bigger than 48dBz also extends, what shows the effect of the high cannon and rocket operations in Gongyi is obviously.

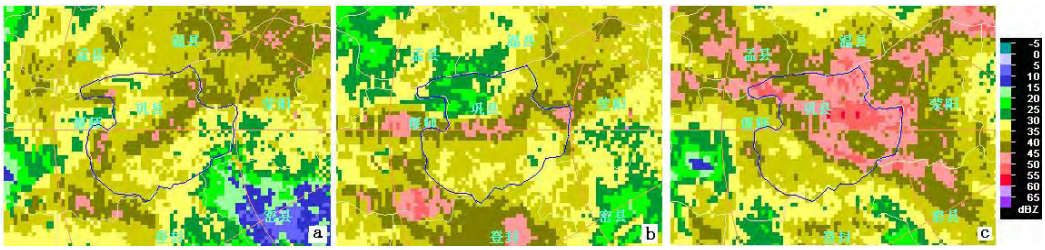


Fig 7 The CR evolution before and after the high cannon rocket precipitation enhancement operation at Gongyi in Zhengzhou (a: CR at 00:13 on 3rd b: CR at 01:08 c: CR at 00:13)

4.3 Analysis of the storm relative mean radial velocity

Storm relative mean radial velocity map (SRM) is similar to the basic velocity products, that is less than the storm tracking information(STI) recognized by the average velocity of all storms. This product can be got by every sample elevation, its maximum distance is 230km, a resolution of 1×1km, the data level is 16. The product can be used to detect concealed movement by storm out of the shear zone (such as the cyclone, divergence and tornado vortex characteristics), so it is extremely useful not only in the analysis of rainfall and convective storms, but also in analyzing the potential of artificial precipitation enhancement.

The SRM of the process shows that in the first half of the main precipitation that is before March 3rd, there is convergence area in Mianchi, Luoyang, Yiyang, to Ruzhou, Baofeng, Pingdingshan, Luohe and Xiping corresponding to the rainfall in the southwest, what makes the continuous precipitation echoe from Nanyang develops and strengthens and then moves to the northeast. Zero speed line through the station shows a NW-SE straight line, what indicates a wide range around the northeast wind field is consistent with the north wind field, in favor of precipitation. About 0.5km lower was the maximum height of NNE wind speed, the SRM maximum of positive or negative is 24m/s, as shown in Fig 8a it's the SRM at 20:10 on March 2nd which has the features of both.

The convergence zone in southwest disappeared at 00:56 on March 3rd (Fig 8b), zero speed line that is still through the station has become a typical S-curve, the warm advection is obvious, the maximum positive or negative SRM increased to 27m/s and the negative speed goes toward radar of the big value (≥24m/s), indicating a much larger positive speed that leaves radar. It shows that the radiation field enhances convergence and the wind field has changed from NNE to NE significantly.

Fig 8c is the wind when operating the aircraft, zero speed line shows the typical S curve, and the negative speed area that is larger than 24m /s is much larger than the positive speed area, which apparently is the convergence field and is favor of rainfall. It shows that the operate timing is correct and the effect is good.

It's visible that, artificial precipitation enhancement should choose such a favorable confluence of precipitation development to enhance the radiation field and to achieve the maximum benefit of the effect.

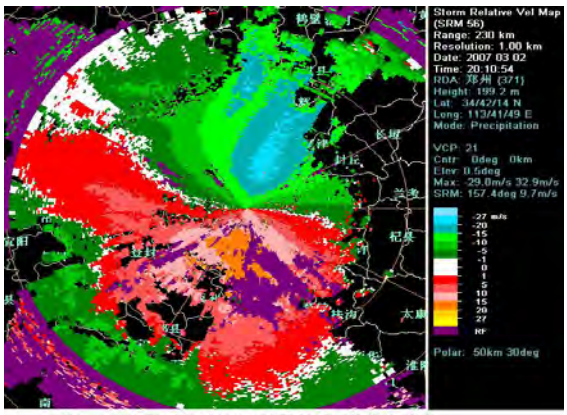


图6a 2007年3月2日20:10风暴相对平均径向速度

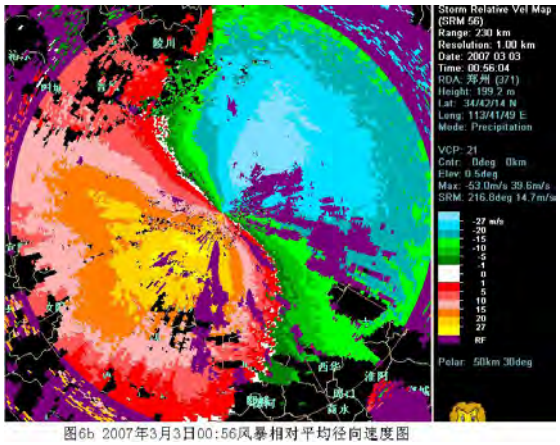


图6b 2007年3月3日00:56风暴相对平均径向速度图

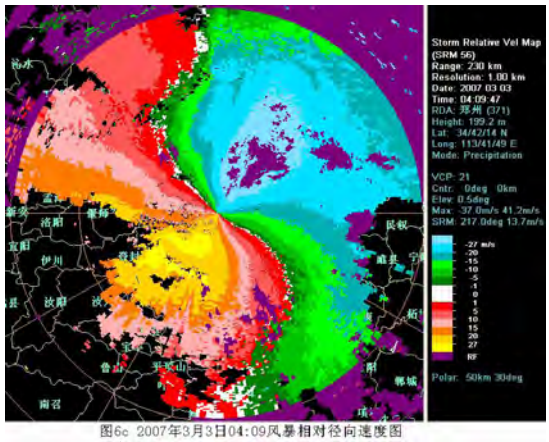


图6c 2007年3月3日04:09风暴相对径向速度图

Fig 8a The SRM at 20:10 on March 2nd, 2007

Fig 8b The SRM at 00:56 on March 3rd, 2007

Fig 8c The SRM at 04:09 on March 3rd, 2007

4.4 Vertical liquid water content

Vertically integrated liquid water content (VIL) is the liquid water equivalent value that the reflectivity data becomes into, it is used to assume that all reflectivity returns are derived from the relationship between liquid water caused by the experience. Value can be exported within a 230km radius of the radar, for each elevation angle and in 4km×4km grid, and then be vertical accumulated. Although there is not all liquid water in the cloud, it can represents the approximate cloud liquid water content in general and cloud precipitation potential of the artificial precipitation for the region to determine a more useful product.

This process is mainly a stability precipitation, the VIL is small. In the early stage on March 2nd, as the precipitation is less than 5mm/h, the VIL is usually 3kg/m^2, local 8 kg/m^2; with the strengthen of precipitation after 19:00, the precipitation in Nanyang and Zhumadian starts to increase, there appears the rainfall larger 5mm/h, corresponding VIL reaches 8 kg/m^2 and local 13 kg/m^2.

It shows that the water vapor content in the cloud of spring storm is much smaller than that of the summer storm (the VIL in summer storm is bigger than 35kg/m^2); therefore, artificial precipitation enhancement in spring should simply select the area that is large tracts bigger than 3kg/m^2 to conduct operations.

4.5 Analysis of wind profile

Wind profile at the T-logP means the horizontal wind (by the VAD algorithm calculated in each stage). To 21km from the ground 30 regular wind feathers can be shown, this product not only shows the most recent addition to the wind/height profile but also shows 10 close wind/height profile(in 5 to 10 minutes intervals). The product is useful to determine low and high level jet, heat advection type, vertical wind shear, thickness of front and the elevation development of the isentropic surface.

During the precipitation period, there is NE wind in the lower and S wind in the middle-high level, the same SW wind in the high level, clockwise rotation of the wind with height, indicating that there is warm advection, precipitation produce a favorable development. Fig 9 is the wind profile of Zhengzhou radar at 20:04-21:05 on March 2nd, we can see the consistent NE wind below 1.2km, the SE wind in 1.2-2.1km, the S wind in 2.4-5.8km and the SW wind in 6.1-9,1km, clockwise rotation.

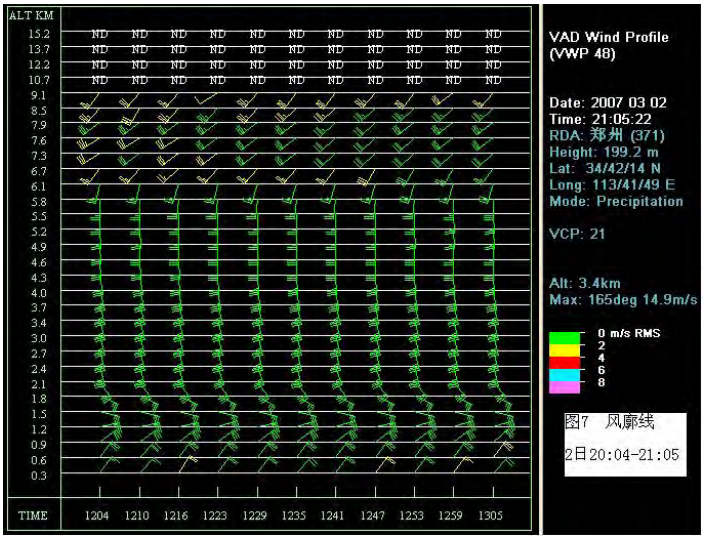


Fig 9 the wind profile of Zhengzhou radar at 20:04-21:45 on March 2nd, 2007

4.6 One hour accumulated precipitation(OHP) products

The accumulated precipitation product of CINRADAR is calculated by sweeping legislation of each group through $Z=300\ I^{1.6}$, and then be accumulated.

The echo whose effect of precipitation enhancement is obvious, one hour cumulus precipitation products is also obvious. Fig 8 is the change of the 1 hour accumulated precipitation before and after the high cannon and rockets operations in Anyang, Linxian, Tangyin and Huaxian at 00:00-01:00 on March 3rd, we can see 44 minutes later, 1 hour accumulated precipitation in Anyang increases to 4.45mm/h from 1.27mm/h, increases to 9.25mm/h after 1 hour and 39 minutes and increases to 22.02mm/h after 1 hour and 51 minutes, the effect can be seen clearly.

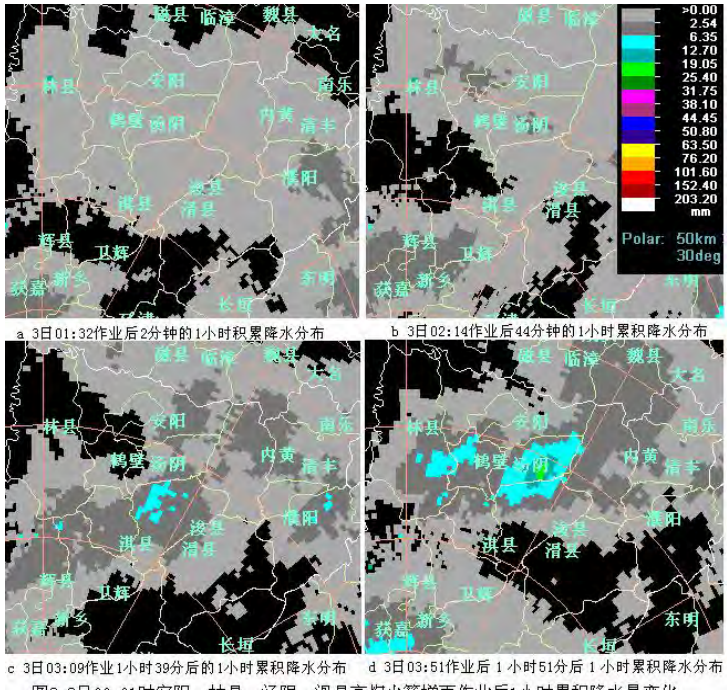


Fig 10 The OHP evolution after the high cannon rocket precipitation enhancement operation in Anyang, Linxian, Tangyin and Huaxian at 00:00-01:00 on March 3rd (a, b, c, d is the OHP after the operation 2 minutes, 1 hour, 1 hour and 30 minutes and 1 hour and 51 minutes, respectively)

5 Conclusions

By analyzing the cloud images, radar and the precipitation in the operational areas and downwind side areas of this artificial precipitation enhancement, we can see the following conclusions that for the future operation of aircraft and high cannon rocket.

1) In satellite images, during the clouds moves to the northeast, on whose right front and rear, the stratus or cumulus clouds will mix continuously and promote itself. It's the best part of the area that artificial precipitation enhancement affect.

2) Contour-intensive parts of TBB is also the perfect area that artificial precipitation enhancement works.

3) The echo development stage should be selected to carry out the work, where the reflectivity is about 30dBz, wind was S-bend or radiation field in the confluence, the vertical liquid water content are more than 5 kg/m^2 and in the period of wind clockwise with height. The effect will be significant.

4) The initially effect of weather modification can be judged using combination of reflectance and one-hour accumulated precipitation.

5) Either the high cannon or rockets or the aircraft artificial, the effect will be significant if only the appropriate time and work area is selected as long as in favorable large-scale weather. It's the key to success to select times and area for artificial enhancement task of aircraft or high cannon and rockets.

References：

[1] Huang Meiyuan, Xu Huaying et.al. Cloud and Precipitation Physics. Beijing. Science Press. 1997.

[2] Niu Shuzhen, Zhao Peijuan, Xi Shiping. The Radar Echo Characteristics Suitable for Artificial Precipitation Enhancement in Spring and Autumn in Henan Province. Meteorology Journal of Henan. 2000/1.

[3] Jin Hua, Wang Guanghe, You Laiguang. The Micro-physical of High-cloud and the Potential of Artificial Precipitation Enhancement in a Precipitation Process in Hennan Province. 14th Session of the National Cloud and Precipitation Physics and Weather Science Conference Proceedings.

[4] Zhou Yuquan, Wu Zhen, Su Aifang . The Multi-scale Condition and the Study on Monitoring and Forecasting in Artificial Precipitation Enhancement. 14th Session of the National Cloud and Precipitation Physics and Weather Science Conference Proceedings.

[5] Wu Zhihui, Duan Ying, Zhang Jin et.al. The Precipitation Characteristics in Different Weather Systems and the Potential Analysis of Precipitation Enhancement by Rocket. Meteorological Science and Technology. 2005/12.

[6] Zhao Ruijin, Yang Baodong, Li Hongbo. The Applications of Doppler Radar Products in the Effect Test of Artificial Precipitation Enhacement. Meteorological Science and Technology. 2005/12.

[7] Hu Ling, Jin Ruijun. Applications of CINRADAR Products in the Precipitation of Discrimination. Meteorological Science and Technology. 2005/12.

[8] Huang Meiyuan, Xu Huaying. Cloud and Precipitation Physics. Beijing. Science Press. 1999.

[9] M.J, Bade et.al. Lu Naimeng et.al. translation, Applications of Satellite and Radar Images in Weather Forecast. Beijing: Science Press. 1998.

[10] Hu Mingbao, Gao Taichang, Tang Dazhang. Analysis and Application of Doppler Weather Radar Data. Beijing: PLA Press. 2000

[11] Li Dashan, Zhang Dengchang, Xu Huanbin et.al. The Situation and Prospects of Weather Modification. Beijing: Meteorological Press. 2002:80-107.

[12] Hong Yanchao, Zhou Feifei. The Study of Evaluation of Potential of Artificial Precipitation Enhancement in Stratiform Cloud System. Vol.30 No.5. Sept. 2006: 913-925.

An analysis of a heavy snow occurred in Shandong Province of China in 2009

Sheng Rifeng
Shandong weather Modification Office, Jinan 250031, China rfs88@sina.com

Ma Zhanshan
National Meteorological Centre, Beijing 100081, China

Wang Jun
Shandong weather Modification Office, Jinan 250031, China

Zhang Hongsheng
Shandong weather Modification Office, Jinan 250031, China

Jiang Peng
Shandong Meteorological Observatory, Jinan 250031, China.

Based on the conventional observational data, Cloudsat satellite (2B-GEOPROF, CWC-RO ,ECMWF-AUX) ,automatic observational precipitation and NCEP reanalysis data (UGRD,VGRD,VVEL,HGT,TMP,RH) , the micro-physical process and dynamic field of Blizzard in the western part of Shandong on 11-12 November 2009 were analyzed. The major conclusions are as follow:

(1) the conventional observational data analysis indicated that the shear line and southwest jet at 700hPa played important roles in Blizzard. Heavy snow occurred under favorite conditions, which was closely related with middle-level convergence and upper-level divergence. The pumping action in upper-level were an important trigger which led to unstable energy release.

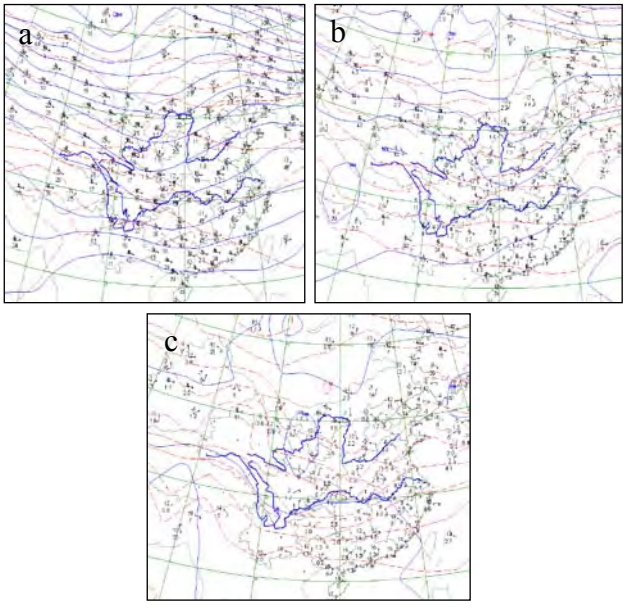


Fig.1 The 500hPa pattern at 20:00(a) on Nov 11,700hPa (b) and 850hPa (c) pattern at 08:00 on Nov 12,2009.（solid lines denote geopotential height line, unit: dagpm; dotted lines denote isotherm,unit: ℃）

(2)The intersection of cold and warm air over snow area formed apparent energy front in horizontal and vertical direction.

(3)Before snowfall, the invasion of cold air in low level triggered the circulation development of snow. During the strong period of snow, the appearance of cyclonic circulation in high-level enhanced transport of southwest warm air. In the late, cold air strengthened and was dominant in low level, which cut off the supply of warm air, so snow gradually stopped.

(4)Comprehensive analysis revealed cloud microphysical processes and vertical evolution to some extent under some dynamic conditions by using Cloudsat satellite, NCEP reanalysis data and L-band radar sounding data, Updraft will help the delivery of water vapor. At the same time, cloud droplets, ice crystal particles, snow crystal particles better mixed, coagulated or condensated with each other in help of updraft. The site of big ice water content were consistent with the area of big vertical velocity ,and big number concentration of ice crystals located at the position of top center of upward motion. L-band radar sounding data reflected vertical evolution of heavy snow cloud under a certain dynamic condition.

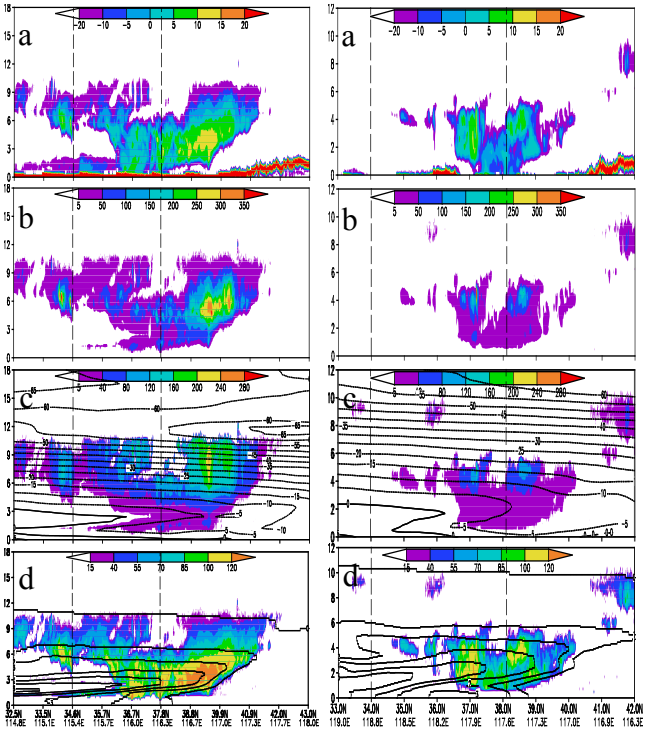


Fig.2 Vertical cross section of Radar reflectivity(unit:dBz),cloud ice-water content (unit:mg/m-3),ice particle number concentration (unit:L-1) and temperature (unit:℃), ice particle radius

(unit: um)and specific humidity (unit: kg/kg) from the CPR at 00:26 BT 11 Nov (a1-d1) and 13:30 BT 11 Nov (a2-d2) 2009 ((a1-d1) are corresponding to the line in Fig.4a and (a2-d2) to the line in Fig.4b).Between the two vertical dashed line was Shandong Province as the satellite passed

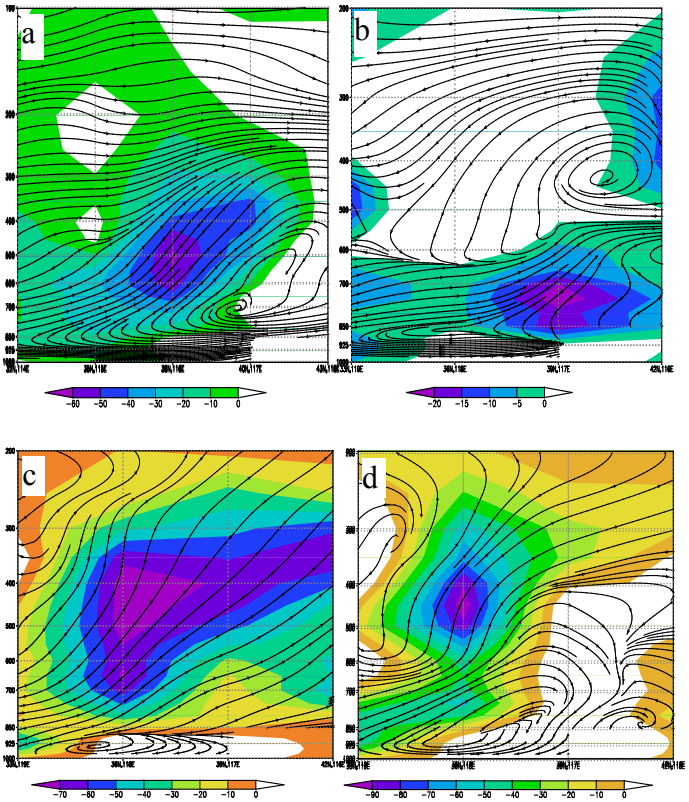


Fig.3 Vertical profile derived from NCEP data along the line in Fig.4a at 02:00(a) on Nov 11;along the line in Fig.4b at 14:00(b) on Nov 11,at 08:00(c) and 14:00(d) on Nov 12,2009.Shaded color denotes vertical velocity(unit:Pa/s)

Refenerces:

Brooks C F. 1920. The nature of sleet and how it is formed. Mon Wea Rev. 48:69-72

Bennetts D A, Hoskins B J. 1979. Conditional Symmetric Instability-a possible explanation for Frontal Rain Bands. Quart J Roy Meteo Soc.105:945-962

Emanuel K A. 1979. Inertial Instability and Mesoscale Convective System Part I:Linear Theory of Inertial Instability in Rotating Viscous Fluids. J Atmos Sci. 36；2425-2449

Frederick S, Lance F. 1985. Bosart Mesoscale structure in the Megalopolitan snowstorm of 11-12 February 1983.Part I:Frontogenetical forcing and symmetric instability.J Atmos Sci. 42:1050-1061

Moors J T, Blakley P D. 1988. The role of frontogenetical forcing and conditional symmetric instability in the Midwest snowstorm of 30-31 January 1982. Mon Wea Rev.116:2155-2171

Toshi H, Yasumi N T. 1999. Riming growth process contributing to the formation of snowfall in orographic areas of Japan facing the Japan Sea. J Met Soc Japan. 77(1):101-115

Yasu M K. 1999. A weak-wind zone accompanied with swelled snow cloud in the upstream of a low-altitude ridge.J Met Soc Japan. 77(5):1039-1059

A sensitivity study of the hailstorm seeding

Vlado Spiridonov[1] and Mladjen Curic[2]
[1]Hydrometeorological Institute of Macedonia, Skupi bb 1000 Skopje, Macedonia
[2]Institute of Meteorology, University of Belgrade, Belgrade, Serbia

1. Introduction

The principle of hail suppression is based on the conceptual models with all uncertainness, which this approach brings itself. Over the past two decades a number of papers have investigated the cloud seeding using numerical modeling. Results of the cloud seeding experiments (Hsie et al., 1980; Orville and Chen, 1992) have revealed that the seeded cloud exhibits the earlier initiation of precipitation which is crucial to the seeding effects, leading to increased precipitation, slight dynamics and microphysics interactions and difference in cloud life history. Farley (1987) found that hailfall decreased and rainfall could be increased in some situations, although some redistribution in hail spectrum can be expected. Aleksic et al., (1992) from their model simulation have found that only 2-3% of the target volume is actually being seeded. DeMott (1995) has quantified four ice nucleation mechanisms for the seeding aerosols. Cloud drops size spectra and its relation to cloud seeding effects of hailstorm are studied by Curic et al. (1997, 2006). In the last decades three-dimensional cloud models started to apply for cloud seeding simulations (e.g. Farley et al., 1994). This study has been focused on two aspects: a three-dimensional simulation of agent transport, diffusion and activation during supercell storm seeding case and the effects obtained from a number of sensitivity experiments by using different initial seeding parameters. Finally the results are summarized and the principal conclusion of the optimal seeding criteria is given.

2. Model

Only few basic characteristics of the model are summarized here. The present version of the model is a three-dimensional, compressible system which is based on the Klemp and Wilhelmson (1978) dynamics Lin et al. (1983) microphysics and Orville and Kopp (1977) thermodynamics. The microphysical parameterization uses the bulk a second-moment scheme for all species. Both bulk mass mixing ratios and number concentrations of cloud water, rainwater, cloud ice, snow, graupel and hail as well as the bulk mixing ratio of water vapor are also predicted in the model. An additional conservation equation is considered for the calculation of agent dispersion

$$\frac{\partial X_S}{\partial t} + \frac{\partial X_S U_j}{\partial x_j} - X_S \frac{\partial U_j}{\partial x_j} = S_{X_S} + E_{X_S} \qquad (1)$$

where X_S is the mixing ratio of AgI particles S_{X_S} is the sink or source term of mixing ratio and E_{X_S} is the subgrid-scale contribution. The activation of AgI is parameterized by the three nucleation mechanisms based on Hsie (1980) and Kopp (1988) which are deposition (including sorption) nucleation, contact freezing nucleation – Brownian collection and inertial impact due to cloud droplets and raindrop. The equivalent radar reflectivity factors for hail and rain are computed on the equations given by Smith et al., (1975) and empirical equation for snow by Sekhon and Srivastava (1970). More detailed informations about the cloud model are discussed by Spiridonov and Curic (2003a, b).

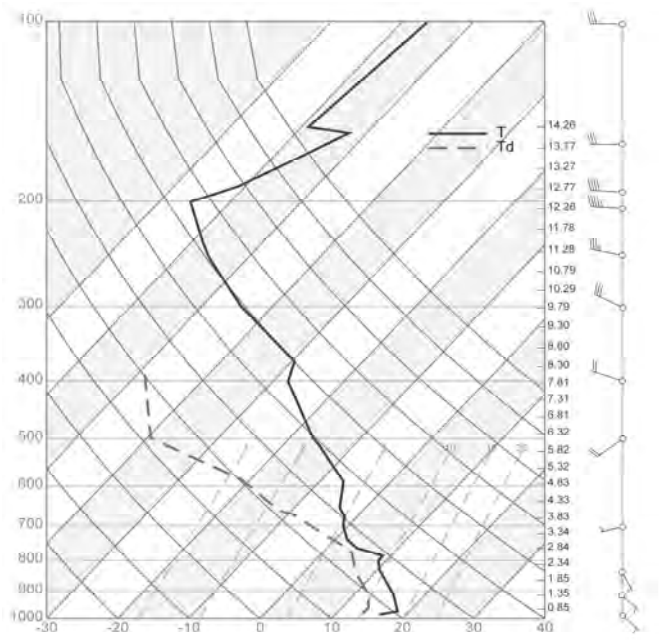


Fig. 1 A representative sounding taken at 01 UCT from Skopje on May 18, 2003

Since the model dispersion of the agent is in its initial phase on a sub-grid scale, the advection and diffusion should be parameterized. This problem is solved by considering the seeding line as the series of the individual spherical puffs by the radius of 10 m. The agent spread is than simulated by the movement and spread of the each individual puff. Its advection is calculated by the wind field bilinear interpolated from the four adjacent grid points. The trajectories of the puffs are computed in the model. The radius σ of these puffs has been calculated for each step as a function of

the turbulent diffusion coefficient Georgopoulos and Seinfeld (1986) by the solution of the equation

$$\sigma_{i+1}^2 = \sigma_i^2 + 2K\Delta K \qquad (2)$$

where K is the diffusion coefficient. Initial impulse for convection is an ellipsoidal warm bubble with the maximum temperature perturbation in the bubble center ($T_0 = 5.6°C$) with exponential decrease towards zero on the bubble boundaries.

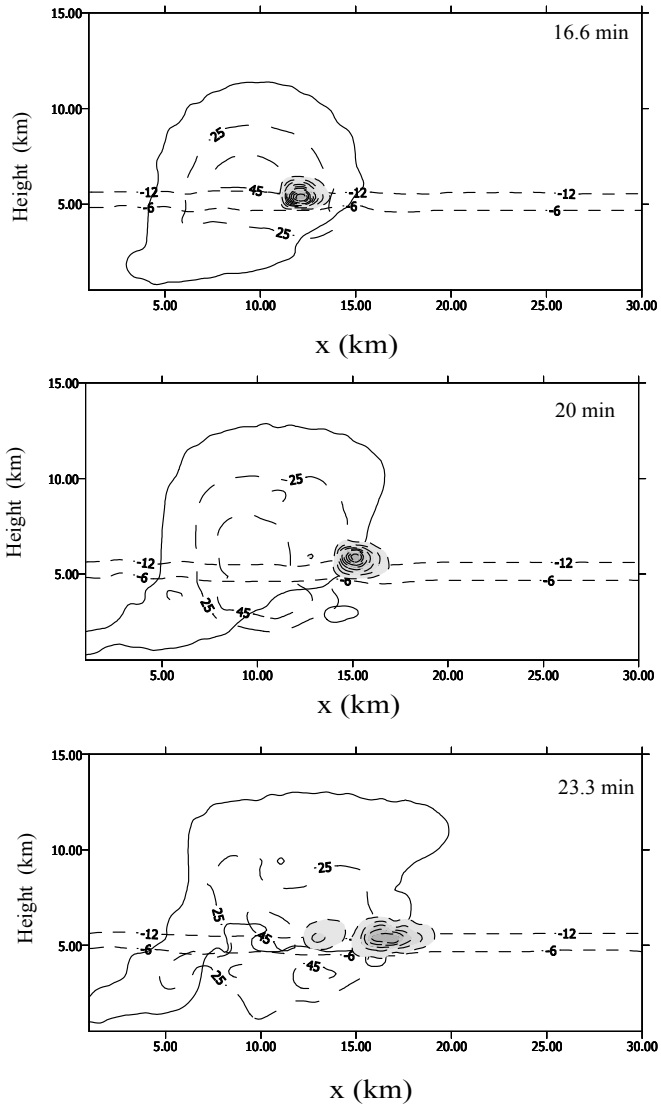


Fig. 2a) Time evolution of the AgI field in the x-z plane at y=15 km at 16.6, 20.0 and 21.6 min. Cloudy areas are outlines by a solid line. Reflectivity contours are given by dashed lines. An outer contour of 0.05 μg kg^{-1} is taken for 16.6 and 20.0 min

The model is chosen to be 30x30x15 km for 3-d runs and 45x15 km for 2-d runs, respectively. The horizontal resolution of the model is 0.5 km; the vertical one is 0.2 km. The temporal resolution of the model is 10 s time step for integration of the dynamics, microphysics and chemistry and a smaller one is (2 s) for solving the sound waves. A representative sounding taken at 01 UTC from Petrovec on May 18, 2003 with the corresponding wind profile is presented in Fig.1. The sounding is dry and stable near the surface and unstable and moist with wind veering above the surface layer, so the cloud develops very quickly in response to the initiating perturbations.

3. Results

The silver iodide agent is directly injected into the simulated cloud at a five minute time interval at 16.6 and 21.6 min, in the area between -8° C and -12°C isotherms and 25dBz-45dBz echo contours at 5.5 and 5km height, respectively. The time evolution of the AgI field in the X-Z cross sections is depicted in Fig.2. After seeding the agent is advected and diffused within

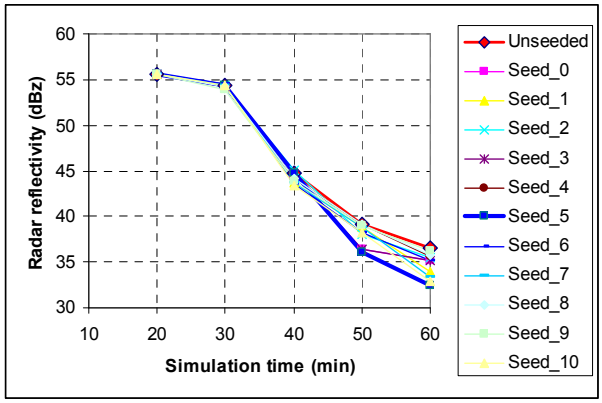


Fig. 3. The time evolution of reflectivity factors of unseeded and seeded case with a different time frequencies of seeding

the cloud by the turbulent flow field. Some of the AgI has been activated, small part tends to be drawn back into the cloud as it descends to the lower levels by the downdrafts, while the large portion is transported outside the target volume above -12°C isotherm. The limited time spread of agent is may be due to the strong air circulation within the cloud. Only 13% of the AgI remains inactivated as a result of less than optimal placement of the seeding agent and the limited advection time of 2-3 min that limits the time available for agent diffusion. The maximum agent spread within the target area during simulation time is less than 60 m from the axis depending on the local turbulence. Most of the AgI has been activated during the first five-minute interval. In order to gain a qualitative understanding of seeding conditions of a hailstorm

Table 1. A model sensitivity experiments

Experiment Time frequency of seeding (min)	*Time repeat of seeding (min)*	*Total rainfall on the ground (kg/m^2)*	*Total hailfall on the ground (kg/m^2)*
Base run	Unseeded	150.51	18.18
A0 (0min)	0	152.90	18.42
A1 (1 min)	1	150.12	18.77
A2(2 min)	2	157.85	18.98
A3(3 min)	3	152.92	18.43
A4(4 min)	4	149.60	18.36
A5(5 min)	5	153.56	18.26
A6(6 min)	6	152.29	18.28
A7(7 min)	7	151.84	18.66
A8(8 min)	8	149.60	18.36
A9(9 min)	9	150.20	18.14
A10(10 min)	10	152.20	18.78

suiting seeding. Table 1 lists the parameters that distinguish the ten simulations performed here. The first run (B), is chosen as a standard non-seeded case which serves as a basis for comparison with other experiments. It is evident that the total rainfall and hailfall at the ground for all experiments increase relative to the base run One sees that the greatest increase of both rainfall and hailfall is observed for a two-minute repeat seeding, for case A2, with percentage values of 4.65% and 4.40%, respectively. The optimal seeding effects are obtained by five-minute seeding interval for the simulation A5, when rainfall and hailfall increase by 2.02% and 0.44%, respectively. Fig. 2 shows the maximum hydrometeor mixing ratios averaged over simulation time as function of the seeding amount in (g/m).

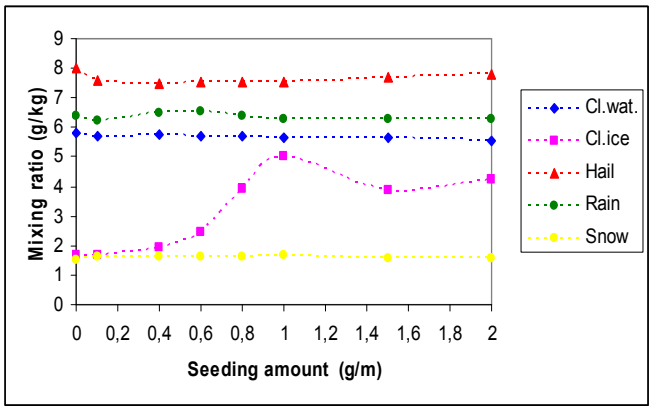


Fig. 2. Mixing ratio of hydrometeors as a function of a seeding amount

Seeding amount marked with (0 g/m) at x-axis is selected as the unseeded case. One sees rainwater mixing ratio increase and hail decrease for seeding amount 0.4 to 0.6 g/m. A peak value of cloud ice mixing ratio agrees with a seeding rate of 1 g/m. The effects of AgI seeding in respect to their microphysics are apparent if we consider the time evolution of reflectivity factors of the unseeded and seeded cloud (Fig.3). There is a slight similarity between the reflectivity echo contours after the initial seeding. The difference in the reflectivity echo fields between these runs becomes more evident as the cloud enters its mature stage.

4. Summary

According to hail suppression hypothesis it is logical to expect significant decrease of hail at the ground as in the other carefully setup hail suppression experiments. Despite positive statistical results from a number of numerical studies our sensitivity experiments indicate peak hailfall depth increased by about 0.44 to 4.40%. This inconsistency may be due to the bulk water parameterization used in our study, which does not recognize the size dimensions of ice particles. This is also a consequence of the limited spread of the seeding agent and the relatively low time of its diffusion and activation in the case of vigorous isolated cells. Finally, numerical models should be enabling to correctly simulate the agent dispersion, witch is in its initial phase on a sub-grid scale. However, it is not possible easy to say that the seeding does not have any effects considering the differences especially in respect to their microphysics.

References

Aleksic, N., B. Telenta and S. Petkovic, 1992: Model simulation of seeding repeat rates for direct injection seeding rockets. J. Wea.Mod., 24, 84-88

DeMott, P. J., 1995: Quantitative description of ice formation mechanisms of silver iodide-type aerosols. Atmos. Res., 38, 63-99.

Ćurić, M., D. Janc, and V. Vučković, 2006: Seeding agent dispersion within convective cloud as simulated by a 3-D numerical model. Meteor. Atmos. Phys., 92, 205-216.

Curic, M., D. Janc, and V. Vuckovic, 1997: The influence of cloud drop size distribution on simulated seeding effects of hail-bearing cloud. J. Wea. Mod., 29, 70-73.

Farley, R. D., 1987: Numerical modeling of hailstorms and hailstone growth. Part III: Simulation of Alberta hailstorm-natural and seeded cases. J. Appl. Meteor., 26, 789-812

Farley, R.D., P. Nguyen and H.D. Orville. 1994: Numerical simulation of cloud seeding using a three-dimensional cloud model. J. Wea.Mod.., 26, 113-124.

Georgopoulos, P.G. and J.H. Seinfeld, 1986: Mathematical modeling of turbulent reacting plumes-General theory and model formulation. Atmos. Envir., 20, 1791-1802

Hsie, E.-Y., R.D. Farley and R. D. Orville, 1980: Numerical simulation of ice-phase convective cloud seeding. J.Appl.Met. 19,950-977

Klemp, J.B. and R.B. Wilhelmson, 1978: The simulation of three-dimensional convective storm dynamics.J.Atm.Sci. 35, 1070-1096

Lin, Y. L. Farley, R. D. and H.D. Orville, 1983: Bulk water parameterization in a cloud model. J.Climate Appl. Met., 22, 1065-1092, 1983.

Smith, P.L, G. G. Myers and H.D. Orville, 1975: Radar reflectivity calculations on numerical cloud model using bulk parameterization precipitation. J. Appl. Meteor., 14, 1156-1165

Orville, H. D. and F.J. Kopp, 1977: Numerical simulation of the history of a hailstorm. J.Atmos. Sci., 34, 1596-1618

Orville, H. D. and J-M.Chen, 1982: Effects of cloud seeding, latent heat of fusion and condensate loading on cloud dynamics and precipitation evolution: A numerical study. J. Atmos. Sci., 39, 2807-2827.

Sekhon, R.S. and R.C. Srivastava, 1970: Snow size spectra and radar reflectivity. J. Atmos. Sci., 27, 299-307

Smith, P.L., G.G. Myers and H.D. Orville, 1975: Radar reflectivity factor calculations on numerical cloud models using bulk parameterization of precipitation. J. Appl. Meteor.., 14, 1156-1165

Spiridonov, V, and M. Curic, 2003a: Application of a cloud model in simulation of atmospheric sulfate transport and redistribution. Part I. Model description. Idojaras, Quart.Vol. 107, No. 2, p. 85-115.

Spiridonov, V, and M. Curic, 2003b: A three-dimensional numerical simulation of sulfate transport and redistribution. Can. J. Phys. 81, 1067-1094.

Weekly Circulation Characteristics of Aerosol and Precipitation and the Possible Influencing Mechanism Analysis in Beijing and Surrounding Areas

Zhanyu YAO Ling HOU
Chinese Academy of Meteorological Sciences, Beijing 100081, China
yaozy@cams.cma.gov.cn

Abstract: Weekly cycles of meteorological parameters have been found in many regions around the world; however, the phase and magnitude of these cycles vary greatly from regions and seasons. Based on the NCEP/DOE reanalysis data and the daily surface station observation data from 1980 to 2009 in Beijing and surrounding areas, the weekend effect of aerosol concentration, precipitation and several other meteorological parameters are analyzed, and a preliminary proof of the possible effects of aerosol on precipitation is given. It is shown that a well-defined weekly cycle appears for the aerosol concentration anomalies, which increase from Sunday to Wednesday and decrease during the later part of the week. The precipitation frequency anomalies, especially for the light rain, also show a significant weekly change, but with an opposite phase distribution comparing with that of aerosol concentration. However, for the anomalies of 24-hourly accumulated precipitation amount, the results are rejected at the 5% confidence level, and pollutant concentration plays a trivial effect on the precipitation amount. By analyzing the characters of weekly change of wind speed, cloud amount, relative humidity and atmospheric stability, it is deduced that the changes in the atmospheric circulation may be triggered by non-adiabatic heating of lower layer troposphere through the accumulation of aerosol, which leads to the change of cloud and precipitation. This provides a possible influencing mechanism of an indirect effect on cloud and precipitation by aerosols.

1. Introduction

Effects by aerosols on climate can be simply divided as short-term effect and climate effect. Human activities have obvious weekly circulation but it has not been found so far that a national weather process has a weekly cycle. Therefore, any weekly effects on climate should more or less have relationship with human activities.

Some observations and researches show that some meteorological variables in some regions have weekly changes. Scientists try to explain these phenomena and it is shown that human activities play an important role on them.

In this study, we find some weekly cycle characteristics of aerosols and meteorological elements in Beijing surrounding areas and try to analyze possible influencing mechanism of an indirect effect on cloud and precipitation by aerosols.

2. Study regions and data

Normal ground weather station observation data, atmospheric pollution index (API), and NCEP/DOE reanalysis data are used. Observation data at 14 ground weather stations from 1980 to 2009 in Beijing and surrounding areas (Fig. 1) are analyzed.

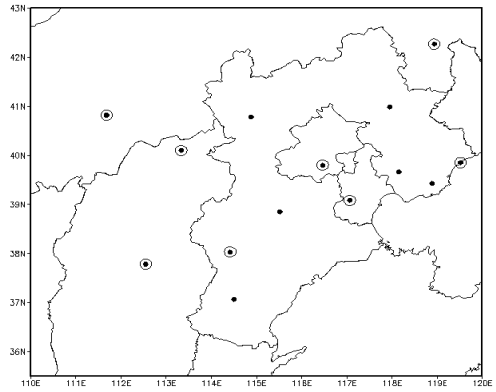


Fig.1 Study region. 14 normal ground weather stations are shown as solid dots and 8 of them, with pollution observations, are also marked with circles.

3. Weekly cycle characters of API

Figure 2 gives the summer average (hollow dot) and yearly average (solid dot) API anomalies within a week from Monday to Sunday in Beijing and surrounding areas.

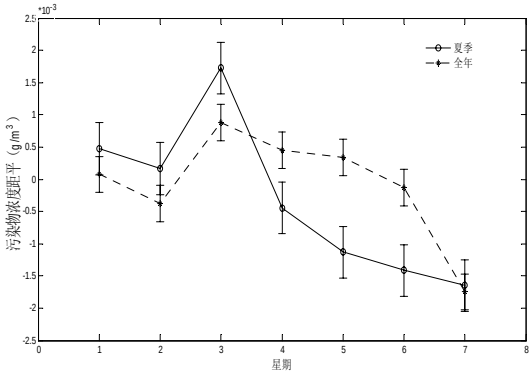


Fig.2 Summer average (hollow dot) and yearly average (solid dot) API anomalies from Monday to Sunday in Beijing and surrounding areas

It is shown that the average API rises to maximum on Wednesday and drops to minimum on Sunday. The summer average API is larger than the

yearly average one in the front part of the week and less in the latter part of the week.

By analyzing the power spectrums of atmospheric pollution concentration measured at all stations in the region, we obtain the regional average power spectrum of atmospheric pollution concentration in Beijing and surrounding areas (Figure 3). It is shown that there is an obvious cycle of 6-8 days which has passed significance test at 0.05 significance level.

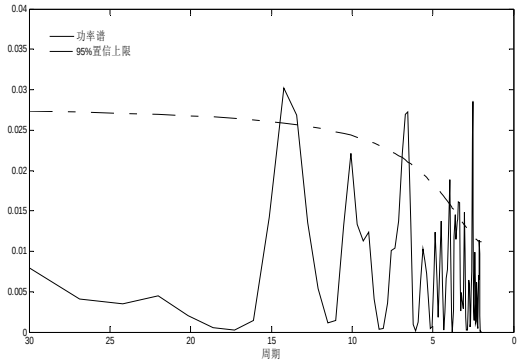


Fig.3 Regional average power spectrum of atmospheric pollution concentration in Beijing and surrounding areas

Similar results can be also found from the average wavelet power spectrum analysis based on atmospheric pollution concentration data from 8 stations. Figure 4a shows an obvious cycle of 4-8 days for the average wavelet power spectrum which has passed significance test at 0.05 significance level. Figure 4b gives the result of band pass filter oscillation based on wavelet analysis, which shows a cycle of 4-8 days and the most obvious weekly cycle oscillation occurs in summer season.

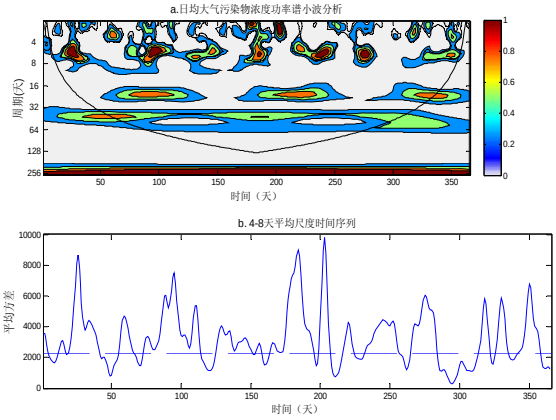


Fig.4 (a) Average wavelet power spectrum of daily atmospheric pollution concentration from 8 stations in Beijing and surrounding areas. The regions inner the black isoline have passed significance test at 0.05 significance level but not for the regions beneath the isoline. (b) Band pass filter oscillation of average wavelet power spectrum with the cycle of 4-8 days (solid line) and the 0.05 significance level (broken line)

4. Weekly cycle characters of precipitation

4.1 Weekly characters of precipitation amount

In order to study if there is a weekly cycle character for daily precipitation amount, one way analysis of variance (ANOVA) method is used to analyze each example. Suppose the daily precipitation amount is equal to each other within a week, when P value is less than 0.05 for two sub-samples in the individual station samples or at least two of four sub-samples in the samples of the sum of daily precipitation amount of 14 stations, it is significant to refuse the original suppose. It is shown by ANOVA based on the individual station samples (Table 1) and the samples of the sum of daily precipitation amount of 14 stations (Table 2) that both of them have not passed the F-test at 0.05 significance level. Therefore it is not significant to refuse the original suppose, that is to say there is no obvious difference among the daily precipitation amount within a week or there is no obvious weekly cycle character for daily precipitation amount.

Table 1 F statistics and P values by one way ANOVA based on the daily precipitation amount samples of individual station

	sub-sample 1		sub-sample 2	
Station	F	Pr>F	F	Pr>F
Hohhot	0.94	0.4626	1.44	0.1965
Datong	1.01	0.4139	0.74	0.6202
Shijiazhuang	1.73	0.112	2.01	0.0615
Taiyuan	1.73	0.1103	1.43	0.2008
Xingtai	0.59	0.7374	0.87	0.5153
Baoding	1.25	0.2754	0.53	0.7821
Chifeng	0.17	0.9845	1.71	0.3186
Zhangjiakou	0.55	0.7741	1.34	0.2357
Chengde	0.98	0.4402	0.65	0.6938
Qinghuangdao	0.75	0.6112	0.33	0.9221
Beijing	0.29	0.9434	0.87	0.5177
Tianjin	0.69	0.6616	0.77	0.5916
Tangshan	1.03	0.4038	1.55	0.1592
Leting	0.65	0.6940	0.42	0.8660

Table 2 F statistics and P values by one way ANOVA based on the samples of the sum of daily precipitation amount of 14 stations

sub-sample 1		sub-sample 2		sub-sample 3		sub-sample 4	
F	Pr>F	F	Pr>F	F	Pr>F	F	Pr>F
1.89	0.0791	0.76	0.5990	0.94	0.4634	0.75	0.6132

The two-tailed T-test statistics is used to further test the average daily precipitation amount of individual station and the regional average daily precipitation amount of 14 stations to see if there are any weekly cycle characters. Suppose the regional average daily precipitation amount is equal to each other within a week, the regional average daily precipitation amount on any two different days within a week are tested one by one by the two-tailed T-test statistics. It is shown (Table 3) that none of them has passed the significance test at 0.05 significance level. Therefore it is not significant to refuse the original suppose, that is to say there is no obvious difference among the regional average daily precipitation amount within a week or there is no obvious weekly

cycle character for the regional average daily precipitation amount.

Table 3 P values by two-tailed T-test statistics based on the regional average daily precipitation amount of 14 stations

	Tue	Wed	Thu	Fri	Sat	Sun
Mon	0.6323	0.7099	0.5505	0.6301	0.7637	0.1471
Tue		0.6461	0.3834	0.9788	0.4550	0.3192
Wed			0.6848	0.6430	0.7572	0.1556
Thu				0.0560	0.9407	0.0697
Fri					0.0795	0.3539
Sat						0.0991

4.2 Weekly characters of precipitation frequency

Due to the higher precipitation frequency in summer than in any other seasons in Beijing and surrounding areas, the precipitation frequency in summer is selected to analyze the weekly characters.

Because it is unknown for the distribution of precipitation frequency, the non-parameter test (Chi-Square Goodness of Fit Test) is used for the analysis of each sample to study the difference of precipitation frequency among each day within a week.

Suppose the precipitation frequency is equal to each other among each day within a week. If the precipitation frequency on any day of the seven days within a week is different from the one on another day, the supposition will be refused.

Table 4 Chi-Square values and P values of total precipitation frequency and light rain frequency of 14 stations in summer analyzed by Chi-Square Goodness of Fit Test. Underlined values have not passed the significance test at 0.05 significance level.

	Total precipitation frequency		Light rain frequency	
Station	χ^2	Pr> χ^2	χ^2	Pr> χ^2
Hohhot	0.9717	0.9867	12.9744	0.0424
Datong	13.0425	0.0418	13.8915	0.0308
Shijiazhuang	12.6705	0.0488	13.4292	0.0375
Taiyuan	23.2582	0.0007	20.0999	0.0027
Xingtai	13.9717	0.0300	13.1414	0.0411
Baoding	15.0641	0.0213	13.2195	0.0401
Chifeng	12.5164	0.0514	2.1414	0.9062
Zhangjiakou	13.9167	0.0305	12.7467	0.0472
Chengde	1.5267	0.9577	2.5307	0.8650
Qinghuangdao	2.5373	0.8643	2.0508	0.9150
Beijing	12.9258	0.0442	14.2553	0.0279
Tianjin	13.8618	0.0312	13.1762	0.0409
Tangshan	14.0424	0.0291	12.8644	0.0461
Leting	17.4526	0.0093	15.7989	0.0149
Regional Average	13.8016	0.0334	18.1176	0.0064

Table 4 gives the statistical analysis of total precipitation frequency and light rain frequency by Chi-Square Goodness of Fit Test. It is shown that among the samples of 14 stations, it has passed the significance test at 0.05 significance level for the total precipitation frequency samples of 10 stations and the light rain frequency samples of 11 stations in summer. It is also shown that for the regional average precipitation frequency of the 14 stations, it has passed the significance test at 0.05 significance level for both total precipitation frequency and light rain frequency.

It can be seen from Table 4 that even though the difference of precipitation frequency among each day within a week is not obvious at some stations, the regional average precipitation frequency has obvious difference among each day within a week in Beijing and surrounding areas. That is to say the precipitation frequency on at least one day of a week is obviously different from the ones on the other days.

In order to reduce noise impact, regional average precipitation frequency of the 14 stations is analyzed. Figure 5 gives the anomalies variation of regional average daily total precipitation frequency and light rain frequency within a week in summer in Beijing and surrounding areas. It is seen that it has the minimum value on Wednesday and the maximum value on Friday for both daily total precipitation frequency and daily light rain frequency. It has the same weekly cycle character for both daily total precipitation frequency and daily light rain frequency.

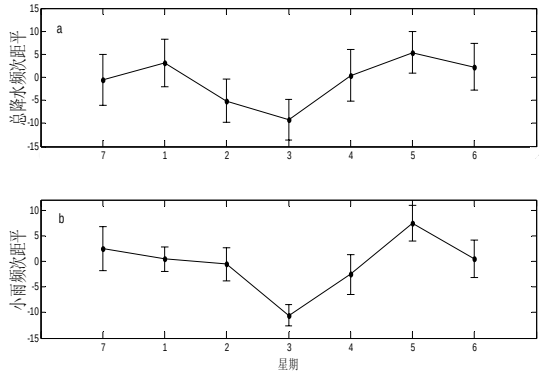


Fig.5 Anomalies variation of regional average daily total precipitation frequency (a) and daily light rain frequency (b) within a week in summer in Beijing and surrounding areas

Further analysis on the daily precipitation frequency on Wednesday and Friday by Chi-Square Goodness of Fit Test supports the result above and they have all passed the significance test at 0.05 significance level for both daily total precipitation frequency and daily light rain frequency.

By analyzing the power spectrum of daily light rain frequency in summer in Beijing and surrounding areas (Figure 6), we can see that there is an obvious cycle of 6-8 days which has passed significance test at 0.05 significance level. It has the similar distribution for the power spectrum of daily total precipitation frequency.

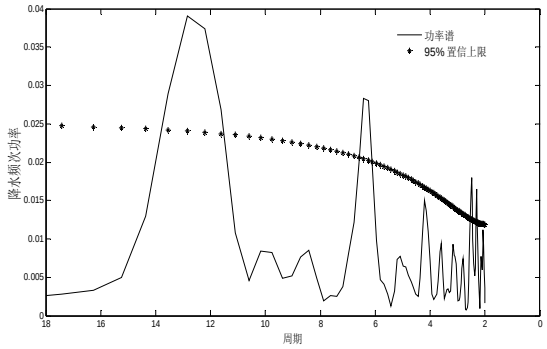


Fig.6 Power spectrum of daily light rain frequency in summer in Beijing and surrounding areas

5. Conclusion and discussion

Atmospheric pollution index (API) and normal ground observation data at 14 ground weather stations from 1980 to 2009 in Beijing and surrounding areas are analyzed to study the weekly cycle characters of atmospheric pollution concentration and precipitation. Several statistical methods are used for significance test. Some results have been taken out as follows:

1) There is an obvious weekly cycle character of atmospheric pollution concentration in Beijing and surrounding areas, which rises to maximum on Wednesday and drops to minimum on Sunday. The anomalies of API have passed the significance test at 0.05 significant level by one-tailed T-test. It is shown by power spectrum analysis and wavelet analysis that there is an obvious cycle of 4-8 days, and its explanation variation reaches as high as 27%.

2) It is not found that there are any weekly cycle characters of either daily total precipitation amount or daily light rain amount in Beijing and surrounding areas.

3) The weekly cycle characters are obvious for both daily total precipitation frequency and daily light rain frequency in summer in Beijing and surrounding areas, which drop to minimum on Wednesday and rise to maximum on Friday. The weekly variations of daily precipitation frequency have passed the significance test at 0.05 significant level by Chi-Square Goodness of Fit Test. It is shown by power spectrum analysis that there is an obvious cycle of 6-8 days and it has passed the significance test at 0.05 significant level.

The possible relation between the weekly cycle character of atmospheric pollution concentration and the weekly cycle character of daily precipitation frequency may be explained as follows. At the beginning of a week, aerosols begin to cumulate in the atmosphere. In the middle of a week, aerosols concentration gets higher and higher in the atmosphere and cloud amount also increases. Affected by both clouds and aerosols, the atmosphere is heated by radiation and it becomes more and more unsteadiness at middle and lower layer of troposphere which leads to vertical motion and strong wind. At the end of a week, the strong wind has led to diffusion of aerosols in the lower atmosphere and the precipitation frequency especially light rain frequency increases obviously.

References

Beaney, G., W. A. Gough. 2002. The influence of tropospheric ozone on the air temperature of the city of Toronto, Ontario, Canada [J]. Atmos. Environ., 36: 2319–2325.

Bell, T.L., D. Rosenfeld, K. M. Kim, et al. 2008. Midweek increase in U.S. summer rain and storm heights suggests air pollution invigorates rainstorms [J]. J. Geophys. Res., 113, D02209, doi:10.1029 / 2007JD008623.

Craddock, J. M. 1965. More rainfall statistics [J]. Weather, 20: 44– 50.

Cerveny, R. S., R. C. Balling Jr. 1998. Weekly cycles of air pollutants, precipitation and tropical cyclones in the coastal NW Atlantic region [J]. Nature, 394, 561–563.

Chunsheng Zhao, Xuexi Tie, Yunping Lin, et al. 2006. A possible positive feedback of reduction of precipitation and increase in aerosols over eastern central China [J]. Geophys. Res. Lett., 33, L11814, doi:10.1029 / 2006GL025959.

DeLisi, M. P., A. M. Cope, J. K. Franklin. 2001. Weekly precipitation cycles along the Northeast Corridor? [J]. Weather and Forecasting, 16, 343–353.

Dominique Bäumer, Bernhard Vogel. 2007. An unexpected pattern of distinct weekly periodicities in climatological variables in Germany [J]. J. Geophys. Res., 34, L03819, doi:10.1029/2006GL028559.

Duan Jing, Mao Jietai. 2008. Effect of aerosol to the regional precipitation in North China [J]. Chinese Science Bulletin (in Chinese), 53(23): 2947-2955.

Gong Daoyi, Guo Dong, Luo Yong. 2006. Weekend effect of daily precipitation frequency in summer of china [J]. Advances in climate change research (in Chinese). 2(3): 1673-1719.

Gong, D. Y., D. Guo, C. H. Ho. 2006. Weekend effect in diurnal temperature range in China: Opposite signals between winter and summer [J]. J. Geophys. Res., 111, D18113, doi:10.1029/2006JD007068.

Gong, D. Y., C. H. Ho, D. Chen. 2007. Weekly cycle of aerosol-meteorology interaction over China [J].J. Geophys. Res., 112, D22202, doi:10.1029 / 2007JD008888.

Liepert B G, Feichter J, Lohmann U, et al. 2004. Can aerosols spin down the water cycle in a warmer and moister world? [J]. Geophys. Res. Lett., 31: L06207, doi:10.1029/2003GL019060.

Liu, D. M., J. Huang, S. P. Gao, et al. 2006. The pollution level and influencing factors of atmospheric particulates from traffic in Beijing city during spring [J]. Earth Sci. Frontiers, 13(2):228–233.

Qian, Y., Daoyi Gong, Jiwen Fan, et al. 2009. Heavy pollution suppresses light rain in China: Observation and modelling [J]. J. Geophys. Res., 114, D00K02, doi:10.1029/2008JD011575.

Ramanathan V, Crutzen P J, Kiehl J T, et al. 2001. Aerosols, climate, and the hydrological cycle [J]. Science, 294: 2119-2124.

Schultz, D. M., S. Mikkonen, A. Laaksonen, et al. 2007. Weekly precipitation cycles? Lack of evidence from United States surface stations [J]. Geophys. Res. Lett., 34, L22815, doi:10.1029/2007GL031889.

Simmonds, I., J. Kaval. 1986. Day-of-the week variation of rainfall and maximum temperature in Melbourne, Australia [J]. Arch. Meteorol. Geophys. Bioclimatol., Ser. B, 36: 317–330.

Uncertainty and the Economic Implications of Weather Modification – Integrating Hypothesis Testing into Benefit-Cost Analysis

Stephen Beare[1], Ray Chambers[2], Scott Peak[3]
[1]Analytecon, 4 Johnston Street, Narrabundah, ACT 2604, Australia, stephenbeare@analytecon.com.au
[2]Centre for Statistical and Survey Methodology, University of Wollongong, Wollongong, Australia. ray@uow.edu.au
[3]Australian Rain Technologies, 23 Hickson Road, Millers Point, NSW 2000 Australia. peak@australianrain.com.au

1. Introduction

The localised modification of weather, intended or inadvertent, is difficult to detect due high level of natural variation in weather conditions and the reliance on observational as opposed to controlled experimental data. As a consequence statistical analysis often generates inconclusive results when using standard scientific precedents with respect to hypothesis testing. In fact, most cloud seeding experiments still do not provide evidence sufficient to reject the null hypothesis of no enhancement, and usually produce data 'not sufficient to reach statistical conclusions' (NRC 2003). However these standard precedents are not always useful in an industry or public policy context when a decision to invest in a rainfall enhancement program or regulate emissions from a power plant is being considered.

Weather modification technologies in general, are relatively low-cost and the prospective economic benefits of increased rainfall can be great. The economic costs of inadvertently caused reductions in rainfall may be equally high. Therefore, it seems appropriate to adopt a framework of decision-making under uncertainty when considering the testing and adoption of rainfall enhancing technologies or monitoring and evaluating the impacts of air pollution.

Expected benefit-cost analysis is perhaps the most common method for decision making under uncertainty. However, this approach has shortcomings when levels of uncertainty are sufficiently high to question whether there is a weather modification effect. A more appropriate approach that integrates hypothesis testing into benefit-cost analysis is developed in this paper. The benefit-cost analysis framework is restructured to admit the distribution associated with the null hypothesis against the alternative associated with the observational data. The objective is to construct an economic measure of acceptable risk .The approach is placed into the context of weather modification trials.

2. Benefit-cost analysis

The benefits and cost of alternative actions should have clear role in the decision process. Statistical measures of error bounds are readily incorporated into benefit-cost analysis. This kind of analysis provides an economic ranking of the options and a measure of risk associated with a particular decision. However, benefit-cost analysis does not resolve the underlying scientific uncertainty nor does it provide a sense of acceptable risk. The latter is because the level of uncertainty or lack of statistical precision does not alter the economic rankings.

We can take a standard benefit-cost approach and take into account the probability of achieving a positive rate of return from a future weather modification trial, given the results from past trials. The focus on benefits of a trial intentionally abstracts from broader benefits of proving the technology if it is in fact effective for simplicity. The costs of the trial are compared to the expected net benefits of additional rainfall. The calculation of these benefits can be quite complex as they depend critically on timing and location of any increase in precipitation. However, the calculation of the benefits is not at issue here. Importantly, the level and variability in the expected net benefits can be weighed against other options for managing the effects of adverse climatic variability such as the purchase of water from other users and agricultural investments in varietal breeding, genetically modified crops, crop management and increased water use efficiency.

A hypothesis-testing framework can also be used to account for the costs of falsely rejecting either the null hypothesis or the alternative hypothesis (there are no opportunity costs associated with a correct decision). In a business or public policy context the cost of falsely rejecting the null hypothesis that there is no effect (that is, the cost of running trials when there is no positive outcome) must be evaluated in light of the foregone benefits of falsely rejecting the alternative hypothesis that there is an effect. In contrast to traditional benefit-cost analysis, this approach can lead to the rejection of an investment with a high-expected return if the level of uncertainty is high enough. A traditional benefit-cost approach allows the comparison of alterative investments but would only reject an option if either negative or same return could be achieved with a greater level of certainty. The hypothesis-based approach has an additional advantage in that it can place a value on information that would increase the precision of the estimated level of enhancement.

3. An alternative view of risk and return

The traditional benefit-cost analysis described in the previous section is predicated on the assumption that the average level of effect is an unbiased, and therefore an acceptable estimate of the true level of the effect. There is uncertainty about that estimate which can be characterised by error bounds. From the average effect and the error bounds, the expected level and variability in net returns is calculated. The decision under uncertainty is simple:

- Any investment option with a positive average net return is viable; and
- If one or more investment options have the same return the option with the lowest variability is preferred.

The scientific process of hypothesis testing gives rise to an alternative perspective on the idea of risk and return. Consider the following standard one-tailed hypothesis test:

- H_o: Effect = 0
- H_a: Effect > 0

Here, risk and return are couched in terms of the direct and opportunity costs of false rejection. That is, the cost of falsely rejecting the null hypothesis H_o versus the cost of false rejection of the alternative hypothesis H_a. This, in turn, is linked to the confidence levels associated with these decisions. Clearly, if the cost of falsely rejecting H_o is far greater than the cost of falsely rejecting H_a it would be rational to try to limit the likelihood of a type-I error and set a confidence level for H_a which is quite high. Conversely, if the cost of falsely rejecting H_o is less than falsely rejecting H_a, it would be rational to try to limit the likelihood of a type-II error and set a confidence level for H_a which is relatively low. It is possible to try and limit the potential for a type-II error by increasing the power of the test through, for example, more extensive trials.

Given the inability to control trial weather, a high level variability in natural rainfall and the lack of longer-term stationarity in weather systems, the capacity to increase the power of the test and reduce type-II error may limited and costly. As a consequence, setting an appropriate level of confidence for H_a becomes the central issue for which commonly used “precedents”, such as the 99 per cent confidence level provide little, if any, guidance.

In comparing the opportunity cost of falsely rejecting the null hypothesis and the opportunity cost of falsely rejecting the alternative it is possible to find a confidence level for a standard one-tailed hypothesis test that equates the two costs. That is, it generates a net economic benefit of zero. This confidence level, in a fiducial or Bayesian context, can be interpreted as a threshold level of risk. For a discussion of fiducial and Bayesian analyses see Hannig (2009).

If the error associated with the estimate of interest generates confidence level below this threshold the best economic option is to accept the null hypothesis even though the net returns under the alternative may clearly warrant an investment or some form of intervention. Alternatively, if the confidence level is above the threshold then the best economic option is to accept the alternative even if by scientific standards the results are not conclusive.

It is also possible to ascribe an ex ante economic benefit to additional experimental data or statistical methods that reduce estimation error (assuming the estimate itself is unchanged). The reduction in error changes the weighting of the opportunity costs, which in turn changes the expected net benefit associated with the preferred option.

4. Application to Weather Modification trial

The new approach described in the previous section is formally set out and then contrasted with traditional benefit-cost analysis using a stylised example. The technique is then applied to data from rainfall enhancement trials conducted in South Australia using a ground-based ionisation technology known as Atlant (Beare et al. 2011). The analysis clearly shows that even with substantively greater levels of uncertainty associated with the estimated level of enchantment, the opportunity cost of foregoing the direct benefits of future trials would be greater than the trial costs.

5. Concluding remarks

In this paper an alternative risk and return framework based on the principles of hypothesis testing was developed. The approach is appropriate for evaluating investment and decisions based on experimental evidence are subject to high degree of uncertainty. The approach yields an economic measure of an acceptable level of risk.

The tool seems particularly useful in the context of weather modification and the observational analysis of natural systems more generally, due to the difficulty of detecting signal against high background noise, when that signal is associated with substantial benefits or costs.

References

Beare, S., R. Chambers, S. Peak, J. Ring, Accounting for Spatiotemporal Variation of Rainfall Measurements when Evaluating Ground-Based Methods of Weather Modification. *Journal of Wea. Modif.* **43**, 44-63, 2011.

Hannig, J., On Generalized Fiducial Inference, *Statistica Sinica*, **19**, 491-544, 2009.

National Research Council (NRC), *Critical Issues in Weather Modification Research*, National Academy Press, pp. 41. 2003.

A short review on Geo-engineering proposals to fight against climate change

Jean-Pierre Chalon
Météo-France, Toulouse, France

Since the beginning of the industrial era, the atmosphere content in greenhouse gases has rapidly increased. In its 4th assessment report (AR4), the Intergovernmental Panel on Climate Change (IPCC, 2007) points out the impact of human's activities and its responsibility for a large part of the changes recently observed in the Earth's climate: increase in global temperature, sea level rise, melting of glaciers and ice-caps...

As expected consequences can become dramatic before the end of the 21st century, numerous geo-engineering proposals have been developed to try fighting against these disturbances.

The average global temperature on our Planet depends both on the quantity of energy received from the Sun, on its absorption by the Earth's surface and on the actions of greenhouse gases preventing a part of the energy emitted by the Earth to escape into the outer-space.

To prevent global warming, the alternatives are therefore either to limit the solar radiation absorbed by the Earth's surface or to reduce the amount of greenhouse gases in the atmosphere. Many of the geo-engineering proposals concern modification in cloud characteristics and are directly linked with weather modification applications.

1. Reducing the solar radiation absorbed at the surface of the Earth

Warming associated with increasing greenhouse gas concentrations could be offset by a reduction of a few percent of the solar radiation that is absorbed by the Earth's surface.

Thus, many ideas have been advanced to develop screens between the Sun and the Planet or to increase the reflective power of the ground.

1.2. Injecting Sulphur in the stratosphere

It has been observed in the past that large volcanic eruptions were accompanied by a fall of a few tenths of a degree in global average temperature; a fall which could last for a few years. Volcanic eruptions eject large amounts of dust and aerosols that reduce solar radiation reaching the Earth's surface. In the troposphere, these aerosols remain only a few days before being leached by precipitations. But those that reach the stratosphere can remain there for several years. As an example, in 1991 the eruption of Mount-Pinatubo, in the Philippines, injected 10 to 20 million tonnes of sulphur dioxide into the stratosphere and, as a consequence, the climate of the Planet underwent cooling of nearly 0.5 ℃ for more than a year.

To exploit this phenomenon, W.R. Cotton (2008) suggests stimulating volcanic activity in order to encourage eruptions that could inject aerosols in the stratosphere. However, he recognizes the difficulty of the task and the need to first study the feasibility, the impact and the side-effects of such an undertaking.

On the same basis, in 1974, Mr. Budyko, of the Observatory of Saint-Petersburg, in Russia, suggested to inject sulphur or sulphate aerosols directly into the stratosphere.

Later on, the idea has been taken again by P. Crutzen (2006), a Nobel Prize in chemistry, who proposed to drop a few million tonnes of sulphur or hydrogen sulphide by using stratospheric balloons at altitudes between 15 and 50 km. At this level, these compounds are converted into tiny sulphate particles that reflect a part of the solar radiation. P. Crutzen noted that the proposed amounts are not exceptional as we already send about 55 million tonnes of sulphur dioxide in the atmosphere each year. To compensate for a doubling of the carbon dioxide concentrations, he estimated the cost of operations to US $25–50 billion per year.

However, sulphur aerosols are very harmful; they cause acid rain that deteriorate forests and are responsible each year, according to the World Health Organization, for hundreds of thousands premature deaths. Furthermore, the method cannot compensate for the local impact of greenhouse gases. Indeed, it would limit radiation, and therefore temperature, but only on the sunlit areas while greenhouse gases warm the whole Planet, on days and nights, and more strongly the Polar Regions that spend six months a year in the dark. The reduction of global warming in the Polar Regions is considered to be an important aspect of the fight against climate change because when highly reflective ice melts it uncovers soil or ocean surfaces (of smaller albedos) which absorb more solar radiation, amplifying the global Earth warming.

A comprehensive study realised by Tilmes et al. (2008) also shows that the proposed method

would destroy part of the stratospheric ozone layer that protects us from highly carcinogenic ultraviolet radiations from the Sun. This concern has to be taken is full consideration while for many years we were looking for ways to restore the ozone layer that is destroyed by impact of chlorofluorocarbons used in aerosol and as refrigerant gases. Other objections have been raised since such an approach could permanently give a milky colour to the sky and have significant effects on our quality of life and on the development of vegetation.

1.3. Making more reflective clouds

The reflecting power of a cloud is a function of its droplet concentration. A higher concentration corresponds to a stronger reflection of the solar energy. Thus, the clouds developing in polluted areas better prevent the ground from solar radiation. Their high concentrations in droplets are due to the presence of numerous aerosols, providing support to the condensation of water vapour.

Conversely, because of the low number of aerosols, clouds over oceans have far less droplets. One could then consider increasing their reflective power by seeding them with hygroscopic nuclei.

Measurements also highlight that, in the track of the ships, the clouds often have higher droplet concentrations than clouds observed in the surrounding areas. This perspective seems to be rather interesting since low clouds such as marine stratocumulus regularly cover about one-quarter of the ocean surface.

J. Latham (2004) rather suggests using particles in solution. To this end, he proposes to construct a fleet of vessels equipped with long chimneys used to send fine sea water particles into the atmosphere.

If they do not reach directly the clouds, these droplets will evaporate and release the salt crystals they contain. This increased number of condensation nuclei present in the atmosphere would then promote the formation of a greater number of droplets in the developing clouds. J. Latham estimated to 1,500 the number of boats necessary to compensate for a doubling of atmospheric carbon dioxide concentrations.

Studies are still needed to estimate the feasibility, cost, and possible side effects of such a project. Clouds with high droplet concentrations being less efficient to produce large drops, the implementation of such a technique could, in particular, lead to a decrease in precipitation watering coastal regions.

1.4. Making a cloud of parasols

R. Angel (2006) imagines covering the space that separates the Earth from the Sun with a multitude of small discs playing the role of umbrellas.

There is a region, at an altitude of about 1.5 million kilometres, where the force of attraction of the Sun is equal to that of the Earth and where small objects can stay in equilibrium. Angel proposes placing in this region small discs, 60 cm in diameter, equipped with a navigation system.

To get a significant effect, it would be necessary to create a 100,000 km long cloud consisting of several thousands billion discs. Even if each disk is very light, the whole set would weight about 20 million tonnes. At the rate of one million disks per minute, it would take about thirty years to implement this cloud.

1.5. Painting deserts in white

Surfaces reflecting light warm less than surfaces absorbing it. The distribution of more or less reflective surfaces that cover the Earth has a significant effect on its temperature.

Thus, when glacier melting replaces white and highly reflective surfaces by dark and more absorbent surfaces, it results both an increase of the absorbed energy and of the surface temperature. As a consequence, several projects aim at increasing the reflective power of the Earth (its albedo) in considering for example painting deserts in white.

However, a simple calculation shows that this type of action can only have very insufficient and limited effects.

On a smaller scale, there are also studies that suggest painting urban buildings in white in order to reduce temperature in urban heat islands that are associated with the absorption of solar radiation by bricks and concrete.

2. Reducing the greenhouse effect

Several methods have also been proposed to reduce the greenhouse effect which maintains a high temperature on the Planet, by dissipating some clouds or by extracting a part of the carbon dioxide from the atmosphere.

As an example, Lackner et al. (1995), at the University of Colombia, in the United States, propose to build "artificial trees" able to collect carbon dioxide from the air and to reduce it in powder that is directly stored in the ground.

2.1. Dissipating cirrus veils and contrails

Cirrus, cirrostratus and condensation contrails produced by aircraft reduce the passage of solar radiation and retain a portion of terrestrial radiation. Considering their overall contribution, it is believed that they participate in the greenhouse effect and thus to the global warming of the Earth (Minnis et al, 2004).

W.R. Cotton (2008) suggests seeding them with carbonaceous aerosols and soot in order to absorb a portion of solar radiation and thus to warm them up sufficiently to evaporate ice particles and to dissipate them.

However, such operations could have an impact on rainfall and on the global water cycle. Moreover, side effects, associated with the presence of large quantities of soot in the atmosphere, remain to be considered.

2.2. Favouring the growth of algae that gobble up the carbon dioxide

The Ocean has a very strong capacity to absorb carbon dioxide. However, only a small part of the waters are in contact with the atmosphere and surface waters are thus quickly saturated. Major transfers take place in the regions of surface cold water diving (or subduction) and in the growth of microorganisms fed with carbon dioxide before pouring into the depths of the oceans.

Lovelock and Rapley (2007) suggest stirring the water to stimulate the growth of phytoplankton, a microscopic marine alga that consumes large amounts of carbon dioxide.

To achieve this, they propose installing in the oceans thousands large tubes (approximately 100 metres long and 10 metres in diameter) which, like elevators, would move up the deep waters to the surface.

As the growth of phytoplankton is favoured by the presence of iron, J.H. Martin (1990) suggests seeding the oceans with iron fillings. Among all of the actual projects envisaged to cool the planet, it is certainly the simplest to implement.

Operations were thus conducted, in 1993 and 1995, off the coast of the Galapagos Archipelago.

Unfortunately, Boyd et al. (2004) show that this technique has no scientific basis and present a non-negligible risk because, before sinking to the depths, the plankton would absorb a portion of the oxygen that fishes need to live. In addition, the absorption of large amounts of carbon dioxide would acidify the ocean leading to the dissolution of a large part of the plankton, a result opposite to that which is looked for.

It should also be noted that the reproduction of plankton produces toxins that are fatal to many organisms that would then be in danger.

2.3. Storing carbon dioxide

Capture and storage of carbon dioxide produced by industry or thermal power plants are part of the methods envisaged to reduce their atmospheric emissions. According to the Intergovernmental Panel on Climate Change (ICCP, 2007), this method could contribute for 10 to 15% of the greenhouse gas reduction efforts.

Several companies, especially in the oil field, work on this subject. The simplest technique is to produce a concentrated carbon dioxide at high pressure that can be easily sent to a place of storage in order to isolate it from the atmosphere. The main proposed techniques of storage are: industrial fixation in inorganic carbonates, deposition in the deep layers of the ocean or injection into the substratum.

Under specific conditions of temperature and pressure, the peridotite, the main rock of the Earth's mantle, reacts with carbon dioxide (CO_2) to form calcites, magnesites or dolomites.

From research developed at Columbia University, this crystallization would allow to store several gigatons (or billion tonnes) of carbon dioxide every year.

However, most of the peridotite, formed by the crystallization of magma, is located at about 30 km depth and only the countries where it is close to the Earth's surface (Oman, Papua, New Guinea, Caledonia, California…) could benefit from such a method.

It seems also possible to directly inject the trapped CO_2 in the oceans, at more than 1 000 metre depth, where most of it could be isolated from the atmosphere for centuries. The retention may be increased by forming solid hydrates or liquid CO_2 lakes at the bottom of the oceans.

However, the possibility to proceed at ocean storage has not yet been demonstrated. It would change significantly the chemistry of waters and their acidity and could be detrimental to marine organisms (lower rates of calcification, breeding...). It is not yet very well known how the species and ecosystems will adapt to such changes in their environment.

Other proposed storage sites are exhausted oil and gas fields, unworkable coal mines and underground salted water tables.

But the implementation of such solutions still presents several technical, economical and societal difficulties. As it is reminded by the tragedy that happened in 1986 in Cameroon during a natural degassing, at high dose of carbon dioxide is lethal. More than 1,000 people have died. Then, because

of the risks of leakage, many associations are opposed to massive storage of carbon dioxide near inhabited areas.

3. Conclusions

If, ideas to cool the Planet are flourishing, most of them still rely on fiction and, at this stage of understanding, their effects are still uncertain. All the possible consequences are not known yet, and some of them could be uncontrollable and far more serious and damageable than the fought effects. Research should therefore be continued. Solutions sometimes arrive when they are the less expected. However, today we should not forget that there is no acceptable solution yet. Reflection on geo-engineering techniques should not prevent us from developing safer and more effective methods to modify our energy consumption and reduce both pollution and the quantity of carbon dioxide we produce on a daily basis.

References

Angel, R., 2006: Feasibility of cooling the earth with clouds of small spacecraft near the inner Lagrange point. *Proceedings of the National Academy of Sciences*, USA, vol 103, 46, pp. 17184-17189, 2006.

Boyd PW, Law CS, Wong CS, Nojiri Y, Tsuda A, Levasseur M, Takeda S, Rivkin R, Harrison PJ, Strzepek R, Gower J, Mckay RM, Abraham E, Arychuk M, Barwell-Clarke J, Crawford W, Crawford D, Hale M, Harada K, Johnson K, Kiyosawa H, Kudo I, Marchetti A, Miller W, Needoba J, Nishioka J, Ogawa H, Page J, Robert M, Saito H, Sastri A, Sherry N, 2004 : The decline and fate of an iron-induced subarctic phytoplankton bloom. *Nature*, 2004 1 April; 428(6982): pp. 549-553, 2004.

Cotton, W.R., 2008: Weather and climate engineering. *17th planned and inadvertent weather modification Conference*. Weather Modification Association, 2008.

Crutzen P., 2006: Albedo Enhancement by Stratospheric Sulfur Injections: A Contribution to Resolve a Policy Dilemma? *Climatic Change*. Springer, 77(3-4), pp. 211-220, 2006.

IPCC, 2007: 4th assessment report (AR4) of the Intergovernmental Panel on Climate Change (IPCC). www.ipcc.ch. 2007.

Lackner, K. S, C. H. Wendt, D. P. Butt, E. L. Joyce, and D. H. Sharp, 1995: Carbon Dioxide Disposal in Carbonate Minerals. *Energy*, 20, pp. 1153-1170, 1995.

Latham, J., 2004: John Latham ponders a plan to counter global warming. UCAR Staff note, May 2004.

Lovelock, J.E. and C.G. Rapley, 2007: These ocean pipes could help the Earth to cure itself. *Nature* 449, p. 403, 2007.

Martin, J. H., 1990: Glacial-interglacial CO2 change: the iron hypothesis, *Paleoceanography*, 5, pp.1-13, 1990.

Minnis, P., J.K. Ayers, R. Palikonda, and D. Phan, 2004 : Contrails, cirrus trends and climate. *Journal of Climate*, 17, pp.1671-1685, 2004.

Tilmes, S., R. Müller, R. Salawitch, 2008: The Sensitivity of Polar Ozone Depletion to Proposed Geo-engineering Schemes. *Science*, 30, Vol. 320, n°5880, pp. 1201–1204, 2008.

Efficiency of Precipitation Enhancement from Convective Clouds at Salt Powder Modification

Belyaeva M.V., Drofa A.S., Ivanov V.N.
RPA "Typhoon",4, Pobedy st., Obninsk, Kaluga Region, 249038, Russia, e-mail: drofa@typhoon.obninsk.ru

Hygroscopic particles from pyrotechnic flares are widely used in a number of projects aimed at enhancement of precipitation from convective clouds (Cooper et al., 1997). At modification with this method hygroscopic particles are introduced into an updraft in the cloud base. The concept of modification is in the transformation of cloud drop spectrum at the initial stage of condensation in such a way that at future evolution of the cloud coagulation processes will be intensified and precipitation formation processes will be enhanced. Hygroscopic particles generated by pyrotechnic compounds have the sizes from 0.3 to 1 μm. The use of larger particles (I – 3 μm), as the investigation results have shown, makes it possible to obtain a more significant modification effect, but the consumption of the agent is by more than the order of the value higher than that of pyrotechnic compounds.

Rosenfeld D. (2005, 2010) proposed to use a polydisperse salt powder NaCl with rather broad particle size distribution functions for cloud modification. Such a powder was tested in the Big Cloud Chamber of SI RPA 'Typhoon' (Russia) (Drofa et al., 2010). The results of the tests supported by the results of numerical simulations demonstrate significant advantages of the powder for obtaining additional precipitation amounts. The essential effect of modification by the salt powder manifesting itself at mass concentrations of the powder introduced is by an order of the value less than at the use of pyrotechnic flares. When the salt powder is used, precipitation can be obtained from small usually non-precipitating warm convective clouds.

The present paper gives (on the basis of numerical simulations) the estimates of modification effect on convective clouds caused by polydisperse salt powders and describes the conditions necessary for maximum positive effect attained with this method.

The analysis of a scenario of cloud drop formation in a convective cloud shows that at the initial stage of condensation the main cloud droplet size distribution spectrum is formed on hygroscopic nuclei with the radii from 0.015 to 0.65 μm. Cloud spectrum maximum is formed on the nuclei of the radii of about 0.02 μm. Just such hygroscopic particles are active condensation nuclei for which unlimited growth at the initial condensation stage is realized. For artificial stimulation of coagulation processes in clouds it is necessary at the initial stage of condensation to transform the droplet spectrum in such a way that the number of large drops will be increased without changes in the conditions of cloud drop formation on atmospheric condensation nuclei. For this hygroscopic particles with the radii over 0.5-0.6 μm should be introduced. The number of additional particles needed for intensification of coagulation events, and the subsequent precipitation formation is determined by the results of numerical simulation.

The size distribution of hygroscopic particles at numerical simulations is described by the function of the form:

$$f(r)=a\, r^{-\mu} \exp(-(r/r_o)^2). \qquad (1)$$

The salt powder particles spectra are of such a form. For the powder presented in (Drofa et al., 2010) the distribution parameters (1) are equal to: μ = 1.5, r_0 = 5 μm; for the powder (Drofa et al., 2011) - μ = 0.5, r_0 = 5.3 μm. An example of calculations of the initial stage of cloud medium microstructure formation at the introduction of the salt powder into the subcloud layer is given in Fig. 1. Here shown are the calculation results of

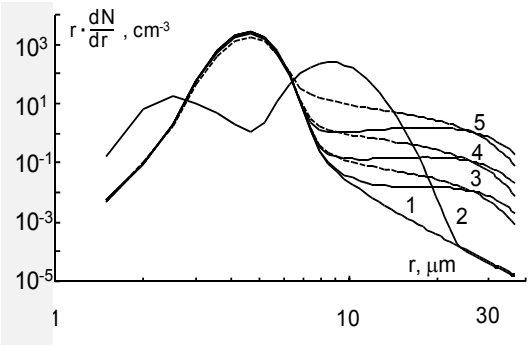


Figure 1. Cloud drop spectra at the 2nd min of cloud formation.
Solid lines – salt powder of RPA 'Typhoon';
dashed lines – powder presented in (Drofa et al., 2010).
1- drop spectrum in the background cloud;
2 - at introduction of salt particles with the radii 0f 1 μm;
3 - at introduction of salt powder with mass concentration of 0.01 mg/m^3; 4 – 0.1 mg/m^3;
5 – 1.0 mg/m^3.

drop spectra in a convective cloud at the level reached by the air mass in 120 s. Physical and chemical characteristics of background aerosol correspond to average characteristics of atmospheric aerosol of the continental origin. Atmospheric conditions are typical for convective clouds of the continental type. The velocity of an air updraft near the cloud base is taken equal to V = 1.5 m/s, the initial air temperature – 10°C, pressure – 900 mb. The Junge distribution was

used as an initial distribution of aerosol particles being atmospheric condensation nuclei:

$$f(r_c)=a\cdot r^{-v} \quad (2)$$

Formula (2) approximates rather well real spectra of aerosol particles in the atmosphere. For continental air masses it is usually accepted that v = 4-5 (Drofa, 2006).

It is evident that a positive effect of cloud modification with salt powders may appear only when a relative number of additionally introduced particles less than 0.5 μm does not exceed the number of active condensation nuclei in the background aerosol. It means that the condition $\mu < v$ should be met. In the opposite case the introduction of additional particles causes an increase of concentrations of particles formed and a decrease of their mean sizes. This effect is called the "oversesding".

As an example in Figure 1 shown are the spectra cloud drop sizes at the introduction into the convective subcloud layer of hygroscopic particles with a narrow size distribution function. NaCl particles with an effective radius of 1 μm and a relative dispersion of size distribution function S=0.3 are used. The number concentration of particles introduced makes 120 cm^{-3}. Such a concentration is optimal for the particles of this size for obtaining maximum modification effect (Drofa, 2006). The mass concentration of particles is 1.1 mg/m^3. As is seen from Figure 1, the introduction of such particles results in the formation of a bimodal cloud drop spectrum, the large-drop fraction in which is determined by the growth of particles formed on salt particles, and the fine-droplet fraction – on the nuclei of the background aerosol. The studies of the effect of modification with such particles have shown (Drofa, 2006; Segal et al., 2007) that at the introduction of salt particles due to a decrease of water vapor oversaturation in a cloud the number of atmospheric nuclei is activated (i.e. they turn into cloud drops) to a lesser extent than in the background cloud. Due to this, the total concentration of cloud drops formed on the background and additional nuclei appears less than in the case when additional condensation nuclei are absent. An average size of cloud drops appears greater at the introduction of particles. Because of this a positive effect of modification with hygroscopic particles with narrow size distributions is reached as the enlargement of cloud drops is the main factor of stimulating gravitation-induced coagulation in clouds and subsequent precipitation formation. One should pay attention at the fact that cloud drops formed on atmospheric aerosol particles are less in size under modification as compared to the background cloud. It means that in this case modification with salt particles results in the changes in conditions of cloud drop formation on atmospheric condensation nuclei.

The modification with salt powder does not lead to such changes even at rather high mass concentrations of the powder introduced. The number of cloud drops formed on the background aerosol particles changes little in this case. As is seen from Figure 1, the introduction of the salt powder into the subcloud level of a convective cloud results in the appearance of large-drop "tail" in the cloud drop distribution. The form of the large-drop spectrum fraction formed on salt particles is determined by the form of salt powder particles spectrum. The spectrum of drops formed on the background atmospheric aerosol particles does not change in this case. As the analysis of the results of numerical simulation has shown, the modification with the salt powder leads to rather more significant intensification of coagulation processes in a cloud (and, later on to enhancement of precipitation formation processes) as compared to the modification by hygroscopic particles with narrow particle size distributions.

The data obtained at the initial stage of condensation (Figure 1) are the basic data for calculations of cloud medium microstructure evolution with the use of a one-dimension numerical model of a convective cloud (Drofa, 2010). The one-dimension model of a convective cloud describes the evolution of a cloud medium in the central part of the cloud at variable with altitude velocity of the air updraft forming the cloud. The model considers parametrically the entrainment of heat and moisture into an air flow from the environment. Activation of atmospheric condensation nuclei occurs in the subcloud layer. At a further updraft of the air mass the evolution of cloud medium microstructure takes place due to the processes of drop condensation growth/evaporation, coagulation, breakdown and sedimentation. Spatiotemporal structure of meteorological parameters and integral characteristics of cloud drop size distribution function are calculated with the model. Liquid water contents of large drops with the radii r>200 μm characterizing precipitation are calculated. From the data referring to the cloud base level calculated are the precipitation intensity and total precipitation amounts.

The calculated temporal trend of precipitation intensity at modification of a cloud of 4.2 km thickness with the salt powder is shown in Figure 2. In this cloud at the stage of its formation realized was the maximum liquid water content of 3.46 g/m^3 and maximum air vertical updraft velocity of 4.5 m/s. The introduction of particles into the sublayer of the thickness from 60 to 240 m is made at the 10^{th} minute of the beginning of the cloud formation. From the graphs in Figure 2 it is seen that with the help of the salt powders precipitation amounts can be by 2-5 times greater. The effect of modification induced by the use of the powder produced at the RPA 'Typhoon', as is seen from Figure 2, is somewhat more pronounced than that presented in (Drofa et al., 2010). In general, the calculation results have shown that the amounts of additional precipitation obtained at cloud

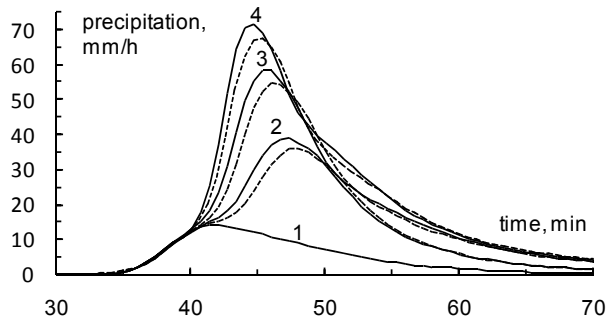


Figure2. Temporal intensity trend of precipitation from a cloud of 4.2 km thickness.
Solid lines – salt powder of RPA 'Typhoon'; dashed lines – powder presented in (Drofa et al., 2010).
1 – without agent, 2 – consumption of salt agent 2.4 kg/km^2, 3 – 12 kg/km^2, 4 – 48 kg/km^2.

modification with the powder of the RPA 'Typhoon' is by 1-2 mm more than at modification with the powder presented in (Drofa et al., 2010). For obtaining similar amounts of additional precipitation with the first powder the needed powder amounts are by 10-15% less.

The calculated total precipitation amounts obtained at modification of warm convective clouds of different thicknesses with the salt powder are given in Figure 3. As is seen from the Figure, at the consumption of more than 24 kg/km^2 additional precipitation amounts can be obtained from the clouds with the thickness H = 2.5 – 3.5 km, i.e. from the clouds that do not usually produce precipitation. The maximum effect of modification – the maximum amounts of precipitation from the clouds – is realized at the consumption of 48 kg/km^2 of the salt powder. In this case

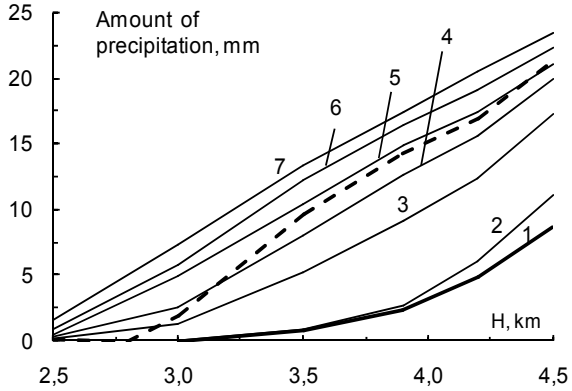


Figure 3. Calculation results of total precipitation amounts from clouds of different thicknesses
1 – without introduction of particles; 2 – introduction of South African flare particles; 3 – introduction of salt powder at the consumption of 2.4 kg/km^2; 4 – 6 kg/km^2; 5 – 12 kg/km^2; 6 – 24 kg/km^2; 7 – 48 kg/km^2.
Dashed line – introduction of 1 μm salt particles at the consumption of 64 kg/km^2.

practically all the cloud drops ate transformed into precipitation drops. After the precipitation falls from the cloud, an insignificant number of cloud drops remains in it. A further increase of the agent amount introduced does not increase the effect of modification.

The calculation results of the modification effect attained with the use of South African pyrotechnic flares (Cooper et al., 1997) demonstrate that significant amounts of additional precipitation are observed only at modifying the clouds with the thicknesses over 4 km. The calculations are made for the consumption of 12 kg of the agent per 1 km^2 of the seeded are. The use of a smaller amount of such particles does not give a significant effect of modification. The result presented here is in agreement with the data of field experiments on seeding with such particles (Mather et al., 1997). As is seen from Figure 3, seeding with a salt powder results in significant precipitation enhancement. At the consumption of 2.4 kg/km^2 of the salt powder the precipitation amounts falling from the clouds with the thickness less than 4 km are greater than at seeding with pyrotechnic particles at their consumption of 12 kg/km^2.

The effect of seeding with polydisperse particles of the salt powder is also significantly greater than that of seeding with large salt particles with narrow particle size distributions. From Figure 3 it is seen that the effect of seeding with the salt particles (the effective radius of 1 μm and optimum weight concentration of 1.1 mg/m^2) at the total salt consumption of 64 kg/km^2 appears to be less than at seeding with the salt powder at the consumption of 12 g/km of the latter.

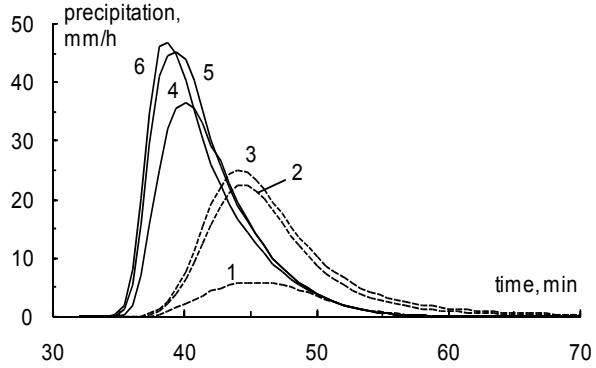


Figure 4. Temporal intensity trend of precipitation from a cloud of 3 km thickness at modification with salt powder at its consumption of 48 kg/km^2.
Solid lines – maximum air updraft V_m = 3.3 m/s; dashed lines - V_m = 5 m/s. 1, 4–drop concentration N=1015 cm^{-3}; 2, 5 – N = 485 cm^{-3}; 3, 6 – N = 305 cm^{-3}.

The results of numerical simulation show that the effect of seeding with the salt powder depends significantly on atmospheric conditions under which a convective cloud is formed. Figure 4 presents the calculation results for precipitation intensity at seeding with the salt powder of the cloud with the thickness of 3 km. Such clouds do

not give precipitation as a rule. Maximum liquid water content of a cloud medium in this modeled cloud reaches 2.56 g/m^3. It should be mentioned that at seeding of a cloud of such a thickness with the liquid water content of less than 2 g/m^3 the modification effect does not practically show itself – precipitation does not form even at very large consumptions of the salt powder. As is seen from Figure 4, the effect of seeding with the salt powder is most pronounced in clouds with power concentrations of cloud drops and at lower velocities of air updrafts.

Thus, the results of the studies carried out demonstrate that the use of polydisperse salt powders for obtaining additional precipitation amounts from warm convective clouds is advantageous against the hygroscopic particles generated by pyrotechnic flares relative to the agent consumption and the modification effect. At seeding with the salt powders additional precipitation amounts can be obtained from warm convective clouds of moderate thicknesses not giving precipitation under usual conditions. In this case the effect of "overseeding", that can appear at modification with fine-disperse hygroscopic particles from pyrotechnic flares, does not show itself.

References

Cooper W.A., Bruintjes R.T., Mather G.K., Calculations pertaining to hygroscopic seeding with flares. *J. Appl. Meteorol*., **36**, 1449–1469, 1997.

Drofa A.S., Formation of cloud microstructure: the role of hygroscopic particles. *Atmos. Ocean. Phys.,* **42**, 326-336., 2006.

Drofa A.S., Studies of a Modification Effect from a Warm Convective Cloud Seeding by Hygroscopic Particles Based on Numerical Simulation Results. *Atmos. Ocean. Phys*., **46**, 346-359, 2010.

Drofa A.S., Ivanov V.N., Rosenfeld D., Shilin A.G., Studying an Effect of Salt Powder Seeding Used for Precipitation Enhancement from Convective Clouds. *Atmos. Chem. Phys*., **10**, 8011-8023, 2010.

Drofa A.S., Eran'kov V.G., Ivanov V.N., Shilin A.G., Yaskevich G.F., Experimental studies of salt powder efficiency at convective cloud modification for precipitation enhancement, 2011 [*in present proceedings]*.

Mather G.K., Terblanche D.E., Steffens F.E., Fletcher L., Results of South African cloud-seeding experiments using hygroscopic flares, *J. Appl. Met*., **36**, 1433-1447, 1997.

Rosenfeld D., Lahav R., The Search for the Optimal Size of Hygroscopic Seeding Particles. *Proceedings of the 16-th Conference on Planned and Inadvertent Weather Modification*, San Diego, USA, 2005.

Rosenfeld D., Axisa D., Woodley W.L. and Lahav R., A Quest for Effective Hygroscopic Cloud Seeding. J. Appl. Met. Climate, **49**, 1548-1562, 2010.

Segal Y, Pinsky M. and Khain A., The Role of Competition Effect in the Raindrop Formation. *Atmos. Res*., **83**, 106–118, 2007.

Analysis of Water Balance and Aridity Index to Detect the Effect of Global Warming in Catchment and Irrigation Area of Jatiluhur Dam

Budi Harsoyo[1], Nora H.Pandjaitan[2], Dwi Putro Tejo Baskoro[3]

[1]Researcher working for The Weather Modification Technology Center, Agency for Assesment and Application of Technology, Indonesia; BPPT Building 1, 19th Floor, MH. Thamrin Street No. 8, Jakarta – Indonesia; email : budi.harsoyo@bppt.go.id ;
[2]Lecturer in Civil and Environmental Engineering Major, Bogor Agricultural University;
[3]Lecturer in Regional Planning Science Major, Bogor Agricultural University

Introduction

The Citarum Catchment Area (CA) with the three cascading dam within it, i.e. The Saguling, Cirata and Jatiluhur dams, has a very strategic role. According to The Jasa Tirta II Public Company (PJT II) as The Caretaker of Jatiluhur Dam which according to Government Regulation No. 94/1999 is appointed as the institution responsible in the water resources management in The Citarum CA, Citarum river flow is utilized to fullfill various water demands in the downstream area with water provision priority as follows, for drinking and households purposes, environmental sanitations, irrigation water needs, electrical plant purposes and industrial demands. In matters of irrigational water needs, Jatiluhur dam provides water supply for farming area with the size of 264.000 hectar acres which are rice crops production centers in the north coast area of West Java.

Therefore with its various vital roles, The Citarum CA needed to be well-managed in order to keep the water provision balanced for the entire year. The Citarum CA water resources potential needed to be determined by way of The Water Balance approach which output could best describe The Citarum CA support rate from the water availability/potential point of view in the upstream area to provide provisions for various needs in the downstream area.

Climate change as a result of global warming had caused an indeterminate seasonal patterns. The length of wet and dry season are no longer balanced and even the timing could not be estimated with great precision. According to Idrus and Mayasari (2008) during dry season, most farming areas along the north coast of West Java often experience draught. Based on those facts, examinations are needed on draught level evident in the north coast areas of West Java which are farming irrigation areas downstream of The Citarum CA by conducting aridity index calculation.

The purpose of this research is to analyze water balance and aridity index in Jatiluhur Dam Water Catchment Area and its irrigational areas in the north coast of West Java while at the same time identified and mapped areas which needs irrigational water supply priorities in Jatiluhur irrigational farming areas in the north coast areas of West Java.

Research Method

Research is performed within PJT II operational environment which has a size of 1.364.072 hectar with the main focus on The Citarum Catchment Area which is The Catchment Area for Jatiluhur Dam and also in the northern coast area of West Java on farming lands which obtained irrigational water supply from Jatiluhur Dam, as shown in Figure 1.

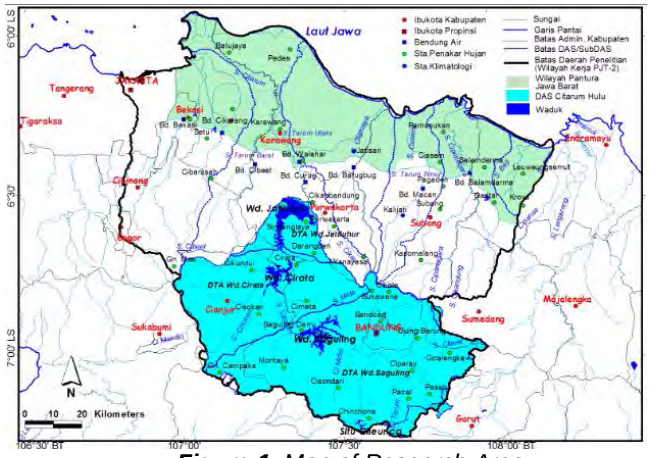


Figure 1. *Map of Research Area*

Rainfall data are analyzed by using 20 years of monthly historical data (1990-2009) from the 43 rain gauge station locations spread throughout the research area, whereas the temperature data is using 2000-2009 data from the 3 weather station location owned by The Indonesian Meteorological, Climatology and Geophysical Bureau (BMKG), i.e., The Jatisari, Kalijati and Bandung Geophysics Station. Both datas are used for water balance and aridity index analysis. Absolute temperature datas are needed to determine the size of evapotranspiration potential (EP).

Water balance is analyzed by way of The Thornthwaite-Mather Method by building a water balance table constructed from its parameters. The calculation is performed with the aid of a water balance program based on The Visual Delphi 5 programming language.

Aridity Index calculations are performed by using The Palmer Method based on the equation below :

$$Ai = 100\ D / PE$$

where : Ai = aridity index, %; D = moisture deficiency (mm) and EP = evapotranspiration potential (mm)

A calculation results are classified according to the criteria shown in Table 1.

Table 1. *Aridity Index Categories*

Aridity Index (%)	Criterias
< 16,7	Draught does not occurs
16,7 - 33,3	Medium draught
> 33,3	Heavy draught

Ref: Sudibyakto, et al (1999)

Spatial analysis with Geographical Information System using the Arcview program version 3.3 was performed to give descriptions on spatial distributions of rainfall conditions, land water balance and aridity index in the research area. From each of those parameters, thematic maps were then made in monthly or total yearly period. Next, those three thematic maps were then overlaid upon each other in order to identify priority areas for irrigation water provision, from the hydro-climatology point of view.

Research Area Rainfall Condition

Rainfall condition in The Citarum Catchment Area and The Northern Coast Area of West Java in the last 20 years (1990-2009) are depicted in figure 2 and 3. Figure 2 depicted monthly rainfall time series in both research areas, whilst figure 3 depicts the sum of yearly rainfall accumulation. From either figures, there are no indications of rainfall decrease either in The Citarum CA or those of the northern coast. Even if we observe at the regressional analysis results in order to deduce the rainfall trends, there is a tendency that rainfall conditions in the last 10 years (2000-2009) tend to be higher compared with the conditions from the first 10 years (1990-1999). This proves that rainfall condition in The Citarum CA or in the northern coast were not influenced by global warming effects if seen from the sum of its yearly rainfall.

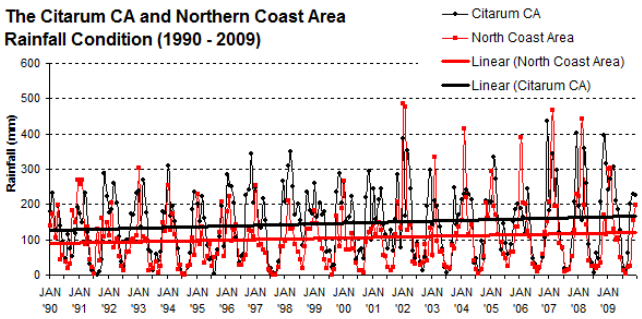


Figure 2. *Research Area Monthly Rainfall Time Series Graph from 1990-2009*

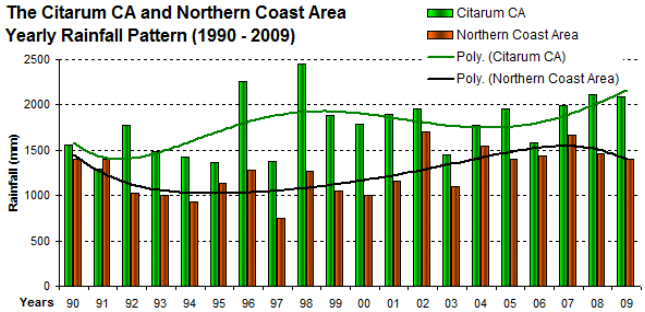


Figure 3. *Research Area Yearly Rainfall Histogram from 1990-2009*

For the last two decades, the lowest rainfall intensities in the northern coast area happened in 1997 (754 mm/year), whereas the highest would be in 2002 (1.703 mm/year), For The Citarum CA, the lowest rainfall intensity happened in 1991 (1287 mm/year). whereas the highest occur in 1998 (2.457 mm/year).

Based on the records of years of El Nino and La Nina events, the year 1991 and 1997 were El Nino years whereas 1998 and 2002 were the La Nina years, so it could be said that rainfall in The Citarum CA or the northern coast were influenced by The ENSO phenomenon.

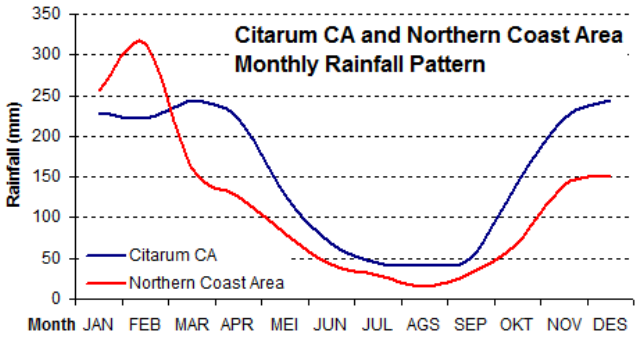


Figure 4. *Research Area Rainfall Pattern*

Figure 4 depicts rainfall pattern in research area which has monsoonal pattern, rainfall peak in The Citarum CA occurs on December (243 mm) and March (242 mm), whilst the lowest occurs on August (41 mm). For northern coast area, highest rainfall occurs on February (315 mm) and lowest on August (15 mm). Except in January and February, on the whole rainfall in The Citarum CA was higher than those of the northern coast area. Rainy season in The Citarum CA happened during the period from November to April (6 months) whilst dry season occurs during the period from May to October (6 months). For the northern coast, dry season is longer than the wet season. New rainy season period last during the month of December to March (4 months), while the period from April to November (8 months) is the dry season.

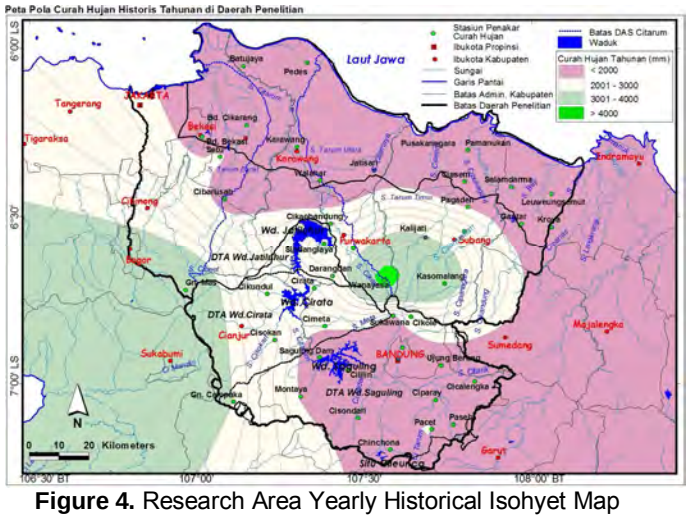


Figure 4. Research Area Yearly Historical Isohyet Map

Total yearly rainfall average in The Citarum CA was 1.856 mm/year. The Sindanglaya area, which was situated in the proximity of Jatiluhur Dam was the location with the highest yearly rainfall in The Citarum CA (3.061 mm/year), whilst the lowest was in the Cicalengka Area (1.257 mm/year). For the northern coast area, its total yearly rainfall average is 1.408

mm/year, the highest of which was located in Bendung Cikarang (1.708 mm/year) and lowest in Pamanukan (1.098 mm/year).

Research Area Water Balance

Averages of each water balance parameters in the research area as the results of running The Visual Delphi Programme is depicted in Table 2 and 3. Based on the rainfall sum difference (P) and evapotranspiration potential (EP), in general, The Citarum CA still experience yearly water surplus, due to the sum of P larger than EP. This is different with the northern coast area which has yearly water deficit, due to the sum of PE that is larger than P. From as much as 1.856 mm entire year total rainfall occuring in The Citarum CA, as much as 1.093 mm (58,9%) evaporates through evapotranspirations. This means that rain water surplus totalling 723 mm (31,1%) could be counted as dirrect runoff, either as surface runoff or as groundwater. For the northern area, from the total entire year rainfall as much as 1.421 mm, 1.136 mm (80,7%) of it evaporates through evapotranspirations and rain water surplus which has the sum of 272 mm (19,3%) could be counted as dirrect runoff.

Water deficit condition in The Citarum CA only occurs as long as 4 months (June to September), whilst to the months beside those, there are water surplus. Averages of all year water surplus total in The Citarum CA is 708 mm. With area size of 464.702, 66 hectar acres then the water surplus total in The Citarum CA is as large as 3.287,9 million m^3/tahun.

For the northern coast area, with the exception of surplus in January up to March, in the next period, this area experience water deficit condition. Averages of all year total water deficit in the northern coast area is as large as -377 mm. With an area size of 372.460,23 hectar acreas then the total water deficit in that area would be 1.404,2 million m^3/year.

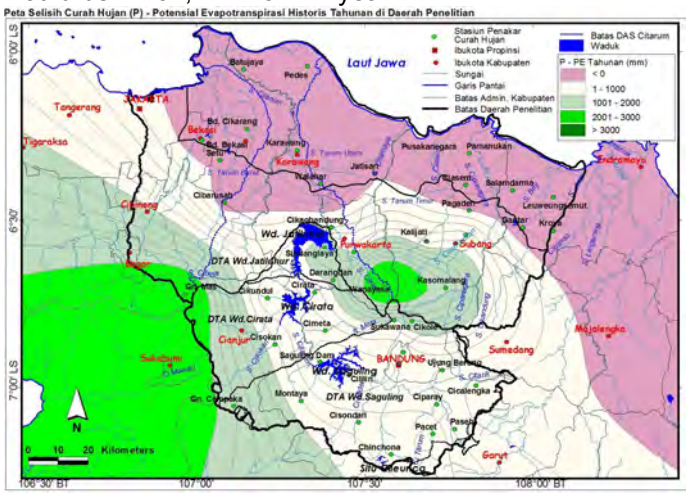


Figure 5. *Map of the difference between Rainfall (P) and Evapotranspiration Potential (PE) Yearly Historical in the research area*

Research Area Aridity Index

On yearly average, The Citarum CA does not experience draught, although draught happened in July, August and September, it is still in the category of medium draught (16,7–33,3%). Draught peak in The Citarum CA happened in September (31,5%), and on the periods of November to April there is not even one location inside the CA experiencing draught. The highest draught potential in The Citarum CA is located in The Cicalengka Area (23,3%), while The Cikole area never experienced draught condition all year round. Area averages for yearly historical aridity index value in The Citarum CA was arithmetically counted to be 7,4% (draught does not occur).



Figure 6. *Map of The Research Area Yearly Historical Aridity Index*

Draught in the northern coast area happened as long as 7 months, i.e. on the period of May to November. The month of May (26,9%) and November (20,4%) is categorized into the medium draught period, whilst the period of months from June to October is categorized into heavy draught period (>33,3%). Draught peak occurs in the month of August with an index value reaching 88,0%. The only months where not even one location in the northern coast experience draught was on the month of February. Locations present in the shores of northern coast (Pedes, Pamanukan, Batujaya and Ciasem(were areas which experience the most severe draught with indexes up to 40% in value. The more south away from the beach, the less the draught intensity would be. Area averages for yearly historical draught index value in the northern coast area, arithmetically is 35,6% (heavy draught)> Draught condition in the research area is depicted quantitatively in Figure 7.

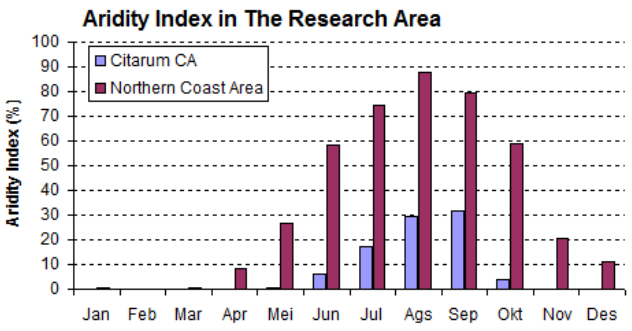


Figure 7. *The Research Area Aridity Index Histogram*

Determination of Priority Area for Irrigational Water Provision

Priority map of irrigational water provision on a farm block in The Jatiluhur irrigational area as a result of cross-matching between isohyet, water balance and aridity index map is depicted in figure 8. Analysis results suggested that northern areas needed to be prioritized for irrigational water supply purposes, as by the climatological pattern in the northern coast area which rainfall decreases as it move to the coastal area.

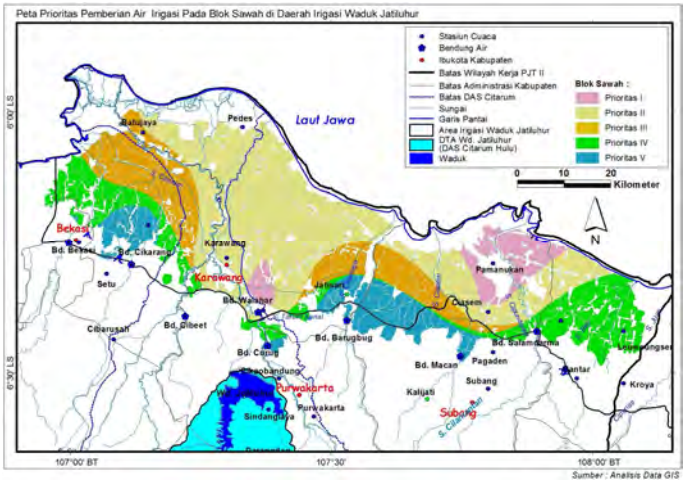


Figure 8. *Priority Map for Irrigational Water Provision on The Farming Block in The Jatiluhur Irrigational Area.*

Conclusion

1. Regressional analysis results of the rainfall data does not indicate any rainfall decrease either in The Citarum Upstream CA or in The northern coast area, there is even a tendency that rainfall condition in the last 10 years (2000-2009) tend to be higher compared to conditions in the first 10 years (1990-1999). This proves that rainfall conditions in The Citarum Upstream CA or The northern coast area does not influenced by the effects of global warming judging from the sum of their yearly rainfall.
2. Dry season period in the northern coast area is longer than its wet season. Rainy season occurs from the month of December to March (4 months), whilst the dry period last from April to November (8 months).
3. Lands in the northern coast areas experiences water deficit all year round due to its evapotranspiration potential being larger than the sum of its rainfall. Surplus condition only occurs for 3 months, i.e. from January to March, whereas from April to December (9 months) lands in The area experience water deficit condition.
4. Spatially, almost all area in the northern coast experience draught in heavy category all year round, with the exceptions of few locations in the southern part in the proximity of hilly topography which are in the medium draught category. Further north to the coastal areas, the higher the aridity index is, Heavy draught in the northern coast area lasted for 5 months, from June to October, with the peak occuring in August.

REFERENCES

Harsoyo, B, Widodo, FH, Syaifullah, D, Nuryanto, S dan Sutrisno. 2007. *Permodelan Hidro-Meteorologi Untuk Perhitungan Neraca Air di DAS Larona Menggunakan Metode Thornthwaite – Mather*. Science and Weather Modification Technology Journal. Vol. 8, No. 1, June 2007. The Deputies of Natural Resources Development Technology, Agency for The Assessment and Application of Technology. Jakarta.

Idrus, H dan Mayasari, R. 2008. *Pengalaman Teknologi Modifikasi Cuaca (TMC) di Wilayah Sungai Citarum*. One Day Seminar Paper in Celebrating The 30th Year of The Founding of The Agency for Assessment and Application of Technology (BPPT). Weather Modification Technology Center, BPPT. Jakarta.

Meyers, G, McIntosh, P, Pigot, L, and Pook, M. 2007. *The Years of El Niño, La Niña, and Interactions with the Tropical Indian Ocean.* Journal of Climate Volume 20. American Meteorological Society. Washington DC.

Sudibyakto, 1985. *Evaluasi Kekeringan Dengan Menggunakan Indeks Palmer di Daerah Kedu Selatan, Jawa Tengah*. Postgraduate Thesis (S2) Postgraduate Faculty, The Bogor Agricultural Institute, Bogor.

Sudibyakto, Suyono, dan Kirono, DGC. 1999. *Analisis Curah Hujan Untuk Antisipasi Kekeringan dan Mitigasinya di Daerah Aliran Sungai Progo*. Majalah Geografi Indonesia, Th.13, No.23, Maret 1999., Faculty of Geography, Gajah Mada University, Yogyakarta.

Tianjin Precipitation Feature and Analysis of Weather Modification Influence

Jin Ruijun Wang Wan Song Wei Wang Zhaoyu
Tianjin Weather Modification Office, Tianjin 300074

Abstract: Based on the precipitation data of 13 observatories in Tianjin from 1986 to 2008， the precipitation characteristics and the weather modification influence are studied in this article. The results show that: the spatial distribution of precipitation is uneven, the difference is small in west-east direction, otherwise large in north-south direction. The rainfall present descending trend from north to south, and the isolines are dense in north while sparse in south, The speed of decreasing rainfall become slow down from north to south. The difference is obvious in different season, the rainy days and precipitation rain fall mainly concentrate in summer, the precipitation is less in spring and autumn while is least in winter. The weather modification doesn't change the correlation coefficient of rainfall in Tianjin, and it also has little influence on the spatial distribution. These relate to the characteristics of weather modification in Tianjin. The weather modification works have influence on probability distribution of the rain-type, but the influence is small. After comparing the probability distribution of different rain-type in 1986-2001 and 2002-2008，we can find that the probability of light-rain days is relative low while probability of moderate-rain days is high after the weather modification works, but these differences are not significant.

Key words: Tianjin; precipitation characteristics; weather modification

1. Introduction

With the rapid development of our economy and society, water shortage has seriously affected the industrial and agricultural production and socio-economic development. Precipitation is an important source of water, so the study of precipitation characteristics is very important for exploiting air water resources. Many people have studied on the precipitation characteristics of whole country or a region[1-6]. There are many factors that affect precipitation and many studies are conducted for natural factors. As man-made factors, weather modification that affects precipitation has been few studied, this paper will study this issue and analysis of the impact on precipitation of weather modification.

Tianjin is located in the northeast part of the North China Plain, belonging to the continental monsoon climate. Most part of Tianjin is plain, to the north is Yanshan while to the east is Bohai Sea which is a landlocked bay. There are four distinct seasons during a year, they are spring, summer, autumn and winter.

In this paper, precipitation characteristics of Tianjin area are analyzed by using daily rainfall data of all stations from 1986 to 2008. Large-scale artificial rainfall in Tianjin was carried out from 2002 and its main operating tools are aircraft, rockets and artillery. Based on analysis of natural precipitation, the impact of operations on the precipitation was studied in this paper by comparing the differences of precipitation characteristics before and after adding human factors.

2. Data

The data we used in this study is daily rainfall material of 13 sites all over the Tianjin city from 1986 to 2008.

3. Analysis of precipitation Feature

3.1. Spatial distribution feature

Figure 1 is the average precipitation distribution of 16 years from 1986 to 2001 in Tianjin area. It can be seen from this figure that the rainfall present descending trend from north to south, and the isolines are dense in north while sparse in south， the decrease rate of precipitation reduced from north to south. The rainfall in the east-west direction is similar which present a symmetrical distribution. So it can be summarized that the spatial distribution of precipitation is uneven, the difference is small in west-east direction, otherwise large in north-south direction.

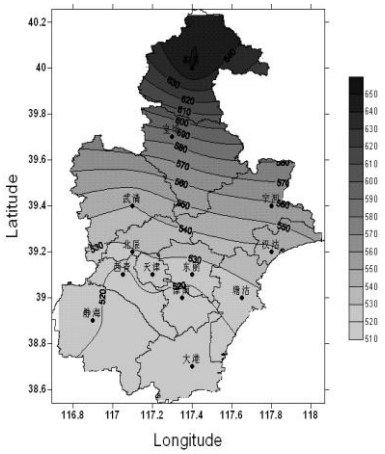


Figure 1. The average precipitation distribution of 16 years from 1986 to 2001 in Tianjin area

Correlation coefficients of 13 districts in Tianjin are calculated in order to further study the spatial distribution of rainfall. Table 1 is the daily precipitation correlation coefficient of 13 observatories. It can be seen from the table: the correlation coefficient of regional rainfall has a relationship with the two relevant regional spatial distance, the closer of the distance the correlation coefficient is bigger and the farer of the distance the correlation coefficient is smaller. Correlation coefficient of the two regions is not the highest each other, such as the largest correlation coefficient of Jixian is Baodi, but the biggest correlation coefficient of Baodi is not Jixian. The correlation coefficient of the two areas is higher when the two regions are similar in area and the regional area is quite small.

Table 1. The daily precipitation correlation coefficient of 13 observatories

	Jixian	Tianjin	Wuqing	Baodi	Dongli	Xiqing	Beichen	Ninghe	Hangu	Jinghai	Jinnan	Tanggu	Dagang
Jixian	1.000	0.410	0.526	0.640	0.399	0.430	0.473	0.445	0.413	0.399	0.398	0.320	0.361
Tianjin	0.410	1.000	0.611	0.571	0.754	0.870	0.800	0.620	0.618	0.726	0.775	0.613	0.598
Wuqing	0.526	0.611	1.000	0.689	0.562	0.638	0.749	0.565	0.511	0.545	0.539	0.462	0.427
Baodi	0.640	0.571	0.689	1.000	0.558	0.598	0.668	0.635	0.581	0.504	0.521	0.452	0.441
Dongli	0.399	0.754	0.562	0.558	1.000	0.708	0.681	0.684	0.704	0.620	0.863	0.730	0.716
Xiqing	0.430	0.870	0.638	0.598	0.708	1.000	0.836	0.625	0.624	0.720	0.763	0.610	0.580
Beichen	0.473	0.800	0.749	0.668	0.681	0.836	1.000	0.664	0.644	0.702	0.685	0.606	0.558
Ninghe	0.445	0.620	0.565	0.635	0.684	0.625	0.664	1.000	0.848	0.536	0.658	0.676	0.574
Hangu	0.413	0.618	0.511	0.581	0.704	0.624	0.644	0.848	1.000	0.549	0.690	0.715	0.617
Jinghai	0.399	0.726	0.545	0.504	0.620	0.720	0.702	0.536	0.549	1.000	0.688	0.576	0.562
Jinnan	0.398	0.775	0.539	0.521	0.863	0.763	0.685	0.658	0.690	0.688	1.000	0.749	0.734
Tanggu	0.320	0.613	0.462	0.452	0.730	0.610	0.606	0.676	0.715	0.576	0.749	1.000	0.770

Dagang	0.361	0.598	0.427	0.441	0.716	0.580	0.558	0.574	0.617	0.562	0.734	0.770	1.000

3.2. Temporal distribution feature

Figure 2 is the distribution of average monthly precipitation from 1986 to 2001 and table 2 （Table omitted） the distribution of assoeted rain days monthly from 1986 to 2001 in Tianjin. It can be seen from the figure and table: the precipitation is mainly concentrate in summer, the rainfall is greater in June, July and August, the total precipitation this three month reached nearly 70% of annual precipitation. Compared to summer, precipitation in spring and autumn is less and the average rainfall of these two seasons is only 30mm that account for just about 25% of annual precipitation. Thus, it can be concluded that the monthly rainfall distribution is uneven and the difference of precipitation is obvious in different seasons.

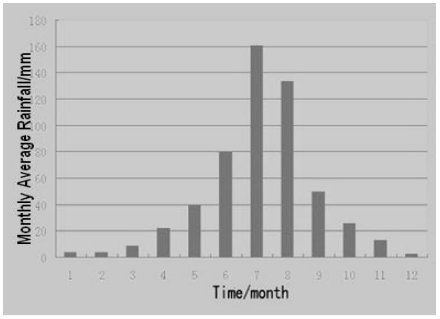


Figure 2. The distribution of average monthly precipitation from 1986 to 2001 in Tianjin

4. Analysis of Weather Modification Influence

Artificial hail suppression is mainly carried out in Tianjin before 2000 and using both rockets and Artillery began from 2001. Aircraft artificial rainfall experiments are carried out from the autumn in 2002. It can be seen from the above analysis that there is no change with the precipitation characteristics after artificial work. So how much influence on precipitation of weather modification will be studied in the following paper.

4.1. The influence on precipitation spacial distribution

The 13 sites are paired and each set of data have 2350 pairs of samples. Random samples are carried out for each set of data and 586 pairs of samples are selected every time, such random sampling done 10000 times and the correlation coefficient to be calculated of each samples. 10000 correlation coefficients can be obtained and then sorted from small to large, the 500th and 9500th of these correlation coefficients are took as the 90% distribution range. Then calculate the correlation coefficient of each set of data from 2002 to 2008 (a total of 586 set of samples) and the results are listed in the following table. The r- and r+ represent low and upper boundary of 90% correlation coefficient distribution. It can be seen from the table 3（Table omitted）hat all the correlation coefficients obtained from the samples of 2002-2008 at the regional distribution of 90% probability which means the significance of correlation coefficient change does not exceed 0.05 except the Beichen and Ninghe this group. It shows that regional rainfall correlation coefficient does not change after artificial precipitation. In other words, artificial rainfall does not increase in precipitation in some locations significantly, because the correlation coefficient of the two areas will change if a significant increase in regional precipitation happen. It means that the artificial rainfall does not play a role? Of course not, the precipitation enhancement operating points almost throughout the entire region of Tianjin,

so each region can obtain equivalent artificial rainfall results even if the cloud seeding work and the correlation coefficient between regions will not be affected by such weather modification work.

4.2. The influence on rainy days distribution

The purpose of artificial rainfall is to increase the precipitation of the Target Area, so it may make the rain type of natural precipitation (rainfall level) changes if the cloud seeding plays a role.

The rainfall is divided into five levels: light rain, moderate rain, heavy rain, rainstorm and heavy rainstorm. Each type of rainy days probability is calculated respectively both of 1986-2001 and 2002-2008.The results are shown in the following table.

As can be seen from the table 4（Table omitted）the probability of moderate rainfall pattern of 2002-2008 is generally higher than that of 1986-2001 but lower for the probability of light rain. Take the July as an example, the light rainfall probability is 64.22% of 1986-2001 and 62.59% of 2002-2008, the moderate rainfall probability is 18.36% of 1986-2000 and 25.71% of 2002-2008.

5. Conclude

(1). Spatial distribution of precipitation is uneven, the difference is small in west-east direction, otherwise large in north-south direction. The rainfall present descending trend from north to south, and the isolines are dense in north while sparse in south, The speed of decreasing rainfall become slow down from north to south.

(2). The difference of precipitation is obvious in different season, the rainy days and precipitation rain fall mainly concentrate in summer, the precipitation is less in spring and autumn while least in winter.

(3). Weather modification has little influence on the spatial distribution. These relate to the characteristics of weather modification in Tianjin.

(4). Weather modification works have influence on probability distribution of the rain-type, but the influence is small. After comparing the probability distribution of different rain-type in 1986-2001 and 2002-2008，it can be find that the probability of light-rain days is relative low while probability of moderate-rain days is high after the weather modification works, but these differences are not significant.

References

[1] Chen GuiYing. Temporal and Spatial Characteristics of Summer Monsoon Rainfall in China in 1991. Meteorological Monthly, 1993, 19（5）: 39-44.

[2] Yang Guang-ji. The Characteristics of Rainfall and Its Tendency Estimate over North China. Plateau Meteorology, 1999, 18（4）: 668-677.

[3] Xu Chenhai, Yao Zhanyu, Chen J inqiang. Analysis of Spatial2temporal Variation of Precipitation in the Upper Reach of the Yellow River and It s Circulation Characteristics. Meteorological Monthly, 2004, 30（11）: 51-54.

[4] Lv Jun, Zhang Jing, Liu Jian. Study on Spatial-Temporal Distribution of Summer Precipitation. Meteorological Monthly, 2006, 32（6）: 48-52.

[5] Lin Shu, Lu Deng-rong. Climatic Change Characteristics of Precipitation in Gansu Province in Recent 40 years. Plateau Meteorology, 2004, 23（6）: 898-904.

[6] GAO Liu-xi, LIU Qin-yu . Analyses on Spring Rainfall Spatial and Temporal Changes of Shandong Province Using EOF. Plateau Meteorology, 2005, 24 (5): 811-815.

DEMANDS OF USERS IN ADDITIONAL PRECIPITATION IN UZBEKISTAN IN THE LIMITS OF THEIR POSSIBLE SUPPLY

(B.Sh.Kadyrov, V.P.Kurbatkin, V.F.Ushintseva. Republic of Uzbekistan)

The main user of consumption of water resources is agriculture. The structure is presented by 4 big regions: big oases, small oases, separate foothills and alpine areas. Within these regions the main and one-two additional types of economical activities are distinguished. Thus, in the big oases the main type of land farming is irrigated farming with a wide spectrum of the planted crops, the main of which the cotton is. On the borders with oasis cattle breeding is developed with cattle grazing on the natural desert and mountain pastures. In small oases the main direction is cattle breeding while the irrigated and dry farming are the additional types of economical activities. In the foothills cattle breeding and irrigated and dry land farming are distributed by the relief - on the mild slopes of the hills the dry farming and partially, cattle breeding (which spreads to the alpine areas) are developed, while in the small river valleys the irrigated farming takes place. In the alpine areas the cattle breeding is the main direction of economical activities while irrigated and dry farming are secondary ones. With such structure of farming the irrigated lands are moistened with the river flow, non-irrigated ones (dry farming) – are moistened with precipitation. In the region the average long-term annual precipitation amount is 200 mm; in mountains (which occupy 1/3 of the region territory) the amount of precipitation is 470 mm. The main mass of atmospheric precipitation is recorded in the cold period (November-March) with the maximum value in February-March while in mountains it is recorded in April-May. The third part of atmospheric precipitation is used for the river flow formation which supplies water for the irrigated land farming, industry and life conditions of human beings. Not more than 20-25% of the precipitation recorded in the region is used rationally while only 15% reaches the irrigated fields. This amount of water does not satisfy the region needs. Furthermore, in the region, in a whole there are no seasons with excessive amount of atmospheric precipitation. This is only possible in the cold vegetation period when with the low air temperature large amount of atmospheric precipitation is recorded.

It is necessary to determine the relationship between water supply of the above mentioned types of economical activities and the amount of atmospheric precipitation including the river flow. Let's use the method proposed in 30-s of 20th century by V.L.Schultz - the well-known hydrologist of Central Asia.

He distinguished the following areas differing one from another by the correlation between the amount of atmospheric precipitation (X) and precipitation (Z):

- zone of flow formation - area of the mountain uplands with the elevation upper than 1000 m a.s.l.; here more quantity of moisture is formed then it is evaporated (amount of atmospheric precipitation is higher than evaporation quantities); here X>Z;

- zone of flow distribution – area of the part of plain and foothills joining the mountains with elevation from 300 up to 700-900 m a.s.l. from which the flow from mountains is evaporated to atmosphere; X<Z [13];

- zone of flow equilibrium – plain area without canal flow; X=Z;

Zone of flow formation of rivers because of the high position is limited by the thermal resources, that is why the farming here is limited mainly by the growing of forage crops. Threshold feeding power of grass on mountain pastures of the region can reach 350 f.u./he (forage units). Mountain pastures occupy less areas then the plain (desert ones). However, the feeding power of grass is not less then 200 f.u./he while on the plain pastures it is not more than 200 f.u./he. Using the correlations between the yield of the pasture grass and amount of atmospheric precipitation it was derived that in the region of syrt uplands of Central Tien-Shan each millimeter of precipitation during winter and three spring decades produces 0,1 c/he of dry mass.

Experiments showed that weather modification (WM) over the mountain pastures should be performed in mesoscale range, then during vegetation of pasture grass about 100 mm can be produced. However, the weight of atmospheric precipitation in mountains is higher, and it is recommended to conduct WM during vegetation period which makes it possible to increase the yield of pasture grass about 30%.

The results of studies conducted before have shown that for the increase of river flow it is necessary first – to cover the Western Tien Shan and Pamir with WM, and then – the Southern margibal Tien Shan. WM on the area of 100-150 thous. km^2 will provide for getting 8-12% in addition to river flow which is sufficient for irrigation of 1 mln. he. As only 1/10 part of the flow of Central Asian rivers is formed on the territory of Uzbekistan, it is rational to conduct WM for the flow increase in the basins of Pskem and Ugam rivers and later – in Angren and Kashkadarja ones. The experiments conducted in Pskem river basin in the beginning of 1960s have shown that it is possible to get additional 3-4% with seeding of stratocumulus cloud, 10-12% - of nimbostratus clouds and up to 5% - of the convective ones. The experiment conducted in the end of 1990s when the seeding was made from the airplane board in the basin of Chirchik river where up to 15% of Syrdarja river flow is formed demonstrated positive results. ~ 400 mln. m^3 was produced at all. In individual points 45-80 mm or 30-50% was produced in addition to the natural sum of atmospheric precipitation during the period of WM within the season or 10-15% to the natural sum of atmospheric precipitation during the season (Table 1).

Table 1

Amount of artificial precipitation (mm) on the experimental (O) and control (K) territories

Territory	Months				Season
	I	II	III	IV	
O	101,5	21.9	18,9	107,9	250,2
K	65,7	15,9	29,1	64,7	175,3
д	35,8	6,1	10.2	43,2	74,9

Zone of the flow distribution (Fig. 1) is the more promising for planting the agricultural crops. There is sufficient quantity of temperature resources for the heat-loving plants, the river water is available for irrigation, and 350–600 mm of precipitation is recorded on the major part of territory during the year.

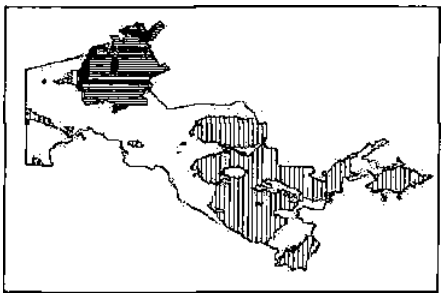


Fig 1. Zone of the flow distribution.

In the zone of the flow distribution the water flow water is enough for irrigated lands with the area of 10 mln. he. That is why the irrigated farming is the main direction of economical activities.

As here the average long-term amount of atmospheric precipitation is 300 mm and more, then the second type of economical activity is non-irrigated farming when it is possible to get high but not maximum yields of cereals on the not irrigated lands because of the deficit of productive moisture.

In this zone it is possible to widen the agricultural farms with the combination of the natural watering and irrigation during the periods of deficit of natural watering.

Usually, the irrigated lands do not depend on the atmospheric precipitation over them. However, the irrigated lands can be extended with increase of snow reserves in mountains due to WM with provision of the increase of river flow.

Traditionally, in the conditions of arid climate the main problem is the water supply during the dry period of year. In CA region the more complicate period is July – September when there is almost no atmospheric precipitation on the major part of its territory. The period from the second part of June up to the second part of October is actually dry.

For the non-irrigated farming precipitation enhancement should be considered in two periods: pre-vegetation (when the mean daily air temperature is less than 4°C) and vegetation one. Periods of December - mid of February and mid of February – mid of May are typical periods. In the cold period of the year it is needed to collect moisture in the upper soil (ground) layer which is accessible for the root system of plants in vegetation period.

The dry hot summer precedes the period of moisture accumulation. From June to October the amount of precipitation can be 1-3 mm. With high position of sun and absence of clouds in summer the soil is dried almost completely. Up to beginning of atmospheric precipitation the soil is dry. That is why in the period of moisture accumulation it is necessary to distinguish between the water passage in the moistened and dry ground. In [1] the mechanisms of passing of the moisture in soil; diffusive, film, film-and-meniscus, capillary and gravitation ones. In the above mentioned studies it was determined that there are holes in soil and their configuration depends on their structure (composition, sizes and packing). We limited our studies with the ground particles which have homogeneous composition and sizes being typical for the main soil types of the plain part of Uzbekistan. However, our estimates on the noted limits will regard the notions of moistening the quantities of which are corrected by experimental data. The results of experimental data [15-18], and results of our studies [7,10-13, 20] are put as basis. These considerations put in the classification of atmospheric precipitation which characterize the penetration and further preservation of moisture in ground.

The results of developmental work on the mechanism of the moisture accumulation in soil have shown that in sandy soil up to 80 % is accumulated and in the fine-dispersion ones – up to 50 %. Then in the cold pre-vegetation period on the plain in the clay loam soil 25-50 mm is accumulated and in the sandy ones - 35-65 mm. In the vegetation period on the plain 55-100 mm and more is recorded. In its eastern part in piedmont area the amount of precipitation is higher and moisture reserve is 1,5 times more then in the eastern one.

In the soil layer with 1cm thickness and S=1 cm^2 base for the provision of the movable moisture the values of 3,5-4,0 mm. 1,7-2,4 mm of moisture will be available for the plant.

Thus, for moistening of the layer with 0,2 m thickness (the roots of cereals in the early phases of the crops development) требуется выпадение осадков в количестве 70 - 80 mm of precipitation is needed on the clay loam soil, and for the layer with 0,5 m thickness up to the state of the least moisture capacity which corresponds to the capillary-weighted, 180-200 mm – for the sandy ones. The uniform process does not produce this amount as there is no upper limit for the precipitation amount during the process on these territories in winter period. The lower limit was considered by the assessment of its preservation in the period between precipitation during the warming-up of soil. In April and October in the 24-h cycle in 15 – 20 cm layer is not more than 3,0 - 3,5° C. In November at the depth of 15 cm the warming-up is not more than 2°C. The it follows out that for protection of moisture against evaporation more than 20mm of precipitation is needed for the single process of precipitation. Considerable moisture accumulation will produce 10 mm and more of precipitation. Возможно The moisture accumulation can also be due to precipitation amount of 5 mm, especially, when period between precipitation is not longer than 10 -15 days.

It is necessary to estimate the available moisture value for individual agricultural crops. Thus, for

agricultural crops with vegetation period of 80-110 days 127-167 mm and и 213-284 mm of available moisture is needed, respectively. Here the moisture evaporated from the soil surface is not accounted for. However, the moisture left in the soil which is also evaporated is not also accounted for. The moisture from the surface of 5-10 cm soil layer lightened with sun will be evaporated. In our conditions the plants can get the mentioned values of moisture in the root system with the amount of precipitation falling in the cold half year which exceeds the quantity of the needed moisture 1,3-1,5 times.

-zone of the flow equilibrium- plain area without canal flow.

In Central Asia for the provision of life conditions in the areas without rivers the water was collected with so-called kyarizes (water collecting galleries). This method is labor consuming, and its use is limited by a small amount of atmospheric precipitation, that is why for the land farming it is necessary to find the regions with precipitation. Peculiar features of the region does not provide for using the experience of the other physical-and-geographical regions with successful keeping of agriculture. For us their agricultural methods can serve only as supplementary method. .

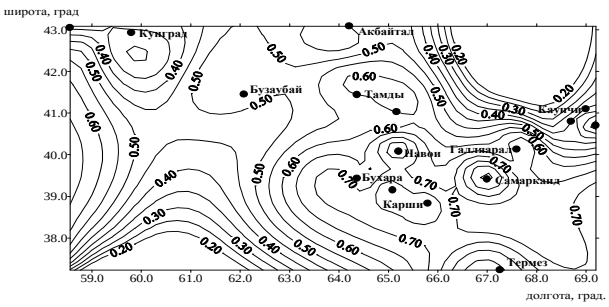
The plain part of Central Asian region with 200mm and 250 mm isohyets occupies 76 and 84 % of the whole territory of Uzbekistan. It was estimated that on this area of Central Asia 110 -130 km^3,is recorded which is consistent with the flow of the main rivers – Amudarja and Syrdaja.

On the plain territory of Uzbekistan the volume of atmospheric precipitation is ~80 km^3. Precipitation is recorded during the rainy period of subtropics from October up to May (in some years they are in September), while in the period from the middle of February up to middle of May (with maximum of precipitation in March) precipitation is characterized by a regime typical for the meso-thermal season by thermal parameters [7].

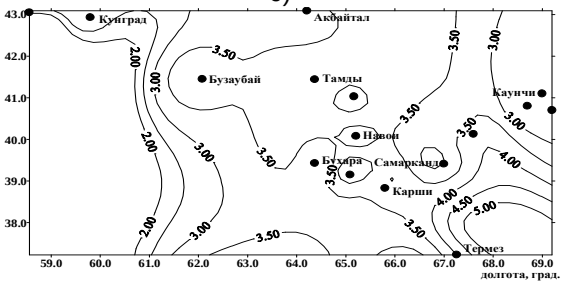
Regarding the water losses for evaporation the estimation of maximally possible evaporation can be made after estimation of evaporability. In the zone of the flow equilibrium the daily evaporability is few millimeters in the cold inter-vegetation period (period of moisture accumulation in soil). In summer the evaporability is 9-12 mm per day.

In the period of moisture accumulation on the major territory of plains in January 60% of precipitation is preserved (Fig. 2а), while in October the evaporability is в 2-5 times higher then the precipitation amount (Fig.2б).

а)



б)



а – January; б – October

Fig. 2. Schematic maps of distribution of the mean long-term evaporability, mm.

In conclusion we consider the water resources of the river flow balance. By the annual precipitation amount the area can be classified as follows: up to 150 mm; from 150 up to 200-250 mm. On the territories with the annual precipitation amount of 150 mm and less the water content available for agricultural crops with vegetation period of 60 days is 20-40%. On the territories with the annual precipitation amount of 150-250 mm the non-irrigated land farming can be developed. In [5] the recommendations are proposed for the preparatory measures on the ground area for guaranteeing that the area from which precipitation is accumulated would be 1.5-2 times more then the area planted with crops. When precipitation amount is 200-250 mm and more the territories can be regarded as appropriate for planting agricultural crops with the period of development of 60-120 days with water supply not less than 80% with application of the elaborated and tested methods of enhancement and intensification of natural precipitation [10,11].

References

1. Ushintseva V.F. Productive atmospheric precipitation. J. NIGMI Proc., Vol.11(256),36-52, 2009.
2. Ushintseva V.F. About water agriculture of a zone of dispersion of a drain. J. NIGMI Proc., Vol.13(258), 52-65, 2010.
3. Ushintseva V.F. Planning and estimation of efficiency of experimental activities for precipitation enhancement in Central Asia, Tashkent: Uzhydromet 113, 2004.
Kurbatkin V. P, Ushintseva V.F. Recommendation on optimization of use of an atmospheric precipitationof a flat part of Uzbekistan. J. NIGMI Proc., Vol.11(256), 66-72, 2009.

Glaciation activity of desert dust, air pollution and smoke from forest fires in convective clouds

Daniel Rosenfeld[1], Xing YU[2], Guihua LIU[2], Xiaohong XU[2], Yannian ZHU[2], Zhiguo YUE[2], Jin DAI[2], Zipeng DONG[2], Yan DONG[2], Yan PENG[2]

[1] The Hebrew University of Jerusalem, Jerusalem 91904, Israel, Daniel.rosenfeld@huji.ac.il

[2] Meteorological Institute of Shaanxi Province, No. 36 Beiguanzhengjie, Xi'an 710014, China

1. Introduction

The heavy air pollution, known as Atmospheric Brown Cloud (ABC), has been research mainly for its radiative effects and cloud condensation nuclei (CCN) activity that act to nucleate larger number of smaller cloud drops, and hence suppress coalescence and warm rain forming processes (Ramanathan et al., 2001). Precipitation in convective clouds with aerosol-induced suppressed coalescence is initiated nucleation of ice crystals that form ice hydrometeors that collect the supercooled cloud water. These ice particles are nucleated by ice forming nuclei (IFN) aerosols. Greater IFN activity of the ABC aerosols mean formation of more ice hydrometeors lower in the clouds, compensating to some extent for the precipitation suppression effect of the CCN activity of the ABC.

The IFN activity of the ABC in clouds is little known. Documentation of the IFN activity of the ABC is challenging because of the wide possible sources of the aerosols composing the ABC, including industrial emissions, burning of low grade fuels and agricultural fires. Air pollution aerosols have been generally considered as having less IFN activity than desert dust aerosol, which are known to be major source of IFN. Szyrmer and Zawadzki (1997), stated in a review paper that "certainly, natural mineral particles dominate the atmospheric nucleation of ice in the conditions of low temperatures of -12° to -15°C or less."

For testing whether this is really the case we focus our study over China and the vicinity, where both pollution and desert dust aerosol abound. Comparative measurements of IFN activity of heavy pollution haze and dust storms were conducted in China using the Bigg cloud chamber (1957), where activated IFN fall into supercooled sugar solution, grow and get counted there. You Laiguang and Shi An-Ying (1964) used the Bigg IFN counter in Beijing and showed that IFN activity of heavy pollution haze with visibility of ~1 km exceeds that of dust storm with similarly low visibility, especially at the higher temperatures (See Figure 1). Subsequent measurements in similar conditions (You Laiguang et al., 2002) had apparently greater detection efficiency of IFN and showed much greater overall concentrations, but air pollution and heavy desert dust had still comparable IFN activity, with desert dust exceeding the pollution activity by a factor of 2 at -15°C, whereas the opposite was the case in the earlier set of measurements.

These measurements contradict the common belief that desert dust dominates the IFN activity of aerosols whereas air pollution mainly act as CCN, except for highly supercooling, e.g., <-30°C. This re-examined here using satellite measurements of cloud and aerosol properties over China and the vicinity.

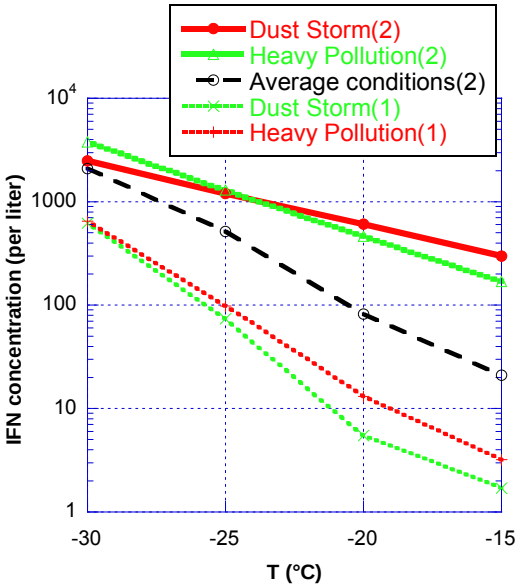


Figure 1: IFN concentrations in heavy pollution haze and dust storms with visibilities of ~1 km in Beijing. The data of (1) and (2) in the legend are from You Laiguang and Shi An-Ying (1964) and from You Laiguang et al. (2002), respectively. Both measurement sets show the same dependency of IFN on T, but apparently with better detection efficiency at the latter set.

2. Methodology

Glaciation temperature (Tg) of growing convective cloud towers was obtained by analyzing the vertical evolution of cloud top particle effective radius (r_e) as a function of cloud top temperature (T), using the methodology that we developed (Rosenfeld and Lensky, 1998) and subsequently applied to many other studies.

Using this method shows the temperature at which the ice phase has sufficiently developed to dominate their radiative signature, but it does not exclude the possibility of have some traces of suercooled water in the m. In order to reach Tg in growing convective clouds, the IFN have to nucleate the first ice crystals at higher temperatures. Therefore, Tg represents the lowest bound of the ice nucleation temperature of the IFN in clouds where glaciation occurs due to primary ice nucleation, as

opposed to secondary ice forming processes that do not involve IFN. Ca ses where r_e>12 μm at the -5 °C isotherm indicate favourable conditions for secondary ice nucleation (Hallett and Mossopp 1974). Glaciation in clouds with r_e<12 μm at -5°C is more likely to occur due to the primary ice nucleation activity of the IFN.

The methodology was applied to the Moderate Resolution Imaging Spectroradiometer (MODIS) onboard the AQUA sat ellite. Scenes were selected for 136 cases with convective cloud clusters for which coinciding measurements of aero sol classification were available from the Cloud -Aerosol Lidar with Orthogonal Polarisation (CALIOP) spaceborne instrument, and for which MODIS-measured aerosol op tical thickness (AOT) measurements were available.

The aerosol types we re: Pristine m aritime; Desert dust; Polluted dust; Contine ntal non-dust, containing the CALIOP classifications of Polluted continental, Clean continental and S moke. Another classification of pollution-free smoke was added, for which smoke from forest fires in remote area s of Siberia to th e north of China was included. The MODIS "Deep Blue" AOT was used for the dust and polluted dust aerosol types, and the 550 nm AO T was used for the other aerosol types.

In order to measure prima ry ice nucleation an effort was made to ide ntify the cases whe re ice multiplication was possible. Eighty six cases were identified as such where r_e>12 μm occurred at T= -5°C, in accordance with the conditions for on set of ice multiplication (Hallett and Mossopp 1974). The geographic distribution and the types of cases a re given in Figure 2.

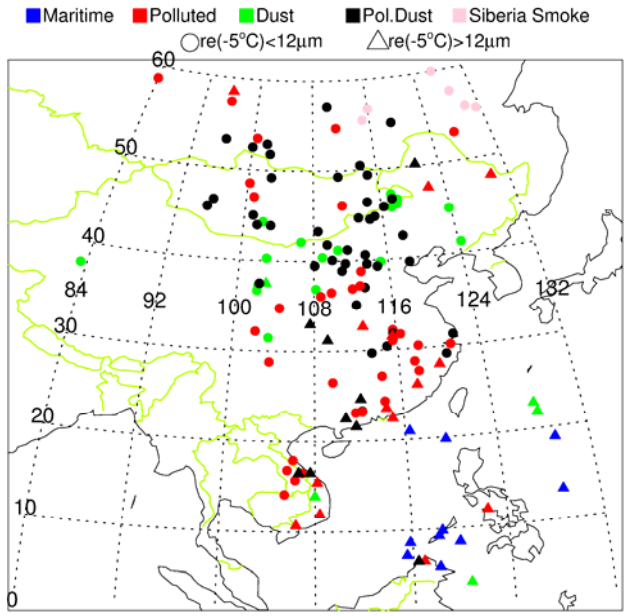


Figure 2: The geographical locations of the cases analyzed in this study. The colour marks the aerosol type according to CALIOP, as sho wn in the legend. Triangles mark cases where r_e>12 μm at the -5°C isotherm, indicating favourable conditions for secon dary ice nucleation. Circles mark the rest of the cases, where glaciation due to the primary ice nucleation activity of the IFN is more likely.

3. Results

The IFN activities of the different aerosol types were compared using cumulative probability functions, shown in Figure 3.

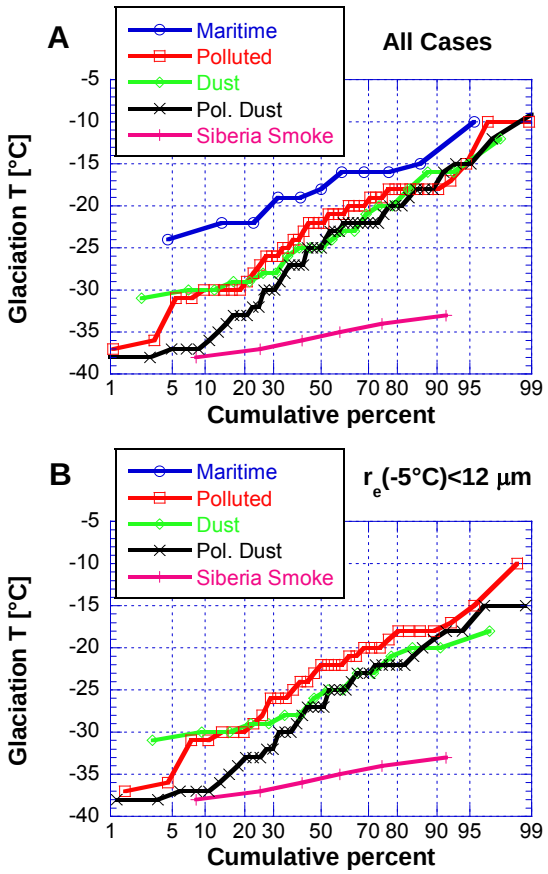


Figure 3: T he cumulative probabilities of glaciatio n temperatures (Tg) for all cas es (A), and for cases with absence of conditi ons for ice multipl ication (B). The number in the abscissa is t he cumulative percentage of the number of cases with Tg lower than t he respective value on the ordinate.

According to Figure 3A, marine clouds glaciate at the hig hest temperatures (median of -1 8°C), followed by continental cloud without dust (-22 °C), clouds in pure and p olluted dust (-2 5°C), and pure smoke from fore st fire (-3 5°C). When excluding the clouds with drops that a re sufficiently large fo r ice multiplication (Figure 3B), the marine clouds are excluded, while the dist inction between dust-free pollution (-22°C) and d usty aerosols (-27°C) is sharpened.

It is expecte d that the aero sol activity would become stronger and in cur glaciation in high er temperatures with greate r values of AOT. This i s observed in clouds with small drop s, in which mo stly primary ice nucleation on IFN is expected to form, as shown in Figure 4A. In contrast, Tg is observed to be lower with increasing AOT in clou ds with large drops that apparently allow seco ndary ice forming processes to cause the cloud glaciation, as shown in Figure 4B. Such clouds were not observed in

AOT>0.8, as evident in Figure 4B, probably because a very heavy aerosol load enforces small cloud drops, regardless of the aerosol composition.

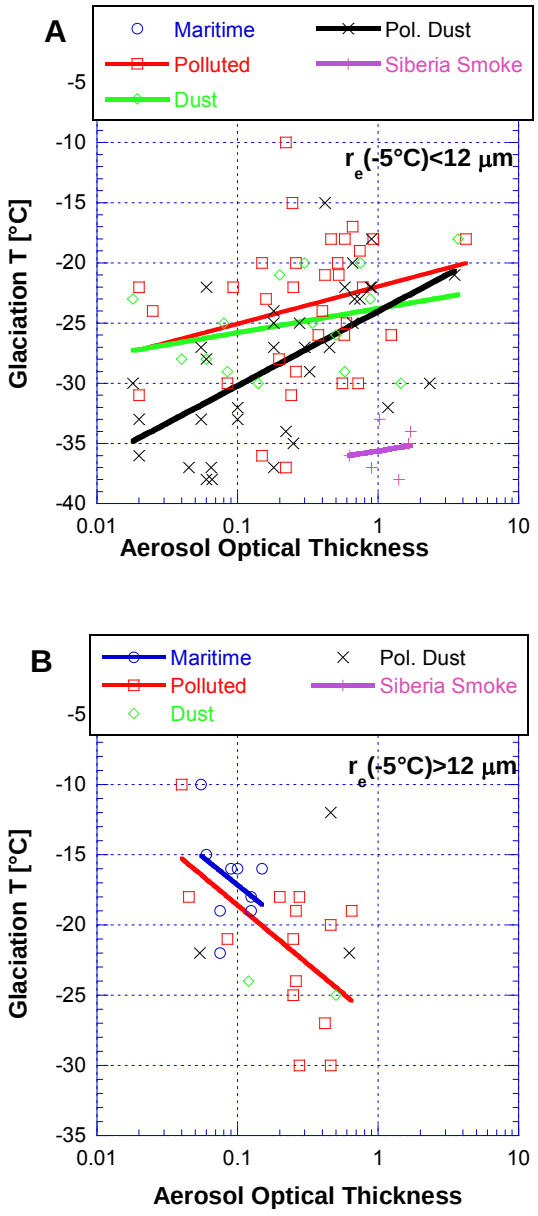


Figure 4: The dependence of the glaciation temperature of the various aerosol types on the aerosol optical thickness, for (A) cloud with small drops, in which mostly primary ice nucleation on IFN is expected to form, and (B) for clouds with suitable conditions for ice multiplication, where most ice is expected to form by secondary ice processes. Best fit lines of Tg with the logarithm of AOT are plotted only for classes with at least 4 cases.

6. Discussion

The main result shows that the Tg without classification to cloud drop size is highest in marine cases and then the pollution. Remarkably convective clouds ingesting pollution aerosols glaciated at warmer temperatures than the dust and polluted dust. Pure smoke from forest fires in Siberia glaciates clouds at the coldest temperature by far.

When focusing on clouds with drops that are too small for ice multiplication (Figure 4A), the differences between the air pollution and the dust become more apparent. For such conditions, Tg increases with AOT. The pollution shows the warmer Tg for the same AOT compare with dust at high AOT. The pure dust has narrower range of Tg values compare with polluted dust, probably because the composition of the polluted dust is more variable than the composition of the pure dust.

At modest and small AOT the polluted dust glaciates clouds at lower temperatures than dust alone, in agreement with the hypothesis that air pollution deactivates IFN activity of mineral dust (Braham and Spyers-Duran, 1974).

Smoke from burning vegetation contributes to both the polluted dust and to the non-dust continental aerosols. The Siberia cases show that pure smoke serve as poor IFN, at least in Siberia. However, smoke from burning vegetation in areas with industrial pollution may release IFN that deposited on the vegetation and rise with the smoke particles.

For clouds with large drops, where r_e at the -5°C isotherm >12um (Figure 4B), the Tg deceases with increasing AOT, reflecting the dominant role of the aerosols impact on cloud drop size over their IFN activity. Apparently, large drops glaciate the clouds by secondary ice forming processes more effectively than IFN do by primary ice nucleation in clouds with small drops.

7. Implications

Until now, the smoke and pollution aerosol effects on precipitation have been recognized mainly through their impact on cloud drop size and respective suppression of drop coalescence. Here we show that, in heavy aerosol loads, their IFN activity becomes dominant in the precipitation forming processes. Furthermore, we show that the industrial air pollution has comparable IFN activity to that of desert dust, in agreement with previous IFN measurements in China. This means that the IFN activity of air pollution might restore some precipitation that is suppressed by the CCN activity of the same aerosols in deep convective clouds. Adding IFN for restoring suppressed precipitation is in fact the objective of glaciogenic cloud seeding for rain enhancement. This means that glaciogenic seeding is superfluous in atmosphere that contains large amounts of industrial pollution and/or desert dust aerosols. On the other hand, clouds ingesting pristine air with relatively small aerosol concentrations develop large drops that allow efficient warm rain processes and high glaciation temperature even without large IFN concentrations. This leaves only lightly polluted clouds as having the potential for very low Tg, where glaciogenic seeding has the potential

to increase Tg and possibly enhance precipitation or suppress hail.

Therefore, the effect of intended glaciogenic cloud seeding is probably by far smaller than the much more massive inadvertent cloud seeding by heavy air pollution and by the natural seeding done by dust storms.

Here we highlighted the implications with respect to cloud seeding. But more importantly, the implication with respect to modification of rainfall, latent heat release and the response of the circulation systems at regional and global scales are far reaching and require much more attention in future research.

Acknowledgements

This research was supported by National Natural Science Foundation of China (Grant 40975087). We are grateful to the supports from Shaanxi Administration of Foreign Expert Affairs and Meteorological Bureau of Shaanxi Province.

References

Bigg, E. K., A new Technique for Counting Ice-Forming Nuclei in Aerosols. *Tellus*, **9**, 394–400, 1957.

Braham, R.R. and Spyers-Duran, P: Ice nucleus measurements in an urban atmosphere, J. Appl. Meteo., 13, 940-945, 1974.

Hallett, J., and S. C. Mossopp, Production of secondary ice particles during the riming process. *Nature*, **249**, 26–28, 1974.

Ramanathan, V., P. J. Crutzen, J. T. Kiehl, and D. Rosenfeld, Aerosols, Climate and the Hydrological Cycle. *Science*, **294**, 2119-2124, 2001.

Rosenfeld D. and I. M. Lensky, Satellite-based insights into precipitation formation processes in continental and maritime convective clouds. *Bull. Amer. Meteorol. Soc.*, 79, 2457-2476, 1998.

Szyrmer W. and I. Zawadzki, Biogenic and Anthropogenic Sources of Ice-Forming Nuclei: A Review. *Bull. Amer. Meteorol. Soc.*, **78**, 209-228, 1997.

You Lai-Guang and Shi An-Ying, The measurement and analysis of ice-nucleus concentrations at Peking during the period from March 18 th to April 30 th in 1963. *Acta Meteorologica Sinica*, **34**, 548-554,1964.

You Laiguang, Yang Shaozhong, Wang Xiangguo, and Pi Jiaxiong, Study of ice nuclei concentrations in Beijing in spring of 1995 and 1996. *Acta Meteorologica Sinica*, **60**, 101-109, 2002.

Weather Modification for Rain Reduction - A Conceptual Design

***Tri Handoko Seto**,Samsul Bahri, Heru Widodo, Erwin Mulyana, Budi Harsoyo, and Mimin Karmini*

Weather Modification Technology Center, Agency for the Asessment and Application of Technology

BPPT 1st building 19th floor, Jl. M. H. Thamrin no. 8 Jakarta, Indonesia

First author's email address: thseto@yahoo.com

1. Introduction

Weather modification technology has been utilized not only for rain enhancement, but also for hail suppression, fog clearing and rainfall intensity reduction. Weather Modification Technology Center carried out experiments in rain intensity reduction in order to overcome floods via competition method in Tuntang area – Central Java during the rainy season of 1995. The result showed that rainfall intensity was decreased to about 15 %. In addition, we had carried out rainfall intensity reduction over The Jakarta area in February 2002. It was considered successful even for only about one week time. The operation was stopped because the adjacent districts complains due to rain occuring more in their areas. This operation is conducted by the jumping process utilization.

Along with more advance research on weather modification technology with the purpose of decreasing rainfall intensity, some countries, such as PRO China and Russia have applied this technology to prevent rain occurrence during some events. Russia has utilized this technology during open door state events, while PRO China applied this technology in Beijing during the opening ceremony of 2008 Olympiad.

The need for weather modification in the form of rain reduction in Indonesia is very high. Open coal mining companies, many located in Kalimantan, require so much of this technology in order to increase its production. Some coal companies which has expressed its interest on using this technology, for instance is PT Adaro Indonesia.

PT. Adaro Indonesia own an open coal mining in South Kalimantan. Its production is influenced by rain occurrence within the mining area. If rain falls, mining activities will be stopped until the top soil is dried and slip free. It may take a while, few hours to days, for it to dry itself. Therefore, It has the potential of reducing PT. Adaro Indonesia coal production. Such events would often occurs during the rainy season. Steady rain from stratiform clouds will even worsened the situation. Stratiform clouds developed mostly in a stable atmosphere, this kind of clouds has a large coverage, produces light rain and may cause overcast. Therefore, the solar radiation needed to dried the slippery soil is also reduced. In order to minimize lost opprotunity due to rain occurrence, PT. Adaro Indonesia consulted the Weather Modification Technology Center (WMTC) to inquire whether the WMTC could help them to alleviate their problem.

The other coal mining companies which has shown interest with this technology is PT Pama Persada. Problems arising in PT Pama Persada is not so much different with those of PT Adaro Indonesia. The same could also be said with regards to other open coal mining estabilishments.

Beside coal mining companies, Provincial Government of Central Java has lately expressed its interest in this technology. Rain reduction weather modification is meant to be used to prevent the occurence of heavy flood on the top of Mount Merapi in Central Java which if happens, will spew out 14 million m3 cold lava which would be disastrous to the surrounding area inhabitants.

This paper is a theoretical review of weather modification for rain reduction and the example of its planned application in PT Adaro Indonesia.

2. Weather Modification Technology for Rain Reduction

Studies on rain intensity reduction has been done by many scientists. These studies have been done both in the laboratory by using some models and also by field experimentations. Those studies are based on the relationship between aerosol, clouds microphysics and precipitation.

Yin et al. (2000) states that based on numerical calculation of hygroscopic seeding impact on convective clouds, seeding agents with a size of less than 2 μm could decrease about 22 – 30 % of precipitation. Givati and Rosenfeld (2004) showed that urban air pollution in California and Israel may reduce about 15 - 25% of yearly rainfall. According to Khain et al. (2005), small cloud condensation nuclei CCN may produce small droplets, which have small collision efficiency, thereby causing deep convective clouds decreasing precipitation.

Competition Mechanism

In a precipitating cloud, precipitation developed when the cloud droplet population become unstable, and also when some droplets grow at the expense of others. The mechanism whereby a cloud microstructure may become unstable involves direct collision and coalescence of water droplet. The most important event for a precipitating cloud is the collision event. In its earliest stage, a cloud is an assembly of tiny droplets numbering in the order of 100 /cm^3 and having radii of about 10 µm. Because efficiency of collision and coalecence is very low (figure 1), this structure is of course extremely stable.

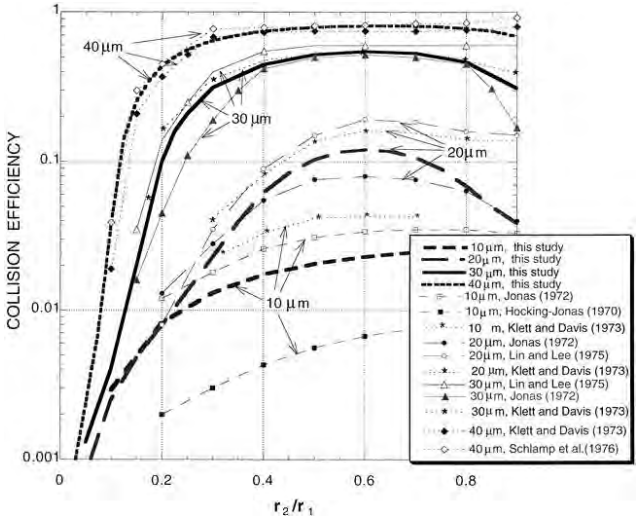


Figure 1. Efficiency of collision and coalesence (Pinsky et.al., 2000).

Introducing super fine hygroscopic seeding agent into the clouds would then initiate the formation of small droplets that will act as competitor to the existing cloud droplets in the water vapor absorption process within the cloud. To conduct the operation, Piper Cheyenne will be utilized to deliver seeding agents in the form of flares. This action would then prevent collision process because within the clouds exists cloud droplets homogenic in size. Once larger droplets are present, collision – coalescence chain reaction would then started.

The best example of competition mechanism is during forest fires events. Because there are too many aerosol present, which have sizes less than 1 µm, produced by forest fires, cumulus clouds barely developed over the fires and vicinity areas.

Jumping Process Mechanism

Collision efficiency intensifies drastically when cloud droplets grew. Collision efficiency of 10% for droplets size of about 10 µm in radii increases drastically to 80% when the droplets size is about 30 µm in radii (Pinsky et al., 2000, see figure 1). The Jumping Process Mechanism is initiated by introducing large hygroscopic seeding agents of about 10 – 100 µm in size into clouds to increase collision efficiency so that rain may occur shortly. It is noted that 10 µm of hygroscopic seeding agents would create more than 30 µm droplets inside the clouds. This mechanism will then be applied to developing clouds that posses the possibilities to produce rain over the entire target area. This activity had been performed during cloud seeding activity to enhance rainfall over small target area.

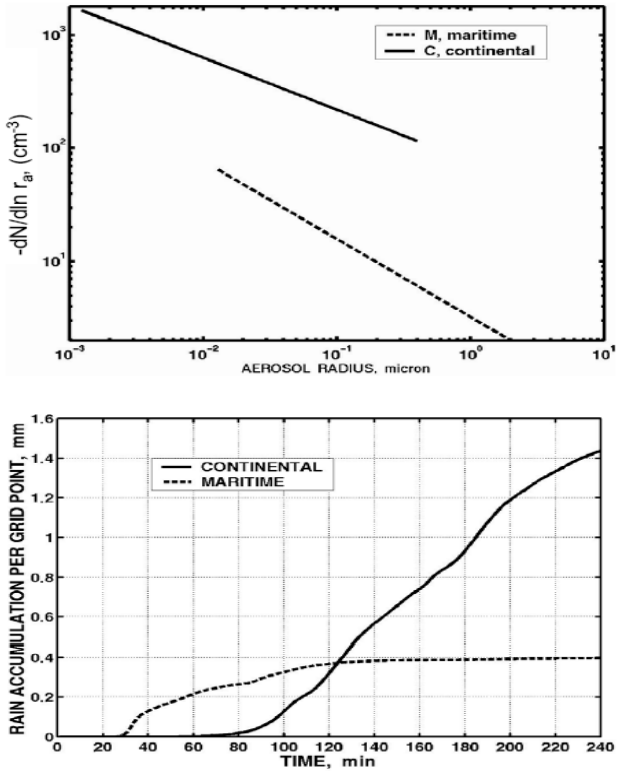


Figure 2. Features of Maritime and continent clouds (Khain et.al., 2005).

Features of Maritime cloud and Continent cloud (Khain et.al., 2005, see figure 2) are:

Maritime Cloud:

- Big aerosol (CCN) size but smaller amount
- Weak updraft
- High moisture
- Quick to rain
- Small rainfall amount

Continent cloud:

- Small aerosol (CCN) size but larger amount
- Strong updraft
- Low moisture
- Slow to rain
- Large rainfall amount

These features agreed well with Pinsky et.al., 2000 in which big aerosol correlates to the acceleration of rain process. Bruintjes et.al., (private communication, 2004) showed that ultra giant aerosol (more than 10 µm in radii) may bypass the CCN population action in determining the initial character of the cloud droplet population, and thus, jumpstart the coalescence process itself.

3. Application of Weather Modification for Rain Reduction

In the application of weather modification technology for PT. Adaro Indonesia, the WMTC will carry out some methods, of how to apply weather modification technology (WMT) and how to evaluate weather modification activities. In response to enquiries, the WMTC conducted field survey in order to study December 2010 cloud formation. Some notes from the survey might be summarized as follows:

1. The present cloud formation seems to be of a typical land cloud formation. In early morning there were stratiform clouds, which then broke up in late morning. Cumulus clouds develop mostly in early afternoon and rain falls in late afternoon.
2. Surface winds were mostly westerly during daylight hours in the rainy season, while during the night time winds were mostly south easterly. Surface wind speeds were mostly about 5 knots.
3. Mining was stopped when rain occurs. The reason is that the top soil during and after rainfall becomes very slippery. The activity would then resume when this slippery condition is no longer present. Therefore, the duration lost due to rain may be calculated as rain duration plus the period needed to dry out the top soil. From data analysis, it could be concluded that the monthly average of lost time as: 140,60 hours in January, 110,92 hours in February, 135,07 hours in March, 128,82 hours in April, 80,46 hours in May, 74,04 hours in June, 59,02 hours in July, 38,02 hours in August, 44,42 hours in September, 60,82 hours in October, 120,83 hours in November and 150,77 hours in December.

In carrying out those two mechanisms, several strategies are applied ;

1. During the early stage of cloud formation, competition mechanism will be initiated by introducing very fine seeding agents of flares by Piper cheyenne aircraft. This would then add more small droplets so that the collision efficiency remains low. As a result, cloud development would become very slow.
2. When there are potential clouds, jumping process mechanism would then be initiated. This is to force rain to occur before it reaches the target area. Therefore, this activity will be done mostly in the upwind area. In order to carried out the jumping process CASA NC 212-200 will be used to deliver seeding agents in powder form.
3. When the water vapor supply is too high and the competition mechanism is no longer sufficient to slow down cloud development, jumping process would then be initiated using CASA NC 212-200. This is done to shorten rain duration. This strategy will also be used when weather condition allow the presence of thick stratiform clouds that may cause longer period light rain.
4. As aircraft would only be flown in daylight, ground base generator will be utilized to start the competition mechanism if needed during night time. For this purpose, four (4) ground base generators will be installed around the target area. However, ground base generators will not be used for the upcoming activity because realization plans for the ground generators still needed to be finalized.

For services to PT. Adaro Indonesia, the WMTC will execute 2 mechanisms in order to reduce rainfall intensity and or rain occurrence over the mining area.

Weather Modification Activities

Weather modification activities will be carried out day and night. During daylight, 2 aircrafts, CASA NC 212-200 and Piper Cheyenne, will be used for weather modification activities. CASA NC 212-200 is used to carry seeding agents in powder form to execute the jumping process. While Piper Cheyenne will be used for seeding agents in pyrotechnics form (flares) to execute the competition mechanism. Flight activities will be guided by flight scientists in executing strategies based on weather data analysis.

During night time, weather modification activities will be carried out through ground base generator. Ground base generator is employed to introduce super fine particles to initiate the competition processes. Operational design of this technology is shown by figure 3.

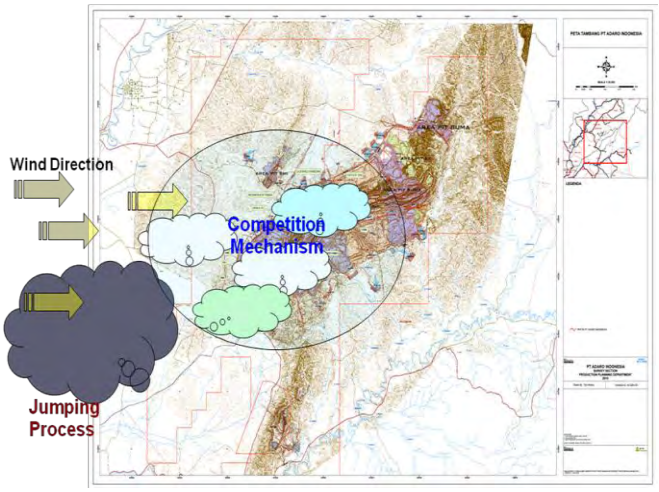


Figure 3. Operational design of weather modification technology for rain reduction at PT Adaro.

4. Summary

1. The need for weather modification technology in the form of rain reduction in Indonesia is very high. Aside from its use in disaster prevention, this technology is very economical as well.
2. Weather modification technology may be applied to reduce rainfall using the competition mechanism and jumping process mechanism.
3. Based on researches and experiences on rainfall reduction, weather modification technology is able to reduce about 15 – 30% of rainfall. By utilizing competition mechanism and jumping process, it is posibble tor reduce more than 15-30% of rainfall.
4. Weather modification activities should be carried out for longer period considering that the possibility of cloud formations is unpredictable. The WMTC suggests that weather modification activities are carried out during rainy season in the area.

Acknowledgements

The author and co-authors are very grateful to WMTC who has given moral and financial support for all weather modification technology for rain reduction assesment and socialization activities. Gratitude owed to PT Adaro Indonesia and The Provincial Government of Central Java which has facilitates us to conduct survey in the mining area and Mount Merapi. Special thanks to WMTC colleagues who have given valuable input and warm discussion for concept improvements and weather modification technology for rain reduction application plan. Thanks owed to Krisna who has dilligently corrected this paper draft. Thank you to all of those parties which we cannot mention individually who has helped in the writing of this paper.

References

1. Givati, A. and D. Rosenfeld, 2004: Quantifying precipitation suppression due to air pollution, Journal of Applied Meteorology, 43, pp.1038-1056.
2. Bruintjes, R. T., V. Salazar, D. Breed, Jia Li, Peter R. Buseck, T. Jensen, K. Ross, S. Piketh, and J. Reid, 2004: Aerosol-Cloud Interactions: Observation Studies of the Effects on Cloud and Precipitation Development.
3. Hsu C. F., S. A. Changnon Jr., F. A. Huff, and K. R. Gabriel, 1981: The assessment of statistical – physical techniques for the evaluation of weather modification operations, State Water Survey Contract Report 286.
4. Khain A., A. Pokrovsky, M. Pinsky, A. Seifert, and V. Philips, 2004: Simulation of Effects of Atmospheric Aerosols on Deep Turbulent Convective Clouds Using a Spectral Microphysics Mixed-Phase Cumulus Cloud Model. Part I: Model Description and Possible Applications, Journal of the Atmospheric Sciences, Vol. 61, pp.2963-2976.
5. Khain, A., D. Rosenfeld, and A. Pokrovsky, 2005: Aerosol impact on the dynamics and microphysics of deep convective clouds, Q. J. R. Meteorol. Soc., 131, pp. 2639-2633.
6. Pinsky M., A. Khain, and M. Shapiro, 2000: Collision efficiency of drops in a wide range of Reynolds numbers: effects of pressure on spectrum evaluation, J. Atmos. Sci., 58, pp. 742-764.
7. Yin, Y., Z. Levin, T. Reisin, and S. Tzivion, 2000: Seeding convective clouds with hygroscopic flares: Numerical simulations using a cloud model with detailed microphysics, Journal of Applied Meteorology.

Radar Investigation of AgI Seeding Efficiency in the Kingdom of Saudi Arabia

Andre A. Sinkevich[1], Terrence W. Krauss[2,3], and Ayman S. Ghulam[4]

1- Main Geophysical Observatory, Karbyshev str. 7, St. Petersburg, Russia,194021 (sinkev@email.com)
2-Weather Modification Inc., Fargo ND, USA
3-Krauss Weather Services Inc., Red Deer, AB, Canada
4-Presidency of Meteorology and Environment, Jeddah, Kingdom of Saudi Arabia

1. Introduction

The Kingdom of Saudi Arabia (KSA) has an area of about 2.25 million km^2, most of which is located in arid regions. Studies have been conducted previously in the KSA to determine if cloud seeding is able to increase the precipitation (Vali, 1991). Starting in November 2006, cloud seeding trials and cloud physics research studies have been conducted in Saudi Arabia by WMI for the Presidency of Meteorology and Environment (PME) in both the central region around Riyadh and the southwest Asir region around Abha.

Carried out experiments show that Cu microphysical characteristics change due to seeding but quantity of additional precipitation is still a challenge in our knowledge. Results of investigations round the world have shown that seeding efficiency change significantly (from 3 to 117%) for different projects (Sinkevich et al., 2001). It is accepted by scientific community that regular efficiency in precipitation enhancement is within 10-25% usually (Sinkevich and Krauss, 2010).

It is important to distinguish seeding efficiency of Cu cong and Cb. Our earlier investigations statistically proofed seeding efficiency of Cu cong (Krauss et al., 2006, Krauss et al., 2010, Sinkevich and Krauss, 2010). Assessments of Cb seeding efficiency are more complicated, especially for multicell Cb when merging processes with feeder cells take place. Detailed statistical analysis of randomized Cb seeding project in the USSR during 1973-1978 (Kornienko, 1982) have shown that for single cell Cb seeding results in 118-160% increase of precipitation amount. The analysis of seeding efficiency for multicell Cb's did not show statistically proofed difference. Our earlier case study has shown very high efficiency of such seeding (Krauss et al., 2007).

This paper examines precipitation characteristics of natural Cu cong and Cu cong seeded with silver-iodide in the Asir region of Saudi Arabia, and observed by weather radar. A variety of radar derived precipitation parameters have been examined, primarily maximum radar reflectivity, precipitation flux, and rain volume. A summary of the storm characteristics and an exploratory statistical analysis of the response variables are presented. We also investigate in a statistical manner the changes in storm (multicell Cb) characteristics derived from radar measurements before and after merging takes place, looking for differences in storm characteristics when the merger involved the seeding of cumulus congestus compared with naturally developing feeder clouds.

2. Cloud seeding methodology and selection criteria

Cloud top seeding was conducted by aircraft flying at an altitude corresponding to the -10ºC level, typically between 6 and 7 km MSL. The seeding aircraft seed Cu cong with 20-g ejectable silver-iodide flares (described at www.iceflares. com). For storms with feeder clouds, the seeding aircraft seed the tops of the developing cumulus towers on the upwind sides of the more mature convective cells, as they grow up through the -10ºC altitude. The ejectable flares are typically dropped at a rate of one 20-g flare every 5 s (500m) during a cloud penetration. Seeding stopped if there were visual signs of glaciation and high ice concentrations.

Several groups of seeded clouds were chosen for the investigation of seeding effects. These were all cumulus congestus clouds; however, the seeding was carried out at different stages of cloud development dependent on proximity of the seeding aircraft to the cloud.

The first group of clouds was seeded without an existing radar echo (minimum detectable signal is approximately 0 dBZ inside 100 km range), but a radar echo formed on the next volume scan (time between scans is 5 minutes). The second group of clouds was seeded when there was a radar echo > 0 dBZ but less than 20 dBZ at time of seeding. The third group of clouds studied was seeded at a stage when a TITAN (Dixon,1993) cell (reflectivity >30 dBZ) had already formed. All clouds chosen for this analysis formed TITAN cells that persisted for more than two radar scans (>10 min of TITAN cell duration).

Naturally developing clouds were chosen for comparison. Clouds were chosen that developed in the close proximity to the seeded clouds in space and time. These clouds were chosen for comparison analysis if they produced a TITAN cell that lasted more than two scans (>10 min duration), similar to the seeded clouds. Their position was within +/- 25

km from the seeded clouds in most cases, though in some cases they were located slightly further. We also tried to choose more or less equal number of naturally developing clouds with the number of seeded clouds, but sometimes there were slight differences on a given day.

A total of 136 single cumulus congestus cells were selected for analysis from 2008 and 2009 in the Asir region, within 100 km range of the Abha radar. All clouds under consideration formed due to day-time heating and the sea breeze, between 09:40 and 14:45 UTC. The most intense development was observed between 11:30 and 13:00 UTC (14:30 to 16:00 local time), and 73% of the clouds in this study formed during this period of time.

Cb's that merged with Cu cong being seeded and Cu cong that naturally developed are analyzed in the second part of the study.

A "Storm" is defined as a thunderstorm that persisted for a long time (typically more than 1 hour), produced a TITAN radar cell and merged with a new developing cell (feeder). A "Feeder" is defined as a cumulus–congestus cloud that developed nearby a larger storm, existed less time than a storm, formed a TITAN radar cell, and then merged with another, pre-existing larger storm. Both storms and feeders formed TITAN cells in this study, and only the merging processes of these types of cells were under consideration. Only one feeder merged in the cases analyzed in this study.

The following radar derived characteristics were analyzed: precipitation flux (Pflux), cell top height, cell mass, maximum radar reflectivity (Zmax), and height of maximum reflectivity.

All of the mentioned data was obtained according to the following radar scans: "zero" time is defined as the time of the scan just before the merging took place. Two scans were analyzed prior to "zero" time i.e.; -5 and -10 min; and 4 scans were analyzed after merging took place i.e., 5 min (first scan after merging), and the following +10, +15, +20 min). This procedure allowed the possibility to study the storm evolution. If any additional merging or splitting took place during these scans the data from these scans was omitted. The same radar characteristics were analyzed for the feeder clouds, but only one scan just prior to merging is discussed.

The period analyzed was June to September 2008. A total of 68 cases of merging were investigated on 31 days, and they included 53 naturally developing clouds and 15 clouds that were seeded.

3. Seeding efficiency of Cu cong

Three groups of seeded clouds were studied: Group I consisted of 28 clouds seeded at a time without any radar echo, and 43 natural clouds for comparison purposes. Group II consisted of 21 clouds seeded when the radar echo was >0 dBZ but <20 dBZ, and 44 natural clouds for comparison purposes. Group III consisted of 13 clouds seeded when the initial radar echo was >30 dBZ, and 19 natural clouds for comparison purposes.

The Group I seeded clouds produced greater maximum reflectivity (ZMAX) and greater precipitation flux (MAX Pflux) than their natural counterparts. The difference in the ZMAX means was 3.3 dBZ.

The probability plots of ZMAX for the 43 natural and 28 seeded clouds are shown in Fig. 1, The maximum values of ZMAX were in the range from 34 dBZ to 64 dBZ. Figure 1 shows a tendency for seeded clouds to have greater maximum reflectivity in comparison with naturally developing clouds. The 95% confidence intervals for the corresponding normal distributions are also shown in Fig. 1.

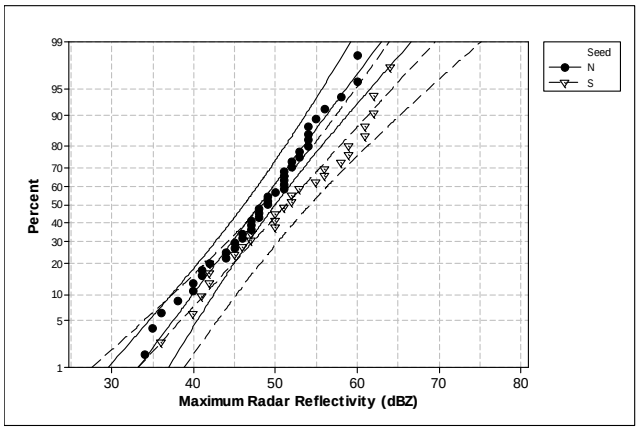


Figure 1: Probability plot of maximum radar reflectivity for 43 natural clouds (N) and 28 seeded clouds (S) that had no-echo at time of selection. The 95% confidence intervals for the corresponding normal distributions are also shown.

The median MAX Pflux for the natural clouds was 148 m^3/s and for the seeded clouds was 193 m^3/s. The differences in the mean for ZMAX and MAX Pflux were significant at the 94% and 93% level respectively. The mean times to reach MAX Pflux for the natural and seeded clouds were very similar; 27.9 min and 26.1 min respectively.

The Group II seeded clouds also produced greater ZMAX and greater MAX Pflux than their natural counterparts. The difference in the mean ZMAX was 1.7 dBZ. The median MAX Pflux for the natural clouds was 61.5 m^3/s and for the seeded clouds was 134.0 m^3/s. The biggest differences between groups was for clouds with ZMAX >50 dBZ and MAX Pflux >100 m^3/s. The positive association with seeding persisted, but the statistical significance was less.

The results of the Group III clouds was dominated by a few large merged-complex storms. Five of the seeded clouds and three of the natural clouds formed large, merged complexes that dominated the radar statistics in favor of the seeded group. The seeded clouds merged with older cells and the effects of seeding could not be determined after merger. A sub-set of cells was selected for further analysis, which was seeded during the first 15 min and did not merge with older cells. This removed

all of the large merged complexes and removed the bias in favor of the seeded group. Unfortunately this reduced the sample size substantially to 6 seeded cells and 12 natural cells. The positive association with seeding persisted, but the statistical significance was low, and must be considered to be very preliminary because the sample size is very small.

The differences between MAX Pflux for the seeded and natural clouds became less as the radar reflectivity at the time of seeding increased. The greatest seeding effects were observed for clouds that were seeded prior to the appearance of a radar echo. The distributions of the response variables to seeding overlap; however, there is a consistent shift to larger values for the seeded cases. The overlap is not surprising because the responses to seeding are highly variable and fall within the range of natural variability.

The authors do not believe that a blind, random selection process would necessarily account for all of the natural variability that exists. This variability is caused by seeding at slightly different times in the cloud development, with slightly different initial conditions, with slightly different seeding amounts, at slightly different locations, with slightly different topography, and slightly different forcing conditions and so on. Therefore, it is not surprising that the differences are not statistically significant at the 95% confidence level. However, this also does not mean that the differences are not positive and sufficient to warrant further assessment and considerations. The results to date have been sufficiently encouraging and suits previous investigations.

4. Impact of merging on storm characteristics and efficiency of seeding feeder clouds

A statistical summary of storm characteristics is calculated from the 3 radar scans before merging, plus 4 scans after merging when the data were available. The time period for these characteristics is 35 min for a maximum of 7 radar scans. The storm data set consists of the TITAN software processing of 417 scans. The storm data set always included one scan before the merging and one scan after the merging. However, if secondary splits or mergers occurred within 3 scans, then those data were excluded.

A statistical summary of characteristics of the associated feeder cells, using the single time-scan just before merging consists of 68 scans with feeder cloud characteristics.

Storm Zmax was rather high. The median Zmax was 56.5 dBZ, and the maximum Zmax was 65 dBZ. Feeder cells had lower values of Zmax; the median was 46.1 dBZ and the maximum was 61 dBZ. The height of maximum reflectivity was similar for both groups and the mean and median values were located at 5.5 and 6.3 km respectively.

The median Pflux for storms (980 m^3/s) was approximately an order of magnitude greater than the Pflux produced by feeder cells (89 m^3/s).

The cell top heights of the investigated storms ranged between 6.6 and 18.6 km. The mean cell top height was 13.5 km. Cell tops were >10 km in 85% of the analyzed cases. The maximum values of cloud top heights could be overestimated due to the presence of high reflectivity cores in the storms and the effects of antenna beam side lobes as discussed by (Krauss et al., 2011). Some of the feeder cells were also rather intense clouds, with maximum top height equal to 17.8 km. Some feeder cells developed significantly during the period of observation, but they were smaller than storms on average. The mean feeder cell top height was 10.4 km. The feeder cell tops did not exceed 12 km in 72% of cases, and the median top height was 9.6 km.

The mass of the investigated storms was significantly bigger than that of feeder cells. Mean storm mass was equal to 1268 ktons and mean feeder cell mass was 173 ktons.

The atmospheric thermo-dynamics characteristics, observed for the days with merging, were studied. The storms were observed when CAPE had very large values. CAPE (mean and median) equalled 4800-4900 J/kg respectively. On 90% of the days, CAPE exceeded 3000 J/kg when merging was observed.

A method to study the merging process was developed; it was based on statistical analysis of storm characteristics prior to and after merging. Such an approach provided the possibility to derive changes in cloud characteristics and to filter them from trends which were the result of cloud development. It also provided the possibility to quantify changes in storm characteristics due to merging.

It was confirmed that merging has a strong effect on storm development. The data analysis shows that an increase in the median of the distribution of maximum reflectivity was observed just after merging and was equal to 4.2 dBZ. The storm mass and precipitation flux also increased significantly. The median mass increased from 385 to 1091 ktons (283%), and Pflux increased from ~475 m^3/s to ~1400 m^3/s (290%).

The investigation of possible differences in storm characteristics after merging with seeded feeders compared with naturally developing feeders was also conducted. It was discovered that in this data set, the non-seeded feeder clouds were more developed than the seeded feeder clouds at the time of merger. There was a tendency of storms to grow prior to merging in the case of non-seeded feeders, and to diminish in the case of merging with seeded feeders. In the opinion of the authors, this was likely due to the seeding pilots choosing to seed feeder clouds that were less severe and having weaker dynamics for safety and comfort reasons. This is not surprising considering the large CAPE values and strong instability.

In the case of merging with non-seeded feeders, an increase in the medians of the distributions of cloud top height (+0.1 km) maximum reflectivity (+5

dBZ), precipitation flux (+1550 m^3/s, 310%) and mass (+700ktons, 275%), and height of maximum reflectivity (+0.1 km) can be attributed to merging. In the case of merging with seeded feeders an increase in all investigated storm parameters was also observed. Median values of all parameters increased in the following way: cloud top height (+5 km), maximum reflectivity (+6.6 dBZ), precipitation flux (+950 m3/s, 337%), cloud mass (+700ktons, 420%), and height of maximum reflectivity (+2.2 km).

To clarify the seeding effect, the data were filtered in order to choose storms with equal mass just before merging. The results showed that Pflux increased after merging in both natural and seeded cases. Even for storms that were "decreasing" at the time of merger, the seeding cases had an increased Pflux after merging, but the values were similar to the natural cases. Therefore, the effects of seeding are within the range of natural variability of the merging effects. Furthermore; any evaluation of cloud seeding experiments must take into consideration and distinguish between cases that merge and cases that do not merge. The merging process has a significant effect on the results, and can lead to erroneous conclusions regarding the seeding if they are not properly taken into consideration.

Acknowledgements

The authors wish to thank the Presidency of Meteorology and Environment (PME) of the Kingdom of Saudi Arabia under the leadership of Prince Turki bin Nasser bin Abdul Azziz for funding the program. Special thanks to Weather Modification Inc. (WMI) which carried out experiments and provided data for current analysis. Roelof Burger of the University of Witwatersrand in South Africa is gratefully thanked for his assistance with the TITAN software. Dr. Paul Kucera of the National Center for Atmospheric Research (NCAR) is acknowledged for his help with the radar data.

References

Dixon M. and G. Wiener, TITAN: Thunderstorm identification, tracking, analysis, and nowcasting - a radar-based methodology. J. *Atmos. and Oceanic Technol.,* **10**, 785-797, 1993.

Kornienko E.E. Results of Cb seeding experiment with the goal of artificial precipitation regulation. J.*Trudy UkrNIGMI*, **187**, 3-25, 1982.

Krauss T.W., W. Shaw, A.A. Sinkevich and V.S. Makitov, Cloud seeding in India and physical and statistical assessment of the results. *Russian Meteorology and Hydrology*, **7**, 24-33, 2006.

Krauss T.W., A.A. Sinkevich, and A.S. Ghulam, Precipitation characteristics of natural and seeded cumulus clouds in the Asir region of Saudi Arabia. J. *of Weather Modification*, **42**, 61-77, 2010.

Krauss T. W., A.A. Sinkevich, N.E. Veremey, Yu. A. Dovgaluk, and V.D.Stepanenko, Investigation of the large vertical depth Cb (Andhra Pradesh province, India, 2004, September 28). *Russian Meteorology and Hydrology*,**1**, 30-42, 2007.

Krauss T.W., A.A. Sinkevich, N.E. Veremey, Yu. A. Dovgaluk, V.S. Makitov and V.D.Stepanenko, Complex investigation of cumulonimbus characteristics developed over the Arabian peninsula in a very dry atmosphere. Part1: in situ observations and numerical modeling. *Russian Meteorology and Hydrology*, **2**, 44-59, 2011.

Vali, G, Aircraft Studies in the Asir. Univ. of Wyoming, Dept. of Atmos. Sci., *Report No. AS163*, 113pp., 1991.

Sinkevich A.A., J.Y. Kim, A.S. Suh, H.S. Chung, Losses in the Korean economy due to lack of routine cloud seeding. *J.of the Korean Meteorological Society*, **37**, 283-294., 2001

Sinkevich, A.A., T.W. Krauss, Cloud seeding in Saudi Arabia, statistical assessment of the results. *Russian Meteorology and Hydrology*, **6**,.26-37, 2010.

Retrieval of Cloud Liquid Water Content Distribution at Vertical Section for Microwave Radiometer Using 2D Tomography

Zhou Jun[1] , Lei Hengchi[1], Chen Hongbin[1], Wang Yanfei[2], Zhao Zhen[1], Ji Lei[3]
1 Institute of Atmospheric Physics, Chinese Academy of Sciences, Beijing 100029,
2 Institute of Geology and Geophysics, Chinese Academy of Sciences, Beijing 100029
3 Beijing Weather Modification Office, Beijing 100089

1. Introduction

The studies of retrieving 2D or 3D distri butions of cloud liquid water content (LWC) from the airborne or ground-based microwave radiometer (AMR or GMR) using tomography begun in the 1980s (Warner and Drake, 1985). So far, some problems still exist. Take the AM R for an example. Firstly, the inverse problem is a limited-angle image reconstruction which is ve ry underdetermined. This paper tries to enhance the well-posedness of this inversion by improving both hardware constitution and retri eval method. Secondly, the radi ative transfer equation (RTE) is non-linear. In springback research, RTE was linearized by Taylor expa nsion (Drake and wa rner, 1988) or solved by linea r iteration algorithm (LI) (Warner and Drake, 1985, Huang et al, 2008a, 2008b) to simplify th e inversion. This paper discusses the relationship between LWC and the n onlinearities of RTE and suggests a nonlinear iteration algorithm (NLI), L-BFGS-B, to solve the inverse p roblem. Finally, there is a l ateral boundary problem i n the microwave tomography because of the restriction of the observation platform. As sho wn in Fig. 1, the Yun-12 plane carrying A MR flies alo ng the clo ud base while two antenna s continue scanning alternatively. If the distribu tion of LWC in the latera l boundary is unknown, some grids will not be scanned by the sl anting antenna which will intensify the underdetermination of the inverse problem. In springback research，the LWC in lateral boundary is simply supposed to be ze ro (Drake and Wa rner, 1988, Huang et al, 2008b) or su pposed can b e obtained from radar or cloud model (Bobylev, 1997). Such assumptions restrict the applicaion of AMR. Besides, there was no discussion about the influence of the uncertainty of the LWC in late ral boundary on retrieval accuracy. In fac t, the micro wave frequency of AMR (31.65GHz) is very sensitive to LWC, so this kind of uncertainty may lead to bad retrieval accuracy. In this pap er, the retrieva l model will fall into two types according to the LWC distri bution in the lateral boundary is kno wn or unknown and they are called LB and NLB for short. LB model will b e used to do some sensitive tests. For NLB model, the nesting retrieval method is developed in order to make th e microwave remote sen sing of LWC distribution s independent of other i nstruments and not limited to the horizontal scale of cloud.

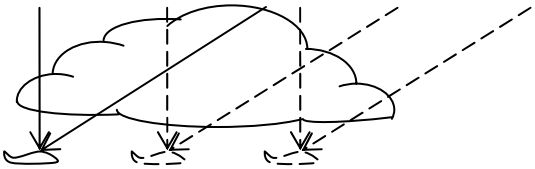


Fig. 1. The diagram of observation

2. Nonlinearity of RTE

RTE can be written as follows:

$$\tau(s_0,s_1)\int_{s_1}^{s_2}\underline{\underline{ka(s)}}T(s)\underline{\tau(s_1,s)}ds \qquad (1)$$

$$=Tb\text{-}Tb(\infty)\cdot\underline{\tau(s_0,\infty)}-\underline{\tau(s_0,s_2)}\int_{s_2}^{\infty}ka(s)T(s)\tau(s_2,s)ds\text{-}\int_{s_0}^{s_1}ka(s)T(s)\tau(s_0,s)ds$$

where τ ,T, ka, Tb and $Tb(\infty)$ represent the transmittance, temperature, abso rption coefficient, observed brightness temperature and the co smic background radiation respectively. S0 denote s the position of the AMR. S1 and S2 denot e the positio n where the beam goes into and out of the retri eval area. At each iteration of LI, the variables with double underline are unknown while the variables with single underline are computed from the outp ut of the last iteration. In this way, RTE tak es the form of the Fredholm integral equation of the first kind. It can b e seen that the nonlinearity of RTE will be strong if the dependence of τ on ka (or on LWC if the background parameters like tempe rature, moisture and pre ssure are known) is strong.

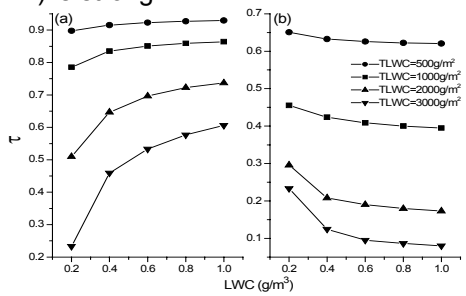


Fig. 2. The variation of τ with LWC, TLWC is amplified by increasing the cloud th ickness (a) up wards and (b) downwards.

Corresponding author address: Zhou Jun, Laboratory of Cloud-Precipitation Physics and Severe Storms (LACS) Institute of Atmospheric Physics (IAP), Chinese Academy of Sciences (CAS). De Sheng Men Wai Qi Jia Huo Zi, Chao Yang District, Beijing 100029, P. R. China. E-mail: xwoman19810919@163.com.

Fig. 2 shows that the dependence of τ on LWC becomes stronger as the total liquid water content (TLWC) increases.

Then the effect of TLWC on the retrieval efficiency of NLI and LI is investigated. To save space, only the conclusion derived from the numerical simulations is given here. NLI possesses broader scope of application, faster convergence rate and retrieval accuracy than LI and the predominance of NLI over LI is more obvious as the TLWC increases.

3. Retrieval method

Considering the horizontal continuity and the possible maximum value of LWC in the nonprecipitating cloud, Tikhonov regularization and double-side constraint are adopted to guarantee the well-posedness of the solution,

$$\min\left\{\left\|\boldsymbol{F}(\boldsymbol{x})-\boldsymbol{b}\right\|_{l_2}^2+\alpha\cdot\Omega(\boldsymbol{x})\right\},\quad 0.0\le \boldsymbol{x}\le 1.0 \qquad (2)$$

where $\boldsymbol{x}$, $\boldsymbol{F}(\boldsymbol{x})$ and $\boldsymbol{b}$ denote the unknown LWC vector, RTE and the observed values, α and $\Omega(\boldsymbol{x})$ denote the regularization parameter and regular term. The discrete form of the norm in $W^{1,2}$ space (W operator) (Wang et al, 2006,2008) and Laplace operator (L operator) (Wen Junhai, 1999) are used as the regular term for LB and NLB respectively. Morozov's discrepancy principle or L-curve method is used to determine the optimum α. The L-BFGS-B algorithm is applied to solve this nonlinear optimization problem. Sometimes mean filter is used to improve the quality of the retrieval image.

4. Numerical simulation

Five cloud types are artificially constructed for numerical simulation. Four of them are shown in Fig.3, where the area in the rectangular frame is the target area and the area out of the rectangular frame is lateral boundary. The fifth type is the homogeneous cloud with LWC of 0.1g/m3. The target area is $4km\times 20km$ and the area of the lateral boundary depends on the angle of the slanting antenna.

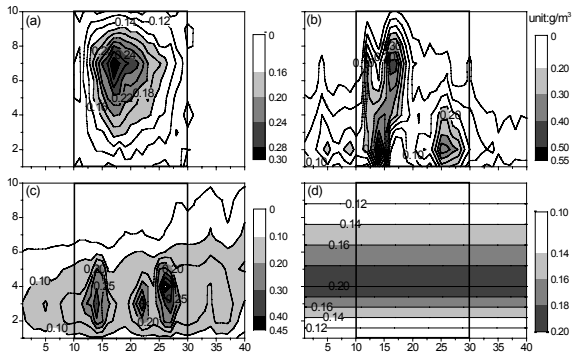


Fig. 3. Simulated 'true values' of LWC of typical cloud types: (a)weak onion cloud (b)broken cumulus cloud (c)stratocumulus cloud (d) horizontal homogeneous cloud; X-axis is the horizontal grid and Y-axis is the vertical grid.

Here are the parameters of the detection system, the flight speed is 70m/s, the beamwidth of antennas is 4.2°,the sampling frequency is 1.7Hz and the noise of the radiometer receiver is 0.2k.

4.1 LB model

4.1.1 The best combination of the double antenna elevation angles

Restricted to the loading capacity of the YUN-12 plane and the instrument itself, the AMR only has two scanning angles. Koldaev et al (1990) and Drake and Warner (1988) took (30°,90°) and (45°,135°) as defaults respectively. This paper determines the best combination of the scanning angles from analysis and numerical simulations. Two factors should be taken into consideration. Firstly, a vertical beam can make the solution more stable because the intercepts of the grids where the beam passes through are equal which means that every unknown has the same importance in the RTE. Secondly, if the angle between the two antennas is closer to 90° the information obtained from them will be less relevant to each other. But if the effective detection distance of AMR and the influence of the antenna sidelobe are considered, the minimum elevation of antenna should be not more than 30°. In conclusion, the best combination of the double antenna angles should be (30°, 90°). The results of numerical simulations (Fig.4) confirm the above deduction.

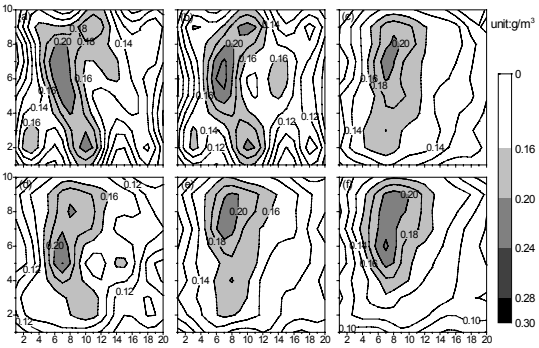


Fig. 4. Retrieval image of weak onion cloud using different combinations of double antenna elevation angles: (a) (30°, 120°); (b) (45°, 135°); (c) (30°, 90°); (d) (45°, 90°); (e) (60°, 90°); (f) (75°, 90°)

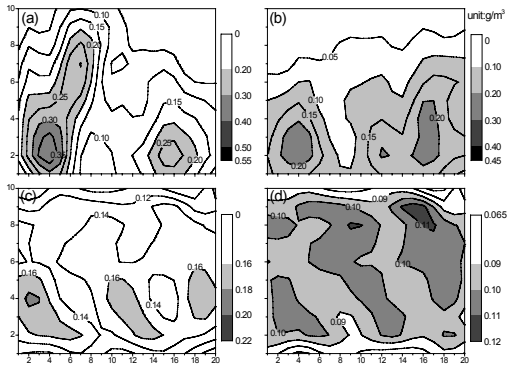


Fig. 5. Retrieval image:
(a) broken cumulus cloud, (b)stratocumulus cloud,
(c) horizontal homogeneous cloud, (d) homogeneous cloud

4.1.2 Retrieval results of five typical cloud types

The retrieval results of the five typical clouds show that the relative error is 8.6% -12.3% and the structure of different cloud types can be mainly showed in the retrieval images (Fig.4-Fig.5). There is some distortion in each image and they are caused by the deficiency of the scanning angles which will be confirmed in the sensitivity tests in next part.

4.1.3 Sensitivity studies

Sensitivity tests have been done to investigate the factors which affect the retrieval accuracy. Conclusions are listed here to save space. Relative error decrease by 4.7%~8.4% (unfiltered) and the distortion of images is reduced obviously when the number of scanning angles increases from two to seven under the present performance index of instrument. If the number of scanning angles continue to increase, the sampling frequency should increase too, otherwise the retrieval image will be worse because of the insufficient detections from each scanning angle. (Fig.6)

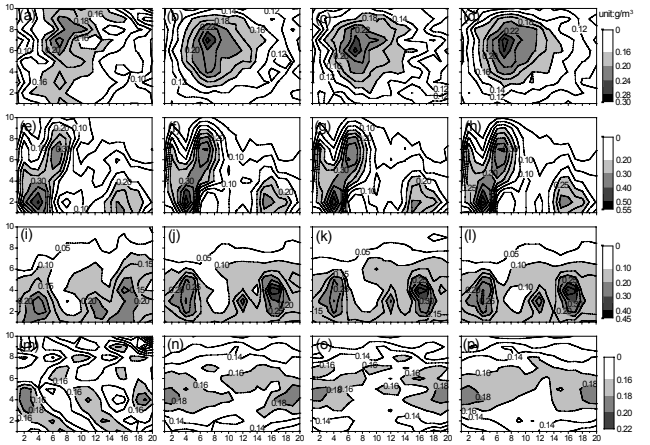


Fig. 6. Retrieval images of (a-d) weak onion cloud, (e-h)broken cumulus cloud, (i-l) stratocumulus cloud and (m-p) horizontal homogeneous cloud with different angle resolution: (a, e, i, h) two projecting angles (sampling frequency is 1.7Hz); (b, f, j, n) seven projecting angles (sampling frequency is 1.7Hz); (c, g, k, o) twenty-five projecting angles (sampling frequency is 1.7Hz); (d, h, l, p) twenty-five projecting angles (sampling frequency is 4.9Hz)

Besides, the retrieval accuracy is improved obviously while the radiometer noise level is decreased through hardware or software technique. The retrieval accuracy varies in different cloud types because of the magnitude of the LWC, the characteristic of the regular operator and the lateral boundary factor. The uncertainty of LWC in lateral boundary affects the retrieval accuracy obviously.

4.2 NLB

Nesting method is developed to retrieve the more general NLB model. In this method NLB model with L operator is used to retrieve the LWC distribution at lateral boundary roughly, then LB model with the W operator is used to retrieve the LWC distribution at target area more precisely. The nesting retrieval result of the clouds whose LWC distribution in target area is unicentric and in lateral boundary is multi-centric, horizontal homogeneous or homogeneous shows that the position of the LWC center in target area is much more accurate than in retrieval area (i.e. the retrieval result of NLB) and the retrieval error in target area is 10.8%~11.4% (Fig.7). The nesting retrieval result of broken cumulus cloud and stratocumulus cloud show that the retrieval error in target area is 12.8% and 16.8% respectively. If the number of projecting angles increase from two to seven, the retrieval error in target area of the above-mentioned clouds decrease by 2.6%~7.1% and the distortion of the retrieval images decrease obviously (Fig.8).

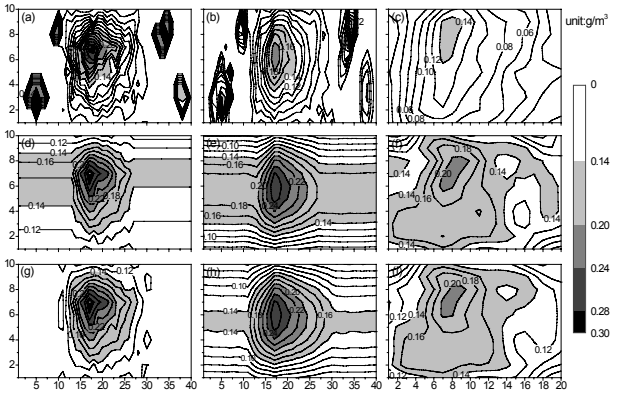


Fig. 7. Simulated 'true values' (a, d, g) and the retrieval images of their retrieval area (b, e, h) and target area (c, f, i) with two scanning angles using nesting method.

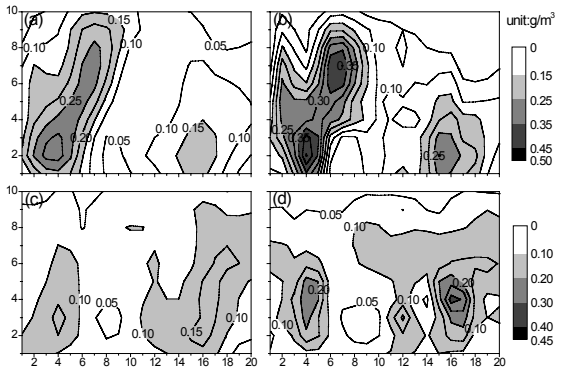


Fig. 8. Retrieval images of (a, b) broken cumulus cloud and (c, d) stratocumulus cloud using nesting method: (a, c) two scanning angles; (b, d) seven scanning angles

5 Discussion

The insufficiency of the scanning angles significantly affects the retrieval accuracy. How to solve this problem through improving the detection pattern or retrieval method is worth further discussing.

Several limiting conditions should be noted in practical application. Firstly, only nonprecipitating cloud or the cloud in which rain rate is less than 1mm/h can be retrieved because the scattering is ignored in the RTE used in this paper. Secondly, the detection must be accomplished quickly enough that the LWC distribution doesn't change obviously. Finally, the flight path should keep straight and

horizontal to make all the beams in the same vertical section.

Acknowledgements

I am grateful to professor Wei Chong and professor Shen Zhilai for their helpful suggestions and continuous encouragement. This research is funded by the national natural science foundations of China (grant No. 40805056 and No. 40775025) and the country plan to support science and technology project (grant No. 2006BAC12B00-01-01).

References

Bobylev L P. Retrieval of liquid water distribution in convective clouds using microwave computerized tomography [J]. *Geoscience and Remote Sensing*, **2**: 830-832, 1997.

Drake J F, Warner J. A theoretical study of the accuracy of tomographic retrieval of cloud liquid with an airborne radiometer [J]. *Journal of Atmospheric and Oceanic Technology*, **5**: 844-857, 1988.

Huang Dong, Liu Yangang, Wiscombe W. Determination of cloud liquid water distribution using 3D cloud tomography [J]. *J. Geophys. Res*., **113**, D13201, 2008a.

Huang Dong, Liu Yangang, Wiscombe W. Cloud tomography: role of constraints and a new algorithm [J]. *J. Geophys. Res*., **113**, D23203, 2008b.

Koldaev A V, Melnichuk Y V, Mironov A F, et al. The application of aircraft microwave radiometric tomography in weather modification experiments [C]. 20th European Microwave Conference, Budapest, Hungary. **2**: 1402-1407, 1990.

Warner J, Drake J F. Determination of cloud liquid water distribution by radiometric data [J]. *Journal of Atmospheric and Oceanic Technology*, **2**: 293-303, 1985.

Wang Yanfei, Fan Shufang, Feng Xue, et al. Regularized inversion method for retrieval of aerosol particle size distribution function in $W^{1,2}$ space [J], *Appl. Opt*., 45, 7456– 7467, 2006.

Wang Yanfei, Yang Changchun, Li Xiaowen. Regularizing kernel-based BRDF model inversion method for ill-posed land surface parameter retrieval using smoothness constraint [J]. *Journal of geophysical research*, **113**, D13101, 2008.

Wen Junhai.. The study of methods about limited angle image reconstruction[D]. Ph. D. dissertation (in Chinese), Xi'an Jiaotong University. **103** pp, 1999.

Forum on "GEO-ENGINEERING AND CLIMATE CHANGE"

On Thursday 6 October 2011, following the WMO Scientific Conference on Weather Modification, an evening Forum related to the "Technical Underpinning and Key Issues on Geo-Engineering Research" is organised at the same venue. This Forum is viewed as an event aimed at encouraging scientific debate in the multidisciplinary fields relevant to Geo-Engineering research and climate change. The participants of the Conference are encouraged to attend the Forum and to contribute to open discussions that will follow introductions of the invited speakers – experts in their respective fields.

Forum Agenda

Chair: Roelof Bruintjes
Panel Members : Roland List, Jean Pierre Chalon, Deon Terblanche, and Masataka Murakami
Rapporteurs:

Thursday 6 October 2011: 20:00 – 22:00

Roelof Bruintjes, NCAR, USA
Introduction to Geo-Engineering and Climate Change (10min)

Jean Pierre Chalon, FRANCE
Geo-Engineering ideas and practicality (10 min)

Roland List, CANADA
Geo-Engineering and environmental and Societal impacts (10 min)

Deon Terblanche, WMO
WMO perspecyives on Geo-Engineering (10 min)

Masataka Murakami
International perspectives on Geo-Engineering (10min)

Open Forum Discussion

Lessons learned from 50 years of cloud seeding in Israel

Zev Levin

Department of Geophysics and Planetary Science
Tel Aviv University, Israel

Rain enhancement in Israel has been going on from the early 1960's to today. It consisted of three experiments and an extended period of operational seeding. These experiments were accompanied by extensive research including measurements, model simulations and statistical analysis. Although questions have been raised about the success of these operations, attempts to transfer the Israeli seeding methods to other countries have failed to show positive results. In the presentation I will show results of our re-analysis of the full period of seeding in Israel and point out the lessons we can learn from this extensive effort. I will also point out that the lessons we learned from our own operations led to a design of a new experiment, Israel 4, in which seeding will take advantage of the orographic setting in the NE of the country.

REINVENTING WEATHER MODIFICATION

Roland List

Department of Physics, University of Toronto, Toronto, Canada

1. The state of weather modification

Over the past 2-3 decades the science of Weather Modification, WM, has barely moved forward. Very few new randomized experiments,designed for statistical evaluation, have been started. No consolidation of testing of several similar operations into one project has been consideredwithin individual countries or internationally. This despite the economic and scientific gains they could produce. Each WM experiment has been and still is small in scale, and often meteorological data collection is minimal and no records are being kept for later extended evaluation. Further, there is little advance in knowledge of the physics of precipitation. Mostly case studies are being presented at the WMO Scientific WM conferences, often with a content which would not let them pass a reviewing process. Further, noscientific synthesis of the results of in-country achievements is being done.

The biggest disappointment is the lack of application of statistical methods as developed by Prof. Ruben Gabriel (2002) whoproposed, among many other things, an assessment of multiple experiments or of Dr. Bernie Silverman's successful statistical assessment of long-duration *operations*. He made statistical processing of operations after 50+ years possible,but opportunities in WM operations are beingsquandered by not leavingsingle areas unseeded for comparison. Further, List(2004) proposed away of assessing the effect of seeding in every seeding unit (day) rightafter execution by a bootstrap procedure which would require a relaxation of the "blindness" rule or its modification. There has been no follow up discussion.

Of note is also the lack of infusion of new ideas and efforts into cloud modeling. Why not discard "mathematical" turbulence and simulate "wake turbulence" with its flow of organized vortices (similar to the global circulation). Turbulent flow is not a continuum of singularities!It follows the Navier-Stokes equations.

The Working Group on Cloud Physics and WM (formerly an EC panel) has not developednew ideas and concepts. It seems to have used its sessions to "*word-smithing"* the WMO Statement on WM and the connected guidelines. It has provided little leadership, if any. Thus, its demotion from the status of Panel of the WMO Executive Council was to be expected. Becoming an entity under the Commission of Atmospheric Sciences, controlled by dynamicists and climate affichionados (don't forget the atmospheric chemists and radiation specialists which are closely attached to climate change), could be suffocating.

Positive achievements are: the application of remote sensing by satellite, the improvement of the delivery systems for seeding agents, and the development/improvement and testing of very effective new seeding materials.WM statistics has reached a very high level -unfortunately, none of the new concepts has been applied.Further, the successful operationaldispersal of warm and cold fog at airports has lost most of its glamor because aircraft landing systems are working now at zero visibility.

In summary, Weather Modification, after some significant successes in its earlier decades (List, 2003), is barely surviving and may not even qualify for palliative care. The scientific community has not spent much effort to understanding the underlying physics, and past progress is being disregarded or has never been understood.

In defence of this situation it has to be stated that the seeding of convective clouds is

very difficult because many details of how clouds work are unknown and very difficult to assess.

Among the specific reasons for the debacle are:

(i) Piece-meal individual experiments;

(ii) Difficulties in getting proper statistical advice;

(iii) Lack of funding to provide adequate scientific and technical infrastructure;

(iv) Lack of funding due to lack of convincing results or proposals with insufficient scientific merit;

(v) Lack of multi-national experiments and/or coordinated and co-evaluated modification experiments;

(vi) Forgotten past achievements;

(vii) The general trend in Meteorology towards larger scales;

(viii) Loss of specialists in cloud dynamics, seeing greener fields in climate change;

(ix) Field not made attractive enough for bright students.

It has become obvious that the *scientific* objective of WM has been forgotten, it has also not been recognized as the main driver of an appropriate program and activity: **UNDERSTANDING THE PHYSICS OF PRECIPITATION IN ALL ITS FORMS**. In this context WM is used to test newly developed science and to see if modification of clouds induces reactions and new processes as predicted.

2. The precipitation treatment in climate change models

The lack of scientific understanding is the reason for the stalled WM. But it is much more than that and also applies to Climate Change Modeling! Precipitation forecasting of convective systems has always been difficult and is not particularly successful – as any forecaster knows. Thus, it was no surprise that (~ 10 years ago) the administrator of NOAA, General Kelly, chided the climate modeling community at a town hall meeting during an AMS annual assembly for the lack of credibility of predicting precipitation in climate forecasts. This has not changed since. There is some basic concept, linking solar input, concentrated mostly in the equatorial regions, to the pole-ward transport of energy involving H_2O. How this is partitioned into longitude and then broken down into 30x30 km pixels is murky, to say the least. Now, climate change modelers are preparing for 10x10 km grids. That also will involve higher resolutions of precipitation climate forecasts. What a travesty!

I have observed that climate modelers are at great pain to explain the basis of precipitation modeling during climate change. One leader told me that it is linked to temperature!?

The secret to proving absurd research results is simple. It is by incorrectly applyingensemble models. Scenario: a group of modelers from the world's top centers is getting together and discusses the issue. One makes a suggestion. In lack of anything better they all agree, go home and run their models based on similar assumptions. Let us now assume that another one, who did not attend the "crucial" meeting, makes the right assumptions. After a while, the model results are then compared in an ensemble model. Guess what: The ones modeling with the agreed upon assumption turn out to be "correct", while the one with the correct model produces outlayer points – and thus, his model has to be rejected. QED.

The *measurement of precipitation* has always been a sore point in Meteorology, considering that ~ 170 different rain gauges have been used all over the world. Precipitation is not only an issue in meteorology but also in agriculture, forestry and other services and institutions. In other words, precipitation data could not easily be assembled and compared on a national, continental or world scale. The algorithm

for this gigantic problem was put together by the DeutscherWetterdienst in Offenbach, which operates the *Global Precipitation Climatology Centre, GPCC*. It *"analyses the monthly precipitation on earth's landsurface based on raingauge station data. It supports global and regional climate monitoring and research and is a German contribution to the World Climate Research Programme (WCRP) and to the Global Climate Observing System (GCOS)"* [from the DWD Webpage].No climate modeler I have met was familiar with this operation and the available datasets.

Precipitation is a factor in climate that is as important as temperature. To me "no rain is desert, rain is life". Thus, it requires respect and not avoidance and circumvention. A group at ECMWF is using statistics to replace cloud physics. "It produces better and reproducible results and does not have the same complexity". Statistics has its place in physics, but not this one. Unfortunately, this approach is getting common in science and engineering – where it becomes detached from and insensitive to science.*We will not, we cannot find a solution to the climate/precipitation question unless we concentrate on the physics.* This takes manpower and time. Example: In 1963 I published a new theory on hail growth including the growth "spongy ice". Within a few month I will submit a new theory based on four *new* variables (instead of the old six), with new insights and simplifications. It is based on 60 years of numerous laboratory and theoretical studies as well as Doppler radar investigations, all condensed into > 130 scientific papers and 29 PhD and 39 MSc theses. Imagine what could be done with 10 dedicated groups?

3. The goal of "Experimental Meteorology, EM"

This title implies that the name "Weather Modification" should be upgraded to "Experimental Meteorology" (or similar), not just because of the witchcraft connotations associated with WM, but also to express the much wider range of the issues. ["Experimental Meteorology" was the title of what is now recognized as the first international conference of both "Cloud Physics" and "Weather Modification", held in Zurich in 1954 (List, 2003). It could also include "Geoengineering", the large scale modification of climate (and hurricanes)[not including the oceans].

Going back to the basics reveals the double purpose of the "old" WM. (i) WM is the test bed for the science we develop in Cloud Physics. All the combined research from the laboratory, observations and measurements in nature, results of models, mathematical assessment procedures, etc. need to be tested in order to establish how nature really works. This requires field experiments for the verification of concepts and theory, through testing of how the clouds react to specific interferences. This is "scientific" WM. (ii) the second step is to apply the established modification to achieve our needs, be they rain enhancement, hail suppression, fog dispersal orsevere storm moderation, etc. These two remain as major objectives.

The purpose of "Experimental Meteorology"could be described as follows:

(i) Development of the physics and dynamics of the formation of clouds and precipitation.

(ii) Development of testing concepts by designing appropriate modification strategies, technologies and evaluation criteria;

(iii) Interference "in the field" with cloud processes to validate newly developed insights and theories of how precipitation is formed in nature;

(iv) Application to changing precipitation in all its forms and at any scale for economic benefits;

(v) *Creation ofa proper basis for the modeling of the precipitation climate*.

This list is to be expanded should geoengineering become part of the new initiative. The private sector should be involved at all times, considering its substantial contributions to our knowledge in WM and its valuable skills and experience.

We should not restrict our activities to day-to-day WM. We must consider the larger issue and concentrate on precipitation in general. Rain

is more than a local phenomenon, it is also a key component of the climate system.

4. Strategy of approach

What is needed is a plan detailing the scientific and technical components and setting specific large and small-scale goals of complex experiments. That may involve new measuring platforms such as fully equipped drones for small scale measurements in large systems, mobile ground Doppler radars to measure particle size distribution and updrafts aloft, Navier-Stokes-based models of turbulence in updrafts, etc.Planning for different research phases is preferable because the financial resources to be asked for are easier to obtain after demonstrating success in a step-by-step program. If no official committee can be setup due to lack of financial resources, then a group of individuals could lay out a scientific plan and find associates to contribute parts. Meetings, if necessary, can always be arranged at the time of conferences where expenses are covered by other bodies.

Remember, the key issue is the science, funding will come later. However, it is advisable to be prepared for a big fight should a piece of the lavish funding of climate change research (at the tune of several billion $/annum) be part of our desires. This would also be the main reason for the climate modelers to defend the validity of their questionable treatment of precipitation – unless a compromise can be reached. It is expected that the Intergovernmental Panel on Climate Change, IPCC, will defend its position up to the last stand.

There are two possibilities: (i) Go through the UN with a proposal to “regulate” and “closely monitor” Geoengineering, GE, with the scientific goals relating to precipitation attached; (ii) to go through WMO Congress or its Executive Committee, EC. I may approach the UN SG about the regulatory issues concerning GE. I know that his advice might be to go through a UN Member (country). This is also the way to proceed with WMO. However, within WMO, there is only one chance for survival: to become a Panel of EC again by a scientifically sound, important and large-scale proposal, independent of CAS. (WMO EC and Congress in particular have a great interest in WM (rainmaking) due to the “overheating” and drying out of many countries.

Should Geoengineering be the goal, then the steering body, the Intergovernmental Panel on Precipitation or IPP would have to be a UN body because it has to deal automatically with economic, legal and re-insurance issues. This would not prevent WMO from becoming the host of IPP, as it is now for IPCC.

In principle, precipitation issues should really be part of IPCC. However,IPCC has not husbanded its scientific resources well by *not*recognizing the need for improving the knowledge of the Physics of Precipitation. It is partner in the suppressing and misjudging of a key component of climate: precipitation. The IPCC would only become acceptable after a total turnover of its leaders, a revamping of its goals and a fair distribution of resources. Further, those resources need substantial expansion. [In my estimation the price tag of testing of a single climate modification concept, including the assessment of its technical feasibility may well be >$100 billion.]

Some of us may know WMO EC members or a WMO Permanent (country) Representative. They could be the conduits for getting Meteorological Experimentation on the meeting agenda. Afterwards, only the quality of the proposal counts. Note that there will be no funding for research alone, direct applications have to be included.

One small example:As the representative of IUGG with WMO I had successfully launched the IAPSAG initiative toassess the impact of manmade aerosols on precipitation at theWMO Congress XIV (2003). The study itself was first led by Prof. Hobbs and, after his death, by Profs. Z. Levin and W.R. Cotton. This study waspublished in book form by WMO and IAMAS, the International Association for Atmospheric Research (Levin and Cotton, 2008). It serves as an example of what can be done by committed top scientists.

5. Final comment

It is up to the Cloud Physics and Weather Modification Community to work out a proposal for Experimental Meteorology. Do we have the leaders, the dreamers, the visionaries and the hard workers to put an exciting scientific plan together to study the Physics of Precipitation with the purpose of establishing how sufficient precipitation can be obtained and maintained in a

changing climate. A further purpose is the substantial improvement of the credibility, quality and predictive power of climate change models. Better understanding of the mechanics of damaging weather systems can and will further lead to their successful modification. This is not easy to achieve, but it is also not pie in the sky.

A footnote: When talking to climate modelers always ask for an explanation of how precipitation is included.

References

Gabriel, R., Confidence regions and pooling – some statistics for weather experimentation. J. Appl., Meteor., 41, 505-518, 2002.

Levin, Z., and W. R. Cotton, Aerosol pollution impact on precipitation: a scientific review. Springer Verlag, Berlin, pp. 407, 2008.

List, R., WMO weather modification activities, a fifty year history and outlook. 8th WMO Scientific Weather Modification Conference, Casablanca, Morocco, 7 April, WMP Report No 39, 1-10, 2003.

List, R., The 1954 International conference on experimental meteorology in Zurich, Switzerland (A historical note), Proceedings 14th Intern. Conf. Cloudsand Precipitation, Bologna, Italy, 19-23 July, Vol. 2, 858-860, 2004.

List, R., Weather modification - A scenario for the future.*Bull. Amer. Met.*Soc., 51-63, January. 2004.

The race for ice.

Gabor Vali
Department of Atmospheric Science
University of Wyoming
Laramie, WY 82070, USA

Cloud seeding seeks an edge in generating more ice crystals than what would form without seeding. This race is not easy to win.

Seeding of supercooled clouds with ice nucleating particles like silver iodide in order to increase rainfall, to dissipate clouds, or to reduce hailstone sizes has been the mainstay of weather modification efforts ever since the discovery of that possibility 65 years ago. The basis for this is the relative paucity of ice particles in clouds that do not reach the temperature required for freezing by homogeneous nucleation (roughly -35°C). However, as is well known, there is enormous variability in how much ice is found at any given temperature so that the opportunities for glaciogenic cloud seeding are very difficult to predict and to quantify. This situation is in stark contrast with the condensation of clouds and the relatively simple relationships between the properties of the aerosol, the CCN, and the cloud droplet populations that develop. Not that there are no outstanding questions in that area as well.

There are three possible approaches to ascertain whether the degree of paucity of ice particles in a given cloud allows seeding to provide a significant margin and thus to consider the cloud "seedable". First, based on general knowledge from prior experience about ice concentrations under prevailing conditions. Second, by numerical cloud models, with assumed ice nucleus concentrations or, at least in principle, with measurements of the ice nucleus content of the air in which the cloud is expected to form. Third, by direct measurements either of the ice particle concentration or of the amount of supercooled water content. One of these methods, or combinations of them, are in use in glaciogenic cloud seeding projects.

The purpose of this paper is to provide a brief review of recent advances in knowledge about the first two of the approaches listed above, i.e. how well can ice concentrations in clouds be predicted. Methods of in situ and remotely sensed measurement techniques are not discussed. By its more usual description of "ice initiation in clouds" the subject of this brief review is known as one of the major unknowns in weather and climate prediction and in climate change estimates.

The basic elements governing of ice formation in clouds are fairly well known qualitatively: ice nucleation, secondary processes and cloud dynamics. Of course, each of these titles covers many complex processes. All of them are subject to the full impact of atmospheric variability on many spatial and temporal scales.

Ice frequencies:

Finding any regularity in the observations of ice particle concentrations in clouds has been an elusive goal. For practically any temperature, the observations may range over a factor of 100, or even more if one includes those below the detection limit and above the overload condition of the in situ instruments. The main generalization possible is that the likelihood of finding supercooled water decreases rapidly as the temperature is lowered from 0°C toward -15°C.

The advances of recent years in this generally unyielding area of research are significant, even if limited. Notable is the degree of detail that is

becoming available through combined in situ and remotely sensed data from clouds of moderate complexity, most clearly from wave clouds. Specially important is that the remote sensing data can provide essentially instantaneous pictures of the quantity and velocity of hydrometeors over very large cloud volumes. This enables diagnoses of processes to be much more complete and more reliable and it allows more demanding model comparisons.

New observations show that ice development in some winter clouds is limited even at temperatures as low as -15C. On the other hand, lofted snow from the surface can introduce ice into clouds essentially forming another variant of the seeder-feeder arrangement.

Progress is also being made in the retrieval of information from remotely sensed (radar, lidar and radiometer) data. Whereas the individual measurements quantify integrated quantities (volume backscatter, attenuation, polarization, etc.), taking advantage of the wavelength dependence of the measurements to the sizes and shapes of particles opens the ways to obtain information on ice water content and perhaps on ice crystal concentration.

Ice nucleation:

All available data on ice nuclei (IN) in the troposphere show large variations in time and location with only very rough general trends like the dependence on temperature. The dependence of IN on readily obtained measures of aerosol composition is highly elusive. Thus, predictions for specific cases are unreliable.

The development of measurement techniques for ice nuclei (IN) have taken a spurt in the last several years. While the measurements still cannot fully reproduce the range of atmospheric conditions that influence the activation of ice nuclei, there is improvement in that regard. There is better understanding of the impacts of the limitations that remain and there is an overall increase in the credibility of the IN measurements. At the last inter-comparison workshop of devices in 2007 significantly greater agreement was found among different instruments than could be demonstrated before. Also, knowledge about the ice nucleating abilities and about the atmospheric abundance of various substances have expanded significantly. These empirical advances are not matched by progress in theory. The fundamental parameters of heterogeneous ice nucleation are known only in rather vague terms as a result of problems associated with theoretical analyses of irreversible processes at the molecular scale and with the characterization of surface irregularities that play a role in ice nucleation.

Cloud seeding:

The other side of the competition is the ability to generate and introduce artificial ice nuclei into clouds. Engineering and logistical challenges are great. Prediction of the dispersion of seeding material is difficult.

The evaluation of what is being achieved in practice by cloud seeding has all the same problems and advances than the determination of ice formation in unmodified clouds.

The race:

Not surprisingly, this race for understanding and perhaps beneficially influencing the multifaceted process of ice formation in clouds is not a single race, but many. Each cloud type, season and location is a new and different race. Each day may bring surprises, because we know little of the competitors themselves and we can't predict with sufficient precision how they will perform. Therefore, we must proceed with caution, not make exorbitant claims and keep accumulating the knowledge and experience that may clarify how the race is going develop.

NUMERICAL MODELING STUDIES IN SUPPORT OF THE WYOMING WEATHER MODIFICATION PILOT PROGRAM

Daniel Breed, Lulin Xue and Roy Rasmussen*

Research Applications Laboratory, National Center for Atmospheric Research, Boulder, CO 80307 USA

1. FORECAST MODEL – WRF RTFDDA

The Weather Research and Forecasting (WRF) model and the Real Time Four Dimensional Data Assimilation (RT-FDDA) system is used in operations to guide forecasters on expected conditions specific to seeding criteria, particularly concerning the existence and persistence of super-cooled liquid water. The WRF RT-FDDA modeling system for the Wyoming Weather Modification Pilot Program (WWMPP) is nested down to a 2 km horizontal grid with 3-hr observation input and nudging of initial conditions, producing 24-hr forecasts. Several display features (maps, cross-sections, site locations, etc.) have been customized to the WWMPP, including plume trajectories from individual seeding generators into the target regions. Figure 1 shows an example of forecast wind trajectories from the AgI generators and cloud water content with the target and control sites denoted by circled red "T"s and circled black "C"s respectively.

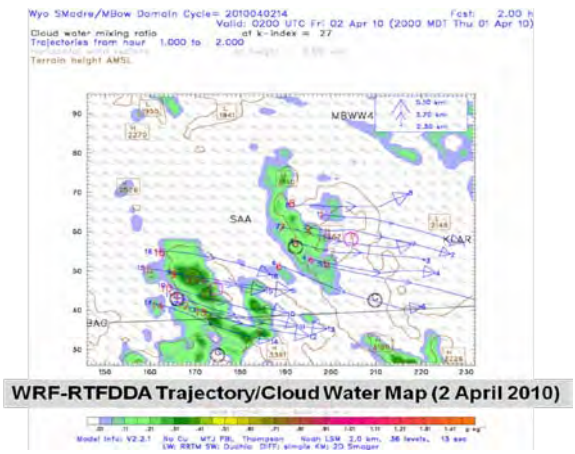


Figure 1. *Example plan-view plot of a 2-hr forecast of cloud water and trajectories over the southern ranges of the WWMPP on 2 April 2010. Cloud water contour scale is at the bottom of the figure. One-hour trajectories (with a 30-min arrow indicator) originate at AgI generators (1-8 in the Medicine Bows; 9-16 in the Sierra Madres). The size of the arrow is scaled to altitude as indicated in the box in the upper right of the plot. Target (T) areas and control (C) sites are denoted. 3-km winds and topographic contours are plotted in the background.*

*Author address: NCAR/RAL, P.O.Box 3000, Boulder, CO 80307-3000, USA. Email: breed@ucar.edu

2. COMPARISONS WITH OBSERVATIONS

Validating the performance of the WRF RT-FDDA system is an important step toward utilizing it as an evaluation tool for the WWMPP. Measurements collected specifically for the WWMPP can be used for comparisons with WRF results. For example, radiometer liquid water path (LWP) is highly correlated to cloud water content in the model output. A qualitative examination of cloud water occurrence in the model compared with radiometer LWP time-series data showed several periods with good agreement between the two. One such period is shown in Figure 2 for the 5 March 2009 case. A more systematic approach of manipulating the model output to simulate a radiometer scan is being developed to allow a quantitative comparison over an extended period time (several seasons) and provide some insights into the performance of the model.

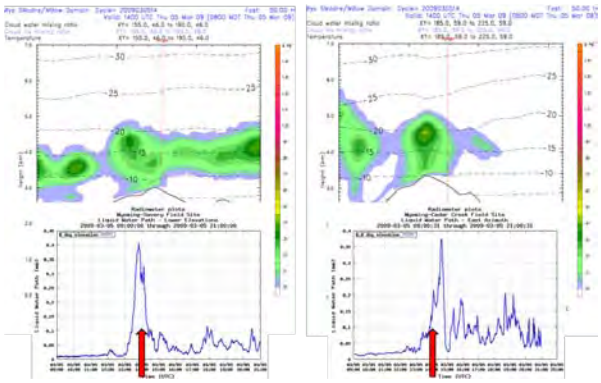


Figure 2. *Cross-sections of WRF-derived cloud water over the Serra Madres (left) and the Medicine Bows (right) with time series plots of radiometer-measured liquid water path indicated below. The red arrows show the time of the model cross-sections.*

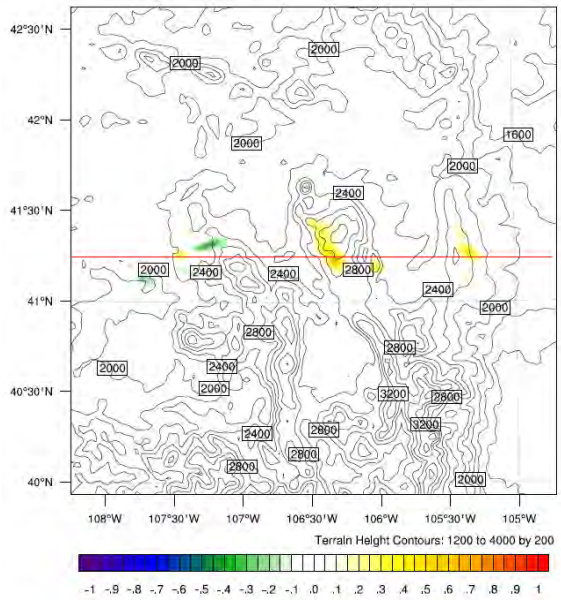
3. DEVELOPMENT OF A SEEDING MODULE

As a first step in evaluating areas potentially affected by seeding, a silver iodide (AgI) point source module was implemented into the Thompson microphysics scheme in WRF. This module follows the parameterization of DeMott (1995), which was based on laboratory studies of the same seeding material employed in the WWMPP. The DeMott parameterization was first used in a modeling study over the Park Range in Colorado (Meyers et al., 1995). Deposition nucleation, condensation freezing,

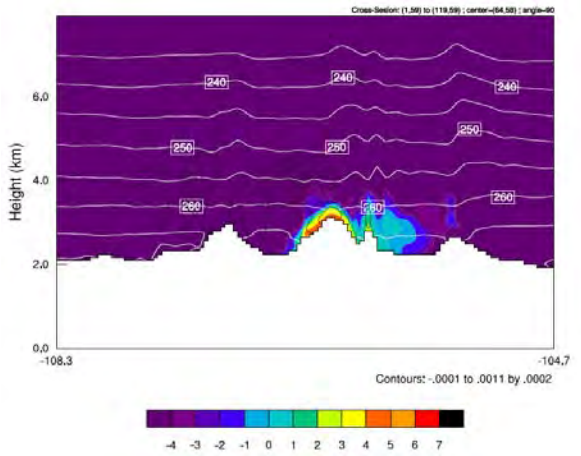
contact freezing and immersion freezing of AgI aerosol are all included in the DeMott parameterization for a variety of temperature and supersaturation conditions. The seeding module uses the parameterization and then allows for number concentrations and mixing ratios of AgI in the air and in different hydrometeors to be tracked in the WRF model. By specifying locations of AgI sources, the seeding module is capable of simulating both airborne seeding and ground-based seeding.

Several idealized and real case simulations have been performed to test this coupled model. Preliminary results show that the model can explicitly simulate the detailed microphysical processes associated with seeding events. Figure 3 illustrates the effects of applying the seeding module to a WRF simulation of a case study in the Medicine Bow area. As can be seen from the yellow shading in Fig. 3(a), the simulated AgI seeding resulted in an increase of about 0.6 mm of snow on the ground over the no-seed simulation. The cross-section in Fig. 3(b), indicated by the red line in Fig. 3(a), further illustrates some of the important processes related to ground-based seeding. For example, the seeding material mixes to a realistic height above the terrain (< 500 m), but also suggests greater dispersion heights downwind of the Medicine Bows due to waves. The cross-section demonstrates the basic conceptual model of seeding in that the seeding material disperses into the boundary layer, gets incorporated into the cloud, and converts supercooled liquid water into ice and snow.

The addition of the AgI seeding module into the WRF model is an exciting application of the model in potentially providing a quantitative evaluation of seeding effects on winter orographic clouds. More recent results will be presented at the conference.



A)



B)

Figure 3. *WRF numerical model output demonstrating effects of an AgI seeding module.* ***A)*** *Plan view map of differences in snow (liquid equivalent) on the ground (in mm) between seeded and no-seed simulations for seeding in the Medicine Bow Range, which is located in the center of the map.* ***B)*** *West to east cross-section (indicated by the red line in* ***A)*** *of temperature in K (white contours), cloud mixing ratio (black contours every 0.2 g/kg starting at 0.1 g/kg), and AgI number concentration in all hydrometeor types (color-shaded areas in logarithmic scale).*

ACKNOWLEDGEMENTS

The Wyoming Water Development Commission (WWDC) of the State of Wyoming is the sponsor of the WWMPP and Barry Lawrence, the program manager representing WWDC, has been extremely supportive in carrying out this work. We also acknowledge the support and efforts of many RAL staff members. NCAR is sponsored by the National Science Foundation.

REFERENCES

DeMott, P. J., 1995: Quantitative descriptions of ice formation mechanisms of silver iodide-type aerosols. *Atmos. Res*., **38**, 63 – 99.

Meyers, M. P., P. J. DeMott, and W. R. Cotton, 1995: A comparison of seeded and nonseeded orographic cloud simulations with an explicit cloud model. *J. Appl. Meteor.,* **34**, 834 – 846.

Numerical Simulation Studies with New Double-moment Explicit Microphysical Scheme in GRAPES

Chen Xiaomin
（**Weather Modification Office of Chongqing, Chongqing 401147, China**
Civillegend@163.com）

Abstract: Based on the dynamic frame of GRAPES model and the Hu Zhijin and Liu Qijun'S cloud physics scheme, a new double-moment microphysical scheme is developed and incorporated in the model. Two Qilian Mountain area precipitation processes and one Chongqing precipitation process are simulated by using the model which contains the new cloud physics scheme.

In the new scheme, both the mixing ratios and number concentrations of cloud water，rain water，cloud ice，snow and graupel are predicted. The influences of the cloud droplet spectrum character and the spectrum growth and change are considered in course of the collision and coalescence of cloud droplets to form raindrops．Use Cotton's(1989) Fletcher Formula and Huffman Formula to describe the ice nucleation process, when temperature is blew 246.15k ,the number concentrations o of ice nucleation must revised. By adding automatic conversion of ice and snow into each other, and cloud water freezing to graupel, the new scheme is incorporated in the GRAPES and becomes a new option in its explicit microphysical scheme. The model which use new cloud physics model is called GRAPES mesoscale cloud resolving model in this paper.

Use the GRAPES mesoscale cloud resolving model, three summer precipitation processes are simulated on August 7 and 10, 2006 in Qilian Mountain area and July 4,2008 in Chongqing . As a whole, model is able to reveal the distribution of precipitation and intensity prediction. The evaluation of the cloud which simulated by the model is basically consistent with the satellite cloud photograph and radar data. Simulate results show that GRAPES mesoscale cloud resolving model has great capability to study microphysics structure of cloud system.

In August, the clouds in the west of the Qilian Mountain region are stratus, mostly due to forced up lift of landform when southwest air stream cross the mountain. The clouds in the east of the Qilian Mountain region are cumulus, mostly due to the horizontal wind shear by the influence of west Pacific Subtropical High. The cloud system of the Qilian Mountain region is constituted by those two different kinds of cloud. In the stratus, cloud ice, cloud water, snow, graupel and rain water can in divide into three layers, the cloud ice and cloud water locate high layer, the snow and graupel locate middle layer ,and the rain water locate low layer. In the cumulus, the distribution of cloud water is wider, other microphysics variables are mixed together.

In Chongqing, the water vapor is extremely rich and the vapor distribution is corresponding to the topographic distribution. Low-level water vapor transport is large, the whole layer of water vapor flux is relatively high. Southwest air flow and terrain together provide favorable condition for the formation of liquid water in Chongqing. There are a large number of water vapor accumulated in the windward slope of northeastern mountains area,

and easy to form a wealth of liquid water. In july 4,2008，a plenty of vapor convert into cloud water in northwest of Chongqing，there is rich in super cool liquid water，less in ice number，low in precipitation efficiency，and the vapor vertical flux is large on 0℃ layer，so it is greater potential for precipitation enhancement。

In order to study the influence of precipitation processes and the macro and micro structures of cumulus by seeding at the different stages and different places, different seeding methods are designed to make seeding simulation for the precipitation process in August 7, 2006 in Qilian Mountain area ,

After seeding simulation, the main analysis results are as follows: The artificial ice crystals seeding in the initial stage of cumulus can lead to wider distribution of rain enhancement than seeding in the development stage. The center region of rain enhancement locate downwind direction of seeding region, and few rain reduce region is found. The center region of rain enhancement in the seeding region, and at the upwind direction there has rain reduce region. The most efficiency of rain enhancement is 10％ when seeding in 500hPa layer ,and 5％ in 400hPa layer. Mostly due to the 500 hPa layer is near 0℃ layer, the increased graupel crystals can melt more quickly , enhance the efficiency of precipitation and make effects of rain enhancement much better.

Numerical Simulation and Seeding Tests on the Stratiform Precipitation in North China

Gao Qian[1] Wang Guanghe[2] Shi Yueqin[2]
[1]Beijing Weather Modification Office, Beijing 100089, gaoqianbjwm@163.com
[2]Chinese Academy of Meteorology Science, Beijing 100081

1 Introduction

Stratiform clouds are a large-scale precipitation system in north China, as well as the primary object of artificial precipitation to alleviate the spring drought. The distribution and translation process of hydrometers can showed by numerical simulation and seeding test on the stratiform precipitation. Meanwhile dynamic mechanism and thermal mechanism can be analyzed so that seeding time, seeding area and seeding amount can be chosen reasonably.

Based on the consistent simulation of natural precipitation with actual rain, seeding tests with different amount and different height were designed. The vertical distribution of precipitation particles, dynamic mechanism and thermal mechanism, as well as the conversion between source and remit were analyzed, providing references for airplane seeding experiments.

2. Description of Model

The numerical model used is the CAMS cloud resolving model that is the MM5 model coupled with CAMS explicit cloud scheme. The center of the simulation was set at (41°N, 114°E), with three two-way nesting in the horizontal direction and grid intervals at 45 km, 15 km and 5 km, 23 vertical layers and model top pressure set at 100 hPa. The Grell scheme for convective parameterization, the Blackadar high-resolution boundary-layer scheme, the lxf scheme for explicit cloud physics and a cloud radiation scheme were used. The model is started using NCEP's 1°×1°reanalysis data available every 6 hours. The simulation started at 08:00 LST 20 March 2008, lasting 24 hours and restarts at the 360 minutes.

3. Comparison between observation and simulation

Both observation and simulation showed a pressure trough near Gansu Corridor at 08:00 LST March 20, moving east while cloud system strengthened. The precipitation began at 16:00 LST. By the time of 08:00 LST March 21, this weather system has moved out of Beijing and Hebei.

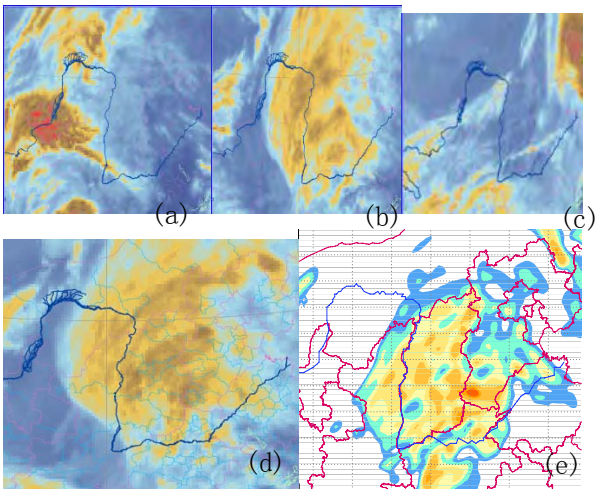


Figure.1 Micaps infrared image: (a)08LST Mar 20,2008; (b)20LST Mar 20,2008; (c)08LST Mar 21,2008; Observed and simulated cloud image: (d)observed;(e)simulated

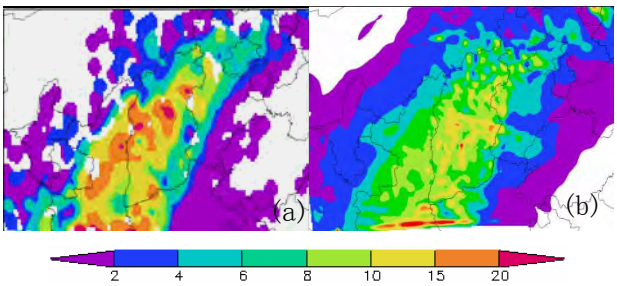


Figure.2 24 hours precipitation:08LST Mar 21,2008(a)observed(b)simulated results of 15km grid

The precipitation core was scatted in Shanxi area from northeast to southwest. Simulation of rainfall was similar to the observation. The simulated distribution of area that has a rainfall amount bigger

than 10mm was larger than observation, but the simulated amount bigger than 15mm was smaller than observation. On the whole, the simulation of precipitation system was consistent to actual situation.

4. Physical and dynamical characteristics

The ice and snow particles distributed widely in the cloud, which can stretch from 750hPa to 250hPa. The ice particles had two core centers around 550hPa at this height temperature was about -10℃.Cloud water mainly distributed below 500hPa. With the highest mix ratio 0.24g/kg existed between 110.5E and 110.75E, right above 650hPa which is also the zero-layer. Below the zero-layer, the two high cloud water mix ratio centers are 0.27g/kg and 0.33g/kg, respectively between 110.4E to 110.5E and 110.65E to 110.8E. Among these three high cloud water mix ratio centers, only the one between 110.5E and 110.75E had lower ice mix ratio that was suitable for seeding test. Meanwhile, an updraft stream were between 110.5E and 110.7E, corresponding to the area with lower ice particles concentration but abundant cloud water.

5. Model seeding tests

5.1 Seeding designs

Different seeding time and area can lead to different effects for seeding tests. When the precipitation system was at the stages of developing and maintaining, seeding at area with updraft and abundant supercooled water can produce good effects. As analyzed in section 4, area of 110.2°-110.7°E, 34.2°-34.5°N, at the time of 15:51 LST met the conditions for rainfall enhancement seeding test(the red rectangle in Figure3). Seeding tests conducted 4 times per minute, lasting 2 minutes. Because of the leapfrog scheme, the actual seeding times per minute was approximately more than twice, each time scattered $1.0*10^{6}$ ice particles per kg. In actual seeding experiments, $1.0*10^{-14}$-$1.0*10^{-15}$g AGI will be needed. Each grid (25km2) needed AGI 400g-40g, 24kg-2.4kg for the entire simulated area. Seeding at vertical level k=12(t=-7.8 ℃), 470min-471min, 475min-476min after model initialized.

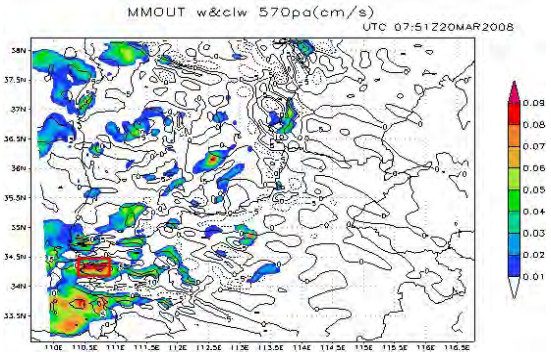


Figure.3 570hPa horizontal distribution cloud water and vertical velocity

5.2 Seeding effects

5 minutes after seeding, rainfall amount in seeding area decreased, the maximum reduction was 0.018mm. 10 minutes later, rainfall enhancement showed, 25 minutes after seeding, rainfall amount increased 0.18mm. Since then rainfall decrease began to show. 95 minutes after seeding, rainfall decrease was bigger rainfall enhancement. The first 15 minutes was rainfall decrease phase; 15-65 minutes was rainfall enhancement phase; after 65 minutes was rainfall decrease phase again.

5.2.1 Microphysical, thermal and dynamical characteristics in rainfall decrease phase

The vertical sections along 34.41°N at 16:01 LST showed there was a significant vapor decrease that can decrease 0.1g.kg around 550hPa. Supercooled cloud water's maximum reduction was 0.06 g/kg. The ice mix ration increased 0.035g/kg, and the ice particle concentration increased 800/L. The snow mix ratio also had a sharp increase. The analysis showed that the maximum water vapor and supercooled water decrease was 0.16g/kg, and the maximum ice and snow increase was about 0.16g/kg. That means these four particles had a balance in a whole. Meanwhile, it was noticed the vapor reduction in seeding area was much bigger than the supercooled cloud water reduction. That meant the vapor

had bigger contribution to the rainfall enhancement.

In the snow source, the collection of supercooled cloud water by snow (ccs) decreased in seeding area, while increasing below seeding area. That meant after seeding, supercooled cloud water in seeding area decreased. Below the seeding area, because of the increase of snow, the collection of supercooled cloud water by snow (ccs) increased, and the collection of ice by snow (cis) increased significantly. The conversion of ice to snow (ais) increased a little. In the graupel source, the collection of raindrop by snow (crs) increased, and the collection of raindrop by graupel (crg) decreased. In the seeding height, the collection of snow by raindrop (csr) and the melt from snow to raindrop (msr) had a sharp increase. After seeding, the melt from graupel to raindrop decreased significantly, which covered an area from 600hPa to 900hPa. That led to the decrease of surface precipitation.

5.2.2 Microphysical, thermal and dynamical characteristics in rainfall increase phase

The surface precipitation increased sharply 25 minutes after seeding. The vertical sections along 34.41°N at 16:21 LST showed the enlarged and east moved vapor decrease area. The cloud water decreased area also moved east. Comparing to 5 minutes after seeding, the ice mix ratio and concentration increase decreased sharply. The snow mix ratio increase also reduced to 0.07g/kg. The graupel mix ratio began to increase, while the rain water mix ratio maximum increase was 0.014g/kg. And the rain can get to the surface. There are two precipitation centers along 34.41°N. The west side of 110.7E had a maximum increase that was about 0.016g/kg. The precipitation enhancement here mainly caused by graupel increase in higher level. The graupel melted into rain in the process of falling to grand. The precipitation enhancement happened to the east side of 110.7E was becaused of the melt of increased snow under zero-level. In seeding area, updraft strengthened, with the maximum increase 3.5cm/s, the updraft was stronger than the downdraft. Temperature raised 0.35°C.

In the snow source, the collection of ice by snow (cis) decreased compared to 5 minutes after seeding. In the graupel source, the collection of raindrop by snow (crs) increased significantly, and the collection of raindrop by graupel (crg) decreased. In the area between 650hPa and 730hPa, both the collection of snow by raindrop (csr) and the melt from snow to raindrop (msr) increased. But at the vertical level between 650hPa and 800hPa, the melt from snow to raindrop (msr) had a sharp decrease. Below 800hPa, the melt from snow to raindrop (msr) was positive and kept on growing. Surface precipitation increased. It showed that, after seeding, the increase of snow led to the increase of the collection of raindrop by snow (crs). So the graupel increased. Below zero-level, the graupel melted into raindrop and the surface precipitation increased.

5.3 Tests with different seeding heights and different seeding amounts

5.3.1 Different seeding amounts

Seeding with different amounts at the 470 minutes after model initialed, which is 15LST Mar 20, 2008. Seeding time was 1 minute. The accumulated rainfall enhancement changed along with the change of seeding amounts. When seeding amount smaller than 10^5/kg, there was no significant effects. When seeding amount was 106/kg, rainfall enhancement could reach 1500kt 40 minutes after seeding. Althouth when seeding amount was 10^7/kg, the rainfall enhancement was better than that of 10^6/kg. But in actual experiment, that amount is hard to conduct. So the appropriate seeding amount was 10^6/kg.

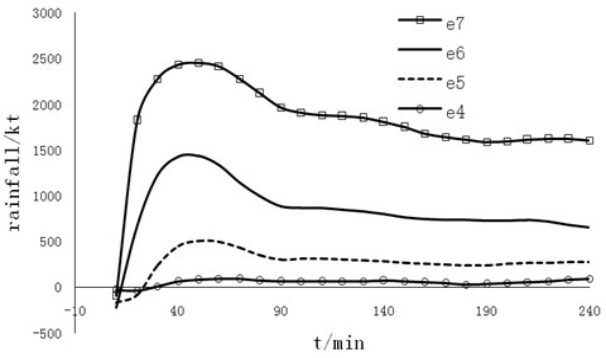


Figure.4 Regional accumulated rainfall of different seeding amount

5.3.2 Different seeding levels

With seeding time and amount stayed the same, seeding tests at different levels led to different effects. When seeding level k=11(t=-5.3°C, p=610hPa), rainfall enhancement was 78.3kt,the smallest in all tests. When seeding level k=12(t=-7.8°C, p=570hPa), rainfall enhancement was1432.7kt. Seeding at level k=13(t=-10.9°C, p=530hPa) can lead to 1417.7 precipitation enhancement. The seeding effect of k =14((t=-14.4°C, p=500hPa) was 550.8kt. Seeding at the level k=12 had the best effect, because this level had abundant cloud water and small ice concentration, and the seeding ice particles can stay a longer time compared to k=13.

6. Conclusions

(1) The results of tests with different seeding heights and different seeding amounts showed 10^6/kg was the appropriate seeding amount. Seeding at the level k=12(t=-7.8°C, p=570hPa) and k=13(t=-10.9°C, p=530hPa) can get good effects. But a higher seeding level meant longer developing time, which also had abundant cloud water and small ice particles concentration, that made k=12 the appropriate seeding level.

(2) When the precipitation system was at the stages of developing and maintaining, seeding at area with updraft and abundant supercooled water can produce good effects. 20 minutes after seeding, rainfall enhancement showed. 50 minutes after seeding there was a precipitation decrease center but precipitation enhancement was the major result. 80 minutes after seeding, rainfall decrease exceeded rainfall increase. After seeding, the water vapor and supercooled water decreased, and the ice and snow increased. That meant these four particles had a balance in a whole. The vapor reduction in seeding area was much bigger than the supercooled cloud water reduction. The water vapor had bigger contribution to the rainfall enhancement.

(3) Above the seeding level, the collection of ice by snow (cis), the conversion of ice to snow (ais) was the main sources of snow. Below the seeding level, the collection of supercooled cloud water by snow (ccs) was the main source of snow. The collection of supercooled raindrop by snow (crs) was the main source of graupel. The increase of snow led to the increase of the collection of raindrop by snow (crs). So the graupel increased. The collection of snow by raindrop (csr) and the melt of snow (msr) were important process of rain enhancement, which happened between 650hPa and 730hPa. The melt of graupel to raindrop (mgr) was the main process of rain enhancement. In the rainfall decrease phase, the melt of graupel to raindrop (mgr) had a sharp decrease, which led to the surface precipitation decrease.The melt of graupel to raindrop (mgr) decreased a lot between the vertical level 6-10 (800hPa-650hPa) in the rainfall increase phase, but below the vertical level 6 (800hPa), it increased. And the more it came to the surface, the stronger rainfall enhancement became. Surface precipitation had increased significantly.

References

Farley R D, Nguyen P and Orville H D. Numerical simulation of cloud seeding using a three-dimensional cloud model[J]. J. Wea. Modif.,1994,**26**(1):113-124

Meryers M P, DeMott P J and Cotton W R. Comparison of seeded and non-seeded orographic cloud simulations with an explicit cloud model[J]. J. Appl. Meteor., 1995,**34**: 834-846

Lou Xiaofeng. Development and implementation of a new explicit microphysical scheme and comparisons of original schemes of MM5.PhD thesis, Peking University,2002

SHI Yueqin. Seeding Numerical Experiments of Cold Front Clouds in South China. Chinese Journal of Atmospheric Sciences(in Chinese),2008,**32**(6):1256-1275

Hu Zhijin,. Discussion on Mechanisms, conditions and Methods of Precipitation Enhancement in Stratiform Clouds[J]. Quarterly Journal of Applied Meteorology, 2011, **12**:10-13

Assessing A New Approach to Tropical Cyclone Modification by Hygroscopic Smoke

Joseph H. Golden[1], Daniel Rosenfeld[2], William R. Cotton[3], William L. Woodley[4], Isaac Ginis[5], Alexander Khain[2]

[1] Golden Research & Consulting Group, Boulder,CO. 80301 USA, joegolden@q.com
[2] The Hebrew University of Jerusalem, Jerusalem 91904, Israel, Daniel.rosenfeld@huji.ac.il
[3] Dept of Atmospheric Science, Colorado State University, Fort Collins, CO 80523 USA
[4] Woodley Weather Consultants, Littleton, CO 80127 USA
[5] Graduate School of Oceanography, University of Rhode Island, Narragansett, RI 02882 USA

1. Introduction

The Department of Homeland Security (DHS) asked NOAA/ESRL in Boulder to organize a workshop on possible new scientific theory and approaches to tropical cyclone (TC) modification in February, 2008. Scientists from around the world presented a number of hypotheses and new ideas. On this basis the DHS funded the Hurricane Aerosol and Microphysics Program (HAMP). The PIs were the authors of this extended abstract. The initial success of HAMP to show plausibility of hurricane modification resonated with the aftermath of STORMFURY that led to an early termination of a scientifically very productive and successful program. One of several tangible results of the program is the recognition that aerosols can affect hurricane intensities, and when taken into account the predictions can be improved. Here we report some of the HAMP observational and theoretical work results of aerosols effects on TCs.

2. The theoretical basis

TCs are energized by the huge amount of latent heat that is released by the condensation of water and its subsequent precipitation. Therefore, it can be expected that changes in the precipitation-forming processes that would change or redistribute the precipitation in the TC would also redistribute the latent heating and respectively affect the dynamics of the storm and its intensity. This concept was first invoked in the Stormfury hurricane-mitigation experiment (Willoughby et al., 1985) that focused on glaciogenic seeding of vigorous, convective, clouds within the eye wall. The Stormfury experiment failed to show a detectable effect on the seeded hurricanes. It is now understood that the amount of supercooled water in the hurricanes is too small to expect much of a seeding effect upon freezing, and this small amount of water freezes naturally quickly above the 0°C level. This is because the cloud drops in tropical maritime clouds become sufficiently large to undergo effective coalescence and produce warm rain well below the freezing level. Much of the rain precipitates without ever freezing.

Much more recently Rosenfeld et al. (2007) and Cotton et al. (2007) independently hypothesized that the invigoration of convective clouds near the periphery of the TC might be achievable by adding hygroscopic aerosols that slow the warm rain-forming processes. This was postulated to take place at the expense of the eye wall by intercepting some of the energy being transported toward the inner core and weaken the storm.

The basis for the cloud invigoration hypothesis was reviewed by Rosenfeld et al. (2008). Adding large concentrations of smoke aerosols to marine tropical clouds can delay the formation of warm rain to above the 0°C isotherm within the cloud. This is done by the nucleating activity of cloud condensation nuclei (CCN) aerosols. Large concentrations of CCN nucleate larger concentrations of smaller cloud drops. The smaller drops are slower to coalesce into rain drops. The cloud water that did not precipitate as rain can either re-evaporate at low levels, or rise with the updraft above the freezing level, creating enhanced amounts of supercooled water, and thereby produce ice hydrometeors with the consequent enhancement of the release of the latent heat of freezing. This added heat release invigorates the convection and may enhance rain amounts in a moist and weakly sheared tropical atmosphere (Fan et el., 2009) Greater amounts of supercooled water with stronger updrafts and more ice hydrometeors are expected to produce more lightning. Simulations show that the invigoration also enhances the downdraft and low level evaporative cooling (Khain et al, 2005; van den Heever and Cotton, 2007).

3. Simulations of aerosol impacts on TC

Rosenfeld et al. (2007) and Cotton et al. (2007) independently simulated TCs with suppressed coalescence, and showed that this reduces their maximum wind intensities. The simulations of Rosenfeld et al. (2007) showed that the suppressed warm rain caused low-level cooling in the lowest 3 – 4 km, probably due to re-evaporation of some of the cloud water that did not precipitate and due to the enhanced colder downdrafts from the invigorated convection at the periphery. The added aerosols in the simulations of Zhang et al. (2009), Carrio and Cotton (2011) and Krall and Cotton (2011) also invigorated the convection at the spiral rain bands and enhanced cold-pools by producing downdrafts and evaporative cooling of rain. These cold-pools blocked the surface radial inflow transporting high θe air into the eyewall, and led to its weakening and widening, in a mechanism similar to that of an eyewall replacement. Convection outside the eyewall was previously observed to introduce air with low

equivalent potential temperature (θe) into the boundary layer inflow, resulting in blocking of the inflow of the warm air to the eyewall (Powell, 1990). In Krall and Cotton's simulations, however, when pollution aerosols were swept into the storm core the storm actually intensified. Subsequently, as aerosol were scavenged before reaching the storm core, only convection in the outer rainbands were intensified, and the storm weakened, consistent with the working hypothesis. That work plus Carrio and Cotton's (2011) targeted seeding simulations suggests that the response to aerosols critically depends on the locations of where the aerosols actually infect the storm.

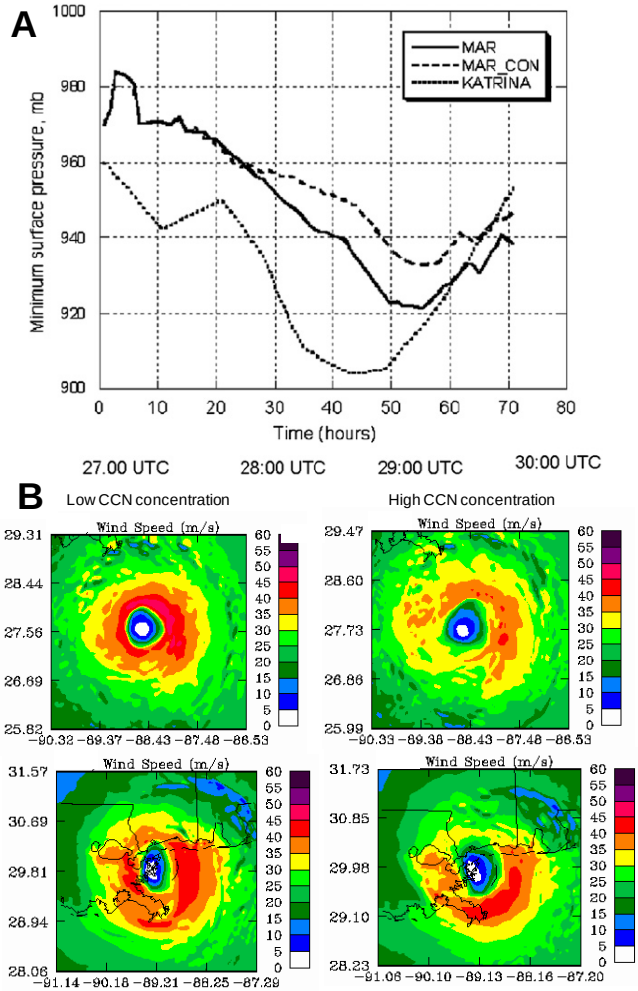


Figure 1. Simulations of aerosol effects on Hurricane Katrina. A. Time dependence of minimum pressure for low (MAR) and high (MAR_CON) CCN concentrations at the periphery of the storm. B maximum wind speed low and high CCN concentrations at the periphery of the storm at 28 Aug. 22 Z (upper row) and during landfall 29th at 12Z (From Khain et al., 2010)

Sensitivity simulations of Hurricane Katrina to the impacts of pollution aerosols showed similar results (Khain et al., 2008a and 2010, Khain and Lynn, 2011) using the Weather Research and Forecast (WRF) Model with the implementation of a spectral bin microphysical (SBM) scheme. Penetration of continental aerosols to the TC periphery caused by the TC circulation approaching the land was simulated. As a result of the aerosol penetration, concentration of CCN (at 1% of supersaturation) increased at the TC periphery (radial distance from the center > ~200 km) from 100 cm^{-3} to about 1000 cm^{-3}. This increase in CCN concentration in the lower atmosphere and successive penetration of these CCN into rain bands at the TC periphery resulted in an increase of 16 hPA in the central pressure of the storm, as shown in Fig. 1a (Khain et al., 2010). Maximum wind speed weakened by 10-15 m/s and the area of strong winds significantly decreased (Fig. 1).

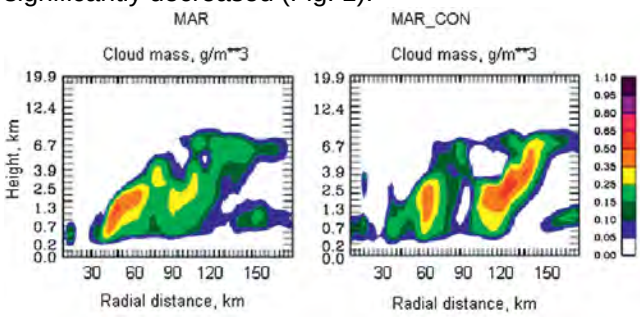


Figure 2: The cross section of azimuthally averaged cloud water content (g/m^3) in simulations (left) maritime and (right) polluted at times when the maximum difference in the TC intensities took place (From Khain et al., 2010). Note that the polluted case (right) developed stronger and more water-rich clouds at the storm periphery, whereas the eye is not well defined and widened.

The simulation showed that penetration of continental aerosol to the TC periphery leads to dramatic intensification of convection at the TC periphery which competes with the convection in the eyewall (see Fig. 2).

Building on the earlier dust simulations of Zhang et al., (2007; 2009), Carrio and Cotton (2011) performed idealized simulations of the direct seeding of CCN in the outer rain band region of a hurricane. The Regional Atmospheric Modeling System was used in those idealized simulations that included a two-moment microphysics scheme which emulates bin microphysics for drop collection, ice particle riming, and sedimentation. New algorithms for sea-spray generation of CCN and precipitation scavenging were added (Carrio and Cotton, 2011). These simulations supported the hypothesis that much of the variability to enhanced CCN concentrations found in the Zhang et al. (2009) simulations was due to the variable intensity of outer rainband convection when the enhanced CCN advected into that region. Moreover, the environmental CCN are not always transported from the storm environment into outer rain band convection as transport is at the mercy of the local flow in those regions. Furthermore, those simulations showed a clear step-by-step response of the hurricane to the direct seeding of enhanced CCN in the outer rainband of the storm as described in the basic hypothesis.

4. Quantitative Relations Between Aerosol Amounts and TC Intensity

Although the observational and modeling evidence suggests that aerosols affect the structure of a TC, the major uncertainty is whether these structural changes are manifested as changes in TC intensity as indicated by the model simulations. Rosenfeld et al. (2011) used observed TC data and forecasted TC data to statistically analyze the relationships between TC intensity and aerosol quantities at the TC's periphery. They separated the aerosol's effect on TC intensity from all other effects by using data of TC prediction models that take into account all meteorological and sea surface temperature properties, but not the aerosols. The models used were the dynamically based GFDL (Bender et al. 2007) and the statistically based SHIPS (DeMaria et al. 2005) models. The hypothesis was that if greater aerosol amounts actually act to decrease storm intensity, the forecast model would tend to over-predict the observed intensities of the more "polluted" storms. Rosenfeld et al. (2011) tested this hypothesis by examining the prediction errors of the maximum sustained wind velocities (dVmax) and their statistical relationship with the aerosol optical depth (AOD) that was calculated by the Goddard Chemistry Aerosol Radiation and Transport (GOCART) hindcast model (Chin et al., 2000). The GOCART was used to obtain aerosols under cloudy conditions and to avoid measurement artifacts due to meteorological conditions. The results showed that the variability of aerosol quantities in a TC's periphery can explain about 8% of the forecast errors of the TC. Indeed, the actual intensities of polluted TCs were found to be on average lower than their predicted values, providing additional evidence for the hypothesis. Quantitatively, an increase in AOD by 0.01 is associated on average with a decrease of 0.3 knots in the peak wind speed. No distinction between aerosol types could be made. It was also found that TC intensity might be more susceptible to the impacts of aerosols during their developing stages and less in the TC's mature and dissipating stages, consistent with the modeling results of Zhang et al., (2009).

5. Summary

Based on the above observations and simulations, our present understanding of the effect of aerosols on tropical clouds and cyclones is summarized in the following links in the conceptual chain, which is illustrated in Fig. 3:

a. Small (sub-micron) CCN aerosols in the form of particulate pollution and/or desert dust nucleate larger numbers of smaller cloud drops that slow the coalescence of the cloud drops into rain drops.
b. The CCN aerosols present in the peripheral clouds of the hurricane slow the rain forming processes there.
c. The delayed formation of rain decreases the amount of early rainout from the rising air; hence more water can ascend to freezing levels as supercooled water where ice precipitation particles form.
d. The greater amount of freezing water aloft releases extra latent heat that invigorates the convection. The invigoration and the added supercooled water are manifested in greater cloud electrification and lightning discharges.

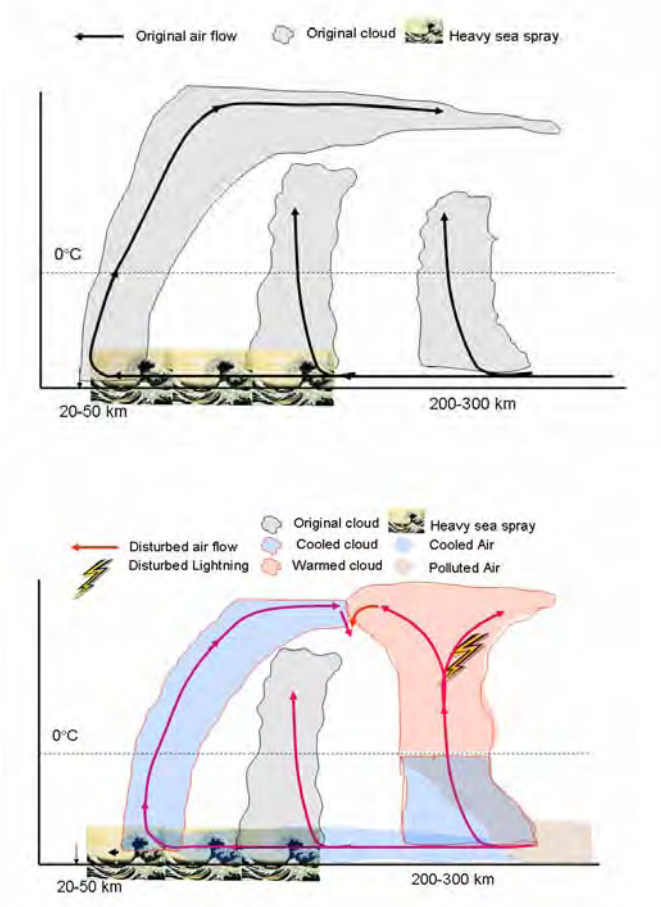


Figure 3: Conceptual model of aerosol impacts on tropical cyclones. The undisturbed and disturbed states are shown in the top and bottom panels, respectively. In the bottom panel, pollution or dust aerosols slow warm rain in the peripheral clouds causing invigoration and electrification of the clouds and warming aloft, coupled with stronger downdrafts and intensified low-level cool-pools. Strong nucleation and precipitation scavenging and sea spray from the rough sea promotes warm rain in the inner cloud bands and eyewall clouds, which reduces the suppression effect due to any remaining pollution aerosols that were not washed down, so that little aerosol-induced invigoration can occur there. The convection in the outer cloud band decreases the inflow towards the eyewall. The cold-pools also partially block the inflow, causing cooling, weakening and widening of the eyewall, leading to weaker winds.

e. The greater vigor of the clouds draws more ascending air at the periphery of the storm, thereby bleeding the low-level airflow towards the eye wall. The weakened convergence towards the center causes the central pressure to rise;

less air ascends in the eye wall, and there is respectively lower maximum wind speed.

f. The intensified ice precipitation in the peripheral clouds melts and evaporates at the lower levels, thereby cooling the air that converges into the center of the storm.
g. Stronger low-level cooling produces cold-pools which favor the intensification of storm cells in the outer rain bands, which transport more water vertically leading to enhanced latent heating and stronger convection in a positive feedback loop.
h. Additional low-level cooling occurs when the cloud drops that did not precipitate and did not ascend to the freezing level re-evaporate.
i. The storm is further weakened by cooling of the low-level air that converges to the center, in addition to the air bleeding effect that was discussed in the first five points. The cooler air has less buoyancy and hence dampens the rising air in the eye wall, thereby weakening further the convergence and the maximum wind speed of the storm.
j. Under hurricane force winds very intense sea spray is lifted efficiently by roll vortices in the BL and induces rain of mostly sea water at the height of the convective cloud base. This restores the warm rain processes and offsets the delaying effect of small CCN aerosols on rain forming processes. Furthermore the core of the TC is nearly saturated at low levels thus cold-pool formation in that region is inhibited. Therefore the CCN aerosol effect would be most effective in the peripheral clouds of the storm, where the winds are still not very strong. Strengthening of the winds there would reduce the sensitivity of the storm to the weakening effect of the CCN aerosols.

These links in the conceptual model are still a hypothesis that requires additional investigation. However, its physical plausibility underline the importance of understanding precipitation forming and evaporation processes in TC clouds and the need to further observe and simulate them and the resultant cold-pools properly in order to obtain additional improvements in TC prediction models.

Acknowledgements

This extended abstract summarizes some of the results of the HAMP research effort that was sponsored by the Department of Homeland Security under Contract Number: HSHQDC-09-C-00064.

References

Bender, M. A., I. Ginis, R. Tuleya, B. Thomas, and T. Marchok, 2007: The operational GFDL coupled hurricane-ocean prediction system and a summary of its performance. Mon. Wea. Rev., 135, 3965–3989.

Carrió, G. G., and W. R. Cotton, 2011: Investigations of aerosol impacts on hurricanes: Virtual seeding flights. Atmos. Chem. Phys., 11, 2557–2567.

Chin, M., Savoie, D.L., Huebert, D.L., Bandy, A. R., Thornton, D.C., Bates, T.S., Quinn, P.K., Saltzman, E.S., and De Bruyn, W.J., 2000: Atmospheric sulfur cycle simulated in the global model GOCART: Comparison with field observations and regional budgets. J. of Geophys. Res. 105, D20, 24,689-24,712.

Cotton, W.R., H. Zhang, G.M. McFarquhar, and S.M. Saleeby, 2007: Should we consider polluting hurricanes to reduce their intensity? J. Wea. Mod., 39, 70-73.

DeMaria, M., M. Mainelli, L. K. Shay, J. A. Knaff, and J. Kaplan, 2005: Further improvements to the statistical hurricane intensity prediction scheme (SHIPS). Wea. Forecast., 20, 531–543.

Fan, J., Yuan, T., Comstock, J. M., Ghan, S., Khain, A., Leung, L. R., Li, Z., Martins, V. J., and Ovchinnikov, M., 2009: Dominant role by vertical wind shear in regulating aerosol effects on deep convective clouds, J. Geophys. Res., 114, D22206.

Khain, A., D. Rosenfeld, and A., Pokrovsky, 2005: Aerosol impact on the dynamics and microphysics of deep convective clouds, Q. J. R. Meteorol. Soc., 131, 2639–2663.

Khain, A., N. Cohen, B. Lynn, and A. Pokrovsky, 2008a: Possible aerosol effects on lightning activity and structure of hurricanes. J. Atmos. Sci., 65, 3652–3667.

Khain A., B. Lynn, and. J. Dudhia, 2010: Aerosol Effects on Intensity of Landfalling Hurricanes as Seen from Simulations with the WRF Model with Spectral Bin Microphysics. J. Atmos. Sci., 67, 365–384.

Khain A., and B. Lynn, 2011: Simulation of Tropical Cyclones Using a Mesoscale Model with Spectral Bin Microphysics, In: Recent Hurricane Research- Climate, Dynamics, and Societal Impacts, Anthony R. Lupo, pp. 197-227, Intech Open Access Publisher Rijeka

Krall, G., and W.R. Cotton, 2011: Potential indirect effects of aerosol on tropical cyclone development. Submitted to Atmos. Chem. and Physics.

Powell, M. D., 1990: Boundary layer structure and dynamics in outer rainbands. Part II: Downdraft modification and mixed layer recovery. Mon. Wea. Rev., 118, 919–938.

Rosenfeld D., A. Khain, B. Lynn, and W.L. Woodley, 2007: Simulation of hurricane response to suppression of warm rain by sub-micron aerosols. Atmos. Chem. Phys., 7, 3411-3424.

Rosenfeld D., U. Lohmann, G.B. Raga, C.D. O'Dowd, M. Kulmala, S. Fuzzi, A. Reissell, and M.O. Andreae, 2008: Flood or Drought: How Do Aerosols Affect Precipitation? Science, 321, 1309-1313.

Rosenfeld, D., M Clavner and R. Nirel, 2011: Pollution and dust aerosols modulating tropical cyclones intensities. Atmospheric Research. Early online publication.

van den Heever, S., and W.R. Cotton. 2007: Urban aerosol impacts on downwind convective storms, J. Appl. Meteor. Climat., 46, 828–850.

Willoughby, H. E., D. P. Jorgensen, R.A. Black and S.L Rosenthal, 1985: Project STORMFURY, A Scientific Chronicle, 1962–1983, Bull. Amer. Meteor. Soc., 66, 505–514.

Zhang, H., G.M. McFarquhar, S.M. Saleeby, and W.R.Cotton 2007: Impacts of Saharan dust as CCN on the evolution of an idealized tropical cyclone. Geophys. Res. Lett. 34 L14812, doi: 10.2029/2007GL029876

Zhang, H., G. M. McFarquhar, W. R. Cotton, and Y. Deng, 2009: Direct and indirect impacts of Saharan dust acting as cloud condensation nuclei on tropical cyclone eyewall development. Geophys. Res. Lett., 36, L06802. doi:10.1029/2009GL037276.

The Numerical Analysis About Water Vapor Budget and Precipitation Efficiency During July-October, 2003 in Shandong Province in China

GONG Dianli LIU Shijun

(*Shandong Weather Modification Office, Ji´nan 250031， China,gdllj@sohu.com*)

1. Introduction

Shandong province is located in the lower Yellow River in China,near the western Pacific Ocean, the influence of East Asian monsoon is obvious.Using the non-hydrostatic model MM5 v3.5, the water vapor budget and precipitation efficiency form 0000 UTC 1 July to 1200 UTC 31 October,2003 in Shandong region in China were calculated,the atmospheric water cycle characteristics were analysed.

2. Methodology

The solid line around Shandong province was composed of 134 calculated points(Fig.1),the closed area was about 15.6×10^4 km^2. Using bilinear interpolation method, the u(x wind),v(y wind),q(water vapor mixing ratio) of MM5 domain2 forecast data(18-km grid spacing) of each pressure level (1000-200 hPa,50 hPa interval) were interpolated to each calculated points, the instantaneous water vapor transportation were subsequently calculated by vertical and horizontal integral along the west(W1-W2), north(N1-N2), east (E1-E2) and south (S1-S2)boundary, the daily accumulated water vapor transportation (12-36h forecast time) were obtained lastly by time integral.

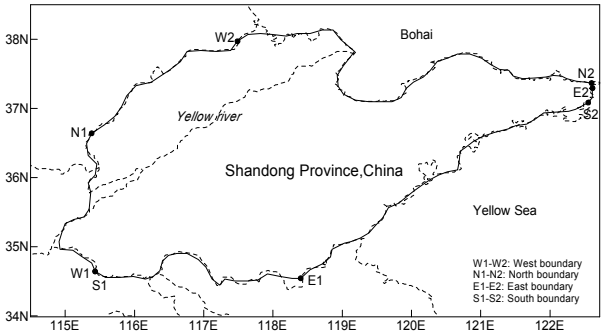


FIG.1 The boundary circled around Shandong province in China(dashed line:real boundary of Shandong,solid line:calculated boundary. West,north,east and south boundary were labeled as black dots).

In the present application,two-way nesting,with a set of two domains(54-,18-km grid spacing) was used to achieve cloud-resolving grid spacing.The model initial and lateral boundary conditions came from T213(Beijing medium range forecasts) data,the upper-air and surface observations were assimilated by analysis nudging in the first 12 hours,the model was initialized at 1200 UTC,and the length of forecast time was 48h.The Reisner graupel schemes were used for two domains, the Betts-Miller parametrization scheme was used for coarse grid, and Grell scheme was used for two nested grid.

3. Results

In the period of July-October(123 days),2003,the simulated average rainfall was 556.1 mm(867.44×10^8 m^3),and the observed average rainfall was 613.8 mm (957.53×10^8 m^3) in Shandong,see Fig.2 and Table 1. The geographical distribution of both results were more consistent except part area.The time series of daily water vapor input,output,average rainfall,et al. listed in Table 1 were shown in Fig. 3.

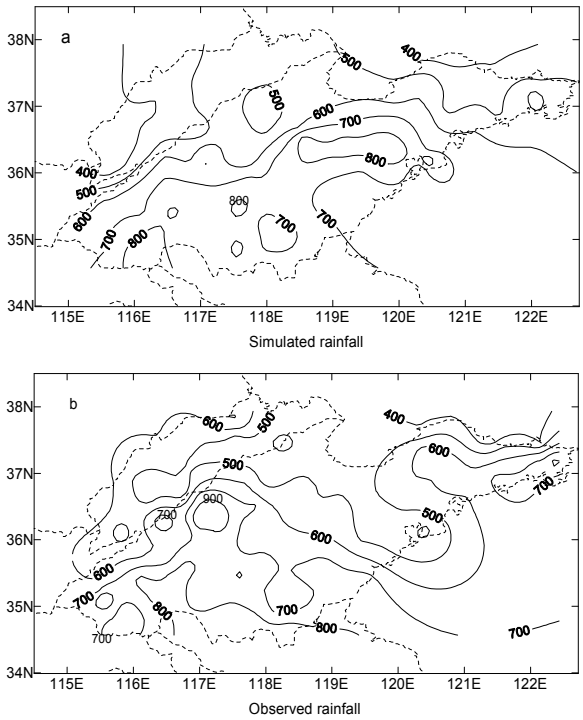


FIG.2 Distributions of the simulated (a) and observed(b) accumulated rainfall(unit:mm) from 1 Jul to 31 Oct, 2003.

TABLE 1. The total amount of water vapor budget,simulated and observed rainfall
(Sum was the cumulative number of 123 days,Minimum,Maxmum and Mean were daily number.Unit:10^8 m^3).

situation	vapor input	vapor output	Net vapor input	Rainfall(MM5)	Rainfall(OBS)
Sum	14393.02	13292.40	1100.62	867.44	957.53
Minimum	20.84	21.64	-51.63	0	0
Maximum	349.63	346.25	96.30	69.01	76.75
Mean	117.02	108.07	8.95	7.05	7.77

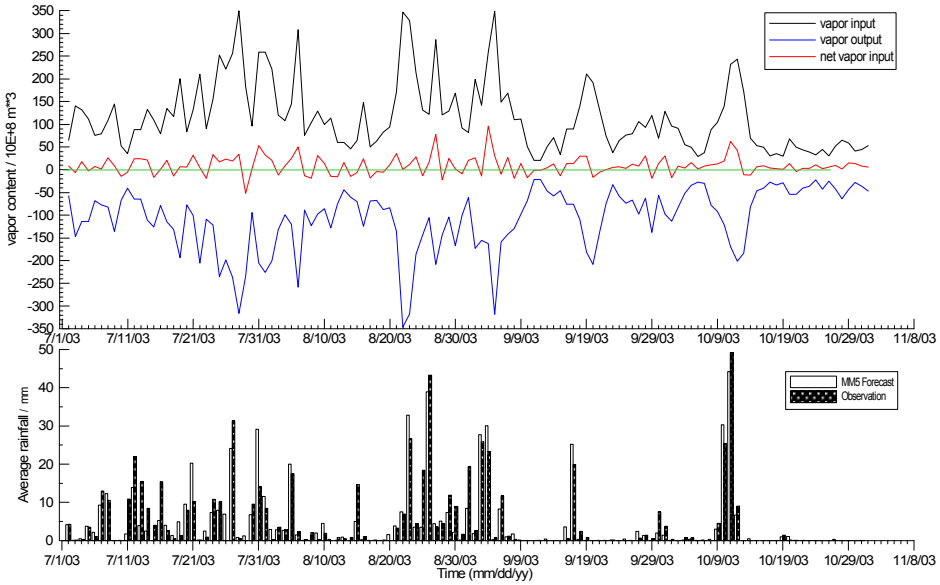


FIG.3 Accumulated daily vapor input(black lines,units:$10^8 m^3$),vapor output(blue lines),net vapor input(red lines),and simulated (hollow histogram,unit:mm) and observed(solid histogram) rainfall over the area of Shandong province from 1 Jul to 31 Oct,2003.

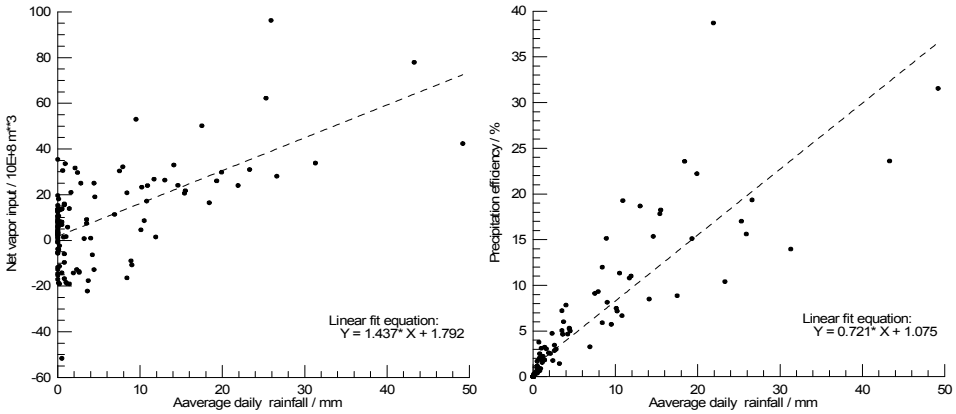


FIG.4 Scatterplot of daily net vapor input(a),precipitation efficiency(b) versus average daily rainfall.

The results indicated,when precipitation weather systems appeared, the amount of vapor input and output were increased obvious, the total net input vapor and precipitation were approximate.Relative to the total amount of water vapor input during 123 days, the average precipitation efficiency was 6.33%,the maximum daily precipitation efficiency was 38.71%, appeared in 12 July,2003. When daily average rainfall was greater than 10 mm, the net vapor input became positive(Fig.4 a),the evaporation can be neglected,the rate of vapor transform to rainfall was very fast of the cloud(Fig.4 b),meanwhile,it's the most active stage of the water circulation.The results are helpful for understanding the characteristics of the water vapor cycle in Shandong area of northern China.

References

Ding Yihui and Hu Guoquan.A study on water vapor budget over China during the 1998 severe flood periods.Acta Meteor Sinica(in Chinese),61(2),129-145,2003.

Application of numerical cloud model in hail suppression of cold clouds

Javanmard, Sohaila[1]; Karimpirhayati, Mahla[2]; BodaghJamali, Javad[3]; Abedini, Yusefali[2]
[1] Atmospheric Science and Meteorological Research Center (ASMERC), Pajuhesh Blvd., Tehran-Karaj Highway, Tehran, I. R. of Iran, sohailajavanmard@gmail.com, sjavanmard2004@yahoo.com
[2]Department of Physics, Zanjan University, Zanjan, I. R. of Iran, Mahla_kp@yahoo.com, Abediniy@znu.ac.ir
[3]University of Environment, standard Squar, Karaj, I. R. of Iran, jbjamali@gmail.com, jbodagh@yahoo.com

1. Introduction

Hail induces many damages to agriculture, transportation, economical affairs in hail prone area over Iran annually (Jamali et al., 2010). In order to achieve hail risk management to decrease eht induced destruction in Iran, application of hail suppression methods is necessary. In order to asses the performance of operational cloud seeding operations and achieve desirable results, application of numerical cloud model is one of the most important tools to assess the seeding effect on hail suppression. In this paper, effects of Silver Iodide (AgI) cloud seeding in order to hail suppression have been examined using one dimensional time dependent numerical cloud model.

2. Hail suppression model

The governing dynamical equations of model is based on Ogura and Takahashi (1971), microphysical parameterization of natural precipitation process is based on Lin et al., (1983), and cloud seeding parameterization is based on Zhen and Heng-Chi (2010).

Ogura and Takahashi model is a time dependent and one dimensional model with bulk parameterization. In this model, the cloud is modelled as a circular air column with a time dependent radius in an environment at rest. All dynamical equations have been formulated in a one dimensional space based on Asai and Kasahara(1967). In Ogura and Takahashi model, nine microphysical processes has been parameterized with four water substances including water vapor, cloud droplet, raindrop and hail.

Lin et al. model (1983) is a two dimensional, time dependent cloud model which it has been used to simulate a moderate intensity thunderstorm. In this model, six forms of water substance (water vapor, cloud water, cloud ice, rain, snow and hail/graupel) are simulated and 32 microphysical processes are considered as shown in Fig .1.

In hail suppression model, dynamic and thermodynamic equations are based on Ogura and Takahashi model (1971) that cloud ice and snow are added and microphysics of natural precipitation is based on Lin et al. model (1983). Three microphysical processes for seeding are added to model that is based on Zhen and Heng-Chi (2010). When AgI is inserted to the cloud base, it affects on six cloud hydrometeors including cloud droplet, raindrop, snow and hail mixing ratios via contact and deposition nucleation, transportation from rain drop to snow and droplet to cloud ice due to seeding.

The equation of the vertical component of velocity in a cylindrical coordinate may be written as:

$$\frac{\partial w}{\partial t} = -w\frac{\partial w}{\partial z} - \frac{2\alpha}{a} w|w| + \frac{2}{a}\tilde{u}_a(w - \tilde{w}_a) + g\frac{T_v - T_{v0}}{\nu_0} - g(Q_c + Q_r + Q_i + Q_s + Q_G + X_s) \quad (1)$$

The first term in the right-hand side of Eq. (1) represents the vertical advection, the second term the lateral eddy exchange, the third term the dynamic entertainment that is required to satisfy the mass continuity between the cloud and the environment, the fourth term the buoyancy, and the last term the drag force that is assumed to be provided by the weight of cloud droplets, raindrops, cloud ice, hail, snow, and AgI.

In this research, dynamical equations with 32 microphysical processes have been coded by Fortran programming according to Javanmard et al. (2010), then three seeding microphysical parameterization have been added to cloud model. Finally, results have been compared before and after seeding.

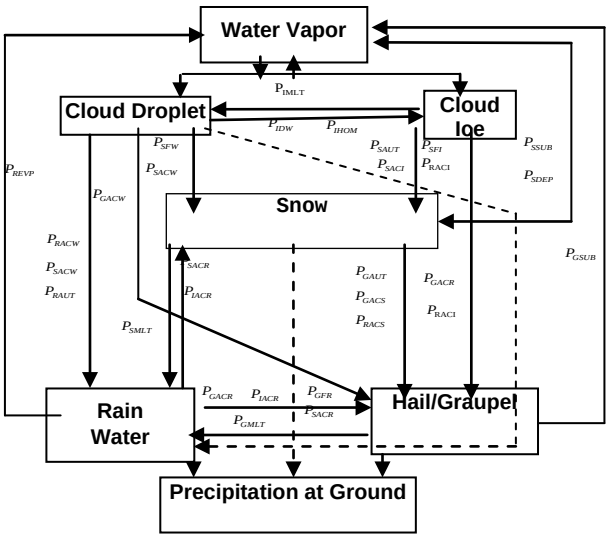


Fig. 1. Microphysical processes in Lin et al. model (1983).

3. Results and conclusion

In this paper, effects of cloud seeding by AgI have been simulated in one dimensional cloud model. It is concluded that as AgI introduced into the

cloud at height about 6.5 km above the surface (temperature less than -20 degree Celsius) within 30 minutes after cloud formation, and with mixing ratio about 2.5*10^{-9} gg^{-1} resulting in rainfall intensity enhancement about %20. Moreover, heterogeneous nucleation of AgI enhanced the cloud ice, so snow increased and rainfall enhanced by melting of snow and cloud ice. On the other hand, cloud ice consumed to produce snow and they did not grow up to reach hail size, so the processes that related to growth of hail decreased strongly.

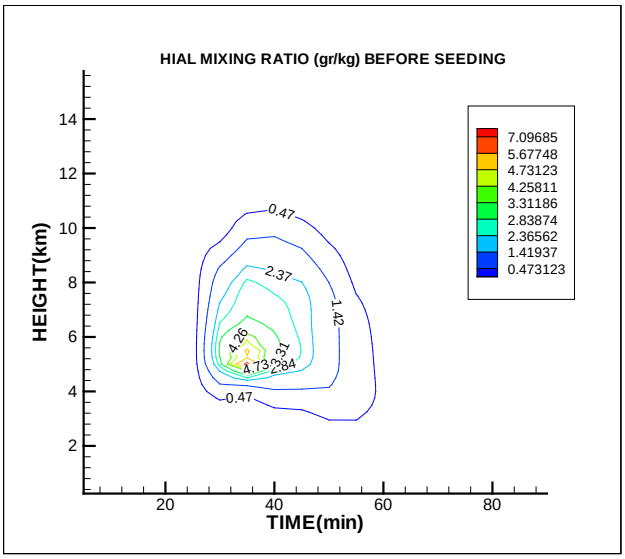


Fig. 2. Hail mixing ratio versus height and time before seeding

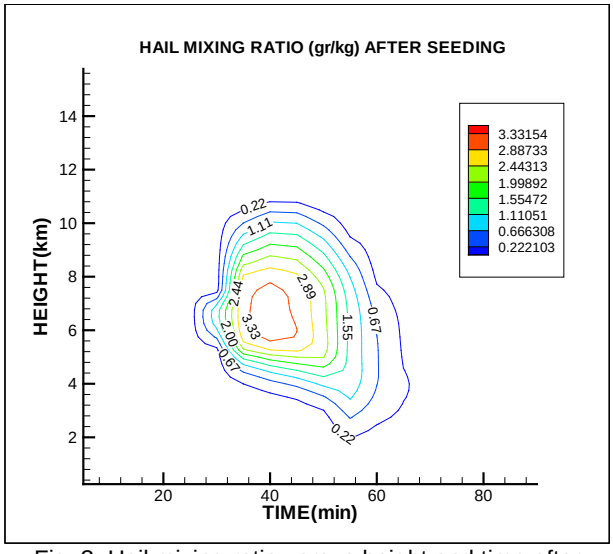


Fig. 3. Hail mixing ratio versus height and time after seeding

The contours of hail mixing ratio versus height and time have been shown in Figs. 2 and 3, which the maximum values of hail mixing ratio are7.1 gg^{-1} and 3.3 gg^{-1} before and after seeding, respectively. Hail mixing ratio has been reduced about %53. From Figs. 4 and 5, the most effective source terms are P_{IACRG} (accretion of rain by cloud ice; produces hail), P_{SACRG} (accretion of rain by snow; produces hail), and P_{GFR} (freezing of rain to form hail) before seeding and they are P_{GDRY} (dry growth of graupel/hail) and P_{GWET} (wet growth of graupel/hail) after seeding. From Figs. 6 and 7, it has been concluded that the most effective sink terms is P_{GMLT} (melting of hail to form rain) before seeding and it is P_{GSUB} (sublimation of hail) after seeding.

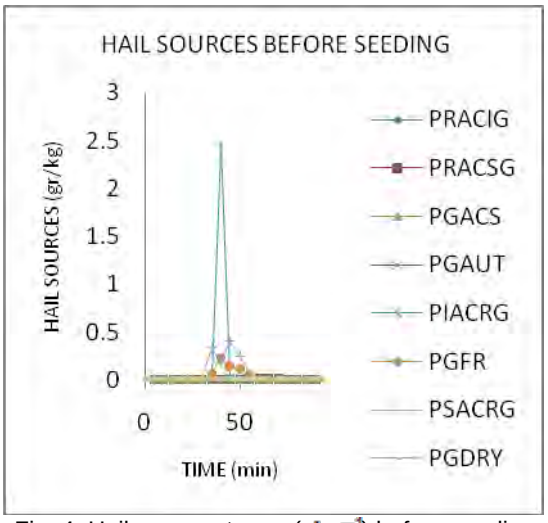


Fig. 4. Hail sources terms (gkg^{-1}) before seeding

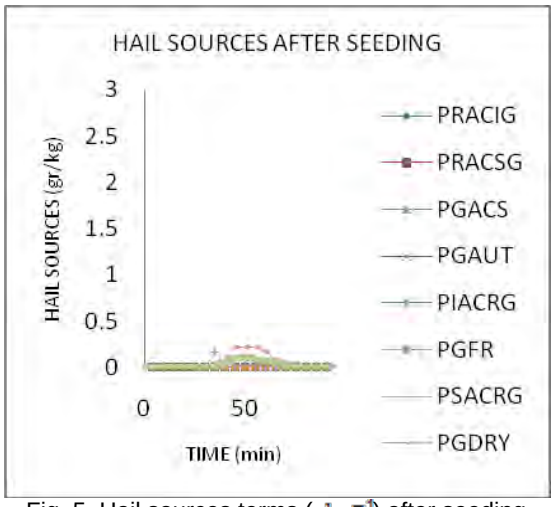


Fig. 5. Hail sources terms (gkg^{-1}) after seeding

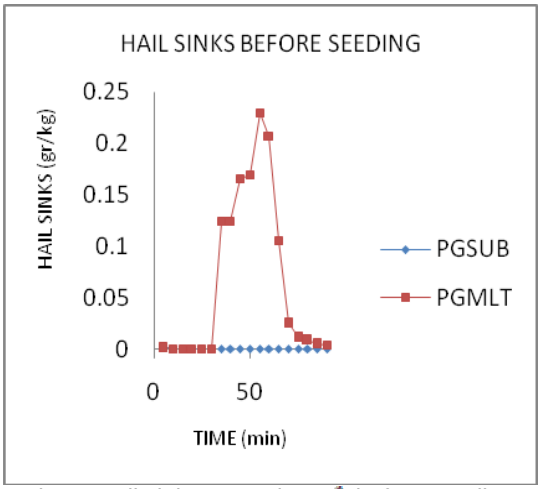


Fig. 6. Hail sinks terms (gkg^{-1}) before seeding

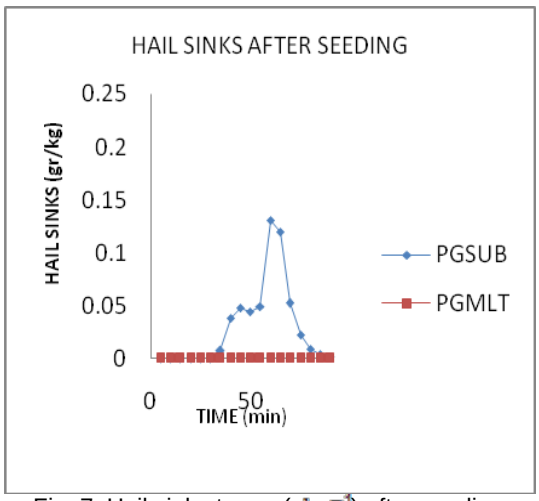


Fig. 7. Hail sinks terms (gkg^{-1}) after seeding

References

Asai T. and A. Kasahara, A Theoretical study of the compensating downward motions associated with cumulus clouds, *J. Atmos. Sci.,* **24**, 487-496, 1967.

Jamali J. B., S. Javanmard and Sh. Fateh, Investigating about hail event in Iran and methods of control and hail suppression, ***14th*** *Geophys. Conf.*, Iran, 2010.

Javanmard S., J. B. Jamali, M. Karimpirhayati and Y. Abedini, Numerical study for role of cold convective cloud parameterization in precipitation pattern at ground**,** ***14th*** *Geophys. Conf.*, Iran, 2010.

Lin Y. L., R. D. Farely and H .D. Orville, Bulk parameterization of the snow field in a cloud model, *J.Climate Appl. Meteor*., 23, 1065-1092, 1983.

Ogura Y. and T. Takahashi, Numerical simulation of the life cycle of A thunderstorm cell, *Mon. Wea. Rev*., **19**, 895-911, 1971.

Zhen Z. and L. Heng-Chi, Numerical simulation of seeding extra-area effects of precipitation using a three-dimensional mesoscale model, *Atmos. Ocea. Sci*., **3**, 19−24, 2010.

METHODS OF MODELING IN CONTROLLING THE PROCESSES IN CLOUDS

(*B.Sh.Kadyrov, V.P.Kurbatkin, Republic of Uzbekistan*)

In Uzbekistan which is in the area of Turan climate (type of the dry subtropics) the main interest is in the activities on precipitation enhancement and hail prevention. These activities are being conducted since the middle of 1960s. During the last decade with the available technical means which facilitate the implementation of different regimes of reagent injection to different parts of the cloud the issue improvement pf seeding technique arose. The basis for this is comprised by:

- knowledge of mechanism of effect of cooling agents and crystallizing agents [2.6];
- tested schemes of the cloud seeding and recommended norms of seeding determined by a small number of cloud parameters which do not require the airborne laboratories;
- the theory of precipitation, both widespread and shower ones which provides the forecasting of clouds and precipitation with indication of their amount [1, 9, 10].

We studied the models of the convective and non-convective clouds on the base of which the possibilities and different ways of managing the processes of dispersion, triggering of precipitation and intensification of natural precipitation from non-convective clouds in operational activities and the ways of prevention of the hail, showers causing the floods and washing-out of soil through the seeding of convective clouds are shown.

By [1] it follows that non-convective clouds are the clouds for which the big horizontal extension (hundreds of square kilometers and more) and low velocities in them during their formation, evolution and disintegration (10^{-5}-10^{-3})ºC/s are characteristic. As the main reasons of condensation processes in clouds are the vertical currents, then the rates of temperature changes can be characterized by vertical velocities. For the analyzed clouds they are 0,1-10 cm/s. These velocities are averaged by space and time in the ranges of: 10 - 100 km by horizontal and – 10^{-1}-1,0 km by vertical; the time range is about one hour.

The considered model of such cloud is presented in [4, 5]. The process of cloud development can be presented as follows. In nimbostratus cloud two stages can be distinguished by the time of development: this is the time before the formation of particles and after with indication of differences in their phase structure with performance of separate functions; and also three layers with possible sublayers: layer of cloud particles formation with the minimum thickness and the vertical extent of which is from several tenths of meters; middle layer of the average growth of cloud particles and precipitation usually with thickness of 2,0 - 2,5 km and the upper layer of formation of precipitation particles with vertical extension up to several hundred meters. The absence of the later one corresponds to the cloud where no precipitation is formed, and in the middle layer the size of the cloud particles is increased.

The characteristic sizes of the clouds and precipitation and the time of their growth are given. The ways of weather modification via the interference to the considered functions of the process of the cloud-and-precipitation formation are presented in brief.

Such idea does not contradict the experimental data and theoretical conclusions. Basing on this model the thin clouds can be dispersed due to the enlargement of the cloud sizes, while with the existence of “jets” over the cloud field it was possible to extract moisture form the cloud in a form of fine crystals. It is possible to deposit liquid moisture from cloud in a form of precipitation. Actually, the clouds with vertical extension up to 600-1000 m can be dispersed. The clouds with positive temperature and thickness of not more than 200-300 m can be dispersed as separate clouds.

Using the tested ways of weather modification the super-cooled clouds with vertical extension up to 1500 m can be dispersed with greater degree of reliability.

The artificial precipitation can be originated from the water-containing stratiform clouds with the layers of negative temperatures.

The seeding of clouds with vertical extent not less than 1.0 km and temperature -15°C and less on the upper limit of cloud layer will be of practical value. When temperature value on the upper limit is near 20 - (-22)° C the stratiform cloud can be converted to nimbostratus cloud in the result of seeding.

When the seeding is conducted for getting the additional precipitation for the purposes of economical activities it is necessary to pay attention to precipitation structure, while the major part of precipitation should be left in the layer under the clouds. By their amount their quantity should be enough not to be lost after their falling on the soil surface and penetrating to a small depth just after the effect on the evaporation. With the model and numerical experiments it is necessary to calculate properly the amount of artificial precipitation which can be produced in the result of seeding comparing it with the useful one. One of these indices is the duration of the cloud process. Amount of precipitation falling out during the uniform process should exceed 2 mm. In autumn in the non-irrigated agricultural lands seeded by the winter wheat it is rational to conduct the seeding if the total precipitation amount (natural and artificial) is not less then 20 mm during the autumn vegetation period.

When the weather modification on clouds is made with the purpose of intensification of the natural precipitation the solution of task is simplified considerably. As a rule, precipitation from these clouds reaches the ground surface. Its intensity is 1.5-3.0 times more, and the duration of such deposition processes in the mean climatic value is ~5 h.

However, during the seeding it is necessary to pay attention to the formation of the sufficient number

of the natural crystals, on the principal possibility of increase of the vertical extent of cloud. In practice it is necessary to pay attention not only on the lower limit of getting the possible additional amount of artificial precipitation during the single process of their falling which was mentioned above (seeding with the aim of precipitation), but also on the upper limit and also on precipitation amount during a season when the seeding is conducted. For example, if we would like to moisten the soil or to increase the surface flow, then the requirements to the parameters of clouds on which WM is conducted will be different.

Limitations in the cloud seeding increase in the regions where the probability of negative weather events (floods, landslides, mudflows, etc.) exists.

Let's consider the role of condensation growth of precipitation particles. Stratiform cloud is presented as three types of layers with distinguishing of two types of development. The first one when the lower and middle part of cloud where the origination and condensation growth of cloud particles take place, are liquid-drop ones in some approximation, and the second stage when the subsidence of crystals in upper part has began, and the cloud in its main part becomes the mixed one. In the purely crystal and purely aqueous clouds the cloud processes of precipitation formation will be very weak because of the slow growth of precipitation particles with the small supersaturation. As it was already mentioned above, the growth of precipitation particles takes place on the border between the liquid-and-aqueous and solid phases where for crystals the supersaturation is 20 times and more then for the drops. The same growth will be for any ice part in the liquid-and-drop cloud. This relates to the rare crystals which were formed in the cloud when the probability and share of which is increased with the decrease of loss of temperature with temperature loss (their growth is described with condensation process) as well as of the subsiding solid precipitation particles the growth of which is described by the process of condensation and coagulation, simultaneously. This is very important aspect which is lost from the view of researches. Small-size snow flakes subside faster than the drops and grain of the same mass. Their velocities are measurable with the tenths of centimeters per second. They will pass through the layer with vertical extent of 400 m and maximum water content during 100-1000 s. During this time the condensation increment will be comparable with coagulation one. For small values of water content (0.1 g/m^3) the snow flakes the mass of which is equivalent to drops with 30-50μ radius due to coagulation process in 2km cloud layer will increase 1,5-1,8 times, and with the higher water content (0.3 g/m^3) – about two times (Fig. 1. 4). Regarding purely condensation growth in 400m layer in the temperature field of -12° C with high falling velocity (0.8 m/s) snow flakes will increase 1.5-2.5 times while with the lower velocities (0.4 m/s) – 2-3 times.

This shows that only the upper part of cloud should be seeded with creation or increment of crystal layer with preservation of the mixed central part with characteristic moisture content which is defined by temperature in a cloud and by the drop sizes.

Present state of knowledge of the laws of movements (sedimentation) of particles in a solid medium gives possibility to estimate the sizes of granules which will enable formation of crystals in the cloud layer with any prescribed vertical extent of its supercooled part. With the rated reagent quantity it is possible to regulate the process of precipitation formation. Using the sets of granules of different sizes it is for example, possible to crystallize the part of existing crystal layer with simultaneous introduction of the small number of bigger granules, to increase sizes of the cloud particles in the inner part of cloud or to deposit the lower part of this supercooled cloud, etc.

In perspective, using the ice-like reagents and regulating the sizes of crystallization nuclei it is possible to work out the methods of seeding of cloud with a big transverse size from a single seeding band. Variations of the granules sizes enable to find the methods of seeding with a delay of time of cloud seeding process which is required in the conditions of the complex orography of Central Asia when the air flights can not be performed because of safety measures. In this situation the seeding can be performed with AgJ aerosol the particle sizes of which are less then "critical" one with the given cloud temperature. The delay of cloud crystallization is possible with seeding the over-cloud layer by the ice-like reagent. It is also possible to work out the methods of the transfer from diffusion of the small round-shape with the high reagent concentration inside to the turbulent diffusion [4, 8, 11] with simultaneous dispersion of these nuclei over the space in the result of turbulent diffusion.

The methods of calculation of extension of zones of the passive admixture (aerosol including the small-size crystals) in the result of turbulent diffusion are worked out both theoretically and experimentally, in particular.

At present it can be stated that it is possible to disperse the clouds, initiate precipitation from clouds from which the natural precipitation does not fall, and intensify the natural ones when seeding the individual classes of clouds. The general typical feature for all these classes of clouds is the existence of the water part with negative temperatures in them. From them it is possible to distinguish the classes of clouds during the seeding of which the highest efficiency and performance for many sectors of human economical activity are reached. For Central Asia they are determined with the assessment of their economical expediency.

We consider some results of simulation of processes of the convective clouds development in the natural process and with the cloud seeding for the prevention of the severe weather phenomena (showers, floods, hail). As the instrument for the conduction of numerical experiments the non-stationary one-and-half numerical model of convective cloud developed by the researches of the State Geophysical Observatory of Russian hydrometeorological administration

and adapted (B.Sh.Kadyrov) was used for the above mentioned tasks.

The data of radiosounding were used as the input information for model. About 400 cases of radiosounding during 1981-1993 were selected. Total number of estimated days was 213. The calculations for the other days were deleted by different reasons.

From the resulted print-outs the following parameters were selected: maximum vertical velocity (Wмax) and maximum horizontal velocity (Umax), depth of the upper (Нв.г) and lower (Нн.г) cloud limits, vertical cloud depth (ΔH), water content in a cloud (QC), rain water content in cloud (QR) and ice content (QI). Further with the processing software the patterns of the change of the mentioned characteristics in time were created.

For the assessment of resource capacity (which in fact is regarded as the dynamical seeding capacity (DSC**)** we used (Нв.г) parameter. With this the increment of the upper cloud limit after imitation of seeding was defined.

The model was adjusted in such a way that in the assessment of the dynamic capacity of seeding the numerical experiments were conducted with the constant parameters responsible for the microphysical processes.

On the base of the model experiments it was estimated that for the precipitation enhancement the optimal concentration of crystals is 100 part/l for convective cloudiness taken as the basic one for conduction of numerical experiments.

The summarized results of calculation with numerical model are given in table below.

Frequency of (%) values of DSC in different months for 1981-1993.

	DSC (km)					N
Months	0	0 - 1,5	1,6 – 2,5	2,6 - 3,5	ΔS>3 ,5	
April	36	15	23	12	14	91
May	31	17	28	10	14	74
June	13	31	25	18	13	48

N – number of cases of radiosounding.

It was estimated that the mean value of DSC with inclusion of all zero values for cloud with 5 km radius was 2,2 km. With elimination of zero values it was 3,6 km.

With this in April the mean value was 1,6 km, and with elimination of zero values it was - 2,7km: in May the mean values were 2,1 km and 3,6 km, and in June - 3,7 km and 5,1 km, respectively.

Thus, in conduction of numerical experiments as in [12] we faced a lot of cases when DSC ("seedability" in their terminology) was equal to zero.

By data of Wiggert V., Sax R.I., Holle R. it follows that the share of such cases was 28 - 33 % of all simulated cases. In one cases the authors of these works regarded them as the false "seedability" while in the others – as the cases which are inappropriate for the cloud seeding. By their data approximately in one of three days DSC has zero value even with the highest radius of the cloud towers.

Unlike them we used the non-stationary model which made it possible to study the change of DSC inside the life cycle of the cloud development. Maximum DSC for us was the particular result while the stationary model gives only maximum value of DSC with the given set of the input data. If the parameter in the simulation of seeding did not exceed the maximum value in the case without seeding, then we regarded this case as zero "seedability". Even when DSC is zero, then within the life cycle of cloud it can not be different than zero. This means that there is seeding capacity within the life cycle. We think that it can be attributed to the resources of precipitation redistribution, as the upper cloud limit remained unchanged in the result of seeding.

Numerical experiments on the study of the process of precipitation formation were conducted for checking different aspects of the seeding techniques. The main attention was paid to the working out of different ways of reagent injection to the convective cloud, both spatially and temporarily.

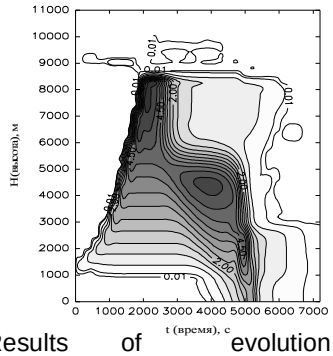


Fig.1. Results of evolution of cloud with 5-km radius in the natural development

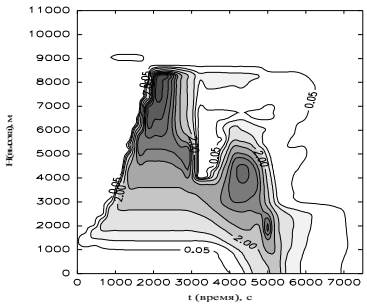
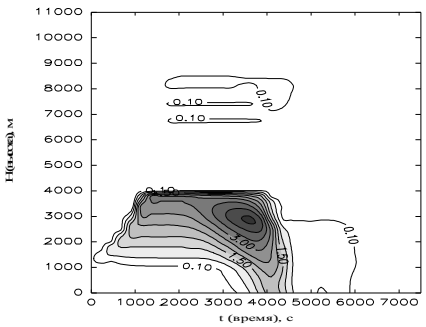


Fig. 2 presents the same process in the first 3000 sec., after which the imitation of point seeding was made at 4000 m elevation.

Fig. 3 presents the same process with the condition of permanent ground-based seeding preceding the development of cloud itself.



It follows that in the first case of seeding (Fig.2) the cloud development was ceased at 5th minute. Later it did not reach the elevation values corresponding to the natural development process. With the uninterrupted seeding of the space up to the formation of cloud the cloud life and its upper limit were reduced. The last option foresees the possibility of prevention of the cloud development in separate valleys with the valley winds by simple means of seeding. The objective of such seedings is the prevention of the severe weather phenomena. The advantage is the target-oriented flow of reagent in the constrained space.

In the result of analysis of numerical experiments it was defined that the higher the blocking level (the limit over which the liquid drops do not pass) is – the more water can accumulate in the cloud. Another important result is that the effect of the level of reagent injection on precipitation intensity is determined. Thus, the regent injection on the level of -16°C isotherm caused the considerable decrease of precipitation intensity due to the certain increase of precipitation area comparing with the results of experiment when the injection of reagent was performed at -6 °C level.

Variation of the level of reagent injection has shown that the effect of shifting of precipitation maximum on the ground is recorded. The lower level of reagent injection resulted in the higher values of the cloud moisture at 7-9 km.

Thus, the conducted numerical experiments have shown that the blocking injection of reagent (injection on the whole lower cloud layer) causes the sharp reduction of the liquid-drop part in the upper part of cloud and change of precipitation intensity on ground surface. The second important result is that depending on the purpose of cloud seeding it is possible to change the process of precipitation formation by the change of the level of reagent injection. For example, if it is necessary to delay the beginning of precipitation, then the blocking seeding with reagent should be at the level of (-4)°C - (-6)°C isotherms, while if it is needed to lessen the precipitation intensity – then the reagent should be injected at the level of (-16)°C. It is also important to note the interesting result regarding the physical efficiency of seeding in the field of low negative temperature values (-22)°C - (-24)°C which demonstrates that seeding in this field regardless the sufficient crystal number can also facilitate the regulation of the process of precipitation formation.

In conclusion we note that the use of results of numerical modeling for the assessment of cloud resources is improved by the estimates themselves, which up to present are based on climatic workouts regarding the ground meteorological data. The improvement is due to the account of physical processes taking place during seeding.

References

1. Kachurin L.G. Physical principles of weather modification. L.: Hydrometepizdat, 463, 1990.

2. Krasnovskaya L.I. Physical principles of seeding of supercooled clouds with cooling reagents. Proc. of CAO.- Vol. 58-78 1964.

3. Kurbatkin V. P., Ushintzeva V.F. On evaluation of different means of bringing the reagent to the supercooled cloud. Proc. of SANIGMI.- Vol. 46(61).. 25-43. 1969

4. Kurbatkin V. P. Structure of nimbostratus cloud and interaction between its separate parts. Proc. of SANIGMI. - Vol. 154(235). 5-26. 1998

5. Kurbatkin V. P. Principles of management of processes in clouds in case of airborne seeding. Tashkent, 166, 2005.

6. Nikandrov V.Ya. Weather modification on clouds and fog. L.: Gidrometeorizdat. 190. 1959.

7. Raist P. Aerosols. Introduction to theory. MIR Publ. House, 287, 1987.

8. Fuks N.S. Mechanics of aerosols. - M.: Proceedings of AcSc of USSR. 351. 1955

9. Shifrin N.S. Kinetics of precipitation formation. Proceed. of SGO. Vol. 31(93). 32-40. 1951

10. Shishkin N.S. Clouds, precipitation and thunderstorm electricity. L.: Gidrometeorizdat. 400. 1964.

11.Shlikhting G. Theory of boundary layer.- M.: Science. 744. 1969.

12. Wiggert V., Sax R.I., Holle R.I. About potential of seeding on summer convective cloud in Illinois (USA) a comparison with observation in Florida and in experiment FASE. J. APP. Meteorol. Vol. 21, 1293-1322,1982.

A three-dimensional numerical simulation of supercell hailstorm seeding over Greece using a cloud model

Theodore Karacostas[1], Vlado Spiridonov[2], Dimitrios Bampzelis[1] and Ioannis Pytharoulis[1]

[1]Aristotle University of Thessaloniki, Department of Meteorology and Climatology, GR- 541 24, Thessaloniki, Greece. e-mail: karac@geo.auth.gr
[2] Republic Hydrometeorological Service, Skupi bb 1000 Skopje

1. Introduction

Based upon the structural and evolutionary properties, convective hailstorms could be classified as single cell, multicell and supercell (Marwitz, 1972a, b). The supercell hailstorm cloud usually consists of one and rarely from more cells. It has horizontal and vertical development more than 30 km and 12km, respectively. Circulation wise, the embryo formation area (EFA), the hail growth region (HGR) and the hail cascade area (HCA) are adjacent within the storm (Karacostas, 1989). Such a circulation supports the regeneration of the ascending airstreams in cloud. Case studies are carried out in order to verify and document the value of the cloud model used in contributing to the understanding of supercell convective storm dynamics and microphysics. The examined supercell hailstorm, which occurred over Greece on the 17 June 2009, is analyzed in this study. Numerical simulation of supercell hailstorm seeding has been performed according to the seeding methodology, seeding hypothesis and seeding rates adopted by the Greek National Hail Suppression Program (NHSP) (Karacostas, 1984 and 1989). The examination of the performance and capability of the model is tested through comparisons between simulated and observed radar reflectivity fields (PPI and RHI) plots, being provided for the selected case study by the TITAN software tool (Thunderstorm Identification, Tracking, Analysis and Nowcasting), (Dixon and Wiener, 1993).

The cloud model formulation is briefly described. The boundary conditions and numerical techniques are then explained, followed up by a brief explanation of the seeding methodology. The analyses continue with the numerical simulation of the supercell hailstorm seeding with the comparative analyses. Finally, the results are followed by discussion and the conclusions are summarized.

2. Model characteristics

Only few basic characteristics of the model are summarized here. The present version of the model is a three-dimensional, non-hydrostatic, time-dependant, compressible system, which is based on the Klemp and Wilhelmson (1978) dynamics, Lin *et. al.* (1983) microphysics, and Orville and Kopp (1977) thermodynamics. The bulk microphysical parameterization uses a double-moment scheme for all species. The activation of AgI is parameterized by the three nucleation mechanisms based on Hsie (1980) and Kopp (1988), which are deposition (including sorption) nucleation, contact freezing nucleation, Brownian collection and inertial impact due to cloud droplets and raindrop. The calculation of agent dispersion is done by using an additional conservation equation. Since, in its initial phase the model dispersion of the agent takes place on a sub-grid scale, the advection and diffusion are represented by individual puffs, which spread in time according to the turbulent diffusion coefficients proposed by Georgopoulos and Seinfeld (1986). The equivalent radar reflectivity factors for hail and rain are computed on the equations given by Smith et. al. (1975) and empirical equation for snow by Sekhon and Srivastava (1970). More detail information about the model, initial and boundary conditions, numerical technique and initialization could be found in Barth et. al. (2007).

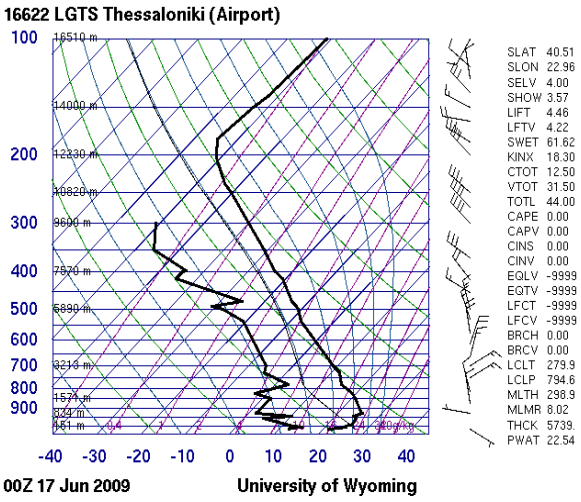


Fig. 1 A representative sounding taken at 00 UTC for Thessaloniki, Greece from University of Wyoming on June 17, 2009

2.1. Initial conditions and initialization

Initial impulse for convection is an ellipsoidal warm bubble with the maximum temperature perturbation in the bubble center (T_o = 2.8°C). The model domain is 61 km x 61 km x 18 km^3. The horizontal resolution of the model is 0.5 km, while the vertical one is 0.2 km. The temporal resolution of the model (time step) is 10 s for the integration of the dynamics, microphysics and chemistry and a smaller one (2 s) for solving the sound waves.

2.2. General characteristics of hailstorm case

The convective cloud observed on 17 June exhibits the general characteristics of the supercell hailstorm. The intensive cloud activity that was observed in the afternoon hours, is registered on the whole territory of northern Greece from 14:47 to 16:03.

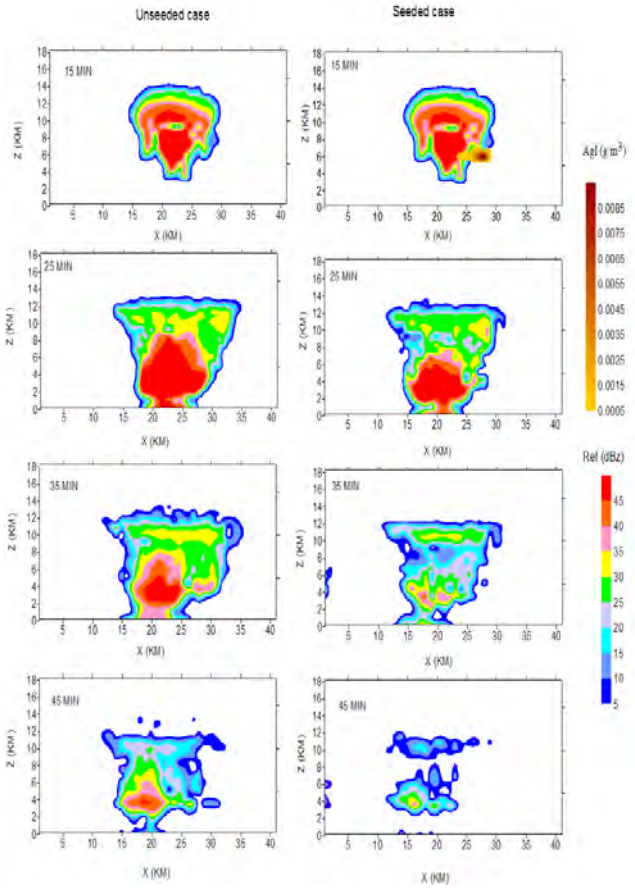


Fig. 2. Model simulated vertical transects of the reflectivities along NW-SE, from 15 to 45 min, at 10 min time intervals. a) Unseeded case. b) Seeded case. A seeding agent placement is shown on the first r.h.s. panel from above.

2.2. General characteristics of hailstorm case, occurred in northern Greece on June 17, 2009

The convective cells with heights up to 5-8 km, exhibited the maximum reflectivity values (around 66 dBz). The maximum observed heights of cloud top were around 15 km. The life cycle of the convective cloud was about 70 min. The hailstorm was moving with mean speed of 55 km/h from NW to SE flow. The dominant observed phenomena were intensive showers, hail and strong wind. Hailfall is registered around 30 min from the beginning of the radar observation.

2.3 Seeding approach

The adopted seeding hypothesis is based on the beneficial competition theory, which is specifically described by Karacostas (1989). In this particular case study, the seeding was conducted at the cloud top and the AgI was introduced within the area bounded by the temperature zones of -10 °C and -8 °C. The preferable areas were chosen to be on the upshear side of the storm and to exhibit strong updrafts and high values of liquid water content and lack of ice. The seeding rate was chosen to be 1 to 2 flares of 20 g every 5 seconds. The time seeding duration was 4 to 5 min, flying back and forth, from SW to NE. The seeding rate, in this particular case study, is ten times larger than the aforementioned. In this case, the aircrafts seeding of this vigorous convective cloud started at its early developing stage, that is, at 15 min, within the main and mostly secondary inflow region, with enhanced updrafts, associated with the new growth zone of the later developed supercell storm, when the reflectivity reaches and exceeds the 35 dBz, between -5° C and -30 °C, at about 6 km height a.s.l.

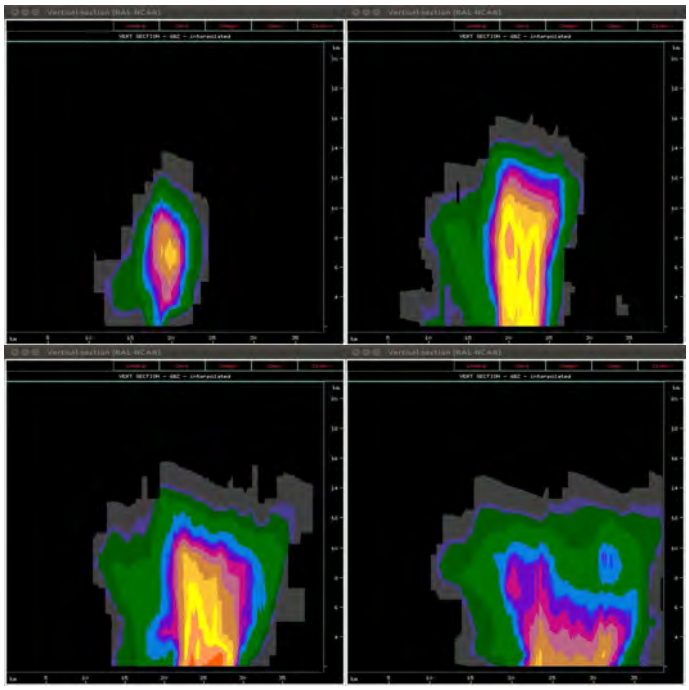


Fig. 3. RHI echoes recorded by TITAN system on 04.08.2007 from 15 to 45 min at 10 min time intervals. The first echoe is observed at 15:03 local time, while the last echo is observed at 15:33 local time

3. Results

3.1 The numerical simulation of hailstorm seeding

Numerical simulation of hailstorm seeding has been performed following the operational hailstorm seeding operational method applying in the Greek NHSP. A three-dimensional numerical simulation has shown a typical supercell hailstorm with intensive growth. The maximum simulated vertical velocity is 27.6 m/s, the cloud top reaches 16.8 km and the total accumulated rainfall at the ground is 55.7 kg/m^2. The maximum simulated radar reflectivity of 70 dBz is slightly lower than the observed radar reflectivity (66 dBz). The max calculated mixing ratio of cloud water, cloud ice, hail, rain and snow is: 7.4, 7.2m 17.5, 9.7 and 5.2 g/kg,

respectively. As it is illustrated in Fig. 2b (top panel), seeding material is correctly introduced at the cloud side, in the main inflow area, in radar reflectivity zone greater than 35 dBz between -8 °C and -10 °C.

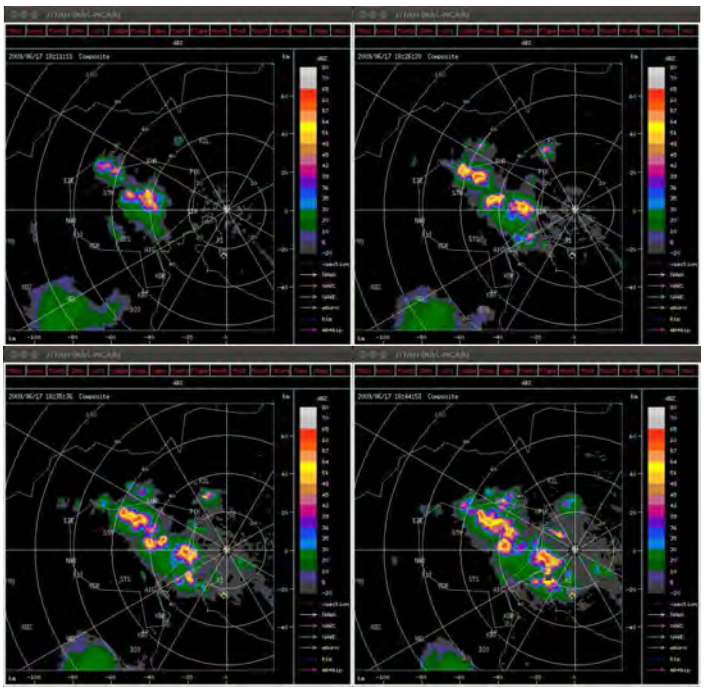


Fig. 4. PPI echoes recorded by TITAN software system on 04.08.2007 from 15 to 45 min at 10 min time intervals. The first echoe is observed at 15:03 the local time, while the last echo is observed at 15:33 local time

The silver iodide aircraft seeding trajectory is well seen in the horizontal cross section plot shown in Fig. 5 (also r.h.s. top panel). Seeding material in convective cloud is realized in 15 min of the simulation time. The positive or negative effects of the hailstorm seeding could be identified by comparing the radar reflectivities (horizontal and vertical transects) in a different time intervals, between the unseeded and seeded cases. A slight difference is noted on the radar reflectivity patterns a few minutes after the seeding, as it is shown in a vertical cross section of the radar reflectivity fields at 10, 20 and 30 min after the initial seeding. The change of the reflectivity structure is also evident at the horizontal cross section of the reflectivity echoes (see Fig. 5a, b). Seeded case, exhibits a slight increase of the reflectivity 10 min after the initial seeding (as it was expected) and rapidly decrease of it at 25 min after the seeding. The RHI plots shown on Fig. 3, and PPI plots at the same time intervals provided from TITAN, show a relatively similar reflectivity patterns. The difference becomes more evident in the cloud mature stage, when intensive rainfall occurs. By comparing vertical and horizontal transects of reflectivity fields at 25, 35 and 45min (Fig. 2 and 5), a distinct picture of the positive effects of hailstorm seeding is obtained. Radar reflectivity in seeded case is substantially decreased 30 min after the initial seeding. A more realistic view of the hailstorm occurred in northern Greece on June 17, 2009 is visualized through a three-dimensional numerical simulation of the cloud.

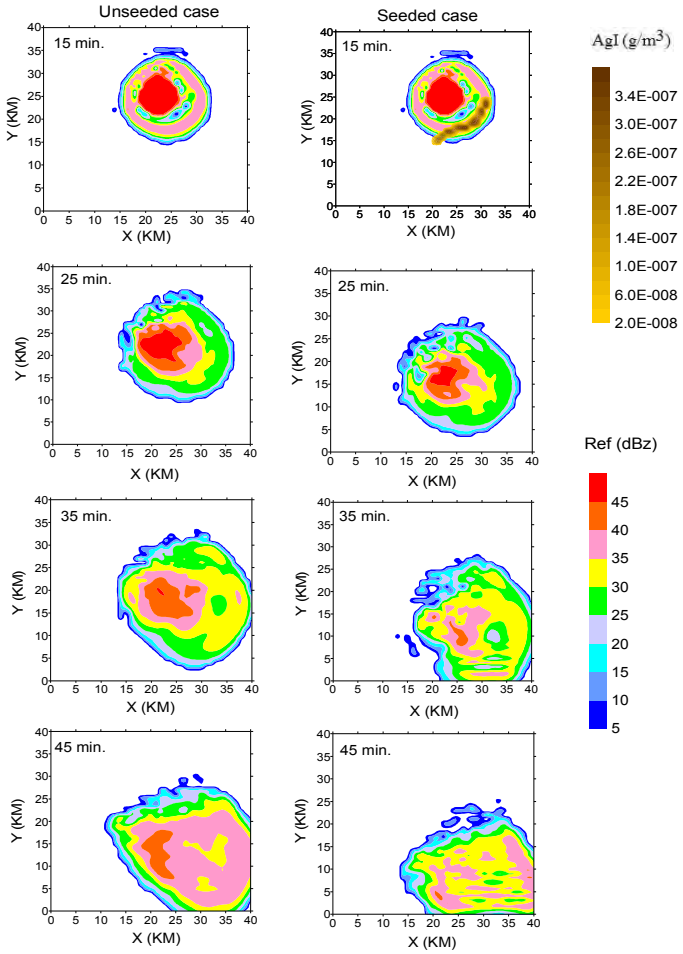
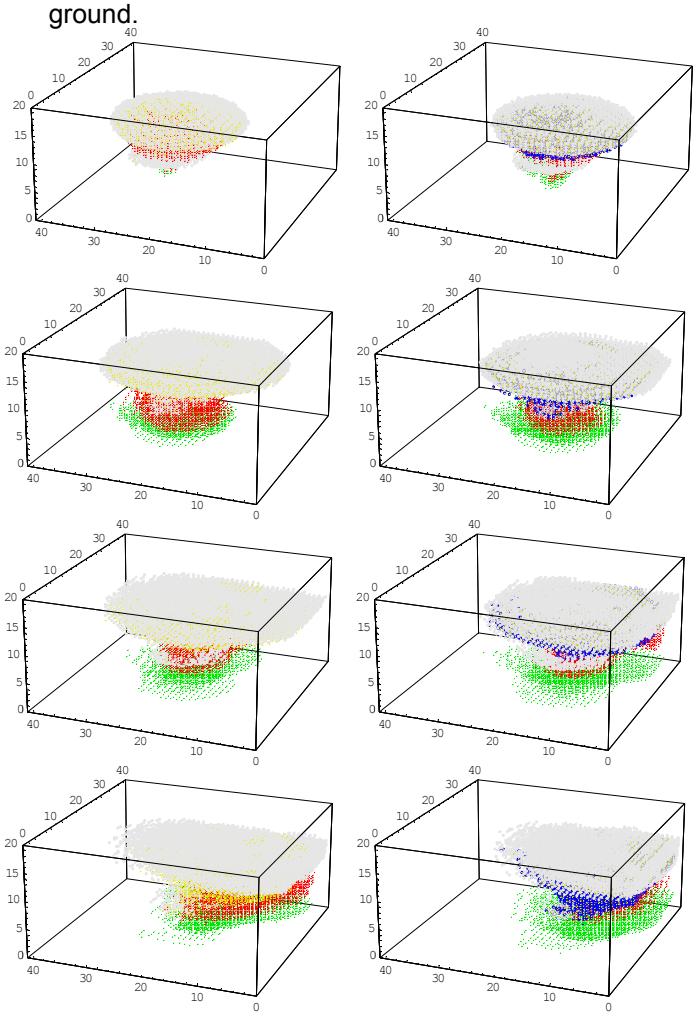


Fig. 5. Model simulated horizontal cross sections of the reflectivity's at height=7 km a.s.l. from 15 to 45 min. at 10 min time intervals. a) Unseeded case. b) Seeded case. A seeding agent placement is shown on the first r.h.s. panel from above.

Fig. 7a, b shows 3-D depictions of the cloud life cycle viewed from the southeast (SE) with hydrometeors (cloud water, cloud ice, hail, rain and snow), expressed through mixing ratios, together with seeding material, which is released by aircraft seeding (see Fig. 7b). The plot size dimensions of AgI have been increased for visualization purposes. It is well seen how seeding material is released in the appropriate place in the inflow region (see blue fields), within the hailstone growing area, during the growing phase. The cloud grows quite rapidly and the upper portion extends towards SE ten min after the seeding. The internal structure and the horizontal extension of the apparent anvil, categorize this cloud as a typical supecell hailstorm. The panels at 25 min show that some of the AgI has been used up and some has been transported to southeast. Most of the seeding material has been activated within the 25 min. It is obvious that seeding has contributed in modification of the cloud environment, which is more visible 20 and 30 min after the initial seeding was performed. Seeded case shows rainwater field increase and slight hailfall decrease in 25 min. The difference between the internal structures of both

cases becomes more evident in 35 and 45 min of the simulation time. AgI seeding has modified the in-cloud volume and caused enhanced rainfall at the ground.



(a) (b)

Fig. 7 Three dimensional depictions of the cloud (cloud water+cloud ice-grey; hail-red, rain-green, snow-yellow and silver iodide-blue color) for the unseeded case viewed from the southeast. Cloud water, cloud ice, rain, hail and snow shown in these panels have 0.01 g/kg as the surface mixing ratios

4. Summary and conclusions

An attempt has been made to simulate a supercell hailstorm seeding occurred on June 17, 2009 in northern Greece using a 3-D cloud model. Seeding experiment is performed according to the seeding hypothesis adopted by the Greek NHSP. Taking into consideration the very fast growing of the hailstones within the supercell storm, it is pointed out the significant importance of delivering the AgI at the right time and place, according to the standard seeing criteria. Even this is a single analyzed case study, the greatest efficiency is achieved if sufficient amount of ice nuclei is introduced in the hailstone growing area during the phase of their formation, when the hailstones are small and the number of large cloud droplets is greater than the number of hailstones.

Simulation of aircraft seeding at the frontal part of the supercell hailstorm, in radar reflectivity zones greater than 35 dBz between the -8 °C and -10 °C isotherms results in cloud modification, change of the internal structure, hailfall decrease and total rainfall increase by 12.5 % with respect to the unseeded case. In spite the fact that this is only a single case study of a supercell hailstorm seeding, the obtained results are quite optimistic, in respect to the obvious potential for modification of cloud environment by applying appropriate cloud seeding with optimal placement, time and seeding amount.

References

Barth, M.C., S.-W. Kim, C. Wang, K. E. Pickering, L. E. Ott, G. Stenchikov, M. Leriche, S. Cautenet, J.-P. Pinty, Ch. Barthe, C. Mari, J. H. Helsdon, R. D. Farley, A. M. Fridlind, A. S. Ackerman, V. Spiridonov and B. Telenta, 2007: Cloud-scale model intercomparison of chemical constituent transport in deep convection Atmos. Chem. Phys., 7, 4709–4731,

Dixon, M. and Wiener, G., 1993: TITAN: Thunderstorm Identification, Tracking, Analysis and Nowcasting – A radar-based methodology. *J. Atmos. Ocean. Tech*. 10, 785-797.

Durran, D. R.: The effects of moisture on mountain lee waves. *Ph.D. Thesis, Massachusetts Institute of Technology* Boston, MA (NTIS PB 82126621), 1981.

Georgopoulos, P.G., and J.H. Seinfeld: Mathematical modeling of turbulent reacting plumes-General theory and model formulation. *Atmos. Envir*., 20, 1791-1802, 1986.

Karacostas, T. S.: The Design of the Greek NHSP. *Proc. 9th Conf. on Wea. Mod.*, A.M.S., Park City, Utah, USA, 1984.

Karacostas, T. S.: The Greek National Hail Suppression Program: Design and Conduct of the Experiment. *Proc. 5th WMO Sci. Conf. on Wea. Mod. And Appl. Cloud Physics*, WMO/TD-269, CHINA, 605-608, 1989.

Klemp, J. B. and Durran, D. R.: An upper boundary condition permitting internal gravity wave radiation in numerical mesoscale models. *Mon. Wea. Rev*., 11, 430-444, 1983.

Klemp, J. B. and Wilhelmson, R. B.: The simulation of three-dimensional convective storm dynamics. *J.Atmos.Sci.*, 35, 1070-1096, 1978.

Hsie, E.-Y., R.D. Farley and R. D. Orville: Numerical simulation of ice-phase convective cloud seeding. *J. Appl. Met*. **19**, 950-977, 1980.

Marwitz, J.D.,: The Structure and Motion of Severe Hailstorms. Part I: Supercell Storms. *J. Appl. Meteor.*, **11**, No. 1, 166-179, 1972a.

Marwitz, J.D., 1972b: The Structure and Motion of Severe Hailstorms. Part II: Multi-Cell Storms. *J. Appl. Meteor.*, **11**, No. 1, 180-188, 1972b.

Marwitz, J.D., 1972c: The Structure and Motion of Severe Hailstorms. Part III: Severely Sheared Storms. *J. Appl. Meteor.*, **11**, No. 1, 189-201, 1972c.

Lin, Y. L. Farley, R. D. and Orville, H. D.: Bulk water parameterization in a cloud model. *J.Climate Appl. Meteor.*, 22, 1065-1092, 1983.

Smith, P.L, G.G. Myers and H.D. Orville: Radar reflectivity calculations on numerical cloud models using bulk parameterization of precipitation. *J. Appl. Meteor.*, 14, 1156-1165, 1975.

Orville, H. D. and Kopp, F. J.: Numerical simulation of the history of a hailstorm. *J.Atmos. Sci.*, 34, 1596-1618, 1977.

Sekhon, R.S. and Srivistava: Snow size spectra and radar reflectivity. *J. Atnos. Sci.*, 27, 299

Study, choose microphics and comulus convection schemes in WRF Model to forecast heavy rain in Vietnam

Truong Ba Kien, Institute of Meteorology, Hydrology and Environment (IMHEN), Vietnam.

Heavy rain is a dangerous meteorology phenomenon which often happening in Vietnam. To predict heavy rain is essential in reduction influences of heavy rain on Vietnam social-economy. However, to forecast heavy rain for VN is very difficult and complex, especially when there are combining of two or more different formations of weather. The precipitation predicting including heavy rain forecasting is more and more better thanks to development of computer and numerical weather forecast models. Precipitation forecast is strongly influenced by the parameterization in the schemes of microphysics and cumulus convection of any model. Therefore, choosing the parameterization for the model is very important in the rain forecasting capability.

This report will study, choose and combinate (if necessary) 9 forecasting options which come from 3 different microphysics schemes: Kessler, EtaGCP, Thompson and 3 different cumulus convection schemes: Kain-Fritsch, Betts-Miller-Janjic, Grell-Devenyi in WRF Model version 3.2 precipitation forecasting in Vietnam. Two domains covering Vietnam and South China Sea with 27 km and 9 km of resolution are chose for 72 hour time range. Results showed that Thompson-Betts-Miller-Janjic (T_B) option is better than 8 remaining with the correlation index for rain forecast are 0.48 (24h forecast range), 0.34(48h forecast range) and 0.32 (72h forecast range). The FBI index at 15mm threshold for rain forecast are 0.43 (for 24h forecast range), 0.34 (for 48h forecast range) and 0.30 (for 72h forecast range).

NUMERICAL SIMULATION OF SEEDING MATERIAL DISPERSION BY GROUND-BASED AgI GENERATORS IN MOUNTAINOUS TERRAIN

Koloskov, B.P.[(1)], Korneev V.P. [(1)], Kleimenova A.V.[(1)], Sergeev B.N.[(2)], Shapovalov A.V.[(3)]

[(1)] Agency of Atmospheric Technologies (Agency ATTEX, ROSHYDROMET)
Novovagankovsky per. 8, Moscow, 123242, RUSSIA
Tel: +7(499)795-2372; Fax: +7(499)795-2134; e-mail: attech@mail.ru

[(2)] Central Aerological Observatory (CAO)
Pervomayskaya 3, Dolgoprudny, Moscow Region, RUSSIA

[(3)] High Mountain Geophysical Institute, Nalchik, RUSSIA

1. Introduction

It is known that ground-based generators are widely used in world practice of weather modification for cloud seeding with the purpose of precipitation enhancement and hail suppression. In particular, in United States, Morocco, Cuba ground generators are used to increase precipitation, while in France, Spain, Brazil - for anti-hail protection. Taking into account that the use of ground-based generators sometimes economically more expedient than the use of an airplane or rocket technology in 2005 ANO "Agency ATTEX" began to create ground-based and firework ice-forming aerosol generators.

To investigate the transport and dispersion of seeding material over the real terrain using different type of ice-forming generators three-dimensional numerical model SeedDisp was developed in “Agency ATTEX".

Description of the numerical model SeedDisp and some results of numerical simulation of glaciogenic seeding material dispersion by AgI ground-based generators in mountainous terrain are presented in this paper.

2. Numerical model SeedDisp

The model is intended for numerical simulation of atmospheric transport and dispersion of seeding material under the seeding by different type of generators. The modeling domain is three-dimensional mesoscale region with sizes from several tens to several hundred kilometers. A relief of terrain is taken into account.

The computations are fulfilled for given air wind and temperature fields, which are formed using upper air sounding and meteorological data. The data are interpolated on a finite-difference grid taking into consideration time change of the data. Atmospheric boundary layer is parameterized just like in the CULPUFF modeling system /Scire et al., 1999, Scire et al., 2000/. The parameterization is based on the energy balance method /Holtslag et al., 1983/. Initial data for computations are prepared on the basis of surface meteorological data.

The model allows to simulate atmospheric transport of seeding materials generated by different type of generators: 1) AgI ground stationary generator, 2) AgI and liquid nitrogen airplane generators, 3) pyrotechnical cartridges, 4) firework generator, 5) rocket generator, 6) dry ice pellets dropped from an airplane. Particles of seeding materials produced by the generators are imputed in discrete times and in those spatial points where generators are located at the times. The locations of ground generators are steady in time, but the airplane and rocket generators work on the trajectory of flight. The pyrotechnical cartridges and dry ice pellets produce the particles under drop from the airplane. The particles are produced as well by the firework explosion on a certain height above surface.

The particles of seeding materials propagate in the atmospheric boundary layer and free atmosphere. Atmospheric transport of the particles is simulated using the puff model /Scire et al., 1999/ for certain initial time after particles release. The puff model represents a continuous plume as a number of discrete packets of the seeding particles. The puff is then allowed to move, evolving in size, strength, etc. When dispersion of the particle concentration becomes comparable with sizes of the finite-difference grid, the concentration is recalculated on the grid. Thereafter the simulation is proceeded using the prognostic Euler equation for the particle concentration.

The equation is integrated by a third-order Runge-Kutta time integration scheme /Wang et al., 2009/. Advective terms of equations are represented by fifth-order schemes on the finite-difference grid. To provide monotonicity of solutions monotonic flux limiter is used. The computations are fulfilled on the finite-difference grid with 101 x 101 x 101 nodes. The model integration employed dx=dy= 2 km, dz=100 m.

3. Some results of numerical simulation of seeding material transport and dispersion

The described numerical model allows to study concrete problems of applied nature. In particular, the model SeedDisp can be used to obtain information about of seeding zones depending on the type, characteristics and operating modes of generators, and the weather conditions considering the topography and characteristics of the terrain.

Taking into account that the test operations of the new AgI ground-based generators planned in the

North Caucasus numerical simulation of seeding material transport and dispersion were performed for network of 22 AgI ground-based generators located at anti-hail fire locations in the Baksan mountainous area of North Caucasian Anti-hail Service (Fig. 1).

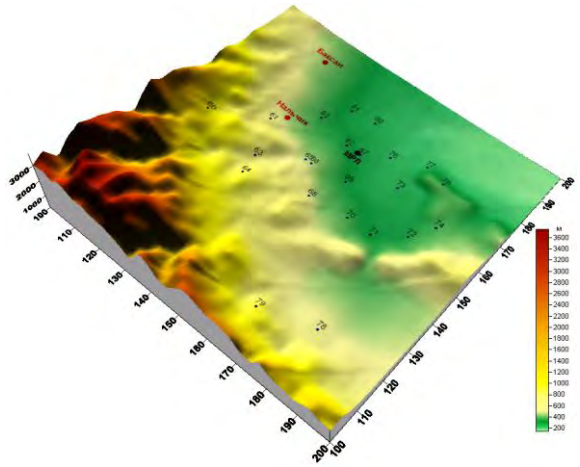


Fig.1. Topography and location of 22 AgI ground-based generators in the Baksan area of 100 km x 100 km.

As an example, Fig. 2 shows the results of calculations of ice-nuclei concentration ($1/m^3$) in the horizontal section at 0.5 km AGL and in the vertical cross-section 3 hours after the activation of AgI generators on May 10 (a) and May 14, 2007(b).

These results demonstrate the existence of substantial differences in the distribution of seeding reagent under different weather conditions observed during these days. So showers and thunderstorms were observed on 14 May and hail on May 10, 2007.

An analysis of results of numerical simulation and data of radar observations of clouds and precipitation collected over the Baksan territory during May-June 2007 led to the following conclusions:

1) The AgI plumes transport, dispersion and ice-nuclei concentration depend on weather conditions, the vertical wind profile, the terrain and the type of underlying surface.

2) It takes (at the least) about 20-60 minutes after the activation of generators (depending on weather conditions) as AgI plumes with ice-nuclei concentration of 10^4 - 10^5 $1/m^3$ reach heights of 1-1.5 km AGL.

3) The length of AgI plume with ice-nuclei concentration more than 10^4 $1/m^3$ is about 10-25 km and the width is about 3-10 km at transport wind speeds of 2-8 m/s. The distance of such zones from generators is from 2-5 to 20-25 km.

4) The three-dimensional numerical model SeedDisp has great potential for use in the development of schemes of the optimal placement of the ground-based generators, taking into account the topography and the type of underlying surface, and also to determine the modes of work of generators in ground-based seeding operations depending on the specific weather conditions.

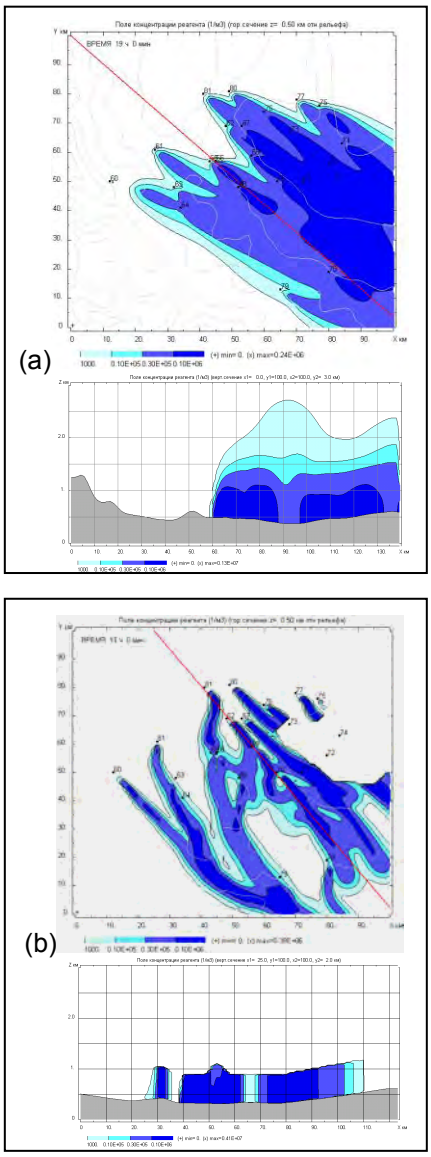


Fig. 2. Examples of SeedDisp model simulations of particle concentration ($1/m^3$) in AgI plum in horizontal and vertical cross-sections on May 10 (a) and May 14, 2007 (b).

References

Holtslag A.A.M., van Ulden A.P. A simple scheme for daytime estimates of the surface fluxes from routine weather data. *J. Clim. and Appl. Meteorol*, V.22, 517-529, 1983.

Scire J.S., Strimaitis D.G., Yamartino M.J. A user's guide for the CULPUFF dispersion model (Version 5). - Earth Tech. Inc., Concord, MA, 1999.

Scire J.S., Robe F.R., Fernau M.E., Yamartino M.J. A user's guide for the CALMET meteorological model (Version 5). - Earth Tech. Inc., Concord, MA, 2000.

Wang H., Skamarock W.C., Feingold G. Evaluation of Scalar Advection Schemes in the Advanced Research WRF Model using Large-Eddy Simulations of Aerosol-Cloud Interactions. - *Mon. Wea. Rev.*, V.137(8), 2547-2558, 2009.

Applications of Doppler Radar Characteristic Parameters in Artificial Hail Suppression Decision Making

Li Hongbin He Yuke Zhao Fansheng Pu Wenyao
(Dalian Weather Modification Office, Dalian, China, lhb7159@163.com)

1 Introduction

China is a large agricultural country as well as one of the countries which suffered serious hail disasters. Artificial hail suppression is an important measure in disaster prevention and mitigation. With the development of atmospheric science and related science and techniques, the ability of hail cloud identification and hail suppression improves continuously.

In recent years, with the rapid development of new-generation weather radar techniques, great progresses(Xu, H.-B., etc., 2004)(Chen, X.-G., etc.,2008) are made in the mechanisms of hail formation and new artificial hail suppression techniques, which provides the basis and foundation of scientific hail suppression operations. Based on the analysis of new-generation radar detection data, different radar parameters are concluded as evaluating indicesof hail suppression operations. To a certain degree, the technical merit of hail suppression is raised. Meanwhile, problems are also noticed. For example, the accurate identification of hailclouds. People often take thunderclouds as hail clouds by mistake and cause economic waste. Especially, a complete, scientific operation scheme design in implementation is not formed. The casualness in determining operational parameters and the use of unreliable seeding methods reduce the effect of hail suppression. After many years of hard work in many places, local hail suppression systems are built. But, practical applications are rare due to problems of systematic operations and unsolved key techniques in operations.

In this paper, the Doppler radar data of 37 hailstorm and thunderstorm cases in Dalian during the years from 2003 to 2008 were processed and analysed. In each case, several main radar parameters and their variations with time were obtained. The identification indices of hailclouds, the types of hailclouds and decision-making index models of hail suppression in Dalian were summarized. On the basis of the latest theories of hail suppression and large amount of practical operations, technical schemes of hail suppressions are designed and proposed. This solves certain technological problems of hail suppression operations to the maximum extent. Operational applications were implemented in 2009 In seven hail suppression cases, timely identification of hailclouds and scientific hail suppression planning can be obtained, which greatly raised standards of technological support and comprehensive benefits.

2 Identification Of Hail Clouds And Discrimination Of Operations

37 hail and severe thunderstorm cases with radar detections were processed(Yu, X.-D, etc., 2006). Here a localized hailstorm event or severe thunderstorm event is seen as a single case. According to the characteristics of hailstorm in Dalian area, hailclouds are classified. The discriminant indices of classifying hailclouds are concluded and the index model of decision-making in hail suppression operation is built in this paper.

2.1 Identifcation Of Hailclouds

For artificial hail suppression, the first step is to distinguish hailclouds from severe thunderstorms, then, decide whether or not to operate, further, choose proper technical scheme. The experience indicates that an effective hail suppression is based on identifying hailclouds efficiently and accurately.

According to the formation theories of hailcloud and the latest research results of hail suppression, the Doppler radar data of 29 detected hailcloud cases are analysed statistically. The discriminant indices and models of spring, summer and autumn hail clouds are derived as follows:

① The height of the strong echo centre ≥ the height of -6°C level;② The height of the strong echo centre ≥

4km, or ≥ 5.2km for July and August;③ The height of the top of the 45dBZ strong echo zone ≥ the height of -30°C level.

If the echo intensity of a strong convective cloud fits to any one criterion above step by step, the cloud can be identified to be a hailcloud which will be seeded. Specifically, determines the height of radar initial echo. If strong echo appears on the top of cloud or 45dBz strong echo top ≥ the height of l -30ºC level, initially, it can be called hail cloud. After this, further identification can be proceed according to the variation of radar characteristic values with time. A hailcloud can be confirmed if it is with an abrupt increasing phenomenon.

2.2 Classification Of Hailcloud And Operational Decision-making

2.2.1 Classification Of Hail Clouds

By analysing the characteristics of 29 hail events detected in Dalian area, the hail clouds are divided into three categories: single-cell hail clouds, multi-cell hailclouds and super-cell hailclouds.

2.2.2 Decision-making Of Hail Suppression Operations

Radar characteristic parameters of echo intensity, echo top, >= 30dBz echo centre height, intensive echo top and VIL in all types of hail clouds are analysed statistically. discriminant indices of hail cloud types, which are also called decision-making indices for hail suppression operation are derived (Table 1.)

From the statistical analysis of characteristic parameters of radar echo,we find that abrupt increasing of characteristic parameters occurs in the initial stage of hail cloud and the height of strong echo centre lies on the upper part of the cloud. On the contrary, no obvious abrupt increasing is observed in thunderstorm clouds. The strong echo centre lies on the lower part of the clouds. The results are consistent with hail cloud theory(Post Training Materials of Artificial Weather Modification, 2003).

Table 1. **Discriminant index of hail cloud types**

Radar parameters hail / cloud types	Intensity (dBZ)	Strong echo centre height(30dBZ)（km）	Strong echo centre(30dBZ) Top height(km)	Cloud top height (km)	VIL (g/m^2)
Strong hail	≥45	5．0-7．5	9--15	12--18	≥25
Multi-cell	≥30	4.0-6．0	7--13	10--17	10-50
Single-cell	≥25	4．0-5.3	6--11	8--16	5-40

2.2.2.1 Radar Parameter Characteristics Of Single-cell Hailclouds

Radar characteristic parameters of 11 single-cell hailclouds are analysed. Take a representative example to discuss, the case occurred on 14:00BJT October 13th 2006. From Table 2 we can see the radar characteristic parameters and their variation characteristics. The abrupt change of 30dBz strong echo centre height and VIL are more obvious than other parameters. After hail falling, the parameters decreased sharply.

2.2.2.2 Radar Paracteristics Of Multi-cell Hail Cloud

Radar characteristic parameters of 13 multi-cell hail clouds are analysed. Radar parameter indices are obtained. Take the case occurred on 13:51 October 13th 2006 in Fuzhou town Wafangdian for example. From table 3 we can see the abrupt change of 30dBz strong centre height and VIL are more apparent than other parameters. After hail falling, the parameters decreased sharply.

2.2.2.3 Radar Parameter Characteristics Of Super-cell Hail Cloud

Take the case occurred on 18:47 BJT October 13th 2006 in Pulandian city for example.From table 4, VIL increases sharply during fluctuation, the maximum value is over 70 kg/m^2. When the hail ended, radar parameters such as height and VIL decreased rapidly.

By analysing radar characteristic parameters and their variation of different types of hail clouds, we can find that in the hail suppression operations, firstly, estimates 30dBz strong echo central height. Then define the type of hail cloud via the abrupt change of radar parameters with time. The first step of effective hail suppression operation is efficient identification of hail clouds.

Table 2. **Hail cloud radar echo parameter variations in Paotai town of Wafangdian City at 14:00BJT Oct 13th 2006**

Radar Parameters \ Time (min)	13:44	13:51	13:58	14:06	14:13	14:20	14:27	14:35
Echo intensity(dBz)	40	40	50	55	55	60	55	55
Echo top(km)	10	12	13	14	13	12	12	13
30dBz strong echo top (km)	7	9	10	11	10	9	9	8
30dBz strong echo central height(km)	4.5	4.5	5	6	4	2	1.5	1.5
VIL(kg/m^2)	1	5	20	30	35	25	15	15

3 Determination Of Operational Scheme

Hail suppression operation scheme includes: elevation angle, azimuth angle, bomb consumption amount and operation mode. During practice, the technical scheme should be made by considering cannon or rocket types, hail cloud types and operational conceptual models. Based on artificial hail catalysis principles, as well as, the latest research results and Dalian's local features, six different operation modes are designed.

3.1 Technical Scheme Of Rocket Opration

3.1.1 Technical Scheme Of Single-cell Hail Cloud

A.Operating Location

According to results calculated by numerical models, the operating location should be chosen at the centre of strong echoes. Specifically：

①Elevation angle：Take the height of strong echo centre as the vertical height of rocket launching notes for H（Convert to local altitude），the horizontal distance between strong echo centre and operating point notes for L. Elevation angle can be obtained by setting the curve parameter of rocket trajectory. ②Azimuth angle：Refer to the identifying method of convective cloud azimuth angle in rocket precipitation enhancement(Li, H.-B, etc., 2005).

B.Operating Amount:According to rocket amount and formula M=0.1V*Q, considering results of numerical models(Duan, Y , etc., 2001),it is estimated that each operation requires 6~10 rockets. The operating time is 10 minutes. Whether or not continue to operate depends on the evolution of radar echoes.

C.Launching Method :fan shaped launching at the height of -6℃layer, opening angle <15 degree.

3.1.2 Technical Scheme Of Multi-Cell Hail Cloud

A.Operating Location :Operating location is set to the strong echo centre of mature cell , newly generated cell. The identifying method is the same as that of single-cell hail cloud.

B.Operating Amount:According to rocket amount and formula M=0.1V*Q, it is estimated that each operation requires 8~14 rockets for mature cell and 6-10 for newly generated cell.

C.Launching Method:Fan-shaped launching at the height of -6℃ layer, opening angle <15 degree.

3.1.3 Technical Scheme Of Super-hail Cloud

A.Operating Location :The operating location should be within the weak echo region(10~30 dBz) in front of strong echo centre of mature hail cloud (or super-cell).

①Elevation angle: The height of -6℃ layer within the weak echo region (30 dBz) in front of strong echo centre is seen as the vertical height of rocket launching. The horizontal distance is the distance between strong echo centre within weak echo region and operating point. Azimuth angle is derived from rocket trajectory parameter.②Azimuth angle：Refer to the identifying method of convective cloud azimuth angle in rocket precipitation enhancement.

B.Operating Amount:According to rocket amount formula M =0.1V*Q, that each operation requires 14~26 rockets. Repeated operations.

C.Launching Method:Fan-shaped launching in the weak echo region , opening angle <15 degree.

3.2 Technical Scheme Of Cannon Hail Suppression

3.2.1 Technical Scheme Of Single-cell Hail Cloud

A.Operating Location:Identifying methods follow the methods discussed above.

①Elevation angle: The height of strong echo centre (convert to local altitude) is served as the height of explosive target H. L is defined as the horizontal distance between strong echo centre and operating point, which can be fixed by referring to cannon

trajectory parameters. ②Azimuth angle：Refer to the identifying method of convective cloud azimuth angle in rocket precipitation enhancement.

B.Operating Amount:According to technical regulation(Operational Regulations of Hail Suppression ,2000) of cannon hail suppression operation，it is estimated that each operation requires 10~30 bombs.

C.Launching Method:Fan-shaped launching at the height of -6℃ layer, opening angle <20 degree.

3.2.2 Technical Scheme Of Multi-cell Hail Cloud

A.Operating Location: The location is set to be at the central part of strong echo of mature, newly generatinghail clouds. Specific method is the same as that of single-cell.

B.Operating Amount:According to technical regulations of cannon hail suppression, it is estimated that each operation requires 20~60 bombs for mature single-cell, 10~30 bombs For newly generating single-cell.

C.Launching Method: Identifying methods follow the methods discussed above.

3.2.3 Technical Scheme Of Super-cell Hail Cloud

A.Operating Location:For mature hail cloud, the operating location is selected to be in the weak echo region which is in front of strong echo centre, that is, "cave points"(Xu, H.-B, etc., 2008).

① Elevation angle：The height of -6℃ layer within the weak echo region (30 dBz) in front of strong echo centre is seen as the height of bomb explosion. The horizontal distance of cannon operation is the distance between strong echo centre within weak echo region and operating point. The distance is derived from bomb trajectory parameter.② Azimuth angle：Identifying methods follow the methods discussed above.

B.Operating Amount: it is estimated that each operation requires 100~200 bombs for super-cell. Repeated operations.

C.Launching Method:Fan-shaped launching at the strong echo centre in weak echo region in front of strong echo centre,opening angle <15 degree.

Whatever rocket or cannon operations, the best operating time should be in the stages of hail cloud generation, abrupt change and developing. The early practical operations is the key to hail suppression.

4 Conclusions

(1) The Doppler radar data detected in hail clouds and severe thunderstorm clouds was calculated and processed by PUPs. Radar main characteristic parameters including echo and their variations with time were analysed. The discriminant index model of hail clouds was summarized.

(2) According to the characteristic analysis of 29 hail events in Dalian area, hail clouds were classified into three categories.,discriminant indices were concluded. Consequently, decision-making index model was established.

(3) According to the latest research results of precipitation enhancement and hail suppression as well as practical work, technical schemes of hail prevention were designed considering different operating tools.

References

Xu, H.-B., Y. Duan and H.-Y. Liu, Hail Cloud Physics and Principles and Design of Hail Suppression. *China Meteorological Press,* 2004.

Chen, X.-G., Y. Duan and D. Wu,Techniques on Rocket Artificial Influence on Weather. Beijing: *China Meteorological Press,* 2008.

Yu X.-D, Operational Applications and Principles of Doppler Weather Radar. Bejing: *China Meteorological Press,* 2006.

R&D Department China Meteorological Agency. Post Training Materials of Artificial Weather Modification.*China Meteorological Press,* 2003.

Li H.-B. D.-P. Zhou and W.-Y. Pu, The Determination of Catalyzing Points and Project Quantity in Rocket Rain Enhancement. *Meteorology*, Vol. 31, No.10, 42-46.,2005.

Duan,Y.,and H.-B. Xu, Research on the location of Rain Enhancement Operation and Catalyst Amount. *Meteorology*, Vol. 59, No.3, 91-98. 2001.

R&D Department China Meteorological Agency. Operational Regulations of Hail Suppression and Rain Enhancement, 2000.

Xu,H.-B.and L-Q.Tian, Physical Meanings of “Cave Channel” in Strong Convective Storm with Its Application. *Journal of Applied Meteorological Science*, Vol.19, No.3, 372-379. 2008.

Contrast and Analysis of Numerical Simulation Results with the Airborne Detection Data of Precipitation Clouds

Junxia Li [(1)], Peiren Li [(1)], Yue Tao [(2)], Lijun Jin [(1)], Gang Ren [(1)]

[(1)]Weather Modification Office of Shanxi Province ,Taiyuan ,China,030032, ljx22258@126.com

[(2)] Weather Modification Center, Chinese Academy of Meteorological Sciences, Beijing,100081

1. Introduction

Deep research has been carried out for the numerical simulation of precipitation structures and the cloud detection using airborne instruments by many experts in China and abroad. But, comparing the numerical simulation results with the airborne detection data and further verifying the authenticity of each other have not been done before. At present, the main products of cloud parametric numerical model include temperature, wind field, height field, water vapor field and the horizontal and vertical distribution of different kinds of cloud particles. Airborne cloud detection system can obtain the data and the images of temperature, humidity, height, flight speed and the distribution of the size, concentration, the images of cloud and precipitation particles. The same physical parameters of both which can be compared are rare. Furthermore, we cannot do the airborne cloud detection at any time and in any places as we want because of the detecting airspace restrictions and weather conditions. So, it is very difficult and unscientific to compare the both data directly.

Therefore, this paper focus on some physical quantities which both of the numerical simulation and the airborne detection have, such as temperature, humidity, height and different images of different cloud particles forms in different vertical orientation. We choose the airborne detection data from two flying detections on on April 20,2010 in Shanxi Weather Modification Experimental Area, and we use the numerical simulation results in the same place and at the same time period. And, we select the data and images information of both to contrast and analyze.

This is the first time we try to contrast airborne detection data with numerical simulation results from a new point of view, the conclusion can be helpful to verify the numerical simulation results. So, which is valuble and meaningful in a certain sense.

2. Introduction of CAMS mesoscale cloud model and airborne droplet measurement equipments

2.1 CAMS mesoscale cloud model

We adopts CAMS mesoscale cloud model to do the numerical simulation. The main products of the model include temperature, wind field, height, water vapor field and the horizontal and vertical distribution of different kinds of cloud particles. The model use T213 forecast data as initial data, and the resolution is 10km.

2.2 The airborne droplet measurement equipment

The detection plane equipped with ZZW-1 temperature measurement sensor and GWS-1 humidity measurement sensor. The response time is no longer than 2 seconds. And, the plane installed Droplet Measurement Equipments，which include CIP and PIP probes. CIP is two dimensional cloud particle image probe(Detection scope: 25micron~1.5mm),and PIP is two dimensional precipitation particle image probe (Detection scope:100~6200micron). In this paper, we would take the different particles image information from these two probes for comparing and analysis.

3. Design of two observation flight routes

The detection plane carried out two cloud detection flights in Shanxi Weather Modification Experimental Area(in Shanxi Prov. China) on April 20, 2010. The first flight was from 10:11am to 12:20am. The plane took off from Taiyuan Wusu Airport，and first flew at 3600m high level, and flew from Jiaochen County to Fenyang County adopting fold lines, then climbed up to 5900m(to Wenshui County)through the clouds,and then flew horizontally from 11:20am, and finally flew downward spirally in the clouds and went back landing.

The second flight was from 15:25pm to 18:30pm. First, the plane flew along the route A→B→C→D horizontally at 3600, and then climbed to 6210m adopting 600 meters for interval hovering between the two spots E and F, and finally went back.(Fig.1 shows the two flights tracks.)

4. Contrast air temperature and humidity changes with the numerical simulation results

4.1 Contrast data of the first flight observation

Of the first flight, when the plane was at 3600 meters high, the temperature was about -3℃. The zero layer was at 3200m. When the plane was at 5000m, the temperature dropped to below -8℃.And the plane was at 5520m, the temperature was -9.2℃. When the plane was flying at the top height of 5870m, the temperature dropped to below -10℃. The humidity conditions were

better during the whole flight. When flight height was 3600 meters, the relative humidity was above 80%.And when flight height was above 4000m, the relative humidity declined because of the increase of snow and ice particles. When flight height was to its peak, the temperature dropped to the minimum, and the humidity fell to 70%. The temperature and humidity increased gradually in the descent stage of the flight when the plane returned.

Fig.2 is the CAMS model simulation results of vertical distribution profile of snow, sleet and raindrop at 10:00am and 12:00am on April 20, 2010. Taiyuan was taken as the center of the profile. In the profile, the vertical axis represents altitude, the horizontal axis represents longitude, the black solid lines are temperature isolines, the shadow is ratio water content of snow, the red isolines are ratio water content of sleet, the green isolines are ratio water content of rain.

We can see from fig.2 that it had precipitation on the ground at that time, and the precipitation were composed of raindrops mainly and a small part of ice particles. From 800hpa and up to 250hpa, the various states of water particles started to increase, and the humidity was better. Zero layer was at 700hpa (about 3100m), and -5℃ layer was close to 600hpa(about 4300m),and -10℃ layer was close to 500hpa(about 5600m).

4.2 Contrast data of the second flight observation

Of the second flight, the temperature turned lower during the period of the plane rising. The plane entered 0℃ layer When the flight height was 3000m.The plane started flying horizontally at 3600m, and the temperature was 2.5℃. The temperature was -4℃ when the flying height was about 4000m. When the plane was above 5000m, the temperature dropped to below -8℃. And, the temperature was below -11.4℃ when the flying height was above 6000m.When the plane was at its peak height of 6217m, the temperature dropped to -11.7℃.The humidity conditions were better during the whole flight. when flight level was upward to 4000m and above, the humidity declined slightly because of the increase of snow and ice particles.

We chose the numerical simulation results of vertical distribution profile of snow, sleet and raindrop at the same period of time (16:00 to 18:00pm) to contrast temperature and height relations(Fig.3). Fig.3 shows that, it had precipitation at that time. The various states of water particles started to increase from 800hpa, and humidity was better. Zero layer was at 700hpa(3100m), and the -5℃ layer was above 600hpa, and the -10℃ layer was close to 500hpa (above 5600m) high.

Table.1 is the temperature and height contrast-references of the two flights detection and numerical simulation results on April 20.

The first flight	0℃ layer	-5℃ layer	-10℃ layer
Airborne detection	3075～3102m	4234～4337m	5600～5633m
numerical simulation	About 3100m	About 4300m	About 5600m

The second flight	0℃ layer	-5℃ layer	-10℃ layer
Airborne detection	2981～3130m	4503～4565m	5750～5782m
numerical simulation	About 3100m	About 4500m	About 5600m

From Tab.1 we can see obviously, the temperature and the height of the numerical simulation and the two airborne detections are coincided better .

5. Comparison different forms of particle images of airborne detection with numerical simulation results

5.1 Comparing data of the first flight observation with simulation results

We adopted the particle images data from CIP and PIP probe to compare and analyse. Fig.4 is the two-dimensional cloud particle images of CIP, and the heights were 2200m, 3660m, 5206m,and 5785m in turn from down to up for rising stage, and the 2910m and 2000m for descent stage. We can see from fig.4, at the 2200m, the cloud particles were round and elliptic liquid cloud drops, and at 3660m(above zero layer), the cloud particles were cylindrical and some irregular shape solid particles, and at 5206m(about -8℃), the cloud particles were mostly branch shape and snowflake, and when the plane upwards to 5785m(-10℃),the cloud particles were mainly of ice crystals. In the period of descent, when the flying height was 2910 m (close to 0℃), the cloud particles were coexistence form of circular particles, branch shape and snow particles, and at 2000m(6.5℃or so), the cloud particles were mainly of big liquid cloud droplets.

Figure 5 is the two-dimensional precipitation particle images of PIP, and the detection heights were 787m(on the ground),1100m,3640m,and 5860m in turn from down to up for rising stage. As we can see, it had precipitation near the ground; at 1100m(10℃),most of the particles were small round and oval raindrops with some irregular particles coexistence, and which can be considered to a small amount of snow, sleet, and ice particles. At 3640m(about -3℃),the particles images were almost of branch, radial, and irregular snow and ice particles. Up to 5510m(about-9 ℃), the particles were most of ice crystals and snow. At 5860m(below -10℃),all of the particles were ice crystals.

This flight began to climb from 3600 meters to 5900 meters from Fenyang, and began to downward spirally near Wenshui. So we choose the numerical simulation results of vertical distribution of the hydrometerors at 10:00～12:00am of Fenyang station and Wenshui station to contrast with the airborne detection images. The fig.6 and fig.7 are the numerical simulation results of vertical distribution of the hydrometerors at 10:00～12:00am on April 20, 2010.

From the fig.6 and fig.7 we can see, the precipitation was appeared below 700hpa(about 3100m), which mainly composed of liquid droplets, and also of a small amount of sleet shape particles. Above 700hpa height, snow shape particles began to increase

gradually, and then increased to the maximum at 550hpa~450hpa(5000m). Upwards to 450hpa,snow particles reduced gradually,and there has small amount of cloud water coexistence, distributing unevenly. The ice crystals appeared above 450hpa.

5.2 Comparing data of the second flight observation with simulation results

Fig.8 is the two-dimensional cloud particle images of CIP. We can see that most of particles in cloud were big elliptic liquid at a height of 2713m (Fig.8). At 3670m height (above 0℃ layer), the shape of particles in cloud was mainly columnar and irregular. At 4300m height (about -4.5℃)，particles in cloud were snow flake and irregular shape particles， and upwards to 6200 m (-11.7℃), particles in cloud had been mainly of ice crystals and snow shape particles. During the process of decline, the cloud particles were circular particles and ice crystals coexist at 4000m height(about -4.4℃).

Fig.9 is the precipitation particle images of PIP. As we can see, it was already had precipitation near the ground (787m and 2200m),and the raindrops were mostly of circular liquid droplets; at 3000m (0℃ layer), there coexisted round and oval little raindrops and some irregular shape snow and sleet particles; at the 3660m(about -2℃), all particles were branch and radial irregular snow and ice particles; when up to 4200m(-4.5℃),most of particles were ice crystals, with a small amount of snow; and to the peak 6209m(below -11℃), all of the particles were ice crystals.

The first flying level of the second flight was 3600m,and then climbed up between the E,F spots(near Fenyang station) from 3600m to 6210m in spiral paths, and then returned and landing. So we choose vertical distribution of hydrometerors in simulation from 15:00 to18:00pm to contrast with the airborne detection image at Fenyang Station (Fig.10).

From the Fig.10 we can see, it had precipitation during the period of time. The precipitation was appeared below 700hpa(about 3100m), and the precipitation mainly composed of liquid raindrops with a small amount of sleet. There were some snow particles from 3000m to 4000m, which indicated that there existed a part of ice state particles participated in the precipitation. When above 700hpa, snow shape particles began to increase gradually, and up to maximum at 550hpa~350hpa(5600m).And continue to upwards, snow state particles gradually reduced, and a small amount of ice crystals appeared above 450hpa.

5.3 Contrast results

Compared the numerical simulation results with the particle images from airborne detection, the ground precipitation were liquid rainfall; and at 3000m(zero layer),liquid, columnar, ice and snow shape particles began to appear coexisting; and above 3600m,most of the particles were branch shape and snow shape particles. The difference was Ice crystals appeared from above 4000m and increased gradually for the airborne detection, but for the numerical simulation, ice crystals appeared and increased from 5600m.

6. Conclusion

In this article, we contrasted and analysed numerical simulation products with the airborne detection data for the first time. And that is a new point of view to verify the authenticity of the numerical model.

(1) We contrast airborne temperature and humidity probes data of the two detection flights with the temperature and height of the numerical simulation data , both do have a good agreement.

(2) According to the results of contrasting the numerical simulation data with the particle images from airborne detection, precipitation was appeared below 700hpa(about3100m). The precipitation was mainly of liquid raindrops, and also have a small amount of sleet shape particles, which indicates that there were part of ice form particles involved in the precipitation. Above 700hpa(zero layer), snow shape particles began to increase gradually, with liquid drops and columnar ice shape particles coexisting, and the content was to the maximum at 550hpa~450hpa(5000m).Then upwards again, snow shape particles reduced gradually. A small amount of ice crystals appeared above 450hpa.

(3) We can see the slightly different is, a few ice crystals began to appear and increase gradually at 4200 meters according to the airborne detection. But the numerical simulation showed that ice crystals began to appear at 500hpa(about 5600m). So, the height of the airborne detection of the ice crystals appeared was below the numerical simulation results. Overall, compared the numerical simulation data with the products of airborne detection, both had good corresponding.

This work should also be continued to think furtherly, and we should find deeper and appropriate points to do the research of contrasting and testing the corrections of numerical model using the practical detection data more scientificly.

References

Mcfarquhar G. M., Black R. A., Observations of particle size and phase in tropical cyclones: implications for mesoscale modeling of microphysical process. *J. Atmos. Sci.,* **61**: 422-439. 2004.

Van Den Heever, Cotton, W.R., The impact of hail size on simulated supercell storms. *J. Atmos. Sci.* **61**: 1596-1609. 2004.

Mcfarquhar, G.M., Henian Zhang, Gerald Heymsfield, Robbie Hood, Jimy Dudhia, Halverson, J.B.,… Factors affecting the evolution of Hurricane Erin and the distributions of hydrometeors: role of microphysical processes. *J. Atmos. Sci.* **127**:127-150. 2006.

Khvorostyanov, V. I., and J. A. Curry, Terminal velocities of droplets and crystals: Power laws with continuous parameters over the size spectrum. *J. Atmos. Sci.*, **59**, 1872-1884. 2002.

Figures

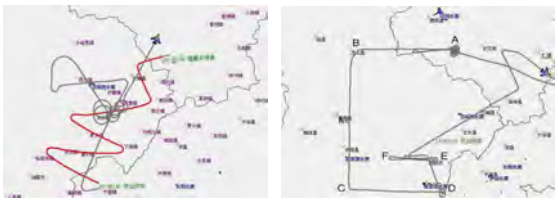


Fig.1 The two flights routes on April,20,2010(The left figure is the first flight,and the right one is the second flight)

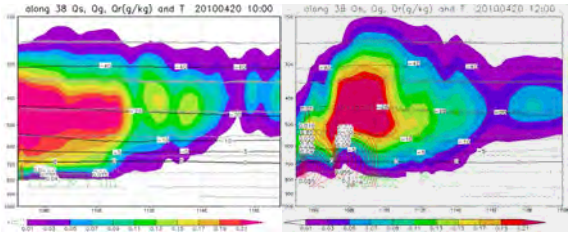


Fig.2 The numerical simulation of vertical distribution profile of snow, sleet and raindrop at 10:00am and 12:00am on April 20, 2010.

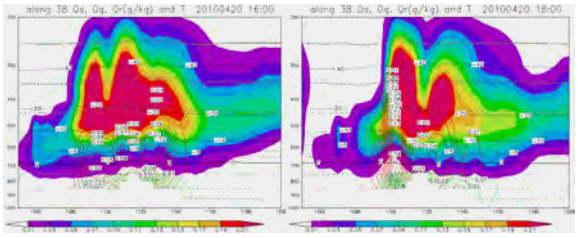


Fig.3 The numerical simulation of vertical distribution profile of snow, sleet and raindrop at 16:00am and 18:00pm on April 20, 2010.

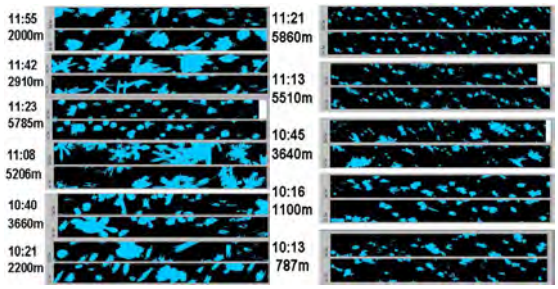


Fig.4 The two-dimensional cloud particle images of CIP at 10:21～11:55am(Left Fig.)

Fig.5 The two-dimensional raindrop particle images of PIP at 10:13～11:21am(Right Fig.)

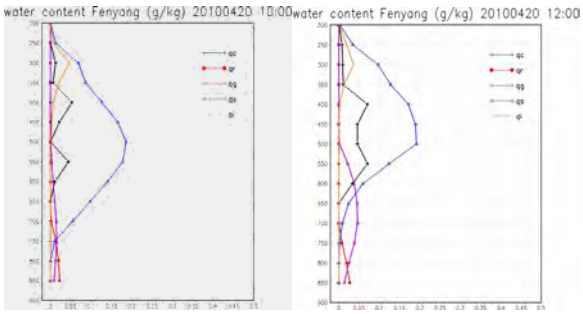


Fig.6 The numerical simulation results of vertical distribution of the hydrometerors at 10:00～12:00am on April 20, 2010, of Fenyang station. (qc—cloud water，qr—raindrops，qg—sleet,qs——snow，qi—ice crystals)

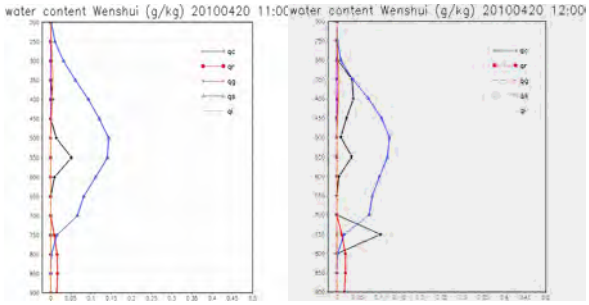


Fig.7 The numerical simulation results of vertical distribution of the hydrometerors at 10:00～12:00am on April 20, 2010, of Wenshui station.

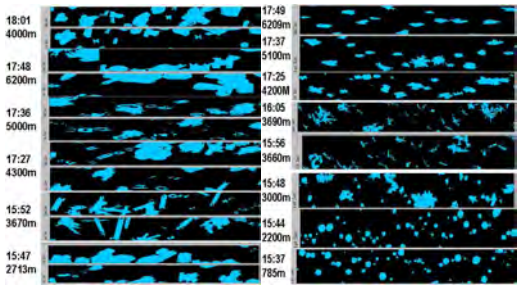


Fig.8 The two-dimensional cloud particle images of CIP at 15:47～18:01pm(Left Fig.)

Fig.9 The two-dimensional raindrop particle images of PIP at 15:37～17:49pm(Right Fig.)

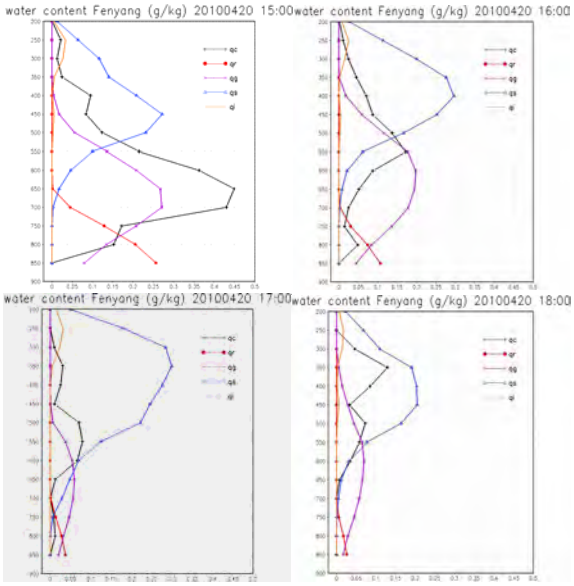


Fig.10 The numerical simulation results of vertical distribution of the hydrometerors from 15:00～18:00pm on April 20, 2010, of Fenyang station.

Numerical simulation of macro- and micro-structures of intense convective clouds with a spectral bin microphysics model

LIU XiaoLi, and NIU ShengJie
Key Laboratory of Meteorological Disaster of Ministry of Education, School of Atmospheric Physics, Nanjing University of Information Science & Technology, Nanjing 210044, China
liuxiaoli2004y@nuist.edu.cn,niusj@nuist.edu.cn

1. Introduction

Spectral (bin) microphysical cloud models have been successfully used for the investigation of different microphysical processes (e.g., Takahashi, 1976; Tzivion et al., 1989; Reisin et al., 1996a; Ovtchinnikov and Kogan, 2000; Ovtchinnikov et al., 2000), effects of cloud microphysics on spatial redistribution of precipitation in the coastal zones (e.g., Khain et al., 1993; Khain et al., 1996), simulation of stratiform clouds and their radiative effects (e.g., Liu and Kogan, 1998; Rasmussen et al., 2002), simulation of cloud seeding (e.g., Khvorostyanov et al., 1989; Reisin et al., 1996a; Yin et al., 2000), and cloud chemistry (e.g., Flossman et al., 1985), etc.

Advances in spectral bin microphysics model development have been achieved in China. For example, cloud droplets are categorized into several bins in a one-dimensional time-dependant model for warm clouds (e.g., Xiao et al., 1988a, b). The water droplet spectral distribution was formulated in a study of the evolution of the particle spectrum (e.g., Xu, 1999). A three-dimensional convective cloud model with discrete mass categories of hail/graupel has also been developed (e.g., Guo et al., 2001a, b). This model can simulate details of the growth and the distribution of hail/graupel particles, which can not be properly depicted by parameterization models. Water and ice processes and their interactions have been simulated by spectral bin microphysics in a study of the mechanisms involved in plateau precipitation systems (e.g., Zhao et al., 2004).

The spectral bin microphysics of the Tel Aviv University model (e.g., Reisin et al., 1996a; Yin et al., 2000) is coupled with 3D compressible non-hydrostatic dynamics (Institute of Atmospheric Physics - IAP, China), and a real convective cloud caes is simulated (e.g., Liu, 2007; Liu and Niu, 2007). Simulation results of the bin cloud model are compared with the results of the IAP 3D hailstorm numerical model (with bulk microphysics) and the observations. It was found that the bin model accurately depicts the updraft velocities and spatial structure of the reflectivity that was observed by Doppler radar. The model is suitable to study severe convection, in particular the formation and evolution mechanism of hailstorms and hail particles.

2. The cloud model

2.1 The dynamic model

The dynamic framework of the model employed in this study is a three-dimensional compressible dynamic model which prognoses 3D velocity of airflows, temperature, pressure and humidity (e.g., Kong et al., 1990; Kong, 1991). The model uses a time-splitting method with a small time step to calculate the sonic wave production term to assure computational stability, while the rest of the terms are calculated using a large time step that is suitable for gravitational and meteorologically relevant waves. The model uses an Euler backward scheme to compute fields at the first time step. The model uses 36x36 grid points in the horizontal with a grid spacing of 1 km. The vertical grid contains 38 points with a grid spacing of 0.5 km.

2.2 Microphysical processes of the model

The spectral bin microphysics includes a spectral description of the CCN, water droplets, ice, snow, and graupel. The warm microphysical processes considered in the model include: nucleation of CCN, condensation, evaporation, collision-coalescence, and binary breakup. The ice microphysical processes include droplet freezing, ice nucleation (deposition and condensation freezing, and contact nucleation), ice multiplication, deposition and sublimation of ice, ice-ice and ice-droplet interactions (aggregation, accretion, and riming), melting of ice particles, and sedimentation of both droplets and ice particles. The mass concentration and number concentration of each bin of individual hydrometeor particle categories are individually solved for in the microphysics scheme. Each type of particles is divided into 34 bins with mass doubling in each bin ($x_{k+1} = 2x_k, k = 1,2,\ldots,34$). The masses at the beginning of the first bin for both liquid and solid phases are 1.598×10^{-11} g. The minimal diameters of droplets and graupel are 3.12 μm and 4.24 μm, respectively. The maximal diameters of droplets and graupel are 8063 μm and 10943 μm, respectively. The detailed microphysics model is described in Reisin et al. (1996b).

3. Case study

3.1 Case description

The model has been used to simulate an observed cloud case that occurred on 29 June 2000 near Bird City, Kansas (Sun, 2005). This was a case studied as a part of the STEPS (Severe Thunderstorm Electrification and Precipitation Study) field project, and its evolution was within the coverage area of the STEPS triple-radar network. The three S-band Doppler Radars consisted of the operational WSR-88D located at Goodland, Kansas (KGLD) and two multi-parameter research radars: the National Center for Atmospheric Research's (NCAR) S-Pol and Colorado State University's (CSU) CHILL units. Wind and electric fields measurements were also taken as well. The 29 June 2000 supercell storm formed just ahead of a dryline with an approaching mesoscale cold front to the north. The initial echo appeared at 2130 UTC. The storm lasted approximately four hours. Environmental winds near the storm were from the south at near-ground level

and veered to the west with height as shown in the 2022 UTC National Center for Atmospheric Research (NCAR) GPS Dropsonde Loran Atmospheric Sounding System (GLASS) sounding released approximately 65 km to the southeast of where the storm initiated; these wind measurements were taken one hour before the storm was first detected by radar (Kuhlman et al., 2006). The sounding data of 2022 UTC were used as the initial input field (Kuhlman et al., 2006). The convective cloud is triggered by a moist thermal bubble disturbance with a horizontal radius of 12 km, thickness 6 km, maximal disturbance potential temperature 1.5 K, and relative humidity 65%. The initial CCN distribution is chosen to be a continental CCN, with exponential size distribution, with number concentration of 700 cm^{-3} (e.g., Liu, 2007).

3.2 Simulation results

3.2.1 Radar reflectivity

During the mature phase of the severe storm, radar reflectivity of the simulating supercell displays similar features to the observations, with a height reaching 13 km and maximum radar reflectivity of 70 dBZ. With the supercell developing, the radar reflectivity of the simulated supercell splits into two centers. Also, strong updraft velocities appear in these two centers.

3.2.2 Graupel water content at large sizes (Diameter>4)

Similar to the total content of all graupel, the graupel with sizes larger than 4 mm initial appear on the left edge of the main updraft at 28 min. At 32 min, there are also two maxima for gaupel larger than 4 mm, with centers of 7 g kg^{-1} and 5 g kg^{-1}, respectively. During the dissipation period of the supercell, most of the graupel on the left side decreases. The falling graupel particles on the left side contribute to downdraft development. During the mature stage of the storm, the maximal graupel water content is located in the mid-upper part of the cloud. The graupel particles initially grow during their ascending process near the left flank of the main updraft and fall down when their terminal velocities overcome the updraft. Some of the falling graupel re-enter the main updraft by transport of the inflow at low-levels and then continue to grow. This recycling growth mechanism contributes greatly to large size graupel formation.

3.3 Effect of CCN concentration on graupel water content

To study the CCN impact, we conducted sensitivity studies on the effect of CCN concentration on the evolution of the severe storm by increasing CCN concentration to 10 times more, and decreasing to 0.1 times less. The simulation experiments are called CCN1, CCN10, and CCN0.1.

When the CCN concentration increases, the concentration of nucleated droplet increases, and droplets compete for available vapor to grow. Subsequently, coalescence between the droplets becomes rarer and the size of droplets generally decreases. When droplets are being transported to the freezing level, they freeze and the total mass of freezing liquid water being converted to ice particle at all gridpoints decreases substantially (Fig. 1a), producing a large number of ice particles that can be transported to the upper levels of the cloud easily. In contrast, as the CCN concentration decreases, the number concentration of nucleation droplets decreases and coalescence between droplets is more active, resulting in larger sizes droplets. Next, the total mass of freezing droplets increases substantially around 19-24 min (Fig. 1a). With relatively large size droplets and frozen ice particles, the coalescence process between ice (graupel) particles and droplets becomes more dominant in the CCN0.1 experiment. There is less mass involved in the coalescence process for graupel in the CCN10 experiment, prohibiting the growth of graupel particles (Fig. 1c). The large number of ice particles produced in CCN10 mainly grow through the deposition process, and are located in the upper part of the convective cloud (Fig. 1b).

When the concentration of CCN is increased by 10 times, in the warm cloud stage there is a small difference in the liquid water content, but with a large increase of concentration of liquid droplets, which means smaller droplet sizes. An increase of the liquid droplet concentration causes an increase of ice crystals, accompanied with a large increase of the concentration of the ice crystals (figure not shown). The large number of ice crystals induces a competition for supercooled water and vapor in the cloud, which inhibits the growth of ice crystals and the formation of graupel, causing the large reduction of graupel water content .

It can be concluded that large levels of CCN can induce a large increase of concentration of liquid droplets, on the one hand inhibiting the coalescence of cloud droplet, i.e., the production of large size liquid droplets; on the other hand, this can produce high concentrations of ice crystals, making the growth of ice crystals challenging and inhibiting the formation and growth of graupel particles. It can be deduced that in heavily polluted areas, the extremely high concentration of CCN has an inhabitory effect on the formation of graupel particles.

The decrease of CCN concentration by 10 times from the base case causes a large decrease of the concentration and content of ice crystals. Concentration of liquid droplets decreases by 10 times, as well, without corresponding evidence of a decrease of the liquid water content (figure not shown). The CCN0.1 case favors coalescence of the liquid droplets and an increase of their diameter. Decreasing the CCN concentration accelerates the droplet coalescence process and broadens the droplet spectrum, and the diameter and concentration of large size drops increases. The freezing of the large droplets favors the formation of graupel particles , with graupel forming earlier at lower levels. For the relatively large sized initial graupel particles, the graupel particles stays longer in the mid-levels of the cloud, and these inhibit the up-down recycling growth process of the graupel. The graupel water content appears to have a different

distribution with respect to the CCN1 experiment. The graupel pellets with diameters larger than 4 mm form at lower levels, with lower maximum values of water content. The decrease of CCN concentration can produce abundant graupel water content, but the production of large size graupel can be significantly inhibited. The reason is that as the CCN concentration decreases greatly, accelerating the coalescence between droplets and producing some droplets with relative larger sizes and also graupel particles with relatively larger sizes. However, it is more difficult for the updraft to move the large graupel particles to the upper portions of the cloud, and the up-down recycling growth process of graupel particles may not be allowed, thus inhibiting the formation of graupel with very large sizes.

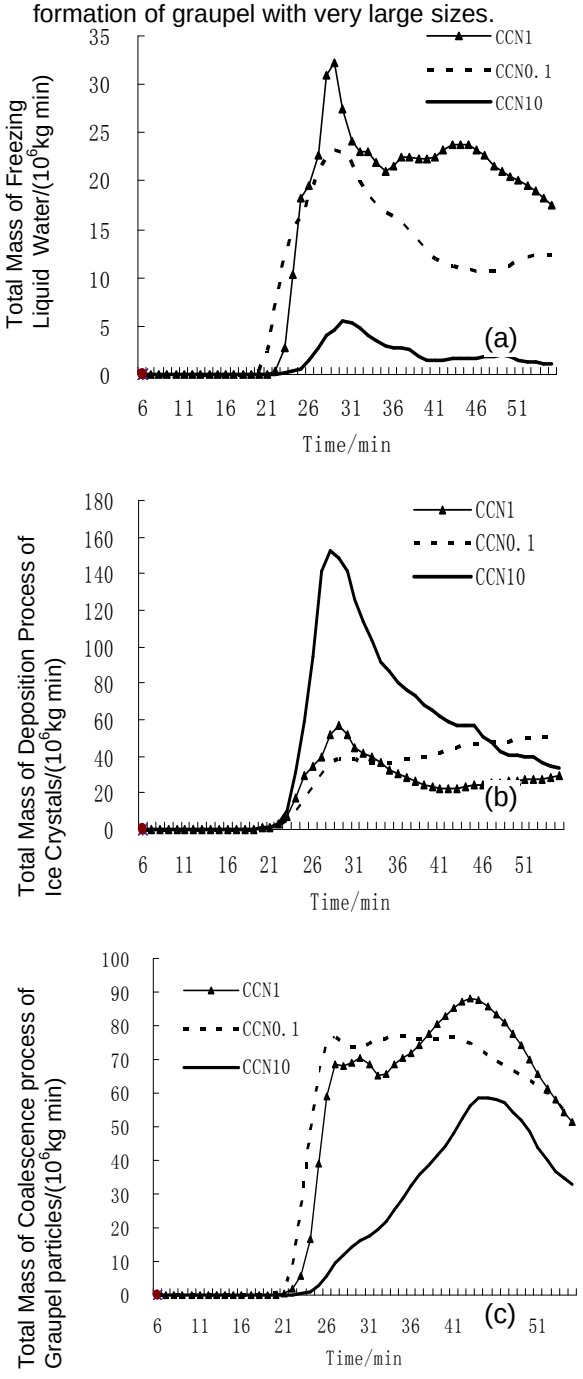


Fig. 1. Time variation of total mass budget of (a) freezing process of liquid water, (b) deposition process of ice particles, and (c) coalescence process of graupel

4. Discussion and conclusion

(1) A cloud model that combines three-dimensional compressible dynamics and detailed bin spectral microphysics is tested with a severe convective storm case. It is found that the model is able to simulate the distribution and evolution of precipitation particles, as well as their relationship with respect to the macroscopic flow field during the mature and severe stages of the storm. The macroscopic and dynamical processes can either support or restrain the microphysical processes. The initial warm-cloud processes not only produce adequate numbers of droplets of certain sizes, but also produces adequate updrafts to move hydrometeors upward and support the development of the supercell cloud dynamically. At the same time, the microphysical processes also affect the dynamical structure of the cell through the latent heating or the gravity loading.

(2) Spectral bin microphysics with a CCN category component can be used to model the effect of CCN on the macro- and micro-physical formation mechanisms of the convective clouds and the development mechanism of the large size graupel. CCN concentration not only varies the number concentration and spectral distribution of liquid droplets in convective clouds, but also modifies the number concentration and the sizes of the ice crystals, as well as the formation and growth mechanisms of graupel. A large increase of CCN concentration can induce a large increase of the concentration of the liquid droplets and ice crystals, inhibiting the formation and growth of graupel particles due to the competition mechanism. Further, the large magnitude decrease of the CCN concentration results in large-size droplets but inhibits the recycling growth of graupel, and can thus limit the formation of graupel of large size.

Acknowledgements

This Work is Supported by the National Natural Science Foundation of China (Grant Nos. 40537034,40805057), Foundation of Key Laboratory of Meteorological Disaster of Ministry of Education (KLME) in NUIST (Grant No. KLME060202), Major Fundamental Research Program of Natural Science Foundation of the Jiangsu Higher Education Institutions of China (Grant No. 06KJA17021), Foundation of Key Laboratory for Cloud Physics and Weather Modification of CMA (Grant No. 2009Z0036), and Foundation of Nanjing University of Information Science & Technology.

References

Browning, K. A., Airflow and precipitation trajectories within several local storms which travel to the right of the winds. J. Atmos. Sci., **21**, 634-639, 1964.

Flossmann, A. I., W. D. Hall, and H. R. Pruppacher, A theoretical study of the wet removal of atmospheric pollutants. Part I: The redistribution of aerosol particles captured through nucleation

and impaction scavenging by growing cloud drops. J. Atmos. Sci., **42**, 583-606,1985.

Guo, X. L., M. Y. Huang, Y. C. Hong, H. Xiao, and L. Zhou, A study of three- dimensional hail-category hailstorm model Part I: Model description and the mechanism of hail recirculation growth. Chinese J. Atmos. Sci., **25**, 707-720, 2001. (in Chinese)

Guo, X. L., M. Y. Huang, Y. C. Hong, H. Xiao, and L. Zhou, A study of three-dimensional hail-category hailstorm model Part II: characteristics of hail-category size distribution. Chinese J. Atmos. Sci., **25**, 856-864, 2001. (in Chinese)

Khain, A. P., D. Rosenfeld, and I. L. Sednev, Coastal effects in the Eastern Mediterranean as seen from experiments using a cloud ensemble model with a detailed description of warm and ice microphysical processes. Atmos. Res., **30**, 295-319, 1993.

Khain, A. P., I. Sednev, and V. Khvorostyanov, Simulation of coastal circulation in the Eastern Mediterranean using a spectral microphysics cloud ensemble model. J. Climate, **9**, 3298-3316, 1996.

Khvorostyanov, V. I., A. P. Khain, and E. L. Kogteva, A two-dimensional non-stationary micro-physical model of a three phase convective cloud and evaluation of the effects of seeding by crystallizing reagent. Soviet Meteorology Hydrology, **5**, 33-45, 1989.

Kong, F. Y., Three-dimensional numerical simulations of hailstorms. Ph. D. thesis, Institute of Atmospheric Physics, Chinese Academy of Sciences, 155PP,1991. (in Chinese)

Kong, F. Y., M. Y. Huang, and H. Y. Xu, Numerical simulation of ice microphysical process of convective cloud, Part □:Construction of cloud and the parameterization of ice cloud processes. Chinese J. Atmos. Sci., **14**, 441-453, 1990. (in Chinese)

Kuhlman, K. M., C. L. Ziegler, E. R. Mansell, D. R. Macgorman, and J. M. Straka, Numerically simulated electrification and lighting of the 29 June 2000 STEPS supercell storm. Mon. Wea. Rev., **134**, 2734-2757, 2006.

Liu, Q., and Y. Kogan, Large eddy simulations of cloud processing of small size aerosols in marine stratocumulus. Preprints Conf on Cloud Physics, Everett, WA, Amer. Meteor. Soc., 329-332, 1998.

Liu, X. L., Research on cloud model with spectral bin microphysics. Ph. D. thesis, Nanjing University of Information Science and Technology, 123PP, 2007. (in Chinese)

Liu, X. L., and S. J. Niu, Development of 3-D convective cloud model based on spectral bin microphysics. Journal of Nanjing Institute of Meteorology, **30**, 617-622, 2007. (in Chinese)

Liu, X. L., and S. J. Niu, Numerical simulation on the evolution of cloud particles in 3-Dconvective cloud. Science in China (D), **52**, 1195-1206, doi:10.1007/s11430-009-0112-1, 2009.

Ovtchinnikov, M., and Y. L. Kogan, An investigation of ice production mechanisms in small cumuliform clouds using a 3D model with explicit microphysics, Part I: Model description. J. Atmos. Sci., **57**, 2989-3003, 2000.

Ovtchinnikov, M., Y. L. Kogan, and A. M. Blyth, An investigation of ice production mechanisms in small cumuliform clouds using a 3D cloud model with explicit microphysics. Part II: Case study of New Mexico cumulus clouds. J. Atmos.Sci., **57**, 3004-3021, 2000.

Rasmussen, R. M., I. Geresdi, G. Thompson, K. Manning, and E. Karplus, Freezing drizzle formation in stably stratified layer clouds: The role of radiative cooling of cloud droplets, cloud condensational nuclei, and ice initiation. J. Atmos. Sci., **59**, 837-860, 2002.

Reisin, T., Z. Levin, and S. Tzvion, Rain production in convective clouds as simulated in an axisymmetric model with detailed microphysics. Part II: Effects of varying drops and ice initiation. J. Atmos. Sci., **53**, 1815-1837, 1996.

Reisin, T, Z. Levin, and S. Tzvion, Rain production in convective clouds as simulated in an axisymmetric model with detailed microphysics. Part I: Description of the model. J. Atmos. Sci., **53**, 497-519, 1996.

Sun, J. Z., Initialization and Numerical Forecasting of a Supercell Storm Observed during STEPS. Mon. Wea. Rev., **133**, 793-813, 2005.

Takahashi, T., Hail in an axisymmetric cloud model. J. Atmos. Sci., **33**, 1579-1601, 1976.

Tzivion, S., G. Feingold, and Z. Levin, The evolution of raindrop spectra. Part □: Collisional collection/break and evaporation in a rainshaft. J. Atmos. Sci., **46**,3312-3327, 1989.

Xiao, H., H. Y. Xu, and M. Y. Huang, Numerical simulation on the formation of cloud drop spectrum in cumulus. Part □: The function of the spectra and concentration of salt. Chinese J. Atmos. Sci., **12**, 121-130, 1988. (in Chinese)

Xiao, H, H. Y. Xu, and M. Y. Huang, Numerical simulation on the formation of cloud drop spectrum in cumulus. Part II: The function of coalescence processes and atmospheric stratification. Chinese J. Atmos. Sci., **12**, 312-319, 1988. (in Chinese)

Xu, H. B., Some questions in studying the evolution of size distribution spectrum of hydrometeor particles. Acta Meteorologica Sinica, **57**, 450-460, 1999. (in Chinese)

Yin, Y., Z. Levin, T. Reisin, and S. Tzivion, Seeding convective clouds with hygroscopic flares: Numerical simulations using a cloud model with detailed microphysics. J. Appl. Meteor., **39**, 1460-1472, 2000.

Zhao, S. X., H. B. Xu, and G. Deli, Numerical simulation of microphysical character of convective cloud precipitation in upper reach of yellow river. Plateau Meteorology, **23**, 495-500, 2004.(in Chinese)

Development of salt-seeding scheme in 3-D convective cloud model and seeding simulations

Xiaofeng Lou, Guanfang He, Zhijin Hu, Xing Zhang
46 Zhongguancun South Avenue,
Chinese Academy of Meteorological Sciences
Beijing 100081, China
louxf@cams.cma.gov.cn

1. Introduction

In this research a salt-seeding scheme is developed in a 3-D convective cloud model (Yu et al, 2001), considering the microphysical processes between salt particle and liquid and ice particles. These microphysical processes are condensation, collection of cloud drops, collection by rain drops, in cold region, salt powder collected by ice and freeze to graupel, collected by graupel and hail.

Two prognostic variables are added: mixing ratio and number concentration of salt particle (Qn and Nn).

2. Descriptions of microphysical processes of salt dissolved drop

Detailed descriptions of salt dissolved microphysical processes with other water substances are as following, where N is number concentration，Q mixing ratia，D diameter，V falling speed，ρ air density，λj particle spectrum slope，E collection efficiency.

a. Salt dissolved drop collection with cloud drop

Ccn=Nn· $\frac{\pi}{4}$ ×Dn2×Vn×ρ×Qc×Ecn

Collection efficiency Ecn (Mason, 1971):

R<10μm, Ecn=0.0

10μm<R<30μm, Ecn=0.01×1.262(R-15)

30μm<R<60μm, Ecn=0.33+0.0585· $\sqrt{R-30}$

60μm<R<100μm, Ecn=0.65+0.003·(R-60)

100μm<R<400μm, Ecn=0.77+0.007· $\sqrt{R-100}$

R>400μm, Ecn=0.89

b. Salt dissolved drop collection with ice crystal

T<273K, ice crystal collected by salt dissolved drop and froze to graupel, Ein=0.7

Cin= $\frac{\pi}{4}\rho A_{mi}\int N_{0i}\left(D_n+D_i\right)^2 D_i^3\exp\left(-\lambda_i D_i\right)dD_i N_n\left|V_n-V_i\right|E_{in}$

=Nn× $\frac{\pi}{4}$ ×Dn2×|Vn-Vi|×ρ×Qi×Ein×(1+ $\frac{8}{D_n\lambda_i}+\frac{20}{D_n^2\lambda_i^2}$)

NCin= Nn× $\frac{\pi}{4}$ ×Dn2×|Vn-Vi|×ρ×Ni×Ein×(1+ $\frac{4}{D_n\lambda_i}+\frac{6}{D_n^2\lambda_i^2}$)

When T<273k, salt dissolved drop collected by ice crystal and froze to graupel，Ein=0.7

Cni= Nn× $\frac{\pi}{4}$ ×Dn2×|Vn-Vi|×ρ×Qn×Eni×(1+ $\frac{4}{D_n\lambda_i}+\frac{6}{D_n^2\lambda_i^2}$)

NCni= Nn× $\frac{\pi}{4}$ ×Dn2×|Vn-Vi|×ρ×Nn×Eni×(1+ $\frac{4}{D_n\lambda_i}+\frac{6}{D_n^2\lambda_i^2}$)

c. Salt dissolved drop collected by graupel

whenT<273k, salt dissolved drop collected by graupel, Avg=500cm0.2s-1, Eng=0.8

$$C_{ng}=\frac{\pi}{4}\rho_w Q_n E_{ng}\int_0^{\infty}N_{0g}\exp\left(-\lambda_g D_g\right)\left(D_g+D_n\right)^2\cdot\left|V_n-V_g\right|dD_g$$

$$=\frac{\pi}{4}\rho_w Q_n E_{ng}\frac{N_g}{\lambda_g^2}\left\{\left[\gamma(3.8)\frac{A_{vg}}{\lambda_g^{0.8}}-\gamma(3)V_n\right]+2D_n\lambda_g\cdot\left[\gamma(2.8)\frac{A_{vg}}{\lambda_g^{0.8}}-\gamma(2)V_n\right]+D_n^2\lambda_g^2\left[\gamma(1.8)\frac{A_{vg}}{\lambda_g^{0.8}}-V_n\right]\right\}$$

NCng=Cng $\frac{N_n}{Q_n}$

d. Salt dissolved drop collected by rain drop

Cnr=

$$\frac{\pi}{4}\rho_w Q_n E_{nr}\ \frac{N_R}{\lambda_R^2}\left\{\left[\gamma(3.8)\frac{A_{VR}}{\lambda_R^{0.8}}-\gamma(3)V_n\right]+AA\right\}$$

AA=

$$2D_n\lambda_R\left[\begin{matrix}\gamma(2.8)\frac{A_{VR}}{\lambda_R^{0.8}}\\-\gamma(2)V_N\end{matrix}\right]+D_N^2\lambda_R^2\left[\gamma(1.8)\frac{A_{VR}}{\lambda_R^{0.8}}-V_n\right]$$

Avr=2100cm0.2s-1, Enr=0.8

NCnr=Cnr $\frac{N_n}{Q_n}$

e. Salt dissolved drop collected by hail

when T<273k,

Cnh=

$$\frac{\pi}{4}\int_{D_*}^{\infty}N_{0r}\exp(\lambda_h D_h)(D_n+D_h)^2 dD_h|V_n-V_h|E_{nh}\rho Q_n$$

Enh=0.8

NCnh=Cnh $\frac{N_n}{Q_n}$

f. Salt dissolved drop condensate in super saturation cloud

Condensation equation of single salt dissolved drop （Hu et al, 1982）:

$$r\frac{dr}{dt}=\frac{(s+\frac{3im_s}{4\pi\rho_L r^3}\cdot\frac{M}{M_s})\cdot D\cdot\rho\cdot q_s\frac{1}{\rho_L}\cdot F_1}{[1+\frac{D\rho q_s LF_1}{K_1 TF_2}(\frac{L}{RT}-1)]}$$

Where r is diameter, s is super saturation; i is Van Hoof，let i=2.5；m_s is quality of single dry salt particle；M and M_s are molecular weight of water and salt; D is water vapor diffusion coefficient；K_1 Air thermal conductivity；F_1，F_2 ventilation coefficient which is function of particle diameter; ρ_L droplet density.

Simplified above equation as following:

$$r\frac{dr}{dt}=0.18\cdot A\cdot\frac{m_s}{r^3}\cdot F_1$$

$$A=D\cdot\rho\cdot q_s[1+\frac{D\rho q_s\cdot L}{K_1 T}(\frac{L}{RT}-1)]^{-1}$$

Where

$$dt=\frac{dr^5}{0.9\cdot A\cdot F\cdot m_s}$$

After integration,

$$S_{VN}=\frac{4.19N_N}{Dt}\left\{R_N^5+[BB]^{0.6}-R_N^3\right\}$$

$$BB=\left\{\left[\frac{2.02\times10^{-7}M_N\rho Q_{sw}\left(1+7.85\sqrt{V_N R_N\rho}\right)Dt}{1+0.162[1-0.0066(T-T_0)]\rho Q_{sw}}\right]\right\}$$

Where M_N is quality of single salt particle.

g. Evaporation of salt dissolved drop out of cloud (Qsw>Qv)

Svn1=

$$\frac{2.83\cdot10^{-6}N_n R_n(Q_{sw}-Q_v)\rho(1+7.85\sqrt{V_n R_n\rho})}{1+0.162[1-0.0066(T-T_0)]\rho Q_{sw}}$$

h. Large salt dissolved drop freeze to graupel in cold region（T<273k）, Am=0.6, Bm=8e-3.

$\frac{dT}{dt}\geq 0.0$, NMng=0.0

$\frac{dT}{dt}\leq 0.0$,

NMng=

$$\frac{Q_n}{\rho_w}B_m A_m Exp[-A_m(T-273+3.2)](\frac{dT}{dt})^{1-0.6A_m}$$

Mng=NMng $\frac{Q_n}{N_n}$

3. Simulation results

Using salt-seeding model, a heavy rainfall case is simulated in west China. A sounding data is used for this model's initial field. Horizontal resolution is 1200 m with 80 *80grids, vertical resolution is 700 m with 30 grids.

With this model, AgI seeding simulations were made, both seeding under cloud base and seeding in cloud can enhance rainfall (Fang, et al, 2005)

Using the salt-seeding model, a series of seeding simulations are made with salt particle size of 20, 30 and 40um, seeding dose from 10^3 to 10^7/kg. Accumulated rainfalls of seeding series of natural and seeded clouds are listed in Table 1.

Seeding with 10^5/kg seeding dose can produce good seeding effect, which can reach 10%. With less dose, such as 10^4 or 10^3/kg, the rain enhancement seeding effect will be limited. Meanwhile with huge seeding dose of more than 10^6/kg, rainfall is reduced. Seeding time point also will affect net rain enhancement amount. Seeded and natural clouds own the same precipitation time period. Positive seeding effect is maintained to the end of precipitation.

Salt seeding not only changes the warm cloud processes, but also changes the graupel and cold rain processes.

Table 1 Accumulated rainfall of seeding series of natural and seeded clouds on 3rd September, 2002 in Henan county, Qinghai province.

No	Seeding tests							rainfall (kt)
	Seeding dose /kg	D(um)	times	time point (min)	Seeding locations			
					Vertical	W-E	S-N grids	
1	Non-seeding simulation							532
2	1.0×10^7	20	1	12	5-6	40-42	38-41	509
3	1.0×10^7	40	1	12	5-6	40-42	38-41	477
4	1.0×10^6	40	1	12	5-6	40-42	38-41	484
5	1.0×10^5	40	1	12	5-6	40-42	38-41	571
6	1.0×10^4	40	1	12	5-6	40-42	38-41	541
7	1.0×10^3	40	1	12	5-6	40-42	38-41	536
8	3.0×10^4	30	2	18	5-6	40-42	42-44	583
9	3.0×10^4	30	2	15	5-6	40-42	42-44	580
10	3.0×10^4	30	2	12	5-6	40-42	42-44	586
11	3.0×10^4	30	2	10	5-6	40-42	42-44	556
12	3.0×10^4	30	2	8	5-6	40-42	42-44	546
13	3.0×10^4	30	2	6	5-6	40-42	42-44	540

Acknowledgements

Support for this research was provided by the National Natural Sciences Foundation of China (40805003) and the Social Commonweal Research Project (2004DIB3J116).

References

Fang W., G. G. Zhneg, G. F. He, Simulation study on the precipitation and seeding process of convective cloud in Qinghai with a 3D cloud model (in Chinese). J. Nanjing Inst. Meteor., 28, 763- 769, 2005.

Hu Z. J. and Z. T. Pan, Research of salt particle seeding of stratiform cloud precipitation (in Chinese). Beijing, China Meteorological Press. 118-122. 1982,

Mason B J. The Physics of Clouds. Oxford, Oxford University Press, 1971.

Yu D. W., G. F. He, et al, 3-D convective seeding model and its application for field experiment (in Chinese). J. Appl. Meteor., 12, 122-132, 2001.

The Use of WRF Model To Support Cloud Seeding Operation: A Study in theCitarum Catchment Area

Mahally Kudsy
Ridwan
Findy Renggono
Faisal Sunarto
Weather Modification Technical Unit , BPP Teknologi –Jakarta-10340

Abstract

This paper presents about the use of WRF modelling to assist weather analysis for cloud seeding operation in the Citarum Catchment Area, West Java, Indonesia. In this study, WRF parameterization was carried out. The parameterized values were used to forecast precipitation during cloud seeding operation. To study the effect of variational run, WRF 3DVAR was run using GDAS data set and doppler weather radar data. The result from this study shows that precipitation precipitation can be better predicted by ingesting radar data into 3DVAR run.

1. Introduction

The Citarum Catchment Area is a very important area in Indonesia because it provides water for rice irrigation and hydropower generation. It's total area covers more then 7000 sq.km. There are 3 cascaded hydropower dams that supply ~ 6000MW electricity and rice field that produce about 30% of national production. **(Figure-1)**

Due to it's strategic value, Indonesian Government and related authorities have conducted many short-termed cloud seeding programs to ensure the provision of water supply for this area. WMTU has conducted 76-months cloud seeding operations since 1980. This year, WMTU has conducted 30 days operation during 18 March- 8 April 2011.

Weather predictability is very important in cloud seeding operation, this can achieved if atmospheric measument can be conducted. In case of instrumentation lack, some efforts must be made to obtain the likely atmospheric condition. Models such as WRF can be use to forecast near atmosphere properties. We have used WRF to study weather seedability during the periode mentioned above.

WMTU has operated a C-band doppler weather radar for several years. It is desired that radar can optimize the operation economy by ingesting into WRF prediction runs. The purpose is to remove some uncertainty during the operation.

WRF has potential use in cloud seeding such as mentioned by several workers (Peckham et.al, 2008; Stone, et.al, 2009). The use of model is very helpful to remove some uncertainty during cloud seeding operation (Levin et.al, 1997)

This paper present the result our first attempt to utilize model in cloud seeding. First, WRF physics parameterization was conducted to obtain correct physical parameters, namely microphysical and cumulus parameters. Subsequently, these parameters were used to forecast rain precipitation within a selected period. Then, WRF 3DVAR was employed using GDAS data set. Finally doppler weather radar data was ingested into 3DVAR WRF runs. Comparison of observed and forecast values are reported here.

2. Method

First , WRF was run using freely available GFS data set obtained from NCAR to generate a 3-day forecast within the domain bounded by (5S-9S, 105E-112E). These domain is much larger in size than the actual area of cloud seeding operation. To obtain the desirable parameters, WRF was run to forecast precipitation of the area outside the cloud seeding period. by varying the microphysics (mp_physics=3,4,6,8) and cumulus parameters (*cu_physics*=0,1,2,3,5). The output of WRF was analyzed for precipitation amout.

Analyses results indicates that for *mp_physics* for this domain does not have strong influence on precipitation, which is contrast to the cumulus parameter. The best cumulus parameter for this study is 5. Table 1 shows the explanation of the parameters studied

The parameters (*cu_physics* and *mp_physics*) which produced the best patterns were used in WRF to predict 3 days condition (24-26 May 2011). Precipitation data obtained from 10 raingages were compared with observed data and compared using point analysis.

WRF variational runs (WRF3DVAR) were made using observational data GDAS data set using PREPBUFR format from NCEP. GDAS data set used in this prediction was taken at the model initialization time (without data update). Finally, for the purpose to improving the results of the prediction, WRF 3DVAR was run using doppler weather data. During cloud seeding period a mobile doppler radar was operated to help locate potentially seedable clouds. The radar data volume itself is very large, so it needs a series of selection and thinning proces before it can be ingested into 3DVAR.

3. Results and Discussion

WRF accommodates a large number of parameterization. Previous studies such as Nepal's study (Regmi, et.al 2011), suggested that parameterization can often be successfully made by directly targeting to the specific problem.

Figure 3 shows that there is no significant in precipitation pattern from WRF output by varying microphysics parameter. Thus subsequent WRF runs were then made by using *mp_physics* = 5. This parameter has been used in operation forecasting by NCEP, where the scheme considers a mixed phase processes

Physical cumulus parameterization in WRF has developed from simple to advanced scheme. Now there are 6 cumulus schemes have been introduced. In general, where grid size is larger than cumulus' scale, WRF is often run without considering Cu (Cu=0). In this study *cu_physics=5* is relatively better than other values, as can be seen in Figure 3.

The results of precipitation prediction from WRF output can be seen in Figure-4. The results were taken from a 3-day forecast (March 24-26, 2011). The results are compared with observed values from 9 raingauges within cloud seeding operation area.

The effect of data assimilation using GDAS and assimilation with doppler weather radar are presented here for comparison. Although WRF 3DVAR is run, the result nearer to the model initial will give the best result. The longer the difference to the initial time, more spurious error will be expected from the result. Figure 4 show the comparison of observed values (OBS), WRF control run without assimilation (CNTL), run with GDAS assimilation (GDAS), and run with GDAS and doppler weather radar assimilation (GDAS+DWR) for March 24.

4. Conclusion and remarks

Observable preciptation increase (or decrease) is the main objective in cloud seeding works,therefore the predictability of precipitation will to extent remove some uncertainty of the result. It is shown from the present study that precipitation can be relatively to some extent accurately predicted.

WRF run can produce preciptation. Using GFS data it can forecast precipitation 72hr- ahead. The accuracy of prediction can be increased by running GDAS data and doppler data ingestion.

There are many indicators that are usually used to predict the atmospheric condition, namely K index, Sweat Index, Index of Coalesence Activity (ICA). In the absence of measurement, it is impossible to measure these indices, while they are very important for conducting cloud seeding. However, with a realible forecast product, such indices can be easily approximated. . According author's study from published papers ICA is one of the best indicator to predict air seedability in cloud seeding the results of a prediction.

Acknowledgement

This paper constitutes a partial report to The Ministry of Research and Technology for their funding support through The Research Incentive Program 2011; and to Weather Modification Technical Services through Global Warming Mitigation Program – 2011.

References

Levin, Zev, Shimon, O. Krichak, and Tamir Reisin. Numerical simulation of dispersal of inert seeding material in israel using a three-dimensional mesoscale model. *J. Appl.* **36**, 474-484, 1997

Murali-Krishna , I. V. and Manickam, V., Global Climatic Change And Weather Modification Technologies, 760pp BS Publicatons Hyderabad – ISSN : 978 -81-7800 -184 -5 (HB), 2009

Peckham, S., Grell, G. A., McKean, S. A., Fast, J. D., and Gustafson, W. I. Annual Report CIRES/Univ. of Colorado & NOAA/ESRL/GSD, Boulder, CO

Regmi, Suman Kumar, Jayaraman Potty, PVS Raju and Itesh Dash: Performance evaluation of WRF model for Nepal, Workshop on Weather Forecasting and Flood Early Warning System in Nepal, 08th Apri 2011, KathmanduRosenfeld, D. and Silverman, BA., Results of On –Top Glaciogenic Cloud Seeding in Thailand, Part 1: The Demonstration Experiment, J. *App. Meteor*., **42**,939-951, 2003.

Stone, R. H., Reno, NV; McGurty, B. M., Farber , R. J., Shaw, B. L., and Clarke, B.: Assessment of the San Joaquin Cloud Seeding Program using WRF based Sub Basin Quantitative Precipitation Forecasts as Formal Controls for Unseeded Precipitation: Preliminary Results obtained from the 2009 and 2010 Winter Seasons, 91st Americam Meteriological Society Meeting, 2011

Woodley, W. L., D. Rosenfeld and BA Silverman, Results of On –Top Glaciogenic Cloud Seeding in Thailand, Part 1: The Demonstration Experiment, J. *App. Meteor*., **42**,920-938, 2003.

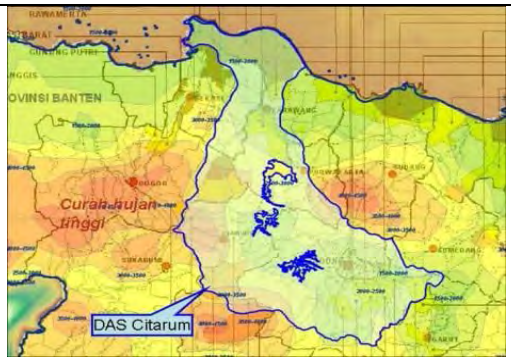


Figure 1 – The Citarum Catchment Area with 3-cascaded dams

Microphysics		Cumulus	
value	scheme	value	Scheme
		0	No cumulus
3	WRF-SM3	1	Kain-Fristch
4	WRF-SM5	2	Bets-Miller-Janjic
6	WRF-SM6	3	Grell-Devenyi
8	New Thompson	5	3D-Grell

Table 1 – Microphysical and cumulus parameters investigated in this study

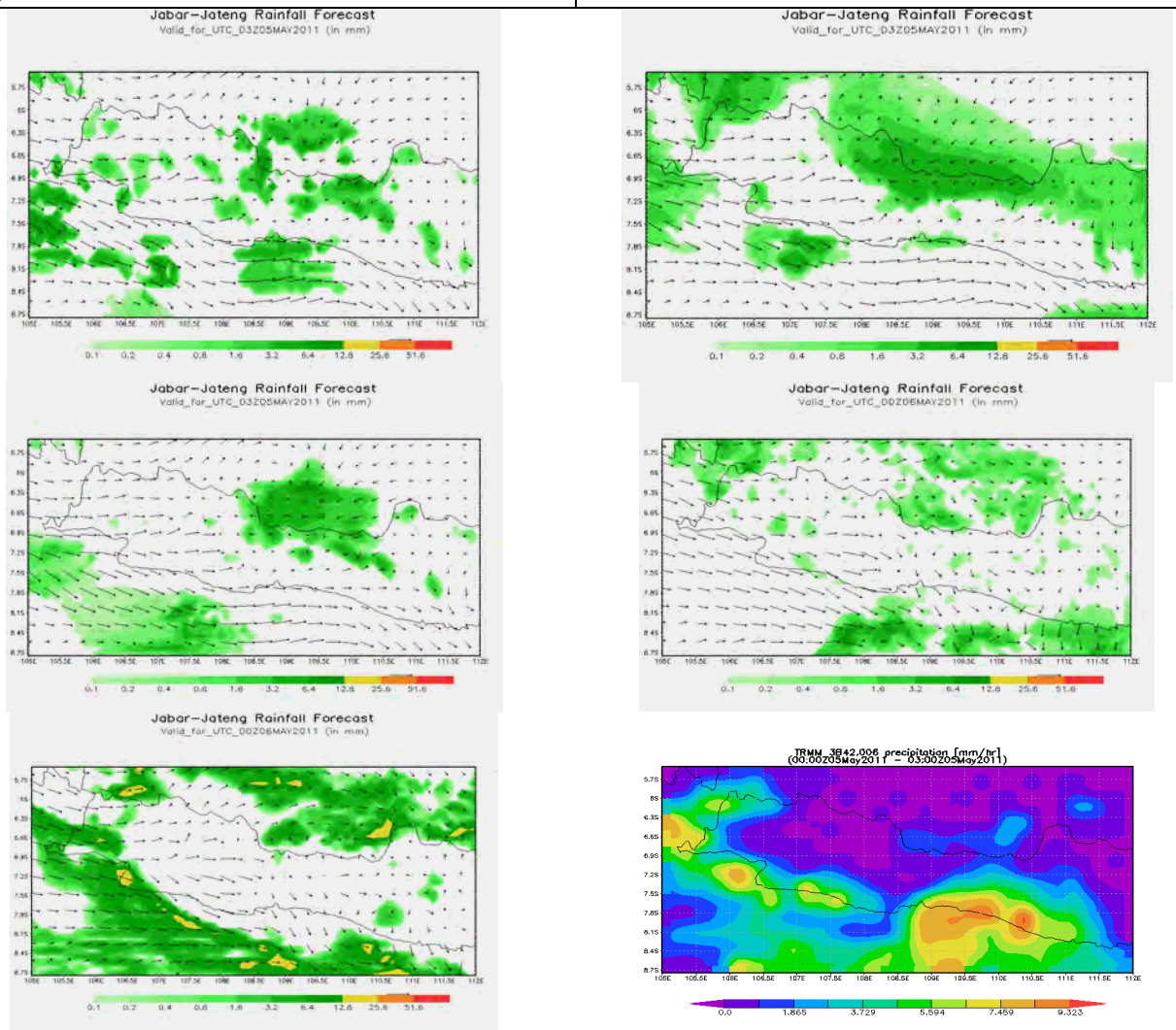


Figure-2: Sample from WRF preciptation output

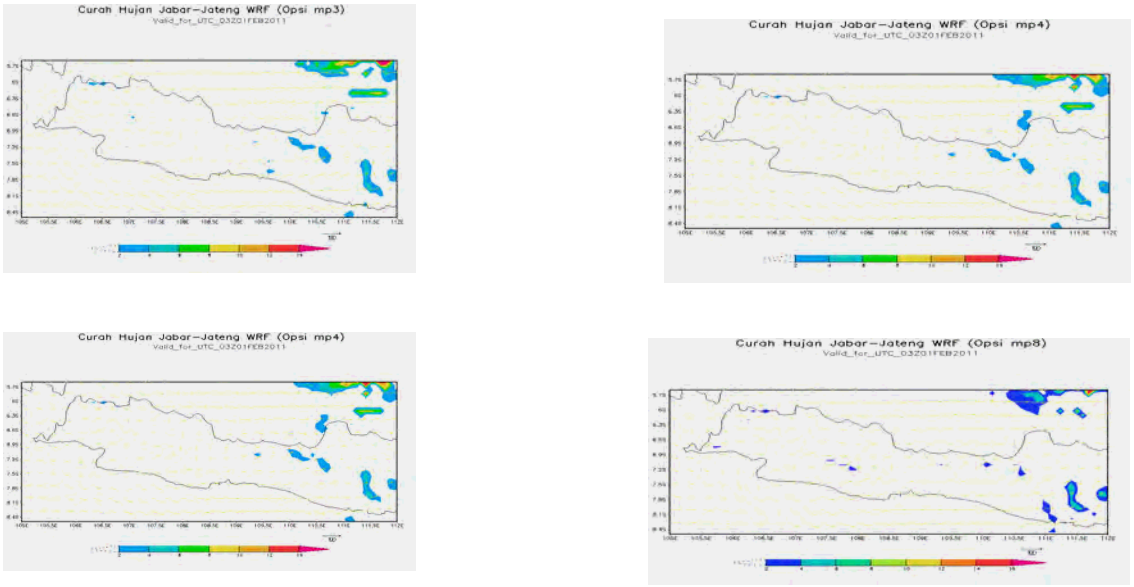


Figure 3: Effect of microphysical parameter on precipitation in WRF

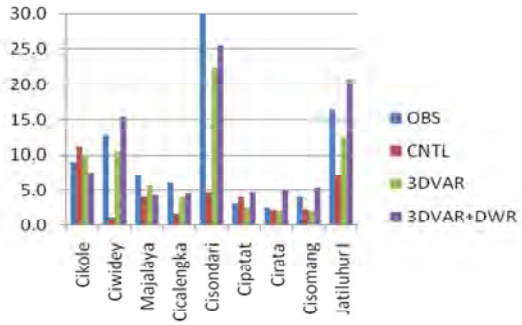


Figure 4: Precipitation comparison of observed, control, 3DVAR with GDAS , and 3DVAR with radar data ingestion

Comparisons of Cloud Microphysical Characters between Mesoscale Model for Artificial Precipitation Enhancement and Satellite Observations

Ma Zhanshan, Liu Qijun

National Meteorological Center of CMA, Beijing, China

Qin Yanyan

National Marine Environmental Forecasting Center, Beijing, China

1. INTRODUCTION

National Meteorological Center (abbreviated to NMC) has developed a new double-moment explicit microphysics scheme in 2006, and coupled it with mesoscale numerical model GRAPES, which established an operational numerical model forecast system for artificial rainfall enhancement in NMC. This system can provide information of cloud microphysical structure, macro properties and synoptic situations over China, which would be beneficial for the development of artificial rainfall enhancement. In order to have a better understanding of the system's performance and accuracy，the comparisons of cloud microphysical characters between the forecasting products and observations is significative and it will put forward an objective and reasonable proposal for improving and optimizing of the microphysical scheme at the same time. In previous studies, many comparisons of model forecast results with satellite data have already been undertaken abroad. For example, J.-P. Chaboureau et al. (2001) has adjusted the ice-to-snow autoconversion threshold of microphysical scheme according to the discrepancy of cloud top brightness temperature between Meso-NH model and METEOSAT observation. William. L. et al. (2006) has evaluated the results of operational NOAA Rapid Update Cycle (RUC) model in term of the analyzed and predicted condensation fields by directly comparing them with NASA Langley research Center (LaRC) satellite-derived cloud products and quantifying the differences. In this paper, we will mainly reveal the forecast performance of cloud characters and their [1]difference compared with MODIS and TRMM observations.

2. DATA AND METHOD

Monitoring and retrieving data, including cloud liquid water, precipitation water, cloud ice water and precipitation ice of 14 levels in vertical direction, which is provided by TRMM microwave imager (TMI) product 2A12 in TRMM satellite orbits, are used to evaluate forecasting ability of artificial precipitation enhancement model to cloud water, rain water, cloud ice and precipitation ice. The column cloud water content of MODIS data is also used to verify cloud macroscopic field.

The following method is used to calculate satellite observation and retrieval data: observed hydrometeor content values on each grid points of model in satellite's observation orbits are calculated by the mean value of all observed satellite data in square area which centers on the grid and has a radius of 0.05°. Comparison and analysis are conducted between satellite monitoring data and model forecast data on grid points.

3. RESULTS

3.1 Quantitative Evaluation

Table 1 shows that results of four types of hydrometeors selected three random cases from both model forecast and TRMM satellite monitoring were compared. Mean value of hydrometeor contents in vertical direction at four different heights (2 -3 km, 4 -5 km, 5 -6 km, 7 -8km) was calculated.

The comparison of vertical distribution of hydrometeors reveals that artificial precipitation model has a better vertical distribution forecast for different hydrometeors, and they were also coordinated with the observation results. The products of the cloud liquid water content and rain water content provided by TRMM satellite and model both showed an increasing tendency with height decreasing and reached its maximum value at 2-3 km, while decreased rapidly at high altitude and reduced to the minimum at 7-8 km. Meanwhile, cloud ice had a contrary vertical distribution. That was its content emerging a gradual increasing tendency with height increasing at the cold zone. There was no cloud ice at low altitude, while maximum appeared at 7-8 km or above. In general the prediction value of model was slightly larger than the average satellite monitoring value, while there were some subtle differences among hydrometeors.

Tab.1 The comparison of hydrometeor mean values in cloud clusters between model and satellite

[1] Corresponding Auther Address: China National Meteorological Center, Zhongguancun South Road 46, Beijing, China; E-mail: mazs@cma.gov.cn

Hydrometeor / height		cloud liquid water（g/kg）		precipitation water（g/kg）		cloud ice water（g/kg）		precipitation ice（g/kg）	
		model	TRMM	model	TRMM	model	TRMM	model	TRMM
mean	2 ~ 3km	0.080	0.050	0.123	0.157	0.0	0.0	0.122	0.153
	4 ~ 5 km	0.037	0.035	0.080	0.075	0.006	0.001	0.189	0.192
	5 ~ 6km	0.010	0.017	0.029	0.016	0.009	0.004	0.270	0.235
	7 ~ 8km	0.007	0.006	0.004	0.002	0.007	0.005	0.192	0.176

3.2 A Case Analysis

On 25 May 2006, there was a heavy rainfall caused by a northeast-southwest shear line at South China. Record in station Guixi of Jiangxi province was 130.01 mm, station Fogang of Guangdong province reached 125.20 mm, and station Jiangyong and Qidong of Hunan province reached 139.0 mm and 118.0 mm, respectively. The following results are the case between model and observations.

3.2.1 Precipitation field

As shown in Figure 1, both locations and patterns of the rainband are very close to the actual situation and the order of magnitudes. The heavy rainfall center at joint part of three provinces was identical to actual situation, while the heavy rainfall center at northeast Jiangxi shifted southwestward slightly.

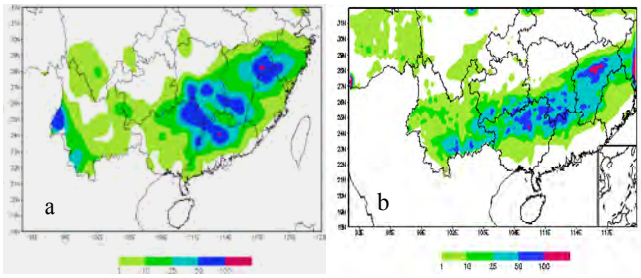


Fig.1 Observed (a) and forecasted (b) rainfall from 1200 UTC 25 May to 1200 UTC 26 May 2006，unit：mm

3.2.2 Cloud Macroscopic Field

Column cloud water content was chosen in order to valuate the model forecasting ability to cloud macroscopic fields during this heavy rainfall process , which shown as Fig.2. The column cloud water content of MODIS distributed from southwest to northeast, which was mostly above 200g/m^3 in the main cloud band (Fig.2a). The high-value area above 800 ~ 1000g/ m^3 lay in north of Guangxi, south of Hunan, north of Guangdong and middle of Jiangxi. Furthermore, there were also some developing convective cloud cluster with high cloud water content in mid Guangxi and northeast of Yunnan. The patter of column cloud water content was well forecasted (Fig.2b) and coincided with MODIS monitoring in Guangxi, Guangdong and Hunan province with the value above 1000g/m^3. The location of forecasted column cloud water content was a little northward in Jiangxi and the value was somewhat greater than observation in northwest of Guangxi.

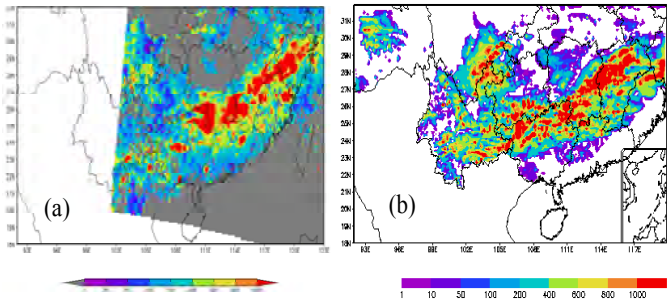


Fig.2 Column Cloud Water Content of TRMM (a) and model (b) at 0300 UTC 26 May 2006, unit: g/m^3

3.2.3 Cloud Microphysical Field

Fig.3a-Fg.3h shows the spatial distributions of hydrometeors content for cloud liquid water, precipitation water, cloud ice water and precipitation ice from TRMM observation and model forecast. TRMM satellite monitoring shows there were cloud bands developing in Hunan, south of Jiangxi, north of Guangdong, mid Guangxi, south of Yunnan, southwest of Sichuan and east of Tibet from 0300 UTC to 0500 UTC on 26 May, and local convection was very strong. The artificial precipitation enhancement model had forecasted the spatial distribution quite well. The spatial distributions of forecasted precipitation water and cloud ice water were very close to those of TRMM satellite observation. And their strong central locations were also good agreement. The forecasted cloud liquid water coincided with TRMM in Guangxi and Yunnan, but missed southwest Sichuan and east Tibet. The centers of precipitation ice for both model and TRMM were located at north of Guangxi, southwest of Yunnan Province, southeast of Tibet. Nevertheless, the distribution of forecasted precipitation ice was slightly greater than that of TRMM, which were mainly concentrated in 0.01-0.05g/kg. The order of magnitudes of all hydrometeor content from model and TRMM were exactly the same and their absolute values are almost in 10^{-3}-10^{-1}g/kg, yet there were trivial differences between different hydrometeors. The cloud liquid water content of model at strong central location was greater than that of TRMM, the maximum value of TRMM was 0.1-0.3g/kg while the result from model was 0.7g/kg. The ultimate difference occurred at southwest Yunnan and this might be related to local complexity of the

underlying surface. The magnitudes of precipitation water and cloud ice was at between 10^{-3}-10^{-2}g/kg, which were smaller than those of TRMM. Magnitudes of maximum value of forecasted precipitation ice content was identical to satellite observation but the distribution range was wider than that of TRMM.

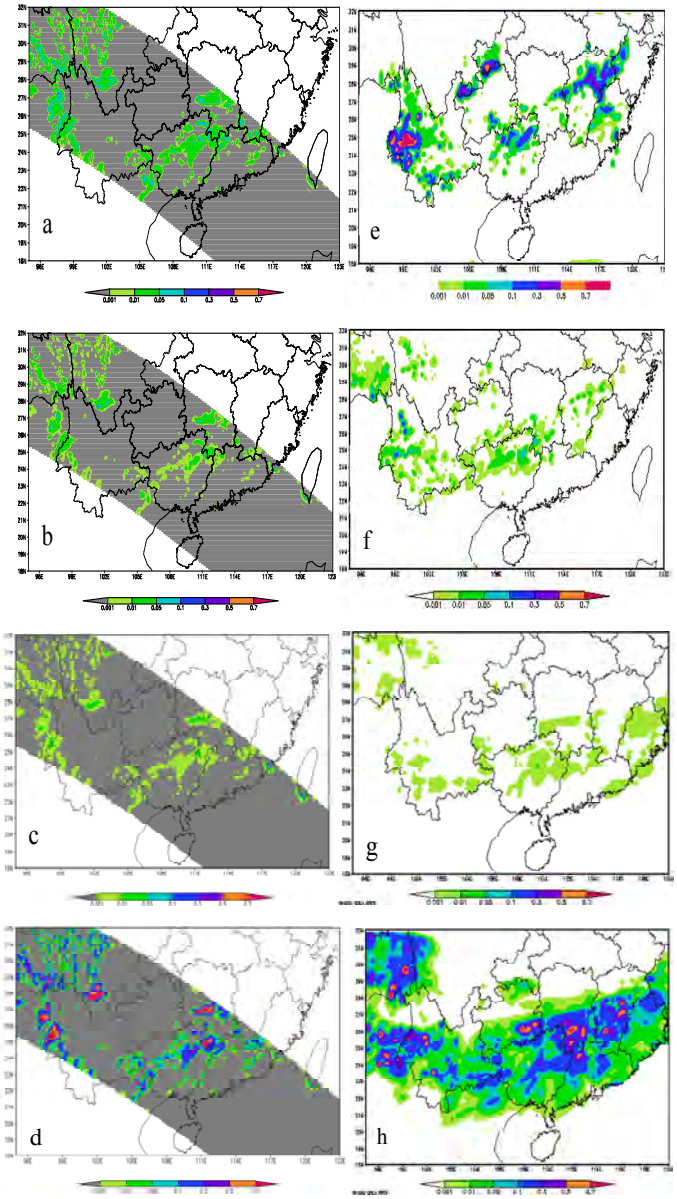
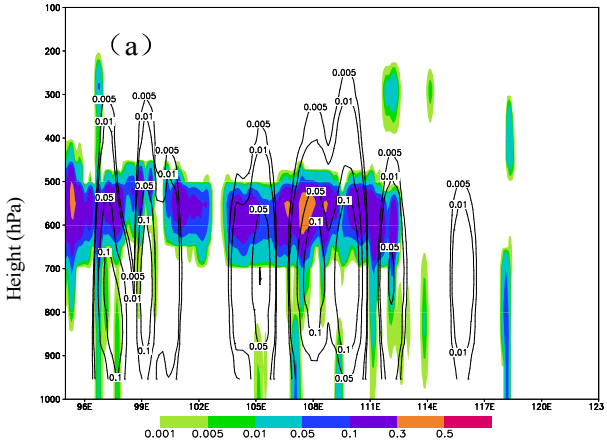
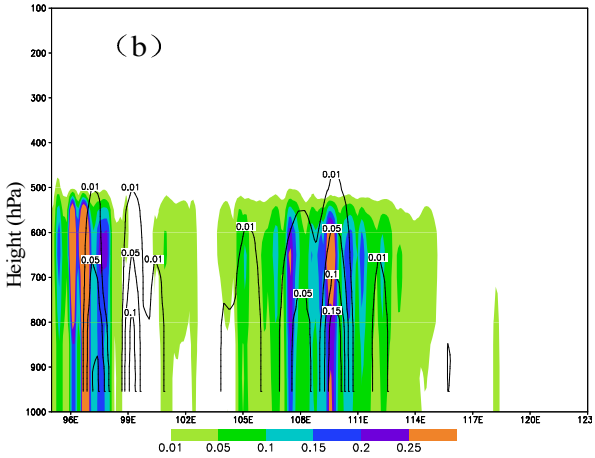


Fig.3 Spatial distributions of hydrometeors at 0300 UTC 26 May 2006, of which a ~ d are cloud liquid water, precipitation water, cloud ice water and precipitation ice of TRMM and e ~ h are those of model forecast, unit: g/kg

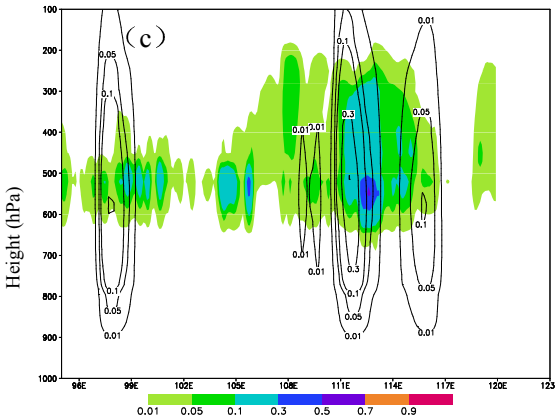
In order to verify the capability of artificial precipitation enhancement model to distributions of vertical hydrometeors content, zonal profiles of cloud liquid water, precipitation water, cloud ice and precipitation ice content of both model and TRMM along the rainfall center were shown in Figure 4. As shown in Fig.4, the distribution scopes of forecasted cloud liquid water was slightly narrower than that of TRMM. TRMM monitoring had a wide scope in vertical direction from ground surface to 300hPa and the maximum content (0.1-0.3g/kg) lay at 850hPa to 600hPa while artificial precipitation enhancement model mainly distributed from 700-450hPa and its maximum content (0.3-0.5g/kg) was at 300hPa height. The vertical distributions of forecasted precipitation water are consistent with those of TRMM very well, which mainly was below 500hPa. Some places must have occurred rainfall process for the precipitation water fell to the ground surface. There were two high intensity centers at about 97 ° E and 109 ° E for both model and TRMM, which one maximum reached 0.1-0.15g/kg and another reached 0.15-0.25g/kg. The precipitation ice of TRMM monitoring located mainly at 800-200hPa and its value was between 0.01 g/kg and 0.3g/kg. There were also two high intensity centers at 98.2 ° E and 112 ° E with maximum value of 0.15g/kg and 0.4g/kg, respectively. The vertical range of forecasted precipitation ice was smaller than that of TRMM with the same top height and a higher bottom at about 600hPa. The forecasted high precipitation ice content was about 0.1-0.3g/kg with maximal value of 0.5 g/kg, and occurred slightly easterly relative to TRMM monitoring. Likewise, the cloud ice of both model and TRMM appeared at 550hPa above with value between 0.001 g/kg and 0.05 g/kg.



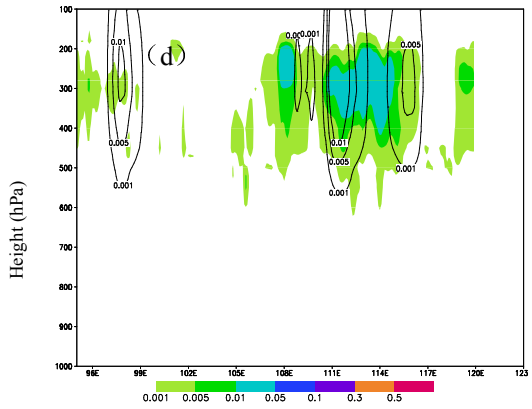
cloudwater contents mixing ratio (g/kg)



rainwater contents mixing ratio (g/kg)



fallout icewater contents mixing ratio (g/kg)



crystalwater contents mixing ratio (g/kg)

Fig.4 Zonal profiles of hydrometeors along 24.2°N at 0300 UTC 26 May 2006, of which a ~ d are cloud liquid water, precipitation water, precipitation ice and cloud ice water with shading denoting model forecast and contour denoting TRMM, unit: g/kg

4. CONCLUDING REMARKS

These preliminary results indicate that the magnitudes of forecasted hydrometeors from artificial precipitation enhancement model coincided with those of TRMM observations generally, yet the forecasted values are slightly larger than TRMM. Vertical distribution characteristics of cloud microphysical fields can be forecasted quite well by model system, which is identical to TRMM satellite monitoring. The distributions and positions of maximum intensity of forecasted cloud liquid water, rain water and cloud ice, as well as values coincided with TRMM observation at seeding height. Forecasted high value areas of precipitation ice agreed with TRMM monitoring, but the areas of precipitation ice content in 0.01-0.05g/kg was larger than that of TRMM. As to vertical distribution, the height range of forecasted rain water and cloud liquid water were in accord with satellite observation. The height of maximum values for cloud liquid water and precipitation ice agreed with TRMM, but their distribution range was narrower than that of TRMM.

References

J.-P. Chaboureau, J.-P. Pinty,J.-P. Mascart, J.-P. Lafore. Mesoscale Cloud Scheme Assessment Using satellite Observations. Ninth Conference on Mesoscale Processes, Fort Lauderdale, FL,30 July-2 August 2001.

William L., Smith Jr., Patrick Minis, Stanley G.Benjamin, Comparison of RUC condensate analyses and forecasts with satellite-derived cloud properties. AMS 14th Conference on Satellite Meteorology and Oceanography. Atlanta, GA, 2006.

Impact of natural production of coastal marine aerosols on convective clouds as simulated using cloud model with detailed microphysics: Comparison to cloud seeding with hygroscopic flares

Rabia MERROUCHI[1], Abdalah MOKSSIT[1], Jacques PIAZZOLA[2] and Mohamed CHAGDALI[3]
Rabia.merrouchi@gmail.com, mokssit.abdalah@yahoo.fr, *jacques.piazzola@univ-tln.fr* and *m_chagdalli@hotmail.com*

[1] National Meteorological Service of Morocco –BP 8106, Oisis. Casablanca-Morocco.
[2] ISITV, Laboratory of Particles Exchange at the Interfaces (LEPI), University of Toulon Var, France.
[3] Laboratory of scientific computing in mechanic, Faculty of sciences Ben M'sick Casablanca, Morocco.

1. Introduction

The marine aerosol is produced by the ocean spray. Under the action of breaking waves, water droplets of large size are projected into the atmosphere. After evaporation of sea water, solid sea salt particles are found in the atmosphere as Aerosols. The chemical composition of this type of aerosol is close to that of sea water. We found essentially chlorine and sodium, but also large amounts of nitrates and sulfates (Masclet & Cachia, 1998). The annual emission rate of the marine aerosol is approximately 10^9 tonnes which represents more than 42% of the total mass of atmospheric aerosols.

The aerosol cloud interaction is a fundamental mechanism influencing the precipitation process. Indeed, the microphysical processes governing the growth of water droplets inside the cloud depends on the initial spectrum and the chemical composition of atmospheric aerosols caught in the updrafts.

The need to introduce an appropriate source term in numerical models of clouds and of dispersion of atmospheric aerosols explains the interest, raised several years ago, of studying the process of generation of coastal marine aerosols produced by the breaking waves. this process is defined by the relationship between witecapping coverage and meteorological parameters (Vignati et al. 2001; Piazzola et al., 2002).

To study the impact of marine aerosols on cloud microphysics and in particular the impact of coastal marine aerosols spectra, numerical simulations were carried out. These simulations have focused on a convective cloud (mixed phase) using different marine aerosols spectrum. The comparison between the results obtained show that some microphysical properties have been modified accordingly influencing the conditions for triggering rainfall and the rain amounts collected at the ground.

2. Material and methods

2.1. The Mediterranean Coastal Aerosol Model

The Mediterranean Coastal Aerosol Model (MEDEX) is based on an extensive series of measurements which were acquired on the island of Porquerolles (France) between 2000 and 2001. During this extended period, large variety of aerosol size distributions were observed for different meteorological conditions which were statistically analyzed to develop an empirical coastal aerosol model. The basic principles of this model is that the aerosol concentration vary differently with the fetch and the wind speed, if the particles are generated from the local sea surface source (sea spray) or are transported from other places (small anthropogenic or continental aerosols). The concentrations are determined by the balance between production and removal, which is strongly dependent on the wind speed. For example, Fig. 1 shows aerosol spectra recorded at a wind speed of about 10 m/s for fetches varying from 13 to 100 km in the study area. The concentrations of coarse particles (> 1 µm), which at longer fetch are assumed to be dominated by sea-salt particles (Cipriano et al., 1987; Monahan et al., 1983), increase with increasing fetch. In contrast, the concentrations of sub-micrometer particles decrease at larger fetch. Thus, the data in Figure. 1 represent an example of the transition from a continental to a marine aerosol as the air mass is advected over the sea, similar to observations by Vignati et al. (1999) and Van Eijk and De Leeuw (1992) in other coastal locations.

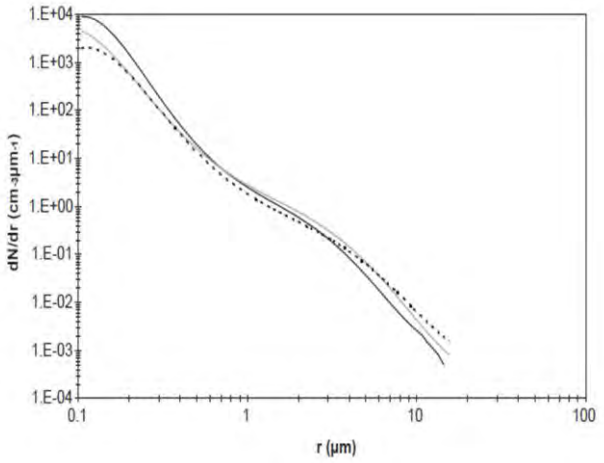


Figure 1. *Aerosol size distributions measured in the Mediterranean coastal area with a surface wind of 10 m/s and at different fetches. The thin curve was recorded at a 3-km fetch, the dashed line was recorded at a 10-km fetch and the thick line was recorded at a 22 km. (Piazzola et al., 2003).*

The Mediterranean coastal aerosol model was written to take into account these typical coastal processes. It is a modification of the Navy Aerosol Model (NAM) developed by Gathman et al. (1983) and it is formulated analogously to the model proposed by Piazzola et al. (2000) on the basis of an aerosol data set acquired on the island. As in the

model NAM, the particle size distribution dN(r)/dr of the coastal aerosol model is calculated as the sum of modified lognormal functions (Piazzola et al., 2005):

$$\frac{dN}{dr} = \sum_{i=1}^{4} \frac{A_i}{f} \exp\ -C_i(\ln(r / fr_{oi}))^2$$

where *i* gives the number of the lognormal component of N(r), r_{0i} are the mode radii (in µm), i.e., r_{01}=0.03 µm, r_{02}= 0.24 µm, r_{03} = 2.0 µm, r_{04} = 10 µm. *f, A_i and C_i* represents respectively the dimensionless humidity growth factor, the concentration ($cm^{-3}\mu m^{-1}$) and the width of the i^{th} mode.

The predictions of the Mediterranean coastal model have recently been compared to the data recorded in other geographical locations (Piazzola and Kaloshin, 2005; Benderski et al., 2004). This confirmed the accuracy of such a model to predict the aerosol size spectra in coastal areas. Indeed, Piazzola and Kaloshin (2005) found 2.6 as the maximum factor by which the modeled aerosol concentration differs from the experimental concentration (68% confidence).

2.2. The Mediterranean Coastal Aerosol Model

The cloud model ExMix (External Mixture) has been developed (Worbrock 1989, Monier 2003 and Leroy 2005) to study mixed-phase clouds by integrating a detailed microphysics of the whole process of formation, growth and precipitation and taking into account the initial thermodynamic profile and the aerosol spectrum in terms of distribution and chemical composition (solubility).

The microphysical part of the model includes all processes governing drop formation, vapor growth, collisional growth, evaporation, melting and glaciations. At the initial time, aerosol particles are considered in equilibrium with the atmosphere following Köhler equation. Droplets and wet aerosol particles can then grow due to condensation or collision/coalescence processes. The digital processing of condensation occurs in two steps: First, calculate the growth speed of the droplet by condensation according to the equation of Pruppacher and Klett, 1980. The advection is then calculated using the scheme of Smolarkieviecz (1983).

Ice crystals are assumed to be of type column (Monier et al., 2003) in cirrus clouds or spherical in the case of mixed phase clouds (Leroy et al., 2004). Ice crystals are formed by heterogeneous nucleation as described by Meyers et al. (1992). Once formed, Ice crystals grow by vapor deposition and riming following Pruppacher and Klett (1997) formulae and also by collision and coalescence.

The process of the coalescence of droplets by larger drops is also represented by Pruppacher and Klett (1997) and the stochastic equation of collision is solved using numerical scheme proposed by Bott (2000).

The model EXMIX was tested for mixed phase clouds (Leroy et al., 2005) by using as reference case the summer convective cloud observed at Miles City the July 19, 1981 during the CCOPE Campaign (Cooperative Convective Precipitation Experiment) held in Montana (USA).

2.3. The Simulations

The sensitive studies were made based on the conducted simulations. Only, the initial aerosol distribution function is modified from a simulation to another. The four initial spectrums used are deduced from following formulae and correspondent coefficients are detailed in Table 1.

$$\frac{dN}{d\ln r} = \sum_{i=1}^{k} \frac{n_i}{\sqrt{2\pi}\log(\sigma_i)\ln 10} \exp\left\{\frac{(\log(\frac{r}{R_i}))^2}{2(\log(\sigma_i))^2}\right\}$$

Where k, n_i, R_i and σ_i are number of the lognormal component of N(r), the total number concentration, the geometric mean radius and geometric standard deviation of aerosol for each mode i.

Spectrum	*Concentration N_i (cm^{-3})*	*Radii R_i (µm)*	*Log (σ_i)*
Continental	N_1= 997	R_1=0.001	$log(\sigma_1)$= 0.328
	N_2= 842	R_2= 0.0218	$log(\sigma_2)$= 0.505
	N_3= $7.1.10^{-4}$	R_3= 6.24	$log(\sigma_3)$= 0.277
Marine (jaenicke, 1988)	N_1= 133	R_1=0.004	$log(\sigma_1)$= 0.66
	N_2= 66,6	R_2= 0.133	$log(\sigma_2)$= 0.21
	N_3= 3.1	R_3= 0.29	$log(\sigma_3)$= 0.4
Costal marine spectrum calculated using MEDEX (U= 20m/s.)	A_1/f= 92634,22	R_1=0.03	C_1= 1,241
	A_2/f = 55,713	R_2= 0.24	C_2= 1,357
	A_3/f = 0,449	R_3= 2.0	C_3= 1,508
	A_4/f = 0,008	R_4= 10.0	C_4= 10
Costal Marine spectrum according to VAGNITI et al, 2001(U=20m/s)	N_1= 152,40	R_1=0.2	$log(\sigma_1)$= 0.278
	N_2= 13,55	R_2= 2.0	$log(\sigma_2)$= 0.301
	N_3= 0,0075	R_3= 12	$log(\sigma_3)$= 0.477
South African Hygroscopic flares –Cooper et al.1997	N_1= 152,40	R_1=0.3	$log(\sigma_1)$= 0.2
	N_2= $1.7*10^{-4}*N_1$	R_2= 1.0	$log(\sigma_2)$= 0.4
	N_3=$3*10^{-7}*N_1$	R_3= 10	$log(\sigma_3)$= 0.6

Table. 1. *Initial aerosol spectrum as a sum of log-normal distribution functions where ni, Ri and σi are the total number concentration (cm^{-3}), the geometric mean radius (µm) and geometric standard deviation of aerosol for each mode* i.

The first simulation was conducted using a continental aerosol spectrum calculated based on aerosol measurements at Puy de Dome (France) in a continental and unpolluted air mass (Sellegri, 2002). The results are compared to those of the second simulation conducted using the marine spectrum given by Jaenicke, 1988. This comparison is made to examine the impacts of introducing marine aerosol spectra on both dynamics and precipitation formation mechanisms. Furthermore, a third simulation was made using as initial aerosol spectrum the coastal marine aerosol distribution calculated by the model MEDEX with the aim to study the importance of the natural processes behind the generation of marine aerosols in coastal areas and their impacts on clouds forming at the vicinity of the generation area.

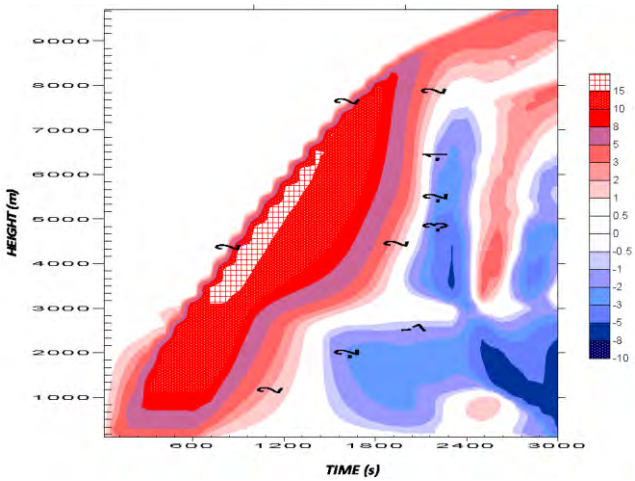
To investigate the importance of parameters induced in the model MEDEX for the calculation of

the coastal marine aerosol spectrum, a fourth simulation have been performed using the coastal marine spectrum provided by the formulation of Vignati et al. (2001) which relates the aerosol concentrations to the wind speed at 10 meters height above the sea surface based on measurements collected in the California coast between 1996 and 1997.

In the final simulation, it's a question to reproduce and investigate the possible effect of a real airborne cloud seeding operation using South African hygroscopic flares. The South African hypothesis (Mather et al., 1997; Cooper et al, 1997) was based on the fact that the seeding particles have the advantage over CCN by being larger in size and more soluble. The observed aerosol spectrum produced by the hygroscopic flares was measured using instrumented Learjet of South Africa that flayed about 50 m behind a seeding aircraft burning two of the flares. The measured size distribution from the flares can be approximated by the sum of three lognormal distributions as shown in table 1.

3. Results and Discussion

Passing from an initial continental spectrum of aerosols to a broad marine aerosol spectrum (Jaenicke, 1988), the updrafts are more prevalent between 4000 and 8000 meters height. The downdrafts in the cloud are shorter but become stronger near the surface beyond 40 minutes of integration. As shown in figure 2.a, precipitating water appears earlier (22 minutes instead of 33 minutes) at lower elevations (5400 instead of 9200 meters). Rainfall reaches the ground more rapidly (37 minutes instead of 48 minutes) and the amount of water collected on the ground is more important with liquid water content up to 2 g/m^3.



Figures 2.a and 2.b

(2.a): *Time evolution of vertical velocity (m/s) (initial marine spectrum –Jaenicke 1988).*

(2.b): Evolution of liquid water content in g/m^3 as a function of height (m) and time (s). The cloud droplets (r <40µm) in black, in blue and colour precipitating droplets (initial marine spectrum –Jaenicke 1988).

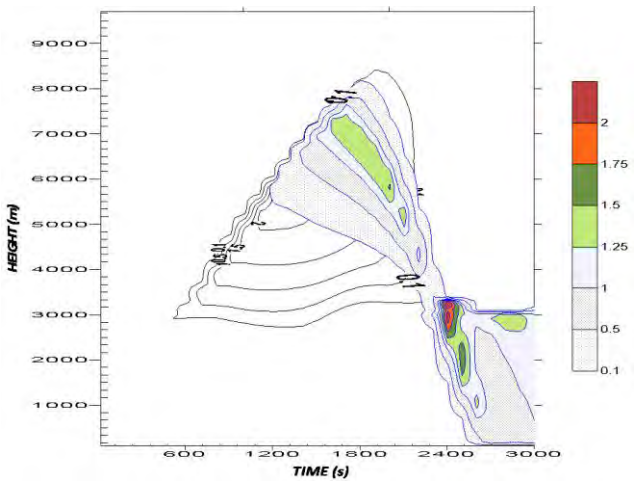
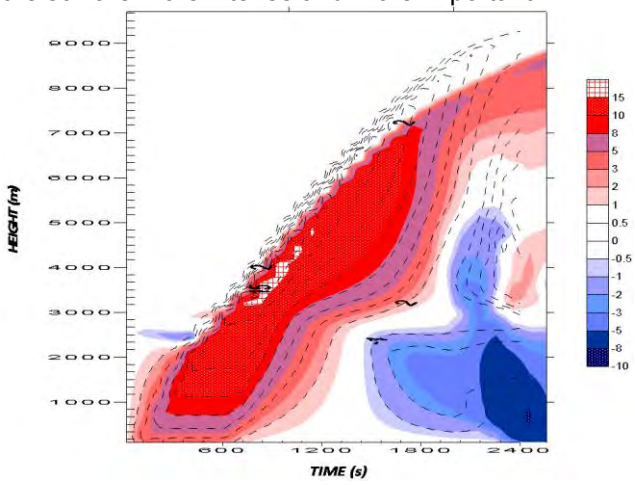


Figure 2.b

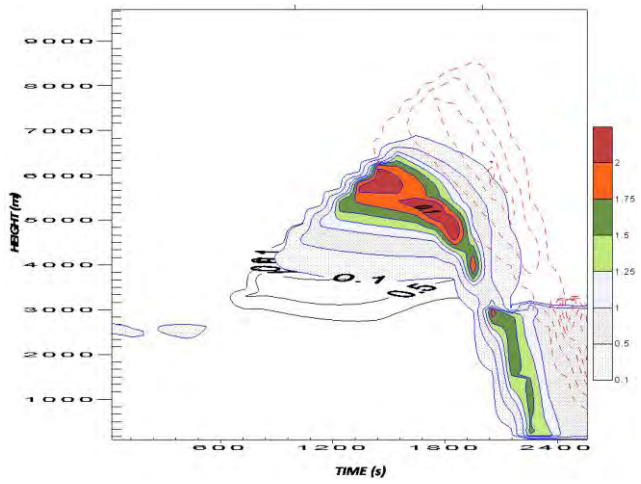
The coastal marine aerosols spectrum predicted by the model MEDEX depends mainly on the strength of the wind at the sea surface and the size of the sea surface under the influence of this wind (fetch). The submicron particles decrease slightly when the wind speed increases while the concentration of giant particles (radii> 2µm) increases with wind speed (Piazzola et al., 2003).

In order to highlight the contribution of wind speed and the fetch, the model MEDEX was forced by a value of surface wind of 20 ms^{-1} and fetch of 30 km. The calculated spectrum is normalized to a relative humidity of 80% in order to compare accurately with various studies related to coastal marine aerosols.

Compared to the first and second simulations, the precipitating particles are more prevalent in the altitudes below 6600m instead of 8400m (Figure 3.b). Indeed, all liquid and solid particles larger than 40µm fall to reach the ground ten minutes earlier. The liquid water content is higher with values exceeding 2g.m^{-3}. The quantities of water reaching the soil are more intense and more important.



Figures (3.a)*: Time evolution of vertical velocity (m/s).*
(3.b) *Evolution of liquid water content in g/m^3 as a function of height (m) and time (s). The cloud droplets (r <40µm) in black, in blue precipitating droplets (Medex calculated spectrum for U=20m/s and Fetch=30km).*



As the first two modes of the spectrum calculated by MEDEX seems to be contaminated by a contribution from continental aerosols, large concentrations of sub-micrometer aerosols are predicted in particular for the nucleation and the accumulation modes (respectively 10^4 cm^{-3} and 10^2 cm^{-3}). The question in this case is to determine if those modes are responsible of the large amounts of precipitation accumulated at the ground. In general, several modeling studies (Reisin et al., 1996; Leroy et al., 2006) and satellite imagery (Rosenfeld, 1999) have highlighted the reduction of precipitation at the ground in convective clouds developing in polluted environments. High concentrations of small atmospheric aerosols are known to reduce the size of cloud droplets, increase cloud albedo and suppress precipitation formation. In contrast, cloud simulations suggest that even low concentrations of large soluble aerosols should promote droplets' growth and rainfall.

In order to address this issue and to investigate the possible effect of the two first modes of the MEDEX predicted spectrum, two new simulations were performed by adopting a strong winds (surface wind speed of 10 m/s and 20 m/s) blowing over a wider sea surface (large fetch of 90 km instead of 30 km) to emphasize the production of large particles to the detriment of submicron particles (Piazzola et al., 2003 (Figure 1)). The concentration of aerosol particles of small size is then reduced by 30% from 9.10^3 cm^{-3} to 6.10^3 cm^{-3} while the production of giant particles (> 2µm) increases starting from 8.10^{-4} cm^{-3} to 2.10^{-3} cm^{-3}.

The results of those simulations are consistent with those already obtained while noting a reinforcement of the vertical negative velocities up to -10 m/s which are associated with a more intense rainfall. The liquid water content is higher with values of more than 2.5 g/m^3 and same behavior reported for predicted rain accumulation on the ground.

To reproduce the cloud seeding operation, we introduce, for the purpose of the fifth simulation, for five minutes in the growth phase of the cloud (between t = 700s and 1000s) and 300m below the base of the cloud the quantity of aerosols given in table 1. It seems that no effect have been induced by the additional quantity of hygroscopic aerosols generated by the two flares. Other simulations were conducted modifying only the concentration of the hygroscopic aerosols which is synonym to the use of more flares. Large amounts of liquid content appear when the number of flares used increases.

Opposite effect is observed when the amount of flares used increases greatly. In this case, simulation shows that the cloud remains in the stage of cumulus congestus with a vertical extension not exceeding 2500 m, low liquid water content (less than 1.25 g/m^3 and no rain at the ground.

5. Conclusion

In this study, four types of aerosol spectrum of different origins were used. If the continental spectrum is more focused on continental fine particles (r <0.1 µm) with major concentrations around 10^3 cm^{-3}, the marine spectrum of Jaenicke, 1988 contains more large particles (between 0.2 µm and 2 µm) with lower concentrations (about 10^2 by cm^{-3} of air). The coastal marine spectra suggested by Vignati et al, 1999; Kaloshin and Piazzola, 2004 are characterized by the presence of giant particles (around 10 µm) but with low concentrations.

Thus, the transition from a continental aerosol spectrum to a marine aerosol spectrum is synonymous to the introduction of aerosol particles of large size. The impact of such change in the initial spectrum of aerosol is much felt in terms of dynamic and microphysical responses of the cloud.

From the dynamic standpoint, there is a reduction of the spatial-temporal coverage of the maximum of the updrafts and a strengthening of the subsidence especially in the lower levels associated with more intense rainfall. The cloud is then composed, in the higher altitudes, by non-precipitating ice particles. In a microphysics point of view, there is an early starting of the process of precipitation (10 minutes earlier) and at lower altitudes (2600m below). Precipitation reaching the ground is more important and more intense.

6. Acknowledgements

Our thanks go to Laboratory of Particles Exchange at the Interfaces (LEPI), University of Toulon for their kind invitation to attend the coastal marine aerosols measurement campaign MIRAMAR and to the Laboratory of Physical Meteorology, University of Blaise Pascal in Clermont Ferrand for their guidance and authorization to use the model EXMIX.

7. References

MASCLET, P., and CACHIER, H., 1998. *L'aérosol atmosphérique: Caractéristiques physico-chimiques.* Anal. mag., 1998, 26, N°9.

PIAZZOLA, J., FORGET, P., and DESPIAU, S., 2002: *A Sea spray generation function for fetch-limited conditions.* Anal. Geophys.,20, 121–131.

LEROY D., WOBROCK W., and FLOSSMANN A. I., 2007: *On the influence of the treatment of aerosol particles in different bin microphysical models: a comparison between two different schemes*. Atmos. Res., 85: pp 269-287.

"The Tenth WMO Scientific Conference on Weather Modification"
Bali, Indonesia, 4 – 7 October 2011

Zawiah Mohd.Taib

"Weather Modification in Malaysia "
Malaysian Meteorological Department, Malaysia

Abstract

Cloud seeding is an important weather modification aspect. In Malaysia cloud seeding operation is carried out to enhance the rainfall over the catchments area so as to improve the water shortage situation. Usually it is carried out during the intermonsoon period whereby the atmosphere is conducive for the formation of moderate cumulus clouds. Another purpose of cloud seeding operations in Malaysia is to create rain to reduce the haze and forest fire problem especially under prolonged dry conditions during the Southwest monsoon. In Malaysia, only warm cloud seeding operations are carried out and these activities have been carried out for more than 30 years.

Several techniques have been tried for cloud seeding over the world but the effectiveness of the technique depends on the types of cloud and atmospheric conditions. Currently, there are 2 techniques being used by the Malaysian Meteorological Department (MMD). The first technique is the spraying of tiny droplets of salt solution into suitable clouds under the right conditions to improve the efficiency of rain formation process in the cloud. The operation involves the use of an aircraft equipped with a spraying system. This technique is carried out with the assistance of Royal Malaysian Air Force's C-130 H aircraft and normally used whenever the country experiences moderate/severe haze during the dry season. Another technique used is called the pyrotechnic hygroscopic flare. Pyrotechnic hygroscopic flare is a combustion technique used in cloud seeding operation by introducing hygroscopic salts into the cloud. This technique is carried out either by using the Mi-17 helicopter equipped with a flare rack or a rental aircraft with a fixed wings system. Both techniques are currently and widely used by other countries such as Thailand and Indonesia.

The cloud seeding activities in Malaysia are mainly operational in nature. The high variability of precipitation, both temporally and spatially in tropical countries, has made evaluation difficult. Preliminary indirect evaluation in Malaysia, using the statistical methods, has in fact indicated that cloud seeding is able to increase the rainfall over the target areas. Recently, MMD has acquired a mobile radar for the monitoring of weather and atmospheric conditions as well as to evaluate the effectiveness of cloud seeding operation in Malaysia. Hopefully with this new mobile radar unit, research in cloud physics as well as cloud seeding techniques can be carried out in order to increase the knowledge in warm cloud seeding, which in turn could further improve the cloud seeding technique in Malaysia.

Currently, in Malaysia, cloud seeding is still being carried out on a request basis to augment water resources so as to charge up water storages of dams and to initiate rain and provide temporary relief whenever the country experiences moderate/severe haze and forest fire during the period of dry season.

A Numerical Study of Macro and Micro Structures of Stratus Precipitation Cloud in Spring of Shanxi Province

Peiren Li [(1)], Junxia Li [(1)], Lijun Jin [(1)], Dongdong Shen [(1)], Gang Ren [(1)]

(1)Weather Modification Office of Shanxi Province , Taiyuan ,China, 030032, lpr640221@163.com

1 Introduction

The CAMS mesoscale cloud model was introduced and Started for business operation in 2009 of Shanxi Province, China. The main products of the CAMS mesoscale cloud model include temperature, wind field, height field, water vapor field and the horizontal and vertical distribution of different kinds of cloud particles. For ice crystals, the model can give the ice crystals number concentration at a certain height, and for other hydrometerors, the model can give the ratio water content. The model use T213 forecast data as initial data, and the resolution is 10km.

This article chose a spring stratus cloud precipitation process on May 16th~17th, 2010, in Shanxi Province as an example for analysis using the output data from the CAMS mesoscale cloud model. We focused on the macro and micro Structures of the stratus cloud, especially the vertical physical structures of the stratus cloud and the precipitation. And finally, we summed up the macro and micro structure features of this stratus cloud and precipitation in spring.

2 Ground accumulated precipitation (From 8:00 am on 16th to 8:00am on 17th, May,2010)

Most areas of Shanxi province had significant precipitation on May 16th~17th, 2010. Most cities and counties had the rainfall of 0.1~25 mm in 24 hours. The maximum precipitation occurred in Jiexiu County, and the 24 hours accumulated precipitation was up to 60 mm.

Figure 1 is the 24 hours accumulated precipitation forecast graph and the graph of real accumulated precipitation on May 16th~17th.(The left is the numerical forcast product, and the right one is the real situation) Contrasting the precipitation range and intensity of the forecast with the real precipitation accumulation on that day we can see that both are coincided better. Strong precipitation appeared in the central and southeast areas of Shanxi Province

3 Numerical simulation analysis

3.1 The horizontal distribution characteristics of the stratus cloud

(1) The distribution of the vertical integrated cloud water from 16:00pm on May 16th to 08:00am on May 17th (Fig.2). We can see from fig.2 that the big range of stratus clouds moved to Shanxi province from the west to the east. The most areas of Shanxi province had been covered with stratus clouds gradually at the time to 8:00am,17th.The areas with rich cloud water were located in the central and southern, especially in the southeast of the province.

(2) The distribution of supercooled cloud water at 500hpa height.(Fig.3 is the cloud water distribution at 500hpa at 18:00pm on 16th and 8:00am on 17th.The shadow is the ratio water content of the cloud (g/kg), the red lines are temperature isolines). From fig.3 we can see, the temperature was about -10℃ at 500hpa.The distribution of the supercooled cloud was uneven. The cloud water became riched from 18:00pm on 16th, and the areas with rich supercooled cloud water mainly located in the south and central part of the north of the Province. The ratio content of the supercooled cloud water was about 0.1~0.7g/kg.

(3)The distribution of ice crystals at 500hpa.(Fig.4 is the number concentration distribution of ice crystals at 500hpa at 18:00pm and 21:00pm on May 16th. And the shadow is the number concentration distribution of ice crystals).Fig.4 showed that there had a small amount of Ice crystals distributed unevenly at 500hpa height. Combined with fig.3 we can see that the supercooled cloud water content was relatively rich and the ice crystals concentration was relatively lower. This type of cloud structures were with better potential of artificial precipitation.

3.2 The vertical structure and temperature characteristics of the clouds

Numerical simulation results showed that the height of the clouds with rich supercooled water was commonly above 700hpa. The thickness of the supercooled cloud water layer was about 4000 meters, and the temperature of the layer was about 0℃～-20 ℃. The ratio water content of the layer was about 0.4g/kg～0.7g/kg. There had a small amount of ice crystals distributed unevenly above 500hpa height. The 0℃ layer was at 600hpa, and the snow(or supercooled water)was very rich above the 0℃ layer. There was existing a strong vertical updraft airflow in the cloud, and the content of snow and ice crystal was very big in the strong updraft airflow areas. In the supercooled area, a lot of ice crystals could stretch up to the height of which temperature was below -40 ℃.The rich snow area appeared above zero layer, and the maximum snow content could reach to 0.21g/kg. Sleet appeared mainly between 750~450hpa, the maximum ratio water content of sleet could reach to 0.35~0.45g/kg. The sleet

melt to raindrops below the 0℃ layer. The rainfall appeared below 700hpa, and the intensity of the rainfall was distributed unevenly. There were a part of ice form particles involved in the precipitation.

3.3 Research of the micro physical structure of the clouds

According to the distribution of the stratus clouds and the 24hours ground accumulated precipitation in Shanxi Province from May 16th to 17th, we chose two stations of Taiyuan City and Jiexiu County to study the vertical distribution state of the different kinds of hydrometerors, and analyzed the physical structures of the hydrometerors using the numerical simulation products.

(1) Fig.5 is the numerical simulation results of vertical distribution of the hydrometerors on May 16th to 17th of Taiyuan station(qc—cloud water ， qr—raindrops，qg—sleet,qs——snow，qi—ice crystals). We can see from fig.5 that various kinds of hydrometerors were mostly concentrated between the 650hpa to 400hpa at 18:00～22:00pm on May 16th, and the amount of the hydrometerors was small. From May 17th, the hydrometerors began to increase gradually. We can see from the picture of 6:00am on May 17th, there were two or more than two maximum peaks of the cloud water distribution, which indicated that the cloud water was distributed unevenly at the time, and the cloud displayed as multi-layer, and there may have fault zones at different height of the clouds. In addition, a large amount of snow crystals of the clouds appeared above 600hpa, and the thickness of the snow layer was very deep, extended from 600hpa to nearly 200hpa, which indicated that the cold process was strong in the clouds. And, the distribution of the snow was continuous，the snow distribution of all the pictures had one maximum peak between 450hpa and 500hpa.The maximum ratio water content of snow was about 0.2-0.35g/kg. A small amount of ice crystals and sleet existed up and below the snow. Ice crystals were mainly distributed above 350hpa height, and the content of ice crystals was very few from the graph. From 12:00am on 17th, the sleet increased gradually under 400hpa height, and reached to the maximum peak at 600hpa.Obviously, a small amount of ice particles were involved in the precipitation. The rain appeared from 550hpa and increased downward gradually, and the maximum content of rain appeared at 850hpa.

Analyzed the disposition of the water content of rain, cloud water and various kinds of ice particles, we could get the conclusion that the cold process was stronger in the cloud, and there were also existed part of the warm cloud process. It showed that a distinct "Seeder-feeder" process was existing during the ice and snow particles dropping from the top to the down in the cloud. In the high-level, the content of cloud water was higher, and the cloud water provided superior "supply" as a good growth conditions for the ice, snow particles seeding from the top. At the same time, we can see at the bottom of the cloud water area, there were a large amount of rain with a small amount of sleet coexistence. The rain water content was larger, and rainfall had appeared on the ground.

(2)The maximum accumulated precipitation of 24 hours appeared in Jiexiu station that day. Fig.6 is the numerical simulation results of vertical distribution of the hydrometerors from May 16th to 17th of Jiexiu station.

From fig.6 we can see that a small amount of ice crystals appeared above 500hpa, and the maximum content was about 0.005g/kg. A lot of the cloud water mainly distributed above 850hpa, and the content was very rich, the deep cloud water layer with too much cold cloud water extended upward to about 400hpa height. The distribution of cloud water content was uneven. there are two or two more peaks, and the maximum water content was up to 0.7g/kg. Two more peaks in vertical showed that there may have fault zones at different height of the clouds. The snow appeared from 600hpa and the content was large. The deep snow layer extended to the higher altitude, which indicated that the cold cloud process was very strong, and the rainfall was mainly composed of the cold cloud precipitation. The distribution of snow was continuous, and the peak located at about 400-500hpa, the maximum content was about 0.35g/kg. And the peak of the cloud water content was at 650-700hpa height. So, the snow peak height was higher than the height of cloud water peak. Sleet appeared below 450hpa and increased downward obviously. The peak of sleet content was at about 600-550hpa, and the maximum content was more than 0.15g/kg. The sleet decreased to the minimum below 850hpa. The rain began to appear from 550hpa and increased downward to the ground. The precipitation accumulation was very big, which was benefit from the large amount of hydrometerors resources, and a lot of ice form particles were also involved in the rainfall. From 11:00am on 17th, all of the ice, snow, sleet and ice particles already began to decrease, and the cloud water was still rich. Later from 13:00pm, the hydrometerors gradually decreased. From the pictures of 13:00pm and 14:00pm, except for a small amount of cloud water there was no other hydrometerors existing. And the distribution of cloud water was extremely uncontinuous. There were no rain and sleet, and the precipitation tended to stop, and later, nearly all hydrometerors were gradually disappeared.

According to the distribution condition of hydrometerors in Jiexiu station, the precipitation mainly composed of cold cloud precipitation process. From the high and low level structure of snow and cloud water, the snow melt to supercooled cloud water during the process of falling down. So, the cloud water content was increased, and the height of snow content peak was higher than the height of cloud water content peak. Sleet was transformed from snow, and grown up through the process of collision and

freezing with supercooled cloud droplets. The rain still mainly came from the conversion of the melting process of ice, snow, sleet etc. from high altitude, and partly from the cloud water transformation.

4 Conclusion

(1) The rainfall on May 16th to 17th ,2010, in Shanxi Province was mainly came from cold stratus cloud precipitation. The cloud contained a lot of supercooled water, and the thickness of the rich supercooled water layer was about 4000～6000 meters. The temperature of the supercooled layer was about 0～-20℃, and the ratio content of the supercooled cloud water was about 0.4 ～ 0.7g/kg, within some ice crystals distributed unevenly.

(2) The structures of the stratus precipitation cloud can be roughly divided into three layers. The first layer(upper layer)was mainly composed of ice crystals and a little snow, and the snow, sleet, and supercooled cloud water were mixed in the second layer(middle layer), and the third layer(lower layer)was mainly of liquid raindrops.

(3) In the early period of the cloud development, the boundary of the first layer and the second layer was located at 350～550hpa height. The second layer was mainly composed of the deep and large amount of snow, and mixed with a little sleet. Along with the growth of the snow and sleet melting and landing, the raindrops in the third layer(warm layer)were led to increase gradually. And in the later stages of the precipitation, snow and sleet content of the second layer decreased, and the water supply from the cold cloud was not as enough as early, and the clouds gradually appeared stratified. So, the precipitation weakened gradually and stopped finally. The sleet came from the transformation of the deep snow layer according to the vertical distribution of rain, cloud water, snow and sleet. The large amount of ground rainfall mainly came from the melting of snow, sleet, and some ice particles of the second layer, and part of the precipitation was from the cloud water transformation. Of the whole rainfall process, the supercooled cloud water, snow and sleet in the second(middle) layer gave the largest contribution to the precipitation

References

Bennetts, D. A., and F. Rawlins, Parameterization of the ice phase in a model of midlatitude cumulonimbus convection and its influence on the simulation of cloud development. *Quart. J. Roy. Meteor. Soc.*, **107**, 477-502. 1981.

Lord, S. J., and J. M. Lord, Vertical velocity structure in an axisymmetric, nonhydrostatic tropical cyclone model. *J. Atmos. Sci.*, **45**, 1453-1461. 1988.

Mcfarquhar G. M., Black R. A., Observations of particle size and phase in tropical cyclones: implications for mesoscale modeling of microphysical process. J. Atmos. Sci., 61: 422-439. 2004.

Van Den Heever, Cotton, W.R., The impact of hail size on simulated supercell storms. J. Atmos. Sci. 61: 1596-1609. 2004.

Gilmore, M.S., Straka, J.M., Rasmussen, E.N., Precipitation and evolution sensitivity in simulated deep convective storms: comparisons between liquid-Only and simple ice and liquid phase microphysics. *J. Mon. wea. Rev.*, **132**,1897-1916. 2004.

Mcfarquhar, G.M., Henian Zhang, Gerald Heymsfield, Robbie Hood, Jimy Dudhia, Halverson, J.B., and Frank Marks JR., Factors affecting the evolution of Hurricane Erin (2001) and the distributions of hydrometeors: role of microphysical processes. *J. Atmos. Sci.* **127**:127-150. 2006.

Locatelli, J. D., and P. V. Hobbs, Fall speeds and masses of solid precipitation particles. *J. Geophys. Res.*, **79**, 2185-2197. 1974.

Mitchell,D. L., Use of mass- and area-dimensional power laws for determining precipitation particle terminal velocities. *J. Atmos. Sci.,* **53**, 1561-1580. 1996.

Khvorostyanov, V. I., and J. A. Curry, Terminal velocities of droplets and crystals: Power laws with continuous parameters over the size spectrum. *J. Atmos. Sci.*, **59**, 1872-1884. 2002.

Figuers

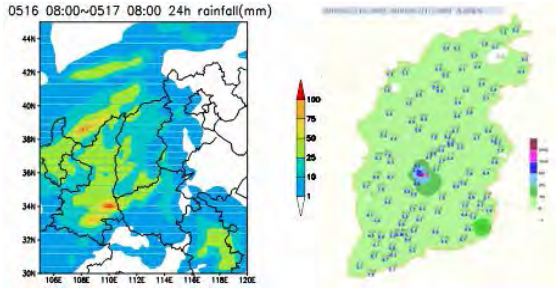


Fig.1 The 24 hours accumulated precipitation forecast graph and the graph of real accumulated precipitation on May 16th~17th.

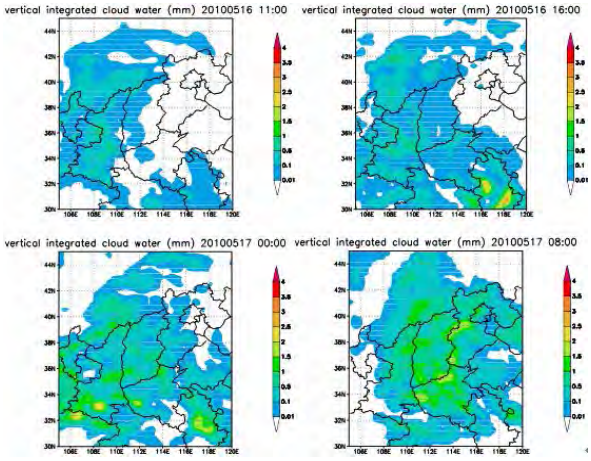


Fig.2 Distribution of the vertical integrated cloud water from 16:00pm on May 16th to 08:00am on May 17th.

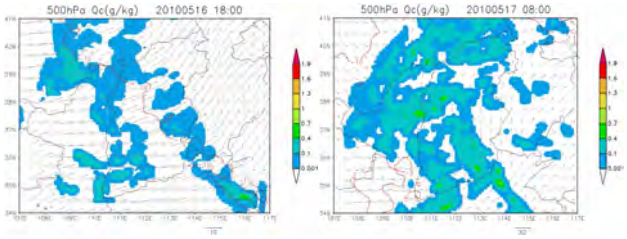


Fig.3 The cloud water distribution at 500hpa at 18:00pm on 16th and 8:00am on 17th .

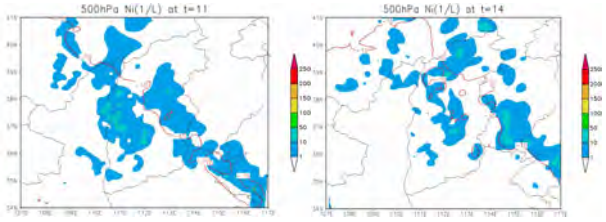


Fig.4 The number concentration distribution of ice crystals at 500hpa at 18:00pm and 21:00pm on May 16th.

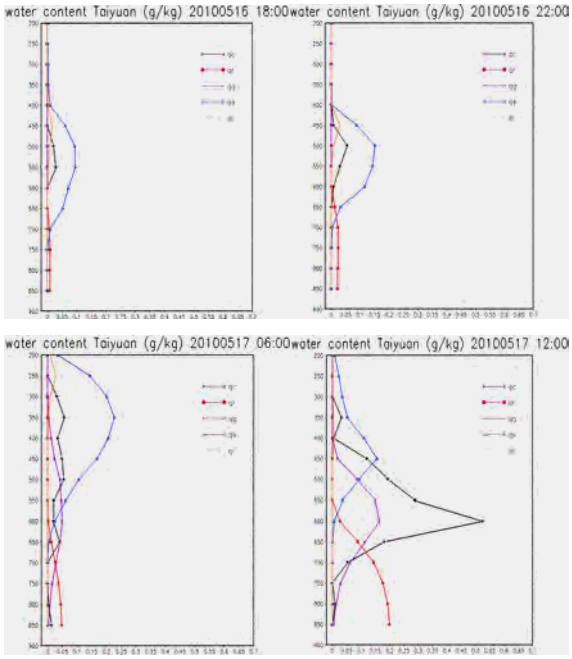
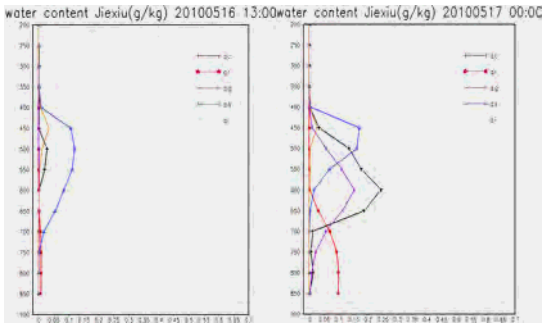


Fig.5 The numerical simulation results of vertical distribution of the hydrometerors on May 16th to 17th of Taiyuan station.



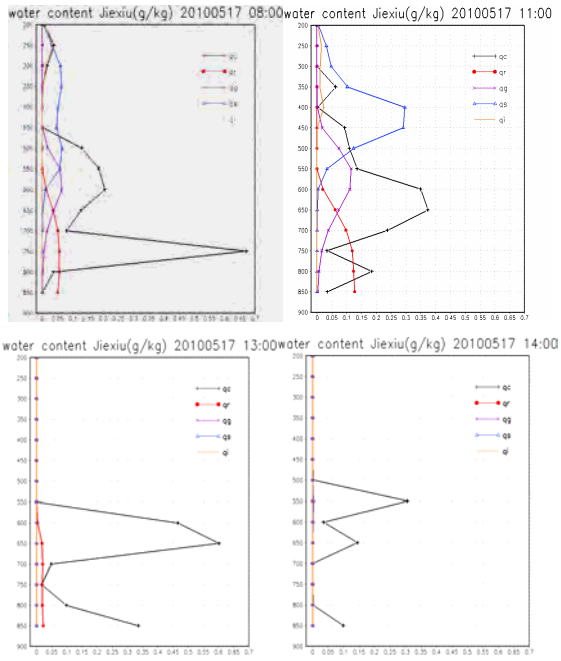


Fig.6 The numerical simulation results of vertical distribution of the hydrometerors from May 16th to 17th of Jiexiu station.

Numerical Seeding Experiments on Stratiform Clouds in Spring in North China

SHI Yueqin
Chinese Academy of Meteorological Sciences(CAMS), Beijing, China, 100081
E-mail: shiyq@cams.cma.gov.cn

1. Introduction

Droughts always appear in North China, which has influenced local agriculture and industry produce. Nowadays, a great number of rainfall enhancements have been carried out in North China, and gained economic and social benefit. In 2005, WMO pointed out that it is urgent that using cloud model investigates optimal seeding method about different cloud type (WMO, 2005).

In this paper, using NCEP reanalysis data and mesoscale model MM5 coupled with CAMS microphysical scheme (LOU, 2002), a case of stratiform clouds precipitation during Apr. 30th and May 1st, 2009 in North China is studied. Based on the reasonable simulation of natural precipitation, numerical experiments of adding ice crystals are conducted to study if there is any possibility to increase the stratiform rainfall.

2. Weather situation and model design

Caused by western trough, the natural precipitation mainly occurred on Apr. 30th night at Zhangjiakou area.

Model center is at (39ºN, 113ºE), three nested domain is used, 27km, 9km and 3km. Vertical layer is 23. Grell cumulus scheme, Blackadar planetary boundary layer scheme, and CAMS explicit moisture scheme are used. The model run begins at 00 UTC, 30th April, 2009, and lasts 36 hours.

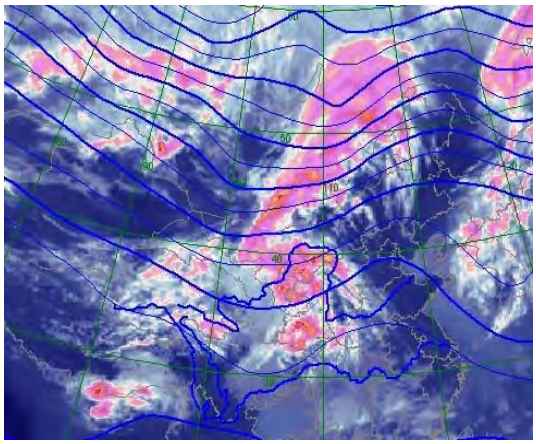


Fig. 1 cloud image and 500hPa height at 1200 UTC, 30th April, 2009

3. Precipitation variation after seeding

Orville (Orville, 1996) concluded that there are three seeding methods about using cloud model to do seeding experiments. The second one is to directly add some ice crystals in the model. This method can be used to study the basic principle of seeding. In the paper, we use this method to do some seeding experiments.

Fig 2 is the temporal evolution of total net surface rainfall increment in domain 3 in different seeding experiments. In the five experiments, we add 10^3 L^{-1} ice crystals except NO. 36 at about -9℃ layer. It shows that seeding in abundant cloud areas can increase more surface rainfall. And seeding with 10^3 L^{-1} can be more effective than 10^2 L^{-1}.

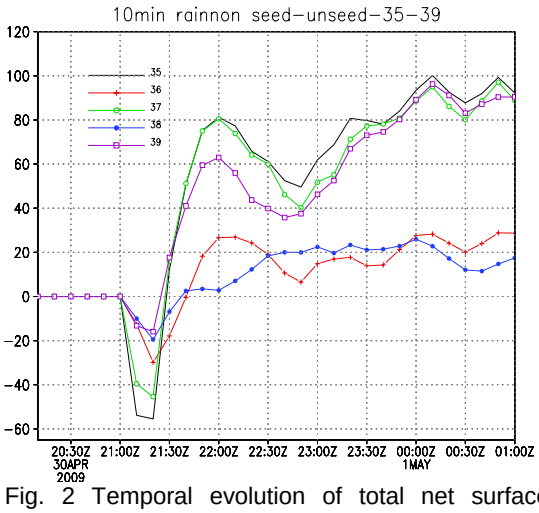


Fig. 2 Temporal evolution of total net surface rainfall increment in different seeding experiments

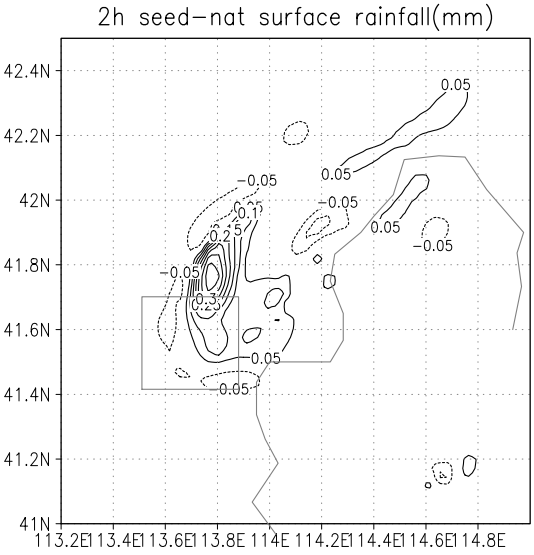


Fig. 3 Net surface rainfall increment (mm) after seeding 120 min. square is seeding area of No.39.

Fig. 3 shows that after seeding 120 min, rainfall increasing areas mainly appear at downwind 20km×30km

scope. The maximum increasing rainfall reaches 0.3mm. Meanwhile, seeding changes rainfall distribution at further scope.

In fact, if an artillery contains 30 g AgI, nucleation ratio is 10^{15}/g, seeding area is 30km × 30km, using 30 artilleries can gain 10^3 L^{-1} in seeding area. It is practical.

4. Analysis of seeding micro-physical mechanics

The source terms of raindrops includes graupel melting into raindrops (Mgr), snow melting into raindrops (Msr), raindrops collecting cloud droplets (Ccr) and cloud droplets auto-conversion to raindrops (Acr). In Fig. 4, in natural cloud, the process of graupels melting into raindrops is the dominant source process of raindrops (Mgr-n). Because of scarce of cloud water in lower layer, raindrops can't grow through collecting cloud water. After seeding, because the source process of graupel decreasing, the melting process of graupel (Mgr-s) disappear. Snow melting into raindrops is the main source process of raindrops after seeding (Msr-s). In convective cloud seeding experiments, graupel melting into raindrops and raindrops collecting cloud droplets are the main source processes of raindrops increasing (SHI et al., 2008).

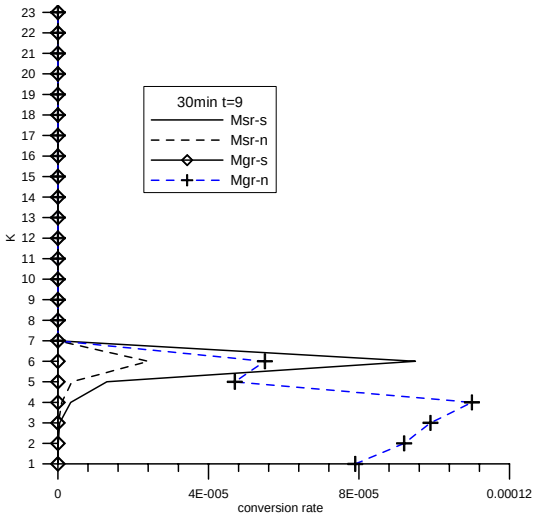


Fig. 4 conversion rate of source terms of rain drops after seeding 30 min at rainfall increasing centre

5. Conclusions

The main conclusions are the following:

The natural precipitation mainly occurred on Apr. 30th night. The simulated occurring time, location and magnitude of precipitation are consistent with observation. But the range of surface rainfall is a little larger than the observation. In the natural clouds, cloud water mainly lies during 0～-12℃ layer. There is no supercooled rain water and little graupel. Ice crystals and snow lie in upper layer, and the mass content of snow is great.

Several tests for different seeding agent dosage, different areas and different temperature are designed. Results show that after seeding 20 minutes surface rainfall start to increase, after seeding 60 minutes the Net Increase Rainfall (NIR) reach a peak, then after 110 minutes NIR decrease a minimum, which is consistent with the results of seeding cold frontal dynamical precipitation (SHI et al., 2008).

Results show that seeding in the area with plentiful supercooled cloud water, less number concentration of ice crystals and updrafts results in the most enhancement of rainfall. The seeding effects with 10^3 L^{-1} artificial ice crystals is better than 10^2 L^{-1} and 10^1 L^{-1}. Continuous seeding effect is better than that of single seeding. Because there is a dry layer in the natural clouds, seeding effects at -9℃ layer is better than seeding at -12℃.

When adding artificial ice crystals, the conversion of ice to snow is increased. Snow grows mainly through the collection of ice and sublimation, which consumes water vapor and supercooled cloud water. Because there is less cloud water, snow can't grow through riming supercooled cloud water. In finally, the melting of snow cause the surface rainfall increasing. The release of a large quantity of sublimation latent heat increases the temperature in cloud, strengthens the updrafts, which indicates that "static seeding" and "dynamic seeding" are correlative each other.

References

Lou Xiaofeng. Development and implementation of a new explicit microphysical scheme and comparisons of original schemes of MM5. Ph.D. dissertation (in Chinese), Peking University, 2002

Orville H D. A review of cloud modeling in weather modification. *Bull. Amer. Meteor. Soc.*, **77**, 1535-1555, 1996.

Shi Yueqin, Lou Xiaofeng, Deng Xuejiao, et al. Seeding numerical experiments of cold front clouds in South China. *Chinese Journal of Atmospheric Sciences* (in Chinese), **32**, 1256-1275, 2008.

World Meteorological Organization. Program on physics and chemistry of clouds and weather modification research. WMP REPORT SERIES, WMO/TD-1294, Geneva, 2005, 7

Recent Progress in Glaciogenic Cloud Seeding over Southeast Australia and Tasmania

Steven T. Siems and Michael J. Manton

Monash University, Melbourne, Australia

1. Introduction

From the 1950s through the 1980s, Australia was at the forefront of cloud seeding research, primarily through the Commonwealth Science and Industrial Research Organisation (CSIRO). Over this time, major field campaigns to test glaciogenic seeding methods were undertaken in the states of New South Wales, South Australia, Tasmania and Victoria. The majority of these campaigns ultimately failed to clearly demonstrate a significant positive effect when employing a double ratio analysis. A more complete history of these early efforts can be found in Ryan and King (1997). Ultimately cloud seeding research within Australia was abandoned by the CSIRO in the 1980s.

Of these field campaigns, there were two notable exceptions: the Snowy Mountains in New South Wales and the central plateau of Tasmania. The seeding trials over the Snowy Mountains (1955-1959) reported 19% increase at the 5% significance level (Smith et al., 1963) In Tasmania the first seeding experiment (1964-1971) reported increases of up to 30% at the 3% significance level at times in the Autumn. A second Tasmanian campaign (1979-1983) reported increases of 37% (Ryan and King, 1997). On the basis of these research programs operational cloud seeding has been undertaken over central Tasmania for much of the past 20 years. A field campaign over the alpine region in Victoria was abandoned before completion. While no significant results were recorded for the target region, a statistically significant increase in precipitation was observed within the buffer region (Ryan and King, 1997).

The southeast region of Australia experienced a prolonged drought from 1997-2009, which has led to considerable interest in these historical cloud seeding experiments including a new glaciogenic cloud seeding experiment in the Snowy Mountains (Manton et al., 2011).

A review of the recent progress made in understanding glaciogenic cloud seeding is presented starting with an analysis of historical cloud seeding records over Tasmania. The positive findings for the Snowy Precipitation Enhancement Research Project (SPERP) are summarised. Consistent with the earlier field work, this experiment has found a positive (14%) increase in precipitation during seeded events at the 3% confidence level, when poorly targeted events are removed. Finally the natural environment over this region is explored through in-situ field observations and satellite observations. In comparison to the Western U.S., high concentrations of supercooled liquid water are commonly present, suggesting that the apparent success in this region can be directly linked to superior cloud seeding conditions.

2. Analysis of Historical Record over Tasmania

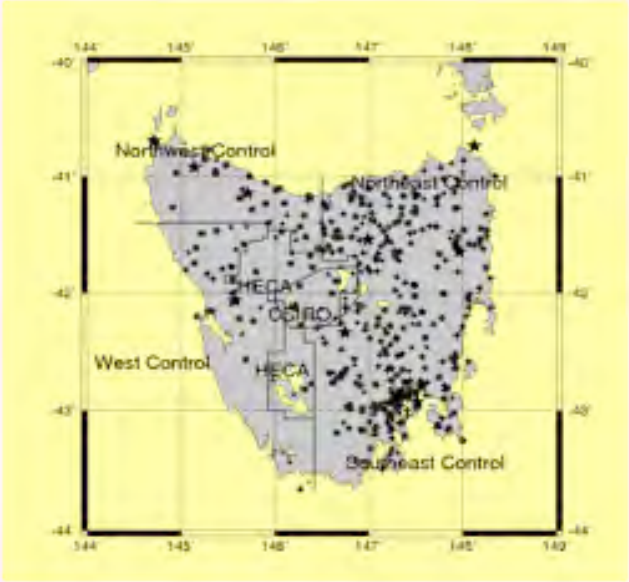


Figure 1. From Morrison et al. (2009) Map of Tasmania highlighting the locations of sites for the period 1960–2005.

In Morrison et al (2009) an analysis of the cloud seeding activity for the period 1960–2005 over a hydroelectric catchment area located in central Tasmania, Australia, is presented (Figure 1.)

The analysis is performed using a double ratio on monthly area-averaged rainfall for the months of May–October. Results indicate that increases in monthly precipitation are observed within the target area relative to nearby controls

during periods of cloud seeding activity. Ten independent tests were performed and all double ratios found are above unity with values that range from 5% to 14%. Nine out of 10 confidence intervals are entirely above unity and overlap in the range of 6%–11%. Nine tests obtain levels of significance better than 0.05 level (Figure 2.)

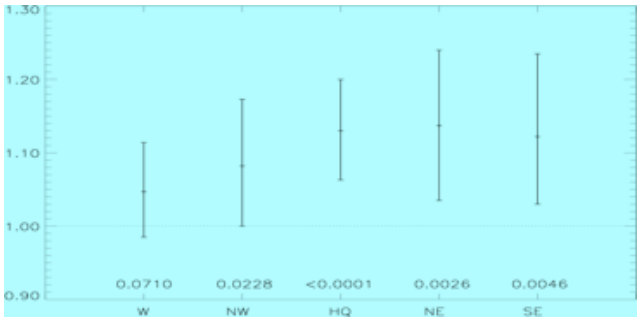


Figure 2. From Morrison et al. (2009.) Double ratios and confidence intervals for the CSIRO targets vs the W, NW, HQ, NE, and SE controls. The bootstrap probabilities for obtaining a double ratio higher than the actual are shown above the horizontal axis.

3. The Snowy Precipitation Cloud Seeding Experiment

In Manton et al. (2011) a description of the Snowy Precipitation Enhancement Research Project (SPERP) is given. SPERP was undertaken from May 2005 to June 2009 in the Snowy Mountains of southeastern Australia with the aim of enhancing snowfall in westerly flows associated with winter cold fronts. Building on earlier field studies in the region, SPERP was developed as a confirmatory experiment of glaciogenic static seeding using a silver chloride material dispersed from ground-based generators. Seeding of five-hour experimental units (EUs) was randomised with a seeding ratio of 2:1. A total of 107 EUs were undertaken at suitable times, based on surface and upper-air observations. Indium (III) oxide was released during all EUs for comparison of indium and silver concentrations in snow in seeded and unseeded EUs to test the targeting of seeding material. A network of gauges was deployed at 44 sites across the region to detect whether precipitation was enhanced in a fixed target area of 832 km2, using observations from a fixed control area to estimate the natural precipitation in the target. Additional measurements included integrated supercooled liquid water at a site in the target area and upper-air data from a site upwind of the target.

In Manton and Warren (2011) a further analysis of the SPERP experiment shows that a substantial source of uncertainty in the estimation of the impact of seeding on precipitation is associated with EUs where the seeding generators operated for relatively few hours. When the analysis is repeated using only EUs with more than 45 generator hours, the increase in precipitation in the primary target area is 14% at the 8% significance level. When applying that analysis to the overall target area, the precipitation increase is 14% at the 3% significance level.

A secondary analysis of the ratio of silver to indium in snow supports the hypothesis that seeding material affected the cloud microphysics. Other secondary analyses reveal that seeding impacted on virtually all the physical variables examined in a manner consistent with the seeding hypothesis.

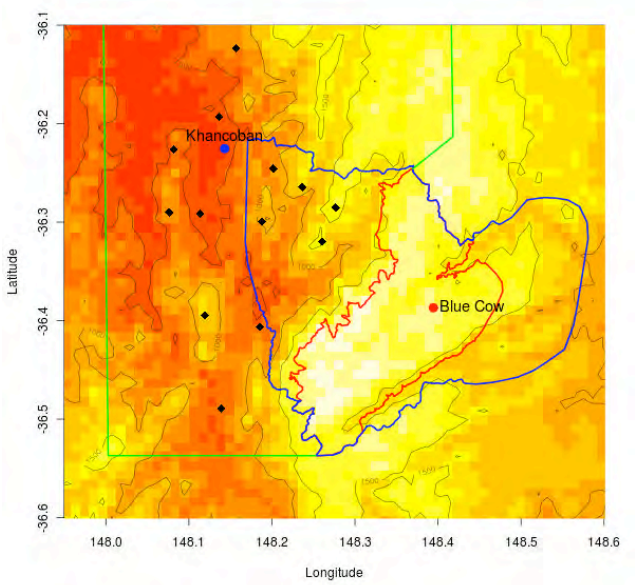


Figure 3. From Manton et al. (2011) Map of Snowy Mountains showing generator sites (black triangles) against the orography, with contours at 500, 1000 and 1500 m; red line shows primary target, blue shows overall target, and green shows control area.

4. In-situ Observations of Supercooled Liquid Water

Tasmania

In Morrison et al. (2010) the cloud structure associated with two frontal passages over the Southern Ocean and Tasmania is investigated. The first event, during August 2006, is characterized by large quantities of supercooled liquid water and little ice. The second case, during October 2007, is more mixed phase.

The evaluated cases are then used to

numerically investigate the prevalence of supercooled and mixed-phase clouds over Tasmania and the ocean to the west with the Weather Research Forecasting (WRF) code. The simulations produce marine stratocumulus-like clouds with maximum heights of between 3 and 5 km. These are capped by weak temperature and strong moisture inversions. When the inversion is at temperatures warmer than 2108C, WRF produces widespread supercooled cloud fields with little glaciation. This is consistent with the limited in situ observations. When the inversion is at higher altitudes, allowing cooler cloud tops, glaciated (and to a lesser extent mixed phase) clouds are more common. The simulations are further explored to evaluate any orographic signature within the cloud structure over Tasmania. No consistent signature is found between the two cases.

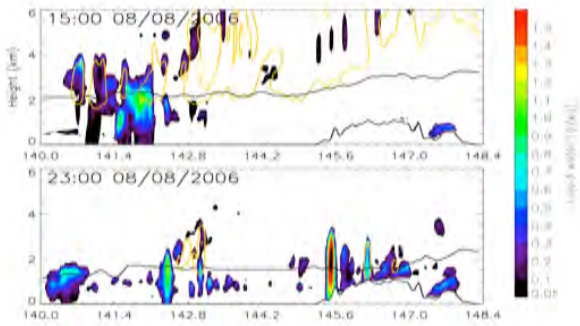


Figure 4. From Morrison et al. (2010). WRF simulations of water and ice to the west of Tasmania (along 42° S). The freezing level is noted to identify regions of supercooled liquid water.

Southeast Australia

Chubb et al. (2011) analysed data from a precipitation gauge network in the Snowy Mountains of South-Eastern Australia to produced a new climatology of wintertime precipitation and airmass history for the region in the period 1990-2009. Precipitation amounts on the western slopes and in the high elevations (> 1000 m) of the Snowy Mountains region experienced a decline in precipitation in excess of the general decline in South-Eastern Australia. The contrast in the decline east and west of the ranges suggests that factors influencing orographic precipitation are of particular importance.

Next a comprehensive discussion of two typical wintertime storms in the Brindabella Ranges of the Australian Capital Territory is considered. Surface observations from automatic weather stations operated by the Australian Bureau of Meteorology, as well as rain gauge data from an independent network, are used to characterise precipitation during these storms. Dual-channel microwave radiometer retrievals provide column-integrated liquid water and water vapour amounts at a mountain-top location, which are compared with MODIS level 2 cloud product data. High resolution numerical simulations are performed with the Weather Research and Forecasting (WRF) model to enhance the interpretation of the observations. The WRF model configuration used is found to be well suited to simulation of wintertime storms in the mountainous Brindabella region. The large-scale dynamics are shown to be well represented, and cloud column-integrated diagnostics compare well with the observed values except during the strongly dynamic frontal passage of the first case. Surface precipitation comparisons are also favourable.

Despite clear dynamical differences between the two storms selected for analysis, the two storms show similarities in the post-frontal conditions. The alpine regions of the Brindabella Ranges experience shallow, supercooled liquid clouds and showery conditions for 12–18 hours following the frontal passage. Numerical simulations suggest that substantial, widespread precipitation is received during this period in elevated

5. Satellite Climatology and Discussion

Morrison et al. (2011) used MODIS satellite imagery to produce a 3-yr climatology of cloud-top phase over a section of the Southern Ocean (south of Australia) and the North Pacific Ocean. The intent is to highlight the extensive presence of supercooled liquid water over the Southern Ocean region, particularly during summer. The phase of such clouds directly affects the absorbed shortwave radiation, which has recently been found to be ‘‘poorly simulated in both state-of-theart reanalysis and coupled global climate models’’ (Trenberth and Fasullo, 2010).

The climatology finds that supercooled liquid water is present year-round in the low-altitude clouds across this section of the Southern Ocean (Figure 5.) Further, the MODIS cloud phase algorithm identifies very few glaciated cloud tops at temperatures above -20°C, rather inferring a large portion of ‘‘uncertain’’ cloud tops. Between 50° and 60°S during the summer, the albedo effect is

compounded by a seasonal reduction in high-level cirrus. This is in direct contrast to the Bering Sea and Gulf of Alaska. Here MODIS finds a higher likelihood of observing warm liquid water clouds during summer and a reduction in the relative frequency of cloud tops within the 0° to -20°C temperature range.

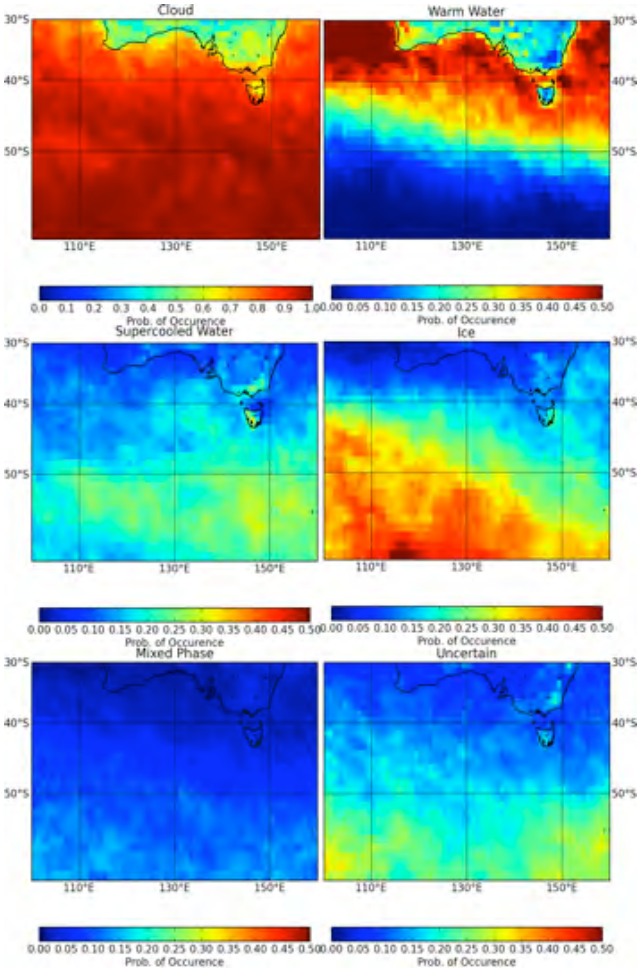


Figure 5. From Morrison et al. (2011). The 3-yr MODIS climatology of thermodynamic phase for the winter months (Jun, July & August.)

This climatology can be further focussed to the cloud seeding regions of Southeast Australia (Figure 6), which reveals peak concentrations in supercooled liquid water along the Australian Great Dividing Range up to the Snowy Mountains. Similar images for cloud seeding regions in the Western U.S. (e.g. the Sierra-Nevada region) find that the conditions for glaciogenic cloud seeding a vastly superior for Tasmania and Southeast Australia.

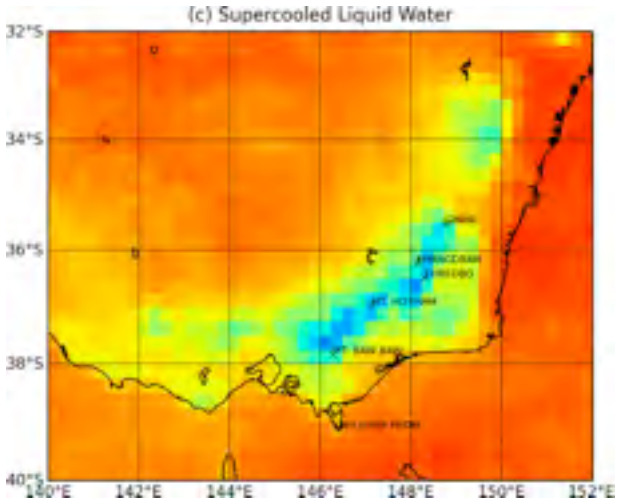


Figure 6. A 5-yr MODIS climatology of supercooled liquid water for the winter months (Jun, July & August.) The scaling is the same as in Figure 5.

References

Chubb, T.H., S.T. Siems and M.J. Manton, 2011: On the decline of wintertime precipitation in the Snowy Mountains of South-Eastern Australia. *J. Hydrometeor.* (in press.)

Manton, M.J., L. Warren, S.L. Kenyon, A.D. Peace, S.P. Bilish and K. Kemsley, 2011: A Confirmatory Snowfall Enhancement Project in the Snowy Mountains of Australia – Part 1: Project Design and Response Variables. *J. Appl. Meteor. Clim.*, (in press).

Manton, M.J. and L. Warren, 2011: A Confirmatory Snowfall Enhancement Project in the Snowy Mountains of Australia – Part 2: Primary and Associated Analyses. *J. Appl. Meteor. Clim.*, (in press.)

Morrison, A.E., S.T. Siems and M.J. Manton, 2011: A Cloud-top Phase Climatology of Southern Ocean Clouds. *J. Climate,* **24**, 2405-2418, DOI10.1175/2010JCLI3842.1.

Morrison, A.E., S.T. Siems, M.J. Manton, A. Nazarov, 2010: A Modelling Case Study of Mixed Phase Clouds over the Southern Ocean and Tasmania. *Monthly Wea. Rev.,* **138**, 839-862, DOI:10.1175/2009MWR3011.1.

Morrison, A.E., S.T. Siems, M.J. Manton and A. Nazarov, 2009: On the Analysis of a Cloud Seeding Data Set over Tasmania, *J. Appl. Meteor. and Clim.*, **48**, 1267-1280, doi: 10.1175/2008 JAMC2068.1.

Ryan, B.F. and W.D. King, 1997: A critical review of the Australian experience in cloud seeding. *Bull. Amer. Met. Soc.*, **78**, 239-254.

Smith, E.J., E.E. Adderley and D.T. Walsh, 1963: A cloud-seeding experiment in the Snowy Mountains, Australia. *J. Appl. Met.*, **2**, 324-332.

Smith, E.J., L. G. Veitch, D. E. Shaw, and A. J. Miller, 1979: A cloudseeding experiment in Tasmania. J. Appl. Meteor., 18, 804–815.

Strategy of seeding using the results of a modelled hailstorm splltting

Vlado Spiridonov[1], Zoran Dimitrovski[1] and Mladjen Curic[2]

[1] Republic Hydrometeorological Institute of Macedonia, Skupi bb 1000 Skopje
[2]Institute of Meteorology, University of Belgrade, Belgrade, Serbia

1. Introduction

The cloud seeding with the goal of producing rain (snow) or suppressing hail is common practice in many areas of the world. Among seeding agents silver iodide (AgI) has been the preferred seeding agent in weather modification for past fifty years. In cloud seeding operations the ground-based generators, rockets or aircrafts are used to inject the AgI particles to the appropriate region of the target cloud. In recent years the numerical models becomes the powerful tool in weather modification research. In the actual paper our primary goal is to find out the seeding zone location that lead to the highest increase in cumulative precipitation compared to unseeded case. We use the cloud-resolving mesoscale model.

Case studies are carried out in order to verify and document the value of the cloud model used in contributing to the understanding of convective storm dynamics and microphysics. Numerical cloud models have contributed substantially to our understanding of supercell storms. Much of our understanding of the sensitivity of convective storms to these environment parameters has been derived from modelling studies that tested a variety of, but often idealized, environmental conditions. A number of three-dimensional cloud models have been developed to simulate the structure, intensity and movement of convective clouds (Cotton and Tripoli, 1979; Klemp and Wilhemson, 1978; Clark, 1979; Tripoli and Cotton, 1982; Xue et. al., 2000; Curic et al., 2007). Convective-scale model or cloud resolving model can be used to obtain general characteristics of these sub-grid processes. The main objective of numerical experiments performed here is to simulate the supercell storm splitting and the proper strategy of seeding a supercell hailstorm. Accurate storm cell identification and tracking that reflect splitting and merging cells is a major challenge in this study.

2. The model

Only few basic characteristics of the model are summarized here. Details can be found Klemp and Wilhelmson (1978) regarding the hydrodynamic equations, turbulence closure and the methods of solutions. The thermodynamic energy equation is based on Orville and Kopp (1977) with effects of the snow field added. The microphysical parameterization uses the bulk a second-moment scheme for all species according to Lin et. al. (1983) and modification in respect to hail spectrum proposed by Curic and Janc (1995, 1997). A special subroutine for a treatment of silver iodide diffusion and parameterization scheme for its activation is developed and applied by Spiridonov and Curic (2006). A more detail information about the convective cloud model could be found in Telenta and Aleksic (1998) and Spiridonov and Curic (2006).

2.1 Initial conditions and initialization

The model is initialized on upper air sounding representing initial vertical profiles of meteorological data for the August 9, 2008 near Skopje, Macedonia (Fig. 1). Upper air sounding indicate unstable atmospheric conditions favorable for convection. Main characteristic of the upper air sounding is weak wind veering in the surface layer and strong wind shear at the middle and upper part of the atmosphere. Vertical profile indicates moisture deficit at 500 hPa pressure level, and increase moisture content at 700 and 300 hPa levels. While the size of the model domain was the same, configured to a 61 x 61 x 16 km^3, the resolution of the model was different. The first numerical experiment is performed with resolution 1km x 1km x 0.5km with a temporal resolution of 10 s for large time. The second run of the model was set up at finer horizontal resolution of 0.5x0.5x 0.25km^3, using a smaller time step of Δt=5s.

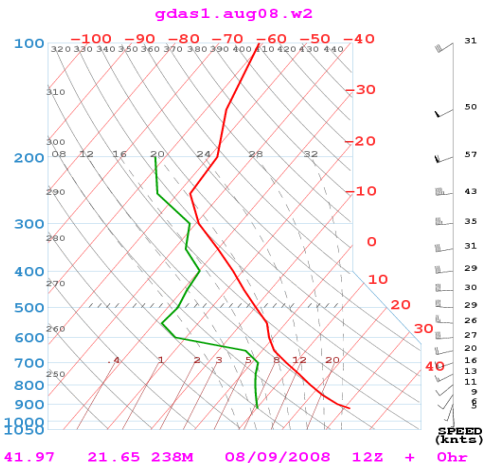


Fig.1 Upper air sounding for Skopje, Macedonia on 09 August, 2008 12 UTC taken from GDAS upper air observations provided at NCEP

3. Results

The structure and evolution of the supercell storm, observed over northern eastern part of Macedonia on 9 July 2008, is described through a combined observational radar analysis and numerical modeling study.

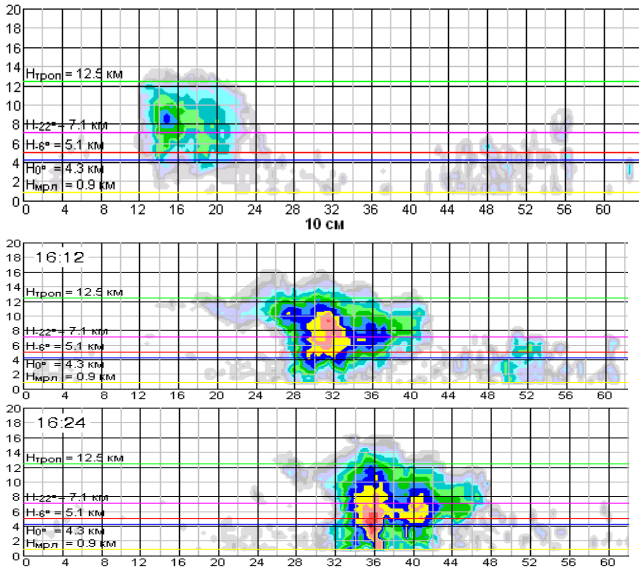


Fig 2a. Observed RHI radar echoes in 15:53, 16:12 and 16:24 local time on 9 August 2008.

3.1. Characteristic of the case study on 9 august, 2008

A severe left-moving thunderstorm occurred on 9 August 2008 in the North-East part of Macedonia along the river valley of Bregalnica. Over 2 h lifetime, the storm was responsible for reports of severe showers and hail, identified as weak tornado. The atmosphere over Macedonia on 09 August 2008 contained the necessary ingredients for the development of severe weather, namely, moisture, instability, and a lifting mechanism. It is evident from radar observations (made by upgraded WSR 74 S) that the supercell due to topography and anticyclone rotating is splitting the thunderstorm on two single cloud cells: left-moving and stationary one (Fig. 2a). By 1553 UTC, thunderstorm that was formed was producing 53-dBZ reflectivity at 10 km distance of the radar location. At 1612 UTC the super cell is splitting inside. The thunderstorm that formed along the river loop and the mountain cusp produced a left mover that traveled eastward along the initial thunderstorm's low-level outflow boundary. This long-lived left mover contained a meso anticyclone and was responsible for numerous severe weather reports. The leftward moving single cell is continuing moving forward to the east with max radar reflectivity over 50 dBz. At 1636 the convective cells are separated at a distance of 30 km from radar site. this turns counterclockwise (cyclonic) (see PPI radar observation shown on Fig. 3a). Vertical and horizontal cross sections of the modeled radar reflectivity are illustrated in Figs. 2b and 3b. Numerical simulation of supercell storm in using finer spatial and temporal resolution shows a more realistic view of the supercell storm structure, evolution and cell splitting.

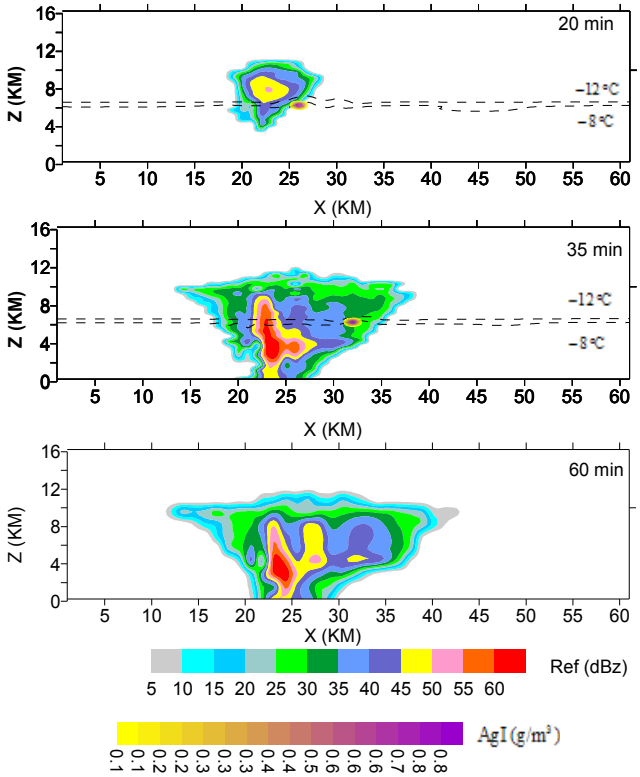


Fig. 2b Modeled vertical cross sections of reflectivity along SW to NE downstream in 35, 50 and 70 min.

It is evident that supercell storm exhibits cell splitting especially early in its lifetime. The reasons for supercell storm splitting involve concepts of fluid dynamics and treatment of sub-grid scale processes, both in the original storm and its environment. This size discrepancy remained throughout the left mover's lifetime. Still, the left mover was considerably smaller than the right mover in area extent. This size discrepancy remained throughout the left mover's lifetime. Even though this storm started small (left), it had no problem dividing itself in two cells, as the result surrounding winds that supported both leftward movers which tend to spin clockwise (anticyclonic) and rightward moving cell which turns counterclockwise (cyclonic). The reasons for supercell storm splitting involve concepts of fluid dynamics and treatment of sub-grid scale processes, both in the original storm and its environment. Both cases show approximately the same reflectivity magnitudes somewhat extensive (>60 dBz) in cloud developing stage and slight decrease and for about 10 to 15dBz in cloud mature stage.

3.2 Numerical simulation of supercell storm Seeding

We perform a set of numerical experiments of AgI seeding for hail suppression (see Tab. 1). Two different approaches are applied in a seeding strategy of such vigorous convective clouds.

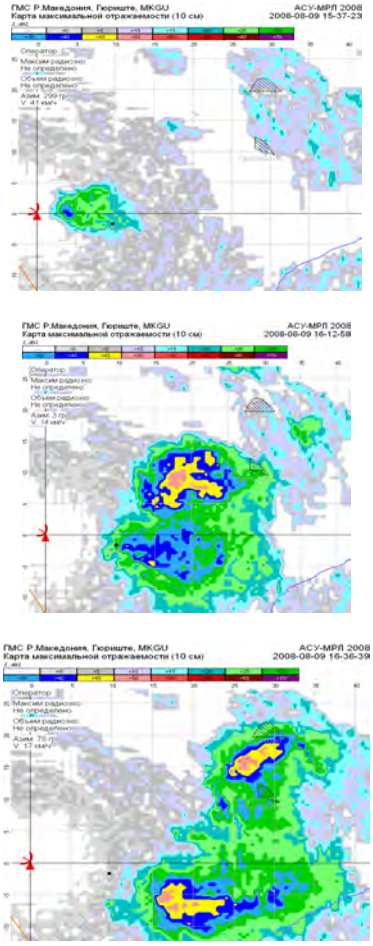


Fig 3a. Radar observation of PPI radar echoes in 15:53, 16:12 and 16:24 local time

The first model test is by AgI seeding of a single cell in cloud developing stage in supercooled frontal part of updraft portion of convective cloud, between -8 and -12 °C isotherms and 25 and 45 dBz (see upper panels in Figs. 2b and 3b). Single cell seeding of supercell storm is carried out using different initial seeding parameters in order to find a proper seeding dose and placement. In the second method the seeding zone is close to the main updraft of the left and right moving parts of the splitte hailstorm.

Table 1. Hailstorm seeding parameters

Hail suppression experiment	AgI dose rate (g/m)	Placement hor.dis. height (km, km)	Seedi time (min)	Hailfall at the ground (kg/m^2)
Non-seed.				10.60
Single-cell Seeding	0.4 0.4 0.4 0.8 0.8 1.6	19, 19, 6.25 22, 20, 6.25 27, 6.25 19, 19, 6.25 22,620, 6.75 19, 19, 6.75	15 20 25 15 20 15	10.50 10.49 10.15 10.15 10.11 10.08
Cell-split. Seeding	0.8 0.8	25, 19, 6.25 32, 36, 6.25	35 35	9.67
Operational seeding	0.8 0.8 0.8 0.8 1.2		30 40 55 75 85	5-30 mm

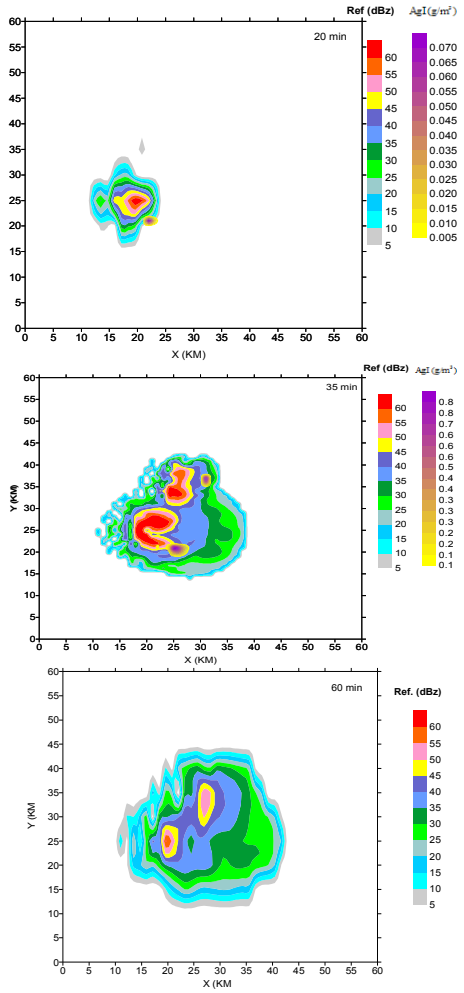
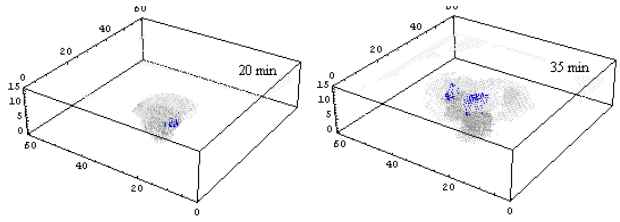


Fig. 3b Modeled x-y radar reflectivity cross sections at z=6.5 km in 35, 50 and 70 min

AgI diffusion in both splitting zones of a cumulonimbus cloud is clearly illustrated in medium pannels of the same figures.



(a) (b)

Fig. 4. 3-D depictions of the total cloud field for the a. seeded single cell case; b. Split cell seeding. The 0.5 g/kg surface is indicated in these panels

AgI diffusion in both splitting zones of a cumulonimbus cloud is clearly illustrated in medium pannels of the same figures. A three-dimensional depictions of agent field evolution in single cell case in 20 min and seeding a spllit cells in 35 min viewed from soutwest is shown in (Figs. 4a,b).

Fig. 5 shows a time evolution of hydrometer mixing ratios of a three different seeding scenarios. Dashed curves of cloud water, cloud ice, hail, rain and snow mixing ratio represent a non-seeding case. A thin bold curves denote a single cell seeding experiment and the solid bold curves

delineate a model running averaged mixing ratios of hydrometeors of a split cell seeding.

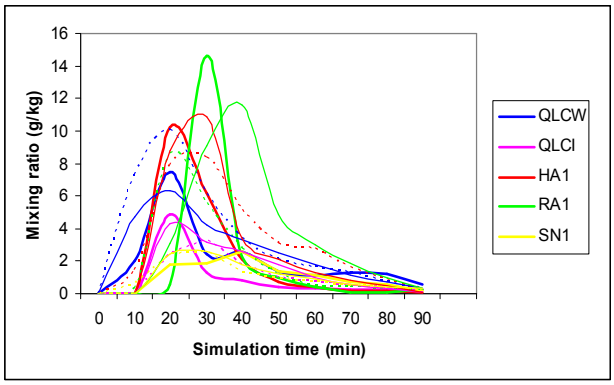


Fig. 5. A time evolution of hydrometeors mixing ratios in a three different seeding scenarios

One sees that both seeding cases exhibit an early formation of rainwater and increase values for cloud ice as result of artificial input of AgI particles in a supercooled zone.

It is also evident that a split cell seeding approach gives a maximum increase of rainwater mixing ratio and hail decrease relative to unseeded case. Comparison shows a difference between a modeled reflectivity of a split seeded relative to unseeded experiment (see yellow and red curves in Fig. 6). In a split seeding case reflectivity decreases in a cloud mature stage that is opposite relative to unseeded case.

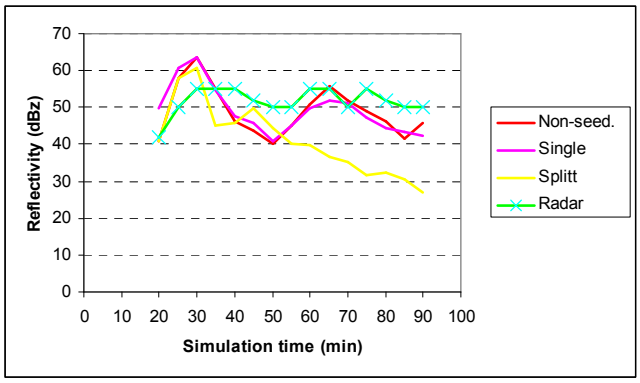


Fig. 6 Radar reflectivity history in (dBz)

4. Conclusions

Three-dimensional numerical simulations have been performed in order to simulate the observational features, including horizontal and vertical dimensions, cyclic behavior and convective core and anvil characteristics. Numerical simulations of the cloud system including of the horizontal and vertical cross sections of radar reflectivity echoes in different time of multicell storm evolution agrees well with observations. In this paper, we intended to show that different scenarios of cloud seeding mast be opplied in order to find out the optimal location of initial seeding zone with respect to increase in cumulative precipitation.from Cb cloud. We found that the highest increase in cumulative precipitation is expected for seeding of the cold part of a cloud if the seeding zone is close to the main updraft. of the left and right moving parts of the splite hailstorm. Clasical scenario of seeding the front side of the updraft will not bring the good results due to the role of the oppositely rotated vortices that transfer large amount of the agent towards the downdraft region. Although we perform experiments for only one among the huge number of strong convective clouds, it is well-known that they are developed under strong directional wind shear, which in turn, induces the vortex formation. With respect to possible loss of seeding material, it is important that the seeding is performed out of the vortex region.

References

Cotton, W.R., and G. J. Tripoli (1979), Cumulus convection in shear flow 3-D numerical experiments. *Atmos.Sci.*, 35, 1503-1521.

Clark, T.L. (1979), Numerical simulations with a three-dimensional cloud model: Lateral boundary condition experiments and multicellular severe storm simulations, J. *Atmos. Sci.* 36, 2191–2215.

Curic, M., Janc, D., and V. Vuckovic (2007), Numerical simulation of Cb cloud vorticity, *Atmos. Res.*, 83, 427-434.

Klemp, J. B. and R.B. Wilhelmson (1978), The simulation of three-dimensional convective storm dynamics, *J. Atmos. Sci.* 35, 1070-1096.

Lin, Y. L., R.D. Farley, and H.D. Orville (1983), Bulk water parameterization in a cloud model, *J.Climate Appl. Meteor.*, 22, 1065-1092.

Orville, H. D. and F. J. Kopp (1977), Numerical simulation of the history of a hailstorm, *J. Atmos. Sci.*, 34, 1596-1618.

Spiridonov, V, and M. Curic, (2006), A three-dimensional modeling study of hailstorm seeding, J. Wea. Mod. 38, 31-37.

Telenta, B., and N. Aleksic (1988), A three-dimensional simulation of the 17 June 1978 HIPLEX case with observed ice multiplication, 2nd International Cloud Modelling Workshop, Toulouse, 8-12 August 1988. WMO/TD No. 268, 277- 285.

Tripoli, G. J., and W. R. Cotton (1982), The Colorado State University three-dimensional cloud/mesoscale model: Part I: General theoretical framework and sensitivity experiments, *J. Rech.Atmos.*, 16, 185-220.

Xue, M., K. K. Droegemeier, and V. Wong (2000), The Advanced Regional Prediction System (ARPS) - A multiscale nonhydrostatic atmospheric simulation and prediction tool. Part I: Model dynamics and verification, M*eteor. Atmos. Physics,* 75,161-193.

Modeling of rainfall enhancement by seeding tropical convective clouds

V Vlado Spiridonov[1] and Mladjen Curic[2]

[1] Republic Hydrometeorological Institute of Macedonia, Skupi bb 1000 Skopje
[2]Institute of Meteorology, University of Belgrade, Belgrade, Serbia

1. Introduction

Convective clouds are characterized by strong updrafts, enhanced transport of heat and moisture in the upper layers and rainfall processes which are activated in very limited time interval and space and with a variable intensities. The cloud seeding for rain enhancment of such clouds is a big challenge and common practice in many areas over the world for more than 50 years. There is a strong scientific evidence and assessment on the status of weather modification from literature (see List et al, (1993), *Cotton and Pielke* (2007), *Rosenfeld and Woodley, (1989, 1993); Silverman* (2001), *Levin and Cotton* (2008). Over the years, there have been a number of projects which showed a more or less confidence for a rain augumentation by applying static glaciogenic seeding of cumulus convective clouds (e.g. Isaac et al. (1982), Dennis, 1980; Mason, 1982; Silverman, 1986; Cotton, 1986 and many others) A comprehensive analysis by Kessler et al. (2007, in Hebrew) and a subsequent summary by Sharon et al. (2008) concluded that seeding enhanced the amount of precipitation by about 30% in storms that produced less that 5 mm per day in Israel. In recent years models become a powerfull tools in weather modification research. Well-designed scientific experiments that include extensive measurements and model simulations are needed to determine whether artificial seeding can modify cloud structures and the effects of the seeding on precipitation enhancement Farley et al (1994); Bruintjes, (1999), Reisin et al., 1996; Cotton et al. (2006), Curic et al. (2007) and many others.

2. Model framework

A three-dimensional non-hydrostatic cloud model with two-moment bulk microphysics scheme has been used to investigate the effects of silver iodide seeding on cloud microphysics, dynamics and precipitation of tropical convective clouds. The model is a set of conservation equations for momentum, energy and mass (air and water contents). An additional conservation equation is considered here:

$$\frac{\partial X_S}{\partial t}+\frac{\partial X_S U_j}{\partial x_j}-X_S\frac{\partial U_j}{\partial x_j}=S_{X_S}+E_{X_S} \qquad (1)$$

where X_S is the mixing ratio of AgI particles, S_{X_S} is the sink or source term of mixing ratio and E_{X_S} is the subgrid-scale contribution. The activation of AgI is parameterized by the three nucleation mechanisms based on Hsie (1980) and Kopp (1988) which are deposition (including sorption) nucleation, contact freezing nucleation – Brownian collection and inertial impact due to cloud droplets and raindrop. These are the sink terms of X_S which can be calculated as:

1.) Contact freezing nucleation-Brownian collection, S_{BC}, and inertial impact due to cloud drops, S_{IC},

$$S_{BC}=-4\pi D_S R_C X_S N_C \qquad (2)$$

$$S_{IC}=-\pi {R_C}^2 X_S N_C V_C E_{CS}; \qquad (3)$$

2.) Contact freezing nucleation-Brownian collection, S_{BR}, and inertial impact due to raindrops, S_{IR},

$$S_{BR}=-2\pi D_S X_S N_{OR}\lambda_R^{-2} \qquad (4)$$

$$S_{IR}=-2.54 E_{RS}\rho^{-0.375} X_S {q_R}^{0.875} \qquad (5)$$

3.) Deposition nucleation due to water vapor at ice supersaturation

$$S_{DN}=\begin{cases} m_s\dfrac{dN_{aD}(\Delta T)}{dt} & \text{when } 5°C\le\Delta T<20°C \\ m_s N_{aD}(\Delta T) & \text{when } \Delta T\ge 20°C \end{cases} \qquad (6)$$

where D_S is a diameter of AgI particles, N_C and V_C the concentration and terminal velocity of cloud droplet, R_C the cloud droplet radius, N_{OR} parameter of the raindrop size distribution, λ_R the slope parameter of rain, E_{CS} and E_{RS} are the collection efficiency of cloud water and rain water collecting AgI particles respectively, ρ the air density, N_{OR} the rainwater mixing ratio, ΔT supercooling and N_{aD} is the number of AgI particles active as a deposition nuclei at a supercooling ΔT, m_s the mass of the AgI particle.

These are the sink terms of X_S, while the initial mixing ratio X_{S0} of agent homogeneously distributed in the seeding zone at the seeding moment is the source term of X_S. A more detail information about the model physics and agent nucleatin mechanisms could be found in Telenta and Aleksic. (1986), Spiridonov and Curic (2006).

2.1 Experimental setup

The static glaciogenic seeding concept has been applied to supercooled cumulonimbus clouds and tested in a tropical region. The lack of rain enhancement in Israel was partly due to the fact that much of the seeding material did not reach the proper heights in the clouds at the right time for it to be effective (see Levin et al, 1997). Often, seeding material that is dispersed from ground generators placed upwind of the target area is used exclusively or as a supplement to airborne seeding. The aim is to disperse the glaciogenic material into as many clouds as possible in the area upwind of the designated target area. We perform a series of numerical experiments on tropical convective cloud seeding by agent AgI using a cloud model. The model simulations are initiated based on seven different upper air soundings for Bangkok, Thailand from 5 to 11 June, 2008. Environmental conditions for all selected cases represent a tropical convective clouds typical for a monsoon period. They are mainly characterized by large moisture content, temperature increase and wind shear and veering in PBL layers. Numerical experiments are configured on domain which covers a region 61 km × 61 km x 20 km in x, y and z directions respectively, with 1 km x 1 km x 0.5 km grid intervals. The seeding agent AgI is introducing in a supercooled cloud zone with reflectivity greater than 25 dBz, between -8 °C and -12 °C isotherms. It is assumed that agent material is instantaneously realized by rocket or airplane in the region of strong updraft. Table 1 lists the initial parametes used as the optimum seeding criteria of a seven different tropical convective clouds .

Tab. 1 Seeding experiments and initial parameters

Tropical convective cloud Date	AgI dose (g/m)	AgI Concentration (g/m^3)	Initial seeding time (min)	Seeding placement x,z (km, km)
05/06/08	1	$1.3x10^{-2}$	15	29, 7
06/06/08	0.4	$5.1x10^{-3}$	25	30, 7
07/06/08	15	$8.8 x10^{-3}$	20	24,6.5
08/06/08	0.2	$2.5 x10^{-3}$	20	28,7
09/06/08	2.0	$2.5 x10^{-2}$	15	26,7
10/06/08	0.6	$7.6 x10^{-3}$	20	28,7
11/06/08	15	$1.9 x10^{-2}$	20	30,6.5

3. Results

Our main task was to model the rainfall enhancement by tropical convective cloud seeding. The effects cloud dynamics and microphysics interactions affected by seeding of AgI are examined. A set of experiments has been performed by seeding tropical convective clouds around the supercooled water region in cloud developing stage in updraft portion of the cloud where maximum cloud modification effects are expected. A proper seeding parameters in sense of optimum dose rate into the proper location and appropriate time is crucial to obtain the optimum effects.

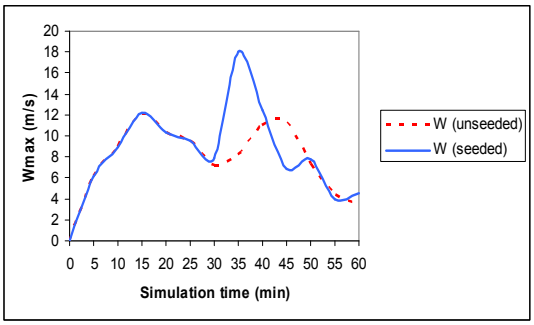


Fig. 1 Time evolution of the simulate maximum updraft (m/s). Unseeded case (dash red curve), Seeded case (blue curve)

The time evolution of the maximum updrafts of unseeded and seeded tropical convective cloud on 5 June, 2008 is shown in Fig. 1. It is seen that the AgI seeding can significantly increase the vertical velocity. Both cases has clearly illustrate that updrafts remain with the same values until 30 min of the simulation time. The great difference is found for about 35 min as the result of agent seeding and downdraft outflow induced by falling hydrometeors in the PBL.

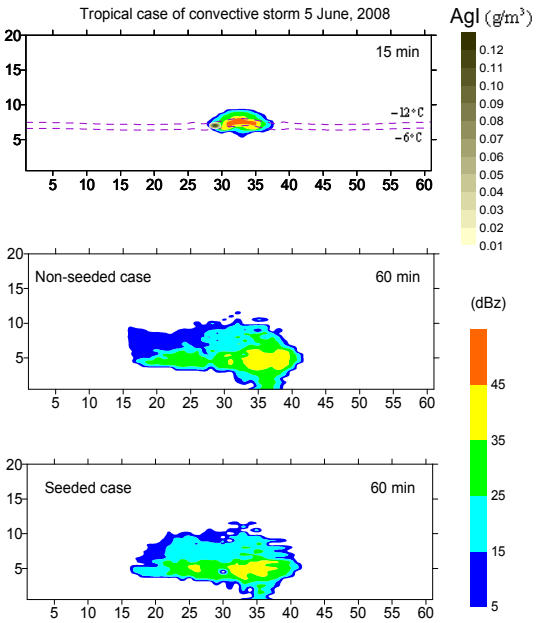


Fig. 2. Cloud seeding of a tropical convective cloud on 5 June, 2008.

Fig. 2 shows an example of a tropical convective cloud seding experiment. Cloud seeding was conducted in the frontal updraft part of the cloud in 15 min of the simulation time on the horizontal distance 29 km in the cloud model domain at 7 km height a.s.l. where the ambient temperature is between -12 and -

8 °C isotherms (see upper panel). The radar reflectivity zone is greater than 25 dBz. Initial seeding amount was 1 (g/m).

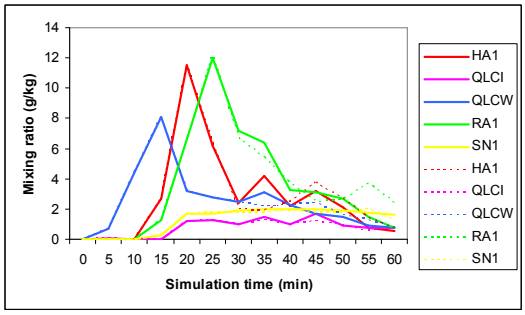


Fig. 3 Time evolution of hydrometeor mixing ratios (g/kg) for unseeded (dash curves) and seeded run (solid curves)

The effect of cloud seeding is evident analyzing the vertical cross section of the radar reflectivity of seeded relative to the unseeded cloud in 60 min of the simulation time as well comparing the time evolution of reflectivity echoes during simulation time (Fig. 4). Seeded case shows vertical expansion of the zone with a radar reflectivity between 15 and 25 dBz mostly containing snow and ice particles and more narrow reflectivity field of 35 dBz. Results from Fig. 5 illustrate that AgI seeding of such tropical convective clouds, has evident effect on the rainfall enhancement at the ground compared with the unseeded process. Our experiments indicate that the total accumulated rainfall at the ground in seeded runs has a larger values relative to unseeded runs. A cumulative rainfall increase from 6 to 35 % is found in all seeded cases and well agree with weathe rmodification findings from the published literature.

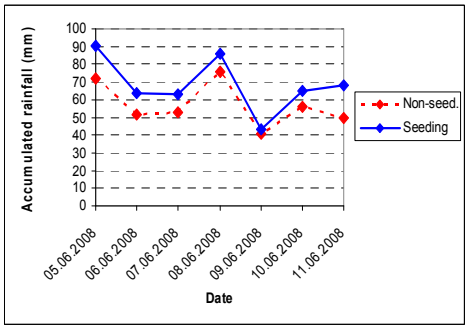


Fig. 6 Comparison of the accumulated rainfall at the ground in (kg/m^2) between unseeded and seeded clouds

When considering a time history of the accumulated rainfall at the ground, seeded case shows an early formation of rainfall and greater difference after 35 min of the simulation time compared to unseeded case. Six seeding tests have been carried out to investigate the effects of seeding at a different release mode (instantaneous or continuous, one grid point or several grid points), and with different amounts of the seeding agent. All of cases are seeded in the region of the strongest updraft when the model cloud top was passing the 10C level at 10min, and produce significant effects.

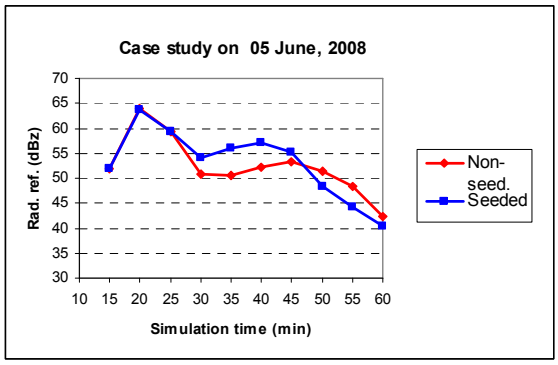


Fig. 4 Radar reflectivity history of unseeded and seeded tropical convective cloud on 5 June, 2008

The cloud seeding results in substantial increases in accumulated precipitation at the surface in all seeded cases (by 6% to 35%) (Fig.7).

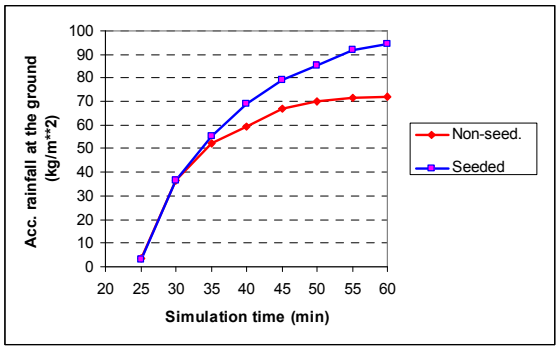


Fig. 5 Time evolution of the modeled accumulated rainfall at the ground

All of cases are seeded in the region of the strongest updraft when the model cloud top was passing the 10C level at 10min, and produce significant effects. The cloud seeding results in substantial increases in accumulated precipitation at the surface in all seeded cases (by 6% to 35%) (Fig.7). There is no accumulated hailfalll at the ground in all simulated tropical cases. Increase of graupel melting and subsequent accretion of cloud water by rain contribute mostly to rain enhancement. The seeding enhances the unloading effect of precipitation mass mainly in the form of graupel, leads to a stronger downdraft outflow and enhanced convergence in the boundary layer, further causes the secondary clouds to form earlier and grow larger. The enhanced updraft increases the inflow and causes the cloud to process more water vapor and thereby cloud water, resulting in increase of accretional growth of cloud water by precipitating particles, finally the precipitation enhancement. These results indicate that silver iodide seeding could significantly influence the cloud dynamics, microphysics and further precipitation of convective storms in a tropical convective clouds. The simulation not only supports the hypothesis of statical seeding, but also demonstrates that the convective cloud with a cold base but a long lifetime has dynamic seeding potential as well.

4. Concluding remarks

The results show that a positive effect of rain enhancement can be obtained when seeding in suitable parts of the tropical convective clouds. A greater benefit in the rain enhancement effect can be gotten when seeding in the early developing stage of clouds. The launching elevation of rockets has a great influence on the effect. The above results obtained are expected to help improving the seeding efficiencies in practice. The study shows that the precipitation in the experiment area is dominated by cold cloud precipitation processes and the ice crystal is the main source of grauple, which is produced by the auto-conversion from ice crystal to grauple and then grows through collecting ice crystals. AgI-seeding should be done before the activation of most ice nuclei start,s o as to enhance rainfall through increasing ice crystals content,and deleting super-cooled cloud water. Otherwise, there will be large amount ice crystals grew in natural clouds, artificial nuclei would be useless. The cloud water amount is reduced and the rain water, ice crystal, graupel and snow amounts are increased after the artificial AgI seeding. The model results show that the cold microphysical processes dominate the hydrometeor production in the simulated storms. Melting of graupel and accretion of cloud water by rain are the major sources of rain water. Conversion of graupel is the largest source of hail formation, contributing about 80%. The intercomparison shows differences in rainfall efficiency attributed to differences in the interaction of cloud dynamics and microphysics and precipitation flux processes.

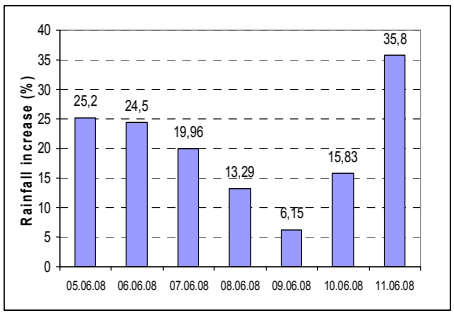


Fig. 6 A cumulative rainfall increase in (%) in all topical convective cloud seeding experiments

However a more comprehensive study with statistical evaluations are essential to give confidence in the outcome of the operations. Concerning seeding effects, this study shows the potential to augment precipitation by AgI seeding of tropical convective clouds.

Acknowledgements
Authors would like kindly to acknowledge to Thai Meteorological Department for provision of initial data and rainfall data for convective case experiments.

References

Cotton, W.R., Testing, implementation and evolution of seeding concepts—A review, Meteor. Monogr. 21, 63–70, 1986a.

Cotton, W.R., Testing, implementation, and evolution of seeding concepts—a review, in Precipitation Enhancement—A Scientific Challenge, edited by R.R. Braham, Jr., AMS Meteorol. Monogr. Ser., 43, 139–149, Amer. Meteor. Soc., Boston, Mass., 1986b.

Cotton, W.R., R. McAnelly, G. Carrió, P. Mielke, and C. Hartzell, Simulations of Snowpack Augmentation in the Colorado Rocky Mountains. J. Weather Modification Association., 38, 58-65, 2006.

Dennis, A.S., Weather Modification by Cloud seeding, 267 pp., Academic Press, New York, 1980.

Isaac, G.A., J.W. Strapp, and R.S. Schemenaur, Summer Cumulus Cloud Seeding Experiments near Yellowknife and Thunder Bay, Canada, J. Applied Met., 21, 1266-1285, 1982.

Farley , R.D., Nguyen, P., and Orville, H.D., 1994: Numerical simulation of cloud seeding using a three-dimensional cloud model. J. Wea Mod., 26, 113-124.

Kessler, A., A. Cohen, D. Sharon et al, Analysis of the cloud seeding in Northern Israel. A report submitted to the Israel Hydrology Institute and the Israel Water Management of the Ministry of Infrastructure, In Hebrew. pp 117, 2002

Levin, Z., S. Krichak and T. Reisin, Numerical simulation of dispersal of inert seeding material in Israel using a three dimensional mesoscale model (RAMS). J. Appl. Meteor., 36, 474 - 484, 1997.

Levin Z. and W.R. Cotton, Aerosol Pollution Impact on Precipitation: A Scientific Review. Springer Press, pp 386, 2008.

List, R. K. R. Gabriel, B. A. Silverman, Z. Levin and T. Karacostas, The Rain Enhancement Experiment in Puglia, Italy: Statistical Evaluation, J. Appl. Meteor., 38, 281-289, 1999

Mason, B.J., A review of 3 long-term cloud-seeding experiments, Meteor. Mag., 109, 335–344, 1980.

Rosenfeld, D., and W.L. Woodley, Effects of cloud seeding in west Texas, J. Appl. Meteor., 28, 1050-1080, 1989.

Rosenfeld, D., and W.L. Woodley, Effects of cloud seeding in west Texas: Additional results and new insights, J. Appl. Meteor., 32, 1848-1866, 1993.

Reisin, T., S. Tzivion, and Z. Levin, Seeding convective clouds with ice nuclei or hygroscopic particles: A numerical study using a model with detailed microphysics, J. Appl. Meteor., 35, 1416–1434, 1996

Silverman, B.A., Static mode seeding of summer cumuli-a review, in Rainfall Enhancement—A Scientific Challenge, AMS Meteor. Monogr., 21, 7–24, Amer. Meteor. Soc., Boston, Mass., 1986.

Silverman, B.A., A critical assessment of glaciogenic seeding of convective clouds for rain enhancement, Bull. Amer. Meteor. Soc., 82, 903–924, 2001.

Sharon, D., A. Kessler, A. Cohen and E. Doveh, A note on the history and recent revision of Israel's Cloud Seeding Program, Israel J. Earth Sci., vol. 57, n.1, 2008.

Spiridonov, V, and M. Curic, (2006), A three-dimensional modeling study of hailstorm seeding, J. Wea. Mod. 38, 31-37.

Telenta, B., and N. Aleksic (1988), A three-dimensional simulation of the 17 June 1978 HIPLEX case with observed ice multiplication, 2nd International Cloud Modelling Workshop, Toulouse, 8-12 August 1988. WMO/TD No. 268, 277- 285.

THE IMPROVEMENT OF CANNON PRECIPITATION ENHANCEMENT OPERATIONS

Wang Yilin[1] *Yao Zhanyu*[2]

[1]*Shandong Institute of Meteorology, Jinan, P.R.China 250031* qxwyl@sohu.com
[2]*Chinese Academy of Meteorological Sciences; Beijing P.R.China 100081* yaozy@cams.cma.gov.cn

1. INTRODUCYION

In previous studies, Abshaev et al. (2003) analyzed the diffusion of a catalyzer (ice nucleating material) in convective clouds. Shen et al. (1983) studied the diffusion of catalyzer regarding exploded cannon shots as point-sources. Diffusion in seeding was also discussed by Yu et al. (2002). However, much work still needs to be done for application. In order to improve cannon precipitation enhancement operations, the cannon precipitation enhancement scheme of practical use is brought forward based on a great number of numerical simulations. The scheme takes into account not only diffusion and transportation from point-sources, but also maximum affected areas with multiple shots at different azimuth and elevation angles. Sensitivity tests are conducted for parameters of large variability, providing a reference value for practical use. The scheme has been coded in the Cannon Precipitation Enhancement Operation Command System, which can determine automatically the optimum azimuth and elevation angles, proper number of shots and other operation parameters. The method of effective seeding area determination can also be used in cannon precipitation enhancement assessment.

2. EFFECTIVE SEEDING AREA

In recent years, cold cloud observation experiments using Particle Measuring System (PMS) probes have been carried out in northern China. Results show that the number of ice crystals in clouds is mostly at the rank of 10^0-$10^1 L^{-1}$. Based on previous studies, for effective seeding, the number of artificial seeded ice crystals should be equal to that of natural ice crystals. The effective seeding area can be defined as the vertical ground projection of the accumulated area where AgI-generated crystals exceeds $10L^{-1}$ after diffusion of cannon shots

3. POINT-SOURCE DIFFUSION

To demonstrate the effect of different eddy diffusivity coefficients (K), areas of concentration of catalyzer AgI q>=10 L^{-1} are simulated，assuming K=20, 40, 80, and 100 m^2s^{-1}. Different asymmetrical single apex curves of effective seeding radius are shown for each K value in Figure 1. The diffusion radius increases with time first, then decreases after reaching its maximum, and ultimately disappears. For

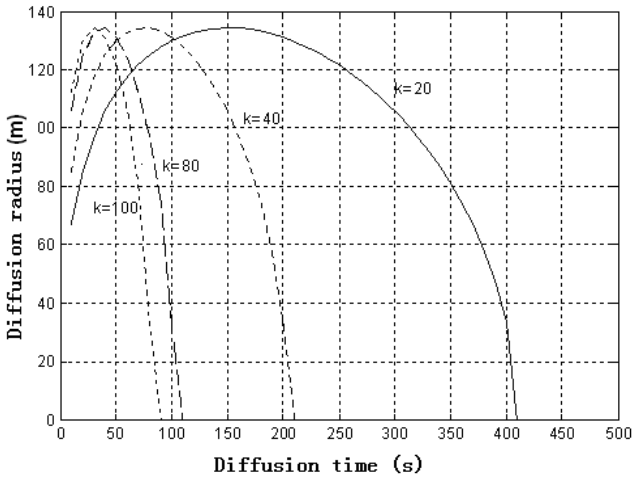


Figure 1. The changes of diffusion radius under different eddy diffusion coefficients

different K values, the maximum value of diffusion radius is the same, which is 135m. For K equals 20, 40, 80 and $100m^2s^{-1}$, diffusion radius reaches its maximum at 150.6s， 75.3s, 37.7s, and 30.1s respectively after explosion, and the time that the diffusion radius disappears is 411s, 206s, 103s, and 84s respectively.

After explosion of a cannon shot, the diffusion of catalyzer AgI from the point-source is governed by two

kinds of movements. The first is isotropic diffusion driven by turbulent eddies, and the second is advection driven by winds. On gradient transportation theory (Shen, 1994),because maximum diffusion radius is the same under different eddy diffusivity coefficients (K), the diffusion area of each shot is only related to time, and different wind speed can only change the transportation distance. For example, when $K=20m^2s^{-1}$, $v=5m\cdot s^{-1}$, simulated areas of AgI consistency exceeding $10L^{-1}$ after explosion at different time of 10s, 75s, 150.6s, 320s, and 400s are shown in Figure 2.

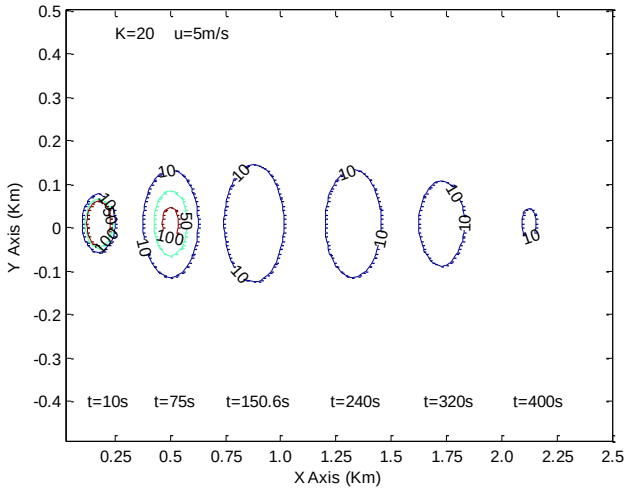


Figure 2 Horizontal distribution of AgI-generated crystals (L^{-1}) at different moments after explosion with $K=20(m^2s^{-1})$, $u=5(ms^{-1})$

4. OPERATION AZIMUTH

In order to get the largest effective seeding area and save shots in cannon precipitation enhancement, a new operation method is put forward, i.e. shooting upwind in a semicircle, as shown in Figure 3. The angle interval of shots is decided according to the principle that no gap is left between cannon shots after diffusion. This operation method also facilitates assessment of operation results after operation.

5. OPERATION ELEVATION AND THE NUMBER OF SHOTS

In precipitation enhancement operations, operation height can be chosen at the levels in cloud with temperatures between -5℃ and −10℃. After operation height is determined, operation elevation is decided according to the parameters of cannon shots (Table 1).

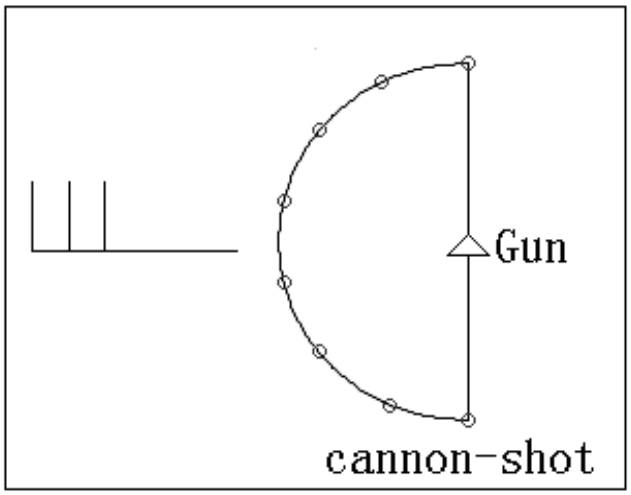


Figure 3 Sketch of operation azimuth. The triangle is the position of the gun; the circles show the positions of the exploded shots delivered at different azimuths.

Table 1 Comparison table of elevation, explosion height and horizontal explosion distance

Elevation	85º	80º	75º	70º	65º	60º	55º	50º	45º
H(m)	4778	4711	4602	4451	4259	4030	3765	3468	3142
X (m)	464	924	1375	1813	2232	2631	3004	3349	3663

According to the relationship between shot range and shot height, the horizontal shot range increases as elevation decreases. In order to get a larger effective seeding area, lower elevation should be used, and azimuth interval between shots should also be decreased while the number of shots increases. Based on the principle of consistency of effective seeding areas, simulations are carried out with different elevations, and the number of shots is given in Table 2. With an elevation of 80º, only eight shots at equal intervals in the semi-circle are needed to get maximum effective seeding area, while 21 shots are needed as the elevation decreases to 60º.

Table 2. Number of shots under different elevations

Elevation	85º	80º	75º	70º	65º	60º	55º	50º	45º
Number	5	8	12	15	18	21	24	27	29

6. EFFECT OF EDDY DIFFUSIVITY COEFFICIENTS ON EFFECTIVE SEEDING AREA

The diffusion equation (omission) shows that eddy diffusivity coefficient and effective seeding area are inversely proportional to wind speed when time is fixed. The larger the eddy diffusivity coefficient, the shorter the time it takes for the catalyzer to reach maxima diffusion radius, and the smaller the effective seeding area. Simulated effective seeding areas under different eddy diffusivity coefficients are shown in Figure 4. For the same wind speed (15m·s^{-1}) and elevation angle (65º), different eddy diffusivity coefficients (20 m^{2}s^{-1}, 40 m^{2}s^{-1}) result in different effective seeding areas of 26km^2 and 13km^2 respectively.

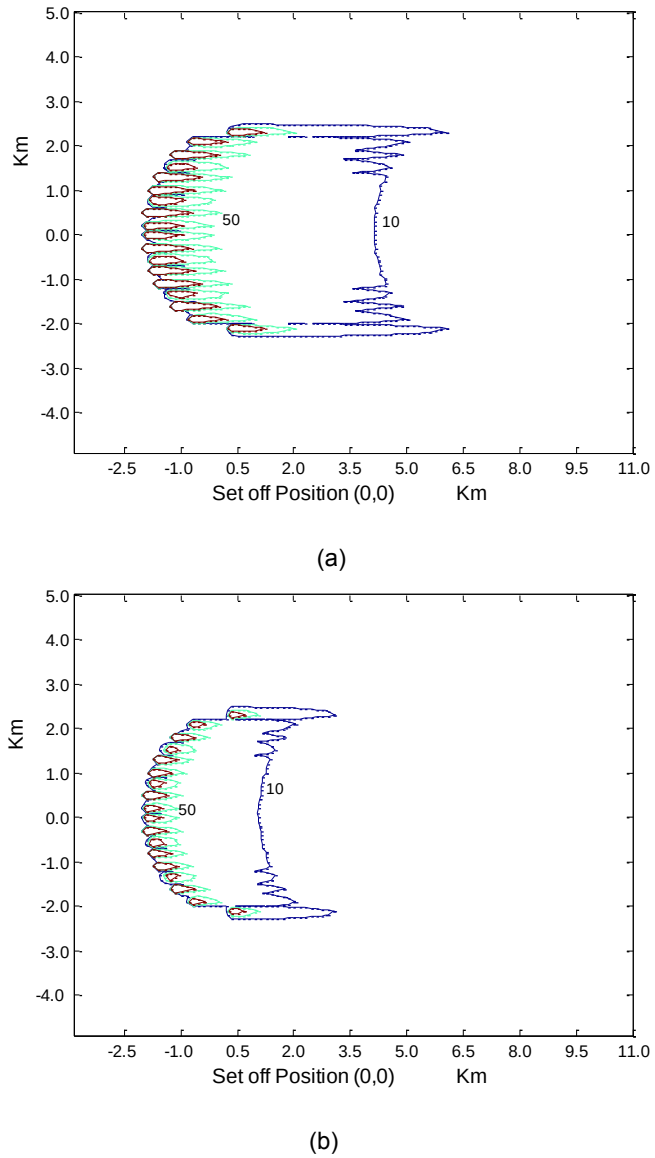


Figure 4. Simulated effective seeding areas (km^2) under different eddy diffusivity coefficients (wind speed is 15m·s^{-1}, and elevation is 65º) (a) K=20 m^{2}s^{-1}, (b) K=40 m^{2}s^{-1}

Simulations were conducted with a combination of different elevation angles, eddy diffusivity coefficients, and wind speeds. The areas of effective seeding are listed in Table 3. For example, with K=20 m^{2}s^{-1}, u=20 m·s^{-1} and the elevation of 60º, 21 shots get an effective seeding area of 39.42km^2.

7. ISSUES OF APPLICATION

There are always no wind observations at the position of the exploding shells at the time of operation. It is practical to substitute for it with data of neighboring levels or from a numerical weather prediction model forecast.

According to observes and calculates, when operating in cumulostratus, the eddy diffusivity coefficient is usually taken empirically as 40m^{2}s^{-1}, and in clouds of strong convections the value is set to 80 m^{2}s^{-1}.

8. CONCLUSIONS

(1) Based on the principle that the number of artificial ice crystals should be equal to that of natural ice crystals, the vertical ground projection of the accumulated area where AgI-generated crystals exceeds 10L^{-1} after diffusion is calculated and can be defined as the effective seeding area.

(2) Operation azimuth is decided based on the operation method, in the case considered here it is shooting upwind in a semicircle with equally spaced intervals. Operation elevation angle is decided based on operation height. The proper number of shots is calculated based on the principle that no gap is left between the effective seeding areas. Precipitation enhancement should be operated with multiple rounds at time intervals determined based on lifetime seeding cloud.

(3) The operation scheme and Cannon Precipitation Enhancement Operation Command System provide an automated and scientific way of cannon precipitation enhancement.

ACKNOWLEDGEMENTS

The authors thank professor Yu kangyuan to provide some material.

REFERENCES

Abshaev, A.M., M.T. Abshaev, and Ya. A. Sadykha, Diffusion of artificial aerosol in cu cong clouds. J. *Russian Meteorology and Hydrology*, **9**, 18-24, 2003.

Shen Yiming, Liu Guixiang, Xu Huanbin et al., The problem of diffusion of point source in the convective clouds. J. *Acta Meteorologica Sinica* **41**(4), 415-425, 1983:

Shen Yiming., The Diffusion of Activators in Cloud. Beijing: *China Meteorological Press,* 48-51, 1994.

Yu Xing, Wang Xiaoling and Dai Jin, Research on simulation of effective range for cloud seeding by aircraft within super-cooled stratus. J. *Acta Meteorogica Sinica*, **60**(2), 205-214, 2002.

Table 3. Comparison table of eddy diffusive coefficient, wind speed and effective seeding area (unit: km^2)

elevation		85°	80°	75°	70°	65°	60°	55°	50°	45°
K=20 (m^2s^{-1})	10 m/s	4.29	7.71	11.31	14.46	17.46	20.46	23.25	25.86	28.17
	15 m/s	6.35	11.37	16.70	21.50	25.64	30.08	34.71	38.36	41.60
	20 m/s	8.42	14.73	21.75	28.35	33.72	39.42	45.54	50.55	54.78
K=40 (m^2s^{-1})	10 m/s	2.21	3.84	5.82	7.38	8.88	10.26	11.88	13.05	14.19
	15 m/s	3.12	5.70	8.37	10.68	12.7 7	15.08	17.34	19.16	20.69
	20 m/s	4.13	7.41	10.89	14.12	16.82	19.83	22.67	25.25	27.35
K=80 (m^2s^{-1})	10 m/s	1.14	2.01	2.97	3.83	4.55	5.27	6.00	6.68	7.19
	15 m/s	1.55	2.90	4.26	5.39	6.41	7.53	8.78	9.54	10.35
	20 m/s	2.03	3.60	5.34	6.98	8.21	9.81	11.16	12.33	13.56
K=100 (m^2s^{-1})	10 m/s	0.93	1.58	2.51	3.09	3.71	4.26	4.76	5.46	6.03
	15 m/s	1.25	2.34	3.42	4.34	5.15	6.18	7.08	7.74	8.40
	20 m/s	1.70	2.93	4.22	5.52	6.75	7.76	9.02	9.86	10.73

Numerical Simulation of Seeding Extra-Area Effects of Precipitation Using MM5

Zhen Zhao [(1)] and Heng-Chi Lei [(2)]

(1) Institute of Atmospheric Physics, Chinese Academy of Sciences, Beijing, People's Republic of China, E-mail: zhaozhen@mail.iap.ac.cn

(2) *Institute of Atmospheric Physics, Chinese Academy of Sciences, Beijing, People's Republic of China, E-mail: leihc@mail.iap.ac.cn*

1. Introduction

The question of "extra-area" effects is prominent among those questions most commonly posed regarding cloud seeding to increase precipitation; that is, whether seeding will affect the weather beyond the targeted temporal or spatial range. A number of researchers have suggested that extra-area effects may have occurred during intensive modification programs (Elliott et al., 1971; Meitín et al., 1984). Field observations over the central Sierra Nevada reported that the effects of cloud seeding with silver iodide persisted for over 90-min after seeding and 100 km downwind of the seedline (Deshler and Reynolds, 1990). The hypotheses that attempt to explain these effects range from direct microphysical effects to mesoscale dynamic effects; however, the cloud seeding extra-area effects have not been investigated using fully interacting mesoscale models yet. The importance of mesoscale processes to the modification of stratiform clouds is the most obvious because the clouds themselves are directly formed from mesoscale meteorological processes.

2. Model description

The three-dimensional non-hydrostatic mesoscale model MM5 was used to test the extra-area effects of stratiform cloud seeding with silver iodide. A two-moment microphysical parameterization for mixed-phase clouds has been established in MM5 (Zhao et al., 2005). The scheme uses a gamma distribution law for rain and for all of the ice species, which predicts mixing ratios and number concentrations of cloud droplets, raindrops, cloud ice, snow, and graupel. A two-moment scheme with the seeding agent field and its effect on clouds was developed in MM5.

2.1 Silver iodide seeding

The simulation of silver iodide seeding that was included in the MM5 two-moment cloud scheme follows (Chen and Orville, 1977; Hsie et al., 1980). Brownian (S_{bc} and S_{br},) and inertial impact (Sic and Sir) collection rates (due to cloud droplets and raindrops, respectively) as well as deposition growth rate (S_{dv}) could be calculated as follows.

1) Collection due to cloud droplets and raindrops are

$$S_{\mathrm{bc}} = \frac{\Delta X_{\mathrm{s}}}{\Delta t} = -2\pi D_{\mathrm{s}} X_{\mathrm{s}} N_{\mathrm{c}} D_{\mathrm{c}},$$

$$S_{\mathrm{ic}} = \frac{\Delta X_{\mathrm{s}}}{\Delta t} = -\frac{\pi}{4} D_{\mathrm{c}}^2 X_{\mathrm{s}} U_{\mathrm{c}} E_{\mathrm{cs}} N_{\mathrm{c}},$$

$$S_{\mathrm{br}} = \frac{\Delta X_{\mathrm{s}}}{\Delta t} = -4\pi D_{\mathrm{s}} X_{\mathrm{s}} \int_0^{\infty} \frac{1}{2} D_{\mathrm{r}} n_{\mathrm{r}} dD_{\mathrm{r}}$$

$$= -2\pi D_{\mathrm{s}} X_{\mathrm{s}} \frac{N_{0\mathrm{r}} \Gamma(2+\alpha_{\mathrm{r}})}{\lambda_{\mathrm{r}}^{2+\alpha_{\mathrm{r}}}},$$

$$S_{\mathrm{ir}} = \frac{\Delta X_{\mathrm{s}}}{\Delta t} = -X_{\mathrm{s}} E_{\mathrm{rs}} \int_0^{\infty} \frac{\pi}{4} D_{\mathrm{r}}^2 U_{\mathrm{r}}(D) n_{\mathrm{r}} dD_{\mathrm{r}}$$

$$= -\frac{\pi}{4} X_{\mathrm{s}} E_{\mathrm{rs}} N_{0\mathrm{r}} \left[\frac{a_0 \Gamma(3+\alpha_{\mathrm{r}})}{\lambda_{\mathrm{r}}^{3+\alpha_{\mathrm{r}}}} \right.$$

$$\left. + \frac{a_1 \Gamma(4+\alpha_{\mathrm{r}})}{\lambda_{\mathrm{r}}^{4+\alpha_{\mathrm{r}}}} + \frac{a_2 \Gamma(5+\alpha_{\mathrm{r}})}{\lambda_{\mathrm{r}}^{5+\alpha_{\mathrm{r}}}} + \frac{a_3 \Gamma(6+\alpha_{\mathrm{r}})}{\lambda_{\mathrm{r}}^{6+\alpha_{\mathrm{r}}}} \right].$$

where X_s is the mixing ratio of the seeding agent, N_c is the number concentration of cloud droplets. The raindrop size distribution is assumed to follow a gamma distribution function of the form

$$n_{\mathrm{r}} = N_{0\mathrm{r}} D^{\alpha_{\mathrm{r}}} \exp(-\lambda_{\mathrm{r}} D).$$

2) The activated seeding agent as deposition nuclei when the air is saturated with respect to water is

$$S_{\mathrm{dv}} = m_{\mathrm{x}} \frac{dN_{\mathrm{aD}}(\Delta T)}{dt}$$
$$= w\frac{\partial[X_{\mathrm{s}} N_{\mathrm{a}}(\Delta T)]}{N_{\mathrm{a}}(20°C)\partial Z} > 0, \quad 5°\mathrm{C} \le \Delta T < 20°\mathrm{C}$$,

$$S_{\mathrm{dv}} = m_{\mathrm{x}} \frac{N_{\mathrm{aD}}(\Delta T)}{\Delta t}$$
$$= X_{\mathrm{s}} \frac{N_{\mathrm{a}}(\Delta T)}{N_{\mathrm{a}}(20°C)\Delta t}, \quad \Delta T \ge 20°\mathrm{C}$$,

where m_{x} is the mass of an AgI particle, and $N_{\mathrm{a}}(\Delta T)$ is the number of nuclei active at the supercooling ΔT (ΔT =273.15-T). The $N_{\mathrm{a}}(\Delta T)$ is computed by (Blair et al., 1973)

$$N_{\mathrm{a}}(\Delta T) = \begin{cases} 0, \Delta T < 5°C \\ 10^3 \exp(-0.022\Delta T^2 + 0.88\Delta T - 3.8), \\ 5^0 C \le \Delta T < 20°C \\ 1.6\times 10^5, \Delta T \ge 20°C \end{cases}$$

The silver iodide particles released in the model interact with cloud water, rain, and water vapor fields to produce ice crystals and snow. The processes in the model are described as follows.

1) Interactions with rainwater

The transformation rate of the mixing ratio (designated by P_{qqq}) and number concentration (designated by N_{qqq}) from rainwater to snow due to seeding are

$$P_{\mathrm{ssr}} = -q_{\mathrm{r}}(S_{\mathrm{br}} + S_{\mathrm{ir}}) \frac{N_{\mathrm{a}}(\Delta T)}{N_{\mathrm{a}}(20°C) N_{\mathrm{r}}} m_{\mathrm{x}}^{-1} \rho, \quad N_{\mathrm{ssr}} = \frac{P_{\mathrm{ssr}} \rho}{m_{\mathrm{s0}}}.$$

2) Interactions with cloud water

The rate at which cloud water transforms to cloud ice due to contact nucleation can be written as

$$P_{\mathrm{isc}} = -q_{\mathrm{c}}(S_{\mathrm{bc}} + S_{\mathrm{ic}}) \frac{N_{\mathrm{a}}(\Delta T)}{N_{\mathrm{a}}(20°C) N_{\mathrm{c}}} m_{\mathrm{x}}^{-1} \rho, \quad N_{\mathrm{isc}} = \frac{P_{\mathrm{isc}} \rho}{m_{\mathrm{c}}}.$$

3) Deposition nucleation

This process is only considered under conditions of saturation with respect to water. The rate (P_{isv}, N_{isv}) is

$$P_{\mathrm{isv}} = N_{\mathrm{aD}}(\Delta T) a_1 m_{\mathrm{x}}^{a_2}, N_{\mathrm{isv}} = \frac{P_{\mathrm{isv}} \rho}{m_{\mathrm{i0}}}.$$

2.2 Silver iodide conservation equations

The equations for the silver iodide mixing ratio X_{s} and number concentration N_{x} are the following:

$$\frac{\partial p^* X_{\mathrm{s}}}{\partial t} = -ADV(p^* X_{\mathrm{s}}) + DIV(p^* X_{\mathrm{s}}) + D(X_{\mathrm{s}})$$
$$+ p^* X_{\mathrm{s0}} + p^*(S_{\mathrm{bc}} + S_{\mathrm{ic}} + S_{\mathrm{br}} + S_{\mathrm{ir}} - S_{\mathrm{dv}})$$,

$$\frac{\partial p^* N_{\mathrm{x}}}{\partial t} = -ADV(p^* N_{\mathrm{x}}) + DIV(p^* N_{\mathrm{x}}) + D(N_{\mathrm{x}}) + p^* N_{\mathrm{x0}}$$
$$+ p^*\{\frac{N_{\mathrm{x}}}{X_{\mathrm{s}}}(S_{\mathrm{bc}} + S_{\mathrm{ic}} + S_{\mathrm{br}} + S_{\mathrm{ir}} - S_{\mathrm{dv}})\}$$.

Here the source terms X_{s0} and N_{x0} represent the seeding agent added at the time of seeding. Thus, the added latent heat due to silver iodide seeding is

$$\frac{d\theta}{dt} = L_{\mathrm{s}} P_{\mathrm{isv}} + L_{\mathrm{f}}(P_{\mathrm{isc}} + P_{\mathrm{ssr}}).$$

The equations for the mixing ratio of water vapor, cloud water, rainwater, cloud ice, and snow and for the number concentrations of cloud water, rainwater, cloud ice, and snow are modified to include seeding effects.

3 Results

3.1 Method of simulation

Between 1200 UTC 12 September and 1200 UTC 13 September 2002, light and moderate rainfall extended from the east of Gansu Province to the north and center of Shaanxi Province and moved across the center of Shanxi Province; this was associated with a mid-latitude low trough that developed mid-level stratiform cloud bands. The model simulation was performed during the same period with a three-domain interactive nested grid domain. The computational domains consisted of a 30-km grid with a mesh size of 109×112 (D01), a 10-km grid with a mesh size of 94×112 (D02), and a 3.3-km grid with a mesh size of 133×109 (D03). The three grids had 33 full-sigma levels in the vertical. Grid-scale precipitation was determined using the mixed phase scheme for D01, the Reisner-2 scheme for D02 and the two-moment scheme for D03.

The simulation of the release of the seeding material was performed for the finest grid only. In the seeding simulation, the horizontal domain of seeding in the D03 was 8×8 grid points centered on the grid point at Yan'an station (36.6°N, 109.5°E). The AgI was released continuously for 30-min at the -5 to -10°C level at 720 min into the model run. Seeding rate was set to

0.2 g s^{-1} in this case.

3.2 Distribution and transport of silver iodide

The simulation of AgI seeding was carried out in the cloud supercooled layer. The updrafts were very weak with vertical motions of approximately 10 cm s^{-1}. Figure 1 shows the distribution of seeding agent at 750 min and 810 min. The AgI drifted with the westerly upper-level wind and was transferred to a downdraft area while moving downward at about 20 m s^{-1}. At 750 min (Fig. 1a), a maximum AgI mixing ratio of 1.2×10^{-7} g kg^{-1} was the value imposed at the center of the seeding domain. As time progresses, the AgI mixing ratio decreased as the seeding agent moved. Most of the AgI particles acted as deposition nuclei in the model. The contact nuclei were captured primarily by cloud droplets, mainly through the Brownian motion mechanism, although this amounts to less than 5%.

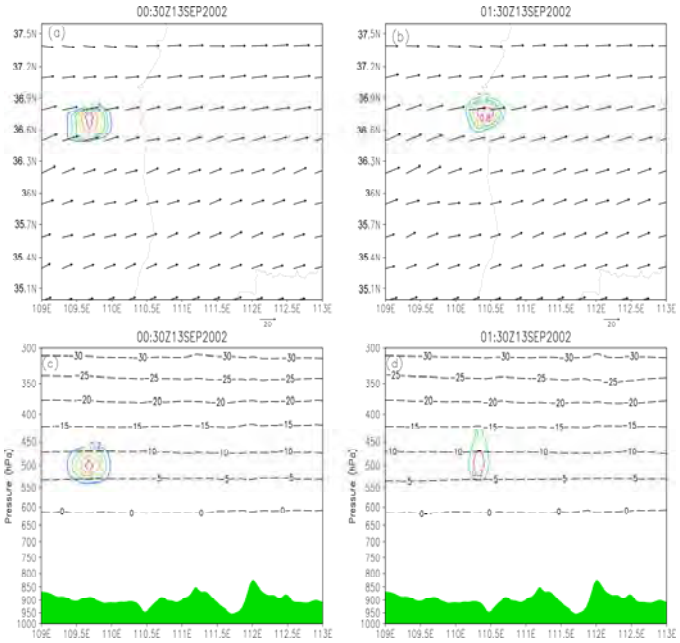


Figure 1 Horizontal cross sections of AgI mixing ratio (10^{-7} g kg^{-1}) and vectors of horizontal winds at 500 hPa (top). Vertical cross sections of AgI mixing ratio (10^{-7} g kg^{-1}) and temperature (dashed lines) along 36.8°N (bottom).

3.3 Evolution of cloud and precipitation processes in seeded and unseeded clouds

The effect of cloud seeding on microphysical quantities was quite significant by 0200 UTC 13 September 2002. Figure 2 shows the differences in cloud hydrometer parameters between the seeded and unseeded cloud. Two hours after the start of seeding, the supercooled liquid water has been depleted to 0.3 g kg^{-1} in the seeded downdraft region where a dissipation zone is obvious. The decreased supercooled cloud water regions have expanded from the seeded levels to the upper levels of cloud. The cloud water content starts to decrease rapidly at about 810 min (60 min after seeding), and after 180 min the depletion ability becomes weak. A large amount of cloud ice of more than 300 L^{-1} increases in the region of supercooled water. The expanding of the cloud ice region corresponds to reductions in the supercooled cloud water region. Cloud ice, via the Bergeron process and contact freezing, acts to diminish the liquid water in the seeded model cloud. The values of the snow mixing ratio increase to 0.2 g kg^{-1} in the seeded case. The more cloud ice that is formed, the more snow that is produced via ice conversion. Rain water increases by more than 0.1 g kg^{-1} in conjunction with the increment regions of snow, which indicates that extra snow melting has enhanced rain formation.

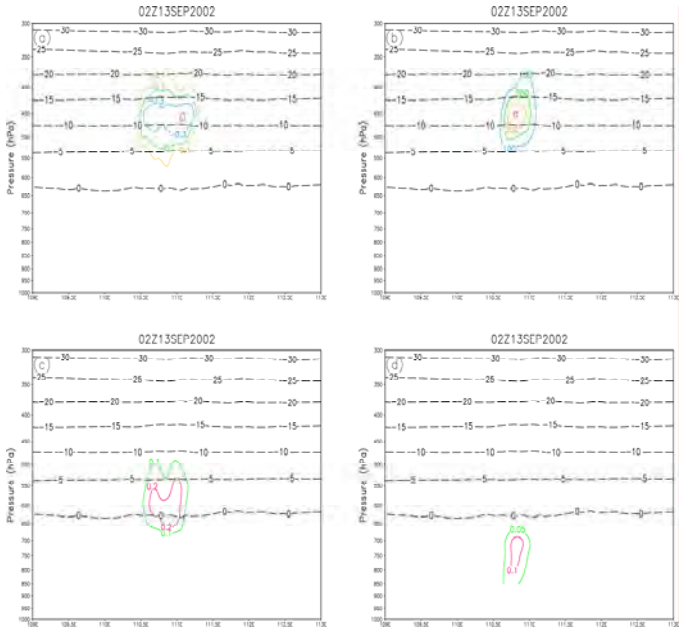


Figure 2 Vertical cross sections of the differences of (a) cloud water mixing ratio (g kg^{-1}), (b) ice number concentration (L^{-1}), (c) snow mixing ratio (g kg^{-1}), and (d) rain water mixing ratio (g kg^{-1}) with and without seeding and temperature (dashed lines) along 36.8°N.

The output of the microphysical processes that describe the interaction of the seeding agent with the cloud yields the following results. Deposition nucleation is the most efficient mechanism for additional cloud ice formation. The increase in the snow melting rate due to seeding contributes mainly to rain enhancement.

Figure 3 shows the distributions of unseeded precipitation and enhanced precipitation after seeding at the surface for a period of three hours. The value is between 0.1 mm and 0.7 mm, which corresponds to a 5%-25% precipitation enhancement over the unseeded case, and the figure shows that considerable redistribution has occurred. An increase in precipitation occurs downwind of the seeding area with distances varying from 80 km to 250 km. The simulated seeding extra-area effects are caused by downwind transport of silver iodide from the seeding source to an area well removed from the intended area of effect.

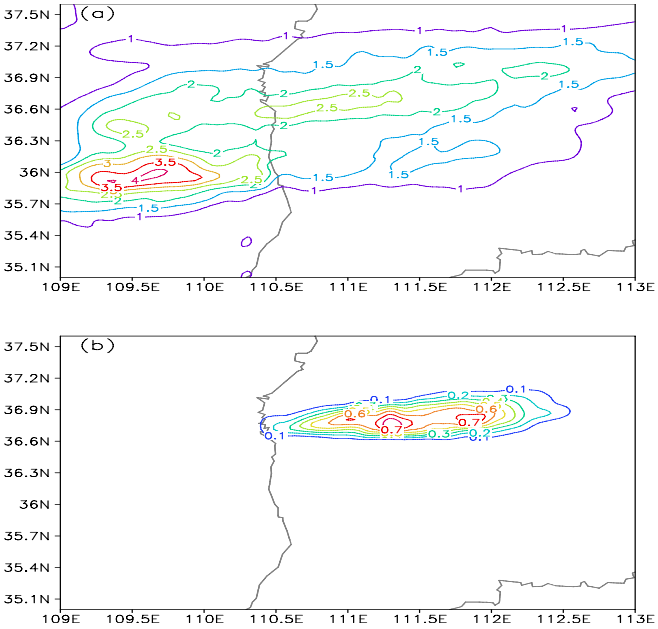


Figure 3 (a) Distribution of simulated precipitation at the surface for unseeded and (b) the augmented precipitation at the surface for seeding (mm) from 0100 UTC to 0400 UTC on 13 September 2002.

4 Conclusions

A three-dimensional mesoscale model MM5 with a two-moment cloud scheme was used to test the extra-area effects of seeding stratiform clouds. Conservation equations were applied to trace the seeding agent in MM5, which is transported with the airflow. For stratiform clouds with silver iodide seeding in the supercooled region, the response of cloud microphysics to seeding was closely related to the transport of the seeding agent. The seeded case produced extra ice and snow in the peripheral regions of the clouds because of the effect of the induced nucleation that was caused by seeding the cloud. Deposition nucleation was the most efficient mechanism for additional cloud ice formation. The model results indicated that seeding could cause extra-area effects that may increase precipitation by 5%-25% in the area downwind of the target location extending to distances varying from 80 km to 250 km.

Acknowledgements

This research was supported by the National Natural Science Foundation of China (Grant No. 40805056) and the Knowledge Innovation Program of the Chinese Academy of Sciences (Grant No. KZCX2-EW-203)

References

Blair, D. N., B. L. Davis, and A. S. Dennis, Cloud chamber tests of generators using acetone solutions of AgI-NaI, AgI-KI and AgI-NH4I. *J. Appl. Meteor.*, **12**, 1012−1017, 1973.

Chen, C.-S., and H. D. Orville, The effects of carbon black dust on cumulus-scale convection. *J. Appl. Meteor.*, **16**, 401−412, 1977.

Deshler, T., and D. W. Reynolds, The persistence of seeding effects in a winter orographic cloud seeded with silver iodide burned in Acetone. *J. Appl. Meteor.*, **29**, 477−488, 1990.

Elliott, R. D., P. St. Amand, and J. R. Thompson, Santa Barbara pyrotechnic cloud seeding test results 1967−70. *J. Appl. Meteor.*, **10**, 785−795, 1971.

Hsie, E.-Y., R. D. Farley, and H. D. Orville, Numerical simulation of ice-phase convective cloud seeding. *J. Appl. Meteor.*, **19**, 950−977, 1980.

Meitín, J. G., W. L. Woodley, and J. A. Flueck, Exploration of extended-area treatment effects in FACE-2 using satellite imagery. *J. Climate Appl. Meteor.*, **23**, 63−83, 1984.

Zhao, Z., H. C. Lei, and Y. X. Wu, A new explicit microphysical scheme in MM5 and numerical simulation. *Chinese J. Atmos. Sci.* (in Chinese), **29**, 609−619, 2005.

EVOLUTION OF BOUNDARY LAYER THERMODYNAMICS, AEROSOL AND CLOUD MICROPHYSICS DURING THE WEATHER MODIFICATION ASSESMENT PROGRAM IN THE SOUTHWEST REGION OF SAUDI ARABIA

Duncan Axisa[1], Lulin Xue[1], Roelof Burger[2], Don Collins[3], Evelyn Freney[4], Paul Kucera[1], Roelof Bruintjes[1] and Peter Buseck[4]

[1]National Center for Atmospheric Research, Boulder, CO, USA
[2]University of Witwatersrand, Johannesburg, South Africa
[3]Texas A&M University, College Station, TX, USA
[4]Arizona State University, Tempe, AZ, USA

1. Introduction

Significant uncertainties exist with aerosol-cloud interactions for which complex thermodynamic and microphysical processes link the aerosol and cloud properties. In order to quantify this thermodynamic and aerosol effect on clouds and precipitation, and to investigate the suitability of these clouds for hygroscopic and glaciogenic seeding, a field campaign was launched in the Asir region of Saudi Arabia as part of a precipitation enhancement feasibility study (Kucera et al. 2010).

In southwestern Saudi Arabia, summertime convection is observed over the mountainous region (often referred to as the "escarpment") that is adjacent to the Red Sea. Ground measurements of aerosol size distributions, hygroscopic growth factor, CCN concentrations as well as aircraft measurements of cloud hydrometeor size distributions were done in this region during the period 5 August 2009 to 31 August 2009. The spatial location of flight tracks is shown in Fig 1. A total of 35 research flights were flown. These flights were designed to study the evolution of droplet coalescence, cloud ice and precipitation hydrometeors in order to understand precipitation formation processes and sensitivities due to thermodynamic and aerosol boundary layer evolution.

2. Surface and airborne instrumentation

Continuous aerosol measurements were made at a surface site located near Abha, just to the east of the Red Sea escarpment. The surface and airborne measurements were linked through a repeatedly employed flight pattern that included multiple low-level orbits around the site. Aircraft measurements were done using the Weather Modification Inc. (WMI) Beechcraft King Air B200. The aircraft was equipped with aerosol spectrometers (Differential Mobility Analyzer, PCASP, CCN counter), a cascade impactor for aerosol filter sampling, cloud drop spectrometers (FSSP, CDP) and optical array probes (CIP, 2DS).

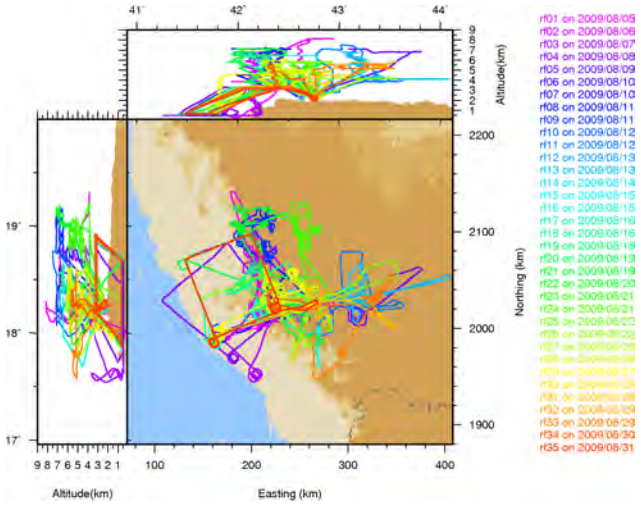


Fig 1: Flight tracks over the southwest region of Saudi Arabia during the August 2009 intensive observation period.

3. Boundary layer evolution and cloud development

The study region is influenced by a diurnal sea breeze mechanism. Southwesterly flow from the Red Sea is lifted orographically along the escarpment causing convective cloud development. To the east of the escarpment, there is a weak to moderate easterly flow from the desert which forces dry air to the region. The interaction between the moist and buoyant airmass from the Red Sea and the dry airmass from the desert creates a moisture convergence boundary that becomes the focus for the initiation of convection. The difference in dewpoint temperature between the airmasses is large (~20°C). Depending on how strong (or weak) the dry flow from the east is on a particular day, the later (or earlier) convective initiation will occur.

Convective clouds form as a series of convective thermals, triggered by surface heating and boundary layer mixing that gradually lifts to higher levels. As these thermals pulse through the lifting condensation level (LCL), small cumulus clouds form. As thermals grow to even higher altitudes, isolated cumulus

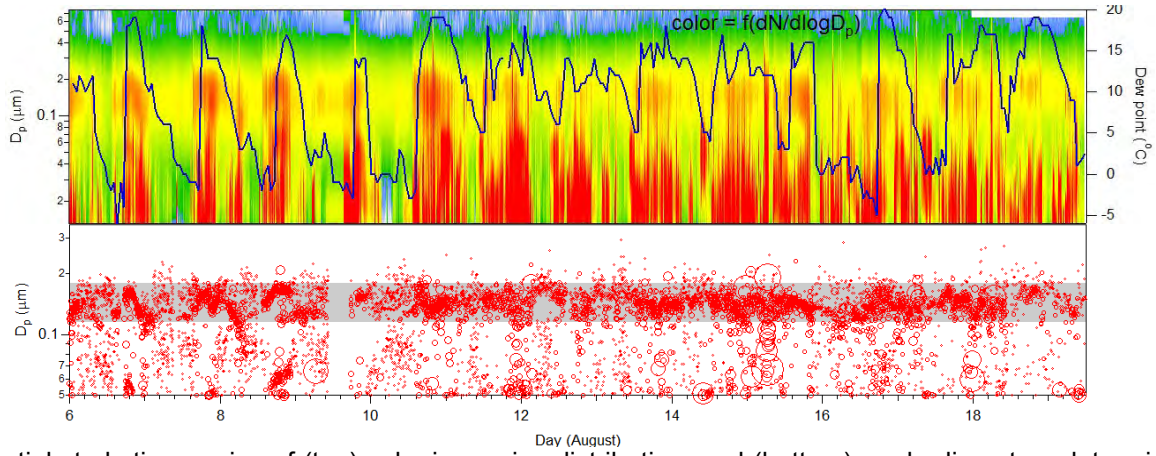


Fig 2: Partial study time series of (top) submicron size distribution, and (bottom) mode diameters determined from lognormal fits of the distributions.

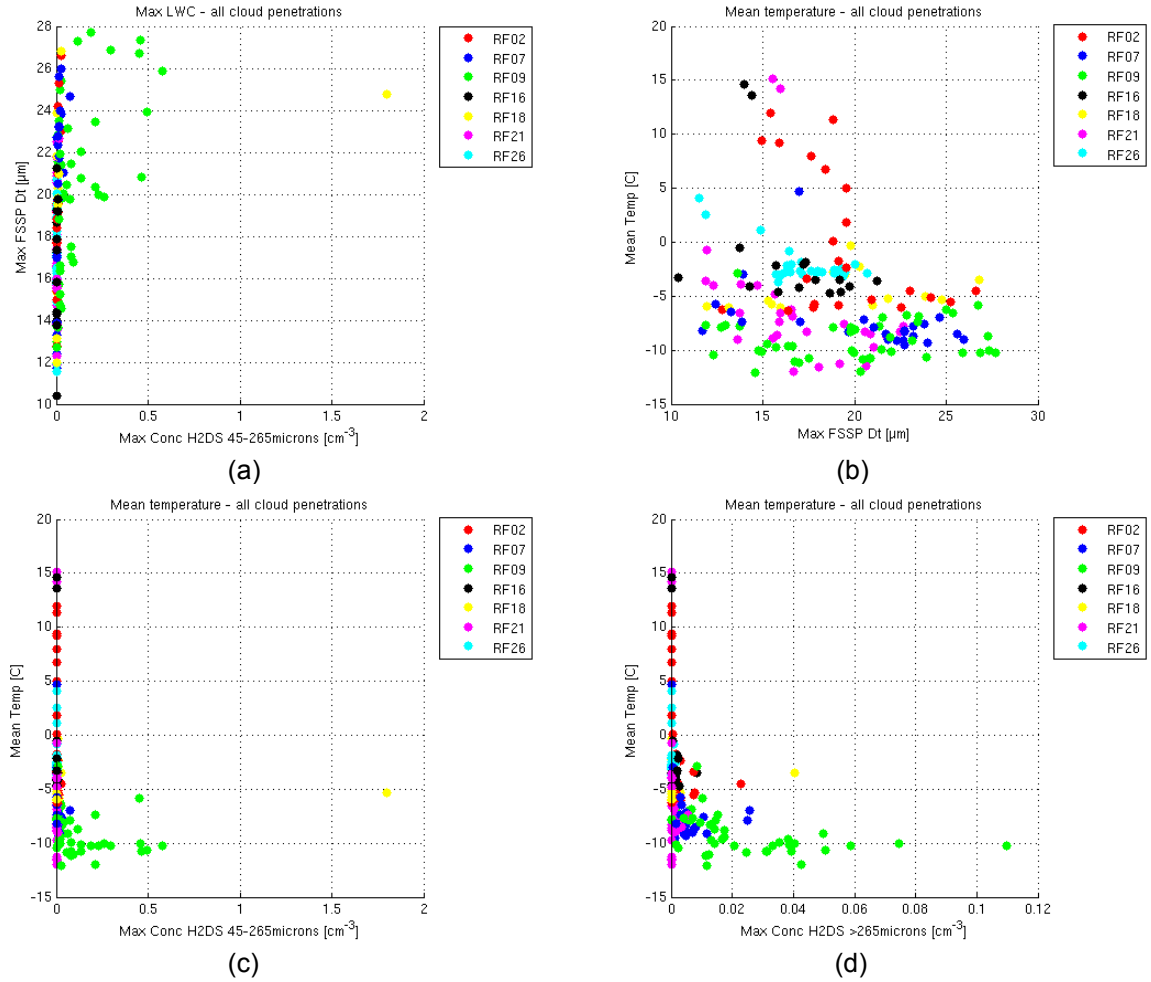


Fig 3: (a) Max FSSP Dt and max 2DS ice particle concentration in the range 45-265 µm for each penetration interval; (b) same as (a) but for temperature; (c) mean temperature and max 2DS ice particle concentration in the range 45-265 µm for each penetration interval; (f) same as (e) but for 2DS ice particle concentration in the range >265 µm.

towers quickly entrain dry air below cloud base resulting in 'break up' of the base. Successive thermal pulses grow the cumulus cloud into a sustainable complex. Strong upper level easterlies cause the convective clouds to tilt, sheer and eventually dissipate.

4. Aerosol and cloud microphysics

Aerosol size distributions and CCN were measured at the surface site. Figure 2 shows a time series of the surface site aerosol size distributions and the mode diameters determined through lognormal fits of the distributions. In the upper panel, the color scale represents the number concentration expressed as $dN/d(\log D_p)$. In the lower panel, each red circle represents one mode and the size of the circle is proportional to the contribution from that mode to the total concentration. The aerosol distributions in this arid environment are characterized by a persistent accumulation mode centered around 0.15 µm and a fluctuating nucleation mode centered around 0.015 µm. The local dew point measured at the Abha airport is superimposed on the upper intensity time series. Though the concentration, size distribution, and properties of the submicron aerosol generally changed very slowly over periods of several hours, as is evident in the intensity plot, an abrupt ~doubling in concentration (and consequently and increase in the CCN concentration) almost always accompanied the increase in dew point that occurred with the arrival of the sea breeze.

Airborne particles were collected from the aircraft for analysis using a particle sampler. Approximately, 600 individual particles were studied from six flights using energy-dispersive spectrometry (EDS) in a transmission electron microscope. Mineral dust, ammonium sulfate, NaCl, and soot where identified as the major particle types. Their compositions are distinctly different in the coarse and fine fractions of all samples.

Our measurements of convective cloud microphysics are summarized in Fig 3. Maximum ice particle concentrations were measured in developing and mature cloud tops at cloud top temperatures down to -15°C. The cloud temperature and ice particle concentration are defined to be the mean and maximum values, respectively, over the penetration interval. To quantify the effect of the broadness of the cloud droplet spectra on the maximum ice particle concentration, we calculate the diameter (Dt) at which the cumulative concentration of droplets with diameter ≥ Dt is 6 cm^{-3} as measured with the FSSP. Therefore a broad drop size distribution would have a high Dt. Figure 4 shows the mean CDP cloud droplet size distribution for RF02, 07 and 09 for Dt smaller and greater than 20 µm. A broader drop size distribution is evident for Dt > 20 µm.

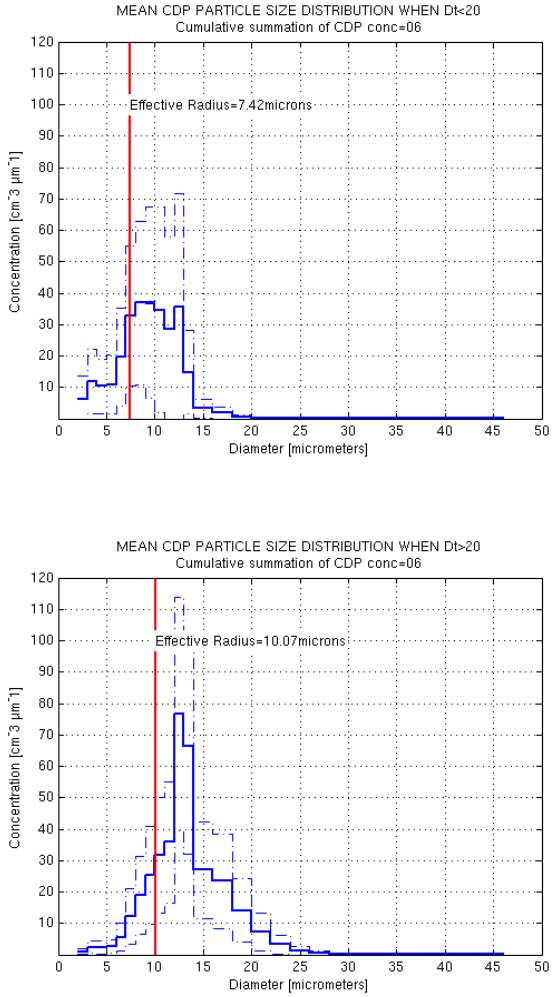


Fig 4: Mean CDP cloud droplet size distribution for RF02, 07 and 09 for Dt < 20 µm (top) and Dt > 20 µm (bottom). Dt is calculated for a threshold concentration of 6 cm^{-3}.

These data show that ice concentrations increase in number at temperatures below -8°C where maximum ice concentrations exceed 100/L (not shown). This sharp increase in ice concentrations is caused by a broader tail in the drop size distribution when Dt > 16 µm. It has also been observed that at temperatures below -5°C Dt exceeds 25 µm. This indicates that at temperatures colder than -5°C the size distribution is broad. Here the development of ice hydrometeors is underway and reaches a maximum at -8°C. Ice crystal types are mostly graupel-like and relatively small initially (<500 µm). It appears likely that these ice particles originate as frozen drops, which then form graupel.

One can speculate that the broadness of the size distribution may indicate that droplet coalescence is active in the early phases of cloud development. The combined growth time of a droplet by condensation and coalescence to a size of, say, 200µm in a typical cumulus cloud is greater than an hour. This is much greater than the lifetime of small precipitating cumulus clouds. It is not well understood which processes produce fast broadening

of the size distribution as is observed here. Some may attribute the source of large droplets to giant cloud condensation nuclei (GCCN) (e.g., Beard and Ochs 1993). Measurements of the aerosol size distribution indicate that the supermicron aerosol concentration could be as high as 50 cm^{-3} up to heights of 4km in some cases. If a small percentage of this coarse mode aerosol is soluble, then GCCN could be the mechanism by which large droplets form.

Formation of ice crystals by primary ice nucleation may also be possible in the heavily dust loaded aerosol although nucleation freezing temperatures of dust particles from the central region of Saudi Arabia were much lower than -8°C. Nevertheless a more detailed analysis including calculations and modeling are needed to understand the occurrence of these ice particles.

5. *Conclusion*

In southwestern Saudi Arabia, summertime convection is observed over the mountainous region in is associated with a diurnal sea breeze mechanism which alters the aerosol physical and chemical properties as well as the boundary layer thermodynamics. The regional aerosol can be characterized by a persistent accumulation mode having hygroscopic properties consistent with a sulfate-rich aged aerosol. The concentration of particles in the accumulation mode, and consequently the CCN concentration, was considerably higher in the air mass behind the sea breeze as in that ahead of it. Aircraft measurements have shown that clouds develop graupel quickly by the freezing of droplets in the 50-200μm range. Once the large droplets form, these quickly freeze and become graupel. Small droplets (<20 μm) remain supercooled and are important in the growth of graupel by riming. High liquid water content (>2 gm^{-3}) can be encountered once the cloud is in the developing stage. Graupel up to 1mm in diameter is present in concentrations reaching 100/L. This increase in ice concentration is caused by a broad tail in the drop size distribution. It appears likely that these ice particles originate as frozen drops, which then form graupel. This process produces graupel showers at temperatures as warm as -8.0°C. The broadness of the size distribution may indicate that droplet coalescence is active in the early phases of cloud development. We attribute the source of large droplets to giant cloud condensation nuclei (GCCN) which are composed of supermicron mineral dust aerosol.

Acknowledgments

This study was supported by the Presidency of Meteorology and Environment (PME) in Saudi Arabia through a contract with Weather Modification Inc.

References

Beard, K. V. and H. T. Ochs III, 1993: Warm-rain initiation: An overview of microphysical mechanism. *J. Appl. Meteor.,* **32,** 608–625.

Kucera, P.A., D. Axisa, R.P. Burger, D.R. Collins, R. Li, M. Chapman, R. Posada, T.W. Krauss and A.S. Ghulam, 2010: Features of the Weather Modification Assessment Project in the southwest Region of Saudi Arabia. J. Wea. Modification, 42, 78-103.

Qualitative Assessment of the Effectiveness of Summertime Cloud Seeding Experiments in South-eastern Sindh-Pakistan.

[1] *Azmat Hayat Khan**

Abstract

In the year 2000, history's worst drought conditions had affected various parts of the country. Pakistan Meteorological Department had initiated summertime cloud-seeding experiments from June 2000 to augment rainfall over drought-hit areas of the country. Southeastern Sindh was severely affected by drought. The initial focus of the experiments remained over this area. Suitable clouds were seeded using two aircraft fitted with liquid dispensers during the month of July 2000. During summertime, clouds formed from maritime air masses which influence SE Sindh area frequently, are too shallow to extend into freezing level. Accordingly the process of precipitation formation in warm clouds was initiated with the nucleation of cloud droplets by hygroscopic aerosols (sodium chloride particles). It is observed that rain formation over the area was dominated by collision and coalescence among droplets. The cloud development was more prominent when seeding was made to developing Cumuli form clouds rather than strateform clouds. Assessment of potential effectiveness of these experiments using a target/control analysis methodology indicated markable increase in precipitation over the target area. Results were also analyzed in relation to La Nina which was influencing during the period. During year 2000, weak La Nina conditions prevailed during April-June period with near neutral conditions during July-September period. Such La Nina conditions were observed in 1984, 1985, 1989 and 2000 (Climate Prediction Centre Analysis). Last 50 years data of target & control stations was analyzed and it was observed that under same set of La Nina conditions, target station received less rainfall compared to control station. However in the year 2000, target station (Chhor) received more rainfall compared to control station (Badin). The comparison of data indicated a markable increase. The selected area was under the grip of the worst drought and success of cloud seeding operations provided considerable relief to the inhabitants. As such, it is evident that there is a significant success in augmenting rainfall over the region.

Keywords: *Cloud Seeding, Drought, Aerosols,*

Precipitation Effectiveness, La-Nina, CPC

1. Introduction

Pakistan mostly consists of hyper-arid, arid and semi arid regions. Some parts of the country remain practically dry for more than 50% of the time in different seasons and therefore, are more vulnerable to drought conditions and call for such measures to be adopted that may augment the water availability; a vital survival entity for every one. Winter rains, which are vital for relief to North Balochistan & NWFP, failed due to strong La-Nina Episode resulting severe drought conditions. The drought situation during the 2nd quarter of year 2000 in southern latitudes of the country pressed the government functionaries to arrange necessary resources for conducting cloud seeding experiments to modify weather and get water to offset some of the impacts of the drought in Sindh and Balochistan.

Accordingly PMD presented a work plan. Pakistan Army and Ministry of Agriculture joined hands and supplied seeding aircrafts and necessary manning for conducting these experiments. PMD is equipped with a network of weather surveillance radar network, satellite ground receiving stations for receiving HRPT & APTs and line links for receiving data of ground observatories & rawinsounde data - essential tools for conducting these experiments.

Primary seeding mode in these experiments was aerial seeding or water spray seeding (after Braham et al. 1957); to inject seeding agent to growing cumulus clouds by specially equipped seeding aircraft. The pilot of aircraft sprayed several hundred liters of sodium chloride solution within and around the periphery of cloud system.

The cloud system was watched at Main Control Center (MOC), Islamabad by a team of experienced meteorologists under the supervision of Dr. Qamar-Uz-Zaman Chaudhary; a scientist of international fame and Director General, Meteorological Services.

MOC was equipped with a network of 5 cm weather surveillance radars and satellite ground receiving stations; vital tools to track and assess the nature of cloud system, to determine the height of cloud and its intensity.

2. OPERATIONS:

A one-month program was conducted from July 1st to July 28th in the CHHOR (target) area. There were limited seeding opportunities during the period. A total of 8 experiments were conducted. The rainfall activity over the area coincides with cloud seeding operations.

3. METHODOLOGY

A target/control evaluation is performed for southeast Sindh area. The evaluation is based on the rainfall activity over target/control area on seeding operation days.

After studying climatic conditions of the area, Badin is selected as control area whereas Chhor is the area (target) where seeding experiments were conducted.

4. CLIMATOLOGY OF AREA

The selection is made on the basis of climatic data for historical data (1961-90 average data), which is appended below. Climatic conditions depict that control station Badin might have receive more rainfall during the month of July than target Area in normal course of weather systems. Detail of various climatic parameters is given as under in Table-1

Climatic Parameter	Chhor	Badin
Cloud Cover	4.5 Okta	4.7 Okta
Wind Speed & Direction	SW/10 knots	SW/11knots
Humidity (0000Z-1200Z)	84% 56%	84% 59%
Rainfall	79 mm	71 mm
Mean Temperature	31.5°c	31.1°c

The area lies in tropical belt and climate is mainly arid. Monsoon currents influence the area. However orography of

**Pakistan Meteorological Department*
Postal Address: Pakistan Meteorological Department, Sector H-8/2,P-O-Box# 1214, Islamabad, Pakistan
Email: dirndmc@gmail.com

the region gives little support in cloud development. As such, meager precipitation is received over the area.

5. Results and Discussion

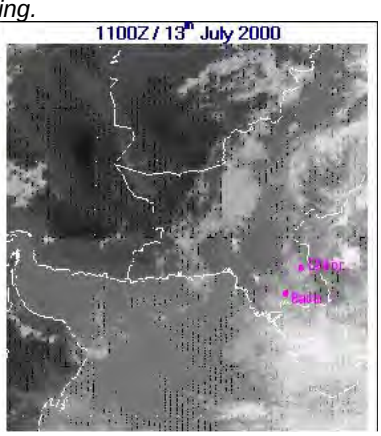
These experiments indicated that cloud system over Southeast Sindh had mildly stable atmosphere that restrict cloud growth, but not so stable that they prelude deep cloud growth when some additional heat is added. Maritime air masses, which influenced the area frequently, contain large amount of super cooled liquid water droplets. As orography of the area provide little support in the cloud development, therefore slight increase of in-cloud temperature with respect to that of cloud environment by seeding process enhanced the cloud buoyancy. The cloud development was more prominent when seeding was made to developing Cumuli form clouds rather than stratiform clouds.

5.1 Experiment No. 1

On 13th July,2000 analysis of weather charts at 00z indicated favorable conditions for cloud development over Southeast Sindh. Synoptic situation on the day was that monsoon low after having developed over Bay of Bengal, was centred over north-eastern Madhya Pradesh (India) and was showing NW moving trend. It had been inducing moist currents in Kashmir, Punjab and Sindh. Forecast for Isolated rainfall was issued for target area. Cloud development was watched by Satellite picture and weather survillence Radar. Latest surface observation at target area supported the remote sensing data and it was decided to seed the area to enhance clouds precipitating efficiency.

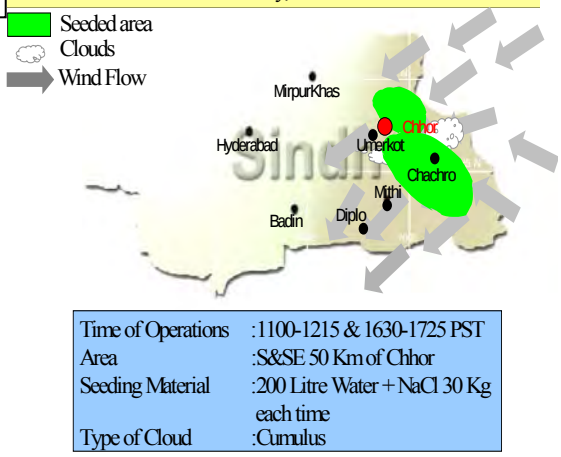
Meteorological Conditions reported from Target/Control Stations and satellite imagery showing cloud cover over the area at the time of seeding.

Meteorological Parameter	Station	
	Chhor	Badin
Wind	S/04	SW/04
Temperature	35.7	34.0
Cloud Cover	St & Sc	Sc & As
Humidity	58	62

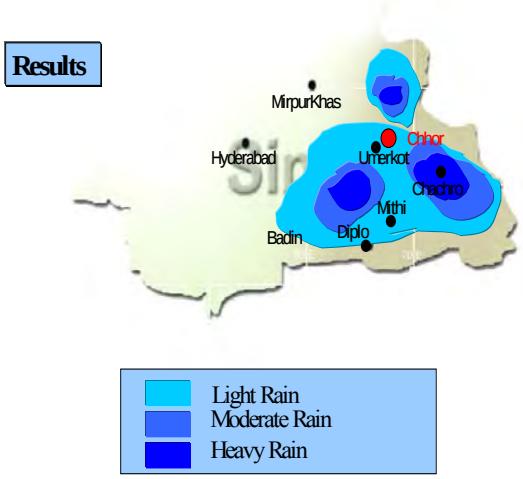


Therefore seeding operation was started at 1100 PST for 75 minutes southeast of Chhor. 3 octa stratocumulus & 2 octa altostratus clouds were available for seeding. Again in the evening at 1630 PST, same area was seeded for 55 minutes. At this time, 3 octa Sc and 2 octa Ac clouds were available for seeding. Moist southeast flows at 850 MB contributed to the development of precipitation efficiency.

Fig.1 RAIN ENHANCEMENT EXPERIMENT IN THAR DESERT
13th July, 2000



Time of Operations	:1100-1215 & 1630-1725 PST
Area	:S&SE 50 Km of Chhor
Seeding Material	:200 Litre Water + NaCl 30 Kg each time
Type of Cloud	:Cumulus



5.2 Experiment No.2

on 14th July 2000, weather charts and remote sensing data reflected promising situation for seeding the area. The seasonal heat low over Balochistan was well marked. The monsoon low was located over central Rajhistan (India) and was slightly weak having NW moving trend. However still it had been a source of moisture incursion over target and control area. Satellite imagery at 10 PST showed scattered convective clouds over SE Sindh. The detail of meteorological conditions and satellite picture is appended below.

Fig-1:Meteorological Conditions reported from Target/Control Stations and satellite imagery showing cloud cover over the area at the time of seeding.

Meteorological Parameter	Station	
	Chhor	Badin
Wind	SW/04	S/08
Temperature	36.5	33.5
Cloud Cover	Sc, Cu & As	Sc, Cu & Ac
Humidity	55	61

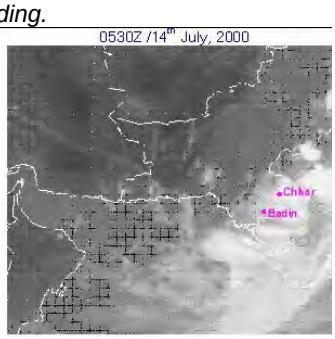
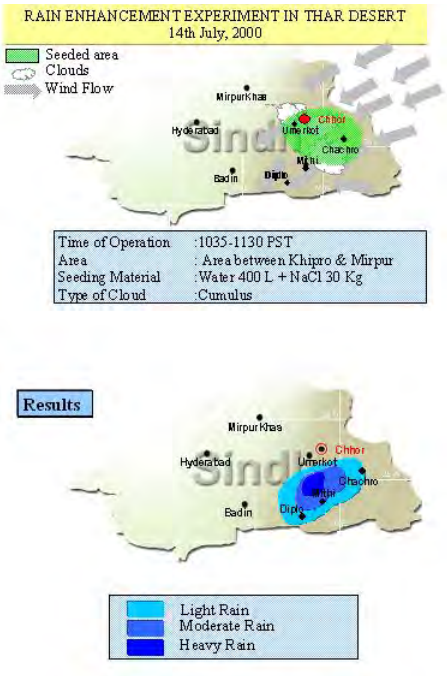


Fig 2



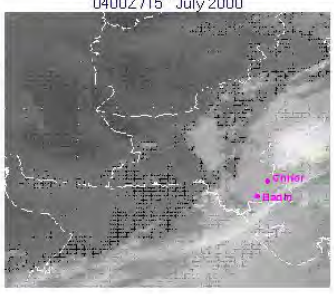
Therefore field staff was instructed to seed the south-easterly sector. Beaver aircraft carrying 30 Kg of NaCl with 400 litres of water was used for seeding. The operation was completed in 55 minutes in two sorties from 1035 PST to 1130 PST. Accordingly moderate to heavy rainfall was reported from the seeded area. The detail is under.
Diplo=62mm, Nagarparker= 22mm, Mithi=20mm.
Control station also received 23 mm of rainfall. Results indicate that dominant contribution seems to be due to monsoon low over Rajhistan (India). However comparison of rainfall pattern of target and control areas supports the contribution of seeding activity in enhancing the cloud precipitating efficiency. Results are also presented in graphic format as Fig. 2

5.3 Experiment No.3

On 15th, there was little change in synoptic situation and monsoon low was located over Rajhistan (India). However a westerly wave was moving across Kashmir, resulting convergence of moisture over northern parts of Pakistan. Chances of rainfall over the target area were bleak. However 3 octa stratocumulus clouds were available for seeding. Beaver aircraft mounted with liquid dispenser and carrying 200 litres of water & 30 Kg of NaCl was used for seeding purposes. The detail of meteorological conditions and satellite picture is appended below.

Meteorological Conditions reported from Target/Control Stations and satellite imagery showing cloud cover over the area at the time of seeding.

Meteorological Parameter	Station Chhor	Badin
Wind	SW / 06	W/08
Temperature	38.5	35.5
Cloud Cover	Sc, St & Ac	Sc, Cu & Ac
Humidity	29	52



However no rainfall was reported from the target area . One reason might be that moisture availability had dropped drastically during previous two days and moisture in the atmosphere was sufficient to produce more rain. Secondly, the concentration of seeding agent was high and probably the moisture content in the atmosphere was less resulting dissipation of clouds

6. CONCLUSION

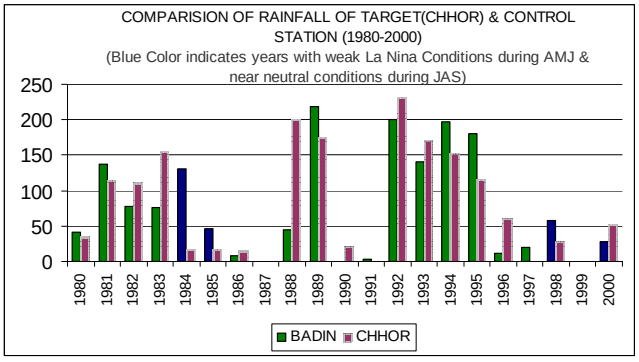
Evaluation of results of any operational cloud seeding program is rather a difficult due to large natural variability in the amount of precipitation over an area. Also, cloud seeding is only feasible when there are clouds and usually only when these clouds are near to or already producing precipitation naturally. Moreover, the apparent differences due to seeding are relatively small. However, being on the order of 5-15 % increase. To establish quantitative relationship, a significant number of years required to have good number of samples. Keeping in view the limitations, qualitative rather quantitative technique has been deployed.

Precipitation data have been used in assessing the effectiveness of cloud seeding experiments. The data have been reported from responsible officers of civil administration from various locations where rainguages were installed for this special project. Detail of rainfall (mm) reported from Target & Control areas for the last 24hour is given below.

Date	Badin	Chhor
13	0	0
14	4	19
15	23.4	32.9
Total	**27.4**	**51.9**
% of normal	**38**	**66**

From 16th July 2001, due to shortage of facilities, the operation centre was shifted to Khuzdar to facilitate drought hit people of that region. It is evident from field observations that rainfall activity over SE Sindh coincided with cloud seeding activity over the area and no rainfall was recorded at target or control station after 16th July 2001 till the end of the month.

During year 2000, weak La Nina conditions prevailed during April-June period with near neutral conditions during July-September period. Such La Nina conditions were observed in 1984, 1985, 1989 and 2000 (Climate Prediction Centre Analysis). Last 50 years data of target & control stations was analyzed and it was observed that under same set of La Nina conditions, target station received less rainfall compared to control station. However in the year 2000, target station (Chhor) received more rainfall compared to control station (Badin). Time series of rainfall data for the last 50 years for Badin & Chhor is as under. Blue bars indicate years with weak La Nina conditions in Apr-June & near neutral conditions in July-Sep period.



The comparison of data indicated a 26% increase. As such, it is evident that there is a significant success in augmenting rainfall over the region.

7. ACKNOWLEDGEMENT

The author is greatful to Dr. Q.Z. Ch. DG PMD for encouragement and guidance in conducting the study. Thanks are also due to Mr. Mehmood Hasnain for producing computer graphics and related material.

8. REFERENCES:

1. Climatic normals of Pakistan, PMD publication, 1993.

2. Braham, R.R., Jr., L.J. Battan, and H.R. Byers, 1957: Artificial nucleation of cumulus clouds and weather modification. A group of field experiments. Meteor. Monogr. 2, 47-85

3. Mason, B.J., 1971: The physics of Clouds, 2nd edition, Clarendon Press, Oxford, 671 PP.

4. Biswas, K.R., and A.S. Dennis, 1971: formation of rain showers by salt seeding. J.Appl.Met., 10 780-784

5. Grant, L.O., and R.E. Elliot, 1974: The cloud seeding temperature window. J. Appl. Met. 13, 355-363

6. Braham, R.R., 1981: Designing cloud seeding experiments for physical understanding. Bull. Ameri. Met Soc., 62, 55-62

7. Cooper, W.A., and R.P. Lawson, 1984: Physical interpretation of results from HIPLEX-1 experiments. J.Climate Appl.Meteor, 23, 523-540.
8. Gagin, A., D. Rosenfeld, and R.E Lopez, 1985: A relationship between height and precipitation characteristics of summertime convective cells in South Florida. J.Atmos. Sci., 42, 84-94.
9. Report on Cloud Seeding Experiments to Augment Rainfall in Pakistan (Part-1, warm Clouds) Sep. 2000

Weather Modification Activities in Indonesia

Samsul Bahri), Halda Aditya, F. Heru Widodo, Tri Handoko Seto*

*)Director of Weather Modification Technology Centre
Agency for the Assessment and Application of Technology- Indonesia.
)samsul.bahri@bppt.go.id

1. Introduction

In 1977, cloud seeding as a Project Research was conducted in Bogor and Sukabumi (West Java Province), and Solo (Central Java Province) as a collaboration with The Royal Rainmaking Thailand. Comprehensive study was conducted for 5 years (1979-1983) at Jatiluhur Dam – Citarum Chatchment Area (West Java Province), in which Saguling and Cirata dams were not built yet. The study was done as colaboration with Perum Otorita Jatiluhur (now Perum Jasa Tirta II), very well known Universities in Indonesia (ITB, IPB, UI), and other related institutions (BMKG, Agriculture Department, and Indonesian Air Force). The conclussion of the study might be said that cloud seeding was favourable to be implemented in tropical area as Indonesia.

In 1985, Cloud Seeding Project Research became the specialized agency under BPPT, namely Weather Modification Technology Center (WMTC). The mission of the WMTC is to provide services on rain enhancement in order to obtain more water over any catchment area, to extinguish forest/field fires, and to clear up smoke for both government and public sectors in Indonesia.

In 2004, weather modification was included in Indonesia's regulation (namely UU no. 7/2004 regarding water resources regulation). It says: "..... Development of function and benefit of rainfall are implemented by developing weather modification technology..." (Chapter 38, Sub chapter 1).

Seeding agents of NaCl in powder form are mostly used. Seeding agents in flare form have been utilized in cloud seeding operation at Larona - Sorowako Chatchment Area (South Sulawesi Province), and at Kotopanjang and Singkarak Chatchment Areas (Riau and West Sumatera Provinces). Collaboration in conducting cloud seeding using flares was started in 1997. In doing so, the WMTC worked with Atmospheric Incorporated (AI) – USA. The WMTC had been collaborated with PT. INCO to carry out cloud seeding activities utilizing flares at Larona-Sorowako Catchment Area, in the period of 2000 – 2009. At this time being, the WMTC is trying to produce hygroscopic flares in collaboration with a company namely PT. PINDAD Indonesia.



Figure 1. Cloud seeding activities conducted in Indonesia.

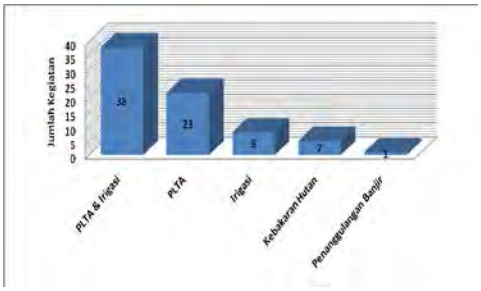


Figure 2. The purpose of cloud seeding activities in Indonesia

Up to now, the WMTC has been carried out weather modification activities in most part of Indonesia region as seen in Figure 1. The purpose of cloud seeding activities were mostly to fill up dams, overcome droughts, extinguish field / forest fires and clear up smoke (Figure 2). In addition, the WMTC is doing experiments to decrease rainfall intensity.

2. Weather Condition

Since 2010 until early 2011, Sea Surface Temperature (SST) anomaly in the equatorial Pacific, especially in the region of Nino 3, 4 and 3.4, were about -1.5 °C. Therefore, Indonesian region in general was influenced by La Nina. Monsoon rainy season (westerlies) occurred in early year. However, rainfall and rain occurrence were very few in West Java in early 2011. Rainfall was only 30% of monthly normal rainfall. We believed that the reason was cooler SST around West Java, especially in north of West Java, in which SST anomaly for the region was around – 0.4 ^{o}C to – 0.6 ^{o}C (Figure 3). Mean while, Dipole Mode that indicates climate activity in Indonesia was almost normal. This indicates that

supply of water vapour into West Java should be normal. These indicators lead to a conclusion that the influence of wet climate anomaly tends to decrease in Indonesia especially in west Java, both globally and regionally.

According to rainfall historical data of West Java, rainfall is high in the months of February and March. Mean while, intraseasonal wave showed that wet anomaly was in Indonesian region in January 2011. However, Indonesia would be dominated by dry anomaly. Moderate wet anomaly is expected to occur in Indonesia in mid February and March. (Figure 4).

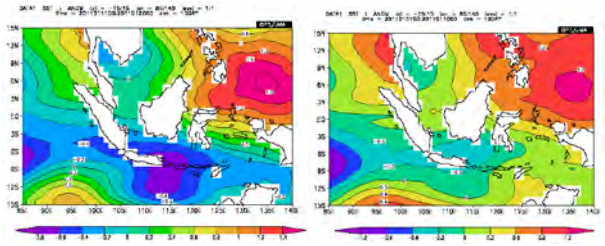


Figure 3. SST anomaly in January 2011.

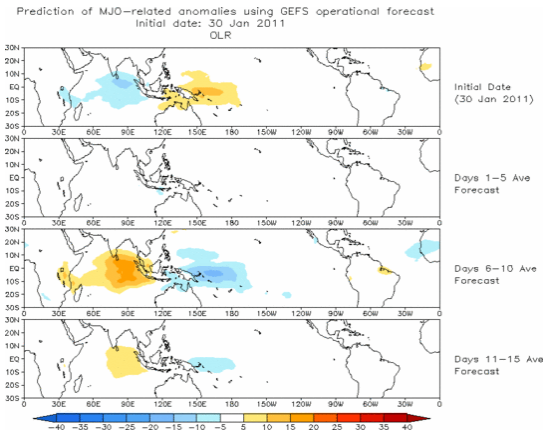


Figure 4. OLR's anomaly in intra seasonal wave. Blue indicates wet anomaly.

In the year of 2010, inflow of Citarum catchment area recorded the highest inflow in the last ten years. However, inflow of Citarum catchment area was very low in late 2010 and early 2011. In this period, the inflow of Saguling dam was recorded only 59 m^3/sec; Cirata dam was only 60 m^3/sec; and Jatiluhur dam was 20 m^3/sec, or total inflow of Citarum catchment area was only 139 m^3/sec. According historical data, inflow of Citarum catchment area for the same period is about 265 m^3/sec. In addition, the inflow indicated to keep decreasing.

Realizing that the three cascade dams within Citarum Catchment area had deficit inflow, PT. PLN (Persero) PT. Indonesia Power and PJT II had requested Weather Modification Technology Center of BPPT to carry out weather modification activity in Citarum catchment area, West Java. The three cascade dams are very strategic. These are used for hydro electric power plant, irrigation, and main supply of fresh water to Jakarta. Weather modification would be utilized to fill up the cascade dams. (Figure 5).

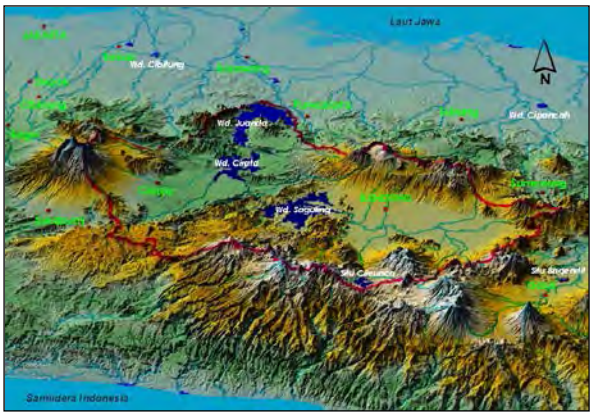


Figure 5. 3-D map of Citarum catchment area, West Java.

3. Cloud seeding activity in 2011

Cloud seeding activity has been carried out in Citarum West Java Province and Kotopanjang Riau Province. Cloud seeding in Citarum area has been conducted during 14 February – 8 April 2011, and in Kotopanjang area has been conducted during 15 May – 10 June 2011 as the first period, next period will begin at October. In this activity, the WMTC has utilized 1 unit of CASA 212-200 Rain Maker version (for Citarum operation) and 1 unit of Piper Cheyenne II (for Kotopanjang operation), 1 unit Mobile X-Band Doppler Radar, 3 units of theodolit-baloon, 58 units of rain gauges (that installed within the Citarum catchment area), 3 units of portable Global Positioning System, 3 units of Single Side Band radio communications, 1 unit of Ground To Air radio and Ground Support Equipments.

During 30 days cloud seeding activities over Citarum catchment area, we did 50 cloud seeding flights. The flight tracks may be seen on Figure 6.

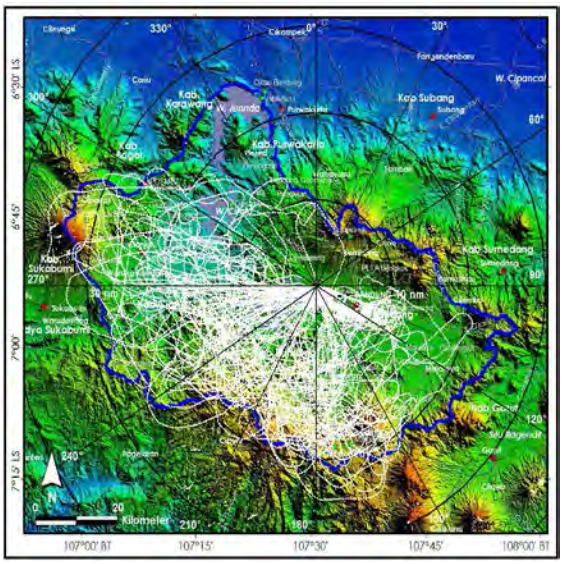


Figure 6. Flight tracks of cloud seeding activities conducted by Casa NC 212-200 in the period of 14 February -15 March 2011.

5. Infrastructure

To carry out cloud seeding using flares, pressurized aircraft such as Super King Air 200, and *Piper Cheyenne II* (Figure 7) were employed. While aircraft of NC 212-200 (Figure 8) were utilized when cloud seeding activities using seeding agents of NaCl. Right now, the WMTC - BPPT has 5 units of Casa NC 212-200 and 1 unit of Piper Cheyenne II.



Figure 7. Piper Cheyenne II (above) for seeding agents of flare, and Burn In Place and Hygroscopic flares (below).



Figure 8. Casa NC 212-200 for seeding agents in powder form.

Mobile X-band Doppler Radar (Figure 9) has been used to support cloud seeding activity. The radar was installed at the airport area in Bandung. It covers up to 150 km-radii. Therefore, it may cover whole Citarum catchment area. However, it has a dead zone of about 7 km. Mobile X-band Doppler radar is employed to monitor cloud type and coverage, rain rate, cloud's position and movement, cloud's thickness, cloud's development, and wind direction, and rainfall prediction. An example of radar's display can be seen on Figure 10.



Figure 9. Mobile X-band Doppler Radar.

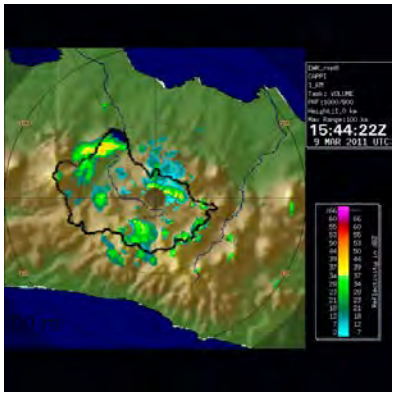


Figure 10. An example of Mobile X-Band Doppler Radar's display.

6. Rain Occurrence

Information of rain occurrence was obtained from 58 rain gauges installed within Citarum catchment area. The 58 rain gauges were distributed as follow: 34 were over Saguling catchment area, 20 were over Cirata catchment area, and 4 were over Jatiluhur catchment area.

Rain occurrence over Saguling and Cirata catchment area for the period of 14 February - 15 March 2011 can be seen on Figure 11.

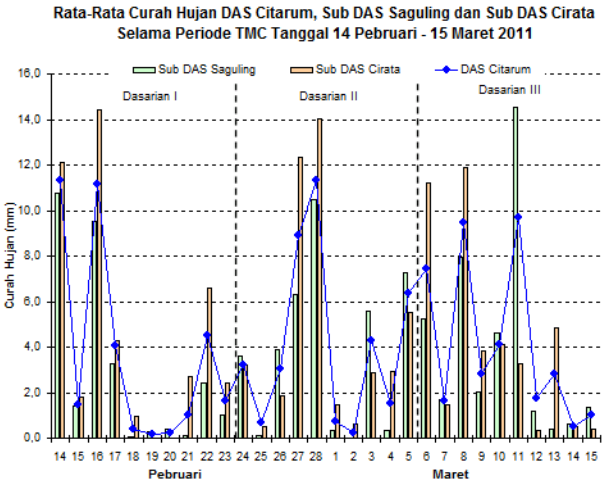


Figure 11. The average of rainfall data of Saguling and Cirata (part of Citarum catchment area) for period of 14 February - 15 March 2011.

Figure 10 shows that rain occurred everyday over Citarum catchment area. High rainfall data were recorded on 14 – 16 and 27 – 28 February 2011, and 6 – 11 March 2011. The highest rainfall in this period was 102 mm. It occurred over Saguling catchment area on 11 March 2011. Some high amount (ranged between 50 – 100 mm) of rainfall were also recorded in this period.

During this period, we observed that rainfall distribution varied over the Citarum catchment area. Rain occurred very sporadic. These indicated that air masses were dry. Spatial distribution of rainfall during this period can be seen on Figure 11.

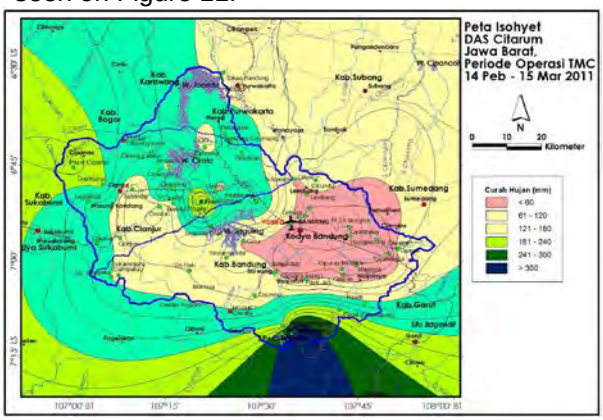


Figure 11. Rainfall Distribution over Citarum catchment area for period of 14 February – 15 March 2011.

7. Conclusion

1)Weather Modification has been conducted in Indonesia since 1983 to overcome water shortage. Weather modification activities were mostly to fill up dams for hydro electric power plant, irrigation and fresh water. Sometimes, weather modification was also carried out to extinguish field/forest fires and clear up smoke during dry season.

2)Weather modification in Indonesia is now playing an important role as tool for national water resources management.

3)Development of weather modification technology is urgently required. The WMTC-BPPT Indonesia needs to collaborate with both International institutions and inter-agencies in order to successfully improve the cloud seeding technique and research in Indonesia.

Acknowledgements

We would like to thanks to the Chairman of BPPT for his support to the 10th WMO Scientific Conference on Weather Modification held in Bali – Indonesia.

References

Erwin Mulyana, and Samsul Bahri, 2011 : *"International Symposium on Weather Modification, Recent Progress in Precipitation Enhancement Research"*, Tsukuba, Japan, March 3-4, 2011.

Samsul Bahri, Heru Widodo, Erwin Mulyana, Tri Handoko Seto, Sutrisno, and Halda Aditya, 2011 : *"Current State of Weather Modification and its prospect in Indonesia., Southeast Asia Hygroscopic Flare Weather Modification Technology Symposium",* Xian, China, April 8-11, 2011.

Weather Modification Technology Centre, Final Report : *"Cloud Seeding for Rain Enhancement over Citarum Catchment Area, West Java province, April 14-March 15, 2011"*, WMTC-BPPT, 2011.

Testing Efficacy of Rainmaking Activities in the Northeast of Thailand

Siriluk Chumchean[(1)] and Walairat Bunthai[(2)]

[(1)] Department of Civil Engineering, Mahanakorn University of Technology, 140 Cheum-Sampan Rd., Nong-chok, Bangkok, Thailand 10530, siriluk@mut.ac.th
[(2)] Department of Civil Engineering, Mahanakorn University of Technology, 140 Cheum-Sampan Rd., Nong-chok, Bangkok, Thailand 10530, bwairat@gmail.com

1. Introduction

During the past decade, weather radar has played more important role in measuring rainfall. It provides detailed information of clouds and precipitation within an operational measurement radius. Therefore, it has been used to assess efficacy of rainmaking activities in several countries. In Thailand, the Bureau of Rainmaking and Agriculture Aviation of the Ministry of Agriculture and Cooperatives has conducted cloud seeding activities for rain enhancement since 1969. Effectiveness of rainmaking activities in Thailand has been evaluated by comparing average rainfall intensity and accumulated rainfall amount of rain-cells that occur inside and outside a rainmaking's benefit area (Chumchean et al. 2010). It is considered that the rainmaking activities are successful if average rainfall intensity and accumulated rainfall of the rainmaking's benefit area are greater than outside the benefit area. It should be noted that the rainmaking's benefit area is assumed to be a conical shape at the height of 1,000 to 10,000 feet from the ground surface which has an approximate area of 20,356 km^2 (Dechyotin, 2008). This area is located perpendicularly to the cloud seeding flight route and it is parallel to downwind direction as illustrated in Figure 1.

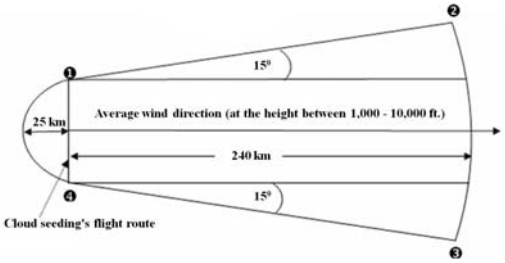


Figure 1. Rainmaking's benefit area (Dechyotin, 2008).

For each of any operational rainmaking day, the rainmaking's benefit area will be assigned by an operational team during their meeting for planning of cloud seeding procedure. Normally, the meeting has been performs at 9 am. The cloud seeding activity starts around 10:00 – 10:30 am and completes around 14:00 – 15:30 pm. However, a number of questions have been raised regarding to an identification of rainmaking's benefit area and effects of cloud seeding on occurrence of artificial rainfall. The objectives of this paper were 1) to examine suitability of the specified rainmaking's benefit area and 2) to test the efficacy of rainmaking activities in the North of Thailand.

2. Data

The 2.5-km **C**onstant **A**ltitude **P**lan **P**osition **I**ndicator (CAPPI) data recorded from the Pimai radar during 2006-2009 were used in this study. The CAPPI products have 6 minutes and 1 km^2 temporal and spatial resolutions, respectively. The Pimai radar is a S-band radar which owned and operated by the Bureau of Royal of Rainmaking and Agricultural Aviation. It is located in Nakorn-ratchasima Province in the Northeast of Thailand as shown in Figure 2.

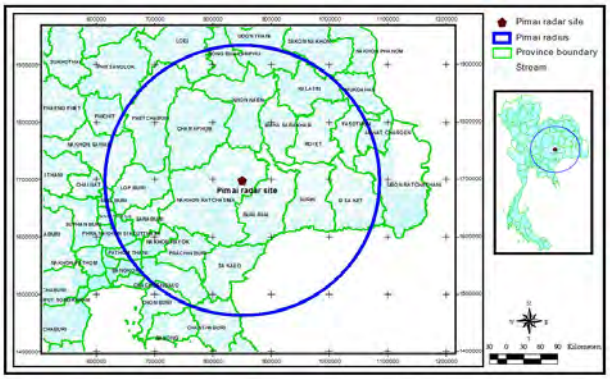


Figure 2 Study area located within 240 km of the Pimai radar site.

Quality control of the reflectivity data was performed. Errors due to radial anomality, ANAPROP, other signals that did not represent rainfall and errors caused by electronic problems were removed from the measured reflectivity data. Reflectivity data that were greater than 53 dBZ were limited to 53 dBZ to mitigate contamination from hail (Fulton et al., 1998). To avoid the effect of noise in the measured radar reflectivity, the reflectivity that are less than 15 dBZ were excluded from the analysis. Based on quality checking of the reflectivity data as mentioned above, 21 rainfall events occurred during the operational rainmaking days between August 2006 to April 2009 were selected to use in this study.

3. Methodology

To examine effectiveness of cloud seeding of an operational rainmaking day, a number of radar pixels that lied within 240 km from the Pimai radar were randomly selected for 100 times regardless whether they were located inside or outside the specified rainmaking's benefit area. At each randomized time, the total area of all randomly selected radar pixels must be equal to the specified rainmaking's benefit area, thereafter referred as "*randomized area*". For each operational rainmaking day, radar rainfall were calculated by converting radar reflectivity into rainfall rate using climatological Z-R relationship of the Pimai radar ($Z=56.5R^{1.5}$) proposed by Chumchean et al. (2009). Thereafter, accumulated radar rainfall, average rainfall intensity and maximum of the average rain rate of the rainmaking's benefit area and the 100 randomized areas were calculated for the entire seeding effect period. In this study, we considered that the seeding effect period was duration between a starting time of cloud seeding procedure and time when rain-cells decayed or moved away from the benefit area.

To investigate differences of rainfall characteristics between rain-cells that fell over the rainmaking's benefit area and the randomized areas of each operational rainmaking day, accumulated rainfall, average rainfall intensity and maximum of the average rain rate of these areas were compared. Statistical testing at 95% and 90% confidence levels with a one-tailed *t-test* was used in the analysis. It was hypothesized that accumulated rainfall, average rainfall intensity and maximum of the average rain rate of the rainmaking's benefit area were higher than the randomized areas. This was because during the operational of cloud-seeding, the hygroscopic materials for rain enhancement were spread into the clouds. These rainmaking materials included sodium chloride, calcium oxide, calcium chloride, urea and dry ice. Sodium chloride, calcium oxide and calcium chloride are accelerators of a collision-coalescence process, leading to the development of rainfall and consequently causing more raining area and high rainfall amount of the cloud-seeding rain-cells (Silverman and Sukarnjanaset, 1999; Plonharn et al., 2008). In addition, urea and dry ice help to increase a condensation at cloud base level, causing more rainfall amounts (Plonharn et al., 2008). The null hypothesis (H_0) and alternative hypothesis (H_1) of this study were defined as follows:

$$H_0 : \mu_s \leq \mu_r \quad (1)$$

$$H_1 : \mu_s > \mu_r \quad (2)$$

Where μ_s and μ_r represented accumulated rainfall, average rainfall intensity and maximum of average rain rate of the specified rainmaking's benefit area (*s*) and randomized areas (*r*), respectively.

4. Results and Discussion

The seeding effect periods of 21 operational rainmaking events used in this study were investigated using radar rainfall data as the results were illustrated in Figure 3. It was found that the average seeding effect period of the 21 operational rainmaking events was about 8.4 hrs which corresponded to the study of Woodley and Rosenfeld (2004). For each operational rainmaking day, accumulated rainfall, average rainfall intensity and maximum of the average rain rate of the specified rainmaking's benefit areas and 100 randomized areas were estimated as the results presented in Figures 4-6.

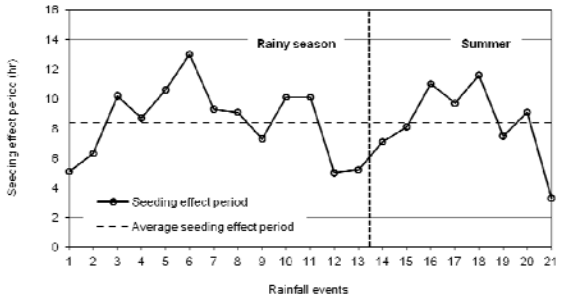


Figure 3. Seeding effect periods

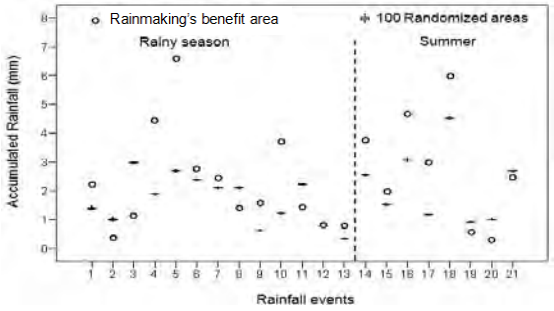


Figure 4. Accumulated rainfall of the specified rainmaking's benefit area and 100 randomized areas.

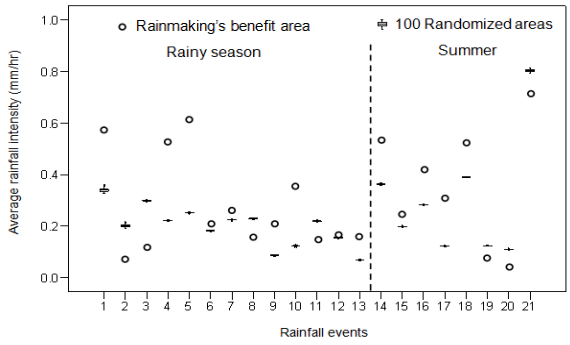


Figure 5. Average rainfall intensity of the specified rainmaking's benefit area and 100 randomized areas.

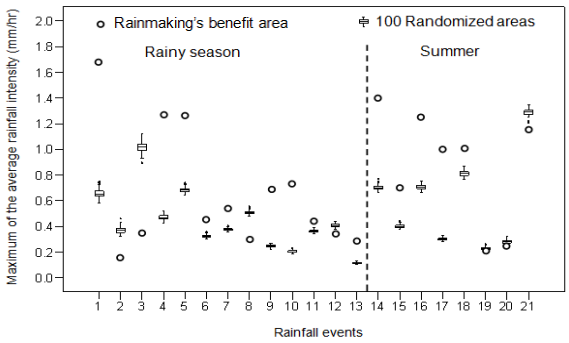


Figure 6. Maximum of the average rain rate of the specified rainmaking's benefit area and 100 randomized areas.

For each rainfall event, *p-value* and *t-value* of accumulated rainfall, average rainfall intensity and maximum of the average rain rate of the specified rainmaking's benefit area and the 100 randomized areas were calculated as presented in Figure 7.

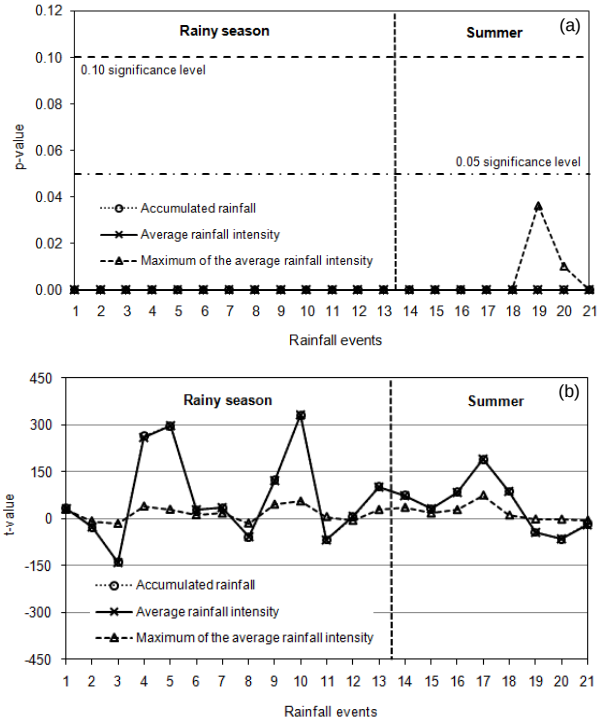


Figure 7. Statistical testing between rainfall characteristics of rain-cells that occurred inside the specified rainmaking's benefit area and 100 randomized areas.

The results presented in the Figures 4-7 showed that 14 in 21 rainfall events had higher average accumulated rainfall, average rainfall intensity and maximum of average rain rate of the specified rainmaking benefit area than the 100 randomized areas. Statistical testing of the differences between the accumulated rainfall, the average rainfall intensity and the maximum of the average rain rate of the specified rainmaking's benefit area and the mean of the 100 randomized areas of these 21 rainfall events were evaluated as the results were established in Table1.

Table 1. Statistical testing of the differences between rainfall characteristics of 21 operational rainmaking days.

Rainfall characteristics	Average of 21 events		*p-value*	*t-value*
	Inside rainmaking's benefit area	Mean of 100 randomized areas		
Accumulated rainfall (mm)	2.48	1.87	0.09	1.35
Average rainfall intensity (mm/hr)	0.30	0.24	0.13	1.16
Maximum of the average rain rate (mm/hr)	0.73	0.48	0.02	2.10

The results from the table 1 showed that the accumulated rainfall of the specified rainmaking's benefit area was higher than the mean of 100 randomized areas at 9% significance level. The maximum of the average rain rate of the specified rainmaking's benefit area was higher than the mean of 100 randomized areas at 2% significance level. The average rainfall intensity of the specified rainmaking's benefit area was higher than the mean of 100 randomized areas but it was not significant at 0.1 level.

The study of Chumchean et al. (2010) indicated that for any operational rainmaking days, amount of rainfall that occurred inside the rainmaking's benefit area corresponded to their upper air conditions. They found that the upper air data that had significant influence to the occurrence of artificial rainfall included showalter (SI), 50 MB lifted index (LI), KI index and average relative humidity (RH) at convective condensation level (CCL). High rainfall amount was observed if SI and LI indexes were low while KI index and average RH at CCL were high. This might be the reason that leaded to the lower accumulated rainfall, average rainfall intensity and maximum of the average rain rate of the specified rainmaking's benefit area when compared to 100 randomized areas for some of the operational rainmaking days where their upper air conditions were not suitable for cloud seeding.

Therefore, to investigate the potential efficacy of rainmaking activities, only the operational of rainmaking days with suitable upper air conditions for cloud seeding were used for statistical testing of the difference between rainfall characteristics of rain-cells that occurred inside the rainmaking's benefit area and the 100 randomized areas. Based on the data used in this study, it was found that the upper air conditions of rainfall events No.3, 20 and 21 were not suitable for cloud seeding. The upper air data of these 3 events were as follows; event No.3: SI = 4.3, LI = 2.2, KI = 29.7, RH at CCL = 70.5%; event No. 20: SI = 4, LI = 1.5, KI = 24.1, RH at CCL = 42.3%; event No. 21: = 3.4, LI = 4, KI = 21.7, RH at CCL = 42%. Thus, only the rest 18 operational rainmaking days were used for the above statistical testing and the results were illustrated in Table 2.

Table 2. Statistical testing of the differences between rainfall characteristics of 18 operational rainmaking days with suitable upper air conditions for cloud seeding.

Rainfall characteristics	Average of 18 events		*p-value*	*t-value*
	Inside rainmaking's benefit area	Mean of 100 randomized areas		
Accumulated rainfall (mm)	2.67	1.81	0.05	1.74
Average rainfall intensity (mm/hr)	0.30	0.21	0.03	2.02
Maximum of the average rain rate (mm/hr)	0.76	0.42	0.01	2.82

From the above table, it was evident that the accumulated rainfall, the average rainfall intensity and the maximum of the average rain rate of the specified rainmaking's benefit area were higher than the mean of 100 randomized areas at 5%, 3% and 1% significance levels. This result showed effectiveness of cloud seeding activities for rain enhancement in the North of Thailand. It also assure that the specified rainmaking's benefit area described in section 1 can be used to represent raining area of artificial rainfall that occurs due to effects of cloud seeding.

6. Conclusions

The results of this study can be concluded as follows:

- The average seeding effect period of cloud seeding activities in the North of Thailand was about 8.4 hrs after the starting time of cloud seeding procedure.
- For the operational rainmaking days with suitable upper air conditions for cloud seeding, the accumulated rainfall, the average rainfall intensity, the maximum of rain rate of the specified rainmaking's benefit area were higher than the mean of 100 randomized areas at 5%, 3% and 1% significance levels, respectively. This showed effectiveness of cloud-seeding activities in the study area.
- The specified rainmaking's benefit area considered in this study can be used to represent raining area of artificial rainfall that occurs due to effects of cloud-seeding.

Acknowledgements

The authors gratefully acknowledge the Bureau of Royal Rainmaking and Agricultural Aviation for funding support by grant No. 23/2552 and providing the data used in this study.

References

Chumchean S. Aungsuratana P. Khommuang A. and Hanchoowong R, Study of rain-cloud characteristics using weather radar data. 18th World IMACS/MODSIM Congress, Cairns, Australia, 3682–3688, 13-17 July 2009.

Chumchean S. Hanchoowong R. and Bunthai W, Comparison between rainmaking and natural rainfall in the northeastern part of Thailand. 5th APHW Conference, Hanoi, Vietnam, 8-10 November 2010.

Dechyotin C, Design and testing of software for estimation of rainmaking's benefit area. Research and development rainmaking technology, Bureau of royal rainmaking and agricultural aviation, Thailand, 2008.

Futon R A. Breidenbach J.P. Seo D.J. Miller D.A. and O'Brannon T, The WSD–88D rainfall algorithm. Weather Forecasting, 13, 377 – 395, 1998.

Plonharn T. Sornboonthai S. and Kleanpratoom S, Hygroscopic Materials for Rain Enhancement. Bureau of royal rainmaking and agricultural aviation, Thailand, 2008.

Silverman B A. and Sukarnjanaset W, Results of the Thailand warm-cloud hygroscopic particle seeding experiment. J *App.Meteol*., 39, 1160-1175, 1999.

Woodley W L. and Rosenfeld D, The Development and Testing of a New Method to Evaluate the Operational Cloud-Seeding Programs in Texas. J *App.Meteol*., 43, 249 – 263, 2004.

Experimental studies of salt powder efficiency at convective cloud modification for precipitation enhancement

A.S. Drofa, V.G. Eran'kov, V.N. Ivanov, A.G. Shilin, G.F. Yaskevich
RPA "Typhoon",4, Pobedy st., Obninsk, Kaluga Region, 249038, Russia, e-mail: drofa@typhoon.obninsk.ru

The studies of an effect of convective clouds seeding with salt powder (NaCl) for precipitation enhancement are made in (Drofa et al., 2010). The experimental results supported by the results of numerical simulation showed that the use of the salt powder has numerous advantages in the effect of modification and in the consumption of the agent against hygroscopic particles generated by pyrotechnic flares (Cooper et al., 1997). The given paper presents the results of experimental studies of the efficiency of a polydisperse salt powder developed at RPA 'Typhoon' (Obninsk, Russia) for stimulating precipitation from convective clouds.

Experimental studies of a salt powder seeding effect on a cloud medium were performed in the Big Cloud Chamber (BCC) of RPA 'Typhoon'. The BCC is designed for modeling convective or stratified clouds and fogs of different origin under the conditions close to those in the real atmosphere. The chamber is a steel airtight cylinder of 18-m height and 15-m diameter. The total volume of the chamber is 3200 m^3.

The process of convective cloud medium formation in the BCC is made through air expansion. For this external air is pumped into the chamber. As a result the air pressure in it is increased to the level of 1300 hPa. The air pressure decrease is made by opening holes in the upper part of the chamber. The air discharge from the chamber through the holes of different cross sections makes it possible to regulate the rate of pressure decrease in the chamber, thus setting a certain velocity of air updraft in the atmosphere during the formation of a convective cloud. Air temperature, pressure, humidity and the chamber wall temperatures are basic parameters for setting thermodynamic conditions in the BCC. These parameters are continuously measured during the experiments in the BCC. In the efforts described in this paper the pressure decrease in the BCC was made with the velocity of air mass updraft in the atmosphere of 1.3 m/s. Relative humidity of air in the chamber before the pressure drop is usually 90 – 96%. The air temperature is 22 – 25ºC.At such values of meteorological parameters a cloud medium in the BCC is formed in 2 – 3 min after the beginning of the pressure lowering. During ≈15 min the process of cloud medium formation in the BCC may be considered adequate to the process of convective cloud formation in the real atmosphere. The total lifetime of the cloud in the BCC is 40 – 50 min. At the chosen mode of air pressure lowering a cloud medium with the drop concentration from 1300 to 1900 cm^{-3} is formed. The liquid water content of the medium grows linearly with time and by 12 min it becomes equal to 0.8 g/m^3. The largest drops in the background experiments reached the radii of 12 μm.

For measurements of cloud medium microstructure the BBC is equipped with the photoelectric particle analyzer developed at RPA "Typhoon". This device is based on measurements of light scattered from particles at an angle of 90º. The operation principle of this device is in the analysis of amplitudes of pulses of light scattered from single particles at their flight through the measuring volume. For this, the calculated dependences of scattered light intensity on a drop size are used. The range of measured drop radii with this meter is within 1 – 50 μm. The number of drop size measuring channels is 360. The photoelectric meter allows one to obtain cloud drop spectra at the time of data accumulation from 1 s at the medium flow rate through the measuring volume over 2.5 cm^3/s. The particle concentrations are determined from the pulse frequency of light scattered from every particle. The particles size distribution function is constructed from the analyzer data. The integral parameters of the size distribution function such as mass concentrations and effective radii of the particles are also calculated.

The agent under study is a specially prepared powder of NaCl with aerosil (SiO_2) used as an anticaking admixture. The measurements of microstructure of the dry salt particles under this study were made in the BCC at the air relative humidity of about 40%. After the salt powder was introduced into the chamber with the pneumatic atomizing nozzle the aerosol was uniformly mixed inside the chamber and measured there. To study the microstructure of the salt powders made a laser and TV aerosol analyzers developed at RPA 'Typhoon' were used.

A TV-analyzer was used for the analysis of larger in size particle distributions. This device analyzes the particles coming into the microscope field of view, the sizes of which are then measured. The range of measured particles radii is from 1 to 50 μm. The number of channels is 200. As the results of TV-analyzer measurements show, the particles with radii over 15 μm are not observed in the samples of the salt powder under study. The analysis of particle images registered with the TV-analyzer showed that the particles with the radii over 6 μm rather frequently have the form of conglomerates of large salt particles with finer salt particles or aerosil stuck to them.

The laser analyzer is designed for measurements of solid aerosol particles

microstructure. It is based on measurements of light scattered from aerosol particles in the range of scattering angles from 60° to 120°. A continuously operating laser at the 0.63 μm wavelength serves as a light source in this analyzer. The laser analyzer operation characteristic is calculated with the account for the geometric peculiarities of its optical scheme. The aerosol under study is supplied via a thin capillary into the region of laser beam focusing. The flow rate of air passing through the analyzer volume is 1 cm^3/s. The laser analyzer makes it possible to measure particle size distributions within the particle radii of 0.1 – 5 μm. The number of particle size measurement channels is 120.

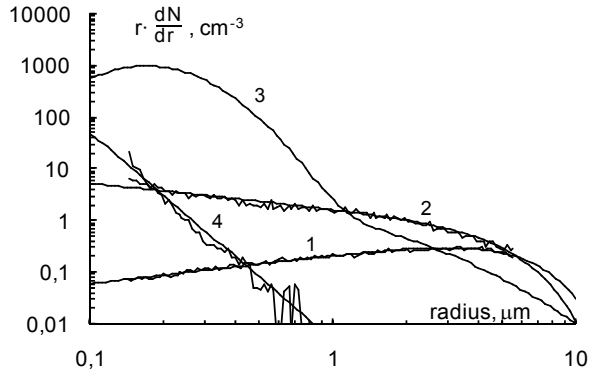


Figure 1. Aerosol particles spectra.
1 – salt powder produced at RPA 'Typhoon';
2 – salt powder presented in (Drofa et al., 2010);
3 – hygroscopic particles of pyrotechnic compound;
4 – background aerosol in BCC.

The results of dry salt particles microstructure measurements made with the laser analyzer are given in Figure 1. The Figure shows the salt particles size distributions for the salt powder developed at RPA 'Typhoon'. Here also shown are the salt particles size distributions for the salt powder presented in […] and the spectra of background aerosol. The measurements were performed at similar mass concentrations (about 0.4 mg/m^3) of salt powders introduced into the BCC. The spectra are obtained during the time of data accumulation of about 10 min. The spectrum of salt powder particles was obtained by subtraction of background aerosol spectrum from the aerosol spectrum in the BCC after the introduction of the salt powder. The spectrums of salt particles, as is seen from Fig. 1, is rather well approximated by the distribution like

$$f(r)=a\, r^{-v}\, exp(-(r/r_o)^2), \qquad (1)$$

where a is the normalizing factor. The values of parameters v and r_0 for the salt powder presented in (Drofa et al., 2010) are: v = 1.5 and r_0 = 5 μm. For the powder of SI RPA 'Typhoon': v=0.5 *and* r_o = 5.3 μm. From comparison of the parameters of the spectra studied it follows that the powder in (Drofa et al., 2010) differs in a larger content of finely-dispersed particles.

For comparison, the particle size distribution of the South African hygroscopic flares (Cooper et al., 1997) is given in Figure 1 at a mass concentration equal to the salt powder concentration of 0.4 mg/m^3. Figure 1 reveals that the South African flares contain a very high number of particles with r<1 μm as compared to the salt powder. At the same time, the particles with r>1 μm are much less in number.

The present paper gives the measurement results of changes of the cloud microstructure in the cloud chamber at the introduction of the salt powder and the estimations of the impact of the salt powder based on the observed changes of the cloud microstructure. The experiments in the BCC on cloud medium modification by the salt powder were performed according to the following method. The pumping of the chamber up to the initial high pressure was made. The salt particles were injected into it by a pneumatic atomizing nozzle. With the help of fans the aerosol was uniformly mixed inside the chamber. The salt particles were introduced into the chamber at a relative humidity of about 96%. By this, the conditions of particles introduction into the subcloud layer of a convective cloud were simulated. The modification effect was assessed from the results of comparing the parameters of the cloud medium with the corresponding parameters during the background experiment (without the introduction of salt particles).

Figure 2 gives the results of cloud drop spectrum measurements at different time steps at the introduction of the salt powder into the BCC with mass concentration of 0.67 mg/m^3. As is seen from Figure, the introduction of salt particles manifests itself in the large-drop cloud spectrum fraction – in the 'tail' of drop distribution the drops formed on salt particles appear. Maximum radius of drops observed in this case reached 16 μm, that is significantly higher than that in the background experiment. Fine-droplet spectrum range did not practically change as compared to the spectra obtained in the background experiment. The spectrum maximum in this range is formed on the background condensation nuclei.

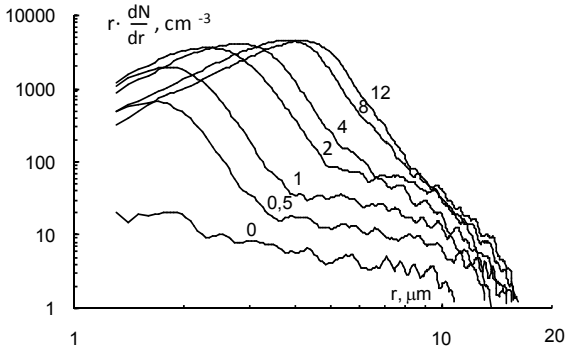


Figure 2. Evolution of cloud drop spectra at introduction of 2 g of salt powder into the BCC.
Numbers at the curves – time after the beginning of cloud medium formation, min

Figure 2 shows a drop spectrum at the initial moment of cloud medium formation. These drops

are covered with water salt particles not-dissolved completely in water.

Temporal variations of cloud drop spectra at the introduction into the BCC of the salt powder with the mass concentration of 8.7 mg/m^3 are shown in Figure 3. As is seen from the Figure, at such significant concentrations of particles introduced a bimodal character of cloud spectrum is clearly defined.

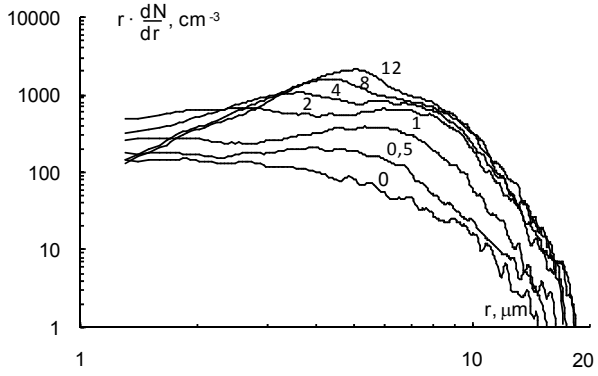


Figure 3. Evolution of cloud drop spectra at introduction of 27 g of salt powder into the BCC.
Numbers at the curves – time after the beginning of cloud medium formation, min

The fine-droplet spectrum mode is formed on the background aerosol (particles), and the large-drop fraction – on salt particles. The spectrum maximum of drops formed on the background aerosol is created later than in the background experiment. This effect can be explained by the fact that at the introduction of a great number of salt particles water vapor supersaturation in the cloud medium decreases, thus resulting in a slower growth of drops formed on background condensation nuclei. The sizes of the largest drops here are considerably greater than in the background aerosol. But due to sedimentation, they fall on the floor of the BCC, and in the spectra measured after the 4th minute of the cloud medium formation large drops with the radii more than 20 μm are not observed. A necessary condition for obtaining the positive effect at modification with hygroscopic particles (additional precipitation from clouds) is a growth of cloud drops caused by the introduction of particles as far as the enlargement of cloud drops is the main factor of stimulating the gravitational-induced coagulation in clouds with subsequent precipitation formation.

The changes in cloud drop sizes in the modification experiments were estimated by us from the changes in their concentrations against drop concentrations in the background experiment. Under similar experimental conditions (the same liquid water contents of the media) the relationship $N_b/N=(r/r_b)^3$ is fulfilled, where r and r_b, N and и N_b are effective drop radii and their number concentrations at modification and in the background experiment, correspondingly. Here, the value of N_b/N characterizes a change in cloud drop sizes under modification. The effect of modification can be considered positive at $N_b/N>1$ (i.e. when the cloud drops become larger). The value of N_b/N may serve an estimate of the effect of cloud modification with hygroscopic particles (Drofa, 2006). The more the value of N_b/N is realized in the subcloud layer, the greater precipitation amounts can be obtained due to modification. The results of cloud drop concentration measurements obtained at different number concentrations of salt particles introduced are given in Figure 4. As is seen from the Figure, with increasing the concentration of particles introduced, the effect of cloud drop enlargement grows practically linearly. From Figure 4 it is also seen that the effect of cloud drop enlargement at seeding with the salt powder of RPA 'Typhoon' is considerably higher than the effect the effect from the powder presented in (Drofa et al., 2010) – to obtain a similar effect of modification considerably smaller number of salt particles are needed. It is explained by the presence of a significant portion of fine-disperse particles on which small cloud droplets not contributing much in the enlargement of cloud drops in their whole population are formed.

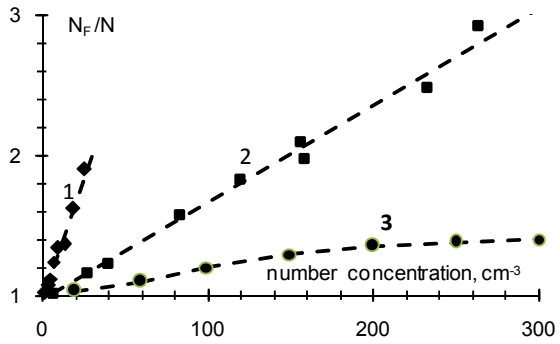


Figure 4. Dependence of cloud drop concentration on the concentration of particles introduced.
1 – salt powder produced at RPA 'Typhoon';
2 – salt powder presented in (Drofa et al., 2010);
3 – particles of South African pyrotechnic compound.

For comparison, the calculation data of cloud drop concentration at seeding with hygroscopic particles from the South Africa pyrotechnic compound are give in Figure 4. The calculations were made with the method proposed in (Drofa, 2006) for the conditions corresponding to the conditions of cloud medium formation during experiments in the BCC. As is shown in (Drofa, 2006), maximum effect of modification with particles having narrow size distributions is achieved at certain concentrations of particles introduced. Their values are determined by atmospheric conditions and the relation of parameters characterizing atmospheric aerosol and the hygroscopic particles introduced. For the conditions realized during the experiments in the BCC the calculation results give the estimate of N_b/N = 1.42. This value is obtained at the

concentration of particles of 300 cm^{-3}. The mass concentration of the pyrotechnic compound introduced in this case is $W \approx 0.05$ mg/m^3. At higher or lower concentrations the value of N_b/N decreases. At mass concentrations $W > 0.14$ mg/m^3 the effect of 'overseeding' appears, i.e. at the introduction of a great number of such particles drop concentration in the cloud grows and the drops average size decreases. Just this is the reason for decreasing the intensity of precipitation formation in a cloud under 'overseeding'. The seeding with the salt powder, as is seen from Figure 4, does not lead to the effect of 'overseeding' at rather high mass concentrations of introduced particles.

As the above-mentioned data show, with salt powders, large drops with the radii over 20 μm are not observed because of their sedimentation onto the BCC floor in the cloud drop spectra obtained during the experiments with salt powders. At the same time, the data on the number of such drops may be rather a significant estimate of the modification effect because the largest drops in the cloud spectrum determine the intensity of coagulation processes for precipitation formation in the cloud. For experimental assessing the number of large drops falling from the cloud medium during experiments the measurements of sediment drops were performed. For this, a platform with the area of 0.5 m^2 was installed on the BCC floor. The mass of this platform during the experiment in the BCC was constantly controlled by an electronic analytical balance. Thus, during the experiment the mass of water collected on the platform due to falling drops was measured.

The measurement results of the mass of water collected during experiments in the BCC are shown in Figure 5. Here shown is the temporal

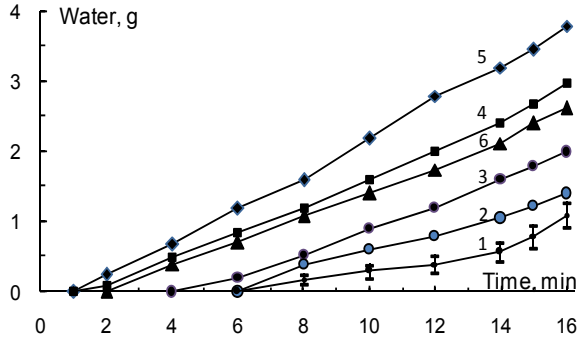


Figure 5. Changing of precipitating cloud drop mass with time in experiments on salt powder seeding.
1 – background experiment; 2 – introduction of 7 g of powder; 3 – 10 g; 4 - 20 g; 5 – 27 g;
6 – introduction of 20 g powder presented in (Drofa et al., 2010).

trend of changes in the mass of water accumulated in the experiments with the introduction of salt powders and in the background experiments. As is seen from Figure 5, precipitation of large cloud drops in the background experiments begins to reveal itself after the 6-th min of cloud medium formation in the chamber. Vertical segments in the graph (background measurements) show the scatter of measurement data in separate experiments. By the 16-th min of experiments from 0.9 to 1.3 g of water were collected. In the experiments with salt powders, as one can see in the Figure, the process of drop settling begins earlier. The mass of accumulated water increases with increasing the mass of the salt powder introduced into the BCC. The data of accumulated water measurements may serve as a comparative estimate of the modification effect at testing different hygroscopic agents. From Figure 5 it is seen that at similar amounts of powders introduced the mass of collected water at seeding with the powder of RPA 'Typhoon' is significantly greater than in the case of the powder presented in (Drofa et al., 2010). So it can be concluded that the effect of large drop formation caused by the salt powder of PRA

Thus the results of experimental studies show that the introduction of the salt powder into a cloud medium under formation results in the formation in the large-drop spectrum 'tail' of an additional number of large drops and in the broadening of drop spectrum. This result is a positive factor for stimulating coagulation processes in clouds and precipitation formation. No effect on the fine-drop spectrum formed on the background condensation nuclei is seen at rather considerable concentrations of the powder introduced. Seeding with the salt powder leads to enlargement of the whole population of cloud drops and to a decrease of their total concentration as compared to the background cloud medium. With an increase o the mass concentration of the particles introduced this effect increases. This effect is also a positive factor for stimulating the transformation of cloud drops into rain drops. At rather high concentrations of the salt powder the effect of 'overseeding' (at which instead of drop enlargement the reduction of their sizes and an increase of cloud drop concentration occurs) is not observed.

References

Cooper W.A., Bruintjes R.T., Mather G.K., Calculations pertaining to hygroscopic seeding with flares. *J. Appl. Meteorol*., **36**, 1449–1469, 1997.

Drofa A.S., Formation of cloud microstructure: the role of hygroscopic particles. *Atmos. Ocean. Phys.,* **42**, 326-336., 2006.

Drofa A. S., Ivanov V. N., Rosenfeld D., Shilin A.G., Studying an Effect of Salt Powder Seeding Used for Precipitation Enhancement from Convective Clouds. *Atmos. Chem. Phys*., **10**, 8011-8023, 2010.

The Study of Distribution Character on Aerosols, Cloud Droplet and CCN over North China Useing Aircraft Observational Data

Duan Ying[1], *Duan Jing*[2] ， *Ju liling*[3]

[1]*Weather Modification Office of Hebei Province, China, 050021,hbwmo@heinfo.net*
[2]*Chinese Academy of Meteorological Sciences, Beijing, China,100081,weatherdj@126.com*
[3]*Hengshui Meteorological Bureau of Hebei Province,China, 053000,qhd12121@sina.com*

1. Introduction

Over the past 20 years, it been studied extensively on the cloud and precipitation physical characteristics, aerosols interaction with clouds in worldwide. For example, Breon, F.-M., D. Tanre et.al (2002), Rosenfeld.D (2000) researched the interaction among aerosol, clouds and precipitation.Shi Guangyu et al (1996) studied the vertical distribution of atmospheric ozone and aerosol by air-balloon.

Since 2000 year, in order to study the distribution character of aerosol, Cloud droplet and CCN in different types of clouds over the North China. A large number of measurements by aircraft during 2005 to 2010 were analyzed. For example, Duan, J., and J. T. Mao (2009), researched for Influence of aerosol on regional precipitation in North China .Shi lixin et.al (2008), using a DMT (Droplet Measurement Technologies) continuous flow streamwise thermal gradient cloud condensation nuclei (CCN) counter installed in a Cheyenne IIIA aircraft, CCN measurements about 20 flights over the North China were completed in the autumn of 2005 and spring of 2006. The CCN distribution characteristic was analyzed inside and outside clouds from the vertical and horizontal measurement. Duan Ying et.al (2000-2010) primarily analyzed the distribution character of aerosol and CCN in different geography environment of north China area.

In this study, based on two observations of the Hebei province in north China at May 27, 2010 ,October 4, 2008, the data of PMS (Particle measurement System) and above-mentioned CCN counter on the aircraft are used, the distribution character of aerosol and CCN is primarily analyzed.

2. Instrument and methodology

Hebei province is located in the north of China, Beijing and Tianjin is surrounded with it, the Bohai sea gulf is in the east of Hebei province. In this study, the data from A Piper Cheyenne ⅢA twin urbo-prop aircraft was used to observe the clouds and precipitation. The aerosol was measured by a PMI (Particle Metrics Inc, USA) Aerosol Spectrum Probe (size range 0.1～3.0 micron). The cloud droplet was measured by a FSSP-100ER probe (size range 1～95 micron). Two-dimensional gravity-scale probe OAP-2D-GA2 (25 ~ 800μm) and OAP-2D-GB2 (150 ~ 9300μm) were used, they are the 2D - C and 2D - P probes can provide two-dimensional particle image. In addition, the aircraft is also equipped with a thermometer, dew point, pressure sensors, GPS and other devices to obtained temperature, dew point, barometric pressure, altitude, airspeed and other data.

In this sduty, the measurement range of FSSP-100ER probe set up as 2 ~ 47μm (range “1”) , so that get the cloud particle concentration, liqiud water content, average particle diameter data, corresponding. CCN were measured by a DMT (Droplet Measurement Technologies, USA) continuous flow streamwise thermal gradient CCN counter.CCN measuring principle with a chemical gradient diffusion chamber (Twomey and Squires, 1959).Since that time, nearly all measurements have used the thermal gradient diffusion chamber. All early measurements were made with static photographic instruments that used batch processing of the samples. In other words, continuous flow chambers using optical particle counters. The supersaturation is set at S=0.3% in observations of this sduty.

Weather Modification Office of Hebei province bought airborne cloud physical instruments from USA and modified a Cheyenne IIIA aircraft in 2004. The instrument for CCN measurement is DMT (Droplet Measurement Technologies, USA) CCN counter.

Specially modified aircraft and airborne equipment for the detection of cloud physics are shown in figure 1.



Fig.1 specially modified aircraft and airborne equipment

3. Results and analysis

3.1 Distribution of aerosol and CCN

In order to understand the distribution characteristics of atmospheric aerosol and cloud physical effects, May 27, 2010, the airborne aerosol probe (0.1-3.0 microns), forward scattering spectrum drops probe FSSP-100ER (range is set 2 ~ 47μm) and cloud condensation nuclei counter were used, the

special detection flight was completed for a stratiform cloud precipitation process. Detection range included the central and southern Hebei province, at same time, the aircraft altitude, the cloud particle and CCN concentration, liquid water content (LWC), average particle diameter etc data were obtained.

Figure 2 shows the detection path of cloud physics aircraft flight. The mainly detection range of the aircraft is in south-central aera of Hebei province, including Shijiazhuang, Handan, Xingtai.

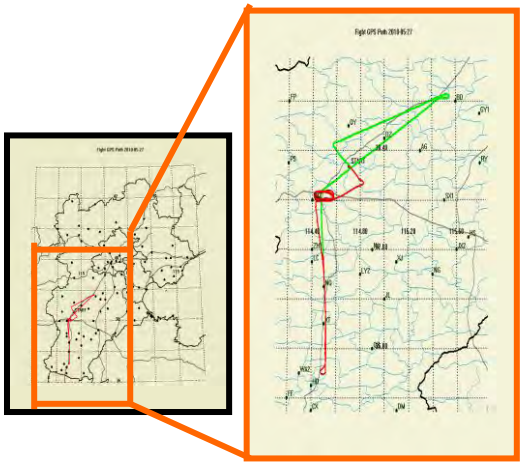


Fig. 2 aircraft flight path at May 27, 2010

Figure 3 shows that the aerosols and cloud condensation nuclei (CCN) with spatial and temporal distribution in the aircraft detection time at May 27, 2010. In figure 3, from Beijing time 11 o'clock start to 14 o'clock, the duration time nearly three hours. The vertical left axis indicates the aerosol and cloud condensation nuclei concentration, the units is cm^{-3}. The vertical right axis indicates height of aircraft flight, its units is meter.

The results shown in the figure 3, light blue curve shows the altitude change with time, the red solid point is the temporal and spatial distribution of aerosol concentration, the black solid point is the spatial and temporal distribution of CCN concentration.

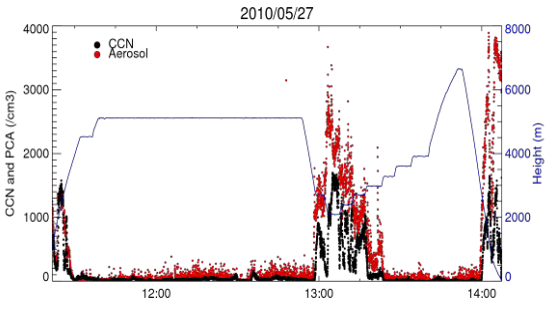


Fig. 3 the temporal and spatial distribution of aerosol and CCN concentration

In the above analysis, the concentration of aerosols and CCN changes are analyzed in the cloud base and inside the cloud. The results show that there is very difference in both cases（figure 4）.

The results shown in the figure 4, light blue curve shows that flight altitude change with time, the red curve is the distribution of aerosol concentration with time, the black curve is the distribution of CCN concentration with time, the green curve is the distribution of cloud droplet concentration with time by FSSP-100ER dada.

Compare of three curves in figure 4, the concentration of aerosols and CCN changes greatly within the cloud base level. Combination of macro-record dada analysis showed that the aircraft detect from 13:20 at the cloud base height of about 3000 meters to 13:24, horizontal flight lasted four minutes, the flight speed is 360 km / h, this flights continued 24 km straight distance. During this time, aerosols and cloud condensation nuclei concentration variation trend is consistent, but their values were the larger of difference between in them, in which aerosol concentration range is 200-600 cm^{-3}, the range of cloud condensation nuclei concentration is 50-150 cm^{-3}.To compare these two values, aerosol concentration is four times with CCN concentration.

On the other hand, the aircraft into to the altostratus cloud at 13:24, the flight height is about 3300 meters , horizontal flight lasted four minutes to 13:28, the flight speed is 360 km / h, the flight continued about 24 km horizontal distance too. During this time, although aerosols and cloud condensation nuclei concentration variation trend is consistent, but compared with the cloud outside (cloud base), their values were less then inside the cloud, in which aerosol concentrations range from 200-600 cm^{-3} reduced to less than 100 cm^{-3} quickly, the range of cloud condensation nuclei concentrations from 50-150 cm^{-3} quickly reduced to less than $10^{1} cm^{-3}$. Cloud droplet (see the green curve) appeared at same time, the results show that the aerosol is heavy consumed in cloud. Because converted to CCN and cloud droplets partly, the concentration of cloud condensation nuclei is reduced quickly.

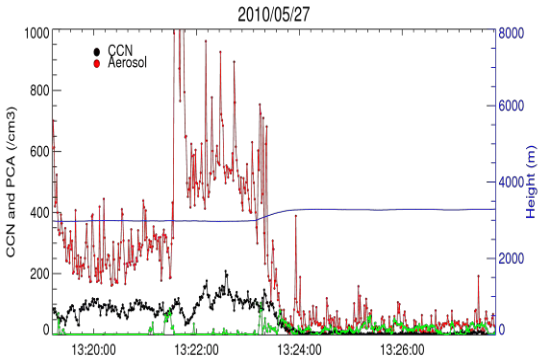


Fig. 4 aerosol and CCN concentrations comparison in cloud outside (bottom) and in cloud

In order to analyze aerosols, cloud condensation nuclei and cloud droplets in cloud base and cloud inside, the corresponding concentration and scale distribution between the spectra shown in figure 5. The results showed that the aerosol concentration and cloud condensation nuclei are very different, in two different conditions of inside and outside of cloud.

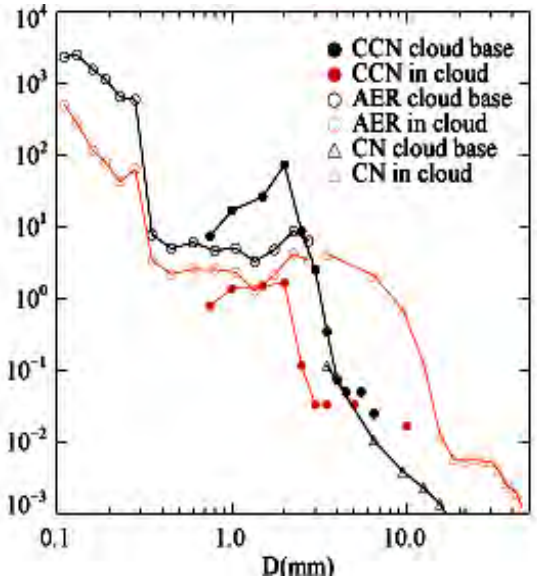


Fig.5 aerosol and CCN spectra comparison inside and outside of cloud

3.2 Distribution of aerosol and cloud droplet

In order to further study the distribution and variation of cloud droplets and aerosols in precipitation process, two flights sounding data getting from airborne PMS system on October 4, 2008 were analyzed. The precipitation in that day is stratiform precipitation.The results show that the distribution of aerosol particles in Shijiazhuang is very different before and after precipitation. Before the precipitation, weather conditions is cloudy and foggy, the average concentration of aerosol particles is $10^3 cm^{-3}$, the maximum concentration is $5.2 \times 10^3 cm^{-3}$, the minimum concentration is $39.3 cm^{-3}$, aerosol particles average diameter is 1.06μm. When it is rainy, the average concentration of aerosol particles is $10^2 cm^{-3}$, the maximum concentration is $2.1 \times 10^3 cm^{-3}$, an order of magnitude of aerosol concentration is smaller than that of previous of precipitation, minimum particle concentration is 16.7 cm^{-3}, average particle diameter is 1.28μm. Scouring effect by precipitation, after precipitation the aerosol particle concentration less than the before precipitation, decreases is very obviously. In addition, beceause of inversion layer aerosol particles concentrations accumulated.

Cloud droplets average concentration is $10^1 cm^{-3}$ on before and after at precipitation, the cloud droplets concentration maximum is $2.7 \times 10^2 cm^{-3}$, the minimum is $12.2 cm^{-3}$. Cloud droplet concentration is smaller than the 1-2 amount of aerosol particles level.

Above results show that the aerosols played an important role in formation of clouds and precipitation processes. It is considered that part of the aerosol particles went into cloud in which they played cloud condensation nuclei through the activation of nuclear, and then formed cloud particles.

This section of the analysis results are shown in Table 1, figures 6 and 7 separately.

Table 1 statistical characteristics of the average number concentration and average diameter of aerosols/cloud particles

Date/ flight	PCASP (cm^{-3})	PCASP (um)	FSSP (cm^{-3})	FSSP (um)
04-f1	961.6	1.05	12.2	5.5
04-f2	1203.3	1.06	39.7	10.5

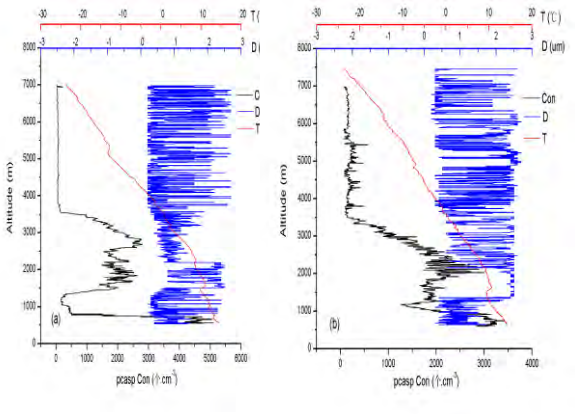


Fig.6 vetical distribution of aerosol particle concentration dring 4-5 October 2008, a. morning of October 4; b. afternoon of October 4.

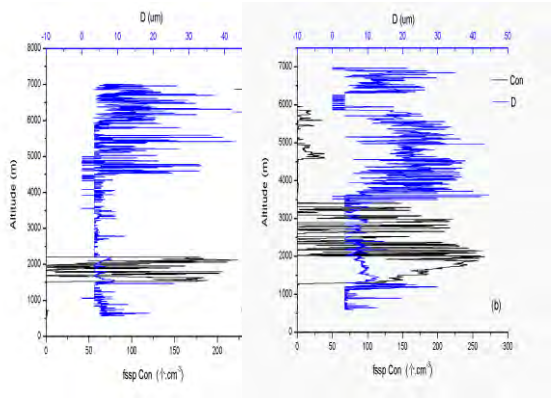


Fig.7 vertical distribution of cloud particle concentration detected with FSSP-100ER during 4-5 October 2008 (a. morning of October 4; b. afternoon of October 4)

Acknowledgements

This research was Jointly funded by National Natural Science Foundation of China (Grant No. 40905058, 40475003), the social commonweal research program (GYHY(QX)2007-6-36) funded by the Ministry of Science and Technology of the People's Republic of China.

Further we thank the staff of attending observation in Weather Modification Office of Hebei Province, China.

References

Breon, F.-M., D. Tanre, and S. Generoso, Aerosol effect on cloud droplet size monitored from satellite, Science, 295, 834– 838, doi: 10.1126/science.1066434. 2002

Duan, J., and J. T. Mao , Influence of aerosol on regional precipitation in North China, Chinese Science Bulletin, 54(3), 474-483, doi: 10.1007/s11434-008-0447-6,2009

Duan ying et.al, an Analysis of the Evolution Characteristics and Physical Cause of Formation about Forty Years Natural Rainfall in Hebei Province .13th Internatoinal Conference on Clouds and Precipitation Proceeding-Volume 1:395-397。,Reno ,Nevada USA ,14-18 August 2000.

Duan Ying, Wu Zhihui et al., An Analysis on Aerosol Variable Tendency and Clouds Physical Effect for Decrease of Natural Precipitation over Hebei Area, 17th International Conference on Nucleation and Atmospheric Aerosols,Galway,Ireland . Springer：C. D. O'Dowd and P. E. Wagner (eds.), ucleation and Atmospheric Aerosols, P507–511, 2007.

Duan Ying, Wu Zhihui, and You Laiguang et.al ,Study on the Variable Tendency of the Aerosol with Low Cloud Days and Drizzle days over the Bohai Sea Gulf Area in North China., the Scientific Assembly of the International Association of Meteorology and Atmospheric Sciences (IAMAS)， PA33-34,August 2-11, 2005.

Duan et.al,: The Study of Macro-microphysical Characteristics of Seeding Clouds for Aircraft Rain Enhancement over North China. 9th WMO Conference on Weather Modification, Antalya, Turkey,2007

Rosenfeld,D., Suppression of rain and snow by urban and industrial air pollution, Science, 287, l793-l796, doi:10.1126/science.287.5459.1793.2000.

Shi L. X., Y. Duan, Observations of Cloud Condensation Nuclei in North China ,Acta Meteorologica Sinica, 22(1) , 97-106,2008.

Shi Guangyu et al, Atmospheric Sounding of the vertical distribution of atmospheric ozone and aerosol by air-balloon. Atmospheric Science, 20(4), P401-407 (In Chinese). 1996.

Airborne radar and lidar studies of ground-based glaciogenic seeding of orographic clouds: preliminary findings and upcoming field campaign plans in Wyoming

Bart Geerts, University of Wyoming
Laramie, WY 82071 USA; geerts@uwyo.edu
Qun Miao, Ningbo University
Dan Breed, NCAR
Roy Rasmussen, NCAR

1. Introduction

The efficacy of glaciogenic seeding of non-precipitating supercooled stratus clouds has been demonstrated more than a half century ago. It is far more difficult to demonstrate precipitation enhancement in naturally precipitating clouds that drape over mountains. Such clouds are more complex mainly because of boundary-layer turbulence (Geerts et al. 2011) and because ice particles can result from interaction with the underlying terrain (Rogers and Vali 1987). Yet such clouds are far more important because they produce much of the precipitation in arid, mountainous regions. Altering the ice nucleation process in such clouds also alters other microphysical processes such as riming, leading to poorly understood changes both in cloud composition and in surface precipitation.

Several studies have attempted to document the cloud microphysical chain of events following AgI seeding of orographic clouds, mainly in the western United States (e.g., Super and Boe 1988; Deshler et al. 1990; Huggins 2007). These studies generally examined individual cases rather than a population of storms. They confirm that it is very difficult to ascertain the effective transport of the AgI nuclei over the target area, and to relate changes in liquid water content and ice particle size distributions in cloud to seeding activity. *Given the complexities of chain-of-events studies, and the statistical uncertainty of outcome-focused randomized experiments, progress in understanding the impact of ground-based glaciogenic cloud seeding is most likely through measurements of cloud microphysical processes by means of modern remote sensing instruments, in particular profiling cloud radars*.

2. Airborne nadir-viewing radar/lidar data

Cloud radars have a high spatial resolution. At mm-wave frequencies, the signal becomes attenuated in heavy precipitation, but this is not a problem for the typically light snowfall rates from orographic clouds. In the present study, data from an airborne profiling W-band Doppler radar are used. The aircraft, the Wyoming King Air (WKA), carried in situ cloud microphysics probes, the Wyoming Cloud Radar (WCR), and the Wyoming Cloud Lidar (WCL). The WCR (http://www.atmos.uwyo.edu/wcr/) is a sensitive 94 GHz (3 mm) Doppler radar with zenith- and nadir-pointing antennas, plus antennas for dual-Doppler measurements below and to the right of the aircraft. The WCL is a 0.355 micron elastic polarization backscatter lidar, also with zenith- and nadir-pointing antennas (Wang et al. 2009). The nadir view provides radar (and lidar) data within ~30 m of the ground, whereas the commonly used ground-based scanning radars can only "look" above complex terrain. The ability to look close to the terrain is important in the evaluation of ground-based seeding since the effect of seeding should be largely confined to the turbulent planetary boundary layer (Geerts et al 2011; Rasmussen et al. 2012, a WRF LES modeling paper in preparation).

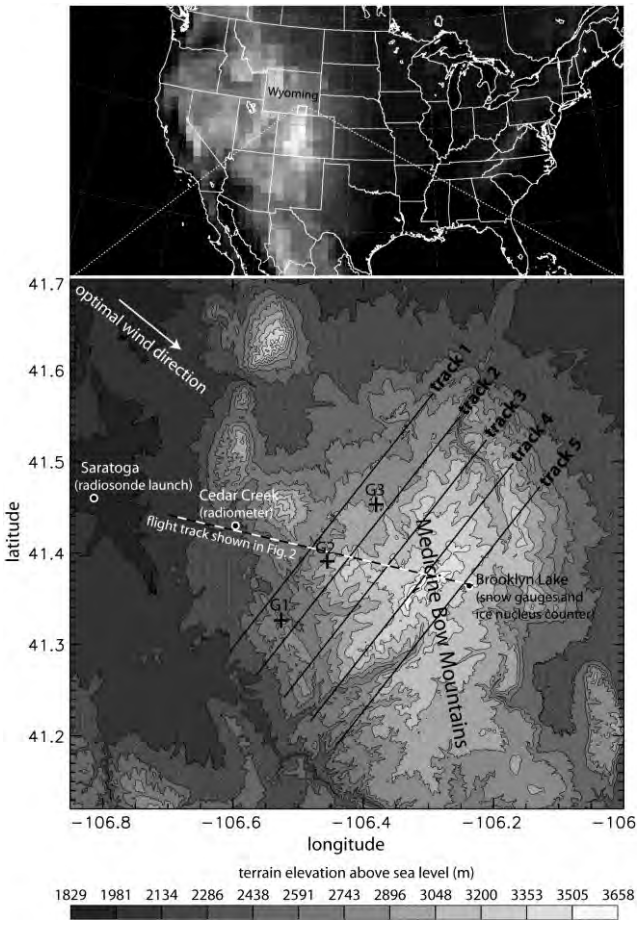


Fig. 1: Terrain map of the Medicine Bow Mountains in the Rocky Mountains, USA, showing the AgI generator sites (G1-G3), the surface measurement sites, and the five fixed flight tracks approximately normal to the wind. The flight level was maintained at about 4267 m above sea level (~607 m above the mountain peak).

3. Flight track and target mountain

A series of five geographically-fixed aircraft tracks was flown repeatedly in winter storms in the vicinity of ground-based AgI generators in the Medicine Bow Mountains of Wyoming, on a total of seven flight days in 2008 and 09 (**Fig. 1**). These generators were operated as part of the Wyoming Weather Modification Pilot Project (WWMPP), an outcome-focused randomized experiment involving two serially aligned mountain ranges (Breed et al. 2008), one of them the Medicine Bow Mountains. This mountain range is about 30 km across and 1,500 m high above the surrounding plains.

4. Sample data

An example of data collected on an along-wind flight track (Fig. 1) is shown in **Fig. 2**. During this flight the wind was westerly at ~14 m s^{-1}, the cloud base (sounding-derived lifting condensation level) was 2.6 km MSL, and the cloud base temperature was -7°C. To a first order, higher reflectivity values imply larger snowflakes, higher backscatter power implies higher droplet concentration, and higher depolarization ratio implies ice rather than droplets. Note the shallow clouds on the left side, well below flight level, detected by lidar (thus cloud droplets are present) and radar (the reflectivity values suggest that some ice is present). Also note the streamers of reflectivity apparently emerging from the surface between 16:07 and 16:06 (x-axis is time, UTC). And note the well-defined cloud top, the lack of deep clouds advected from the west, and the turbulent eddies in the boundary layer.

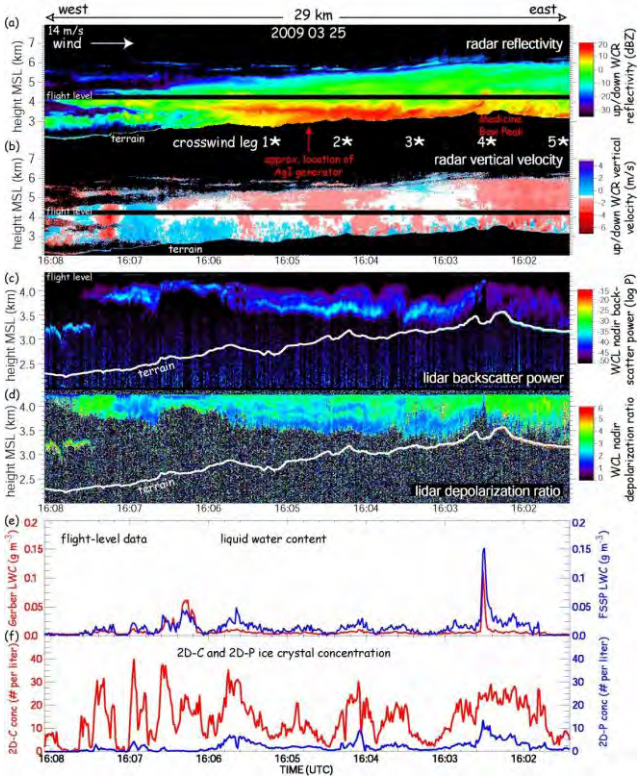


Fig. 2: Along-wind transect of Wyoming Cloud Radar (WCR) data (panels a and b) and Wyoming Cloud Lidar (WCL) data (panels c and d) on 25 March 2009. Also shown are flight-level estimates of liquid water content from the Gerber PVM-100 and the FSSP probes (panel e) and of ice particle concentrations from the 2D-C and 2D-P probes (panel f).The radar data are shown above and below flight level, which is within the black belt in the top two panels. This belt is the radar blind zone centered at flight level. The lidar data are shown only below flight level.

5. Composite results

On all 7 flights, AgI generators were off during the first 2 hours and on during the next 2 hours. Generally we flew two repeats of the five legs (labeled #1 to #5 in Fig. 1) under "no-seed" condition, followed by the same under seed conditions. A total of 70 passes during seeding and 44 passes without seeding were flown on the 7 flights over the legs downwind of the AgI generators (legs #2 to leg #5). The 2D WCR data, at a resolution of ~30 m both in the vertical and along-track dimensions, can be synthesized in the form of a *frequency-by-altitude display* (FAD) (Yuter and Houze 1995). These displays are derived as follows for no-seed (**Fig. 3**a) and seed (Fig. 3b) conditions. All WCR data collected along the four legs (#2 to #5)(Fig. 1), excluding the aircraft turns between the legs, are remapped as a function of height above ground level (AGL), and the occurrences of reflectivity values are then counted in bins with dimensions of 0.5 dB and 30 m, for all range gates and all profiles, the total number of which is listed in Fig. 3a and b. The vertical resolution (30 m) equals the WCR range resolution. The value shown in Fig. 3a or b is this count in each bin, normalized by the total count of all occurrences in all bins. Thus the summation of all bin values in Fig. 3a or b equals 1.0. The value of such summations in three smaller boxes is also shown in Fig. 3a and 3b. The numbers shown in these boxes actually are percentages of the total: for a box covering the entire domain, the corresponding number would be 100%. The normalized bin values in Fig. 3b are subtracted from those in Fig. 3a to yield Fig. 3c. The "data presence" curves in Fig. 3a and 3b is the percentage of WCR range gates with reflectivity values above the noise level (-25 dBZ) at any height AGL. The depression in the "data presence" curves between 1.0-1.5 km is an artifact due to the radar blind zone centered at flight level. This artifact clearly also affects the FADs, but it does not affect the distribution or mean value at any height.

An increase in low-level (below 800 m AGL) reflectivity on the 7 flights (Fig. 3c), each with a no-seed period followed by a seeding period, occurred notwithstanding slightly stronger updrafts (not shown) and thus higher reflectivity values aloft (Fig. 3c) found on average during no-seeding periods. Theory (Matrosov 2007) and a comparison between flight-level snow rate and near-flight-level radar reflectivity (Geerts et al. 2010) indicate that the observed reflectivity increase just above the surface corresponds with a ~25% increase in snow rate during seeding. We conducted 1000 random resamplings of all flight passes irrespective of

seeding action. Each resampling had a matching number of passes on each leg (#2 to #5), to eliminate the strong terrain effect. This resampling indicates that the observed enhancement of high reflectivity values (>10 dBZ) in the boundary layer during AgI seeding has a mere 2.2% probability of being entirely by chance (Fig. 3d).

Geerts et al. (2010) make several physical considerations in support the hypothesis that the increase in near-surface reflectivity (Fig. 3c) indeed is attributed to AgI seeding. For instance, The increase is deeper on days with shallow convection (which effectively mixes the AgI nuclei) and more shallow on days with highly stratified flow and a shallow turbulent boundary layer. Also, the reflectivity increase is found mostly on legs #2-#3 just downwind of the AgI generators (Fig. 1), and less on the more distant legs #4-#5.

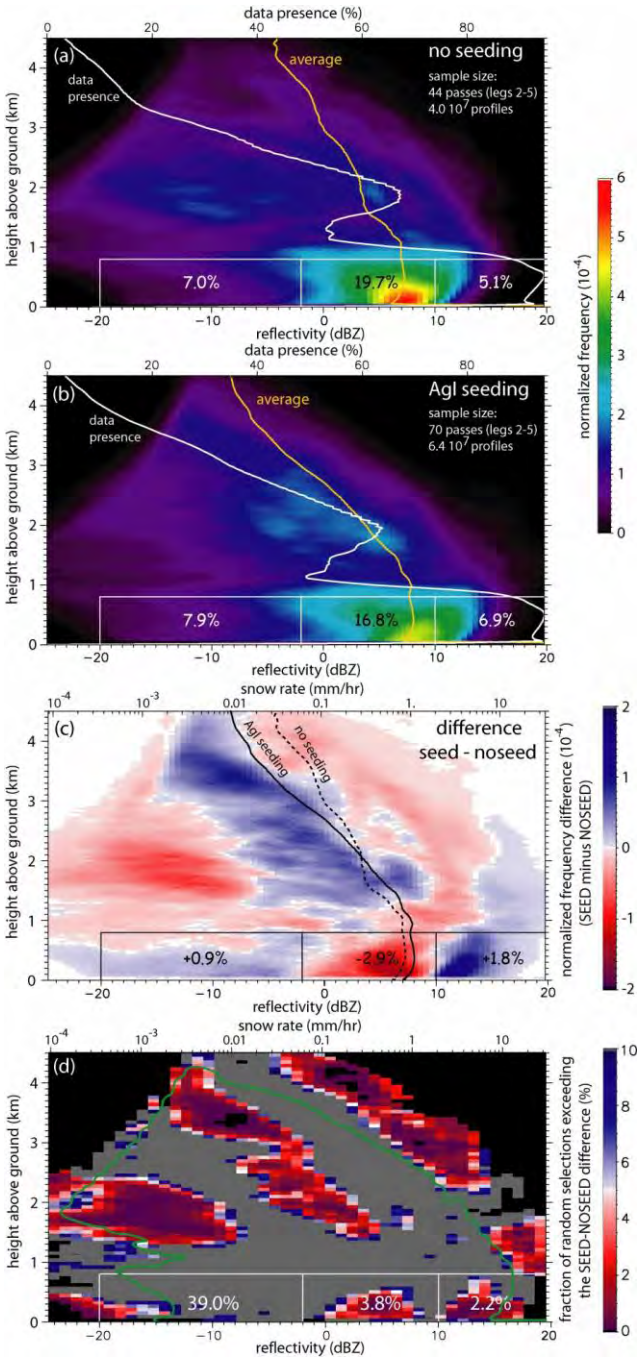


Fig. 3: Normalized FAD of WCR reflectivity (Z) for all flight legs downwind of the AgI generators on seven flights, during (a) no-seed and (b) seed conditions. Also shown are cumulative normalized frequencies in three boxes near the ground, expressed as a percentage, the mean reflectivity profile (yellow line) and the "data presence" (white line), i.e. the percentage of WCR range gates with radar echo as a function of height. The difference between the data in (b) and in (a) is shown in (c), together with the mean profiles from (a) and (b), and the difference within the three boxes. Panel (d) shows the percentage of differences between randomly selected subgroups that exceeds the observed seed minus no-seed reflectivity difference (shown in c). The white numbers in (d) show the same, not at the bin level but within the same three boxes. In the grey areas there is a more than 10% probability that the seed minus no-seed difference is by chance. Bins with an absolute normalized seed minus no-seed frequency difference of less than 10^{-5} (i.e., usually bins of extremely high or low reflectivity) are shown in black. The green contour comprises 90% of the cumulative data frequency. The snow rate (S), shown in the upper abscissa of (c) and (d), is inferred from $S=0.11\ Z^{1.25}$ (Matrosov, 2007).

6. ASCII campaign 2012

Supported by a National Science Foundation grant, the ASCII (AgI Seeding Cloud Impact Investigation) field campaign will be conducted between 4 January and 4 March 2012 over the Sierra Madre, a Continental Divide range in southern Wyoming (**Fig. 4**). This field campaign builds on the 2008-09 pilot project, which involved just 7 flights and lacked snow measurements on the ground. ASCII has two core objectives:

- to deploy relatively new instruments both to study fundamental orographic precipitation processes and to investigate how glaciogenic seeding affects the size distributions and concentrations of supercooled water and ice particles in orographic clouds (lead: Geerts);
- to model the observed cases, in order evaluate the model by means of composite observations, and to assess how upstream conditions (moisture, temperature, stability, concentrations of ice nuclei and cloud condensation nuclei) influence how ground-based glaciogenic seeding affects cloud properties and surface precipitation (lead: Rasmussen)

The ASCII field campaigns has the following elements:

- 100 WKA flight hours (rather than 30 in the pilot project), with the WCR and WCL on board, as well as several new particle probes (CDP, CIP) and aerosol probes (CCN counter, P-CASP);
- 72 radiosondes to be released from a site upwind of the mountain, plus a meteorological station;
- deployment of a mobile dual-polarization X-band Doppler radar (Doppler on Wheels),upwind of the Sierra Madre;
- a liquid water passive microwave radiometer, ceilometer, and Ka-band micro-rain radar, present as part of the Wyoming Pilot Project (WWMPP);

- establishment of a research station on the mountain pass ("Battle Town site" in Fig. 4), with the University of Colorado precipitation research station (Ka-band micro-rain radar, two Parsivel disdrometers, radiometer) a SPEC Cloud Particle Imager, a hotplate snowrate sensor, an ETI snow gauge, and snow chemistry samples.

The WKA flight patterns are shown in Fig. 1. Both single flights and double flights will be conducted. The single flights involve two 5-leg "ladders" before seeding, and the two 5-leg ladders during seeding. The double back-to-back flights with a refuelling stop involve the same patterns, plus some along-wind legs and an aerosol leg to sample the concentration of cloud-active aerosol in the upwind air mass (Fig. 4). In addition, some flights will be dedicated to the study of blowing snow and its impact on orographic clouds.

ASCII collaborators include Dan Breed and Roy Rasmussen (NCAR), Katja Friedrich (University of Colorado), Terry Deshler (University of Wyoming), Qun Miao (Ningbo University), and David Kristovich (University of Illinois, Champaign-Urbana).

More details about ASCII can be found at http://www.atmos.uwyo.edu/~geerts/ascii/.

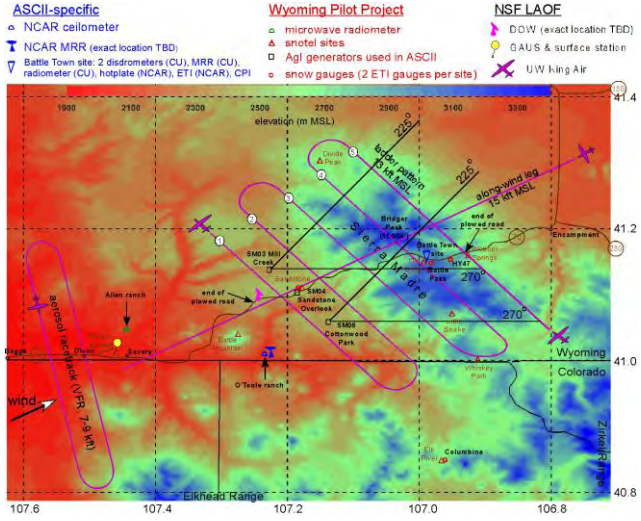


Fig. 4: Proposed sampling strategy during ASCII. The underlying color field is the terrain.

7. Summary

Data from an airborne vertically-pointing mm-wave Doppler radar (Fig. 2) have been used to study the cloud microphysical effect of glaciogenic seeding of cold-season orographic clouds. Geographically fixed flight tracks were flown downstream of ground-based silver iodide (AgI) generators in a pilot project over the Medicine Bow Mountains of Wyoming (Fig. 1). Composite data from seven flights, each with a no-seeding period followed by a seeding period, indicate that radar reflectivity was higher near the ground during the seeding periods (Fig. 3), resulting in a ~25% higher snowfall rate during the seding periods. Several physical considerations support the hypothesis that the increase in near-surface reflectivity can be attributed to AgI seeding (Geerts et al. 2010). While the increase in near-surface reflectivity and thus snowfall rate are statistically significant, caution is warranted in view of the large natural variability of weather conditions and the small size of the pilot project dataset. A larger campaign scheduled for early 2012, ASCII, should provide more robust evidence for the impact of seeding on orographic clouds and precipitation, through ~15 flights with cloud radar and lidar data, plus scanning X-band dual-pol Doppler radar data, and a state-of-the-art snow research station on the mountain crest.

Acknowledgements

The operation of the AgI generators was supported by the WWMPP, which is funded by the State of Wyoming. The seven WKA flights in 2008-09 and the data analysis were financed by the University of Wyoming Water Research Program. The ASCII field campaign is supported by the National Science Foundation grant AGS-1058426. Our thanks go to the WWMPP for operating select AgI generators and launching radiosondes in the pilot project, at no cost to the authors and at no direct benefit to the WWMPP. Thanks also to those involved with the field work, in particular the Weather Modification Inc. crew, coordinated by Bruce Boe, and the WKA flight crew.

References

Deshler, T. D., W. Reynolds, and A.W. Huggins, 1990: Physical response of winter orographic clouds over the Sierra Nevada to airborne seeding using dry ice or silver iodide. *J. Appl. Meteor.* **29**, 288-330.

Geerts, B., Q. Miao, Y. Yang, R. Rasmussen, and D. Breed, 2010: An airborne profiling radar study of the impact of glaciogenic cloud seeding on snowfall from winter orographic clouds. *J. Atmos. Sci.*, **67**, 3286–3302.

Geerts, B., Q. Miao, and Y. Yang, 2011: Boundary-layer turbulence and orographic precipitation growth in cold clouds: evidence from profiling airborne radar data. *J. Atmos. Sci.,* in press.

Huggins, A. W., 2007: Another wintertime cloud seeding case study with strong evidence of seeding effects. *J. Weather Mod.*, **39**, 9-36.

Matrosov, S.Y., 2007: Modeling backscatter properties of snowfall at millimeter wavelengths. *J. Atmos. Sci.*, **64**, 1727–1736.

Rogers, D.C., and G. Vali, 1987: Ice crystal production by mountain surfaces. *J. Climate Appl. Meteor.*, **26**, 1152-1168

Super, A. B. and B. A. Boe, 1988: Microphysical effects of wintertime cloud seeding with silver iodide over the Rocky Mountains. Part III: Observations over the Grand Mesa, Colorado. *J. Appl. Meteor.*, **27**, 1166-1182.

Yuter, S., and R.A. Houze, 1995: Three-dimensional kinematic and microphysical evolution of Florida cumulonimbus. Part II: Frequency distributions of vertical velocity, reflectivity, and differential reflectivity. *Mon. Wea. Rev.*, **123**, 1941–1963.

Wang, Z., P. Wechsler, W. Kuestner, J. French, A. Rodi, B. Glover, M. Burkhart, and D. Lukens, 2009: Wyoming Cloud Lidar: instrument description and applications. *Optics Express*, **17**, 13576-13587.

The Development of Hygroscopic Cloud Seeding Flare In Indonesia: Evaluation and Measurement of Distribution Particles

Haryanto, U.[1], *R. D. Goenawan* [2], *and D. Harsanti* [3]
Badan Pengkajian dan Penerapan Teknologi (BPPT)
BPPT Building I, 19th floor, Jl.M.H.Thamrin No.8 Jakarta 10340 Indonesia
untunghuth@yahoo.com [1], rdjokog@yahoo.com [2], dini.harsanti@bppt.go.id [3]

ABSTRACT

Research and development of hygroscopic cloud seeding flare was conducted in 2010 and funded by BPPT Insentive Program 2010. Using pyrotechnics composition of Potassium Perchlorate, Magnesium and Sodium Chloride in powder form and shellac solution as binder and then pressed with 150 kg/cm^2. Results from ground test by ignite it on installation flare test facility have been produced heavy smoke, with burning duration 4.0 – 4.5 minute. Smoke then analyze using cascade impactor and shows that dominant particles (44.2%) have diameter 1.1 – 2.1 micron, followed by 25.15% of particles sized with 0.7 – 1.1 micron in diameter. Flame temperature was about 1.100 - 1.300^{o}C.

Key Words : pyrotechnic, seeding agent, particles size distribution, cascade impactor

1. Introduction

In Indonesia, long term Cloud Seeding Operation using flare was introduced by Atmospheric Incorporated – AI (US cloud seeding operator) in 1998 to fill up Towuti and Matano Lake, South Sulawesi. After that cloud seeding operation was continued, conducted by Weather Modification Incorporated collaborated with NCAR and BPPT (UPT Hujan Buatan), the last operation was conducted in 2010. The purpose of the cloud seeding operation was to recovery or established water lake level after drop due to deficit rainfall during drought season over Larona Catchment Area (Matano, Mahalona and Towuti Lake).

All of new cloud seeding devices that were used for the operations imported from USA and purchased from ICE (Ice Crystal Engineering). Development of Hygroscopic cloud seeding Flare in Indonesia started in 1999, simple hand made hygroscopic flare manually production was demonstrated in Sorowako and success ignited from AI cloud seeding aircraft, followed by demonstration operational program for 30 days on May 1999 using Indonesia flare. The pyrotechnic chemical compositions are oxydizer, fuel, coloring agent, sodium chloride and binder. The chemical compositions of pyrotechnics ignite by e-match which surrounded by black powder composition and trigger by DC-current source from cloud seeding aircraft. Base on research and development carried out by BPPT researchers, modification was made to simplified pyrotechnic compositions and igniter. Some prototype of production was sent to aerosol laboratory to analyze the particle size distribution.

2. Physical Characteristics Indonesia Hygroscopic Cloud Seeding Flare (IHCSF)

IHCSF look likes as tube with dark brown color, with white color cap, and electric cable along the tube and sealed with laminated transparent plastic, and two ringed red electrical tape. Weight of each flare is about 1 kg. (Table 1).

Table 1. IHCSF Looking from outside

Looking at	***Description***
Casing (tube)	- outer diameter : 6,3 cm
	- inner diameter 5.9 cm
	- length 30 cm
	- material : spiral cellulose, strengthen by parafin liquid
Cable	40 cm long from e-match (electric ignitor) head to the end of cable
Sticker	Label description of IHCSF ingredients
Transparent Laminating	Protect flare from wet
White Color Cap (Choke)	Protect igniter and e-match from wet
Red Color electrical tape	To tighten cable position
Stopper (plug)	Wood, diameter 5.8 cm, fixed by glue to stop the flame.

Pyrotechnics composition consists of Potassium perchlorate ($KCLO_4$) as oxydizer, Magnesium (Mg) as fuel, Shellac as binder, and Sodium chloride as seeding agent. The black powder for a prime is modified from original black powder composition (KNO_3 + Sulfur + Charcoal) due to environment effects of sulfur, stability and for more safety reasoning. Original composition of primer have been modified become simple composition that consist only $KClO_4$ (oxydizer) and charcoal (fuel). Using $KClO_4$ for primer also make more easy to manage the kinds of pyrotechnics material for producing hygroscopic flare. These primer compositions have capable to ignite the pyrotechnics composition due to produce high flame temperature.

On the early development of cloud seeding flare, PVC pipe was used as flare tube. By observation during burning on ground test, deformation on PVC tube before its burned have block the flame, so it was abandoned and replaced by spiral cellulose tube.

3. Method of Production

3.1 Preparing step

The three main tools used for flare production are Ball Mill, Pneumatic Presser, Molding, and Un-molding tools. Each of pyrotechnics material grinded using Ball Mill to reduce size until passing to sieve 100 mesh separately. Some of pyrotechnics materials are ready for use, such as Magnesium and Sodium chloride. The tube must have prepared by immerse it into hot liquid paraffin of about 3 minutes and then stopper must filled in tube and fixed by glue. Shellac then dissolved in denatured alcohol with weight ratio 250 g : 1000 g and kept rest for 24 hours, or until all of shellac well dissolved.

3.2 Weighing, mixing, and filling

All of pyrotechnics material weighing for each flare and each of material placed into suitable plastic bag, as seen in Table 2:

Table 2. Weighing of pyrotechnics material for each flare unit.

No	Pyrotechnics material	Weight (gram)
1	Fuse / Primer ($KClO_4$ + Charcoal)	15
2	Tube	235
3	Coloring Agent	15
4	$KClO_4$	495
5	Mg	60
6	NaCl	90
7	Binder	90
Total		***1000 (approx)***

Material no 4, 5, 6, and 7 then mixed well and after that it was filled -by small part repeated- into the tube which is fitting on mould, and compact it using pneumatic pressure with 150 kg/cm^2 force for 5 minutes. If all of material was filled and pressed, space on tube remain near 2 cm long from edge of tube. This space used for filling fuse or primer (material 1, 2, and 3) and then plug the white cap. Tighten the cable using red electrical tape that ringed around tube and then wrapped the flare using transparent laminating span using hot air. The final of Indonesia flare product can be seen in figure 1.

4. Ground Test and Flare Test Installation

4.1 Ground Test

A number of flares are burned on ground (ground test) for some purpose, i.e. for measurement of burning rate (g/sec or cm/sec) characteristic of flame, tube observation during and after burning, flame temperature, smoke intensity, color of flame and smoke, residual material, etc.

4.2 Flare Test Installation Facility

Flare Test installation is a part of Aerosol Laboratory under National Nuclear Agency (BATAN), located at Pasar Jum'at - South of Jakarta. Installation consists of burning flare compartment, blower as exhaust smoke, and sampling unit, i.e. cascade impactor flow meter, and pump (Figure 1). Filter paper deployed on each of cascade and labeled as same as it's placed on cascade number. After smoke sampling, each of filter then analyzed to determine the particles sized distribution. The Filtering cascade characteristics that used for analysis shown in Table 3.



Figure 1. Flare test installation and Unit of Cascade Impactor. Top left: flare mounted on burning chamber and ready to ignite. Top right : Complete burning chamber. Bottom left : Flare ignite and burn. Top right : Cascade impactor unit and flow meter.

Table 3. Range diameter of each Cascade

No. of Cascade	1	2	3	4	5
Range of Diameter (micron)	>9.0	5.8 – 9.0	4.7 – 5.8	3.3 – 4.7	2.1 – 3.3

No. of Cascade	6	7	8	9
Range of Diameter (micron)	1.1 – 2.1	0.7 – 1.1	0.4 – 0.7	<0.4

The impaction technique is based on the inertial impaction of the aerosol particles onto a collection surface. When aerosol particles are traveling in a gas flow, an obstacle forces the gas to bend and move around it. Some of the aerosol particles with a high inertia will not be able to follow the gas stream, but continue traveling in their original direction, i.e. straight forward, and impinge on the obstacle's surface. The inertial impactor is an application of this principle. An aerosol flow is accelerated through a nozzle. Downstream of the nozzle, the flow is impeded by an obstacle, an impaction plate, which deflects the flow in a new direction, usually by 90º to the original one. All particles with an inertia higher than a certain value will impact on the impaction plate in the ideal case. Smaller particles will follow the flow without hitting the impaction plate. This value of inertia may be translated into an aerodynamic diameter by calibration. This diameter is called the cut-off diameter, and is one of the characteristics of an inertial impactor (Hung N. Nguyen, 2007)

5. Result and Discussion

5.1 Particles size Distribution related to the Optimal Size

Results of analysis shown that dominant distribution of aerosol fraction on smoke samples from Indonesia Flare burning have particle size range 1.1 – 2.1 micron (44.2%) in diameter, followed by 0.7 - 1.1

micron (25.15%) in diameter, and 2.1 – 3.3 micron (13.58%) in diameter. Percentage the other range of particles size diameter are relatively small, and it's can be omitted. Complete percentage of weight and range corresponds to diameter of particle shown in Table 4 and Table 5 (Flare Manufacture Industry, 2010).

Base on results above, it can say that Indonesia Flare having dominant particles cumulative distribution in range 1.1 – 9.0 micron (GCCN or coarse aerosol) with portion 60.11%. Aerodynamic diameter of Indonesia Flare plotted on Figure 3. We also analyze ICE Flare (Table 5), and result showed that both of flares have similar distribution characteristics, tested with same method in same laboratory (Figure 2).

Table 4. Analysis Result of Indonesia Flare

Particles Diameter (µm)	Weight (gr)	% Weight on each cascade (INA Flare)	Aerodinamic Median Mass Diameter (µm)	Standard Deviation Geometri (σg) (µm)	Consentration Mass (µg/m³)
> 9,0	0.002490	4.07			
5,8 – 9,0	0.000710	1.16			
4,7 – 5,8	0.000120	0.20	5,56	1,26	273500
3,3 – 4,7	**0.000590**	**0.96**			
2,1 – 3,3	**0.008310**	**13.58**			
1,1 – 2,1	**0.027050**	**44.21**	1,12	1,77	2167
0,7 – 1,1	0.015390	25.15			
0,4 – 0,7	0.006530	10.67	0,57	1,26	23740
< 0,4	0.000003	0.0054			
Total weight	0.061193				

Burning duration : 4.0 – 4.5 minute

Table 5. Analysis Result of ICE Flare

Particles Diameter (µm)	Weight (gr)	% Weight on each Cascade (Flare ICE)	Aerodinamic Median Mass Diameter (µm)	Standard Deviation Geometry (σg) (µm)	Concentration Massa (µg/m³)
> 9,0	0.002423	2.32			
5,8 – 9,0	0.000433	0.41			
4,7 – 5,8	0.000493	0.47	5,97	1,26	882100
3,3 – 4,7	**0.001543**	**1.48**			
2,1 – 3,3	**0.006743**	**6.46**			
1,1 – 2,1	**0.051310**	**49.12**			
0,7 – 1,1	0.037250	35.66	0,55	1,26	38060
0,4 – 0,7	0.004267	4.08			
< 0,4	0.000003	0.00			

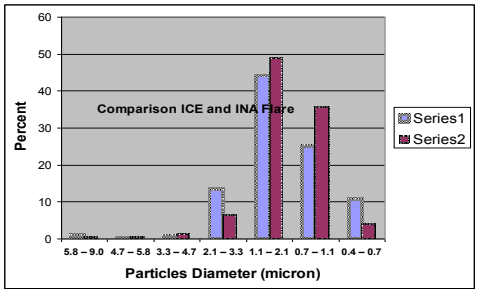


Figure 2. Comparison Distribution particles INA Flare (Series 1) and ICE Flare (Series 2).

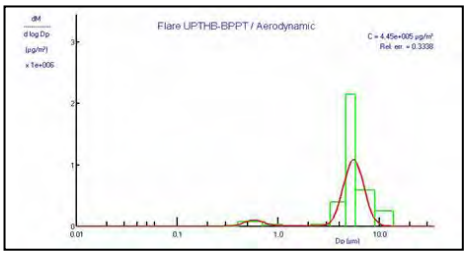


Figure 3. Plot of Aerodynamic diameter INA Flare. Maximum number distribution corresponds to 1.1 - 2.1 micron in diameter

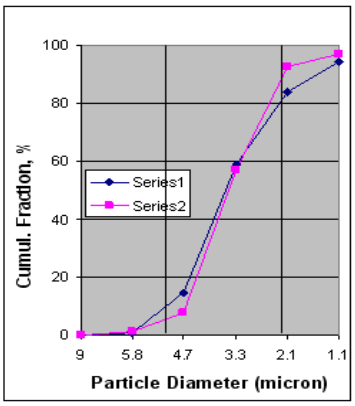


Figure 4. Cumulative fraction as function of Particles Diameter. Series 1 : INA Flare, Series2: ICE Flare

Segal et al (2004) and Kuba et al (2010) base on simulation using model have been found that the maximum raindrop production on ground occur when seeding agent particle sized range between 1.5 – 2.5 in radius injected into the cloud. The near range 2 – 5 sized diameter of optimal size of salt powder seeding agent also found by Ronen et al (2006), Rosenfeld et al (2007; 2010), and Axisa et al (2007). According to optimal size of seeding agent using to produces maximum rainfall on ground, only 14.54% of mass of the INA flare within in the range and this value is almost near doubled of ICE Flare (Table 5 and Figure 4). It may have consequence to use more number of flare in field if both of them are use for operational to reach 100% optimal particles size fraction.

5.2 Primer Composition and e-match

Primer and e-match are crucial to first fire. An example of first fire composition used in pyrotechnics or fireworks is black powder. Black powder as primer is very hazardous material to handle and only used in small quantities. In order to reduce sensitivity, black powder moistened with water and dextrin to become paste form. Other types of primer composition include Magnesium, Potassium Nitrate, and Barium peroxide.

Primer of Indonesia Flares used a special composition that not used black powder. The composition are mixed of Potassium Perchlorate and Charcoal in powder form (about 150 mesh) with weight ratio 15 : 5. This composition is more stable, less sensitive and safe to manufacture process compared with Black Powder. Source of heat comes from nickel-copper wire (diameter of 0.2mm), which was joined to electrical cable and soldered onto double sided of PCB card, then immerse into pyrogen liquor, becomes e-match. If cable connected to DC source, it becomes cinder and rapidly ignited the primer and flame propagate to main composition until it stopped at the end of tube.

Several tests indicate that temperature generated from primer flame is about 450-500^{o}C, measured using laser gun thermometer. This flame temperature is high enough and capable to generate heat to burn the main compositions. The most of flares are succeed to ignite main composition in many events of ground test. It shown that quality of prime

composition is good to ignite main composition of Indonesia Flare (Table 2).

Some flares are dud. After evaluation this flares, the problems comes from two kinds of malfunction of primer, i.e. dryness of primer composite ion, and variation length of nickelin wire as consequences of Ohm's law : I = E/R, R = ρL/A = E/I and E = IR, (Ohm's law). In Standard Operating Procedures (SOP) for Indonesia Flares Manufacture (Flare Manufacture Industry, 2010), the nickelin 0.2 mm diameter with L = 1 cm must be used. Total impedance at the end of wire is 0.8 – 1.0 Ohm, ignite with 9 V DC (1 A). Before mixed for primer uses, each of $KCLO_4$ and charcoal powder are drying with open with temperature 50^{o}C separately for 12 hours. Recently no flares dud if processed and tested using Indonesia Flare SOP Manufacture procedures.

5.3 Flame Temperature of Burning Main Composition and Burning time

Measuring burning time on ground test indicates that duration of burning time are varies between 4 to 4.5 minutes. This is count since appear the first flame until flame was disappear. The first flame comes from composition of prime of about first 5 second. The measure of Flame temperature was conducted after the first of 5 second flame appear. Data from ground test and sampling smoke indicates that flame temperature varies between 1.100 to 1.300^{o}C. Variation might be rise due to angle position and distance from heat source to temperature sensor, and due to covered the flame by residual of flare tube. On actual condition, residual of flare tube do not covered or blocked the flare flame because flare is mounted on wing of seeder aircraft and high speed of wind vibrated and destroyed the residual.

5.4. Indonesia Flare Manufacture

After long periods of research and development, BPPT joined with PT Pindad – one of Indonesia army industries – to manufacture Indonesia Flare. The constraints of $KCLO_4$ as the main pyrotechnic chemicals material and some others materials for this industry were supported by LAPAN (National Aeronautics and Space Agency) and PT Pindad. The prototype of Nul-series Flares produced by PT Pindad and now being tested on BATAN Aerosol Laboratory to analyze it's particle size distribution. The next step action in 2011 is to conduct flare certification product for National Standard Indonesia (SNI) quality.

6. Concluding Remarks

1. Indonesia Flare (Hygroscopic Cloud Seeding Flare) has been developed by BPPT Since 1998 and PT Pindad was started on 2010 for Nul Series production. Some of National Research Agency such as LAPAN and BATAN were supported and contributed for material and testing of particle size distribution.
2. Base on evaluation above and result of flare testing on BATAN aerosol laboratory, Indonesia Flare having characters i.e. flame duration are 4.0 – 4.5 minutes, resistant 0.8 – 1.0 Ohm and have dominant particles (44,2%) 1.1 – 2.1 micron in diameter, followed by 25.15% of particles sized with 0.7 – 1.1 micron diameter. The flame temperature was about 1100 - 1300^{o}C. No flare dud reported after processed and tested followed by SOP Manufacture Indonesia Flare.
3. The Nul-Series production manufactured by PT Pindad by supervision of BPPT Scientist and Engineer. Some National Research Agency are involved and supported of development program.

Acknowledgements

This research funded by The Research Insentive Program 2010 under title Flare Manufacture Industry – IPF/47. Many Thanks to Dr. Eko Poedjadi and his colleagues on BATAN Aerosol Reseach Laboratory, and also for Ir. Henny and her colleagues in LAPAN Pyrotechnics Division. Special thanks for colleagues at PT Pindad in Pyrotechnics and Munitions Division for warm and hospitality cooperated during Nul Series Manufactured in Turen (Malang) on Sepember 2010. The authors also thanks to many person in BPPT (UPT Hujan Buatan) who are involved and supported on this research and the Nul Series Manufactured.

References

Axisa,D., D. Rosenfeld, and W.L. Woodley, Microphysical Signatures Of Hygroscopic Seeding with 2-5 Micron Salt Powder Using Aircraft And Sulfur Hexaflouride (SF6) Tracer, 2007.

Drofa A.S., V.N. Ivanov, D. Rosenfeld, and A.G. Shilin. 2010. Studying an effect of salt powder seeding used for precipitation enhancement from convective clouds. 2010. Atmospheric Chemistry and Physics,10,8011 – 8023,2010.

Flare Manufacture Industry (original in Indonesian), Report of Insentive Reseacrh IPF/47 2010. UPT. Hujan Buatan BPP Teknologi, 2010.

Hung N. Nguyen, Chemical and Morphological Characterisation of Aerosol Particles in the Tropopause Region, 2007.

Kuba, N., and M. Murakami, Atmospheric Chemistry and Physics, 10,3335-3351, 2010.

Rosenfeld, D., D. Axisa, W. L. Woodley, and R Lahav.. A Quest For Effective Hygroscopic Cloud Seeding, 2010.

Rosenfeld, D., R. Lahav, D. Axisa, and W.L. Woodley, Observed micro physical effects of hygroscopic seeding in cloud volumes tagged by SF_6 tracer, 2007.

Segal,Y., A. Khain, M. Pinsky, D Rosenfeld, Atmospheric Research 71, 3-34. www.elsevier.com/locate/atmos, 2004.

Lahav, R., D. Rosenfeld, The Search For The Optimal Size of Hygroscopic Seeding Particles, 2006.

Investigating on Microphysical Clouds Parameters Using Satellite TRMM-TMI

Sohaila Javanmard[1], Samane Golestani[2] ,Javad BodaghJamali[3], Yusef A. Abedini[2]

[1]Atmospheric Science and Meteorological Research Center, Tehran, I. R. of Iran, sohailajavanmard@gmail.com

[2] Zanjan University, Zanjan, I. R. of Iran, Samaneh.golestani@gmail.com

[3] University of environment, standard Square, Karaj, I. R. of Iran, jbjamali@gmail.com, jbodagh@yahoo.com

1. Introduction

Clouds are very important component in hydrological and ene rgy cycle of Earth's climate. Although the critical role of clouds in the Earth's radiation balance has been widely recognized for many years, they are still the major source of large uncertainties in climate predictions by general circulation models(GCMs) (Huang et al. 2005).

The liquid water and ice content of clouds are one of several components of the atmospheric water budget that has influence on the Earth's radiative energy balance. Because of the strong interactions between cloud water, cloud ice and radiation, clouds may play an important part in global climate (Greenwald et al. 1993).

The estimation of cloud liquid water and cloud ice and other meteorological quantities (e.g., precipitable water, surface winds, precipitation, and others) over the ocean and land from space-borne passive microwave instruments has a long history that spans more than two decade. Basharinov et al. (1969) and Akvilonova et al. (1973) were among the first studies to utilize such measurements (Greenwald et al. 1993).

For these reasons and to investigate on melting level it is essential that we understand how cloud liquid water, cloud ice, precipitation water and precipitation ice are maintained on a global scale, how they are distributed in space, and how they varies from season to season and year to year.

In this paper, in order to investigate on the spatial and temporal distribution of the microphysical cloud parameters, mean seasonal and ann ual precipitation water, precipitation ice, cloud water and cloud ice have been analyzed for time period (1998-2005) over Iran country using Grads (Gridded Analysis and Display System) software under Linux operating system.

2. Data and methods

2.1. Study area

Iran country (25º-40º N, 45º-60º E) has been selected as the study area in this research. Iran located on the desert belt and is one of the world's most mountainous countries. Iran with mean annual rainfall 250 mm in the average of the whole country ranging from 50 mm in the deserts to 1600 mm in the Caspian sea compared to global rainfall with 860 mm is classified as an arid or semi-arid country (specially in eastern and central regions).

2.2. TRMM satellite data (3A-12 V6)

The Tropical Rainfall Measuring Mission (TRMM) is a joint mission between the National Aeronautics and Space Administration (NASA) of the United States and Japan Aerospace and Exploration Agency (JAXA). The objectives of TRMM are to measure rainfall and en ergy (i.e., latent heat of condensation) exchange of tropical and subtropical regions of the world. The primary rainfall instruments on TRMM are the TRMM Microwave Imager (TMI), the precipitation radar (PR), and the Visible and Infrared Radiometer System (VIRS). The space segment of TRMM is a satellite in a 402.5-km circular orbit with a 35.8 inclination angle. It was scheduled to be launched in the summer of 1997.

The Tropical Rainfall Measuring Mission's (TRMM) Microwave Imager (TMI) is a nine channel passive microwave sensor designed to provide quantitative rainfall information over a wide swath under the TRMM satellite. By carefully measuring the minute amounts of microwave energy emitted by the Earth and its atmosphere, TMI is able to quantify the water vapor, the cloud water, and the rainfall intensity in the atmosphere (Kummerow et al. 1998).

The data used i n this study are TRMM-TMI monthly products (3A-12 V6) which are global belt (40°S - 40°N) monthly average of surface rain rate (mmh^{-1}), convective surface rain rate (mmh^{-1}), stratiform surface rain rate (mmh^{-1}) and 14 v ertical layers (surface until 18 k m above surface) hydrometeor contents (cloud liquid water (gm^{-3}), precipitating water (gm^{-3}), cloud ice (gm^{-3}), precipitating ice (gm^{-3}) and latent heat ($degh^{-1}$) for 0.5 x 0.5 degree grids. In this research TRMM-TMI monthly data have been downloaded from the website (URL:ftp:disc2.nasacom.nasa.gov/data/TRMM/Gridded/3A-12 V6).

3. Results and conclusion

3.1 Precipitation water and precipitation ice

A comparison between the precipitation water (gm^{-3}) and precipitation ice (gm^{-3}) in different vertical levels has been carried out over Iran. Time series of monthly areal average of precipitation water (gm^{-3}) and precipitation ice (gm^{-3}) in three different vertical levels during the years 1998 through 2005 over Iran have been shown in Fig. 1.

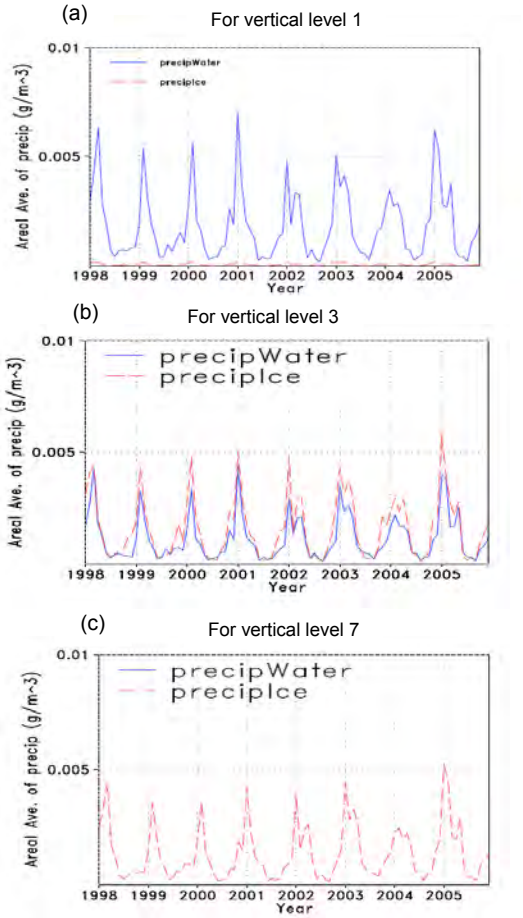


Figure 1. Comparison of time series of monthly areal average of precipitation water and precipitation ice (gm^{-3}) in vertical (a) Level 1 (surface to 0.5 km above surface), (b) Level 3 (1.0-1.5 km above surface) and (c) Level 7 (3.0-3.5 km above surface) for 1998-2005 over Iran.

It revealed that in low vertical levels, main part of precipitation is in form of precipitation water. Maximum of areal average of precipitation water in Iran mostly occurs in winter season (December, January and February). And at the surface the maximum amount of areal average of precipitation water is about 0.005 (gm^{-3}). Gradually with increasing height and also decreasing temperature, precipitation water amount decreased and amount of precipitation ice increased.

In vertical level 3 (1.0-1.5 km about surface) areal average of precipitation water and precipitation ice are nearly same, with maximum amount less than 0.005 (gm^{-3}). And from vertical level 7 (3.0-3.5 km above surface) to the top, precipitation ice supplies all amount of precipitation. The maximum amount of areal average of precipitation ice in vertical level 7 is about 0.004 (gm^{-3}). Although at these altitude with increasing height the amount of areal average of precipitation ice decreased, as in vertical level 14 (14.0-18.0 km above surface) its maximum amount is about 0.001 (gm^{-3}). It has demonstrated the melting of ice at low levels very well. Although it should be noticed that melting level displaces in different seasons of year, and in cold months of year it displaced to lower altitude.

3.2 Cloud water and cloud ice

Also an analysis on the cloud water (gm^{-3}) and cloud ice (gm^{-3}) in different vertical levels has been carried out over Iran. Mean seasonal cloud ice (gm^{-3}) and cloud water (gm^{-3}) for winter season (December, January and February), namely DJF, in three different vertical levels during from 1998 through 2005 over Iran have been shown in figure 2.

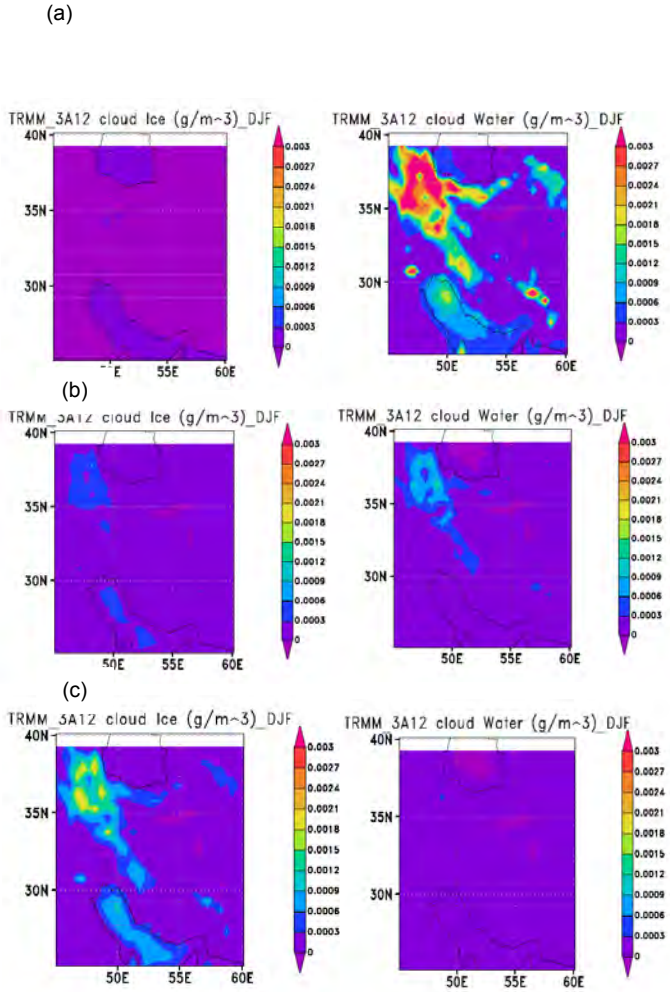


Figure 2. Comparison of mean seasonal cloud ice (gm^{-3}) and cloud water (gm^{-3}) over Iran during time period 1998-2005, for winter (Dec., Jan., Feb.), in vertical (a) Level 3 (1.0-1.5 km above surface), (b) Level 7 (3.0-3.5 km above surface) and (c) Level 11 (6.0-8.0 km above surface) .

An investigation on these two parameters shows that in all seasons of year at altitude of less than 1-1.5 km above the surface there is no cloud ice. While in these altitude cloud water has maximum

values about 0.002-0.004 (gm^{-3}). These values vary in different seasons. With increasing height the amount of cloud ice increased. As at altitude 3-6 km above surface, cloud water and cloud ice have same amount with values about 0.0006-0.001 (gm^{-3}). At altitude 6-18 km above surface with decreasing temperature cloud water is reduced to zero while cloud ice increased and have maximum values about 0.001-0.002 (gm^{-3}).

Comparison between the precipitation water (gm^{-3}) and precipitation ice (gm^{-3}) at different vertical levels revealed that melting level displaces in different seasons of year. The most amount of monthly total surface rainfall is related to precipitation ice in higher levels (above melting/freezing level) and precipitation water (below the melting/freezing level).

The amount of cloud ice and c loud water depends on the height and t ime and v ary from season to season and place to place.

References

Akvilonova, A. B., A. Y. Basharinov, A. K. Gorodetskiy, A. S. Gurvich, M. S. Krylova, B. G. Kutuza, D. T Matveyev, and A. P. Orlov, Cloud parameters measured from the Cosmos-384 satellite, Atraos. Oceanic Phys., **9**, 187-189, 1973.

Basharinov, A. Y., A. S. Gurvich, and S. T. Yegoro, Determination of geophysical parameters from data on thermally-induced radioemission obtained with the Cosmos 243 satellite, Dokl. Akad. Nauk SSSR., **188**, 1273-1276, 1969.

Greenwald J. Stephens G. Vonder T. Jackson D, A Physical Retrieval of Cloud Liquid Water Over the Global Oceans Using Special Sensor Microwave/Imager(S SM/I) Observations. *J. Geophysical Research*., **98**, 18,471-18,488, 1993.

Huang J. Minnis P, Advanced retrievals of multilayered cloud properties using multispectral measurements. *J. Geophysical Research.*, **110**, D15S18, 2005.

Kummerow C. Barnes W. Kozu T. Shiue J. and Simpson J. The Tropical Rainfall Measuring Mission (TRMM) Sensor Package. *J. Atmospheric and Oceanic Technology,.* **15**. 809-817. 1998.

X-band dual linear polarimetric radar wave attenuation impact On hail identification

Jianli Ma

Beijing Weather Modification Office, Beijing, China, 100089,lz_majianli@163.com

Abstract

Electromagnetic wave of X-band (3cm) dual linear polarimetric radar going through a large area of light rain can lead to strong attenuation， when passing through heavy rain or hail region, it may completely decay, and form reflectivity typical V-notch。Generally ，hail are accompanied by heavy rain, when hail area behind heavy rain , the attenuation of waves caused by rain lead to the radar polarimetric parameters do not reflect the actual parameters of hail characteristics， so it is required to do attenuation correction. Reflectivity decay rate (A_H, unit: dB / km) and the differential reflectivity decay rate (A_{DP}) have a linear relationship with differential phase-shift rate (K_{DP}) , which is used for attenuation correction, ϕ_{DP} need to do quality control before correction. and H_{DR} parameter to identify hail is based on the Z_H - Z_{DR} distribution relationships. A case of heavey rain with hail show that the identification parameter of H_{DR} is consistent with the ground hail after using revised reflectivity and differential reflectivity.

Key words: X-band dual linear polarimetric radar , Hail recognition , Attenuation correction

1. Introduction

In June 2008, the Beijing Weather Modification Office began to use a X-band dual linear polarimetric radar to carry out artificial hail suppression. Electromagnetic waves of radar will result in attenuation when go through the atmosphere, clouds, precipitation particles, and the attenuation consists of two parts, one part of energy is absorbed by the particle, and the other is scattered by particles, so that the original incident direction of electromagnetic energy has been weakened。

2. Hail Parameter HDR and Attenuation Correction

The scattering figure for Z_H and Z_{DR} by taking different types of precipitation samples as follow,

$$f(Z_{DR})=\begin{cases}35, & Z_{DR}<0\\ 35+13.75Z_{DR}, & 0\text{dB}<Z_{DR}<1.6\text{dB}\\ 55, & Z_{DR}\geq 1.6\text{dB}\end{cases}$$

H_{DR} is defined as:

$$H_{DR}=Z_H-f(Z_{DR}),\ \text{when}\ H_{DR}>0,\ \text{it's hail.}$$

The attenuation of electromagnetic waves caused by rain lead to the radar polarimetric parameters do not reflect the actual parameters of hail characteristics， so it is required to do attenuation correction. Bringi proposed reflectivity decay rate (AH, unit: dB / km) and the differential reflectivity decay rate (ADP) have a linear relationship with differential phase-shift rate (KDP) , which is used for attenuation correction in this paper ,and attenuation correction formula is as follows：

$Z_{HA}(r)=Z_H(r)+2\,a1\phi_{DP}(r)$， $Z_{DRA}(r)=Z_{DR}(r)+2a2\phi_{DP}(r)$； $Z_H(r)$， $Z_{DR}(r)$ are the reflectivity and differential reflectivity values at the distance r, $2\,a1\phi_{DP}(r)$ ， $2\,a2\phi_{DP}(r)$， are the revised values at distance r

by using the differential propagation phase shift, $Z_{HA}(r)$, $Z_{DRA}(r)$ are revised results after correction , a1=0.22db/deg, a2= 0.033db/deg。ϕ_{DP} need to do quality control before correction. the methods are as follows: Select the a radial, from the first bin begin to look for more than 10dBZ echo corresponding ϕ_{DP} value, and find 14 consecutive this value to average to estimate initial differential phase , namely, $\phi_{DP}(0) = E(\sum_{i=1}^{14} \phi_{DP}[i])$, using 14 points moving average to get each bin ϕ_{DP} .

3. Case Study

On July 22, 2009, a strong convective storm from the northwest of radar moving to the southeast, the ground observations indicate that hail start to fall at the 15:40 in the area of strong echoes through, time lasted for 15-20 minutes， hail are accompanied by heavy rain, when hail area behind heavy rain , the attenuation of waves caused by rain lead to the radar polarimetric parameters do not reflect the actual parameters of hail characteristics.Fig.2 gives out the attenuation feature of reflectivity of X-band dual linear polarimetric radar, Fig.3 gives out the correction reflectivity of X-band dual linear polarimetric radar Compared with S-band radar reflectivity. Fig.4 and Fig.5 show the comparison of hail identification before and after correction.

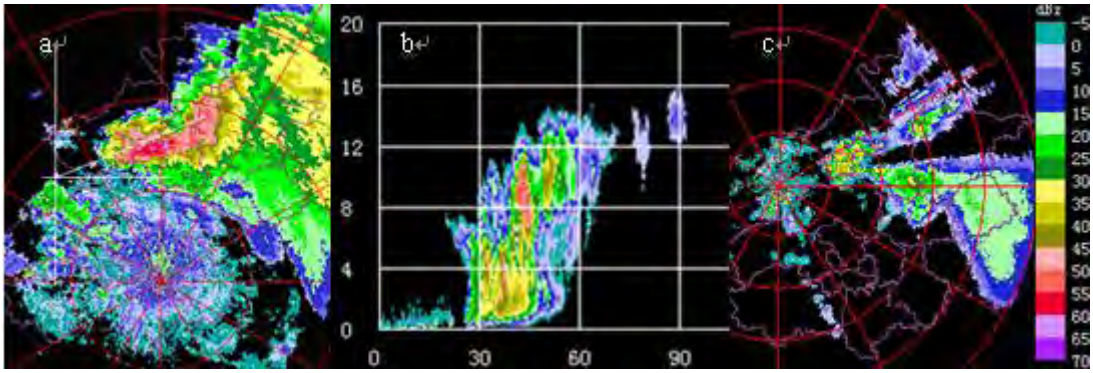


Fig.2 (a) Beijing Nanjiao Cinrad/SA radar combination reflectivity at 15:42 July 22,2009 (b) X-band dual linear polarimetric radar RHI reflectivity at 15:45 July 22,2009 (c) X-band dual linear polarimetric radar 3.4 ° PPI reflectivity at 15:46 July 22,2009.

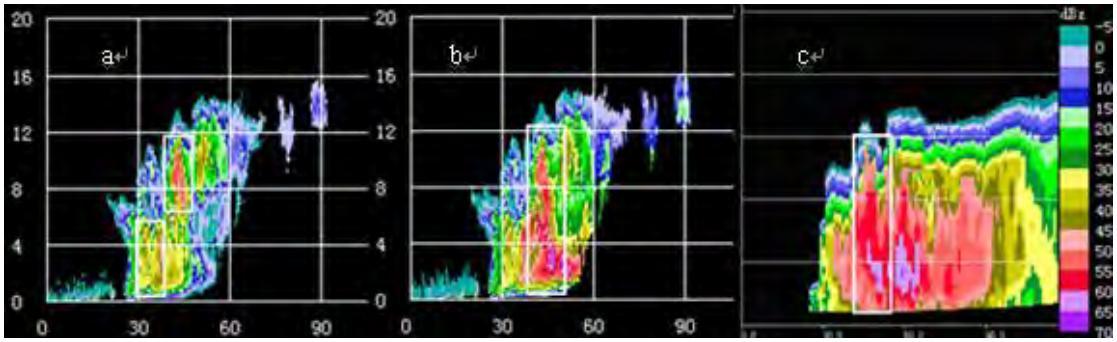


Fig.3 Comparison of the reflectivity before and after correction (a) X-band dual linear polarimetric radar RHI uncorrected reflectivity at 15:45 (b) X-band dual linear polarimetric radar RHI corrected reflectivity at 15:45 (c) the vertical section reflectivity of Beijing Nanjiao Cinrad/SA radar along the direction of X-band dual linear polarimetric radar RHI scan azimuth at 15:42

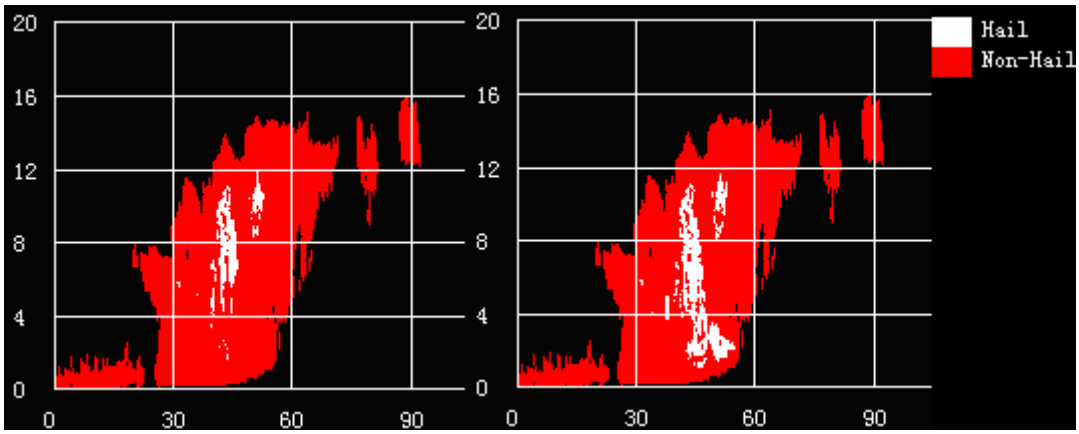


Fig.4 X-band dual linear polarimetric radar RHI hail Identification (a)before correcting (b)after correcting

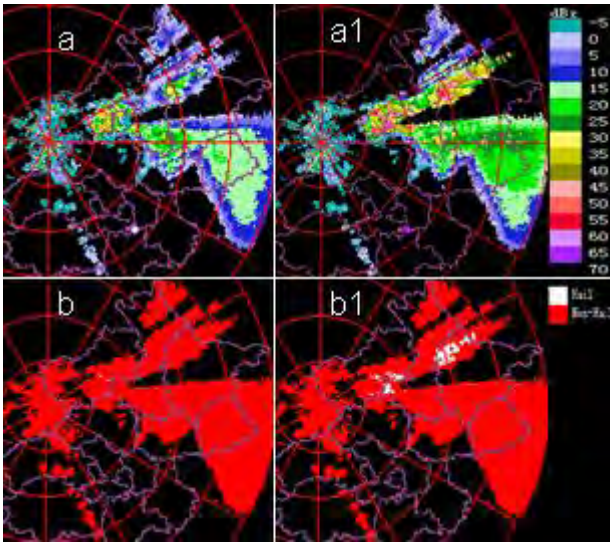


Fig.5 X-band dual linear polarimetric radar 3.4 ° PPI at 15:46 July 22,2009

(a)uncorrected reflectivity，(a1)corrected reflectivity

(b) hail Identification before correcting (b1) hail Identification after correcting

5. Conclusions

(1) Waves of X-band dual linear polarimetric radar will result in severe attenuation after through the region of convective weather, if not doing attenuation correction, will cause considerable error for identification of hail.

(2)The corrected reflectivity of X-band dual linear polarimetric radar is high consistency of the S-band radar ,indicating ϕ_{DP} revised method is effective , reflectivity and differential reflectivity after correction are more effective identification of hail;

(3)The function of recognition hail of X-band dual linear polarimetric play an important role on hail suppression , and can effectively reduce the losses caused by hail.

References

Aydin , K. , T. A. Seliga , and V. Balaji. Remote sensing of Hail with a Dual Linear polarization radar[J] . J . App . Meteo , 1986 , 25 : 1475~1484.

Bringi V N , Keenan T D , Chandrasekar V. 2001. Correcting C band radar reflectivity and differential reflectivity data for rain attenuation : A selfconsistent method with constraints [T] . IEEE TransGeosci Remote Sens , 39 : 1906~1915

Liping Liu, 1993: Preliminary Research For Method Of Hail Detection With C Band Dual Linear Polarization Radar.[J] , Plateau Meteorology , 12 (3) :333-337.

Junwu Cao, Liping Liu , 2006: Hail Identification with Dual-Linear Polarimetric Radar Observations, Meteorological[J]. Monthy, 32 (6):13-19.

Lingbo Qi, Hui xiao, MeiyuanHuang, 2002 : A numeric study of hail identification using dual-polarization radar[J], Chinese Journal Of Altmospheric Sciences, 26 (2) , 230-240.

TWENTY- FIVE YEARS OF CLOUD SEEDING ACTIVITY TO MODIFY WEATHER CONDITIONS IN CITIES

Koloskov, B.P. [(1)]., Korneev V.P. [(1)]., Beryulev G.P.[(2)], Danelyan B.G.[(2)], Stasenko V.N.[(3)]

[(1)] Agency of Atmospheric Technologies (Agency ATTEX, ROSHYDROMET)
Novovagankovsky per. 8, Moscow, 123242, RUSSIA
Tel: +7(499)795-2372; Fax: +7(499)795-2134; e-mail: attech@mail.ru

[(2)] Central Aerological Observatory (CAO)
Pervomayskaya 3, Dolgoprudny, Moscow Region, 141700, RUSSIA
e-mail: secretary@cao-rhms.ru

[(3)] ROSHYDROMET, Moscow, RUSSIA

1. Introduction

During the last twenty-thirty years considerable work has been done in Russia on the development of methods and technical means to dissipate some forms of clouds and preventing or substantially reducing precipitation amount over protected areas. The practical objectives of cloud seeding activity were to reduce municipal expenses for snow removal and clearing the roads and streets in large cities, to create favorable meteorological conditions for carrying out social programs, sporting competitions or some other situations when the necessity may arise to reduce the rainfall.

The first experiment on practical application of these opportunities was carried out to mitigate the consequences of Chernobyl disaster in 1986 /Beriulev et al. 1990/. Since 1995 the organizations of ROSHYDROMET conducted more than 40 experimental projects on improvement of weather conditions in areas of the large cities – Moscow and St.Petersburg (Russia), Tashkent (Uzbekistan), Astana (Kazakhstan) /Bedritsky et al., 1996, Belyaev et al., 1996, Korneev et al., 2003, Koloskov et al., 2007/. The main purpose of these activities was the dispersal of clouds and reduction or prevention of precipitation over the protected areas. The technology of rain mitigation has been successfully used during Beijing 2008 Olympic Games opening and closing ceremonies /Zhang Qiang et al., 2011/.

Some results of twenty-five years activities on cloud seeding operations to modify weather conditions over large cities are presented in this paper.

2. Cloud seeding concepts

Four basic concepts of cloud dispersal and precipitation redistribution are generally used depending on a weather conditions, type of clouds and intensity of precipitation processes /Korneev et al., 2003, Koloskov et al., 2007/:

1. Dispersal of stratiform clouds.
2. Destruction of convective clouds or reduction of the intensity of shower rains and thunderstorms by a dynamic seeding technique /Petrov 1986, Belyaev et al. 1987/.
3. Premature initiation of precipitation from clouds on the windward side of the target area with the purpose of formation of a “precipitation shadow”, i.e. reduction of precipitation over the given site.
4. Reduction of rainfall intensity over the target area by intensive seeding the rain-producing clouds moving toward it, aimed at weakening the mechanism of precipitation generation through the “overseeding” of clouds, i.e. creating excessive concentrations of ice crystals.

All these concepts are based on the use of unstable state of atmospheric processes. Of the various types of instability, those with most potential for local modification of precipitation and cloud-formation processes are the phase instability of cloud water (existence of supercooled liquid water) and the convective instability of the atmosphere.

3. Technical means

The described methods can be implemented using instrumented aircraft of different types – IL-18, AN-72, AN-12, AN-30, AN-26, AN-28, AN-32, M-101T "Gzhel" and SU-30. Aircraft instrumentation includes data acquisition system, technical means to release silver iodide pyrotechnic flares, devices for cloud seeding using granulated dry ice, liquid nitrogen generators of ice particles and systems for dropping the packages with coarse-dispersion powders opening automatically after their release.

Each aircraft participated in cloud seeding operations is equipped with data transmission system “Land–Aircraft–Land” /Petrov, et al., 2007/. This system allows to display the locations and flight paths of aircraft on monitor of the ground based automated weather radar system, as well as send aboard the aircraft radar maps of distribution of cloud and precipitation in region of works.

Management of works and control of the results performed by MRL-5 meteorological radar equipped with the AKSOPRI or MERCOM automated radar system.

4. Results of an improvement of weather conditions

Analysis of the radar and raingauge information collected in more than 40 experimental cloud

seeding operations to modify weather conditions in cities showed that: 1) in 38% of cases (Fig. 1, area 1) there were no need to seed clouds due to the fine weather; 2) cloud seeding with 6 to 12 aircraft caused the destruction of stratiform and precipitating convective clouds in 25% of cases (Fig. 1, area 2), and 3) considerable, 3-10 times decrease of intensity and amount of precipitation (Fig. 2) was obtained over the protected territories in comparison with rain fallen over control areas in 37% of cases (Fig. 1, area 3).

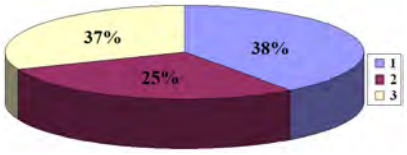


Fig.1. Results of works on cloud seeding to modify weather in cities.

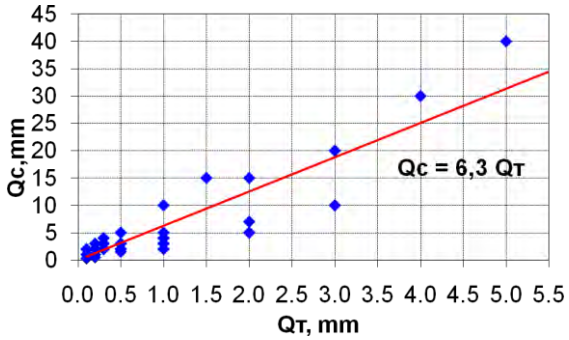


Fig. 2. Precipitation over the protected (Q_T) and control (Q_C) areas.

The results obtained demonstrate perspectivity of the methods and technical means developed in Russia for redistribution summer and winter precipitation. The problem of redistribution and reduction of precipitation in a given area is very important when working to eliminate the consequences of accidents at nuclear power plants, particularly the disasters at Chernobyl (Soviet Union) in 1986 and Fukushima I (Japan) in 2011.

References

Bedritsky A.I. and Chernikov A.A. Cloud seeding to protect Moscow from rain on 9 May 1995 – *WMO Bulletin*, Vol. 45, No 1, 60-64, 1996.

Belyaev V.P., Zatsepina L.P., Zontov L.B., Petrov V.V., Seregin Yu.A. Some results of field experiments designed to reduce convective activity of multi-tower clouds. – *Trudy CAO,* issue 164, 3-10, 1987 (in Russian).

Belyaev V.P., Beriulev G.P., Vlasyuk M.P., Danelyan B.G., Koloskov B.P., Korneev V.P., Melnichuk Yu.V., Chernikov A.A. A case study of cloud seeding over Moscow on 9 May 1995. – *Russian Meteorology and Hydrology*, No.5, 47-55, 1996.

Beriulev G.P., Zatsepina L.P., Zontov L.B., Sergeev B.N., Seregin Yu.A., Chernikov A.A., Kornienko E.E., Maksimov V.S., Khusid S.V. An experience of artificial regulation of precipitations with the purposes of eliminating the consequences of disaster on Chernobyl nuclear power plant. – *Weather Modification on hydrometeorological processes. Proc. of the All-Union Russian Conference*, L., Hydrometeoizdat, 233-238, 1990 (in Russian).

Koloskov B.P., Korneev V.P., Petrov V.V., Beriulev G.P., Danelyan B.G., Chernikov A.A., Shchukin G.G. Cloud seeding operations to modify weather conditions over cities: 2003-2006. – *Proc. of Ninth WMO Scientific Conference on Weather Modification (Antalia, Turkey, 22-24 October 2007)*, WMP - No.44, 2007.

Korneev V.P., Petrov V.V., Diadyuchenko V.N., Stasenko V.N., Beriulev G.P., Koloskov B.P., Chernikov A.A.Results of cloud seeding operations to modify weather conditions over cities. – *Proc. of Eight WMO Scientific Conference on Weather Modification (Casablanca, Morocco, 7-12 April 2003)*, WMO/TD-No.1146, 227-230, 2003.

Petrov V.V. An investigation of the evolution of horizontal wind field near convective cloud tops seeded with powders in a coarsely dispersed aerosol. – *Trudy CAO,* issue 162, 49-57, 1986 (in Russian).

Petrov V., Egorov O., Melnik S. and Skuratov S. “Land – Aircraft – Land” data transmission system. – *Proc. of 9th WMO Conf. on Weather Modification (Antalia, Turkey, 22-24 October 2007)*, WMP - No.44, 2007.

Zhang Qiang, H. He, M. Huang, H. Y. Li, J. Z. Liu, X. Ma, Koloskov B.P., Korneev V.P. Brief introduction of the rain mitigation operations during Beijing 2008 Olympic opening ceremony. - *18th Conference on Planned and Inadvertent Weather Modification (Seattle, Washington, 23–27 January 2011), 2011.*

Observations of Hygroscopic Flare Particles at Various Relative Humidity

Terrence W. Krauss[1], Duncan Axisa[2], and Roelof Burger[1]
1. University of the Witwatersrand, Johannesburg, South Africa
2. National Center of Atmospheric Research, Boulder, Colorado, USA

1. Introduction

From November 2006 to April 2010, cloud physics research studies and exploratory cloud seeding using glaciogenic and hygroscopic pyrotechnics for precipitation enhancement were conducted in Saudi Arabia by Weather Modification Inc. (WMI) for the Presidency of Meteorology and Environment (PME). An instrumented cloud physics aircraft and sophisticated aerosol ground instrumentation were used to document the precipitation processes and background aerosols. Scientists from the National Center of Atmospheric Research (NCAR), Texas A&M University (TAMU), and the University of the Witwatersrand in South Africa provided scientific support and analysis. This paper reports on airborne and ground observations of the aerosols produced by hygroscopic flares from Ice Crystal Engineering (ICE) used during the project in the southwest Asir region of Saudi Arabia.

2. Motivation For This Study

The size spectrum of the droplets formed at cloud base, in the initial stage of cloud formation, determines the subsequent development of cloud microstructure, rate of large drop formation, development of coalescence processes, and precipitation formation. Cloud physics and aerosol measurements indicate that the Saudi Arabian southwest region aerosol can be characterized by a persistent accumulation mode having hygroscopic properties consistent with a sulfate-rich aged aerosol. The concentration of particles in the accumulation mode, and consequently the CCN concentration, are considerably higher when influenced by the sea breeze of the Red Sea, compared with the CCN originating from inland sources.

Aircraft measurements have shown that clouds in the Asir region often develop graupel quickly by what appears to be the freezing of large droplets in the 50-200μm range. Once the large droplets form, these quickly freeze and become embryos for graupel.

Hygroscopic cloud seeding for rain enhancement has been conducted extensively in many countries (for example: China, India, USA, Mexico, South Africa, Saudi Arabia, Thailand). The hygroscopic seeding in convective clouds is aimed at accelerating the conversion of cloud water to precipitation (see Bruintjes, 1999; and Silverman, 2003). Three main conceptual models have guided the most recent hygroscopic seeding experiments:

A: Increasing the concentration of rain embryo particles: Seeding with ultra-giant CCN (size >10 μm), which serve as embryos for raindrops.

B: The enhanced tail effect: Seeding with giant CCN (diameter between 1 and 10 μm) adds drops to the large end tail of the droplet size distribution (DSD), and hence accelerates the further widening of the DSD and leads to formation of rain drops (Segal et al., 2004).

C. The competition effect: Seeding with giant or large CCN (diameter near 1 μm), for greater competition for the vapor, decreasing peak super saturation at cloud base, and hence reducing cloud drop number concentrations and broadening the cloud drop size distribution (DSD). This causes larger drops that coalesce faster into rain drops (Cooper et al., 1997).

Hygroscopic flares produce a size spectrum of aerosol particles (Cooper et al., 1997). The optimum size of particles to be used for hygroscopic cloud seeding for precipitation enhancement purposes is a current topic of scientific research and debate (see e.g. Segal et al., 2004; Rosenfeld et al., 2010).

The purpose of this paper is to present both airborne and surface observations of the smoke plume of the ICE hygroscopic flares, at different relative humidity, to document the dry and solution particles produced by the flare, compared with the background aerosol size distributions. These observations are intended to help assess the possible roles of the different rain enhancement seeding hypotheses that are applicable in the region.

3. The Activation Of Cloud Droplets

Many aerosols are soluble in water, and form a droplet of aqueous solution as water condenses onto them. The vapour pressure over a solution is lowered by the presence of the solute and hence growth of the droplet is energetically favourable. The fractional reduction in vapour pressure due to the presence of a solute is given by Raoult's law. Each individual Köhler curve is specific to the amount and composition of solute in the growing droplet (i.e. the dry radius, rs) and composition of the initial aerosol particle. In Figure 1, the super-saturation over the droplet is plotted as a function of the increasing wet radius of the aqueous droplet, r, formed as the dry aerosol particle dissolves in the accumulating water. The dashed line indicates ambient water vapour super-saturation, S = 0:15% which exceeds the critical super-saturation for (NH4)2SO4 particles with dry diameter > 0:1 μm, so these aerosols will activate

and grow into cloud droplets. Smaller particles remain as unactivated haze particles. Indicated drops (corresponding, for example, to a dry diameter of 0.05 μm) show how these haze particles return to their equilibrium curve through condensation or evaporation.

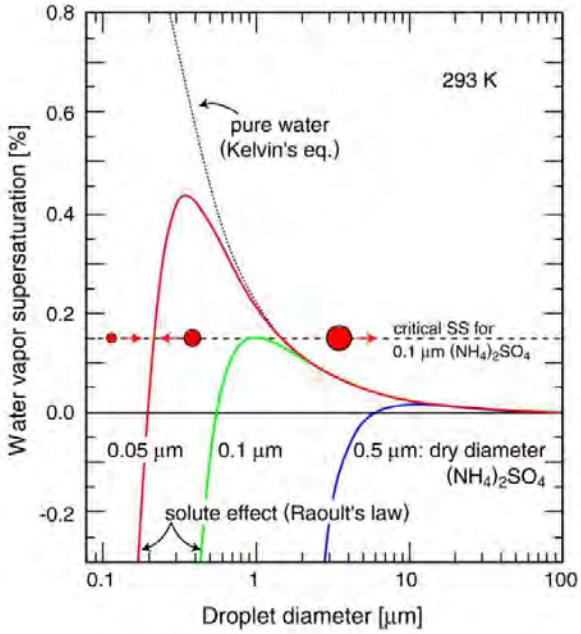


Figure 1: Köhler curves at 293K for pure water (dotted line) and a range of dry diameter (denoted by colour) of (NH4)2SO4 particles (solid lines). Taken from Andreae and Rosenfeld (2008) after Seinfeld and Pandis (1998).

Aerosols are traditionally categorised into fine particles (approx. D < 1 μm) and coarse particles (D > 1 μm). The fine particles are further split into the Aitken (or nucleation) mode (0:005 < D < 0.1 μm) and the accumulation mode (0.1 < D < 1 μm). From Fig. 1, one can see that a dry ammonium sulphate particle of 0.5 μm diameter produces a solution droplet of approximately 8 μm diameter at saturation (cloud base).

4. The Importance Of CCN Size On Rainfall

Segal et al., (2004) conducted numerical simulations to show the dependence of total parcel rain produced in seeding cloud parcels of different depths (Mediterranean thermodynamic conditions) on the radius of seeding nuclei in the case of a narrow natural CCN spectrum [log(r2) = 0.2]. They concluded that the deeper the parcel, the smaller the optimum radius. The optimum CCN radius depends, therefore, on the dynamic properties of clouds. They also concluded that when clouds are of small depth, seeding nuclei should be of a large size to lower the level of collision triggering to allow precipitation formation in these parcels. In deeper clouds, droplets have a longer time to grow. So that in deeper clouds, droplets formed on CCN of a smaller size can trigger collisions as well. As a result, the optimum radius of seeding nuclei decreases with the increase in the cloud parcel depth, as shown in Fig. 2.

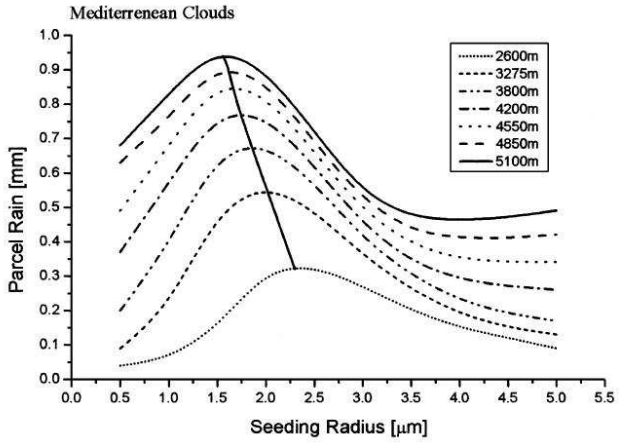


Figure 2: Parcel rain for cloud parcels of different depth as a function of the radius of the seeding nuclei (Segal et al., 2004).

Although the optimum seeding radius varies very little (approx. 1.5 to 2.5 μm), the enhancement effect for deep clouds which would typically be targeted by convective cloud seeding projects (e.g. >4000 m) is substantial for particles in the radius range 1 μm to 3 μm (2 to 6 μm diameter) .

5. Surface Aerosol Measurements

Continuous aerosol measurements were made at a surface site located at the PME Training Center near Abha, located just to the east of the Red Sea escarpment. The surface and airborne measurements were linked through a repeatedly employed flight pattern that included multiple low-level orbits around the site. Submicron and super-micron size distributions were measured at the surface using a differential mobility analyzer and a TSI, Inc. Aerodynamic Particle Sizer (APS), Model 3321. A Droplet Measurement Technologies (DMT) CCN counter (CCNc;) was operated together with a tandem differential mobility analyzer (TDMA) to measure super-saturation resolved CCN concentration and hygroscopic growth of size-resolved particles as the RH to which they are exposed is raised from <15% to 85%.

6. Aircraft Aerosol Measurements

The WMI Beechcraft King Air B200 was equipped to make cloud microphysical and liquid water content measurements. In addition, a PMS Passive Cavity Aerosol Spectrometer Probe (PCASP) and a DMA were operated on the aircraft to characterize the below-cloud aerosol size distribution. A pair of DMT CCN counters were operated on board the aircraft in order to provide 1 Hz measurement of CCN concentration at a single super-saturation and slower (~0.002 Hz) measurement of CCN spectra over a range in super-saturation.

7. Hygroscopic Flare Smoke Characterization

Three flights were conducted to measure the size distribution of the Ice Crystal Engineering (ICE) hygroscopic flare smoke. The flights were done by flying 200 to 300 m behind a seeding aircraft burning hygroscopic flares at various dosages and atmospheric relative humidity (RH). The size distribution of the flare smoke was measured and samples were obtained for chemical composition analysis. Table 1 provides a summary of the three flights that were conducted to characterize the flare smoke.

Table 1: Summary of flare smoke flights.

Date	Altitude (m)	Temp (℃)	Number of 1kg flares (kg/min)	RH (%)
20090809	7130	-7.0	6 (1.5)	8
20090812	3900	13.0	3 (0.75)	43
20090829	5200	-3.0	4 (1.0)	73

Figure 3 shows the combined size distribution of the flare smoke from the airborne DMA, PCASP and FSSP. What is unique about these measurements is that the complete aerosol size distribution (0.01 to ~10 μm) is now available for flare smoke. Previous measurements of flare smoke were done in the range of 0.1 to ~10 μm (Cooper et al.1997 and Ghate et. al. 2007). Both of those studies showed that observed size distributions of cloud droplets in seeded clouds experience a distinct broadening in comparison to the non-seeded case. This results in a higher number of larger cloud droplets (>15 μm) which enhance the collection process and thus precipitation formation. Furthermore, the cloud droplet number concentration decreases resulting from a preferred activation of the larger particles which reduces the super-saturation. Thus, smaller particles do not get activated and the total number concentration is reduced. This is referred to as the 'competition effect'. Another possible effect is the ''raindrop embryo effect' in which giant soluble particles can immediately become raindrop embryos. In some cases, one of the effects may be active, while in other cases, both effects may become effective, depending on the updraft velocity (i.e. super-saturation) and the amount and size of seeding particles. Rosenfeld et. al. (2010) discuss that the potential broadening of the drop size distribution at cloud base by the competition effect occurs when the seeding agent has still not diluted much, and hence affects a very small cloud volume that dilutes quickly. Therefore, the main expected effect of the giant CCN is probably serving primarily as raindrop embryos.

At the measured concentrations of smoke smaller than 0.1 μm the number concentration of CCN can be very large if these fine particles activate as CCN. Rosenfeld et. al. (2010) discuss that nucleant sizes and amounts are major considerations in hygroscopic seeding. According to model simulations, the CCN aerosols can be too small (radius < 0.25 μm) that they suppress precipitation or they can be too large (radius > 2.5 μm), resulting in early precipitation that truncates the convective cycle. Drofa et. al. (2010) conducted numerical simulations with a 1-dimensional warm cloud model to show that the effect of modifying clouds with hygroscopic particles depends on the cloud vertical thickness – the more the thickness, the greater the precipitation amounts. Numerous studies have been published that caution operational programs on the operational use of hygroscopic seeding using pyrotechnic flares. In principal flares should produce more coarse mode particles to introduce giant CCN in clouds.

Energy-dispersive spectrometry (EDS) data of smoke particles collected on 20090812 indicated signals for K, Cl, and Mg.

8. Flare Smoke Measurements At The Surface

Figure 4 shows the combined size distribution of the flare smoke from the ground measurements using the DMA and APS. The ground measurements were conducted on August 22, 2009 at approximately 1300 UTC. The surface temperature was 24 C and the RH was 78%. It must be mentioned that the DMA dries the aerosol through a naphion while the APS does not. The RH inside the APS is not exactly known since the flare burn produces some water vapour. Another caveat is the DMA measures the mobility diameter while the APS measures the aerodynamic diameter of the particle or solution droplet as the case may be. The affects of coincidence of multiple particles for the APS at high concentrations are not known at this time, but they are assumed to be negligible.

9. Discussion

According to Fig. 3, it appears that in Saudi Arabia the dust loading is so high in the boundary layer that the coarse mode of the flare smoke size distribution is not distinguishable from the background aerosol except in measurements done above the boundary layer (where dust is not present at high concentrations). This brings into question the effectiveness of flares in regions with a high dust loading. The chemistry and hygroscopicity of the dust would have to be studied in order to determine whether additional hygroscopic flare material would be beneficial to the broadening of the DSD.

The ground measurements (Fig. 4) indicate 1 to 2 orders of magnitude increase in the activated droplet spectrum at 78% RH, for the size range of particles (e.g. diameter > 5 um) thought to be important for the enhancement of precipitation within deep convective, continental clouds.

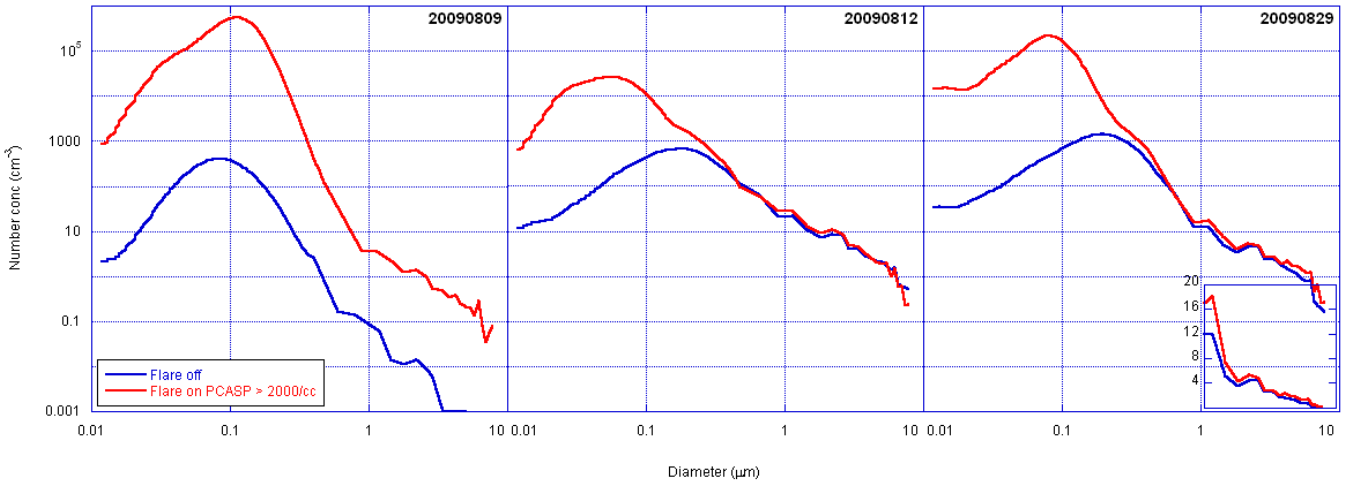


Figure 3: The combined aerosol size distribution of the flare smoke from the airborne DMA, PCASP and FSSP for the flights listed in Table 1, compared with the ambient aerosol size distribution at the same level. The panel at the left was collected at 8% RH above the boundary layer, the middle panel at 43% RH within the boundary layer, and the panel on the right was collected just below convective cloud base at 73%

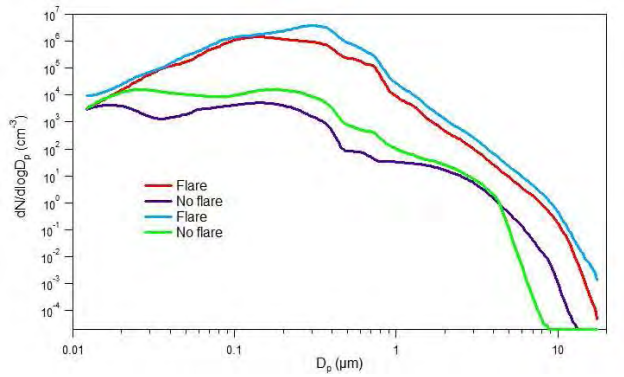


Figure 4: The combined aerosol size distribution of the flare smoke from the ground measurements using the DMA and APS.

Optimization of the flare size distribution should be considered (i.e. increasing the coarse fraction and decreasing the fine fraction in the flare smoke). Determining the minimum dry diameter of activation in the aerosol predominant in the study area and conducting updated simulations such as those done by Cooper et al. (1997) are needed.

Experiments using a burning chamber and a cloud chamber are needed to measure the cloud activation properties of flare smoke in an appropriately diluted and environmentally controlled flare burn experiment.

The measurements in this study suggest that the ICE hygroscopic flare particles fall within the range of suitable (if not optimal) particles for both enhancing the tail of the DSD and also in providing Giant CCN. The effect of dilution of the seeded plume within the cloud volume has not been addressed in this paper, although it is considered to be potentially important.

Acknowledgements

The authors are grateful to Prof. Don Collins and Dr. Runjun Lee at TAMU for providing the DMA and APS data from the airborne and ground measurements. The EDS analysis was provided by Peter Buseck and Evelyn Freney at Arizona State Univ.

References

Andreae, M.O., and D. Rosenfeld, 2008: Aerosol–cloud–precipitation interactions. part 1. the nature and sources of cloud-active aerosols. Earth-Science Reviews, 89(1-2):13–41.

Bruintjes, R. T., 1999: A review of cloud seeding experiments to enhance precipitation and some new prospects, *Bull. Amer. Meteorol. Soc.*, **80**, 805– 820.

Cooper, W.A., R.T. Bruintjes, G.K. Mather, 1997. Calculations pertaining to hygroscopic seeding with flares. J. Appl. Meteorol., 36, 1449–1469.

Drofa, A. S., V. N. Ivanov, D. Rosenfeld, and A. G. Shilin, 2010: Studying an effect of salt powder seeding used for precipitation enhancement from convective clouds, Atmos. Chem. Phys. Discuss., 10, 10741-10775.

Ghate, V.P., B.A. Albrecht, P. Kollias, H.H. Jonsson, and D. W. Breed, 2007: Coud seeding as a technique for studying aerosol-cloud interactions in marine stratocumulus, Geophys. Res. Lett., 34, L14807, doi:10.1029/2007GL029748.

Rosenfeld, D., D. Axisa, W. L. Woodley, and R. Lahav, 2010: A quest for effective hygroscopic seeding. Submitted to J.of Appl. Meteor.

Segal, Y., A. Khain, M. Pinsky, and D. Rosenfeld, 2004. Effects of hygroscopic seeding on raindrop formation as seen from simulations using a 2000-bin spectral cloud parcel model. Atmos. Res., 71, 3–34.

Seinfeld, J.H., and S. N. Pandis, 1998: Atmospheric Chemistry and Physics: from Air Pollution to Climate Change. John Wiley, New York.

Silverman, B. A., 2003: A critical assessment of hygroscopic seeding of convective clouds for rainfall enhancement. *Bull. Amer. Meteor. Soc.*, **84**, 1219-1230.

Contact:
Terry Krauss twkrauss@gmail.com
Duncan Axisa Duncan.Axisa@gmail.com
Roelof Rurger roelof.burger@wits.ac.za

Overview of CAIPEEX – Cloud-aerosol interaction experiment over Indian region

Kulkarni, J. R., Maheshkumar, R. S., Morwal, S. B; Padma Kumari, B., Mahen Konwar, Deshpande C. G., Joshi R. R., Bhalwankar R. V., Pandithurai G., Safai P.D., Narkhedkar S. G., Dani K. K., Nath A., Sathy Nair., Sapre V. V., Puranik P. V., Kandalgaonkar S., Mujumdar V. R., Khaladkar R. M., Vijayakumar R., Thara V. P. and B. N.Goswami

1. Introduction

Weather modification studies in India were started by Indian Institute of Tropical Meteorology (Murthy et al, 1975, 1976, Parasnis et al., 1982; Murthy et al., 2000). These initial experiments were focussing on group of clouds rather than individual cloud samples. Although conditions of cloud seeding were identified in these early experiments, verification and establishment of guidelines could not be done. Since these early experiments, there has been considerable increase in the aerosols and cloud-aerosol interaction in the monsoon environment was less understood in respect to the microphysics. Thus the need for a research based cloud seeding program was emphasised.

Under the auspices of the Ministry of Earth Sciences (MOES), IITM has started a new program to study the path ways through which aerosols may impact cloud and precipitation process. **C**loud **A**erosol **I**nteraction and **P**recipitation **E**nhancement **EX**periment (CAIPEEX) were conducted over Indian region with cloud microphysical and aerosol observations over several locations. This constituted both pre-monsoon and monsoon conditions. In addition, new flare technology for cloud seeding was tested for Indian clouds. Several state of the art instruments for cloud microphysics were first time used in CAIPEEX.

The first phase of the experiment was conducted in 2009 to document the aerosols and microphysical characteristics of clouds and environmental conditions over different regions of the country (Figure 1) and under different monsoon conditions with the help of an instrumented research aircraft.

Phase II of the experiment constituted both research flights and cloud seeding flights originating from Hyderabad. This location was chosen to give specific emphasis to the rain shadow region. There are drastic differences in the cloud microphysical characteristics as we move from the Western Ghat region towards east. The cloud droplets are numerous and are much smaller over the rain shadow region compared to that over the coastal regions. Both flares and salt powder were used for seeding. The main aim of this paper is to give an account of the phase I experiment and how it was possible to characterise the regions amenable for seeding with overview research flights during year I.

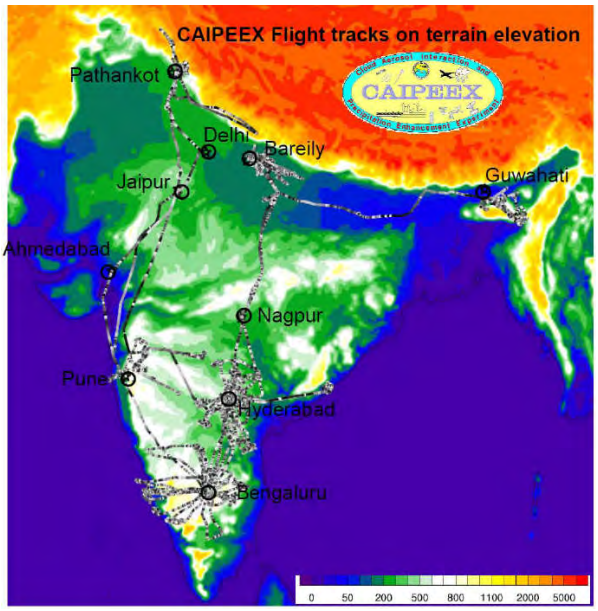


Figure 1. CAIPEEX research flight tracks during phase I of the experiment.

2. Research findings:

Several research findings were noted for the first time. For example:

- Dramatic ways that aerosols influence the cloud microphysics in clouds growing in the polluted and moist environments is noted for the first time in the monsoon clouds. A companion paper (Prabha et al) the same conference will give details of this important finding.
- An elevated aerosol layer and multiple layering over different parts of India
- Drastic difference in the vertical distribution of aerosols near the foot hills

of Himalayas with elevated layer depth up to a height of 5-6 km.

- Black carbon vertical profiles over different regions showed layering effects, which as severe consequences for vertical heating/cooling rates
- A critical effective radius of 14 microns seemed to be important for the clouds sampled during CAIPEEX
- Relationship between the warm rain depth and the CCN concentration

Phase II first year experiment was conducted with additional observations of trace gases and radiation. There were very specific mission oriented flights to investigate the cloud microphysical characteristics of clouds in the Bay of Bengal (Figure 2), where continental nature of the clouds is lost and a more pristine environment with fewer cloud droplets is found. Cloud droplet number concentration decreased drastically over the Arabian sea.

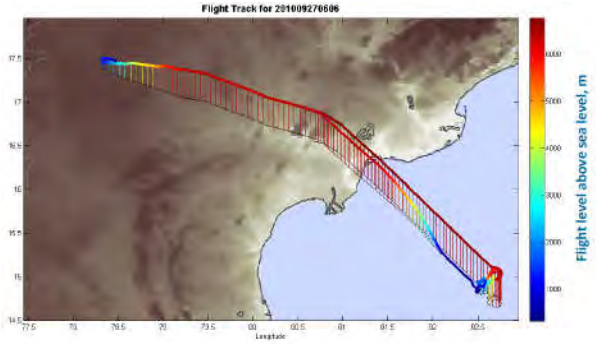


Figure 2. Flight track over the Bay of Bengal

3. Cloud seeding objective

There was a research aircraft and a seeder aircraft during the Phase II of CAIPEEX. About 200 hrs of flying was completed by both aircrafts. The research aircraft was flown for 120 hrs and the seeder aircraft was flown for 80 hours. The cloud seeding operations were carried out mostly using the seeder aircraft. Hygroscopic salt powder (of size 1-10 micron) and flares (particle size 0.1 – 1 micron) were used as the seeding material. SF_6 gas was used as the tracer to identify seeded cloud. Using tracking software, coordination between the aircraft was established. Telemetry link was utilized for communication between radar and aircraft, to monitor and guide the aircraft for seeding operations. About 15 coordinated seeding missions were conducted successfully and seeding signatures were observed in the seeded cloud volumes. About 1600 kg of salt powder and about 100 flares were utilized during the seeding missions.

4. Acknowledgements

We are grateful to the Ministry of Earth Sciences, Government of India for support without which this experiment would not be possible. We are also thankful to the National Steering Committee headed by Shri D. R. Sikka for guidance and encouragements. We are thankful to our consultant Prof. D. Rosenfeld of The Hebrew University of Jerusalem and his team for critical guidance and advice during the conduct of the experiment and data quality assessment.

References

Murty, A.S.R., Mary Selvam, A. and Ramana Murty, Bh. V., Summary of observations indicating dynamic effect of salt seeding in warm cumulus clouds. *J. Appl. Meteor.,* 1975, 14, 629-637.

Murty, A.S.R., Mary Selvam, A., Paul, S.K., Vijayakumar, R. and Ramana Murty, Bh. V., Electrical and microphysical measurements in warm cumulus clouds before and after seeding. *J. Appl. Met.,* 1976, 16, 1295-1301.

Murty, A. S. R., Selvam, A. M., Devara, P.C.S., Krishna, K., Chatterjee, R. N., Mukherjee, B. K., Khemani, L. T., Momin, G. A., Reddy, R. S., Sharma, S. K., Jadhav, D. B., Vijayakumar, R., Raj, P. E., Manohar, G. K., Kandalgaonkar, S. S., Paul, S. K., Pillai, A. G., Parasnis, S. S., Londhe, A. L., Bhosale, C. S., Morwal, S. B., Safai, P. D., Pathan, J. M., Indira, K., Naik, M. S., Rao, P. S. P., Sikka, P., Dani, K. K., Kulkarni, M. K., Trimbake, H. K., Sharma, P. N., Kapoor, R. K. and Tinmaker, M. I. R., 11-year warm cloud seeding experiments in Maharashtra, India. *J. Wea. Modif.*, 2000, 32, 10-20.

Parasnis, S. S., Selvam, A. M., Murty, A. S. R. and Ramana Murty, Bh.V., Dynamic responses of warm monsoon clouds to salt seeding. *J. Wea. Mod.,* 1982, 14, 35-47.

Analysis of Radar and Airborne Data for Artificial Seeding Effects

Lei Ji[1], Jianli Ma, Hongyu Li, Wei Zhou, Qiang Zhang, Jianzhong Liu
Beijing Weather Modification Office, Dept. of Beijing Meteorology Bureau, Beijing, China

1. Introduction

The evaluation of the effects of artificial ice nucleants on clouds and precipitation is a difficult task. In general, it requires careful physical measurements and statistical evaluations. Daniel Rosenfeld(2005), Xing Yu and Jin Dai(2005), Hobbs(1973,1981),and T.W.Krauss(1987) has given some useful analysis.

From 2003, most of the work has been carried out on the artificial seeding in Beijing. We describe below a case study conducted on 24 August 2008, in which artificial seeding was carried out.

The rest of this paper is laid out as follows: In section 2, general procedures and the data used for analysis is described. Section 3 presents the results of radar data to illustrate the changes in the cloud before and after seeding. PMS data obtained by aircraft are presented in section 4. Finally, summary and conclusions are described in section 5.

2. General procedures and the data

On 24 August 2008, a nonprecipitating, altocumulus cloud was situated at the north edge of Mentougou District in Beijing city at 1100 UTC. Cheyenne ⅢA 3626 aircraft was used as the seeding and particle observation platform with airborne silver iodide end-burning pyrotechnic (each contains 25g AgI) generators and PMS equipments including PCASP-100X, FSSP-100, OAP-2DGA2, OAP-2DGB2, so that Information on the microphysics structure of the cloud before and after seeding could be obtained. Pressure altitude probe, temperature probe and dewpoint thermometer was also set on the plane. An S-band radar located at Beijing Weather Observatory was used to record the displacement of echoes, echo size, and characteristics on every scan (PPI). Winds were from 300º at about 1m/s that obtained from Rawinsonde in Beijing at 6km at 1200 UTC.

The aircraft made three passes at about 6km, and the average flight speed was 360km/h. The first seeding procedure began at 1108 UTC at 6km and was seeded at a rate of approximately 2.2g AgI per kilometer along a line 45km long (four airborne silver iodide end-burning pyrotechnics at a time were used). The temperature of this level was from -15.5℃ to -16.3℃.

Several other airborne silver iodide end-burning pyrotechnics were also used after the first seeding procedure, however, there was no significant change have been found. On the one hand, the environment was not suit for seeding as the cloud trended toward dissipation, on the other, the pyrotechnics generators had some burning problems.

We will analyse the first seeding procedure from radar and aircraft data as follows.

3. Radar studies

The radar echo patterns at 6km before and after seeding with flight path that was in a clockwise direction (white line, a-b-c-d-a in Fig. 1a.) are given in Fig.1. The seeding operation started from point E (at 1108 UTC), passed to point B (at 1112 UTC), and finished in point F (at 1114 UTC).

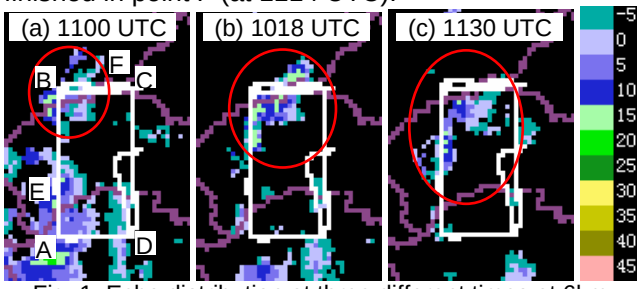


Fig. 1. Echo distribution at three different times at 6km

We can find that a clear echo track like "r", of which the regions were corresponding to the seeding route, appeared after seeding (Figs. 1b and 1c, inside the red circle). The echo intensities in the north part of the route enhanced, whereas the south part of the echo dispersed rapidly.

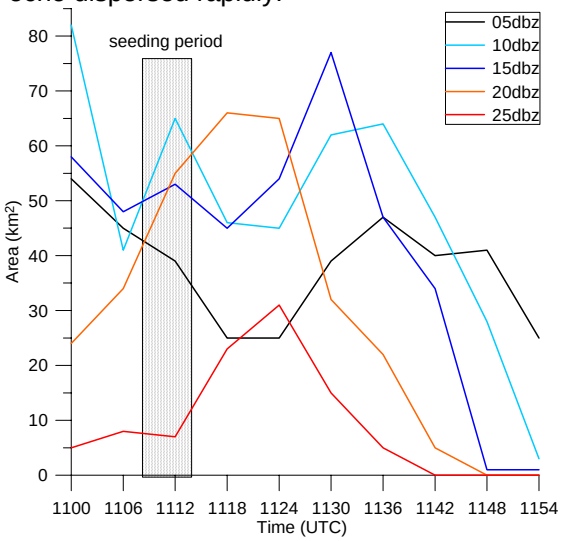


Fig. 2. radar echo areas with different levels at 6km

Fig. 2. gives the area of different radar echoes at 6km. It shows that the echo areas between 16dbz and 25dbz increased rapidly while the areas of echo below 15dbz decreased between 1118 and 1124

[1] Corresponding author address: Lei Ji, Beijing Weather Modification Office, Dept. of Beijing Meteorology Bureau, Beijing, China, e-mail: xman1982426@163.com.

UTC after seeding. That is to say significant changes in some part of the cloud were produced just 10 minutes later after seeding.

However, the echoes became weaker after 1130 UTC while the areas of echo below 15dbz enhanced, and no precipitation reached the ground. There was no radar echo above 25dbz. The radar echoes at 5.5km or lower levels were also enhanced after 1124 UTC (Figure omits here), which was about 12 minutes later than the higher levels.

4. Microphysical studies

It can be seen from Fig. 1 that the cloud moved mainly southward, which cause the seeded cloud out of the flight path between turning points B and C when the second pass began at 1127 UTC about 17 minutes after seeding. The cloud had been dissipated when the third pass began at 1142 UTC. We will compare the seeded portion of the cloud between turning points A and B on first aircraft pass as unseeded with the portion on the second pass as seeded.

We missed the best detection time between 1118 and 1124 UTC because we could not confirm the condition of the seeded cloud by eyes in the evening and there was no radar data on the plane.

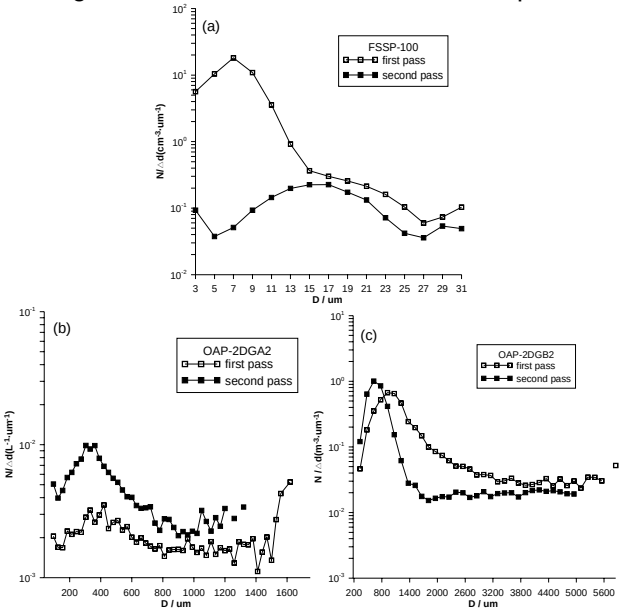


Fig. 3. Spectrum distribution determined before and after clouding seeding by PMS

As shown in Fig.3, the average number of cloud droplets which smaller than 31um (Fig. 3a) and bigger than 1200um (Fig. 3c) in diameter decreased after seeding, but increased when the ice droplets' diameter between 36um and 1200um (Fig. 3b).

It can be inferred that the depletion of the smaller particles was no doubt due to their collection by the larger ice particles and the process of Bergeron-Findeison could be accelerated when AgI particles came into the cloud, especially the droplets smaller than 15um in diameter.

Fig. 3b shows that the number of cloud droplets from 36um to 600um in diameter increased 3-5 times after seeding, while the number of cloud droplets between 600um and 1200um in diameter increased less than 2 times. We can also see from Fig. 3c that the number of cloud droplets decreased sharply between 1200um and 2400um in diameter. One rational explanation of this phenomenon may be that the increasing of Cloud droplets between 36um and 1200um in diameter made the process of coagulation and condensation more easily, especially the cloud droplets between 1400um and 2400um in diameter that grown bigger and fallen down to lower levels at last, which might cause the enhancement of radar echoes at lower levels.

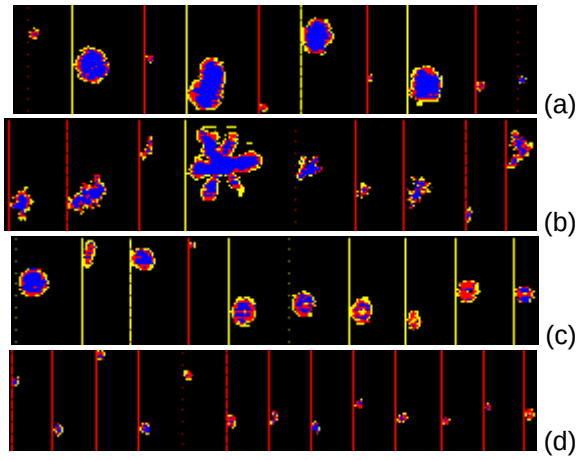


Fig. 4. Cloud droplet images determined by PMS before (a, b) and after (c, d) cloud seeding

The predominance of graupel、rimed snow crystals and their polymers in the cloud was confirmed by the first aircraft pass (Figs. 3a and 3b), which illustrated that there was certain concentration of supercooled cloud water where the environment was suit for cloud seeding. About 17 minutes later, a mass of platelike ice crystals with equal size had became the primary components of the seeded cloud during the second aircraft pass (Fig. 3c), unrimed snow crystals and their polymers which were smaller and less than before were also observed (Fig. 3d), which meant that the supercooled cloud water had been used up. The seeded cloud was glaciated, nearly featureless, and consisted almost entirely of unrimed and unaggregated ice particles.

The reason why the echo enhancement lasted for only about 12 minutes and there was no echo above 25dbz, as shown in Fig. 2, might be that with the exhaustion of supercooled cloud water and the diffusion of crystals, the concentration of ice particles in the seeded cloud decreased which directly leaded to the dissipation of the cloud.

5. Summary and conclusions

The main purpose of this study is to physically evaluate the effects of artificial seeding.

The effects on the cloud on 24 August 2008 can be seen from S-band radar just about 10 minutes after seeding. However, only the environment with supercooled cloud water is suit for seeding. The more concentration of supercooled cloud water, the stronger the seeded cloud can grow up, otherwise,

both intensity and duration of the seeded cloud would be restricted.

The seeding promoted glaciation and some microphysical changes occurred in the cloud. The concentration of ice particles with sizes between 36um and 1200um in diameter increased several times that made the process of coagulation and condensation more easily; steeply dissipation of particles with sizes smaller than 15um in diameter could illustrate the reduction of supercooled liquid water content; the fall of ice particles larger than 1200um in diameter might cause the enhancement of radar echo at lower levels; a large amounts of unrimed and unaggregated ice crystals, such as platelike particles and unrimed snow crystals and their polymers which grow at the relatively low supersaturations, were appeared in the seeded cloud.

The experiments plan should be improved. We should make the first return to the seeded cloud at about 10 minutes after seeding in order to obtain the best data for physical evaluation, and several other passes are valuable. Flight path should be adjusted properly when the seeded clouds move. More experiments should be carried out in the future.

Acknowledgements

The authors gratefully acknowledge the assistance of Qiang Wei, Yajiang Ying and Lei Wang in collecting aircraft data. The efforts by the pilot and supporting staff at the Tri-star General Aviation (Cheyenne ⅢA 3626) were particularly valuable.

References

Daniel Rosenfeld, Xing Yu and Jin Dai, Satellite retrieved microstructure of AgI seeding tracks in supercooled layer clouds. *J. Appl. Meteor*, **44**, 760-767, 2005.

Hobbs, P. V. and L. F. Radke. Redistribution of Snowfall Across a Mountain Range by Artificial Seeding: A Case Study. *Science*, **181**, 1043-1045.1973.

Hobbs, P. V., J. H. Lyons, J. D. Locatelli, K. R. Biswas, L. F. Radke, R. R. Weiss, and A. L. Rangno. Radar Detection of Cloud Seeding Effects. *Science*, **213**, 1250-1252. 1981.

T.W.Krauss, R.T.Bruintjes and J.Verlinde. Microphysical and Radar Observations of Seeded and Nonseeded Continental Cumulus Clouds. *J.Climate Appl. Meteor.* **26**, 585-606. 1987.

Xing Yu and Jin Dai, Daniel Rosenfeld, Hengchi Lei, Xiaohong Xu, Peng Fan, Zhengqi Chen. Comparison of simulations of transport and diffusion of seeding material within stratiform cloud in rain enhancement with NOAA satellite data. *J. Appl. Meteor*,, **44**, 749-759. 2005.

Initial part discussion of cloud merger

Li Yanwei Niu Shengjie
Nanjing University of Information Science & Technology, 210044, China
E-mail: liyw0507@163.com

1. Introduction

Merger of clouds plays an important role on evolution of clouds forming and precipitation process. A large amount of papers(Bennetts et al., 1982; Tian, 1991; Doernbrack, 1997; Knupp et al., 1998; Carey et al., 2000; Jirak et al., 2003;) have shown that Merger often happens between clouds or cloud clusters. Cloud merger is the expression of enlargement and enhancement of clouds, which has significant effect on genesis of precipitation system. Simpson et al. (1980) observed some merger processes in south Florida in the summer of 1973, they proposed that although there was only 10% merger happened in three days in observing area, but 86% precipitation was formed by this part of merger. Furthermore, merger often generate in original stage of clouds, as well as in other stages. After merger, the characteristics of clouds and precipitation change a lot, particularly showing as the enhancement of intensity, height, horizontal scale, precipitation efficiency and lightening frequency. Merger of convective clouds can lead to much more severe and highly-developed precipitating system.

In order to discuss the merger mechanism, many research deeply analyzed the merger process and environment condition using methods of observation and numerical simulation, most of essays（Tao et al., 1984; Ackerman et al., 1988; Westcott et al., 1989, 1994; Chu et al., 2000; Lee et al., 2006; Pozo et al., 2006; Danhong Fu et al., 2007 ） support a similar conclusion: Surface convergence and wind shear is essential to merger. The genesis of merger processes are mainly because of the cold outflow of convective clouds, which inspires cloud bridges between nearby cells, and initial merger happens at lower part of the clouds.

We found through observation, however, sometimes merger initially develops from the lower part of clouds, while sometimes from the upper part. Merger initially from lower part often emerges in original stage or developing stage of cloud body, while the other ones often happens in mature stage. The above shows that there are different types of merger, which is not mentioned in previous study. This type of merger is equally important in development of clouds, so that we choose a merger case in mountainous area of Southwest China to reveal this type of merger in a new sight of view.

2. Environmental support of merger

2.1 Analysis of weather situation

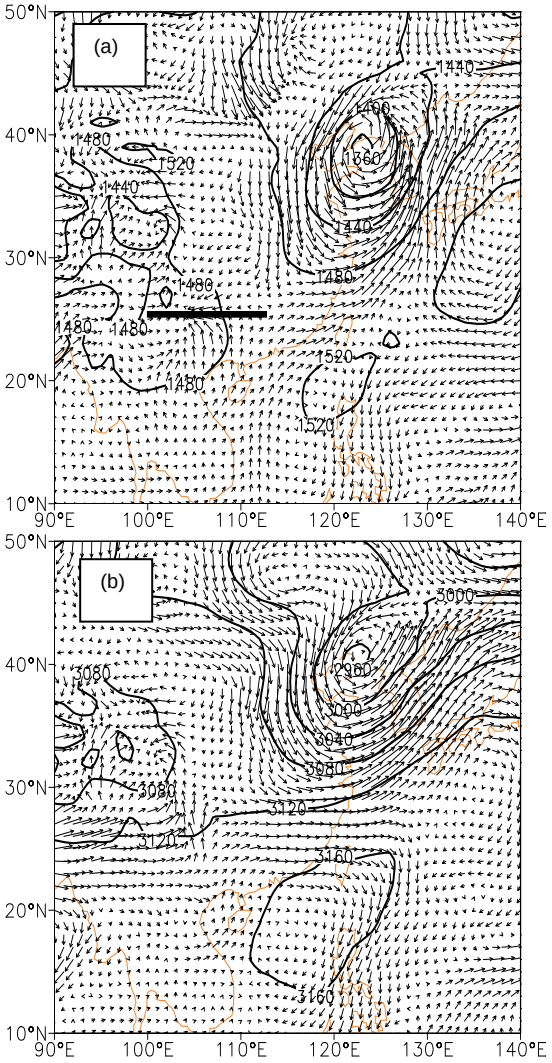


Fig.1 height(gpm) and wind vector(m/s) fields on May 17th in 2005: (a) on 850hpa level, (b) on 700hpa level

This paper begins with case analysis, and a merger process happened in Southwest mountainous area (mainly in Guizhou Province) from May 17th-18th, 2005, is studied. Supportive synoptic background of this merger process is mainly represent in this three aspects: (1) On 850hPa synoptic field, Moving speed of Northeast cold vortex was high, which led to deposit of cold air behind the cold vortex, so that the Northern part of Guizhou was mainly affected by North cold airflow. Meanwhile, southwest airflow stroke Guizhou Province. As a result, a convergent line was formed on level of 850hPa (With longitude from 104~112, shown as the black line in Fig 1a). Correspondingly, a stationary front was also generated on the surface, and most of Guizhou Province was in cold area. (2) Between 700hPa (Fig 1b) and 850hPa (Fig 1a), it existed vertical wind

shear, which was advantageous to development of clouds.

2.2 Analysis of atmospheric stability

Atmospheric unstable energy of Guiyang is analyzed; and the result shows that the air on the evening of May 17th was potentially unstable, which had active effect on convection. Thus the air was easier to be lifted by external force or topography and then convective cells were able to emerge and merge.

2.3 Analysis of divergence field

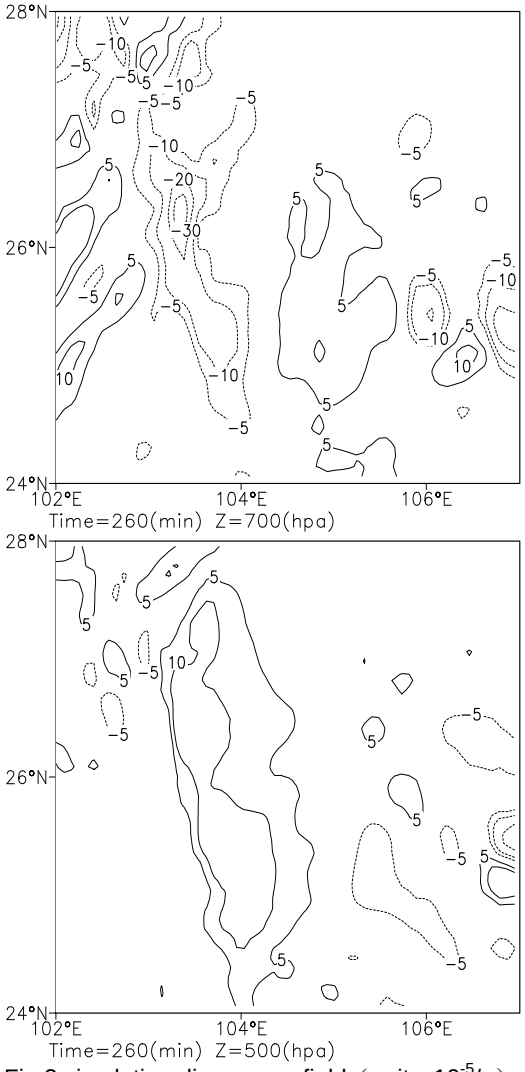


Fig.2 simulation divergence field（unit：10^{-5}/s）

It is time for rapid development of convective cells when observation began for 260min, so we depict the distribution of divergence field on different vertical level, as shown in Fig 2. After analyzing the divergence field on 700hPa and 500hPa, we find that under that certain weather background, lower level near the clouds (700hPa) is convergent while the upper level (500hPa) is divergent. This pattern has advantages to transmit vapor and energy from the environment into the clouds. At this moment, convergence on 700hPa is almost the strongest, and then become weaker. Furthermore, strong convergent field moved from west to east, with the same direction of where clouds move.

3. Observation of merger of convective clouds

Instruction of merger during development of clouds (Shown in Fig 3): at 22:50, May 17th, there are two larger convective clouds displaying in Guiyang radar pictures which merged by some small convective cells; at 00:00, May 18th, these two convective clouds continue to develop and merge small convective cells, and finally become two relatively larger convective cloud clusters; at 02:00, May 18th, these two cloud clusters finally get together as one wide-ranged precipitation system with long duration.

By comparing vertical section of radar echo patterns (shown in Fig1b~d), it found that merger can initially develop from lower part of clouds (Fig1b-c), as well as the upper part (Fig1d). Those processes which develop from lower level often happen between newly-generated cells. The clouds are developing and have short distance between each other. And those processes developing from upper part often happen between relatively large clouds. In this situation, each clouds is already has several column-like convective echoes, and with wide horizontal range. No matter what type of merger it may be enhancement of clouds and enrichment of height can be found after merger.

4. Conclusion & Discussion

This paper discusses merger process of clouds based on observation, and finds that: the initial merger position of clouds varies from the lower part of clouds and upper part of it. Those ones which develop from the lower part initially are often found between vigorous convective cells while those ones develop from the upper part are found between mature convective cloud clusters.

Further analysis of forming mechanism of these two types of merger can be taken by numerical simulation. Limited by space, this part will not be discussed in paper.

Acknowledgements

This work was supported by the Natural Science Foundation of China (Grant No. 40975086).

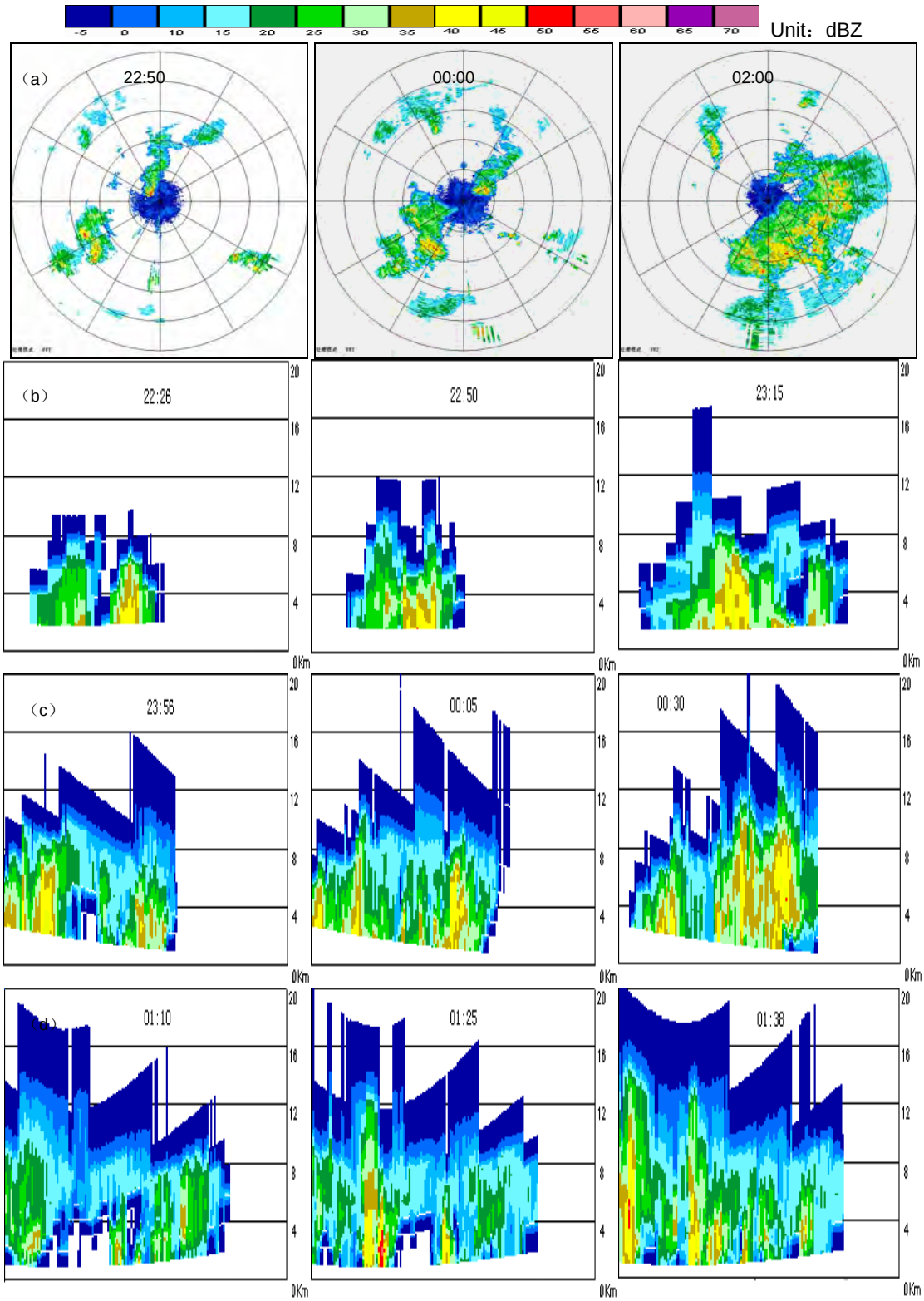


Fig.3. Process of clouds merger (a) PPI radar reflectivity of Guiyang at elevation 1.5°; (b) Cloud merger process from middle and below part at azimuth 240°; (c)cloud clusters merger process from middle and upper part at azimuth 220°; (d) cloud clusters merger process from middle and upper part at azimuth 90°. Color shading denotes radar echo.

References

[1] Ackerman Bernice, Kennedy Patrick C, On the merger of two small convective radar echoes[J]. *Annalen der Meteorologie*, 2(25): 440-442, 1988.

[2] Bennetts DA, Bader MJ, Marles RH, Convective cloud merging and its effect on rainfall[J]. *Nature*, 300(5887): 42-45, 1982

[3] Carey Lawrence D, Rutledge Steven A, The relationship between precipitation and lightning in tropical island convection: a C-band polarimetric radar study[J]. *Monthly Weather Review*, 128(8): 2687-2710, 2000.

[4] Chu Chang-Min, Lin Yuh-Lang, Effects of orography on the generation and propagation of mesoscale convective systems in a two-dimensional conditionally unstable flow[J].

Journal of the Atmospheric Sciences, 57(23): 3817-3837, 2000.
[5] Doernbrack Andreas, Broadening of convective cells[J]. *Quarterly Journal of the Royal Meteorological Society,* 123(540): 829-847, 1997.
[6] Fu Danhong, Guo Xueliang, A Cloud-resolving Study on the Role of Cumulus Merger in MCS with Heavy Precipitation[J]. *Advances in atmospheric sciences*, 23(6): 857–868, 2006.
[7] Fu Danhong, Guo Xueliang, The role of cumulus merger in a severe mesoscale convective system[J]. *Chinese Journal of Atmospheric Sciences,* 31(4): 635-644, 2007.
[8] Jirak IL, Cotton WR, McAnelly RL, Satellite and Radar Survey of Mesoscale Convective System Development[J]. *Monthly Weather Review,* 131(10): 2428-2449, 2003.
[9] Knupp Kevin R, Geerts Bart, Goodman Steven J, Analysis of a small, vigorous mesoscale convective system in a low-shear environment. Part I: Formation, radar echo structure, and lightning behavior[J]. *Monthly Weather Review,* 126(7):1812-1836, 1998.
[10] Knupp Kevin R, Geerts Bart, Tuttle John D, Analysis of a small, vigorous mesoscale convective system in a low-shear environment. Part II: Evolution of the stratiform precipitation and mesoscale flows[J]. *Monthly Weather Review*, 126(7):1837-1858, 1998.
[11] Lee BD, Jewett BF, Wilhelmson RB, The 19 April 1996 Illinois Tornado Outbreak. Part I: Cell Evolution and Supercell Isolation[J]. *Weather and Forecasting*, 21(4): 433-448 2006.
[12] Lee BD, Jewett BF, Wilhelmson RB, The 19 April 1996 Illinois Tornado Outbreak. Part II: Cell Mergers and Associated Tornado Incidence[J]. *Weather and Forecasting*, 21(4): 449-464, 2006.
[13] Pozo D, Borrajero I, Marin JC, A numerical study of cell merger over Cuba - Part I: implementation of the ARPS/MM5 models[J]. *Annales Geophysicae*, 24(11): 2781-2792, 2006.
[14] Pozo D, Borrajero I, Marin JC, A numerical study of cell merger over Cuba - Part II: sensitivity to environmental conditions[J]. *Annales Geophysicae*, 24(11): 2793-2808, 2006.
[15] Simpson Joanne, On cumulus mergers[J]. *Archiv fuer Meteorologie, Geophysik und Bioklimatologie*, 29(1): 1-40, 1980.
[16] Tian Shengchun, Effect of merging of the convective cloud clusters on occurrence of heavy rainfall[J]. *Advances in Atmospheric Sciences*, 8(4): 499-504, 1991.
[17] Tao WeiKuo, Simpson Joanne, Cloud interactions and merging: numerical simulations[J]. *Journal of the Atmospheric Sciences*, 41(19): 2901-2917, 1984.
[18] Westcott Nancy E, Kennedy Patrick C, Cell development and merger in an Illinois thunderstorm observed by Doppler radar[J]. *Journal of the Atmospheric Sciences,* 46(1): 117-131, 1989.
[19] Westcott Nancy E, Merging of convective clouds: cloud initiation, bridging, and subsequent growth[J]. *Monthly Weather Review*, 122(5): 780-790 1994.

Aircraft Measurements of Aerosols、Clouds and Precipitation Over Beijing

Ma XinCheng　Huang MengYu　Jin Hua　Zhang Lei　Zhang Qiang
Beijing Weather Modification Office，Beijing China, 100089
e-mail: fellow_007@163.com

1、Introduction

Beijing Weather Modification Office (BWMO) obtained the materials of the aerosols、clouds and the precipitation physics structure by airplane since 2005.This paper involves the vertical distribution of aerosols and its impact on the chemical reaction study, the macro and micro structural features of clouds and the precipitation formation mechanism, the effect of Aerosol or CCN on clouds etc.

2、Vertical distributions of aerosol particles

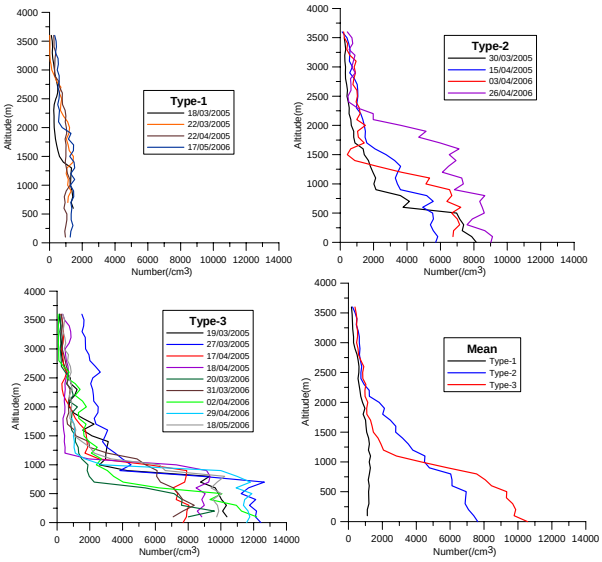


Figure 1, Vertical distributions of aerosol number density for type-1, type-2, and type-3, and averaged values

In this study, aerosol vertical distributions of 17 in-situ aircraft measurements during 2005 and 2006

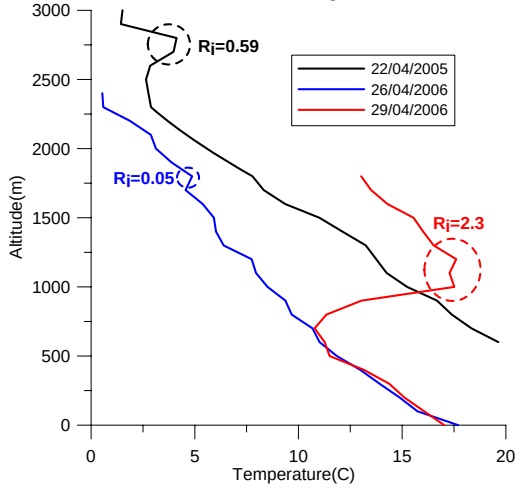


Figure 2, The calculated Ri number at the top of the PBL height under 3 typical conditions.

springs are analyzed. The 17 flights are carefully selected to exclude dust events, and the analyses are focused on the vertical distributions of aerosol particles associated with anthropogenic activities. The results show that the vertical distributions of

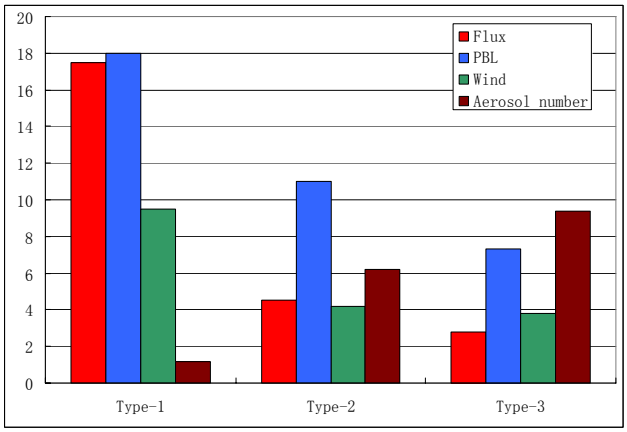


Figure 3, The averaged values for the wind flux, the PBL height, averaged wind speed and the aerosol number concentrations in the PBL for the 3 type conditions. Red is for wind flux (m^2/s x 1000); blue is for the PBL height (m x 100);green is for wind speeds (m/s);and brown is for the aerosol number concentrations(#/cm^3·1000).

aerosol particles are strongly affected by weather and meteorological conditions, and 3 different types

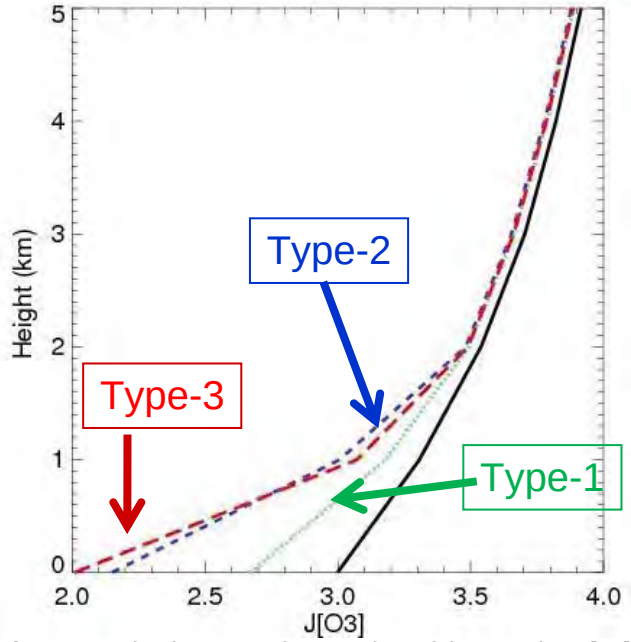


Figure 4, The impacts of aerosol particles on the J[O_3] values (1/s x 10^{-5}) under 3 type aerosol conditions. Black is the J[O_3] values under clear sky; green is the effects due to the type-1 aerosol distributions; blue is the effects due to the type-2 aerosol distributions; and red is the effects due to the type-1 aerosol distributions.

of aerosol vertical distributions corresponding to different weather systems are defined in this study. The measurement with a flat vertical gradient and low surface aerosol concentrations is defined as type-1; a gradual decrease of aerosols with altitudes and modest surface aerosol concentrations is defined as type-2; a sharp vertical gradient (aerosols being strongly depressed in the PBL) with high surface aerosol concentrations is defined as type-3. The weather conditions corresponding to the 3 different aerosol types are high pressure, between two high pressures and low pressure systems (frontal inversions), respectively. The vertical mixing and horizontal transport for the 3 different vertical distributions are analyzed. Under the type-1 condition, the vertical mixing and horizontal transport were rapid, leading to strong dilution of aerosols in both vertical and horizontal directions. As a result, the aerosol concentrations in PBL (planetary boundary layer) were very low, and the vertical distribution was flat. Under the type-2 condition, the vertical mixing was strong and there was no strong barrier at the PBL height. The horizontal transport (wind flux) was modest. As a result, the aerosol concentrations were gradually reduced with altitude, with modest surface aerosol concentrations. Under the type-3 condition, there was a cold front near the region. As a result, a frontal inversion associated with weak vertical mixing appeared at the top of the inversion layer, forming a very strong barrier to prevent aerosol particles being exchanged from the PBL height to the free troposphere. As a result, the aerosol particles were strongly depressed in the PBL height, producing high surface aerosol concentrations. The measured vertical aerosol distributions have important implications for studying the effects of aerosols on photochemistry. The J[O3] values are reduced by 11%, 48%, and 50%, under the type-1,type-2 and type-3 conditions, respectively. This result reveals that atmospheric oxidant capacity (OH concentrations) is modestly reduced under the type-1 condition, but is significantly reduced under the type-2 and type-3 conditions. This result also suggests that the effect of aerosol particles on surface solar flux is an integrated column effect, and detailed vertical distributions of aerosol particles are very important for assessing the impacts of aerosol on photochemistry.

3、The precipitation formation mechanism

A detailed analysis of macro/ micro structure for midlevel clouds has been conducted based on data including airborne DMT PMS (Droplet Measurement Technologies Particle Measuring System) , radar , satellite and weather chart etc. obtained from field campaign on 18 August 2010 in Beijing, and the precipitation formation mechanism is preliminarily discussed. The results show that the midlevel clouds on the mountain in Beijing had apparent stratification structure with deep cold cloud area、middle warm cloud area and big vertical height (less than 7 km),but it had high super cooled water content with a maximum value of 1.1g/ m^3 in the warm cloud area. The CIP/PIP probe shows that aggregation is a major growth mechanism 、 riming have an important contribution to precipitation formation in cold cloud area and melting in 0℃ layer 、 collision and coalescence in the warm layer play a major role in maintaining precipitation.A negative correlation between the number concentration and the diameter of cloud particles is found near 0℃ layer. The number concentration of droplets in the region of strong updraft is smaller than that in the region of weaker updraft. The accumulation region of particle concentration is found below 0℃ layer due to the updraft effect.

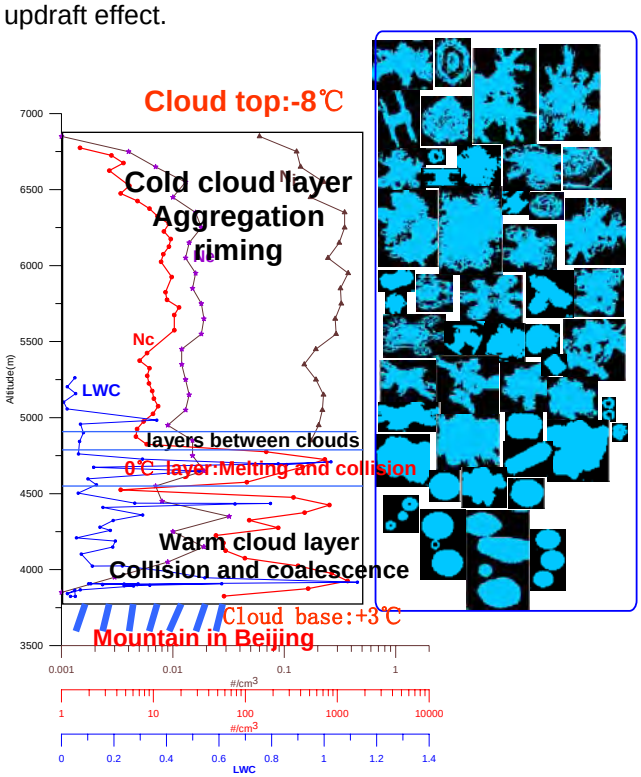


Figure 5,Sketch map of the precipitation formation mechanism

4、the effect of Aerosol or CCN on clouds

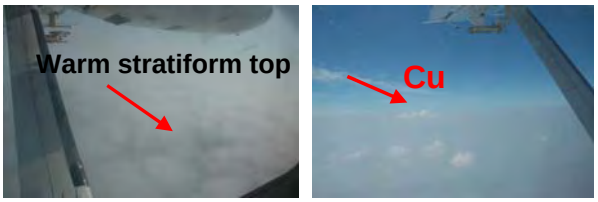


Figure 6, Warm stratiform and Cu around Beijing area

Warm stratiform and Cu microphysical parameters including cloud droplet number concentration (Nc),CCN, liquid water content (ql) and effective diameter (D) around the Beijing area during 2008 are summarized. Warm stratiform is often single layer witch the thickness is about 300m and often not easy to create the ground precipitation. The Nc of warm cloud has a maximum value of 500-800cm^{-3}, the effective diameter (D) is very small. The

result show that the relation between aerosol particle and CCN(NCCN, SS=0.3%) concentrations: Nccn=0.33Na-1366.25(Figure 7), The Relationship between CCN and cloud droplet concentration in stratiform and Cu show that An increase in aerosol concentrations Na causes an increase in drop concentration Nd in stratiform, but not around Cu.

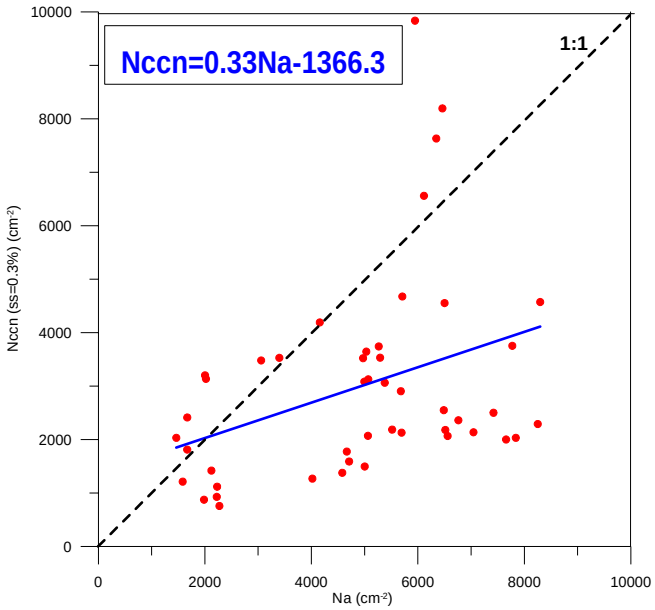


Figure 7, Relation between aerosol particle and CCN(NCCN, SS=0.3%) concentrations

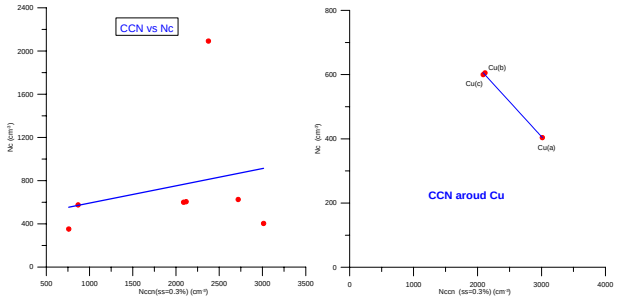


Figure 8, The Relationship between CCN and cloud droplet concentration in stratiform and Cu

Acknowledgements

This research was supported by the Beijing Excellent Talent Fundation under grant No. 20081D0200800058 and the National Important basic research and development plan projects under grant No.2011CB403401.

References

Jeffrey L.Stith,James E. Dye,Aaron Bansemer,and Andrew J.Heymsfifld, Microphysical Observations of Tropical Clouds,J.A.M, 41(11), 97-117, 2002.

Houze R A,Hobbs P V.Organization and Structure of Precipitating Cloud Systems.Adv.Geophys.24:225-315,1982

Kleinman L I,Daun P H。《Vertical distribution of aerosol particles,water vapor,and insoluble trace gases in convectively mixed air 》。J Geophys Res,1991,96(D1):991-1005

Kim Y J,Sievering H,Boatman J F 。《Airbone measurement of atmospheric aerosol particles in the lower troposphere over the central United States》。J Geophys Res,1988,93(D10):12631-12644

Fouquart Y,Bonnel B,Brogniez G,et al。《Observations of Saharian aerosols:Results of ECLATS field experiment, Part I:Broadband radiative characteristics of the aerosols and vertical radiative flux divergence》。J Climate Appl Meteor,1987,26(1):38-52

Isaac G A,Leaitch W R,Strapp J W,et al。《Summer aerosol profiles over Algonquin Park,Canada》。Atmos Environ,1986,20(1):157-172

Guinot, B., Jean-Claude, R., Helene, C.,Wang, P., Bai, J.Yu, T., 2006. Impact of vertical atmospheric structure on Beijing aerosol distribution. Atmos. Environ. 40,5167–5180.

Deng.x.j,Tie.x,Wu.D,etc.Long-term trend of visibility and its characterizations in the Pearl River DeltaRegion(PRD).China. Atmos. Environ. 42,1424–1435.

Han,S.Q,Bian,H.,Tie X.Xie,etc.Impact measurements of nocturnal planetary boundary layer on urban air pollutants:from a 250-m tower over Tianjin,China,J.Hazard.Mater,2006,162,264-269.

Wu,D.,Tie,X.,Li,C.C.,etc.An extremely bad visibility event over the GuangZhou region:a case study.Atmos.Environ,2005,39:6568-6577.

Artificial rainfall enhancement program in Cuba by convective cloud seeding. Acheivements and shortcomings in the period 2005-2010.

Daniel Martínez, Carlos A. Pérez, Guillermo Puente, Félix Gamboa, Sadiel Novo, Ibis Rivero, Graciela Angulo, Ismael Pomares, Alexei Gamboa , Elsa Velazco , Michel Rodríguez, Ernesto Chang
Institute of Meteorology, La Habana, Cuba. C.P. 11700
Tel-Fax: 537-881-3411 e-mail: daniel.martinez@insmet.cu

Victor Petrov, Boris Koloskov,
Agency of Atmospheric Technologies (Agency ATTECH, ROSHYDROMET)
Novovagankovsky per. 8, Moscow, 123242, Russia.
Tel: +7(495)255-2372; Fax: +7(495)255-2134; e-mail: attech@mail.ru

Zhanyu Yao
Chinese Meteorological Administration. Baijing. yaozy@cams.cma.gov.cn.

1. Introduction

To mitigate the effect of a severe drought which affected the Eastern part of Cuba in 2004 and the beginning of 2005, the Cuban Government decided to support the development of an operational and research Rainfall Enhancement Program. This Program was composed by a research project, designed to continue and complement the previous research program, developed in the 80s-90s and an operational cloud seeding project to enhance precipitation in the areas most affected by drought.

2. EXPAREX

The research project of this Program was the Randomized Convective Cold Cloud Seeding Experiment in Extended Areas (EXPerimento aleatorizado de siembra de nubes en AReas EXtensas, EXPAREX), based in silver iodide seeding from the tops of growing convective clouds, which design, general description and physical foundations were presented in Martínez et al. (2007) and Pérez et al., (2008). This experiment is being implemented in Camagüey and the adjacent provinces of Ciego de Ávila and Las Tunas from August 2005 as the continuation and complementation of the previous results of PCMAT (Koloskov et al., 1996).

The experimental units were defined as the group of clouds located within a circle having a radius of 25 km and centered at the location of the initial treatment. The target clouds within the experimental unit were growing convective clouds having, at least 0.5 g/m3 of supercooled cloud water (SCW), updraft velocity greater than 5 m/s and top temperature of -7 to -20oC, as described in detail in Martínez et al. (2007). The clouds were seeded from an instrumented An-26 aircraft, under the dynamic seeding hypothesis. The glaciogenic reagent applied in the experiment is the pyrotechnic mixture of the Russian flares PV-26. This mixture has an output of $1.7x10^{14}$ glaciogenic nuclei per gram at -10 ^{o}C and $7.0x10^{13}$ at -6 ^{o}C. The flares burn during 40s and have a descending burning track of 1.5-2 km in moderate updraft.

The recommended flight level is near to the -7oC isotherm (5700-6000) m. Experimental units are selected jointly by the aircraft and ground team leaders, though the final decision corresponds to the aircraft. As soon as an experimental unit is selected, the envelope enclosing the randomized treatment decision is open by the seeding operator without any notice to any other member of the staff. The operator proceeds consequently for the rest of the clouds in the experimental unit, and the envelope is closed again after finishing working on it. In any case, the leading scientist gives the instructions to seed in the appropriate moment, but if randomized decision is “no seed”, he disconnects the launcher system and presses the buttons simulating seeding, so that the rest of the staff can’t notice the type of treatment actually applied. The experimental unit is being treated with subsequent penetrations of different cloud towers which are considered as apt for seeding.

For the control and track of cloud cells and precipitation, automated MRL-5 radar is used. The characteristics of the radar are the following: wavelength: 10.15 cm (S band); and peak power 510 kW; minimum detectable signal -136 dB/W; frequency; pulse duration 2.0 μs; beam width 1.5^{o}. With the radar and aircraft information, it is possible to follow the time evolution of cloud characteristics according to their development stage.

One of the main tasks of a floating target cloud seeding experiment is to determine the speed and direction of the target. The floating target tracking algorithm (Novo et al., 2007) is based on the hypothesis that the experimental unit will follow the average movement of the surrounding storms. At the treatment instant, which is taken as initial time for tracking, all present storms are identified. The circumference defining the experimental unit boundary is displayed, centered at the treatment point and extending to a radius of 25 km. In the next scan, every storm in the radar’s field of vision is tracked by choosing the new center positions that are located at

the minimum distances from the centers in the previous scan, provided a certain limit distance is not attained. After all the storms have been identified in the new step, their displacement vectors are obtained. An average displacement vector of the storms contained inside a radius of up to 100 km neighborhood of the treated cloud is then calculated. This average displacement vector is assigned to the experimental unit. As output of the processing program, an image with the last maximum reflectivity map and the subsequent positions of the superimposed experimental unit circle is obtained, and also a text file including date, time, coordinates of the center and the main parameters of the seeding circle for every instant, as well as for the total tracking time. Rainfall rates "R" are estimated from radar reflectivity "Z" using a empirical standard Z-R relationship between these magnitudes, and is calibrated every day by the raingauge network of the area, (Gamboa el al., 2005).

An exploratory experiment was made from August 22 to October 10th, 2005, in which 21 experimental units were processed The randomization scheme was not applied in this season. However, the flight and seeding methodology of the EXPAREX experimental design were applied and the pilots and scientific crew were trained in locating and following the target in communication with the ground radar coordinator. In target clouds, SCW was measured to evaluate the ability of the flight leading scientist to choose appropriate clouds.

Figure 1 shows the frequency of occurrence of the mean and maximum values of SCW in the 2005 clouds. The analog distribution is shown for the clouds measured in the 1987-1990, during PCMAT. These are qualitatively similar, regarding the form of the distributions, but the mode, the mean and the maxima are, respectively of 0.4, 0.32 and 0.759 gm-^{3} for 2005 and of 0.8, 0.5 and 1.03 gm^{-3} for the period 87-90. The main reason for that decrease in SCW was the lower mean flight level temperature in 2005 (-10^{o}C), relative to 1987-1990 (-7,7^{o}C). Consequently, in the following experimental seasons the flight level was lowered from 6000 to 5700. The measured SCW distribution for 2006-2007 seasons are very near with PCMAT clouds, as shown in Fig. 2.

In 2006, the beginning of the experiment was delayed because of logistic reasons and it began as late as September 29, and continued until October 15. In 2007, the experiment extended from August 17 to October 4th. The following two years, the experiment could not be accomplished because of financial limitations, but it was continued in 2010, from September 1st to October 4th..

In the whole experimental period, 28 units were processed. Table 1 shows a list of the processed experimental units, including their lifetime T and the total rainfall volume Q produced by each of the units in kilotons, corrected using an adjustment coefficient obtained by comparison of the radar-estimated value with the raingauge network (Gamboa et al., 2005).

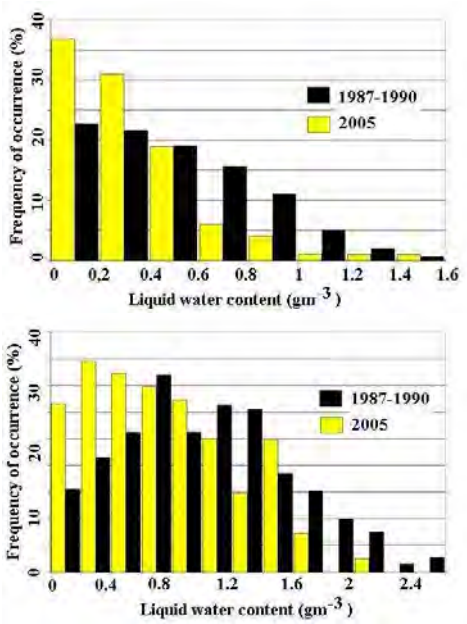


Fig. 1. Supercooled water content in EXPAREX clouds measured in 2005, as compared with PCMAT clouds.

Table 1. Date, time, lifetime and water volume of the processed experimental units.

#	Initial date-time (lst)	T (min)	Q (kT)
1	20061003-14:20	240	55273
2	20061006-15:20	400	12841
3	20061010-13:50	60	16
4	20061010-14:50	290	1141
5	20061011-14:50	350	1450
6	20061012-14:45	115	35
7	20061014-15:15	525	25391
8	20070824-14:05	550	9388
9	20070827-13:35	300	12133
10	20070830-14:00	275	5535
11	20070831-13:15	290	1453
12	20070910-14:05	540	4868
13	20070911-13:30	520	24378
14	20070915-13:40	705	6704
15	20070917-14:15	540	13014
16	20070918-14:30	615	4241
17	20070922-13:55	230	1029
18	20070927-13:15	655	14473
19	20070928-13:45	355	4975
20	20071004-13:25	595	11158
21	20100901-14:05	460	7363
22	20100905-15:00	240	7418
23	20100909-14:45	420	8949
24	20100911-14:40	350	8783
25	20100916-14:20	270	5972
26	20100921-13:15	260	1616
27	20100926-13:25	240	5475
28	20101002-13:55	710	1496

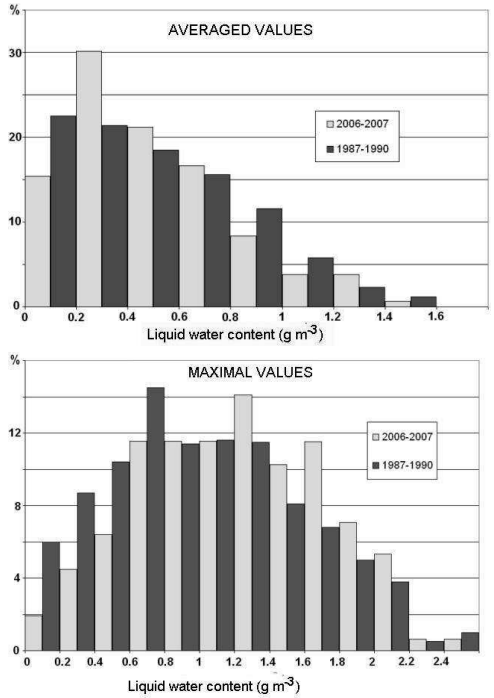


Fig. 2. Supercooled water content in EXPAREX clouds measured in 2006-2007, as compared with PCMAT clouds.

According to the experimental design, 120 experimental units have to be reached to evaluate the experiment. Therefore, the seeded/not seeded condition of each unit is still unknown.

3. Operational cloud seeding in the Eastern part of Cuba

From 2005, an operational cloud seeding project was started in the province of Holguín, in the Eastern part of Cuba with the participation of advisers from the Chinese Meteorological Administration. In 2006 an An-26 aircraft was used for cloud seeding with Long B-2 Chinese flares, similar to the Russian PV-26 used in EXPAREX. The seeding methodology differed from the one used in EXPAREX in the fact that the clouds not always were penetrated, but sometimes were seeded from above the top, which allowed working on the side secondary towers of vigorous cloud systems. 154 convective clouds were seeded in about one month (July), most of them located in the western part of the Holguin province (fig. 3).

For a rough estimate of the rainfall increment, a non randomized historic regression method was applied. The Holguin province was selected as seeding area, and the Guantanamo province, which is located leeward of Holguín, was selected as control. The historic linear correlation coefficient of rainfall in July for both provinces was 0.73, significant at a 99% level. The estimated increment for July, 2006 was of nearly 30%.



Fig.3. Eastern part of Cuba, including the experimental and operational areas.

In subsequent years, the An-26 aircraft for this project was no more available, and it was replaced by a Yak-40, equipped with a launching system for PV-26 Russian flares. In 2007, 71 clouds were seeded in September, most of them in Holguín. In 2008, 82 clouds were seeded from June to September, and in 2009, 180 clouds were seeded from June to October.

From 2005 to 2006, a network of 23 silver iodide ground generators, manufactured by the Chilean enterprise HIDROMET, were installed in the Holguín province and some surrounding locations, near to mountainsides under the hypothesis that orographic lifting and thermal convection could serve as transport agents to carry the reagent up to the clouds. This network worked with stability till 2010. Subsequent numerical studies using a dispersion model showed that the concentration of reagent in the active regions of the clouds is not enough to produce seeding effect (González et al., 2009).

To estimate the effect of the integral operational program in Holguín, a historic regression approach was applied, using the seasonal rainfall totals for the western districts of the province as seeded area, and the eastern districts, located leeward of the seeding area, as control area. Fig. 4 shows the Holguin province, and the two areas. The district of Antilla (green in the map) was excluded from the regression for its peninsular character.



Fig. 4. Seeded (yellow) and control (white) areas for the estimation of seeding effect in Holguin for the period 2005-2010.

Rainfall totals were calculated for the quarter August-October of each year in the period 1964-1998.A linear correlation coefficient of 0.81 between the two sets of rainfall totals was found, with 95% significance level. Fig. 5 shows the scattering plot with the linear regression line. Dotted lines show the estimation errors of the variable 'y' (quarterly rainfall in the seeded area) as a function of the variable 'x' (quarterly rainfall in the control area).

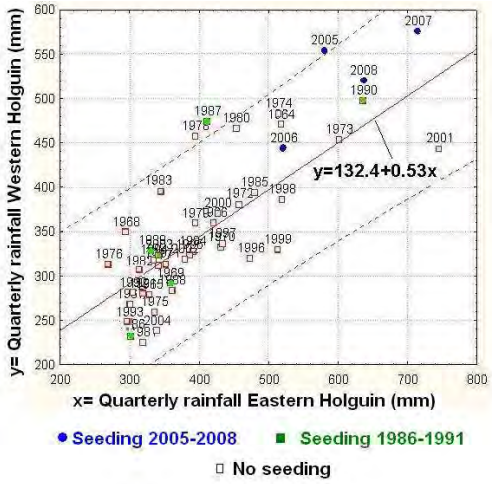


Fig 5. Historical regression line for quarterly rainfall in Eastern (control) and Western (seeded) Holguín for August-October.

In Fig. 5, the blue circles indicate the rainfall totals corresponding to the quarters from 2005 on, where operational seeded was accomplished, either from ground-based generators or from aircraft, or both. The green squares show the totals corresponding to the period 1986-1991, when massive cloud seeding was applied in Western Holguin. The empty squares indicate the years in which no cloud seeding was applied. As can be seen from the plot, in all the quarters of the recent cloud seeding period, rainfall in the seeded area exceeded the regression line forecast in 5%-10%, but is was not enough to exceed the error interval, except 2005, where it is practically on the error border line. This is valid also for the former seeding seasons in 1987-1990, except for 1986 and 1988, when quarterly rainfall was less than the regression forecast.

Acknowledgements

The authors thank the Cuban Government and particularly the Institute for Civil Aeronautics for coordinating and financing the Cuban Artificial Rainfall Enhancement Program.

References

Gamboa F., Pérez C.A, Martínez D. y Gamboa A. (2005): El radar meteorológico camagüeyano como una herramienta para la coordinación científica de vuelo y evaluación de los experimentos de incremento artificial de las precipitaciones. III Congreso Cubano de Meteorología. 5 al 9 de diciembre del 2005. La Habana, Cuba.

González Y.,Martínez D y Borrajero I., 2009: Simulación numérica de la dispersión del yoduro de plata emitido por los generadores terrestres en la región oriental de Cuba" V Congreso Cubano de Meteorología. Diciembre del 2009. La Habana, Cuba.

Martinez D., Perez C. A., Koloskov, B.P., Korneev V.P., Petrov V.V, Gamboa F. and Novo S., 2007: Randomized Convective Cold Cloud Seeding Experiment in Extended Areas in Cuba (EXPAREX). Ninth WMO Scientific Conference on Weather Modification (Antalya, Turkey, 22-24 October 2007). WMP No. 44. WMO TD. No. 1406.

Novo S. ,Martínez D., , Pérez C. A., Koloskov B. and Gamboa F., 2007: Radar tracking method for cloud seeding experimental units over Cuba). Ninth WMO Scientific Conference on Weather Modification (Antalya, Turkey, 22-24 October 2007). WMP No. 44. WMO TD. No. 1406.

Pérez-Sánchez Carlos A., Martínez D., Petrov V.V, Pomares I, Koloskov, B. P.3, Gamboa, F., 2008: An exploratory analysis of the potential for rainfall enhancement in the randomized convective cold cloud seeding experiment in extended areas in Cuba (EXPAREX). Proceedings of the 15th International Conference on Clouds and Precipitation. Cancun, July 7-11, 2008.

Japanese Cloud Seeding Experiments for Precipitation Augmentation (JCSEPA)
--- New Approaches and Some Results from Wintertime and Summertime Weather Modification Programs ---

Masataka MURAKAMI[1] and JCSEPA research group

[1]Meteorological Research Institute, Tsukuba, Japan

1. Introduction

In populated areas of central and western part of Japan, we have had a potential problem of water shortage. For the last twenty years, we had the problem of water shortage almost every two or three years, especially in Kanto and Shikoku district.

In the summer of 2006, MRI, in cooperation with 10 other research organizations, launched the five-year research project (2006-2011) “Japanese Cloud Seeding Experiments for Precipitation Augmentation (JCSEPA)” to aim drought mitigation and water resources management. We carried out summertime weather modification project around Sameura Dam and wintertime project around Yagisawa Dam. Sameura dam is the main water supply for Shikoku district, where they have droughts most frequently in Japan. Yagisawa dam is one of main water supplies for Tokyo Metropolitan area.

In this paper some results from our wintertime and summertime weather modification projects are briefly described.

2. Outline of JCSEPA

Our project, JCSEPA, is made of 4 sub-programs; analytical study by using past meteorological and hydrological data, remote sensing study by using multi-wavelength active and passive sensors, airborne and ground-based in-situ measurement study, meteorological and hydrological numerical modeling study and cloud chamber experiments (Fig. 1).

JCSEPA has three main goals. The first one is to investigate the causes of drought at different areas in Japan by analyzing past meteorological and hydrological data and identify typical weather pattern during drought. The second one is to develop a sophisticated weather modification technology for orographic snow clouds. The third one is to investigate the possibility of rain enhancement by hygroscopic seeding (hygroscopic flare and salt micro-powder) in warm season.

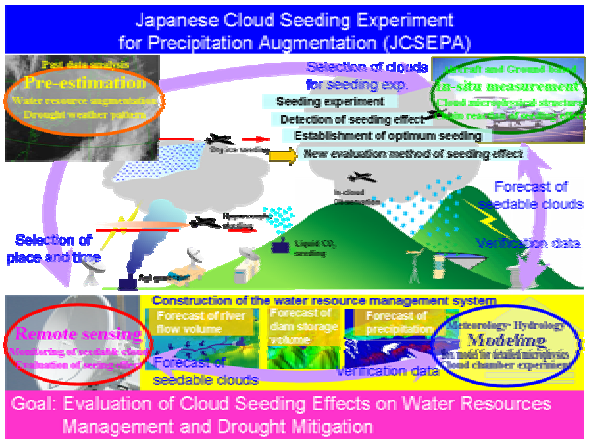


Fig. 1 Outline of JCSEPA

3. Wintertime weather modification technology

In the central and northern parts of Japan, where large portions of water resources rely on snow-melted water from mountain areas, little snow in winter and subsequent little rainfall in Baiu season bring about a serious problem of water shortage. We investigated the effectiveness of snowpack augmentation as a preventive measure for drought mitigation.

If we evaluate and/or predict seedable clouds quantitatively and seed clouds with high seedabilies selectively, we can save seeding time and

materials. Figure 2 shows the appearance frequency of clouds with different seedability ranks calcurated by the multple-regression method, which is based on the relation between windward meteorological and microphysical parameters and the simulated enhancement of the catchment precipitation. The sum of appearance frequencies for clouds with seedability ranks A to E reached 20 ~ 30 % of the time.

Seeding experiments using an instrumented aircraft demonstrated that additional precipitation particles were produced in clouds with supercooled cloud droplets 20 ~ 30 min. after dry-ice pellet seeding. Ice crystal concentrations in seeding curtains were initially more than 1000 particles/L and decreased to ~ 100 particles/L in 20 ~ 30 min. due to turbulent diffusion and aggregation (Fig. 3). Figure 4 shows radar reflectivity calculated from 2D images in seeding curtains and their surroundings as a function of the distance from mountain peak. The calculated radar reflectivity in seeding curtains increased by 3 ~ 5 dBZ as compared with their surroundings. Simultaneous radar observations sometimes showed a significant increase in dBZ in seeding curtains.

Cloud seeding with dry ice pellets in the numerical model is simulated in a realistic way, by predicting dry ice pellet concentrations, and calculating evaporation rate of dry ice pellet and production rate of ice crystals. Figure 5 shows the seeding effect during the whole winter of 2006/2007. Warm color indicates an increase in accumulated precipitation and cold color a decrease due to cloud seeding. Over the catchment area, cloud seeding causes an increase in seasonal surface precipitation by 17%. We may have much more increase in seasonal surface precipitation if we apply the optimum seeding method.

We evaluate the effects of cloud seeing on Dam water storage by using a combination of NHM and land surface model, which represent snowpack, snowmelt and runoff processes as well as land-atmosphere exchange processes. With

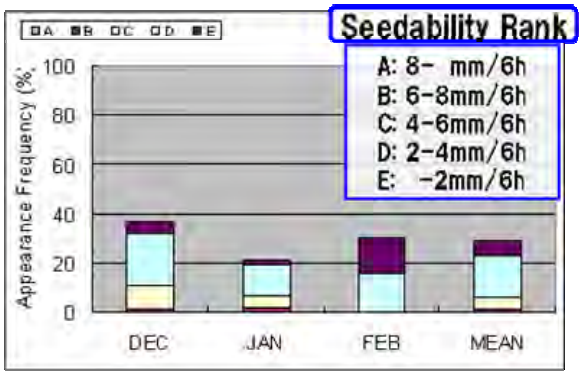


Fig. 2 Appearance frequency of clouds with different seedabilities.

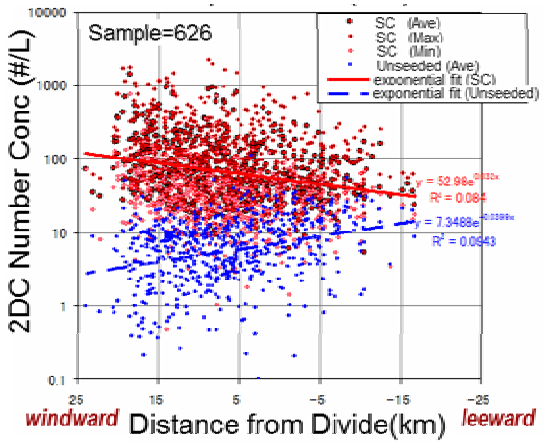


Fig. 3 Evolution of ice crystal number concentrations in seeding curtains (red) and their surrounding (blue) as a function of the distance from the devide.

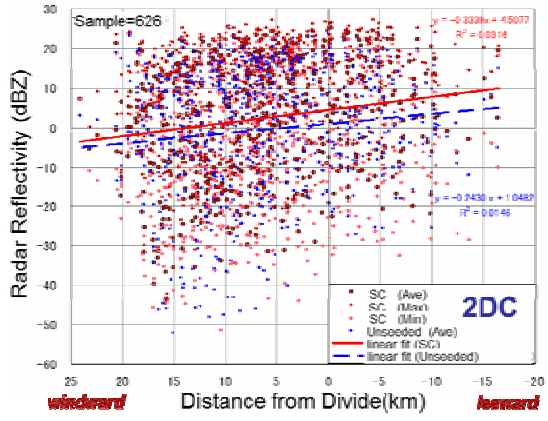


Fig. 4 The same as Fig. 3 except for radar reflectivities calculated from 2DC images

the cloud seeding during the whole winter season, dam water storage increases from 70 % to 100 % at the end of June (Fig. 6).

4. Summertime weather modification technology

For the last four years, we also have carried out a basic study on hygroscopic seeding through dynamic cloud chamber experiments, numerical seeding experiments and small-scale field seeding experiments.

We have tested salt (NaCl) micro-powder and hygroscopic flare as seeding materials so far. Salt micro-powder includes chemical compounds other than sodium chloride to prevent particles from sticking together.

Figure 7 shows an example of hygroscopic seeding experiment in the dynamic cloud chamber. Upper panel shows a time evolution of number concentrations of particles larger than 0.3 microns in black, larger than 1 micrometers in red and larger than 10 micrometers in green for the unseeded case. For the seeded case, droplets larger than 10 microns show up much earlier than the unseeded case.

By using the hybrid cloud-microphysics model, we investigated the effect of hygroscopic seeding on surface precipitation. This model can simulate the activation process of CCN, including giant CCN precisely although dynamic frame of cloud model is prescribed. Interactions between microphysics and dynamics are not included, so we look at seeding effect only from the microphysical viewpoint.

All types of hygroscopic seeding materials produce significant positive effects only for clouds with large updraft velocity (w > 0.5 ms-1) at early stage of their life cycle.

NaCl micro-powder with log-normal size distribution (mode radius of 0.5um) produced significant positive seeding effects by increasing the number of large droplets and decreasing the total number of cloud droplets if total mass of seeding particles is large enough. On the other hand, hygroscopic flare particles (CaCl2) with bi-modal log-normal size distribution (mode radii of 0.1 and 0.8 um) usually produce slightly negative seeding

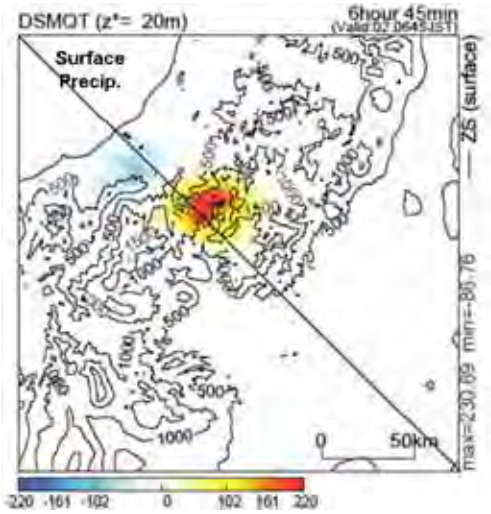


Fig. 5 Seeding effect on seasonal surface precipitation.

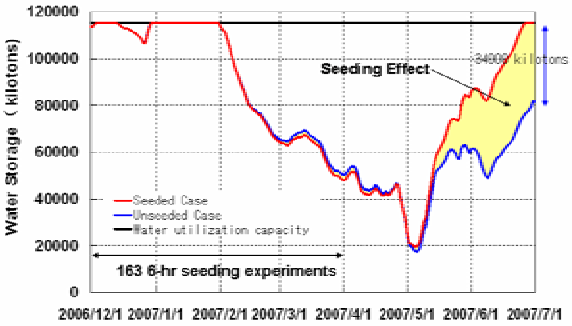


Fig. 6 Dam water storage for the seeded case (red) and unseeded case (blue).

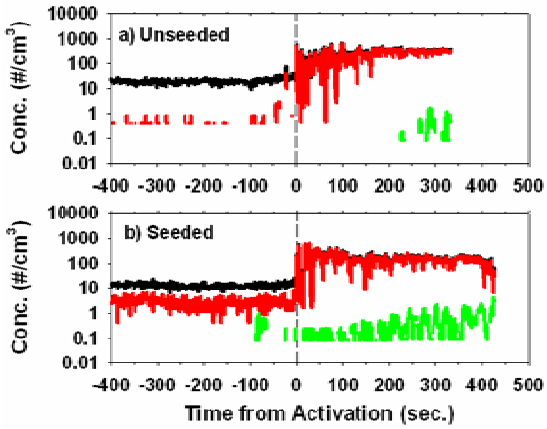


Fig. 7 Time evolution of number concentrations of particles larger than 0.3 mm (black), larger than 1 mm (red) and larger than 10 mm (green) for unseeded (upper panel) and seeded (lower panel) cases.

effects due to large increase in total number of cloud droplets although the onset of surface precipitation is advanced for 10 - 20 min. due to direct formation of raindrop embryos (Fig. 8).

Seeding effects on the total surface precipitation are sensitive to BGCCN, seeding particles and cloud types. Especially for hygroscopic flare seeding, slight changes in size distributions of BGCCN and seeding particles could change even the sign of seeding effects. Therefore more intensive study is needed for better understanding of hygroscopic seeding

In order to investigate the effects of hygroscopic seeding on real clouds and the relation between BGCCN and microphysical structures of unseeded clouds, we have carried out aircraft observations. Regarding hygroscopic seeding in real clouds, what we can do at present is to detect a broadening of initial cloud droplet size distribution toward larger sizes. Only from aircraft seeding experiments, it is rather difficult to trace a chain reaction of microphysical processes, leading to an additional rain formation.

Lastly Figure 9 shows preliminary results for the appearance frequency of summertime clouds suitable for cloud seeding in qualitative sense. We defined cloud types based on cloud top temperature and cloud thickness obtained from a combination of several active and passive remote sensor data. Results show that about 10 percents of clouds may have possibility for hygroscopic seeding and another 10 percents of clouds for glaciogenic seeding. We are still continuing to improve the algorisms for a better evaluation of summertime seedable clouds.

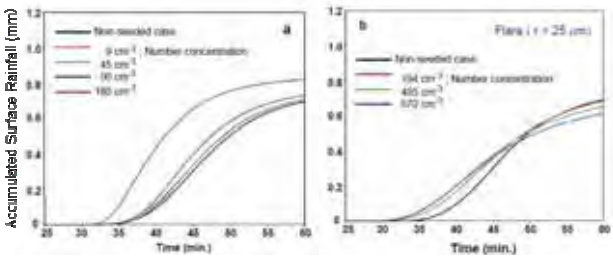


Fig. 8 Accumulated surface rainfall as a function of elapsed time for salt micro-powder seeding (left) and hygroscopic flare seeding (right).

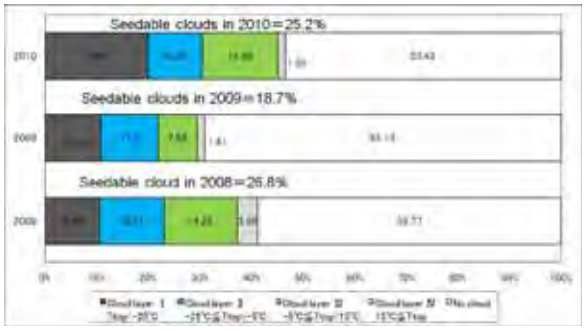


Fig. 9 Appearance frequency of clouds suitable for glaciogenic (-25C<T<-5C) and hygroscopic (-5C<T<15C) seeding.

5. Conclusion

As a part of JCSEPA, we have developed a sophisticated weather modification technology for orographic snow clouds; a monitoring technique for quantitative evaluation of seedable clouds, physical and statistical evaluation techniques of seeding effects, and. water resource forecast system combining NHM and hydrological model. By using these techniques, it is shown that glaciogenic (dry-ice pellet) seeding of mixed-phased orographic clouds forming over the windward mountains of Yagisawa Dam is effective

We have also investigated the possibility of rain enhancement by hygroscopic seeding (hygroscopic flare and salt micro-powder) in warm season on the basis of laboratory experiments, numerical simulations, monitoring of seedable clouds and small-scale airborne seeding experiments. The results we obtained so far showed that hygroscopic seeding of warm clouds may be effective under limited conditions

Hygroscopic seeding of cold, convective clouds is reported to be effective although there remain many arguments about the effectiveness. More intensive study is needed to conclude the effectiveness of hygroscopic seeding of warm and cold clouds.

Russian Technology for Regulation of the Processes of Atmospheric Precipitation Formation, Prevention of Formation and Fall of Hailstones and Fogs Dispersion

P. A. Nesmeyanov, V. P. Korneev, M. S. Reznikov, V. N. Yemel'yanov, V. O. Sapozhnikov
Russia, Moscow Region, 3, Academika Silina St. RF-141313
p.nesmeyanov@mail.ru

There are presented the basic aspects of development, manufacture and application of the Russian facilities for impact on hydro-meteorological processes with the purpose of hail hit prevention, stimulation and redistributions of precipitation, creation of favourable weather conditions on the certain territory. The problems of investigation and development of new compositions of elevated-efficiency ice-formation agents for arming of antihail rockets, ground and aircraft precipitation-stimulating means and means of fogs and low overcast dispersion are considered. Characteristics of the developed Russian technology of active influence on hydro-meteorological processes in comparison with foreign analogues are presented.

Microphysical signatures of aerosol-cloud interaction in the monsoon environment during CAIPEEX

Thara V. Prabha(1), A. Khain(2), R. S. Maheshkumar(1), G. Pandithurai(1), J. R. Kulkarni(1), and B. N. Goswami(1)

1. The Indian Institute of Tropical Meteorology, Pune, India
email: thara@tropmet.res.in
2. Department of Atmospheric Sciences, The Hebrew University of Jerusalem, Israel
email: Khain@vms.huji.ac.il

Abstract

Cloud Aerosol Interaction and Precipitation Enhancement EXperiment (CAIPEEX) was conducted over the Indian subcontinent during 2009 and 2010 with aircraft observations of cloud microphysics and aerosols. Several examples from these measurements for bimodal drop size distributions are noticed that are attributed to in-cloud nucleation and droplet evaporation (Prabha et al 2011). It is noted that boundary layer aerosols could be lifted up in the deep convective cloud and could get nucleated at elevated layers due to increase in supersaturation in the cloud updrafts (Pinsky and Khain 2002). The presence of in-cloud nucleation is noticed most often in moist environments. The concentration of small droplets decreased in the monsoon environment with high water vapor content in the boundary layer (Figure 1). However, there are situations where concentration of small droplets increased in the highly moist and polluted conditions (indicated as B in Figure 1), similar to the clouds profiled in the marine moist and relatively cleaner conditions (indicated as A in Figure 1).

The relative role of the presence of aerosols and of moisture availability is investigated using systematic evaluations with the help of observations of CAIPEEX and numerical models. Bin microphysical scheme is employed in the study for detailed investigations for selected clouds.

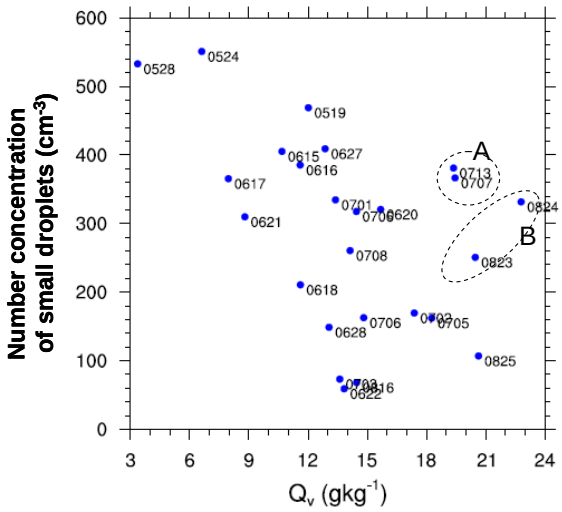


Figure 1. The relationship between the boundary layer water vapor and the number of smallest droplets in the clouds profiled during the CAIPEEX. Each symbol represents observations of a day (labeled as month and day: mmdd)

References:

Pinsky, M. and A. P. Khain, 2002: Effects of in-cloud nucleation and turbulence on droplet spectrum formation in cumulus clouds. Quart. J. Roy. Meteorol. Soc., 128, 1–33

Prabha T.V, A. Khain, R. S. Maheshkumar, G. Pandithurai, J. R. Kulkarni, M. Konwar and B. N. Goswami, 2011, Microphysics of pre-monsoon and monsoon clouds as seen from in situ measurements during CAIPEEX, Journal of Atmospheric Sciences doi: 10.1175/2011JAS3707.1

Compared Radar Reflectivity with Heavy Rain Droplet Size Distribution

Pu Jiangping[1] Zeng Wenhua[1] Yao Zhanyu[2] Zhang Wei[1] Li Yongyi[1]
1. Institute of Meteorology, PLA University of Science and Technology, Nanjing, 211101
2. Chinese Academy of Meteorological Sciences, Beijing,10086

Abstract

Using OTT-Parsivel Laser Particle Spectrometer at Nanjing in East China, several times heavy rain droplet scale & velocity spectral data aquatic from Mt. Lushan weather stations (elevation 1300meters) Compared to the plain deep convective clouds heavy precipitation, the rain droplet size distribution (DSD) with two elevation of deep convective cloud precipitations were significant features which spectrum width is wider than plain. As the Lushan station located at 1300 meters above sea level on an isolated hilltop, at the observation moments, the authors felt was the development of a strong convective cloud, the sky darkened can hear thunder, clouds with strong wind enveloped in the station. It can be observed in large-scale rain droplets and captured by digital camera. The pictures using digital camera directly show the big rain particles. It can be judged, the DSD information of observed the precipitation is almost the bottle of the heavy raining cumulus clouds. General DSD observations on the surface station is that the droplets in clouds fall running thought after several kilometers with cloud outside the dry air environment, warming and melting, touching and broken, evaporation, etc., after the whereabouts of the status of the process. Contrast these two types of DSD data for the study of deep convective clouds in the rain system, we compare Radar observation with OTT out put reflectivity data which were calculated by Rain DSD, the distribution of particle structure is very useful.

Introduction: Based on at different altitudes precipitation particles observation, the heavy rain droplet particles micro-physical parameters of a comparative analysis was Droplet Size Distribution (DSD) and velocity spectra at different heights. Results showed the width of DSD at bottom of convective clouds is much wider than on surface observation. Mountain station, the observed spectral width of DSD in general exceeds 11mm, drop rate of same scale particles in the initial cloud bottom moment were greater than their speed reach ground. The concentration of raindrops falling at cloud bottom is always greater than they landing to the ground. DSD at various stages, smaller particle concentration which diameter were less than 1mm located in the bottom cloud is than of particle spectra above ground about an order of magnitude. Various stages of precipitation particle spectra, located in the cloud is less than 1mm at the bottom of the particle number concentration is the concentration of particle spectra above the ground about an order of magnitude. This shows that the rain droplet concentration produced by the cloud physical processes is larger than the concentration we obtain of conventional on ground-based observations and can generate a lot of big droplets than we realize that convective clouds that may exist in larger particles. Conjecture is due to convective clouds of ice-phase process in the formation of large-scale ice, snow and graupel particles in the melting process of the formation of large drops, however, this suppose remains to be confirmed by direct the aircraft cloud physical parameters measurement.

1. Observation: June 24, 2006 beginning 12:23 noon in local time, to detect precipitation particles, precipitation ended 14:24 pm, the whole process of precipitation is about 2 hours, accumulated precipitation 38.29mm, equipments to detect the greatest rain intensity is 269.33mm/h. Rainfall intensity of precipitation began to increase dramatically with the naked eye can be observed that the whereabouts of a huge rain particle size (compare with normal deep convective cloud precipitation). The main precipitation mount are concentrated before 13 o'clock, the heavy rainfall continued for half an hour later sharply reduced, converted to a more stable array of precipitation. Figure 1 shows accumulated precipitation for the Lushan station precipitation changes. The observation obtained total of 481 groups copy of the data collected, the data sampling interval is 15 seconds, an average particle diameter of 0.57mm, the largest particle appears in the 10~12mm, the average particle concentration of 1896.33 / m3, the largest concentration of particles to 18420.68 / m3. Figure 2 shows the overall average precipitation this logarithmic distribution curve of particle concentration. Particle scales less than 2 mm accounted for the vast majority of all particles. The proportion of smaller particles decreases as

well as larger particles increased when precipitation intensity tends to stable. The large particles of more than 6 mm, even to 12mm, almost exclusively in the mature stage of deep convective cloud precipitation that is, the second phase of this precipitation. Rainfall intensity and other parameters influenced by the larger particles, precipitation of small particles stabilized stall the contribution of these parameters remained stable, while the contribution of large particles relatively huge fluctuations.

2. Analysis: Precipitation in convective clouds can be divided into five stages: the instantaneous rainfall intensity maximum appears in the first phase, the second phase of the accumulated precipitation mount maximum, followed by three stages of the contribution to total precipitation is small but sustained a long time(figure1.). Rainfall intensity, Liquid water content, the radar reflectivity factor and particle numbers concentration of these parameters change in precipitation is quite similar characteristics, are the first stage, reaches its maximum, the second phase remained at a high value on the third phase of rapid decreased slightly during the fourth stage of the increase will be gradually reduced until the fifth stage of the end of precipitation. In fact, the various stages of precipitation are just width of spectrum of changes in the overall spectral changes in smaller type.

The changes in raindrop size distribution is very complex, the second and fourth phase of a number of raindrop size distribution is relatively stable, at the beginning of precipitation, convective precipitation and precipitation decreased the end of these stages and raindrop size distribution seemed more cluttered, no obvious change in law. From the five phases can be seen that the average raindrop size spectra of drops of this general trend of precipitation: lines decreased gradually narrow spectral width, rainfall tends to be stable lines up the middle to bulge.

The original instrument collected 32 channels data by diameter 1mm intervals re-divided into seven files, in order to facilitate analysis of a measure of the contribution of precipitation particles. To this end, various stalls were calculated the concentration of particles of the particles, moisture content, rainfall intensity, radar reflectivity, momentum, kinetic energy contribution to the percentage shown in Figure 3. Concentration of particles increases with the diameter of the percentage decreases rapidly in line with the negative exponential distribution, in a sense similar to the raindrop size distribution, the number of particles less than 1mm of total precipitation in the majority (89.36%), indicating that deep Convective precipitation is still dominated by small particles, bold particle's existence. Showing a bimodal distribution of water content characteristics of 1-2mm, and 3-4 between the two great values, the percentage of the remaining smaller number of files that overall water content of less than 5mm in diameter of particles more evenly distributed between the various files the percentage share of water content in between 15-19%, from 4 mm in diameter began to increase with the percentage share of water content decrease. From the distribution of rainfall intensity, although the highest concentrations of small particles, but the contribution of rainfall intensity is among the lowest, accounting for almost nine-tenths of the small particle contribution to the rainfall intensity of only 4.8%, the greatest contribution is 3-5mm between the particles, together accounted for 43.3% of the total rainfall intensity. The distribution of radar reflectivity and the rest of the distribution of several parameters significantly different from the greatest contribution of the particles is greater than 6 mm, followed by 4-5mm particles, particles less than 1 mm the contribution of the radar reflectivity of only 0.5%. Momentum and kinetic energy distribution similar to the major contribution comes from large particles of more than 3 mm. If you set aside consideration of 6 mm or larger particles, then particle concentration was found negative exponential distribution, moisture content bimodal-shaped distribution, the distribution of the remaining four parameters are more similar to side with the small particle diameter increases, the share the percentage increases, up to 4-5, maximum, and then begins to decrease.

3. Conclusion: The precipitation changes in raindrop size distribution is very complex, a few with the rain from above the amount of

spectrum-related terms, the second and fourth phase of the raindrop size distribution is relatively stable, the third phase of the raindrop size distribution changes in the most complex, there is no obvious rule. DSD shows the rainfall at each stage of this process as a whole the average raindrop size distribution. The first phase of the raindrop size distribution in small drops and large drops of client-side particle concentration of large spectral width is also the largest, relatively smooth lines to the end of the second phase droplets and large drop-side concentration of particles decreased, and the spectrum wide-narrow end of the spectrum maximum small drops began to fall relatively smooth, but in 2-7mm between the concentration of particles than the first phase of a significant increase in spectrum in the range upward, 7mm above the rapid concentration of particles reduced. The third phase of the concentration of particles in diameter than the previous two phases have significantly reduced the spectral width is reduced to 6mm in the vicinity, its spectrum showed a clear bimodal shape, a peak in the vicinity of 3mm, the fourth phase of spectral type with the first Similar two-stage, the diameter of particle concentration profile with the previous period magnitude and spectral width equivalent to the size of particles in the spectrum of middle-segment upward, the last phase of spectral width significantly narrower particle concentration dropped to the lowest spectrum in the 2-4mm between the relatively straight section shows that the particles within this diameter, the number of relatively uniform magnitude in a few / cubic meter. From the changes in raindrop size distribution point of view, of convective precipitation drop spectra in the whole process is generally consistent with exponential distribution, the highest concentration of small particles the initial stage of precipitation, there will be large particles, probably because of the crushing of large particles caused by the concentration of small particles Great. In the convective precipitation maturity, reduce the concentration of small particles, large particles appeared to reduce the frequency, and the maximum diameter is also reduced, but the concentration of medium-sized particles increased, the spectrum is reflected in the increase of concentration with diameter less a small trend slowed in the stability of convective precipitation into precipitation after a weak showing similar characteristics. Of convective precipitation by heavy rainfall into a stable transition in the weak precipitation drops more clutter spectrum, in addition to the small particles near the end of a peak external 3mm peak also appeared, from the actual spectral type of view in this period is often apparent in The multi-peak shape, particle concentration appear within a few diameters, and apart from the small particle end of the peak concentration is smaller than the previous two phases, the large particle end of the peak concentration were significantly higher than the first two stages of the same diameter, concentration of particles larger files, But the peak value of the stalls are constantly changing, from the diameter of bias changes in degree and kurtosis can also be seen at this time the spectral type is volatile. In the precipitation side of the end of droplet concentration of particles have been for a sudden increase, then gradually lines down, in the process, gradually reduce the number of particles makes the lines often break the case, that is, a few stalls in the middle of the particles are not measured, but in a larger number of stalls on the particles was measured.

Acknowledgments. This work was partially supported by the National 973 Foundation of China MOST (2010CB950804).

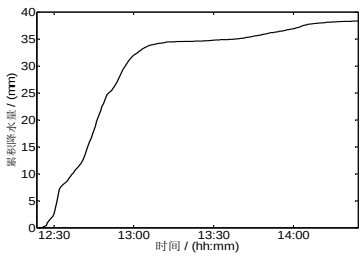


Figure 1 Heavy Rain Convective Precipitation

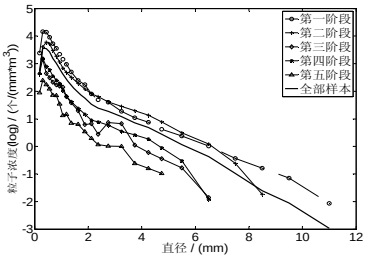
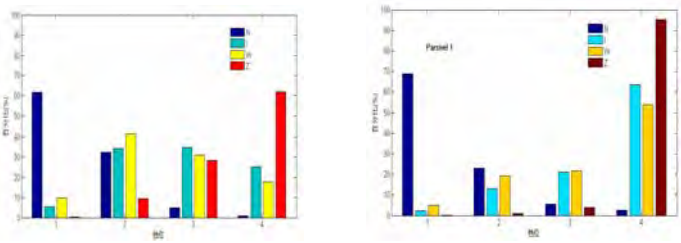
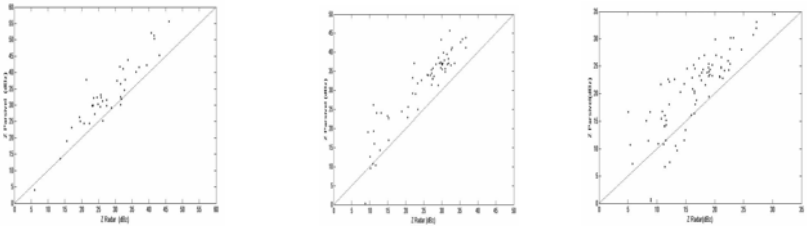


Figure 2 The average raindrop size distribution



(a)Nanjing (plain area) (b) Mt. Lushan (mountain area)

Figure 3. The profile of the contribution of particles compareing



(a). Heavy rain convective cloud (b). Mixed cloud (c).Stratus cloud

Figure 5 Dots chart between Radar and OTT

Table1 Radar reflectivity compared with calculated by DSD in Convectiv/ Mix/ Stratus cloud

Precipitation type	Sample numbers	Biase (dBz)
Convective cloud	150	6.7
Mixed cloud	525	6.7
Stratus cloud	284	1.8

References

[1] Marshall J.S.、W.M.K. Palmer，The distribution of raindrops with size, J.Meteor., 1948,5,165-166

[2] J.Testud，S.Oury, P.Amayenc，The Concept of “Normalized” Distribution to Describe Raindrop Spectra, A Tool for Hydrometeor Remote Sensing，J.Phys. Chem. Earth(B), 2000, 25(10), 897-902

[3] Abe Delfin Ochou, Armand Nzeukou, Henri Sauvageot, Parametrization of drop size distribution with rain rate, J. Atmospheric Research, 2007,84,58-66

[4] Hu, R. Srivastava, Evolution of the Raindrop Size Distribution by Coalescence, Breakup and Evaporation, Theory and Observations. J. Atmos. Sci., 1995,52,1761-1783

[5] Brown, Coalescence and Breakup-induced Oscillation in the Evolution of the Raindrop Size Distribution. J. Atmos. Sci., 1989, 46,1186-1192.

[6] Chen Baojun, Li Hua, Liu Ji into three types of precipitation cloud raindrop size distribution pattern [J], Journal of Meteorology, 1998,14 (1), 8 ~ 11

[7] Hong-Yan Liu, LEI Heng-pool, data analysis, ground-based raindrop spectra of stratiform cloud and precipitation characteristics of convective clouds [J], Atmospheric Sciences, 2006,30 (4) ,693-702

[8] Pu Jiang Ping, Zhao Guogiang, Cai Ding-jun, Parsivel laser particle precipitation in the meteorological field spectrometer and its application [J], Meteorology and Environmental Sciences, 2007,30 (2) ,3-5

[9] Zheng Jiaoheng, Chen Baojun, raindrop size distribution function of the choice: MP and the comparative study of Gamma distribution [J], Meteorological Sciences, 2007,27 (1) ,17-24

[10] Atlas, D., and C. W. Ulbrich (2006), Drop size spectra and integral remote sensing parameters in the transition from convective to stratiform rain, Geophys. Res. Lett., 33, L16803,

[11] Atlas, D., C. W. Ulbrich, F. D. Marks Jr., etal. (2000), Partitioning tropical oceanic and stratiform rains by draft strength, J. Geophys. Res., 105, 2259–2267,

[12] Battaglia, A., E. Rustemeier, A. Tokay, U. Blahak, and C. Simmer (2010), PARSIVEL snow observations: A critical assessment, J. Atmos. Oceanic Technol., 27, 333–344,

[13] Chang, W. - Y., T. - C. C. Wang, and P. - L. Lin (2009), Characteristics of the raindrop size distribution and drop shape relation in typhoon systems in the western Pacific from the 2D video disdrometer and NCU C - band polarimetric radar, J. Atmos. Oceanic Technol., 26, 1973 – 1993,

[14] Lee, C. K., G. W. Lee, I. Zawadzki, and K. - E. Kim (2009), A preliminary analysis of spatial variability of raindrop size distributions during stratiform rain events, J. Appl. Meteorol. Climatol., 48, 270 – 283,

[15] Ulbrich, C. W., and D. Atlas (2007), Microphysics of raindrop size spectra: Tropical continental and maritime storms, J. Clim. Appl. Meteorol., 46, 1777–1791,

[16] Tokay, A., P. G. Bashor, E. Habib, and T. Kasparis (2008), Raindrop size distribution measurements in tropical cyclones, Mon. Weather Rev., 136,1669–1685

Lake and Land Breezes on Lake Towuti and Their Effect on Convection in Larona Catchment Area, Sulawesi, Indonesia

Findy Renggono, Erwin Mulyana, Tri Handoko Seto, Budi Harsoyo, Djazim Syaifullah

frm_68@yahoo.com
Weather Modification Technology Centre, Agency for the Assessment and Application of Technology, Indonesia

1. Introduction

Nickel production at the Sorowako plant is dependent on the availability of water from the lakes surrrounding Sorowako in Sulawesi. Low water levels in the lakes feeding the hydro-power stations at Larona and Balambano could limit the amount of hydropower more than those which can be generated. In order to overcome this problem, PT INCO has been conducted cloud seeding for precipitation enhancement purposes for the region. Previous studies found that lake breezes effects seemed to enhance rainfall during the night along the shores of Lake Matano (NCAR, 2006), but there are no further studies regarding lake breezes effect in this region.

From studies of Lake breezes, it was found that lake and land breezes could best develop only when the synoptic or gradient winds are very light to non existent, and they need partly to mostly clear skies to allow solar heating to warm the land. Laird *et al.* (2001) showed in Michigan Lake that the first-degree factor influencing the lake breeze is synoptic rather than local (thermal gradient) and also found negative correlation between the wind speed of the opposing synoptic wind and the sea breeze frequency. Scott and Huff (1996) found that the presence of Lake Michigan imposed a net cooling of summer mean temperature as large as 28^{o}C within 80 km of the shoreline. Individual lake-breeze events could also play an instrumental role in providing cool temperatures to relieve metropolitan areas in coastal regions, such as Chicago, Illinois, and Milwaukee, Wisconsin, during intense heat waves (Kunkel et al. 1996).

The Larona Catchments Area (LCA) is located at South Sulawesi, Indonesia (Fig. 1). It is composed of a large body of water, three cascade lakes, and land. This composition is believed to have prevented potential cumulus cloud to develop originally within the LCA. It seems that potential cumulus clouds which develop into rain cloud or thunderstorm within the LCA, originally came from outside of the LCA by way of advection.

The purpose of this study is to investigate the characteristics of lake breezes and their effects on convection in the Larona catchments area.

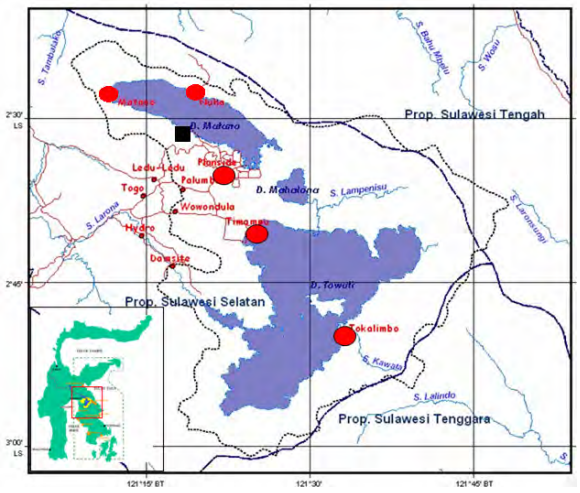


Figure 1. Map of Larona Catchment Area showing the location C-Band Radar (black-shaded square), and surface stations (red circle).

Tabel 1. Location of Radar and AWS

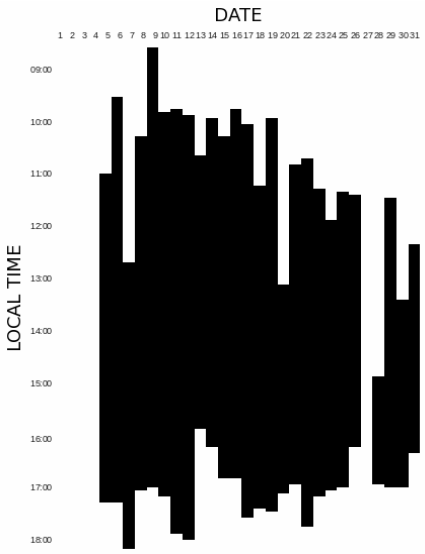
Station Name	Latitude	Longitude
C-band Radar	2.53S	121.35E
Timampu	2.66S	121.43E
Plant Site	2.57S	121.38E
Tokalimbo	2.81S	121.57E
Matano	2.46S	121.22E
Nuha	2.45S	121.34E

2. Data and Method

The LCA as the target area for cloud seeding program, is about 2,477 km^2. There are three lakes in the LCA, namely the Matano (166 km^2), Mahalona (24 km^2) and Towuti(562 km^2) lakes. The Map of LCA can be seen in Figure 1.

This study used a variety of data to examine Lake Towuti lake breezes. Surface wind observations, rain gauge and weather radar are used. In this abstract paper, it is only observation on March 2010 is shown, but the result from observation on November 1999 to March 2010 will be presented during the conference.

Tabel 2. Radar data availability



Hourly surface wind observations were used to investigate lake breezes events. There are 5 locations of automatic weather stations around the catchments area (red-circle on Figure 1). The Latitude and longitude coordinate of each stations are shown in table 1.

The C-band radar is located at the south part of Lake Matano (black-square on Figure 1). It is used to detect the precipitating cloud and their propagation. The radar observation was only available during the cloud seeding project, i.e. only on daylight. Radar data availability is also shown in Table 2.

3. Precipitation climatology

The Geographical position of LCA, in which it is close to the equator and located between Bone Gulf at west side and Tolo Gulf at east side, causes unique rain characteristic. Rain might occur in either wind condition, westerlies or easterlies direction. Larger water body (3 lakes) inside the catchments area causes local dynamic circulation which influences weather pattern and rain occurrence in this area significantly.

Based on the result of Aldrian et.al. (2003) which analyzed rainfall data using the REMO model, this region has rainfall type between the anti-monsoonal and monsoonal type, and also has a strong influence on El-Nino event. This causes the peak of the rainy season to occur in April-May and the peak of dry season occurring in August to October.

Figure 2 shows annual variation of rainfall in the plant site from 1977 to 2006, located about 7 km southeast of the radar site. It is shown here that the peak of rainfall occurs on April (dark shading) and the dry condition (without shading area) occurring around

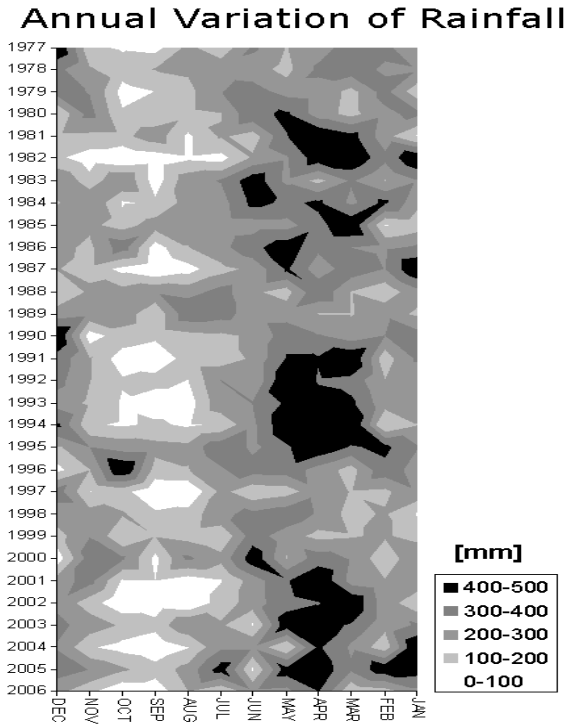


Figure 2. Annual Variation of Rainfall at Plant Site

September-October. Rainfall peak reached more than 400mm/month on 1980-1981, 1991-1995, and 2001-2005, whereas on strong El-Nino year (1997), rainfall seemed fewer than other years.

4. Case study on 10 March 2010

El Niño phenomenon appeared in weakened to moderate strength in March 2010. Also the suppressed convection lessened in Indonesia (Maritime Continent) in early March. In mid to late March, convective cloud formations were much better. Therefore, cumulus clouds could developed well in the LCA.

There was tropical depression (TD) east of the Philippine and TC IMANI south west of southern part of Sumatera. Wind direction was mostly northeasterlies, while sea level pressure ranged

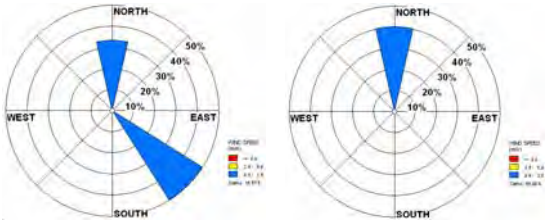


Figure 3. Surface wind at Timampu on 10 March 2010 12-17 LT (left) and 19-23 LT (right)

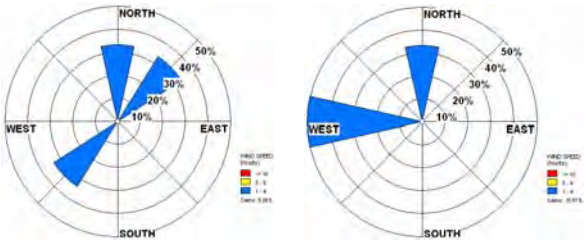


Figure 4. Surface wind on 10 March 2010 12-17 LT at Plantsite (left) and Nuha (right)

about 1012 – 1014mb and 1010 mb, in early March and mid to late March respectively.

Surface wind observations are plotted at 5 stations. Timampu station, which is located in the northwestern shore of Lake Towuti, detected northerlies and southeasterlies wind on 12 -17 LT. Southeasterly wind is suspected to originate from Lake Breeze. But in the contrary, land breeze are found during night time. Figure 3 shows the wind rose for Timampu station during daylight (12-17LT) and night time (19-23 LT). The northerly component

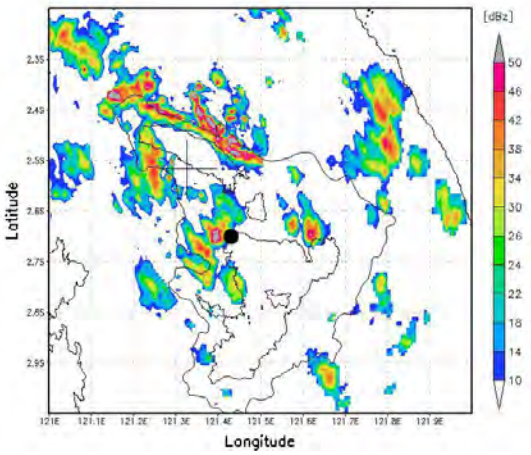


Figure 5. Radar reflectivity on 10 March 2010, 11.25 LT. Cross is radar location, and shaded circle is Timampu station.

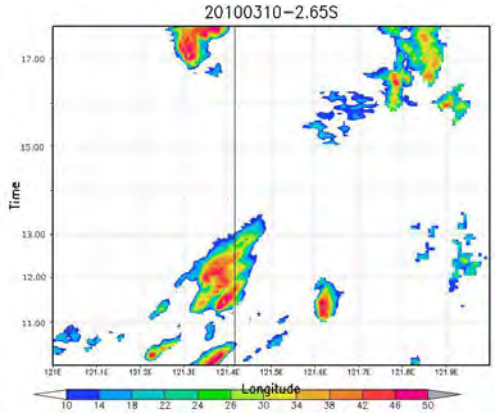


Figure 6. Time-Longitude of radar reflectivity at 2.65°S on 10 March 2010 10.00-18.00. Solid line is Timampu.

during the daylight maybe related to cumulus clouds which developed southwest side of Timampu station.

Lake breezes are also found at Tokalimbo station, where wind dominantly blew from the west. The other three stations (Plantsite, Nuha and Matano) could not identify Lake Breeze event clearly due to topographic and weather conditions (Fig. 4).

Figure 5 is the radar reflectivity composite on 11:25 LT. This figure shows that on LCA, precipitation cloud occurred at west Timampu, west radar site and north site of Lake Matano. The cloud propagation is from west to east.

The lake breezes met the warm air and produce a lake breezes front at the lake shore. Cloud formed over the Timampu area and surface observation also detected rainfall on 12 LT. Temperature drop was also found during this time. The west-east propagation of cloud over Timampu station is shown in figure 6.

5. Observation of Lake Breeze on March 2010

During March, potential clouds are more frequently observed. Radar observation results from 5th to 19th March showed that during those days potential clouds occurred over Larona catchments area. Clouds growth are mostly in northeast and South of East Matano, and also Southeast to West Towuti, and Sorowako area. During the period of 20th to 31st March, potential clouds started to grow at daylight in north Matano, northeast Mahalona, west and southeast of Towuti. The potential clouds formation started at daylight period. Potential clouds formation occurred at west, north to northeast of Matano area and then at north to east of Mahalona area and also north, west, northeast, and southeast of the Towuti area. These potential clouds entered the Larona catchment area at early afternoon.

Surface wind on March 2010 at Timampu shows that the wind mostly blew from the northwest-north direction, but during daylight it is was also found that the south easterlies component was dominant. Figure 7 shows the time-wind direction for March

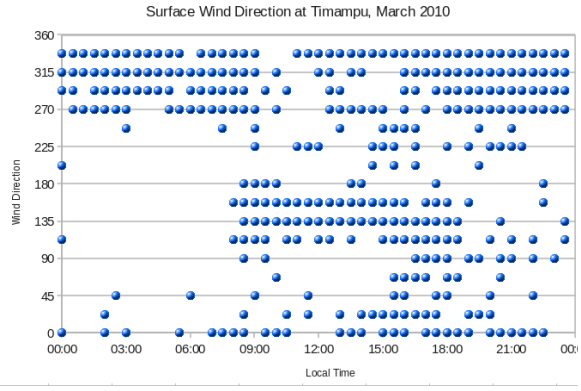


Figure 7. Surface wind direction at Timampu on March 2010.

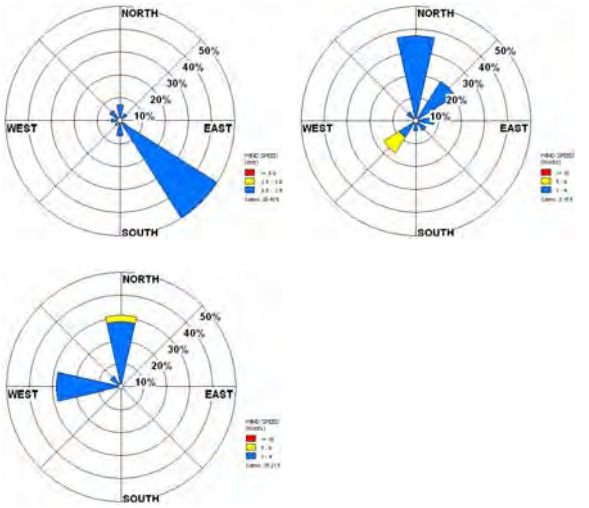


Figure 8. Wind Rose for Timampu (upper left), Plantsite (upper right) and Tokalimbo (lower left) on March 2010, 12-17LT

2010. The wind direction on 09.00-18.00 is from ESE to SSE.

Windrose diagram at Timampu for March 2010 12-17 LT also shows that wind direction southeasterly dominant (fig. 8 upper-left). This means that in the afternoon most of the lake breeze were found at Timampu.

Tokalimbo has westerlies and northerlies component (Fig. 8 lower left). Lake breeze at Tokalimbo was not too strong, as there is a small of island in the western part of the station. At Plantsite the wind came dominantly from the north part of the station. The wind at this station had less impact from Lake Breeze.

The accumulation of radar reflectivity for March 2010 is shown in figure 9. On March 2010, precipitation cloud mostly accumulated at the north side and southwest side part outside the catchments area. Inside the catchments area there are only few clouds were found over Lake Towuti and Matano. The precipitating clouds were found west of Lake Towuti

6. Summary and Discussion

The Lake Breezes events on Larona catchment area were investigated. Preliminary result of one month surface wind observation found that the Timampu and Tokalimbo station, which is located at lake shore of Lake Towuti, are affected by Lake Breeze. The distribution of precipitating cloud observed by radar also showed that the cloud propagation from west to east were blocked by the lake breezes, and the cloud formed over the lake shores.

In the near future, the study of lake breeze in this region will be done by extending the

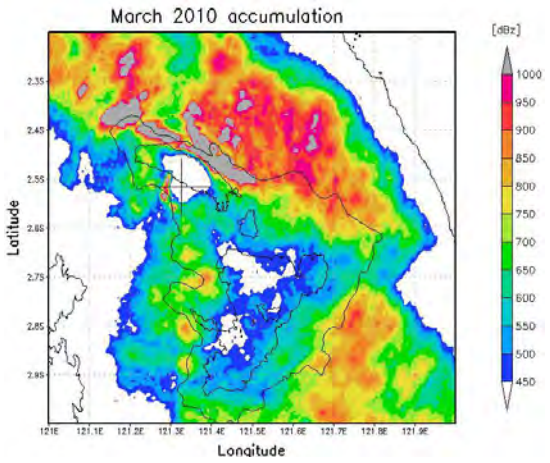


Figure 9. Accumulation of radar reflectivity for March 2010.

observational data and also discovering appropriate method to investigate lake breeze event.

Acknowledgements

This work was carried out as a Weather Modification Project, funded by the Weather Modification technology Center, BPPT and PT Valle Inco. The authors would like to thank Mr. Andi Suntoro of PT. Valle Inco for used of the radar and Mr. Kaimudin for providing the surface meteorological data. They thank to Mr. Krisna Aditya for his careful reading of the original manuscript with constructive comments.They would also like to thank all UPTHB staff for data collection and making the climatological data used in this study available.

References

Aldrian, E., R. D. Susanto, Identification of three dominant rainfall regions within Indonesia and their relationship to sea surface temperature, *International Journal of Climatology*, **23**, 1435-1452, DOI: 10.1002/joc.950, 2003

Kunkel, K. E., S. A. Changnon, B. C. Reinke, and R. W. Arritt, The July 1995 heat wave in the Midwest: A climatic perspective and critical weather factors. *Bull. Amer. Meteor. Soc*., **77**, 1507–1518, 1996.

Laird, N.F., Kristovich, D.A.R., Liang, X.Z, Arritt, R.W., Labas, K., Lake Michigan Lake Breezes: Climatology, Local Forcing, and Synoptic Environment, *J. Appl. Meteor.*, **40**, 3, 409-424, 2001.

NCAR, Feasibility Study for the Augmentation of Rain in Sulawesi, Final Report, 2006

Scott, R. W., and F. A. Huff, Impacts of the Great Lakes on regional climate conditions. *J. Great Lakes Res.,* **22**, 845–863, 1996.

New Development in the Senegalese Rain Enhancement Program "BAWAAN": Investigating key components in support to operations.

Dr. Abdoulaye SARR

National Meteorological Agency of Senegal (ANAMS)

Aéroport International LSS de Dakar

B.P.: 8257 Dakar-Yoff

Dakar, Senegal.

E-mail: layesarr@voila.fr ; abdoulayesar@gmail.com

1. Introduction

A growing number, of rain enhancement programs is noticed in Sahel region mostly because of rainfall variability affecting rain fed agriculture predominant in the area. This region has experience the longest and most devastating drought in the 70s and 80s. That drought began from late 60s (Nicholson 1993; Le Barbé and al. 2002) for almost three decades.

A slight recovery has been noticed since the mid 90s but the interannual variability of rainfall is still characterized by a seesaw between wet and dry years. In the context of global change, projections for future decade are not optimistic about this vulnerable part of the world in terms of temperature (increase in most scenarios) and precipitation (decrease).

In 2002, a severe rainfall deficit occurred again in most countries of Sahel and governments as well as the International Community faced a costly food supply to people in rural areas. Immense losses were noticed in the livestock.

This situation prompted our Government to start putting in place a rain enhancement program to help mitigate the devastating effects of rain deficit in general and also develop the technical and scientific capabilities of Senegal Met Service. .

The trial phase, of the Senegalese rain enhancement program (SENREP), will end this year. This governmental program started in 2005 with support and cooperation of Kingdom of Morocco, which was supplying all air seeding planes and staff. This year, a new phase is reached by the program "BAWAAN" with the acquisition of two King-Air 200 aircraft. One of them is equipped with up-to-date probes to enhance research capacities. This critical cloud seeding year, which represents the last phase of the trial period is conducted with the technical and scientific assistance of Weather Modification Inc. a well known organization in the field.

In this paper, after presenting the program design, the new equipments and other means available are shown with an emphasis placed in the modeling capacities developed to support the program.

2. Climate of Senegal, and design of the programme.

- ***Climate of Senegal***

Senegal is roughly situated between 12.40° and 16.60°N in latitude and 11.5°W and 17.5°W in longitude. It is

the most western country of the Africa main land continent. Therefore it is bordered to the west by the Atlantic Ocean. The annual rainfall is between 1500mm in the south and around 300 mm to the north, where we have the Senegal River.

The northern and central parts of the country are more sensitive to climate fluctuation. That's why the target area of the programme covers the agricultural and livestock lands as shown in Figure 1.

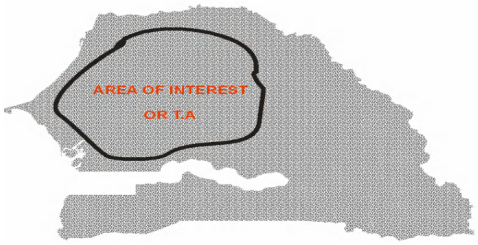


Figure1. Target Area of Bawaan Program

- ***Design of Bawaan Programme***

Ground generators and air seeding are the two components used in the program. The programme head quarter (HQ) is located at the National Meteorological Agency of Senegal (ANAMS), which is in charge of the technical management of the program. Two secondary centres Linguere and Koungheul each supervising five (5) ground generators lcated east of the country.

A telecommunication system based on VHF and HF radio is established between the HQ, the CSs and the generator sites (cf fig.2).



Fig.2: Ground generator sites east of the country and air seeding case with ejectable pyrotechnic flares.

A rain enhancement program requires also mandatory equipment to monitor and forecast convective cloud. An S band 10 cm Doppler radar has been purchased and installed at Linguere located at around 250 km North-East of Dakar. The maximum range of the radar is 480 km with the effective signal around 240 km covering the target area. A remote control/display of the radar from Dakar is available and TITAN system should be implemented this. The forecasting centre (FC) is also equipped with Meteosat Second Generation (MSG) reception workstations. Global models from Meteo-France, UK Met Office, ECMWF are available and used by forecasters. Other models like GFS are obtained via internet and used are lateral and boundary conditions of the meso scale model.

3. Operations

The seeding period covers the rainy season, from June 15 to October 15. As already stated, the number of operations is year dependant and we expect to reach it maximum this year because of the availability of the two King-Air aircrafts and the TITAN software system.

The evaluation method of the program should be scientifically well designed. Although air and ground seeding are used in many programs, the effects are still difficult to be identified and Braham's (1996) listed a few points associated with that and reported in Bruijtus (1999): The large natural variability mentioned above and illustrate in Figure 4 for the case of Sahel, and the incomplete understanding of the physical processes involved. Bruitjes et al. (1999), in a review of cloud seeding experiments, listed the difficulties and progresses made in the field and

mentioned the Israeli experiments (Gagin and Neumann 1981) who provided the strongest evidence to date that static seeding of convective cold-base continental clouds can cause significant increases in precipitation on the ground. However, Rango and Hobbs (1995) have questioned the validity of the Israeli experiments. From their reanalyses of the Israli I and II experiments they claim that seeding-induced increases Israeli I were contaminated by a type I statistical error (i.e., a lucky draw). In addition, they claimed that naturally higher precipitation in the north target area on seeded days during Israeli II could have been mistaken for a seeding-induced change in precipitation.

We also believe that this is the strategy to follows to further convince the funding organisations or governments. New advanced techniques in observation (radar, satellite etc) and modelling could help better understand all processes associated with clouds and precipitation over a region like Sahel. An International experiment like AMMA, started in 2006 is an opportunity in improving our understanding of mechanisms and scale interactions in rainfall process over Sahel. A key feature in rain producing systems is the African Easterly Waves (AEWs) detected mainly at 700 hPa.

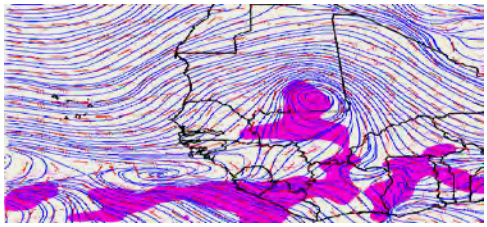


Fig. 3: streamlines at 700 hPa over West Africa showing a deep wave and associated moisture.

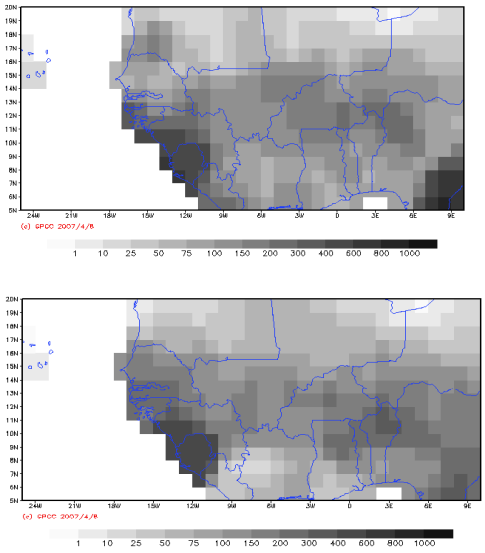


Figure 4. Spatial representation of rainfall amount during July months of 2006 (upper panel) and 2005 (lower panel). Data are from GPCC at 1° resolution using gauge data.

Figure 4 shows the spatial distribution of a specific month (July) between two contrasting years, 2005 and 2006. This coarse dataset highlight the difference over Senegal, as well as over other parts of West Africa in general, and particularly over Sahel. This is an indication of the high interannual variability of rainfall in this region.

This again shows that we need to be cautions when assessing the seeding effects with rainfall recorded. During the implementation phase of the program, the rain gauge network was increased mainly within the target area. If the design is well set, this will enable in at least five years a best assessment, in terms of added rainfall due to cloud seeding.

The Bawaan program has a hydrologic component which is essentially and a large number of storage basin are built in many locations for capturing the flowing water (Figure 3). Certain basins can last many months after the end of the rainy season and have a multi usage for agriculture mainly horticulture, beverage for various animals. The former biodiversity is even recreated in some places with the reappearance of species of animals,

plants, bird etc. Raising of fish is also an activity done in large basins. These activities give added incomes to the rural people living around the basin and also those in the chain of activity. This system also enables keep in place people to avoid exodus and contribute to poverty reduction.



Figure 5: Storage basin, lasting months after the end of the rainy season

Any economic assessment should take this into consideration

4. Modelling Activity

We are working on the selection of a control area, but the south/north gradient and the configuration of the country and wide target area make it difficult. We believe the sampling using the TITAN will be very helpful for the evaluation process.

A modelling component is also undergone for this programme. Different models are used for specific purposes. A non-hydrostatic model (WRF-ARW) as stated above is used during the operations for forecasting and planning purpose. A two way nesting technique is used to have high resolution outputs to help forecasters as additional information to the outputs from the global models and other. A parent domain covering West Africa and the eastern Atlantic Ocean is used at 45 km horizontal resolution with 38 vertical levels. We nest two other domains at respectively 15 and 5 km horizontal resolution centred in Senegal. The run length is 72 hours and delayed start times for nested domains

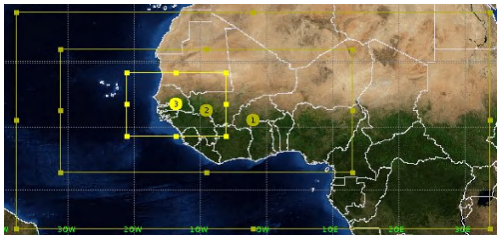


Fig. 6: wrf configuration for Bawaan (SENREP program).

The other modelling activity is a hindcast of past seasons using the regional climate model RegCM which has an aerosol module to investigate the aerosol (including dust) impacts on rainfall in this area.

5. Perspective

A diagnostic study is conducted using observed and simulated vertical profiles in order to understand appropriate key parameters and instability indices for favorable conditions. A combination of satellite and radar echoes will help, in a few years, compute and define indices associated with ideal meteorological conditions for cloud seeding operations.

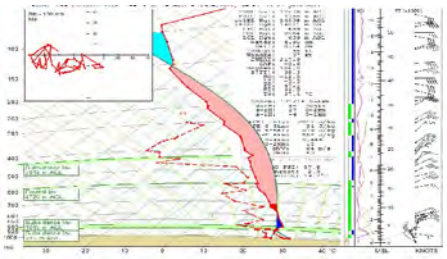


Fig. 7: Vertical profile and key parameter during a day of appropriate seeding conditions.

References:

Gagin A.and J. Neuman , 1981: The second Israeli randomized cloud seedingexperiment: Evaluation of results. *J. Appl. Meteor.*, **20,** 1301–1311.

Nicholson S. E., An overview of rainfall fluctuations of the last decade. *Journal of Climate*, 6, 1463-1466, 1993.

----------,B. Some, and B. Kone, A note on recent rainfall conditions in West Africa, including the rainy season of 1997 ENSO year. J. Climate, 13, 2628-2640, 2000.

Le Barbé, L., T. Lebel, and D. Tapsoba, Rainfall variability in West Africa: A hydrological perspective. *J. Climate*,15(2), 187-202, 2002.

Weather Modification Program using Flare Technique at South Sulawesi, Indonesia – A Technology Transfer

Tri Handoko Seto*, *Samsul Bahri**, *Halda Aditya**, *Moch. Muchlis**, *Mahally Kudsy**, *Moh. Husni**, *Yusef Tiansyah**, *Rino B. Yahya**, *Heru Widodo**, *Mimin Karmini**, *and Andi Suntoro*****

**Weather Modification Technology Center, Agency for the Assessment and Application of Technology*
BPPT 1st building 19th floor, Jl. M. H. Thamrin no. 8 Jakarta, Indonesia
***PT. International Nickel Indonesia*
Bapindo Citibank Tower 22nd floor Jl. Jenderal Sudirman Kav. 54-55 Jakarta, Indonesia

First author's email address: thseto@yahoo.com

1. Introduction

To preserve water resource within Larona Catchments Area, located in the District of East Luwu, South Sulawesi Province holds a key role. The reason is that the production process of PT International Nickel Indonesia (PT. INCO) depends strongly on the electric hydro power plant of Batubesi. Water supply of the PLTA Batubesi is coming from the three lakes, namely Matano, Mahalona and Towuti. These lakes are located in Larona Catchments Area (LCA). The electric hydropower of Batubesi is the only source of electric power for PT. INCO. Therefore, to maintain the water storage is the critical factor in yearly nickel production of PT INCO. Accordingly, PT INCO has utilized cloud seeding program to enhance rainfall in the LCA in order to maitain the availability of water resource. If water level of lakes of Matano and Towuti decrease, cloud seeding activity is be carried out. Cloud seeding using flare in South has started since 1998.

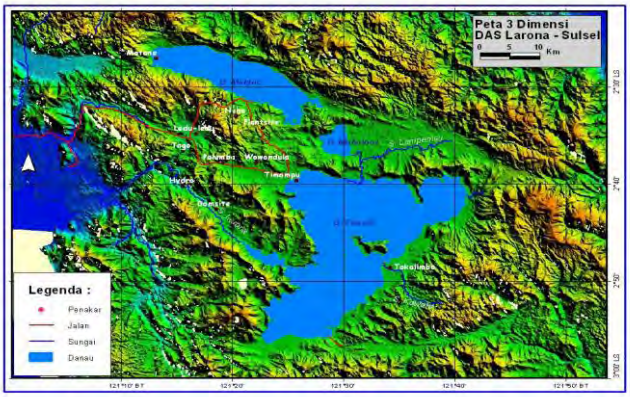


Figure 1. Map of Larona Catchment Area.

The total area of Larona Catchments Area, as the target area for cloud seeding program, is of about 2,477 km^2. There are three lakes in the Larona, namely Matano, Mahalona and Towuti. The Map of Larona Catchments Area can be seen in figure 1. The target area is the watershed of the three lakes (Matano, Mahalona, and Towuti) that feed the two power stations at Larona and Balambano.

Geographical position of LCA, in which close to equator and located between Bone Gulf at west side and Tolo Gulf at east side, causes in unique rain characteristic. Rain might occur in either wind condition, westerlies or easterlies. Larger water body (3 lakes) inside the catchments area causes in local dynamic circulation influences weather pattern and rain occurrence in this area significantly. The effect of lake's breeze and topographical terrain towards air circulation is that subsidence will prevail over the major part of catchments area. Therefore, clouds develop in the catchments area slightly later than those outside. Cloud seeding using flare technique has been conducted when seedable clouds are available in the target area and the vicinity.

Some institution who participate in this program are:

- PT International Nickel Indonesia (INCO), Soroako, Sulawesi, Indonesia.
- Weather Modification Technology Center (WMTC), Agency for the Assessment and Application of Technology (BPPT), Jakarta, Indonesia.
- Atmospherics Inc. (AI), Fresno, California, USA.
- Weather Modification Inc. (WMI), Fargo, North Dakota, USA.
- National Center for Atmospheric Research – Research Applications Laboratory (NCAR/RAL), Boulder, Colorado, USA.

2. Facilities and Instrumentation

Operations Center

The radar and operations control center are located at the Soroako airport (2.53 °S, 121.35 °E) at an elevation of 1388 feet MSL (423 m). Radar data from the WMI weather radar were accessible at this office. The Operations Director performed his duties

from the airport. Forecasting and nowcasting tools were available via Internet and local area network (LAN) lines. These tools included access to the MM5 and other real-time forecasts, weather station information via the internet, satellite imagery, and radar data.

The airport facilities included fuel, hangar space, a dedicated tug, flare storing facilities, and office space. Communications with the aircraft were conducted from this location. Aircraft tracks were displayed at the Operations Center, along with real-time temperature and pressure data from the aircraft.

Airborne instrumentation

An instrumented Piper Cheyenne II twin engine turboprop was used for cloud seeding experiments and microphysical measurements of clouds and aerosols. An array of instrumentation (figure 2) was installed during the evaluation and assessment phase of the field project and included:

- Particle Measuring System [PMS] Forward Scattering Spectrometer Probe [FSSP] (able to detect cloud droplets between 2 and 47 μm diameter)
- PMS Passive Cavity Aerosol Spectrometer Probe [PCASP] (able to measure concentrations and sizes of aerosol particles between 0.1 and 3.0 μm diameter)
- PMS 2D-C Optical Array Imaging Probe (able to detect cloud and precipitation particles between 25 to 800 μm diameter)
- Cloud Liquid Water (CLW) sensor
- Cloud Condensation Nuclei counter (CCNC)
- Cloud seeding racks for 24 hygroscopic flares
- Glaciogenic Cloud seeding material (up to 24 BIP and 306 ejectables)
- GPS system for determining position, ground speed and for estimating winds
- Temperature, pressure and dewpoint sensors
- Data recording system

The data from all of the instruments was recorded every second during flight and select variables were telemetered (radioed) to the operations center in Soroako for real-time data display to aid in the training and direction of flight operations from the ground. The aircraft was capable of carrying only two microphysical measurement probes at a time. Consequently, probes were alternated depending on the mission objectives (aerosol-cloud interactions or precipitation development in clouds) for the day. The FSSP was used for large aerosol and cloud droplets (usually mounted all the time), the PCASP for aerosol characterization (concentrations and sizes) for aerosol-cloud interactions, and the 2D-C for precipitation development studies.

Aircraft analysis software, both commercial and NCAR-developed, was used to examine and summarize the aerosol characteristics, cloud droplet characteristics and precipitation formation processes in clouds in the Soroako region. The measurements obtained with these instruments in combination with radar, satellite and numerical modeling simulations, will be discussed in subsequent sections of this report.



Figure 2. The Piper Cheyenne equipped for seeding and cloud physics measurements.

This instrument package has been designed such that all parameters related to evaluating the seeding potential for Soroako, Indonesia clouds could be assessed. These include microphysical instruments to characterize the natural and seeded precipitation processes, and instruments to characterize the local thermodynamic structure of the atmosphere in which clouds develop.

Radar

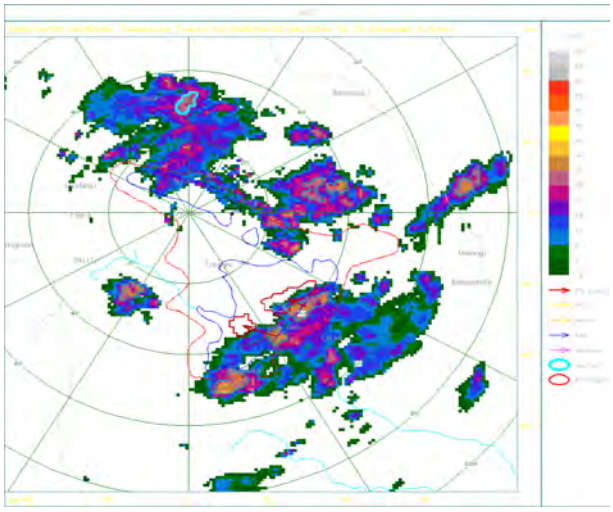


Figure 3. Radar display of precipitation's reflectivity on 22 April 2008, at 12:52 LT.

One of the primary evaluation tools for the Soroako rainfall enhancement project was the WMI C-band weather radar installed at the Soroako airport. The WR-100 radar manufactured by Enterprise Electronics Corporation was located 2.53° S, 121.35° E at an elevation of 423 meters (MSL). The radar was calibrated at the beginning of

operations in March and again at the end of May, with regular calibration checks conducted during the operational period to ensure proper performance during the season.

The TITAN software (Dixon and Weiner, 1993) provided the capability of data display and archival of radar data. With TITAN, the characteristics of rainstorms are capable of being monitored to understand: 1) the large-scale organization of the storms, 2) their frequency of occurrence, 3) their spatial distribution in the area of study and, 4) their history of size and intensity. Figure 3 shows an example of radar display.

3. Feasibility Study

In order to assess the feasibility of any future precipitation enhancement potential in clouds in the Soroako region, it is extremely important to obtain observations in a well-designed measurement program. The aerosol and microphysical measurements determines if seeding could be beneficial and help determine what the optimal seeding method would be that may have potential for enhancing precipitation in clouds in the region. The potential for such manmade increases is strongly dependent on the natural microphysics and dynamics of the clouds that are being seeded (in this case microphysics means the size and concentration of water droplets and ice inside clouds). These factors can differ significantly from one geographical region to another, and even during and between seasons in the same region. In some instances, clouds may not be suitable for seeding, or the frequency of occurrence of suitable clouds may be too low to warrant the investment in a cloud seeding program. Both factors need to be evaluated in a climatological sense. It is therefore important to conduct preliminary studies on the microphysics and dynamics of the naturally forming clouds prior to commencing a larger, operational experiment. It is also important to conduct hydrological studies relating rainfall with river flows and reservoir levels, and to determine hydrological regions where reservoir catchments are most efficient. Seeding could then be optimized by preferentially targeting these more efficient watersheds.

If shown to be feasible, the cloud seeding technique should then be evaluated using a randomization procedure to demonstrate statistically that the seeding method works, and to quantify the increase in rainfall achieved. This approach is similar, for example, to what is commonly done in medical trials with a new drug. Such a randomized statistical experiment would become the second phase of a future program.

Scientists from the Research Applications Laboratory (RAL) of NCAR, in collaboration with WMI of Fargo, North Dakota in the U.S. and WMTC in Indonesia, assisted PT INCO by conducting a feasibility study for rainfall enhancement via cloud seeding in the Soroako region. The feasibility study included the latest technologies that have been developed in this field combining an airborne laboratory with surface weather radar to evaluate and assess seeding operations. The collaborative work entailed all aspects of the project, including cloud physics and radar meteorology, and built on the experience obtained in programs in other parts of the world.

4. Seeding Activities

Flight activities for cloud seeding were carried out based on the availability of cumulus clouds observed by weather radar installed at the Sorowako airport. If radar display showed some cumulus clouds that are able to develop into a storm in target area, seeding aircraft would be taking off to seed the clouds. Before 2009 there were three types of flares mounted on aircraft on each flight. There were hygroscopic flare which ignited at just below of cloud base, AgI Burn in Place flare that ignited at the level of about -6^0 C isotherms (middle of the cloud) and AgI Ejectable flare which ignited at top cloud level when needed. Cloud seeding flights were ended at about 18:00 pm daily.

Before take off, the pilots, flight scientist and the weather observer, held a meeting to discuss cloud development and movement. We then decided which clouds to be seeded within the region. The pilots and an observer at radar site kept communicating to up date radar observation. The observer would guide which could is better to be seeded based on radar reflectivity. The observer on the radar site also had to observe weather condition over the run way to be informed to the pilots. This was to avoid the run way was closed by incoming clouds.



Figure 4. Superimposed flight seeding tracks for the period of January – May 2008.

When the aircraft reaching cloud base of intended cloud to be seeded, a BIP-CN was burn as seen on Figure 10. This burning may continue as needed. While BIP-IN and ejectable flares would be used if the clouds were deep and had strong up draft. Seeding activity, mostly was about one and a half

hours. Figure 4 shows a sample of flight track. Table 1 shows the amount of flares used and result in lake inflow in each cloud seeding program.

Year	Flare used	Result (million m^3)	Flight sorties
1998	496 HBIP, 235 EBIP, 150 EJ	230.84	89
1999	480 HBIP, 366 EBIP, 1025 EJ	1818.13	**
2000	539 AI, 120 BPPT	2250.5	71
2008	704 HBIP-12, 90 EBIP-77, 159 EJ-300	246.2	138
2009 - 2010	1313 HBIP-12, 1 AgI	297.2	112

Table 1. Flare used and result from cloud seeding program in South Sulawesi

Note: HBIP: Hygroscopic Burn in Place Flare
EBIP: AgI Burn in Place Flare
EJ: AgI Ejectable Flare
For year 2000, all using HBIP, with 120 flare made by BPPT

5. Summary

- As one of the largest and most cost-eficient nickel producers in the entire world, PT International Nickel Indonesia (PT INCO) has low-cost electricity which is received from the hydro-power facilities that it owns, which provide approximately 80 percent of electric energy needed..
- To preserve water resource at Larona catchment area, PT INCO carried out weather modification to enhance rainfall since 1998.
- Under colaboration with international some institutions, weather modification program at Larona catchment area has been conducted using some modern equipmments to introduce both of glaciogenic and hygroscopic seeding agent.
- This program also improves the capability WMTC in cloud seeding program using flare technique and weather observation using radar especially for cloud seeding activity.

Acknowledgements

The author and co-authors are very grateful to PT INCO who has given financial support for all weather modification project during 1998-2010. Gratitude owed to Pak Tony Dengkeng, Ibu Shinta, Pak Wisnu, Pak Warto, and all PT INCO colleagues who worked closely and been a good teamwork. Special thanks to WMTC colleagues for a very good teamwork along the program. We would like to thank Dr. Roeloft Bruintjes for his inspirations, encouragements, and discussions throughout this work. Thanks owed to Krisna who has dilligently corrected this paper draft. Thank you to all of those parties which we cannot mention individually who has helped in the writing of this paper.

References

1. Dixon M. And G. Weiner, 1993: *TITAN: Thunderstorm identification, tracking, analysis and nowcasting – A radar-based methodology,* J. Atmos. Oceanic Technol, 10, 785-797.

2. Weather Modification Technology Center, Final report: Cloud seeding project at PT. INCO Sorowako, 1998, Jakarta, Indonesia.

3. Weather Modification Technology Center, Final report: Cloud seeding project at PT. INCO Sorowako, 1999, Jakarta, Indonesia.

4. Weather Modification Technology Center, Final report: Cloud seeding project at PT. INCO Sorowako, 2000, Jakarta, Indonesia.

5. Final report, Feasibility study for the augmentation of rain in Sulawesi, 2006, National center fr Atmospheric Research, Boulder, USA.

6. Weather Modification Technology Center, Final report: Cloud seeding project at PT. INCO Sorowako, 2008, Jakarta, Indonesia.

7. Weather Modification Technology Center, Final report: Cloud seeding project at PT. INCO Sorowako, 2010, Jakarta, Indonesia.

Observations of Haze Aerosols over North China During Autumn 2009

Lixin Shi[1,2] , Xiaobo Dong[3], Feng Lu[3] and Xiangfeng Hu[3]
[1]Key Laboratory of Meteorology and Ecological Environment of Hebei Province, 178 Tiyu South Street, Shijiazhuang, China, shi-lx@hotmail.com
[2]Key Laboratory for Cloud Physics and Weather Modification of CMA
[3]Weather Modification Office of Hebei Province, 178 Tiyu South Street, Shijiazhuang, China, xb.dong@hotmail.com

1. Introduction

Aerosols are an important factor of climate change due to their radiative impact on the Earth's energy budget and the substantial increase in their global mean burden from preindustrial times to now. Aerosols influence climate directly by scattering and absorbing radiation and indirectly through their influence on cloud microphysical and dynamical properties (IPCC 2001). North China is one of the most important economic centers in China. The rapid development and industrialization in the region in recent years and high energy consumption, air pollutant emissions are increasing steadily and the regional environment is deteriorating. North China is one of the four main regions in China heavily afflicted by haze (Lee and Savtchenko 2006). The observation of haze over North China is very important to the study of the effect of anthropogenic emissions on the environment. Many aircraft observations of aerosol and cloud condensation nuclei (CCN) have been done over this region (Zhang et al. 2006; Shi and Duan 2008; Yin et al. 2009), but the haze aerosol observation is still lacking.

The paper is to present the measurements of haze aerosol and CCN over North China during autumn 2009.

2. Instruments

A Piper Cheyenne ⅢA twin turbo-prop aircraft was used for the observations. The aerosol was measured by PMI (Particle Metrics Inc, USA) Passive



Fig.1 Shijiazhuang Location Map

Cavity Aerosol Spectrum Probe PCASP-100X (range 0.1-3 μm). Aerosol particles were divided into 15 unequally sized bins and were recorded at 1-s intervals. CCN were measured by a DMT (Droplet Measurement Technologies, USA) continuous flow streamwise thermal gradient CCN counter (Roberts and Nenes 2005). The instrument can operate between S = 0.1% and S = 2% at sampling rate of 1 Hz. In this study, CCN measurements were made at S = 0.3%.

3. Observations

Aircraft observations of aerosol and CCN were conducted over Shijiazhuang urban area, the mid-south of Hebei Province in North China (Fig.1) during autumn 2009. Shijiazhuang is the capital of Hebei Province, and also is one of the most polluted cities in China. Table 1 summarizes the observations of five flights. For comparison, two clear days and three haze days are chosen in the study (Fig.2 and Fig.3).

Table 1 Summary of observations for five flights

Date	Time (BT)	weather
20 September 2009	1508-1515	Clear
9 October 2009	1504-1511	Haze
16 October 2009	1941-1948	Clear
24 October 2009	1615-1623	Haze
25 October 2009	1607-1615	Haze

The method of spiral ascent or descent in the troposphere was used for the vertical measurements. Fig.4 shows an example of flight track on 16 October 2009. Usually, the observation height was from 600 to 4500 m. Except for flight on 24 October, the max altitude was 3000 m.



Fig.2 The photos on clear days taken on 20 September 2009 and 16 October 2009.

4. The characteristics of aerosol and CCN

Fig.5 shows the vertical distributions of aerosol concentration and Fig.6 shows the temperature profile for the five flights. It can be seen



Fig.3 The photos on haze days taken on 9 October 2009, 24 October 2009 and 25 October 2009.

that aerosols mainly concentrated on the levels from near surface to the low level of troposphere and the concentration generally decreased with height increasing. Usually there exists the inversion layer in troposphere, and the inversion in low level can result



Fig.4 Flight Track on 16 October 2009. A is the airport and B is Shijiazhuang urban area.

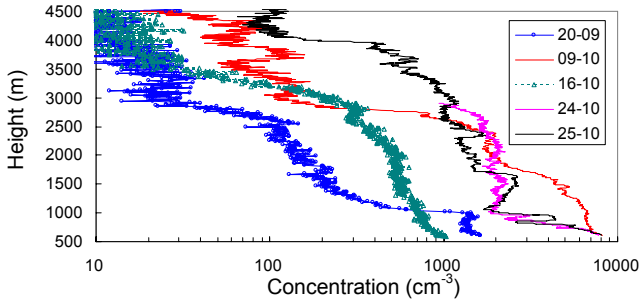


Fig.5 The aerosol concentration profiles for five flights on 20 September, 9 October, 16 October, 24 October and 25 October 2009.

in the cumulation of high aerosol concentration in boundary layer. There is great difference of aerosol concentration between clear days and haze days. The max aerosol concentration on haze days was 8110 cm^{-3}, 7784 cm^{-3} and 8084 cm^{-3}, respectively corresponding to 9 October, 24 October and 25 October. The max concentration on clear days was 1614 cm^{-3} and 1030 cm^{-3}, respectively corresponding to 20

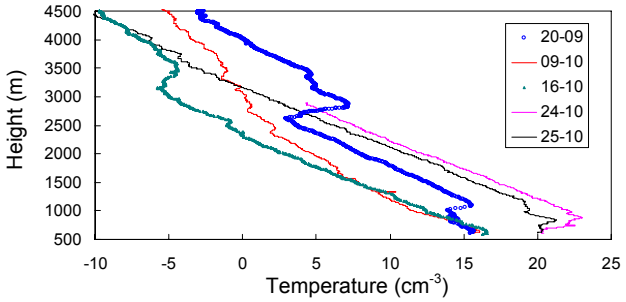


Fig.6 The temperature profiles for five flights on 20 September, 9 October, 16 October, 24 October and 25 October 2009.

September and 16 October. The average concentration from 600 m to 2500 m was 4116 cm^{-3}, 2672 cm^{-3} and 2470 cm^{-3} on haze days and 476 cm^{-3}, 597 cm^{-3} on clear days. There was more than 4 times difference in concentration of aerosol in boundary layer between haze days and clear days.

The CCN concentration has the similar vertical distributions as aerosol concentration (Fig.7). Most CCN concentrated on the boundary layer and also

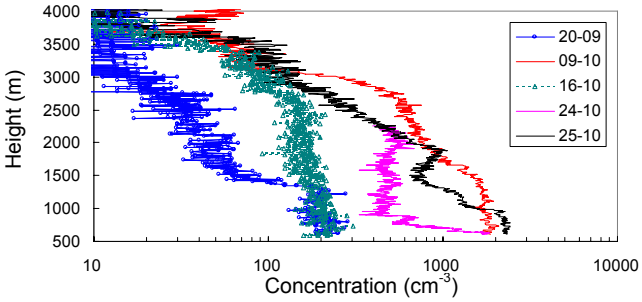


Fig.7 The CCN concentration profiles for five flights on 20 September, 9 October,16 October, 24 October and 25 October 2009 (S=0.3%).

affected by low level inversion. It suggests that the main source of CCN is from surface. It is consistent with the early result obtained in North China (Shi and Duan 2008). On haze days, the max CCN concentration was 2081 cm^{-3}, 1852 cm^{-3} and 2432 cm^{-3}, respectively corresponding to 9 October, 24

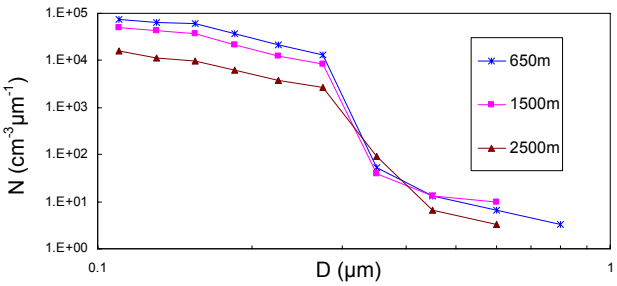


Fig.8 The aerosol spectra at different height on 9 October 2009.

October and 25 October. The max concentration on clear days was 284 cm^{-3} and 305 cm^{-3}, respectively corresponding to 20 September and 16 October. The average concentration from 600 m to 2500 m was 1263 cm^{-3}, 579 cm^{-3}, 1093 cm^{-3} on haze days, and 104 cm^{-3}, 174 cm^{-3} on clear days. There was more than 3 times difference in concentration of CCN in boundary layer between haze days and clear days. The CCN average concentration on 25 October was higher by one order of magnitude than that on 20 September.

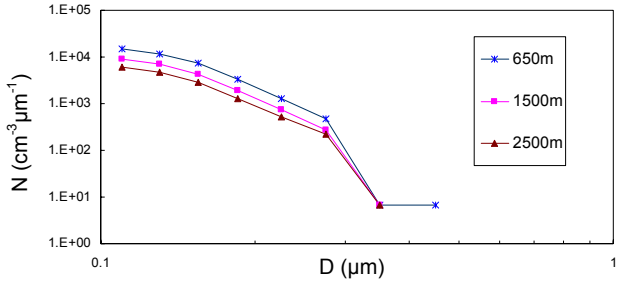


Fig.9 The aerosol spectra at different height on 16 October 2009.

Two kinds of aerosol spectra at different height for haze day on 9 October and clear day on 16 October are shown in Fig.8 and Fig.9. It was cloudy in the morning and turned to fine in the afternoon 9

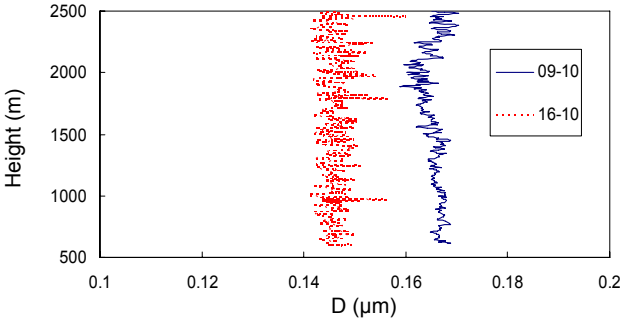


Fig.10 The vertical distributions of aerosol mean diameter on 9 October 2009 and 16 October 2009.

October. There was strong wind weather on 16 October until evening and the atmosphere was clean. Here the 100 m depth average represents a certain height value, e.g. the 650 m aerosol spectrum was averaged from 600 m to 700m. Both on haze day and on clear day, it can be seen that the aerosol spectra have the similar distribution. All the spectra at different height had single peak distribution with peak diameter was 0.11 μm. The spectrum was wider near surface, and with height increasing, the aerosol concentration decreased. On clear day, the max spectrum width (0.45 μm) was narrow, but it was 0.8 μm on haze day. On clear day, the aerosol concentration was only one fifth of that on haze day at 650 m and 1500 m. The bigger and high concentration haze aerosol particles can result in the poor visibility.

Fig.10 gives the vertical distributions of aerosol mean diameter on 9 October and 16 October. Below 2500 m, the mean diameters of aerosol have less change either on haze day or on clear day. It shows the aerosols were well mixed in the low level. But the mean diameter (about 0.16-0.17 μm) was larger on haze day than that (about 0.14-0.15 μm) on clear day. According to Shijiazhuang meteorological observatory surface measurement data, the relative humidity (RH) was 17% at 1900 BT on 16 October, and RH=52% at 1500 BT (RH=83% at 0800 BT and RH=71% at 1100 BT) on 9 October. It suggests that the aerosol particles may become larger by hygroscopic growth under haze weather conditions.

5. Summary

Five flights aerosol observations over North China during autumn 2009 are analysed. There is great difference of aerosol microphysical character between haze day and clear day. This difference obviously concentrates on the boundary layer. The max haze aerosol concentration 7784-8110 cm^{-3} here, is similar to the former result 2437-8760 cm^{-3} measured over Beijing and its adjacent area of Hebei Province on haze days during autumn 2004 (Fan et al. 2007). Generally, Shijiazhuang's aerosol concentration is higher than that over Beijing, and the air pollution is more serious. To find the difference between clean air aerosols and haze aerosols in detail, more observation work should be done and aerosol chemical composition should be analysed in the future.

Acknowledgements

This research was supported by National Public Benefit Research Foundation Contact GYHY200806001, Key Laboratory for Cloud Physics and Weather Modification of CMA Contract 2009Z0034, and New Technology popularization project of CMA Contract CMATG2010M21. We thank the technicians of Yupeng Deng, Yan Jiang, Zhijun Zhao and Zuohui Qi, also Xinjian Huang and other members of the Cheyenne IIIA crew for help in collecting data.

References

Fan Y., Guo X., Fu D., and Li H., Observational Studies on aerosol distribution During August to September in 2005 over Beijing and its surrounding areas. *Climatic and Environmental Research* (in Chinese), **12**, 49-62, 2007.

IPCC, Climate Change 2001: The Scientific Basis, Contribution of Working Group I to the Third Assessment Report of the International Panel on Climate Change. *Cambridge University Press*, 881 pp, 2001.

LEE Y.C. and A. Savtchenko, Relationship between air pollution in Hong Kong and in the Pearl River Delta region of South China in 2003 and 2004: An Analysis. *J. Appl. Meteor.climatology*, **45**, 269-282, 2006.

Roberts G. C. and A. Nenes, A continuous flow streamwise thermal gradient CCN chamber for atmospheric measurements. *Aeros. Sci.Tech.*, **39**, 206-221, 2005.

Shi L. and Duan Y., Observations of Cloud Condensation Nuclei in North China. *Acta Meteo. Sinica,* **22**, 97-106, 2008.

YIN Y., Duan Y., Zhang Y., Shi L., Yang Z., Wu Z., and Li Y., Airborne measurements of the spatial and spectral distributions of aerosol particles over Hebei area, northern China. *Proc. of SPIE*, **7490**, 74900X1-8, 2009.

Zhang Q., Zhao C., Tie X., Wei Q., Huang M., Li G., Ying Y., and Li C, Characterizations of aerosols over the Beijing region: A case study of aircraft measurements. *Atmos. Environ.*, **40**, 4513-4527, 2006.

A Study of the Characteristics of Atmospheric Water Vapor and Its Relationship with Precipitation Using GPS Data

Su lijuan[1] Dabuxilatu[1] Lu shiqing[1] Deng xiaodong[2] Yan bing[1]

(1 Inner Mongolia Meteorological Institute, Hohhot 010051, China; 2 Inner Mongolia Center of Ecology and Agriculture Meteorology, Hohhot 010051, China)

The technology of sensing water vapor using ground GPS is a new method of the atmosphere observation. It senses the content of water vapor in the atmosphere using high-precision ground GPS, through measuring the GPS signals about the amount of delay in the atmosphere. The sensing of water vapor of ground GPS has high resolution and millimeter level accuracy, which can fill the lack of data's accuracy in time and space to provide fast-changing water vapor information. This information is very important on the choice of weather modification operating conditions and precipitation forecast. With using GPS equipment, we finished the water vapor observation and tested the quality of the data. Then we analyzed of the relationship between the monthly changes and precipitation through the comparison with the calculated sounding data of water vapor.

1. GPS / MET observation experiments of water vapor

The tests chosed the observation points equipped with sounding, ground-based observation of meteorological services business and the LAN of meteorological services business. The three test stations were laid in: Inner Mongolia Meteorological Institute of Hohhot at N 40°50'26.7 ", E111°39'16.5" and altitude 1050.551m; Hohhot Baita Airport at N 40°51'34.2 ", E 111°49'33.7 " and altitude 1076.451 m; Erenhot weather station at N 43°38'53.8", E111° 58'5.5 " and elevation 941.5 m. There were the sounding station and ground observation station around Inner Mongolia Meteorological Institute of Hohhot. The GPS observation points were located in the sounding station and ground-based observations of the Bureau of Meteorology Erenhot. Hohhot Baita Airport is equipped with six elements ground automatic observation stations.

2. Data and quality analysis

This data used in the paper began from January 1 to October 31 in 2008. It included the GPS/MET monitoring data, the meteorological sounding data, the ground observation data and conventional ground-based precipitation data. The data was collected by the instrument of GPS/MET at the rate of one time for 15 seconds; the high degree of the satellite was 15. We received the real-time data from each observe station through the network , and the data file was formatted every 15 minutes in every station. And at the same time, we did some management of the data to convert the raw data into the Rinex format needed in the solver package of the vapor.

Meanwhile, to text the validity of the data , this study used the professional data quality analysis software Translate Edit Quality Check(TEQC) to conducted a data quality test, the data was concluded by the observation data of 10 consecutive days from January 1 to 10 in 2008, and 960 data files from every station. In this text, we got the average data quality for each station, and statistically analyzed the data quality of the three stations.

The effective acceptance ratio of the research institute station is 98.88%, mp1 is 0.22, mp2 is 0.24, and the effective acceptance ratio of Baita is 91.01%, mp1 is 0.28, mp2 is 0.30, while the station of Erlianhaote is 99.93%、0.13、0.24, respectively.

According to the principles of data quality inspection, if the effective acceptance ratio of the data exceeds over 85% and both mp1and mp2 are all less than 0.5, then the data can be used effectively. Therefore, the observation data of the three stations are all standard effective available.

3. Calculation method

Gamit software was used on GPS/data processing,

and IGS actual star calendar was adopted to calculate the zenith per hour delay. Each hour, zenith the troposphere delay is the sum of zenith statics delay Z_h and wet Z_w and a delay. It can be written as:

$$\Delta D_z = \int_L (n(s)-1)ds =$$

$$10^{-6}\int_z 77.6\frac{p_d}{T}dz + 10^{-6}\int_z\left(27\frac{e}{T} + 3.73\times10^5\frac{e}{T^2}\right)dz = Z_h + Z_w$$

Zenith statics delay Z_h can be calculated by ground pressure p_0 (hpa):

$$Z_h = (2.279 \pm 0.0024)\frac{p_0}{f(\lambda, H)}$$

$f(\lambda,H) = (1-0.00266\cos(2\lambda)-0.00028H)$, λ is for the latitudes, H is for altitude (km).

Wet delay Z_w is calculated by the following formula:

$$Z_w = 10^{-6}\int_z\left(77.6\frac{e}{T} + 3.73\times10^5\frac{e}{T^2}\right)dz = 10^{-6}\bullet P_W\left|R_v\left|k_2' + k_3\frac{\int_z\frac{e}{T}dz}{\int_z\frac{e}{T}dz}\right|\right|$$

P_w is for atmospheric precipitation, R_v = 461.495J·kg^{-1}·K^{-1}, as the gas constant of water vapor.

$$T_m = \frac{\int\left(\frac{e}{T}\right)dz}{\int\left(\frac{e}{T^2}\right)dz}$$

T_m is average temperature, which can be determined by experience coefficient: $T_m = a + b\bullet T_s$ Bevis gave the experience: a=70.2，b=0.72[1]。.

Therefore, the atmosphere rainfall can be calculated by the following formula:

$$P_W = \prod Z_w,\quad \prod = 10^6[R_v[\frac{k_3}{T_m} + k_2']]^{-1}$$

4. Analysis of water vapor

4.1 Contrast on monthly change of water vapor and sounding calculated value

It can calculate a water vapor value calculated by GPS/MET listed inversion each observatory each hour, and then it can conclude the water vapor average value daily and monthly.

Vapor curve were almost the same with each other by the two sets of instrument measurement inversion of vapor curve in White tower and Research institutes, showing that the stability of GPS/MET listed instrument was very good, and the gap was that research station was 0.1156 mm slightly higher. After compared water vapor retrieved by GPS / MET with water vapor sounding calculation, we found that overall water vapor retrieved by GPS / MET is slightly higher than the value of sounding calculation. The difference of value changes with seasonal changes was not obvious, and it was very stable as well as comparable. The water vapor value from white tower was 1.96 mm higher than sounding calculation and 2.0767 mm higher than research institutes. Average GPS/MET listed inversion of vapor value was 2.0189 mm higher than sounding calculation value. According to GPS/MET listed inversion of vapor map, showing that water vapor content standing on Hohehot state on average monthly from high to low in turn for July, August, June, September, April, May, October, March, January, on average, summer water vapor content was the most as 24.79 mm, followed by autumn as 14.1 mm, spring as 9.55 mm, winter was the least as less than 5 mm.

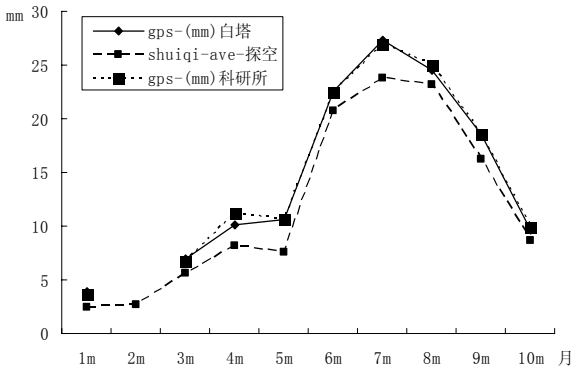


Fig.1 Air vapor month trend from GPS contrast to sounding in Huhhot

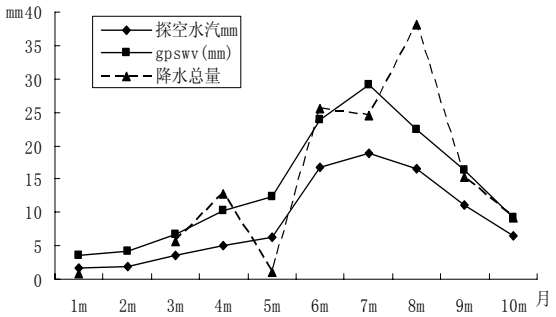


Fig.2 Air vapor month trend from GPS contrast to sounding in Erlianhot and precipitation

Overall the value of water vapor calculated by GPS/MET listed inversion was higher than that by sounding calculation, the absolute difference value was obviously with season change over time, and for the

basic present out of water vapor obviously was the same change trend on month changing, namely: the gap between them is bigger with the increase of vapor, too. After the gradually increased in January-July, it decreased with water vapor reduction. But difference value percentage of water vapor (sounding) and the changing trend of water vapor, was by contrast, the more water vapor, the smaller percentage value. Overall the gap with water vapor value calculated by GPS/MET listed and sounding calculation was higher in Erlianhot stood than that in Hohehot, average GPS/MET listed inversion of water vapor was 4.996 mm higher than sounding calculation.

According to GPS/MET listed inversion of vapor map, showing that water vapor content standing on Erlianhot state on average monthly from high to low in turn for July, June, August, September, May, April, October, March, February, January. On average, summer water vapor content was the most as 25.15 mm, followed by autumn as 12.75 mm, spring as 9.77 mm, winter was the least as 3.82 mm.

4.2 The relation between water vapor changes and precipitation

It can be seen from Figure 3 that monthly changes in average content of water vapor are in consistently with precipitation and the corresponding monthly precipitation is also higher when monthly mean water vapor is high, so which can explain that the content of water vapor has a good indication for the forecast of precipitation and the selection of conditions in artificially affect weather.

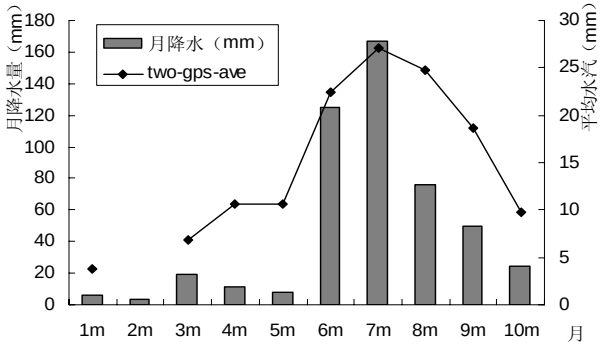


Fig.3 Air vapor month trend from GPS contrast to precipitation in Huhhot

Fig.4 shows the hourly changes of water vapor in August in Huhhot. Purple dots marked in circles represent the time with precipitation. From the fig.4, the characteristics of the water vapor changes can be show in the precipitation mechanism, namely, there is a certain stage of moisture accumulation before the precipitation, and then produce precipitation only when water vapor accumulated to peak, because the water in clouds may has reached saturation. In addition, precipitation generated in the stage of water vapor decline, probably due to consumption of a large number of water vapor. After the start of precipitation, the atmospheric total water vapor reduces quickly.

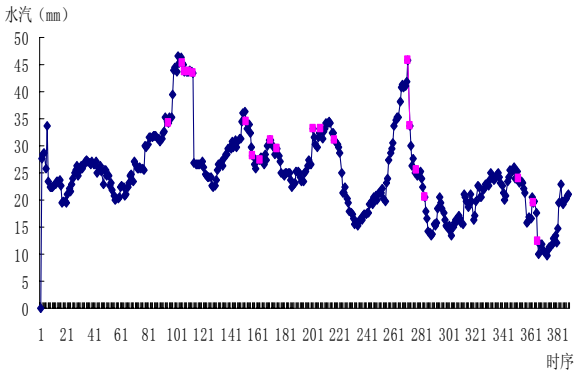


Fig.4 Air vapor sequence change from GPS on May

4.3 A case study

There's been a big rainfall process in hohehot area in July 30-31, 2008. This process started from the continuous rain at 11:00 on the 30th and the precipitation has been maintained to 14:00 on 31th. The total rainfall is 97mm, reached rainstorm level. Fig.6 shows the changing curves of water vapor from 0:00 on July 29 to 7:00 on July 30. Purple line in the figure represents the precipitation period.

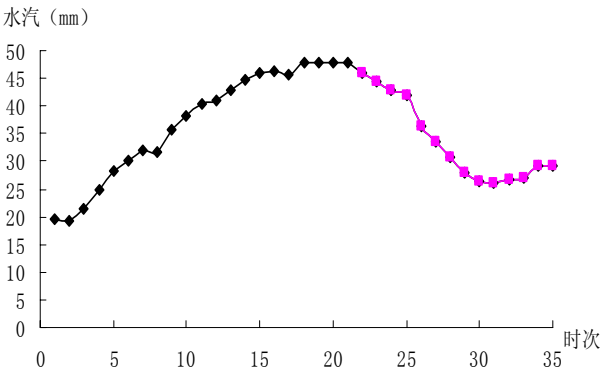


Fig.5 Air vapor change from 0:00 on July 29 to 7:00 on July 31

From fig.5 we can see that, water vapor began to

accumulate gradually at 0:00 on July 29. After the two phases of accumulation water vapor reached to peak at 5:00 on July 30, then maintained 6hours and state rain at 11:00. After the start of precipitation the water vapor declined rapidly to lowest value at 2:00 on July 31, then, there are compensation mechanisms allow the accumulation of water vapor again. Precipitation remained until at 14:00 on the 31th.

5 Conclusion

1) The three observatories quasi-geoids data is effective and reliable.
2) The maximum average water vapor content presents in summer, reaching about 25mm, autumn, and spring followed, and the winter was the lowest with only 5mm or less.
3) Water vapor retrieved by GPS / MET is higher than the sounding calculated value, In Hohhot stood about high 2mm, in 4.996 mm Erlianhot standing tall.
4) Water vapor retrieved by GPS / MET is closely related to rainfall in this site. Before precipitation occurred there is a certain stage of the accumulation of water vapor, and then produce precipitation only when water vapor accumulated to peak, because the water in clouds may has reached saturation. In addition, precipitation generated in the stage of water vapor decline, probably due to consumption of a large number of water vapor. After the start of precipitation, the atmospheric total water vapor reduces quickly

A Study Of Micro-physical Characteristics and Seedability Of Cold Stratiform Clouds In North China

Sun hongping[1] Li peiren[1] Yan shiming[2]

(1 Weather Modification Office of Shanxi Province , Taiyuan China 030032 , fengdichen@sohu.com

2 Shanxi Institute of Meteorological Sciences, Taiyuan China ,030002)

Introduction

Precipitation of stratiform clouds were detected with the particle measurement technology (DMT) in Shanxi test area 0n 11-12 March 2009 . The aircraft made vertical and synthetic detecting flying purposefully. the micro-probe data obtained in the cloud processing, analysis, and to find the cloud cooled water content in the cloud distribution, while Gu zhen-chao three-layered model of stratiform cloud to analyze the cloud structure, precipitation formation and precipitation of stratiform cloud microphysical characteristics, in order to better understand the structure of precipitation and cloud formation mechanism of natural rainfall, provide a theoretical basis for artificial rainfall operations.

1 Weather Background

On 11-12 March 2009, there was a large range of stable stratiform precipitation process in North China. Rainband was basically northeast - southwest direction, the move are basically the same as the upper trough.

2 Flight probe program design

This probe uses Y-12 aircraft, using airborne cloud particle probes from the United States DMT (Droplet measurement technologies) company introduced, CAPS (Cloud Aerosol and Precipitation Spectrometer), CCN (Cloud Condensation Nuclei Counter) and other probes. March 11, 2009 08 pm, rain clouds began to go over the western, to understand the cloud microphysical structure of different levels, access to specific stratiform precipitate formation in North China, the new understanding of potential and mechanisms analysis of artificial rainfall, we conducted a series of vertically stratified cloud detection. 600 meter spacing between layers, starting from the cloud base, spiral, each level flight for 5 minutes, after the genting , the interval is still 600 meters , vertical layered down until the security level. This method can give particle spectrum flight phase state, with Vertical distribution with height of moisture and other continuous, through the analysis of the vertical distribution of particle spectra, can deduce the main physical processes of precipitation formation.

From the ground to upper air, the atmosphere is stable, the air humidity, Zero level is at 850 hPa (1500 m) near. It is a cold cloud precipitation process.

3 Cloud microstructure characteristic and seedable analysis of artificial rainfall

According to Gu zhen-chao three-layered model of stratiform cloud l, there are three lavers in maturity stages of stratiform cloud, where the first layer is ice layer, the second layer is super-cooled water layer, the third layer is warm layers. The aircraft detected in the mid to late in the process of precipitation, there is only the second and third tiers, with the second layer (mixing layer) thickness of 3-4 km, a temperature range of 0 - 17.7 □, the third layer (warm layer) thickness of about 0.6 km, the main objective of the program to detect is the mixed layer.

3.1 Cooled water content characteristics of the cloud

According to the CDP probe data, time series in the probe, the average cooled water content in the cloud is 0.012g/m^3.we calculate the change of cooled water content with height from 0 □ .In order to facilitate comparative analysis, calculate the cloud super-cooled water content with the height of each one hundred meters intervals by height from 0 □. calculated by the cloud of super-cooled water content from 0 □ height distribution shown in Figure 1.

As can be seen from Figure 1, vertical distribution of the cloud cooled water content from 0 ℃ height: in height 100 m from 0 ℃ , the super-cooled water is low. With the height of from

0 ℃ to increase, the super-cooled water content increase, in the probe process, the super-cooled water content maximum come out in height of the 400m from 0 ℃, at its maximum value, respectively 0.416g/m^3; later with a height of from 0 ℃ to increase, the super-cooled water content decreases rapidly , at 600m height from 0 ℃ , come up to the minimum, until Genting, the super-cooled water content maintain low levels. This generation and distribution structure is related to the weather of Shanxi Province.then, according to the statistics history of exploration data, in Shanxi Province in the precipitation of stratiform clouds, above 300 ~ 500 m layer from 0 ℃ the cloud updraft at the maximum speed , entrusted with most of the droplets, so in this height range of super-cooled water content produced a large value area.

This precipitation process, in height 100-600m (altitude 1500-2000m) from 0 □ the super-cold waters is too rich, let analysis the cloud micro-physical Characteristics .

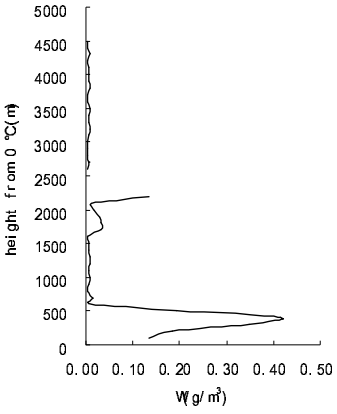


Fig. 1 Vertical distribution between the content cold water in cloud with height from 0 □ during detecting on 11 March 2009

3.2 The vertical distribution of cloud micro-physical

By the height of the cloud particle concentration distribution can be seen, changes in cloud droplet concentration with height turn multimodal distribution, and undulating, LWC and N has a good positive correlation, correlation coefficient is 0.84. 0 □ layer near the cloud droplets, cloud particles spectrum, ice particle spectrum, scale precipitation changes in particle concentrations are large, messy image layers indicating that there are rapid change of particles state in the zero phase. after maintaining Low in 1650 a high degree of increases and then rapidly decreased near to zero, then increases with height, cloud droplet concentration of 1800m near the maximum 452 / cm^3, LWC also increase up to the maximum. in the height (altitude 1500-2000m) rich super-cooled water near, the average diameter of cloud droplet concentrations are positively correlated with, but above 2000 meters the concentration decreases rapidly as the cloud droplets, cloud droplets of average diameter turn a clear jump in, negative correlation .

Particle concentration, mean diameter CIP, PIP probed, distribution with height tell us. the height (altitude 1500-2000m) rich super-cooled water near, a little change in particle concentration, more consistent, and CIP, PIP probe showed the average diameter ,the particle concentration turn more obvious anti-correlation, large cloud droplet diameter corresponding to small cloud droplets concentration, the average particle concentration CIP probed is 10-2 / cm^3 magnitude, average particle concentration PIP measured is 10-3 / cm^3 magnitude, in the cloud ,especially in the cold (0 □ layer above) laye, particles concentration CDP probed is about four orders of magnitude what CIP probed, indicating The number of particles less than 25μm in diameter are more.

In the height (altitude 1500-2000m) rich super-cooled water near, the average particle diameter has a little change, the average diameter of three probe are 8.01μm, 385.18μm and 165.28μm. Description Cloud particles in cold clouds, the average diameter is less. It can be seen from Figure 2, in the supercooled water-rich zone, in the down process to detect particles, the diameter increases, we can see where Raindrops hitting and growth, cloud droplets condensating and growth.

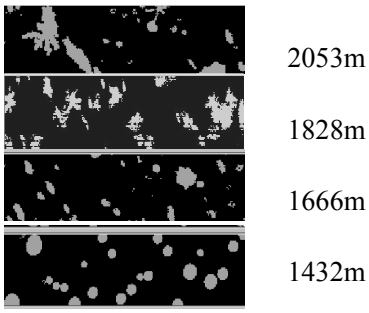


Fig. 2 Two-dimensional particle image

Hobbs has been suggested that when using FSSP-100 probe observed, cloud total concentration of particles larger than 2μm over 107/m^3 or 10/cm^3 time, as the cloud water area. You

lai-guang(1994) pointed out that basis can be understood as the determination, experience and theory show that the ice core nucleus of self-inhibition, ice crystals concentrations in the natural cloud can not exceed 10^4 / L or 10/cm^3. According to this criterion, it seems that when the cloud droplets concentration exceeds 10/cm^3, the clouds have been super-cooled water there, the introduction of an appropriate amount of artificial ice nuclei that could make it into precipitation. Concentrations of cloud droplets at this stage up to 451 / cm^3, an average of 163.6 / cm^3, while the concentration of ice crystals only 10^{-2} a / cm^3 magnitude, rich in supercooled water, with great potential for artificial rainfall.

3.3 Cloud particle characteristics change over time

In order to understand the different detection time , the cloud microphysical structure , precipitation distribution characteristics, the precipitation formation mechanism , the seedability of artificial precipitation, the detection of line added to the radar echoes, Figure 3 shows the detection process the CDP to detect the particles concentration in the cloud N1, L water content, CIP probe to detect the number of large particles of the cloud concentration N2, T for the detection of temperature, we refer to the configuration of the four physical conditions, such as the detection time is divided into shown the different sections, average of the various sections of the cloud are shown in Table 1, the following the seedability artificial rainfall analysis is made separately for each segment.

Tab1. Cloud micro-physical values sampled with DMT probe and seedability

Section No	C_1	C_2	C_3	C_4
N_1/cm^{-3}	181.15	150.38	40.37	209.8
L/(g/m^{-3})	0.1	0.06	0.005	0.005
N_2/cm^{-3}	0.06	0.07	0.05	0.04
T (℃)	-1.47	-0.35	0.09	0.63

It can be seen from Figure 3, the cloud droplet concentration N within a maximum of 432 / cm^3, the minimum is only 0.11 / cm^3, a difference of four orders of magnitude. C_1 segment is the aircraft down , Slightly larger changes in the micro-physical value , LWC maximum 0.42g/m^3, the smallest almost 0g/m^3, C_1 section of cloud droplet number concentration, liquid water content and number concentration of ice crystals appear peak, in this layer the growth of precipitation particles is active . in C_2 segment aircraft continued to decline, reducing micro-physical changes, C_3 segment 20:08:34, aircraft reach the level of 0 □and flight. Radar echo from the RHI (figure omitted) shows a clear zero-layer melting layer bright band, near the melting layer bright band echo intensity has increased, caused by the snow, ice melt and precipitation particle collision in the clouds and reflected there is a clear ice-water conversion layer in the stratiform precipitation. C_4 segment near the zero level detection, changes in micro-physical value is still large.

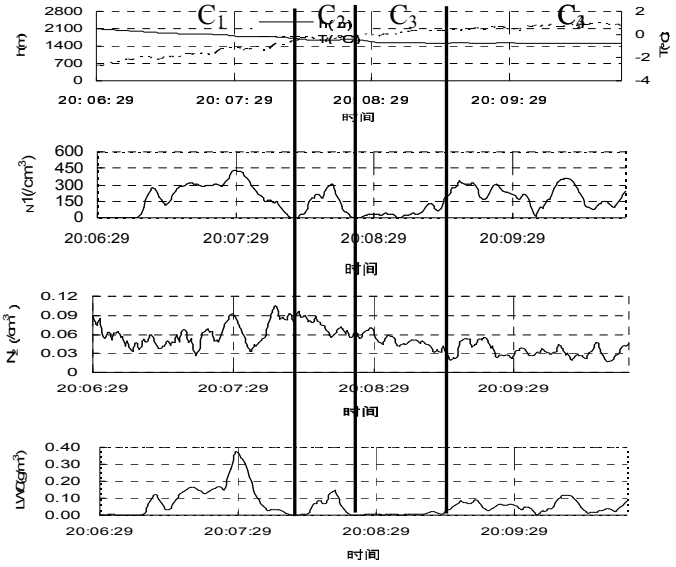


Fig. 3 Variations of the Cloud micro-physical values with time sampled with CDP probe

Reference to the configuration of the four physical conditions, given the various layers of the probe particle spectrum as shown. Figure 4 shows the distribution of the cloud particle spectrum, super-cooled water rich in the over 2000m, 1800m, 1500m cloud droplet particles spectrum turn bimodal distribution, and the spectral width is significantly greater than the super-cooled water has a low level of 1700 m height, 0 □ layer 1500 m peak diameter is 29μm, 1700 m peak diameter is 24μm, we can see the main the LWC come from the large-scale cloud droplet. Figure 4 shows the four types showed a high degree of cloud droplet spectrum bimodal distribution, which is related to the large particle fall in high levels, cloud particle concentration value in the period are higher than LWC lower time. Shows that iin the LWC less time there are snow crystal polymer, more ice, a small amount of smaller scale supercooled cloud droplets, and higher LWC time can be significantly found the dominated presence of supercooled cloud droplets,

indicating ice crystal particles produced ion in the cloud consume the supercooled cloud droplets, making the supercooled water content decreased, Cloud droplets concentration of each range reduce and the particle spectrum wider , the particle number concentration of scale precipitation increase and spectrum broader.

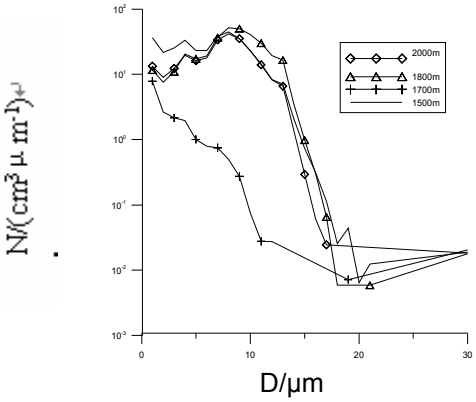


Fig. 4 The particless spectrum distribution

You lai-guang(1994) have discussed the cloud particle phase state,to distinguish the problem that when the ice crystals and cloud droplets are present, the particle spectrum is discontinuous and come out a second peak, which suggested the approach that with the cloud particle scale spectrum distribution to determine the cloud particles phase-state. Figure 4 shows the particle spectra of this detection , we can see, the section which the particle spectrum to detect a second peak, the N_1 on this section is not more than 30/cm^3, but often to a very substantial water content, but the emergence of second peak in the particle spectrum marks the ice particles on the corresponding section of may exist, which gives the water content is actually false, the artificial rainfall, there is no meaning, conversely, the sections where the N_1 is below 30/cm^3, the particle spectral shapes are like this, it can be considered only when N_1 is no less than 30/cm^3, the corresponding area will be seedable.

4 Conclusion and discussion

Based on integrated analysis of the cloud data obtained by digital radar , the particle mea-suring system (DMT) the main cloud physical pa-rameters used to identify cloud seedability are proposed. Calculated cloud water content from 0 □ over layer height (1500m) in the vertical distribution: the cloud water content had a maximum in height above 0 □ 400m at its maximum, respectively 0.416g/m^3, then as the distance 0 □ layer height increases, the cloud cooled water content decreases rapidly to 0 □ layer height of 600m above the base at the lowest, followed until the cloud, the cloud had to maintain low water content.Only when the relevant cloud particle concentration obtained by CDP probe of DMT is larger than 30/cm^3 , has the cloud area certain seedability. Furthermore , when the particle concentration obtained by CIP probe of DMT is less than 10/cm^3 , the cloud is highly seedable and otherwise it is not seedable.

In cloud, droplet concentration with height is multi-peak distribution, and the undulating, LWC and N has a good positive correlation, correlation coefficient is 0.84. 0 □ layer near the cloud droplets, cloud particle spectrum, ice particle spectra, particle-scale precipitation changes are large, rich in supercooled water near the height (altitude 1500-2000m), the average diameter of cloud droplet concentrations were positively correlated with, but above 2000 meters the concentration decreases rapidly as the cloud droplets, the average diameter of cloud droplets there is a clear jump, and the concentration is negative correlation.

Key word: Micro-physical Characteristics ; Seedability; Cold Stratiform Clouds

References :

[1] RutledgeSA, HobbsPV , The mesoscale and microscal structure and organization of clouds and precipitation inmid-latitude cyclones. VIII:Amode lforthe “seeder feeder” process in warm front alrainb ands .J.Atmos.Sci.,1983 40:1185~1206

[2] RangnoAL, HobbsPV. Ice particles in stratiform cloudsithe Arcticand possible mechanisms for the production of higice concentrations.J.Geophys.Res.,2001,106:15065~15075

[3]HeymsfieldAJ. Precipitation development in stratiformic clouds: A microphysica land dynamical study.J.AtmosSci.,1977,34:367~381

[4]OrvilleHD, FarleyRD, HirschJH. Some surprisingre-sults from simulated seeding of stratiform-typeclouds.JAppl.Meteor.,1984,23:1585~1600

[5]BergeronT. Berden Mechanisumsder Ausgiebige Niederschlage. Ber.Deut.Wetterd.,1950,12:225~232

[6]HobbsPV, MatejkaTJ, HerzeghPH, etal. Theme-soscale and microscale structure and organization of cloud and precipitation in midlatitude cyclones.I:Acasestudyofcoldfront.J.Atmos.Sci.,1980,37:568~596

[7]HerzeghPH, HobbsPV. The mesoscale and microscal structure and organization of clouds and precipitation in mid-latitudecyclones.II:Warm-frontalclouds.J.Atmos.Sci.1980,37: 597~611

CLOUD BASE AEROSOL CHARACTERISTICS AND IMPLICATIONS FOR MICROPHYSICS FROM THE QUEENSLAND CLOUD SEEDING RESEARCH PROGRAM

Sarah A. Tessendorf, Courtney E. Weeks, Roelof T. Bruintjes, Duncan Axisa*

National Center for Atmospheric Research, Boulder, CO

1 INTRODUCTION

This paper presents in situ aerosol measurements, for the southeast Queensland region, that were collected during the Queensland Cloud Seeding Research Program (QCSRP; Tessendorf et al. 2010, 2011a). Having a good understanding of the natural aerosol that are present in the atmosphere and affecting cloud droplet formation is paramount toward understanding such implications on precipitation formation or whether or not using hygroscopic cloud seeding techniques could enhance rainfall in a given region. The goal of this study is to define the typical aerosol regimes observed in the southeast Queensland region, and present representative characteristics of each of those regimes. Such representations can be used for further detailed study of the precipitation processes in the region, including initializations for cloud resolving microphysical models.

2 DATA SET AND METHODS

The measurements were collected during the QCSRP between November 2008 and February 2009 in southeast Queensland, near Brisbane, Australia. The South African Weather Service (SAWS) Aerocommander was flown into and around clouds in the region equipped with a suite of microphysical instrumentation to obtain measurements of aerosol and droplet size spectra. Fine-mode aerosol measurements were obtained with a Differential Mobility Analyzer (DMA; Stolzenburg et al. 1998), accumulation mode aerosol were measured by a Passive Cavity Aerosol Spectrometer Probe (PCASP-100X), and when flying out of cloud a Forward Scattering Spectrometer Probe (FSSP; Dye and Baumgardner 1984) was used to measure coarse mode aerosols. However, it should be noted that the small sampling volume of the FSSP limits its ability to measure coarse particles that are often present in very low concentrations and the FSSP was always being run in cloud droplet size range mode since it was primarily used to measure cloud droplet spectra in cloud. A DMT single column Cloud Condensation Nuclei (CCN-100) counter (Roberts and Nenes 2005) was used to sample the CCN concentration.

For sampling sub-cloud aerosol at cloud base (hereafter, “cloud base aerosol”), the aircraft orbited below solid cloud bases, maintaining a constant altitude and remaining in the updraft as much of the time as possible. After obtaining a cloud base aerosol sample, the aircraft always ascended to collect measurements of the initial cloud droplet spectra, at roughly 300 m above cloud base. Terrain occasionally impacted the aircraft’s ability to fly at this altitude in cloud, and thus the aircraft would ascend to its minimum safe altitude to conduct these cloud base passes. For the purposes of our analysis, we only consider those cloud base passes that were within 300-600 m of cloud base. Furthermore, for our purposes we wanted to avoid analyzing data from the portions of cloud passes through cloud edge or areas with precipitation falling from above, therefore we only focused on FSSP measurements with a minimum concentration of 20 cm^{-3}, and excluded measurements with any particles measured larger than 100 μ m (as measured by a Cloud Imaging Probe; CIP).

2.1 Back trajectory modeling

The Hybrid Single-Particle Lagrangian Integrated Trajectory (HYSPLIT) model (Draxler and Rolph 2010) driven by Global Data Assimilation System (GDAS) output was used to calculate 120-hour back trajectories in order to get an air mass history for each measurement. The back trajectories, shown in Fig. 1, illustrate the wide variety of source regions.

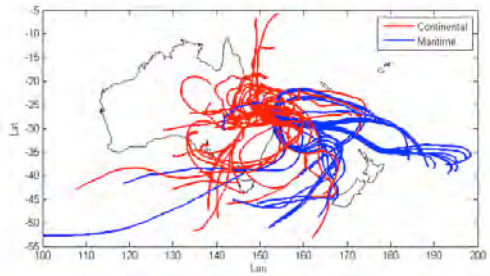


Figure 1. 120-hour HYSPLIT back trajectories for each cloud base aerosol measurement color-coded into two regimes based on how much time each trajectory spent over land below 2 km: maritime regime <= 12 hrs over land below 2 km (blue) and continental regime > 12 hrs (red).

3 REGIME CLASSIFICATION

Using the modeled back trajectories for each of the 69 cloud base aerosol measurements collected, we empirically determined different aerosol regimes that were observed in the region. Using the hours a

* *Corresponding Author:* Sarah A. Tessendorf, NCAR/RAL, P.O. Box 3000, Boulder, CO 80307. Email: saraht@ucar.edu

trajectory spent over land within the boundary layer (estimated at 2 km; hereafter, “hours over land”) as a primary influential factor on the measured aerosol conditions, we determined that splitting the data set into two regimes produced significantly distinct aerosol regimes (in aerosol concentration, as well as aerosol size spectra): maritime, identified as <=12 hours over land, and continental, with >12 hours over land (see Fig. 1). With this classification, the two regimes exhibited generally distinct and more uniform PCASP concentrations than the season-wide dataset; however, there is still a fair amount of variability within each regime (Fig. 2a). These two regimes also exhibit distinctly different CCN concentrations, both at 0.3% supersaturation (Fig. 2b) and across all supersaturations, on average, for those measurements with supersaturation (SS) cycles (Fig. 3).

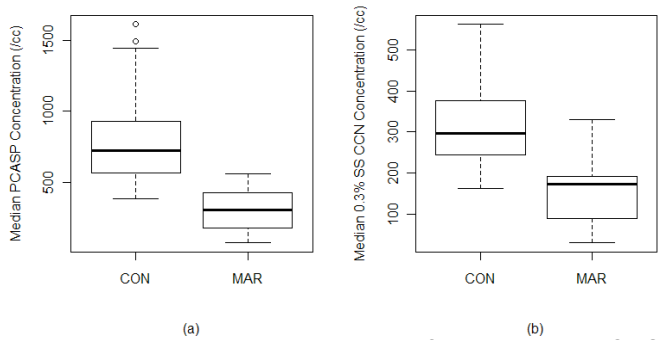


Figure 2. Box and whisker plots of (a) median PCASP aerosol concentration and (b) median 0.3% SS CCN concentration split by regime (MAR: <=12 hours over land below 2 km; CON: >12 hours over land below 2 km).

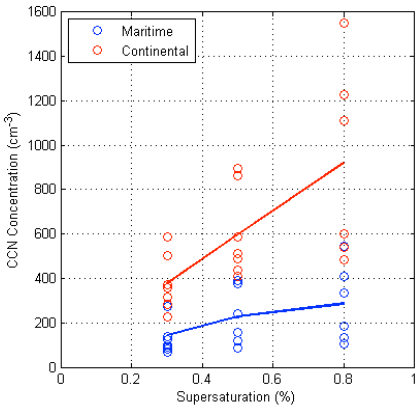


Figure 3. CCN concentrations at varying supersaturations measured during cloud base supersaturation cycles, colored by maritime (blue) and continental (red) regimes. The solid line connects the mean CCN concentration at each supersaturation for each regime.

3.1 Other influential factors

The variability in the measurements that still exists after classifying the regimes by the hours each trajectory spent over land can be explained by other influential factors, such as the number of fires along a trajectory, the proximity of the trajectory to the city of Brisbane (defined as the city center point at 27.5 S, 153.02 E), and the amount of rainfall in the prior 12-hour period before the measurement was taken.

For the maritime air masses, there was little relationship between aerosol concentrations and hours over land (Fig. 4a); however the aerosol concentrations exhibited a considerable increase as the trajectories get closer to Brisbane (Fig. 4b). The continental concentrations were highly dependent on the number of fires observed along the trajectory (Fig. 4c), while showing less dependence on hours over land and no relationship with distance to Brisbane (Figs. 4a-b). Both regimes’ aerosol concentrations were affected by recent rainfall (Fig. 4d). While noisy, the trend suggests that the concentrations will be lower with greater rainfall, as would be expected due to precipitation scavenging (e.g., Kerker and Hampl 1974, Barlow and Latham 1983).

Based on these additional influences on aerosol concentration, each regime was broken into two sub-regimes (Fig. 5): a city-influenced maritime regime was defined for maritime trajectories with at least one time step along the trajectory that was < 50 km to Brisbane; and a fire-influenced continental regime was defined for continental trajectories with >1000 proximity fires. The *remaining* measurements in each of the maritime and continental regimes were then included in respective “background” sub-regimes.

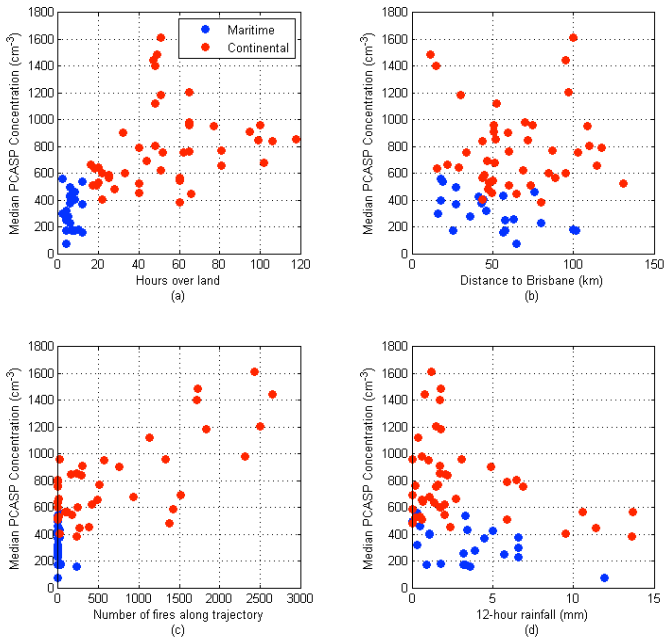


Figure 4. PCASP aerosol concentration variation based on the a) hours over land below 2 km, b) distance to Brisbane, c) number of fires within 200 km of (and 12 hrs prior to) the trajectory, and d) 12-hour rainfall of each back trajectory colored by maritime (blue) and continental (red) regimes.

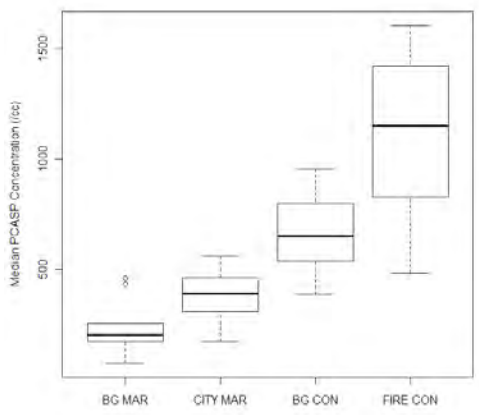


Figure 5. Box and whisker plots of median PCASP concentration for each of the sub-regimes: background maritime (BG MAR), city-influenced maritime (CITY MAR), background continental (BG CON), and fire-influenced continental (FIRE CON).

4 REGIME CHARACTERISTICS

4.1 Thermodynamic environment

In addition to differences in aerosol, there may be inherent environmental differences between these regimes that could affect cloud microphysical processes. Thermodynamic factors such as moisture and instability have been investigated revealing that cloud base heights are consistently lower in the maritime regime (Fig. 6). This suggests more humid surface conditions, although the cloud base temperatures were quite similar between the two regimes on average. Precipitable water and instability (measured by the Total Totals index) were quite similar between the regimes also (not shown).

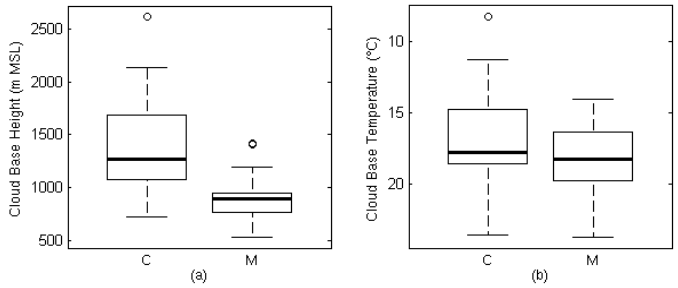


Figure 6. Box and whiskers plots of (a) cloud base height and (b) cloud base temperature from 00Z Brisbane airport soundings on the day of each measurement.

4.2 Aerosol characteristics

The maritime and continental regimes also have unique features in the full aerosol size spectra created by combining measurements from the DMA, PCASP, and FSSP[1] (Fig. 7). Despite substantial variability in the measurements, the mean spectra highlight the tendency for the maritime regime to have a stronger coarse mode of aerosol particles compared to the continental regime. Aerosol composition measurements indicate that the coarse mode was dominated by mineral dust, even in the maritime regime (not shown). Interestingly the fine modes in both regimes are quite similar.

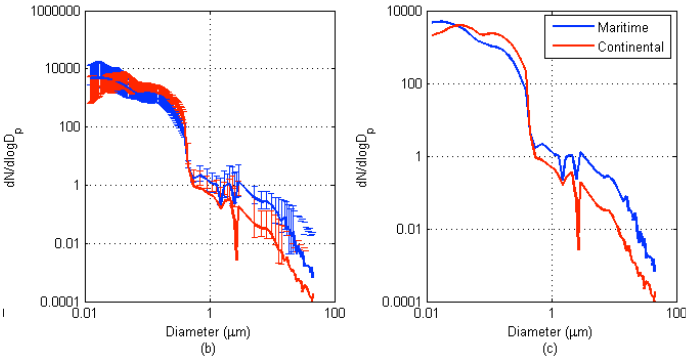


Figure 7. Mean aerosol size spectra for the maritime (blue) and continental (red) regimes. Whiskers denote the range of 25th and 75th percentile for each regime on left, but have been removed for clarity on right.

4.3 Cloud microphysics

We used three different methodologies for calculating the typical droplet concentration, mean diameter, and size spectra 300-600 m above cloud base that could result from nucleation on the aerosol particles measured below cloud base (see Tessendorf et al. 2011b for more details). The steady-state method requires a minimum 3-sec period of steady and high liquid water content and drop concentrations. The maximum method takes a mean of the drop spectra characteristics over the course of a 3-second period; plus or minus one second from the 1-Hz maximum measurement. The "binmax" method is based on Yum et al. (1998) and averages data points in the bin with the highest concentration that also contained at least three 1-Hz data points.

Droplet concentration and mean diameter results using the steady-state and maximum methods were surprisingly very similar on average in both the maritime and continental regimes (Table 1), with the maximum method resulting in the highest drop concentration measurements. The "binmax" method yielded the most notable differences between the two regimes, in a manner that would be expected given the lower (higher) aerosol concentrations and thus lower (higher) droplet concentrations in the maritime (continental) regime (Table 1). Mean droplet diameters were also larger in the maritime regime than the continental regime.

[1] Due to the small sample volume of the FSSP and extremely low concentrations of large particles, there is considerable noise in the coarse mode end of these spectra.

The maritime cloud base droplet spectra, on average, were generally broader due to a tail of larger droplets, as indicated by the difference in the concentration of drops larger than 20 μm between the two regimes. The mean diameter was significantly different between the regimes (i.e. larger in the maritime regime) under the binmax method only. This tendency for a tail of larger drops in the maritime regime could be the result of droplet nucleation on larger aerosol particles (exhibited in the coarse mode of Fig. 7).

Table 1. Average cloud droplet concentrations ("Conc"), mean diameter ("Diam"), and concentrations of droplets greater than 20 μm ("Conc>20") by regime for each of the three calculation methods. Standard deviations ("StdDev") and p-values ("P") are also provided.

Method	Regime	Conc	StdDev	P	Diam	StdDev	P	Conc>20	StdDev	P
Steady-state	MAR	411	135	.94	12.1	1.7	.13	5.9	7.8	.03
	CON	431	111		11.1	0.8		1.7	1.5	
Maximum	MAR	596	62	.30	11.1	1.2	.54	4.0	5.2	.65
	CON	534	113		11.1	0.8		2.6	3.6	
BinMax	MAR	353	207	.41	12.8	2.3	.01	7.9	9.0	.08
	CON	414	154		10.9	1.6		3.4	7.7	

5 SUMMARY

Two general regimes (maritime and continental) were identified based on the hours each measurement's back trajectory spent over land. However, within each of these two regimes there was still substantial variability in aerosol concentration related to other factors, such as proximity to Brisbane or proximity to fires.

The most notable thermodynamic difference between the regimes was cloud base height, which was consistently lower in the maritime regime. This environmental influence on the clouds that formed under the maritime regime could have contributed to higher concentrations of coarse mode (dust) aerosol particles by nature of the measurements being taken closer to the ground. Cloud base droplet spectra also tended to have a tail of larger drops in the maritime regime compared to the continental regime, which may be the result of the differing aerosol conditions. By having defined these aerosol regimes in a quantitative way, we hope that future observational studies in the region can further diagnose the potential effects of the aerosol and that numerical modeling studies can help fill in the gaps where our observations are incomplete and unable to control for aerosol differences alone.

Acknowledgements

This research was sponsored by the Queensland Government Department of Environment and Resource Management through the Queensland Climate Change Centre of Excellence. The authors acknowledge the NOAA Air Resources Laboratory (ARL) for the provision of the HYSPLIT transport and dispersion model and Christine Wiedinmyer (NCAR) for providing the processed MODIS fire data.

REFERENCES

Barlow, A.K. and J. Latham, 1983: A laboratory study of the scavenging of sub-micron aerosol by charged raindrops. *Quart. J. Royal. Met. Soc.,* **109**, 763–770

Draxler, R.R. and Rolph, G.D., 2010: HYSPLIT (HYbrid Single-Particle Lagrangian Integrated Trajectory) Model access via NOAA ARL READY Website (http://ready.arl.noaa.gov/HYSPLIT.php). NOAA Air Resources Laboratory, Silver Spring, MD.

Dye, J.E. and D. Baumgardner, 1984: Evaluation of the forward scattering spectrometer probe: I. Electronic and optical studies. *J. Atmos. Ocean. Tech.*, **1**, 329-344.

Kerker, M., and V. Hampl, 1974: Scavenging of aerosol particles by a falling water drop and calculation of washout coefficients. *J. Atmos. Sci.*, **31**, 1368-1376.

Roberts, G.C., and A. Nenes, 2005: A continuous-flow streamwise thermal-gradient CCN chamber for atmospheric measurements. *Aerosol Sci. and Tech.*, **3**, 206-221.

Stolzenburg, M., N. Kreisberg, and S. Hering, 1998: Atmospheric size distributions measured by differential mobility optical particle size spectrometry. *Aerosol Sci. and Tech.,* **51**, 402-418.

Tessendorf, S.A., and Co-authors, 2010: Overview of the Queensland Cloud Seeding Research Program. *J. Wea. Modification*, **42,** 33–48.

Tessendorf, S.A., and Co-authors, 2011a: The Queensland Cloud Seeding Research Program. *Bull. Amer. Meteor. Soc.*, in review.

Tessendorf, S.A., C.E. Weeks, R.T. Bruintjes, and D. Axisa, 2011b: Cloud base aerosol characteristics and implications for cloud microphysics in Southeast Queensland. Preprints, *18th Conf. Planned and Inadvertent Weather Modification,* Amer. Meteor. Soc., Seattle, WA.

Yum, S. S., J. G. Hudson, and Y. Xie, 1998: Comparisons of cloud microphysics with cloud condensation nuclei spectra over the summertime Southern Ocean, *J. Geophys. Res.*, **103**, 16,625–16,636.

Monitoring Atmospheric Precipitable Water Using MODIS Satellite

Xilatu Dabu[1] Shiqing Lu[1] Lijuan Su[1] Chengcai Li[2] Bin Yan[1]

(1 Inner Mongolia Institute of Meteorology, Hohhot 010051, China;

2 Department of Atmospheric Sciences, Peking University, Beijing 100871, China)

Abstract

Since atmospheric precipitable water plays a very significant role in weather modification, weather forecast, climate change, atmospheric radiation transport, etc., accurate fine monitoring aqueous vapour appears especially important. Along with the development of satellite technology, many earth observations technology developing from ground-based observation into space-based observation gradually. Based on the high spatial and time resolution and the constantly improving of the precision, the Satellite observation (SATOB) gradually become the main earth observation techniques.This paper using the GPS data and surface humidity parameter (surface vapour pressure, surface dew point) to correct the parameters which using the surface humidity parameter, geographical latitude, sea level elevation, etc. to calculate the total of atmospheric water-vapour content equation. Based on this, we study and establish a method using the MODIS satellite near-infrared channel to monitor atmospheric precipitable water. By this, the method to monitor atmospheric precipitable water under cloud cover is explored.

1. Data

This paper based on the GPS data of Beijing Fangshan, Hohhot (2 sets) Erlianhot and surface humidity parameter (surface vapour pressure, surface dew point) to correct the parameter which using the surface humidity parameter, geographical latitude, sea level elevation etc. to calculate the atmospheric precipitable water equation.

We choose total four typical month (October 2006, January, April and July 2007)of surface dew data from126 surface sites in Inner Mongolia , calculated the atmospheric precipitable water vapor during each observing time level, then screened，as inspection objective for test.

The projection way of Near-infrared serene atmosphere and cloud top Upward atmospheric precipitable water vapor products adopt conformal spherical projection, the longitude range of the projection area is 97°E～127°E, Latitude range is 34°N～54°N(covering the whole area of the Inner Mongolia),the resolution is 0.01°×0.01°.

2. Research results and analysis

2.1 MODIS Near-infrared serene atmosphere and cloud top upward atmospheric precipitable water vapor calculation mode

The scatterplot figure corresponding with MODIS Near-infrared serene atmosphere and cloud top Upward atmospheric precipitable water vapor products and surface dew point material given in Fig. 1. Figure 1 shows the result of atmospheric precipitable water vapor calculated by surface point temperature slants big obviously, the result is correspond with the phenomenon which is found by Liu in Qinghai-Tibet Plateau that the MODIS Near-infrared serene atmosphere and cloud top upward total of atmospheric water-vapour slants small.

In order to further revealed the reason why the MODIS near-infrared serene atmosphere and cloud top upward total of atmospheric water-vapour slants small, combined with surface observation of synoptic elements，we divided the condition into clear skies(the total cloud cover low-level cloud cover is less than or

equal to two) and total cloud cover low-level cloud cover is Greater than or equal to three, in this two conditions, the two products are compared & tested in detail.

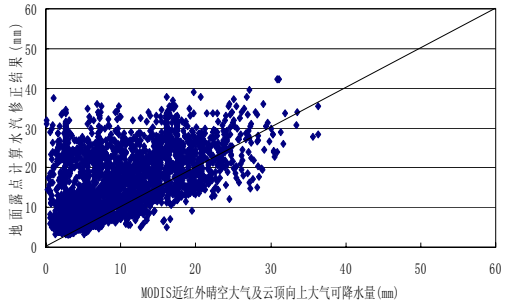


Fig. 1 The precipitable water retrieved from MODIS near IR datas

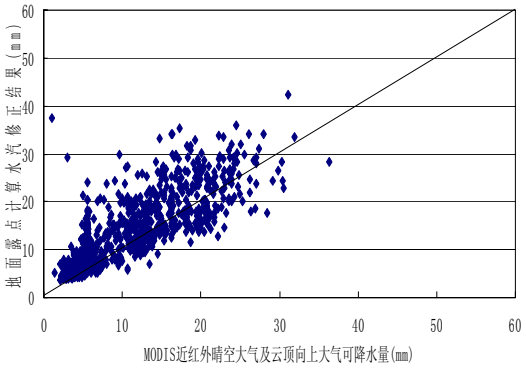


Fig. 2 The contrast between atmospheric precipitatable water which retrieved from MODIS near IR datas and which calculated by corrected Ground Dew Point datas

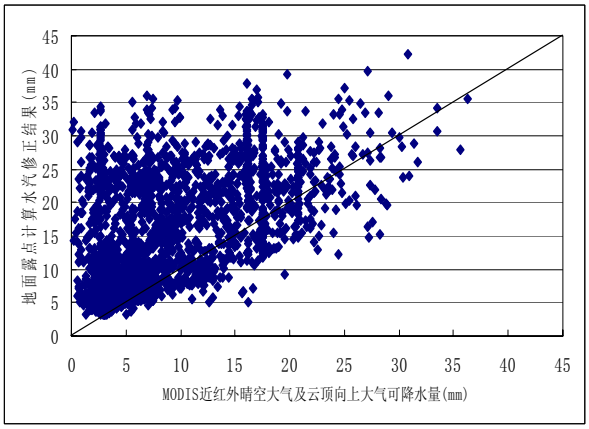


Fig. 3 The contrast between atmospheric precipitatable water which retrieved from MODIS near IR data and which calculated by corrected Ground Dew Point data (cloud mass more than 3)

As showed in Fig. 2, what can be seen from the clear skies scatter plot is the sample points distributed relatively uniform between the two sides of the line y＝x, This suggests that under clear skies conditions, the product of MODIS Near-infrared serene atmosphere and cloud top upward atmospheric precipitatable water could response clear skies precipitatable water accurately. In Fig. 3, the cloud cases, we can see that the negative impacts of cloud cover on MODIS near-infrared serene atmosphere and cloud top upward atmospheric precipitatable water inverse algorithm precision is significant.

2.2 Establishing the arithmetic model of MODIS satellite Near-infrared (the cloud cover area) atmospheric water vapour inventory arithmetic

The MODIS satellite near-infrared channel arithmetic could reflect serene atmosphere precipitatable water accurately, but it is a imperfection to the MODIS data that the water of cloud top downward vapor can not be inversed, the all-weather inversion atmosphere precipitatable water could not be done. precipitatable water is Particularly important when the cloud existing, so it is necessary to correct the algorithm of the MODIS near-infrared serene atmosphere and cloud top upward total of atmospheric water-vapour product in order to obtain cloud cover sector atmospheric water content in cloud cover sector.

The research which is found by Liu in Qinghai-Tibet Plateau that the MODIS near-infrared serene atmosphere and cloud top upward total of atmospheric water-vapour slants small mentioned that

$$PW_{corrected} = PW * (\frac{P}{P_0})^{-0.9} \qquad (1)$$

$PW_{corrected}$ is MODIS near-infrared serene atmosphere and cloud top upward total of atmospheric water-vapour which is after revised. PW is the MODIS near-infrared serene atmosphere and cloud top upward total of atmospheric water-vapour before revised. P is the station pressure of pixel point. P_0 is air pressure at sea level.

In the thinking of the relation which offered by Dr. Gao of NASA in this text, we imports the cloud top pressure that completed retrieval result as variable quantity, replacing that like spot ground pressure, setting up the model that MODIS near-infrared gallery

of the cloud-covering region about the calculating of the total of atmospheric water-vapour :

$$PW_{clounm\text{-}cloud} = \exp(-0.4585 * \ln(\frac{p_{ctp}}{p_0}) + \ln(PW)) + 0.3166 * PW \quad (2)$$

$PW_{cloumn-cloud}$ is total of atmospheric water-vapour of MODIS near-infrared after revised; PW is the total atmospheric water-vapour of MODIS near-infrared in the fine day and the cloud top upward; P_{ctp} is the cloud top of the pixel spot; P_0 is the sea level pressure.

Under the condition that not revised, as Fig. 4, scatter plot of precipitatable water which calculated by corrected Ground Dew Point data and which retrieved by MODIS near IR. The inversed data of the total atmospheric water-vapour of MODIS near-infrared in fine day and cloud top upward. As in Fig. 5,the scatter plot of precipitatable water which calculated by corrected Ground Dew Point data and which retrieved by MODIS near IR and corrected by NASA Dr. Gao's formula, the revised data of the atmospheric precipitatable water which calculated by corrected Ground Dew Point data and which retrieved by MODIS near IR has obviously decreased.

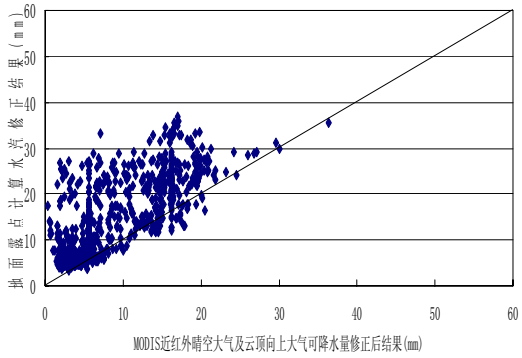


Fig. 4 Scatter plot of precipitatable water which calculated by corrected Ground Dew Point data and which retrieved by MODIS near IR in cloud area

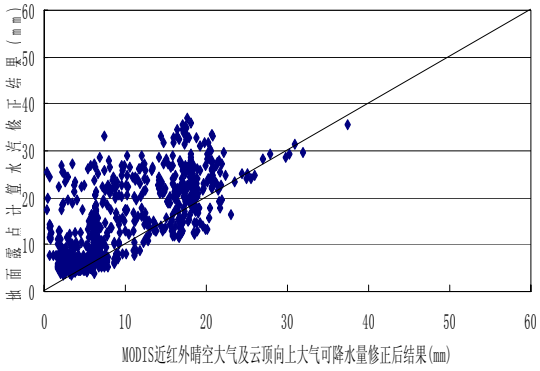


Fig. 5 Scatter plot of precipitatable water which calculated by corrected Ground Dew Point data and which retrieved by MODIS near IR and corrected by NASA Dr. Gao's formula in cloud area

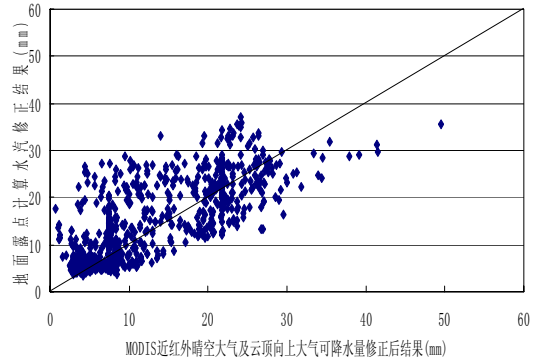


Fig. 6 Scatter plot of precipitatable water which calculated by corrected Ground Dew Point data and which retrieved by MODIS near IR and corrected by this task formula in cloud area

Figure 6 is the scatter plot of the total water vapour of the modeling result and the calculated ground dewpoint. Contrasting with Fig. 4 and Fig. 5, each point in Fig. 6 have well-distributed between the two sides of the straight line of 'y=x', which indicated that the revised MODIS near-infrared total water vapour content in the atmosphere of cloud covering area and the revised water vapour content calculated by ground dew-point have better coherence.

The error of mean square root between the unrevised value of MODIS observation and the total water vapour content calculated by ground dewpoint is 63.1454 mm^2; The error of mean square root between the MODIS near-infrared total water vapour content in cloud atmosphere and the total water vapour content which calculated by Ground Dew Point data supplied by NASA Dr. Gao is 37.3838 mm^2.The coefficient of correlation r=0.7479 and the sample capacity is 815

which improving the precision of observation obviously.

3. Conclusions

1) It’s available that using the NASA method in the fine area, and there’s a good corrected effect of the method of Dr.Gao.

2) The revised MODIS near-infrared total water vapour content in the atmosphere of cloud covering area and the revised water vapour content calculated by ground dew-point have better coherence. Though the spot in the picture is more scattered, and the precision is not the best, it’s feasible by using the method to revise the total atmospheric water-vapour of the MODIS near-infrared and the cloud top upward in business before the more authoritative revisal algorithm appeared. It can make up insufficient about MODIS inversing the total atmospheric water-vapour in cloud area.

Effects of Giant-Particle Seeding on Cloud Microphysics and Precipitation Derived from Mesoscale Cloud-resolving Numerical Simulation

Xueliang Guo
Chinese Academy of Meteorological Sciences, Beijing 100081, China, guoxl@cams.cma.gov.cn
Danhong Fu
Institute of Atmospheric Physics, Chinese Academy of Sciences, Beijing 100029, China, fudanhong@mail.iap.ac.cn

1. Introduction

The size of seeding particles might be critical in warm cloud rain enhancement since the cloud condensation nucleation and coalescence processes are closely related with size of aerosol particles. Johnson (1982) obtained that giant (>1 μm in radius) and ultragiant (>10 μm in radius) aerosol particles will produce a tail of large drops in the cloud-droplet distribution, and then these drops will significantly accelerate the development of precipitation by the coalescence process. Yin et al. (2000) showed that the coalescence between water drops can be enhanced while adding of the giant cloud condensation nuclei, and found that the most effective particles were those with radii larger than 1 μm, especially those larger than 10 μm. Zhang et al. (2006) concluded that the role of giant CCN on precipitation formation in warm, stratiform clouds is only important when the concentrations of CCN larger than 5 μm are high. However, some studies showed that the particles size might not be essential to the formation of raindrops for some clouds such as a maritime cloud (Takahashi, 1976; Takahashi and Lee 1978).

Due to the inconsistent conclusions obtained in previous studies, the further investigations are necessary by designing more detailed numerical experiments as well as field measurements (Orville, 1996; Bruintjes, 1999; Ma et al., 2007; Guo and Zheng, 2009). In this study, a WRF-based mesoscale cloud-resolving study was conducted to investigate the effects of giant particle cloud seeding on cloud microphysics, dynamics and precipitation. The cloud formation, intensity and evolution as well spatial and temporary distributions for seeded and un-seeded clouds are presented and compared. cloud lifetime, intensity, time evolutions of cloud microphysics and

2. Model setup and initiation

The study area was chosen around Beijing urban regions where the aerosol background number concentration was around 1026cm^{-3} which was primarily produced by air pollutants and composed of small-size particles. The seeded aerosol number concentration was 1000cm $^{-3}$ with sizes larger than 1 μm in diameter, which is called giant particles in the study. The seeding duration was 10 min started from 7:30 and ended at 7:40. The seeded height was at 2.5-3.5 km which is just located near cloud base. WRF-model was initialized with NCEP data and run for 24 hours.

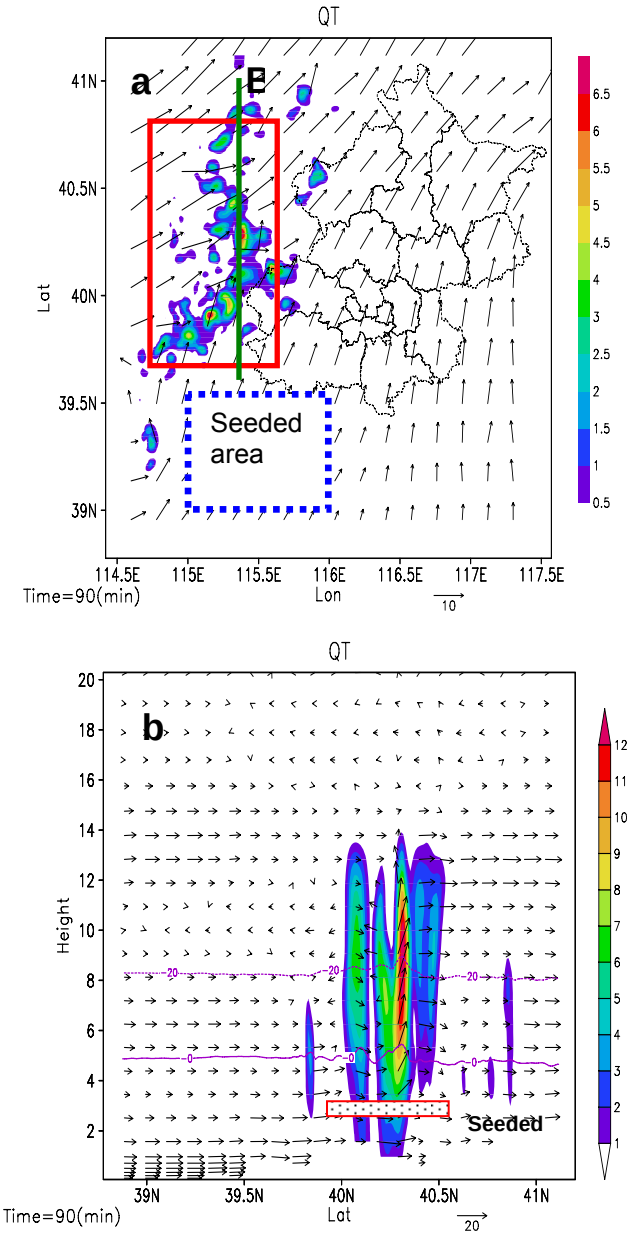


Fig.1 (a) The horizontal cross section indicates the seeded area, and (b) the seeded height is indicated in the vertical cross-section along AB in Fig.1a . The levels for 0℃ and -20℃ are also indicated in Fig.1b.

3. Results

Comparing of un-seeded case with seeded case, we found that the cloud seeding with water-soluble aerosols in size over 1.0 μm in diameter may induce substantial changes of cloud microphysics, dynamics and precipitation.

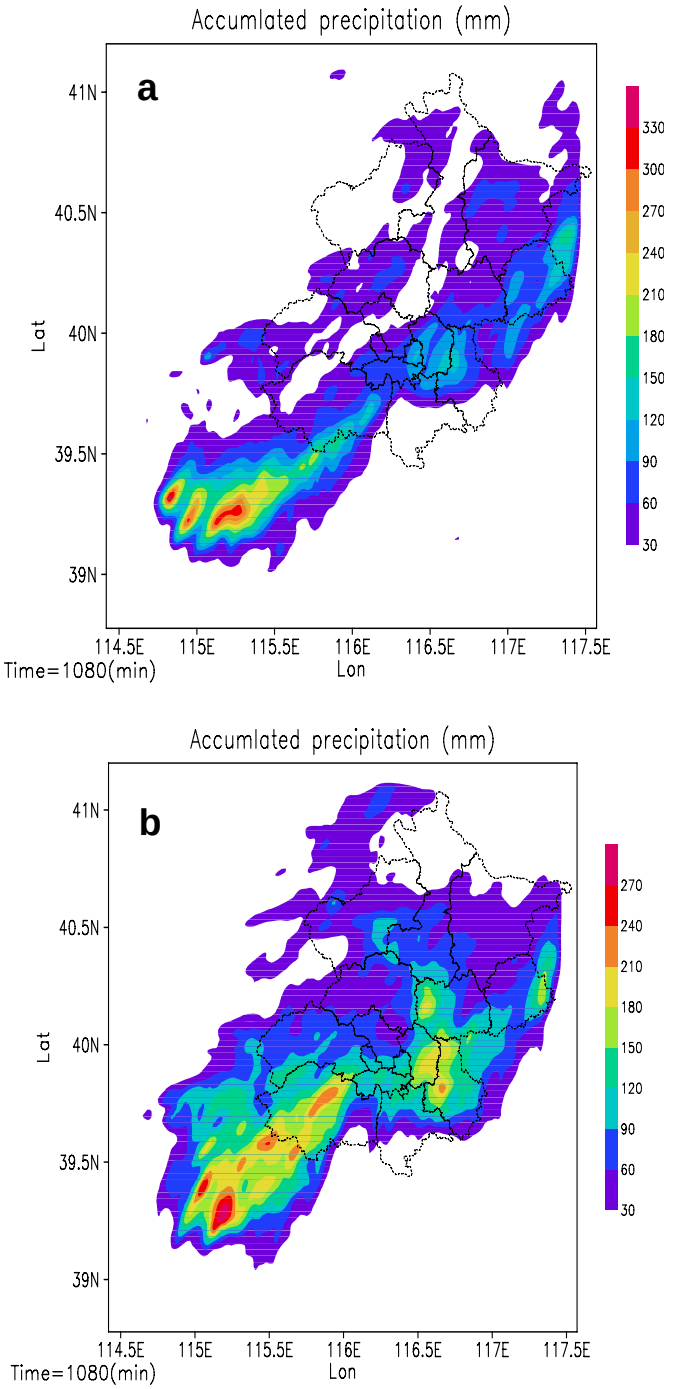


Fig.2 The accumulated precipitation (mm) is shown for the (a) un-seeded case and (b) seeded case based on the seeding method shown in Fig.1.

It also indicates that the seeding also has high impact on cloud ice processes, such as the increase of ice particles concentration. The influential time for seeding is around 3-4 hours. The maximum surface rain intensity, rain amount and the accumulated precipitation are greatly changed, in which the rain intensity is increased, but the maximum precipitation amount is decreased and surface accumulated precipitation is increased. The maximum increase of surface accumulated precipitation may be 41%.

The surface precipitation distribution is also changed from the concentrated type for un-seeded case to the more dispersed type for seeded case.

Acknowledgements

This research has been jointly sponsored by the Chinese Natural Science Foundation (Grant 41005072 and 40575003) and the Key Sci & Tech Supporting Project of the Ministry of Science and Technology of China (Grant No. 2006BAC12B03).

References

Bruintjes, R. T., A review of cloud seeding experiments to enhance precipitation and some new prospects. Bull. Amer. Meteor. Soc., **80**(5), 805-820,1999.

Guo, X. L. and G. G. Zheng, Advances in weather modification from 1997 to 2007 in China. Adv. Atmos. Sci., **26**(2), 240-252, 2009.

Johnson, D. B., The role of giant and ultragiant aerosol particles in warm rain initiation. J. Atmos. Sci., 39, 448-460,1982.

Ma, J., X. Guo, C. Zhao, Y. Zhang, and Z. Hu, Recent progress in cloud physics research in China. Adv. Atmos. Sci., **24**(6), 1121-1137, 2007.

Orville, H. D., A review of cloud modeling in weather modification. Bull. Amer. Meteor. Soc., **77**(7), 1535-1555, 1996.

Takahashi, T, Warm rain, Giant Nuclei and Chemical balance-A numerical model. J. Atmos. Sci., **33**, 269-286, 1976.

Takahashi, T, S. Lee, The nuclei mass range most efficient for the initiation of warm cloud showers. J. Atmos. Sci., **35**, 1934-1946, 1978.

Yin, Y., Z. Levin, T. G. Reisin, and S. Tzivion, The effects of giant cloud condensation nuclei on the development of precipitation in convective clouds - A numerical study. Atmos. Res., **53**, 91-116, 2000.

Zhang, L., D. V., Michelangeli, P. A. Taylor, Influence of aerosol concentration on precipitation formation in low-level, warm stratiform clouds. Journal of Aerosol Science, **37**(2), 203-217, 2006.

Hail types and Distribution of Related Factors

Yuwen Sun[1,2]，Wei Liu[3]， Zhijun Zhao[1]， Anying Shi[1]，Yan Jiang[1]
1 Weather Modification Office of Hebei Province，Shijiazhuang,China, 050021；
2 Hebei Province Meteorological and Ecological Environment Laboratory,Shijiazhuang, China, 050021；
3 Shijiazhuang Meteorological Burea, Shijiazhuang, China, 050081;

Abstract : Currently, many researchers have studied the hail cloud system from different aspects. Mainly including: the relationship between development of the thundercloud and the changing of meteorological elements; the analysis of the distribution character of hail spectrum; observation of the micro-structure of the hail cloud with the satellite and radar; distinguish the hail cloud from thundercloud with the lighting counter; simulate the micro-scale physics of the hail and test the effectiveness of hail suppression, etc. These play an important role in the forming of theories of hail forecast and hail suppression.

To improve detect result, China has developed some devices, such as dual polarization radar and a line polarization radar; semiconductor refrigeration hail slicer; hail slicer like machine tool; lighting counter; electric field instrument in the air; inverted atmosphere mean electric filed instrument; smart rain gauge, etc. These devices could help us understand the natural better. However, there is not a device that used to decide hail quantity.

In 1987 AnYing Shi et.al discussed the error of measuring hail by developing “Automatic hail rain sub-detector ". Huanbin Xu described part of the data measured by the instrument, summarized the distribution of factors about hail in the trial of the "Hail suppression and hail cloud physics works" .It put the observation technology of hail to a big step forward and will play a key role on the hail forecast and hail suppression. However, the focus of discussion was different, so the difference between hail categories was not given; The potential implications of the three physical factors, the amount of hail 、rainfall and the ratio K was not deeply studied. And thus we can not understand the continuous, comprehensive, integrated feature of hail and rain.

With regards to this, automatic hail rain sub-detector was laid out at Weixian, Shangyi, Chicheng, Wanquan, Zhuolu, and Chongli of Zhangjiakou in Hebei province and has obtained 16 times of self-recording paper about hail weather system. By doing the rain hail sub-file and simultaneously reading analysis of the achieved self-recording paper of hail weather system detected from automatic hail rain sub-detector, we obtained the 5 types of hail and the distribution of related factors：1.hail whose intensity is in a super large class;2.hail whose intensity is in subclass;3. hail which has a large total amount with a devastating disaster;4.hail whose amount shows a pulse surge;5. weak hail cloud with a long duration, hail in a small amount and a weak intensity. Making thorough research to the character of the five classers will guide the study of the structure of hail cloud and hail from the generation of embryos and will provide observational data for the simulation of hail formation and floor. It also will help us understand the production, development and disappearance of the hail clouds, enrich the theory and improve the effect of hail suppressionhail suppression.

Keywords: hail rain sub-detectors; hail type;

related factors; distribution

Acknowledgements

This research was supported by technology plan projects of Hebei province contact 11277107D, and the research of fog and haze by aircraft observations contact 10ky14 which was developed by Hebei meteorological burea.

References

[1] Jie Zhang, Wenli Li, Fengqin Kang et.al. Analysis and Satellite Monitor of A Developing Process of Hail Cloud, PLATEAU METEOROLOGY, 23(6), pp758-763, 2004.

[2] Shuangxi Fu, Lin An, Fengqin Kang et.al. Application of VIL in Identification of Hailstorms and Estimation Error Analysis. PLATEAU METEOROLOGY, 23(6), pp810-814, 2004.

[3] Yanbin Huang, Zhenhui Wang. Identification of Thundercloud and Hailproducing Cloud Based On Lightning Counting Data. JOURNAL OF NANJING INSTITUTE OF METEOROLOGY, 24(2), pp275-280, 2001.

[4] Fengqin Kang, Qiang Zhang, Yongxing Qu et.al. Simulating Study on Hail Microphysical Process on the Northeastern Side of Qinghai-Xizang Plateau and Its Neighbourhood, PLATEAU METEOROLOGY, 23(6),pp735-742,2004.

[5] Zhiguo Liu, Jianhong Tao, Xiwen Wang et.al. Effect Analysis of a Hail Suppression by Anti-hail Gun Based on INRAD/CC Products. ARID METEOROLOGY, 24(3), pp23-30, 2006.

1. Yuwen Sun, Weather Modification Office of Hebei Province, China, 050021; E-mail: sunyun288@163.com.

NEW ADVANCES IN AUTOMATION OF ANTI-HAIL ROCKET TECHNOLOGY

Abshaev M.T.[(1)], Abshaev A.M. [(2)], Kuznecov B.K. [(2)], Kotelevich A.F. [(2)], Guzoev T.H. [(2)], Balakova N. [(2)]
Chochaev H.H. [(3)], Yakushkin B.V. [(3)], Ponomarenko R.N. [(4)], Trifonov V.S. [(4)]
[(1)] High Mountain Geophysical Institute, 360030, Lenin av. 2, Nalchik, Russia, abshaev@mail.ru
[(2)] Hail Suppression Research Center "ANTIGRAD"
[(3)] Northern Caucasus Antihail Service of Roshydromet
[(4)] Joint-Stock Company "Sevkavrentgen"

1. Introduction

Successfulness of hail prevention is provided by perfection of technology and quality of implementation of the concepts put into its basis. Transience of hail formation leads to that seeding of hail and hail dangerous clouds are carried out in conditions of critical time shortage. Therefore, efficiency and accuracy of seeding objects (SO) recognition, allocation of seeding zones and delivery of reagent in the field of the future hail formation is very important. The solution of these problems can be achieved on the basis of automation of the listed anti-hail operations.

The current Russian rocket technology of hail suppression [Abshaev M. T, Abshaev A.M., Malkarova A.M., 2010] provides automatic recognition of SO, place allocation of seeding zones and development of commands by means of radar system "ASU-MRL" [Abshaev M.T., Abshaev A.M. at all., 2007]. Thus rocket seeding of SO is carried out by means of a network of remote rocket points (up to 30 per one radar center), having 1–2 hand-operated rocket launchers, VHF radio station, 4 persons staff (2 in each rotary operating crew), inhabited and working premises, rockets warehouse, etc. Maintenance of the personnel and the infrastructure of such points increases the protection cost price. Year after year it becomes more difficult to keep the trained personnel of these points because of necessity of round-the-clock duty in the field conditions.

Problems of operative transfer and execution of commands to rocket seed by remotely controlling a network of distant automatic rocket launchers are considered in this paper.

2. Anti-hail rocket launcher «Elia-2»

In 2006 – 2009 Hail Suppression Research Center "ANTIGRAD" (Nalchik, Russia) developed, tested, prepared for a serial production and put into operational application a new automatic rocket launcher (RL) "Elia-2" which is the second generation of the launcher "Elia" [Abshaev M.T, Abshaev A.M., Kuznetsov B.K., 2009].

RL "Elia-2" (fig. 1) is intended for launching of anti-hail rockets with dynamic start "As", "Alan-3" and jet start "Alazan-6", "Alazan-9" in two control modes:

- Automatic control by commands from the computer of the automated control system "ASU-Elia" via wireless communication and management system without distance restriction;
- Semi-automatic management by commands from the panel of wireless remote control on distance not less than 100 m;



Fig. 1. Automatic anti-hail rocket launcher "Elia-2"

RL "Elia-2" consists of the base device, rotation mechanisms by azimuth and vertical angles, replaceable directing devices package, encoders of angular position, GPRS/EDGE modems, a device for control and communication, mini meteorological stations and systems of independent power supply. Replaceable packages with directing devices for rockets of different types are unified on seat sizes. Power supply is provided by accumulators charged by solar panels.

The communication and control system provides:

- Control of the launcher's state (azimuth, elevation angle, presence of rockets in each guide cell, level of accumulators charge, self-testing information, temperature, pressure and humidity of the air on the position;
- Automatic targeting to the sun for orientation control;
- Automatic transmission and execution of commands to launch the demanded quantity of rockets with accuracy of ±0,5 degrees and prevention of launching rockets to forbidden sectors (fig. 2);
- Logging the date, time and coordinates of launched rockets and their types.

An alarm is produced before the launcher's rotation and launching of each rocket. Rocket launch registration is carried out by a circuit break and acoustical signal specific for each type of rockets. In case of rocket launch failure an appropriate warning is produced.

The programmable controller has a memory device for storage of settings (serial number of RL, 11-digits identification number, geographical coordinates of its position, forbidden sectors for rockets, etc.).

Table 1. Technical characteristics of RL "Elia-2"

Parameter	Value of parameter with a package of replaceable guides for different rockets type		
	Alazan-6	Alazan -9	As, Alan-3
Quantity of guides, pieces	16	20	36
Length of guides, mm	2000	2000	1800
Dimensions, mm: – Length – Width – Height	 2055 1320 1400	 2055 1320 1295	 1875 1320 1295
Mass, kg	190	195	215

Layout of guides: parallel;

Angular position of rockets loading in degrees:

– By elevation angle: 0 degrees;

– By azimuth: without restriction.

Targeting sector in degrees:

– By elevation angle: from 0 to 78 degrees forbidding rockets launch below 45 degree;

– By azimuth: any with restriction of rockets launch into forbidden azimuth sectors;

Speed of rotation, not less than:

– By elevation angle: 12 degrees/sec;

– By azimuth: 15 degrees/sec;

Rotation step by angles: 1 degree.

Accuracy of angles aiming; ± 0,5 degrees.

Life cycle: not less than 15 years.

Preparation to use the launcher includes: leveling, orientation by the sun (moon, North Star), checking the communication system and control system, training and certifying the staff.

In 2010 – 2011 it were exploited 47 launchers "Elia-2" in two anti-hail projects in different climate geographical regions.

3. Program-technical complex «ASU-Elia»

The program-technical complex "ASU-Elia" is created for management of remote launchers network. It allows to:

1. Control and guide an unlimited number of remote RL from one monitor via radio and cellular communication channels;

2. Perform data packets exchange between Command Center and several rocket points in a parallel mode.

3. Conduct full automatic control of rockets launch process while logging rockets quantity, coordinates and launch time.

4. Increase the speed of hail and hail dangerous clouds seeding by increasing the efficiency of commands transmission, execution and control of execution of rockets launch commands and by simultaneous parallel transmission of commands to several RL.



Fig. 2. Rockets launching from RL "Elia-2"

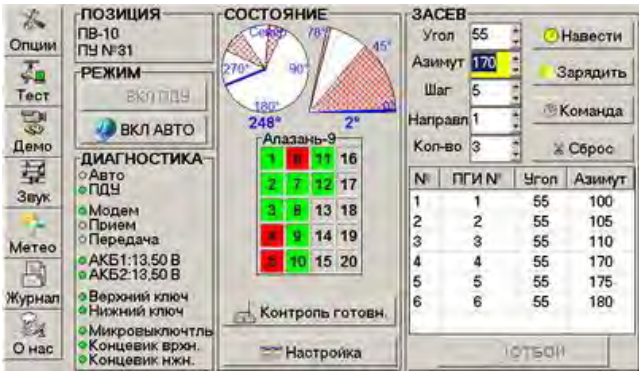


Fig. 3. Screen of remote control panel

5. Collect data from the automatic meteorological stations built into "Elia-2" and to build maps of space distribution of temperature, humidity, pressure, precipitation amount, hail kinetic energy above the background of regional map.

6. To deploy thin-staff automatic system of hail suppression (fig. 5).

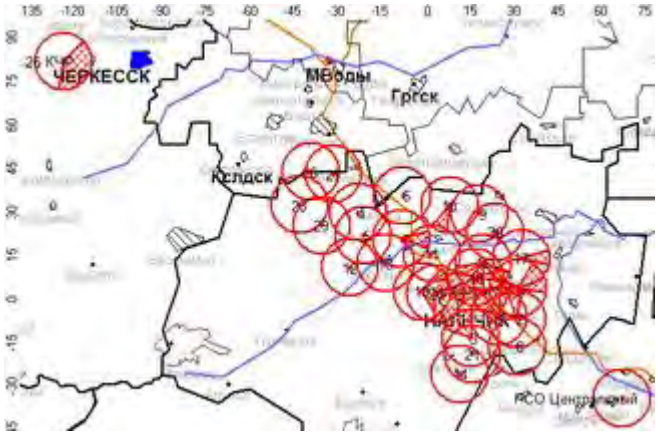


Fig. 4. Position of RL “Elia-2” (red circles) of the Northern Caucasus Anti-hail Service

4. Perspectives

1. Replace morally and physically out-of-date manual launchers with the modern automated ones with high shooting rate.

2. Increase of hail suppression efficiency due to the increase of rocket launching efficiency and elimination of the human factor (errors and temporal delays of commands execution).

3. Reduction of projects cost via creation of unfrequented rocket points and avoidance of expenses for their infrastructure.

4. Full automation of anti-hail operations chain by integration of rocket launchers control system "ASU-Elia” into radar control system of hail suppression "ASU-MRL”.

5. For registration of the hail drop-out fact and calibration of indications of automated radar control system "ASU-MRL" development of the built in sensors of hailstones and precipitation amount is being conducted.

5. Conclusion

The new automatic anti-hail rocket launcher "Elia-2" and system of remote control by a network of distant launchers via cellular and radio communication channels “ASU-Elia” are developed, tested and implemented into commercial operation, allowing implementation of thin-staff rocket technology of hail suppression.

Their application in hail suppression practice has provided increased accuracy, efficiency and physical efficiency of clouds seeding.

Acknowledgements

We express gratitude to all participants of development, batch production, maintenance and exploitation of launchers "Elia-2".

References

Abshaev M.T., Abshaev A.M., Malkarova A.M.: Guiding manual 52.37.731-2010. Organization and carrying out of hail suppression, Nalchik, 86 p., 2010.

Abshaev M.T., Abshaev A.M. at all.: New means of hail suppression // 9th WMO Conf. Weather Mod. – Antalya, Turkey, 375 – 378, 2007.

Abshaev M.T., Abshaev A.M., Kuznetsov B.K.: Patent for the invention of Russian Federation No 2267914. Automatic antihail rocket launcher, 2009.

Abshaev M.T., Abshaev A.M., Sulakvelidze G.K., Burtsev I.I., Malkarova A.M. etc. Development of rocket and artillery technology for hail suppression. – In the book “Achievements in Weather Modifiaction”, UAE, Abu Dhabi, 109 – 127, 2006.

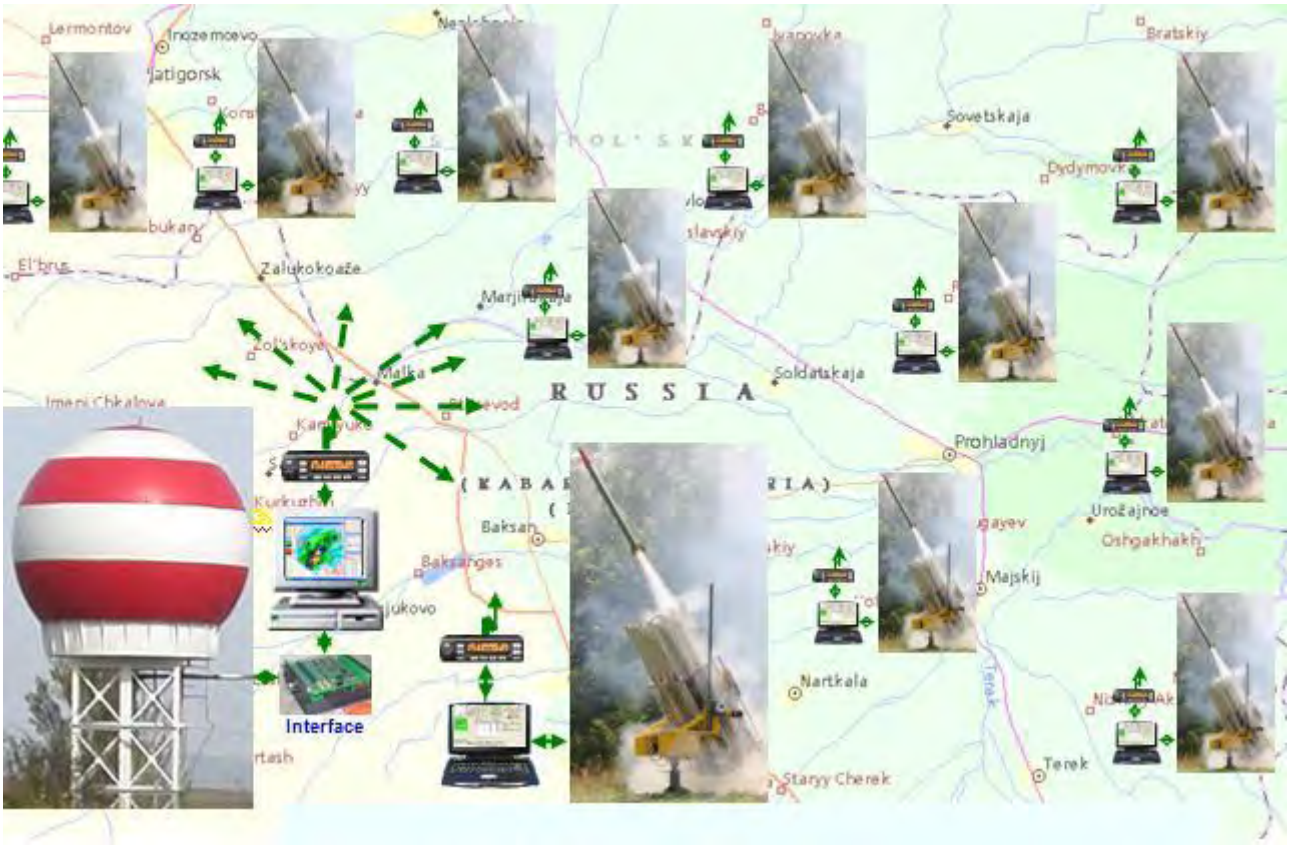


Fig. 5. Scheme of automatic rocket system for hail suppression

Efficiency of Precipitation Enhancement from Convective Clouds at Salt Powder Modification

Belyaeva M.V.[1], Drofa A.S.[2], Ivanov V.N.[3], Ridwan[4], Kudsy M.[5], Haryanto U.[6], Goenawan R.D.[7]
RPA "Typhoon"[1,2,3] 4, Pobedy st., Obninsk, Kaluga Region, 249038, Russia, e-mail: drofa@typhoon.obninsk.ru
BPPT[4,5,6,7] Building I, 19th floor, Jl. MH Thamrin No. 8 Jakarta 10340, e-mail: ridwan@bppt.go.id

Hygroscopic particles from pyrotechnic flares are widely used in a number of projects aimed at enhancement of precipitation from convective clouds (Cooper et al., 1997). At modification with this method hygroscopic particles are introduced into an updraft in the cloud base. The concept of modification is in the transformation of cloud drop spectrum at the initial stage of condensation in such a way that at future evolution of the cloud coagulation processes will be intensified and precipitation formation processes will be enhanced. Hygroscopic particles generated by pyrotechnic compounds have the sizes from 0.3 to 1 μm. The use of larger particles (l – 3 μm), as the investigation results have shown, makes it possible to obtain a more significant modification effect, but the consumption of the agent is by more than the order of the value higher than that of pyrotechnic compounds.

Rosenfeld D. (2005, 2010) proposed to use a polydisperse salt powder NaCl with rather broad particle size distribution functions for cloud modification. Such a powder was tested in the Big Cloud Chamber of SI RPA 'Typhoon' (Russia) (Drofa et al., 2010). The results of the tests supported by the results of numerical simulations demonstrate significant advantages of the powder for obtaining additional precipitation amounts. The essential effect of modification by the salt powder manifesting itself at mass concentrations of the powder introduced is by an order of the value less than at the use of pyrotechnic flares. When the salt powder is used, precipitation can be obtained from small usually non-precipitating warm convective clouds.

The present paper gives (on the basis of numerical simulations) the estimates of modification effect on convective clouds caused by polydisperse salt powders and describes the conditions necessary for maximum positive effect attained with this method.

The analysis of a scenario of cloud drop formation in a convective cloud shows that at the initial stage of condensation the main cloud droplet size distribution spectrum is formed on hygroscopic nuclei with the radii from 0.015 to 0.65 μm. Cloud spectrum maximum is formed on the nuclei of the radii of about 0.02 μm. Just such hygroscopic particles are active condensation nuclei for which unlimited growth at the initial condensation stage is realized. For artificial stimulation of coagulation processes in clouds it is necessary at the initial stage of condensation to transform the droplet spectrum in such a way that the number of large drops will be increased without changes in the conditions of cloud drop formation on atmospheric condensation nuclei. For this hygroscopic particles with the radii over 0.5-0.6 μm should be introduced. The number of additional particles needed for intensification of coagulation events, and the subsequent precipitation formation is determined by the results of numerical simulation.

The size distribution of hygroscopic particles at numerical simulations is described by the function of the form:

$$f(r)=a\, r^{-\mu}\, exp(-(r/r_o)^2). \qquad (1)$$

The salt powder particles spectra are of such a form. For the powder presented in (Drofa et al., 2010) the distribution parameters (1) are equal to: μ = 1.5, r_0 = 5 μm; for the powder (Drofa et al., 2011) - μ = 0.5, r_0 = 5.3 μm. An example of calculations of the initial stage of cloud medium microstructure formation at the introduction of the salt powder into the subcloud layer is given in Fig. 1. Here shown are the calculation results of

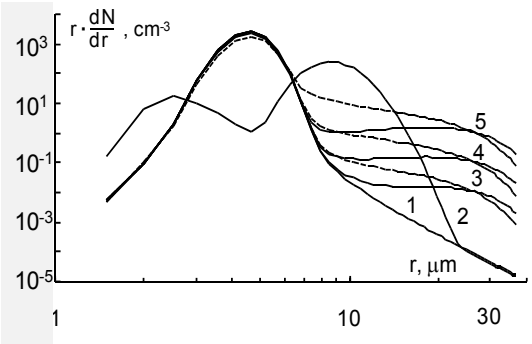


Figure 1. Cloud drop spectra at the 2nd min of cloud formation.
Solid lines – salt powder of RPA 'Typhoon';
dashed lines – powder presented in (Drofa et al., 2010).
1- drop spectrum in the background cloud;
2 - at introduction of salt particles with the radii 0f 1 μm;
3 - at introduction of salt powder with mass concentration of 0.01 mg/m^3; 4 – 0.1 mg/m^3;
5 – 1.0 mg/m^3.

drop spectra in a convective cloud at the level reached by the air mass in 120 s. Physical and chemical characteristics of background aerosol correspond to average characteristics of atmospheric aerosol of the continental origin. Atmospheric conditions are typical for convective

clouds of the continental type. The velocity of an air updraft near the cloud base is taken equal to V = 1.5 m/s, the initial air temperature – 10°C, pressure – 900 mb. The Junge distribution was used as an initial distribution of aerosol particles being atmospheric condensation nuclei:

$$f(r_c)=a\cdot r^{-v} \quad (2)$$

Formula (2) approximates rather well real spectra of aerosol particles in the atmosphere. For continental air masses it is usually accepted that v = 4-5 (Drofa, 2006).

It is evident that a positive effect of cloud modification with salt powders may appear only when a relative number of additionally introduced particles less than 0.5 μm does not exceed the number of active condensation nuclei in the background aerosol. It means that the condition $\mu < v$ should be met. In the opposite case the introduction of additional particles causes an increase of concentrations of particles formed and a decrease of their mean sizes. This effect is called the "oversesding".

As an example in Figure 1 shown are the spectra cloud drop sizes at the introduction into the convective subcloud layer of hygroscopic particles with a narrow size distribution function. NaCl particles with an effective radius of 1 μm and a relative dispersion of size distribution function S=0.3 are used. The number concentration of particles introduced makes 120 cm^{-3}. Such a concentration is optimal for the particles of this size for obtaining maximum modification effect (Drofa, 2006). The mass concentration of particles is 1.1 mg/m^3. As is seen from Figure 1, the introduction of such particles results in the formation of a bimodal cloud drop spectrum, the large-drop fraction in which is determined by the growth of particles formed on salt particles, and the fine-droplet fraction – on the nuclei of the background aerosol. The studies of the effect of modification with such particles have shown (Drofa, 2006; Segal et al., 2007) that at the introduction of salt particles due to a decrease of water vapor oversaturation in a cloud the number of atmospheric nuclei is activated (i.e. they turn into cloud drops) to a lesser extent than in the background cloud. Due to this, the total concentration of cloud drops formed on the background and additional nuclei appears less than in the case when additional condensation nuclei are absent. An average size of cloud drops appears greater at the introduction of particles. Because of this a positive effect of modification with hygroscopic particles with narrow size distributions is reached as the enlargement of cloud drops is the main factor of stimulating gravitation-induced coagulation in clouds and subsequent precipitation formation. One should pay attention at the fact that cloud drops formed on atmospheric aerosol particles are less in size under modification as compared to the background cloud. It means that in this case modification with salt particles results in the changes in conditions of cloud drop formation on atmospheric condensation nuclei.

The modification with salt powder does not lead to such changes even at rather high mass concentrations of the powder introduced. The number of cloud drops formed on the background aerosol particles changes little in this case. As is seen from Figure 1, the introduction of the salt powder into the subcloud level of a convective cloud results in the appearance of large-drop "tail" in the cloud drop distribution. The form of the large-drop spectrum fraction formed on salt particles is determined by the form of salt powder particles spectrum. The spectrum of drops formed on the background atmospheric aerosol particles does not change in this case. As the analysis of the results of numerical simulation has shown, the modification with the salt powder leads to rather more significant intensification of coagulation processes in a cloud (and, later on to enhancement of precipitation formation processes) as compared to the modification by hygroscopic particles with narrow particle size distributions.

The data obtained at the initial stage of condensation (Figure 1) are the basic data for calculations of cloud medium microstructure evolution with the use of a one-dimension numerical model of a convective cloud (Drofa, 2010). The one-dimension model of a convective cloud describes the evolution of a cloud medium in the central part of the cloud at variable with altitude velocity of the air updraft forming the cloud. The model considers parametrically the entrainment of heat and moisture into an air flow from the environment. Activation of atmospheric condensation nuclei occurs in the subcloud layer. At a further updraft of the air mass the evolution of cloud medium microstructure takes place due to the processes of drop condensation growth/evaporation, coagulation, breakdown and sedimentation. Spatiotemporal structure of meteorological parameters and integral characteristics of cloud drop size distribution function are calculated with the model. Liquid water contents of large drops with the radii r>200 μm characterizing precipitation are calculated. From the data referring to the cloud base level calculated are the precipitation intensity and total precipitation amounts.

The calculated temporal trend of precipitation intensity at modification of a cloud of 4.2 km thickness with the salt powder is shown in Figure 2. In this cloud at the stage of its formation realized was the maximum liquid water content of 3.46 g/m^3 and maximum air vertical updraft velocity of 4.5 m/s. The introduction of particles into the sublayer of the thickness from 60 to 240 m is made at the 10^{th} minute of the beginning of the cloud formation. From the graphs in Figure 2 it is seen that with the help of the salt powders precipitation amounts can be by 2-5 times greater. The effect of modification induced by the use of the powder produced at the RPA 'Typhoon', as is seen from

Figure 2, is somewhat more pronounced than that presented in (Drofa et al., 2010). In general, the calculation results have shown that the amounts of additional precipitation obtained at cloud

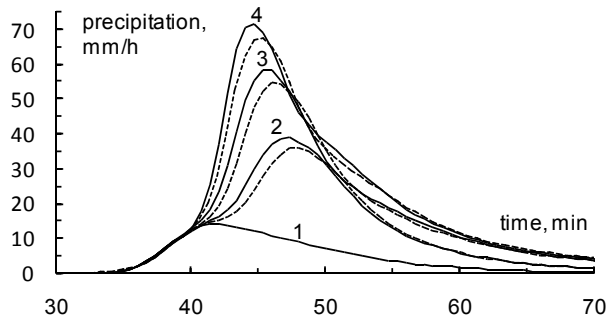


Figure2. Temporal intensity trend of precipitation from a cloud of 4.2 km thickness.
Solid lines – salt powder of RPA 'Typhoon'; dashed lines – powder presented in (Drofa et al., 2010).
1 – without agent, 2 – consumption of salt agent 2.4 kg/km^2, 3 – 12 kg/km^2, 4 – 48 kg/km^2.

modification with the powder of the RPA 'Typhoon' is by 1-2 mm more than at modification with the powder presented in (Drofa et al., 2010). For obtaining similar amounts of additional precipitation with the first powder the needed powder amounts are by 10-15% less.

The calculated total precipitation amounts obtained at modification of warm convective clouds of different thicknesses with the salt powder are given in Figure 3. As is seen from the Figure, at the consumption of more than 24 kg/km^2 additional precipitation amounts can be obtained from the clouds with the thickness H = 2.5 – 3.5 km, i.e. from the clouds that do not usually produce precipitation. The maximum effect of modification – the maximum amounts of precipitation from the clouds – is realized at the consumption of 48 kg/km^2 of the salt powder. In this case

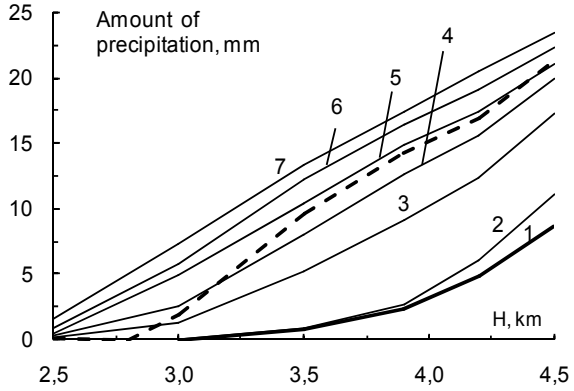


Figure 3. Calculation results of total precipitation amounts from clouds of different thicknesses
1 – without introduction of particles; 2 – introduction of South African flare particles; 3 – introduction of salt powder at the consumption of 2.4 kg/km^2; 4 – 6 kg/km^2; 5 – 12 kg/km^2; 6 – 24 kg/km^2; 7 – 48 kg/km^2.
Dashed line – introduction of 1 μm salt particles at the consumption of 64 kg/km^2.

practically all the cloud drops ate transformed into precipitation drops. After the precipitation falls from the cloud, an insignificant number of cloud drops remains in it. A further increase of the agent amount introduced does not increase the effect of modification.

The calculation results of the modification effect attained with the use of South African pyrotechnic flares (Cooper et al., 1997) demonstrate that significant amounts of additional precipitation are observed only at modifying the clouds with the thicknesses over 4 km. The calculations are made for the consumption of 12 kg of the agent per 1 km^2 of the seeded are. The use of a smaller amount of such particles does not give a significant effect of modification. The result presented here is in agreement with the data of field experiments on seeding with such particles (Mather et al., 1997). As is seen from Figure 3, seeding with a salt powder results in significant precipitation enhancement. At the consumption of 2.4 kg/km^2 of the salt powder the precipitation amounts falling from the clouds with the thickness less than 4 km are greater than at seeding with pyrotechnic particles at their consumption of 12 kg/km^2.

The effect of seeding with polydisperse particles of the salt powder is also significantly greater than that of seeding with large salt particles with narrow particle size distributions. From Figure 3 it is seen that the effect of seeding with the salt particles (the effective radius of 1 μm and optimum weight concentration of 1.1 mg/m^2) at the total salt consumption of 64 kg/km^2 appears to be less than at seeding with the salt powder at the consumption of 12 g/km of the latter.

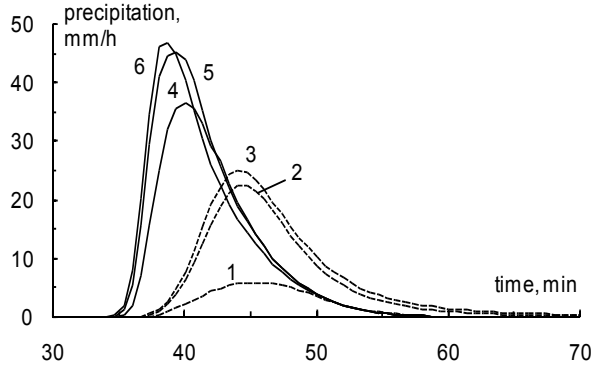


Figure 4. Temporal intensity trend of precipitation from a cloud of 3 km thickness at modification with salt powder at its consumption of 48 kg/km^2.
Solid lines – maximum air updraft V_m = 3.3 m/s; dashed lines - V_m = 5 m/s. 1, 4–drop concentration N=1015 cm^{-3}; 2, 5 – N = 485 cm^{-3}; 3, 6 – N = 305 cm^{-3}.

The results of numerical simulation show that the effect of seeding with the salt powder

depends significantly on atmospheric conditions under which a convective cloud is formed. Figure 4 presents the calculation results for precipitation intensity at seeding with the salt powder of the cloud with the thickness of 3 km. Such clouds do not give precipitation as a rule. Maximum liquid water content of a cloud medium in this modeled cloud reaches 2.56 g/m^3. It should be mentioned that at seeding of a cloud of such a thickness with the liquid water content of less than 2 g/m^3 the modification effect does not practically show itself – precipitation does not form even at very large consumptions of the salt powder. As is seen from Figure 4, the effect of seeding with the salt powder is most pronounced in clouds with power concentrations of cloud drops and at lower velocities of air updrafts.

Results of those numerical simulation consistent with observation in field. Indonesia experienced conducted cloud seeding operational in Larona Catchment Area (Sulawesi) and Citarum Catchment Area (Java) shows that during cloud seeding with favorable atmospheric condition in Larona Catcment Area in April 2005 resulting 3 times more total rainfall comparing to the operational in Citarum Catchment Area which was conducted under unfavorable condition in February 2011 due to occurence of convective storm formed (Haryanto etal, 2011). One of the significant different of atmospheric condition of those of two areas was atmospheric cloud base temperature (Tccl) - derived from analysis of sounding atmosphere - which was significant role on coalescence activity in convective cloud.

Thus, the results of the studies carried out demonstrate that the use of polydisperse salt powders for obtaining additional precipitation amounts from warm convective clouds is advantageous against the hygroscopic particles generated by pyrotechnic flares relative to the agent consumption and the modification effect. At seeding with the salt powders additional precipitation amounts can be obtained from warm convective clouds of moderate thicknesses not giving precipitation under usual conditions. In this case the effect of “overseeding”, that can appear at modification with fine-disperse hygroscopic particles from pyrotechnic flares, does not show itself.

References

Cooper W.A., Bruintjes R.T., Mather G.K., Calculations pertaining to hygroscopic seeding with flares. *J. Appl. Meteorol*., **36**, 1449–1469, 1997.

Drofa A.S., Formation of cloud microstructure: the role of hygroscopic particles*. Atmos. Ocean. Phys.,* **42**, 326-336., 2006.

Drofa A.S., Studies of a Modification Effect from a Warm Convective Cloud Seeding by Hygroscopic Particles Based on Numerical Simulation Results. *Atmos. Ocean. Phys*., **46**, 346-359, 2010.

Drofa A.S., Ivanov V.N., Rosenfeld D., Shilin A.G., Studying an Effect of Salt Powder Seeding Used for Precipitation Enhancement from Convective Clouds. *Atmos. Chem. Phys*., **10**, 8011-8023, 2010.

Drofa A.S., Eran’kov V.G., Ivanov V.N., Shilin A.G., Yaskevich G.F., Experimental studies of salt powder efficiency at convective cloud modification for precipitation enhancement, 2011 [*in present proceedings]*.

Haryanto, U., D. Harsanti, R.D. Goenawan, K. Adithya, Analysis of Storm Category and Coalescence Activity: Relationship to The Daily Mean Catchment Rainfall (Cases Cloud Seeding Operational in Larona and Citarum Catchment Area). *Paper submitted to Tenth WMO Scientific Conference on Weather Modification, Bali October 2011*.

Mather G.K., Terblanche D.E., Steffens F.E., Fletcher L., Results of South African cloud-seeding experiments using hygroscopic flares, *J. Appl. Met*., **36**, 1433-1447, 1997.

Rosenfeld D., Lahav R., The Search for the Optimal Size of Hygroscopic Seeding Particles. *Proceedings of the 16-th Conference on Planned and Inadvertent Weather Modification*, San Diego, USA, 2005.

Rosenfeld D., Axisa D., Woodley W.L. and Lahav R., A Quest for Effective Hygroscopic Cloud Seeding. J. Appl. Met. Climate, **49**, 1548-1562, 2010.

Segal Y, Pinsky M. and Khain A., The Role of Competition Effect in the Raindrop Formation. *Atmos. Res*., **83**, 106–118, 2007.

Estimation of the deposited silver-iodide in the Hail Suppression Project in Serbia

Mladjen Ćurić and Dejan Janc

Institute of Meteorology, University of Belgrade, 11000 Belgrade, Serbia, curic@ff.bg.ac.rs

1. Introduction

Hailstorms are considered to be among the most devastating weather manifestations. The devastation encouraged operational hail suppression activities to be undertaken in many countries (e.g. Ćurić,1990;Dessens,1998).“Hail suppression project” in Serbia uses the anti-hail rockets to inject the silver iodide agent into the hail clouds (one rocket has 400 g of mixture with 10-20% of AgI agent). The target area is between isotherms of - 8℃ and -12℃ and radar echo contours of 25 and 45 dBZ. This project has a very dense network of stations with rocket launchers (the mean distance between sites is 5 km) in operative use continuously over forty years. The total target area is 77.498 km^2 with 51.069 km^2 of agricultural area. The voluntary observers reported days when hail and other precipitation types (classified in nine categories) from Cumulonimbus (Cb) clouds occurred at their stations. All hailstorms moving over target area were monitored by S-band radar detectors located at 13 radar centers presented in Fig. 1. The launching site is shown in Fig. 2.

There are minor number of studies dealing with aftereffects of weather modification activities. Most of these studies investigate the persistent



Fig. 1.The radar centers in Serbia.

effects of cloud seeding (Bigg and Turton, 1988; Mother et al., 1990; Bigg, 1995). Ćurić and Janc (2008) tested the hypothesis about the presence of silver-iodide seeding agent over 100 km downwind from the point where the agent was released and corresponding inadvertent enhanced precipitation. They demonstrated that the cloud seeding produces the enhanced cumulative precipitation (about 50%) 110 km far from the mass center of initial seeding area. This effect was observed if the AgI agent can be injected by chance in downwind direction with respect to the target cloud during seeding.



Fig. 2. A launching site.

The spatial distribution of the deposited AgI agent may give us an information about the possible water pollution (Cooper and Jolly, 1970; Goettl and Davies, 1978) as well as possible persistent effects of enhanced precipitation. The importance of such investigation increases if the huge amounts of silver iodide agents are deposited. Our primary goal is, therefore, to establish the method for estimation of deposited silver-iodide agent during hail suppression activities within “Hail Suppression Project” in Serbia.

2. Method

An analysis of the operational “Hail Suppression Project” in Serbia that used silver iodide dispensed from anti-hail rockets was performed for the period 1981-1986 to estimate the seeding agent amount reaching the surface of the target area. We want to show whether amounts of silver iodide exceeds the threshold of 1 μg/m^2 (Bigg and Turton, 1988) from one seeding event, which in turn, may be of importance for an analysis of apparent after effects of seeding. This period is selected due the largest silver-iodide consumption (the maximum is over 10^3 kg per a season, 4.4 tones for 1981-86 period). This can be viewed from Table 1 under assumption that the agent used contains 10% of silver iodide.

Table 1. The anti-hail rockets (AHR) fired in 1977-2006 period.

year	1977	1978	1979	1980	1981	1982	1983	1984	1985	1986
AHR	14495	11465	11730	9947	11494	17687	21868	16641	16938	26094

year	1987	1988	1989	1990	1991	1992	1993	1994	1995	1996
AHR	10758	17477	17046	6812	13185	15638	10122	9284	5795	4685

year	1997	1998	1999	2000	2001	2002	2003	2004	2005	2006
AHR	9691	4157	300	3399	5564	12786	10379	15914	12263	11811

The radar observations give us the possibility to estimate the precipitation area associated with a seeded hail cell. It is well known that this area is often much smaller than the analyzed target area independently of a storm type. The main assumptions of our method for estimation of the deposited AgI are as follows: Each seeding operation was performed according to the seeding criterion; Both activated and non activated agent particles reach the ground; Analyzed precipitation area is associated only with a single hail cell which satisfies the seeding criterion; 60% of the seeding agent would be fall down bellow or close to the storm; The agent particles are uniformly distributed within the accumulated precipitation area at the surface. In such a way, we performed estimates of the seeding agent amount reaching the ground after seeding.

Our analysis is performed for the area monitored by S band radars located near Valjevo and Užice (Fig. 3). The area is composed by the plain in the northern part and a mountainous region in the southern part. This terrain was selected because it causes many peculiarities in the analyzed hailfall patterns. The Machva plain is situated in the northern part of this area (bounded by the rivers Drina, Sava and Kolubara). The mean height is 200 m (m.s.l.). The most prominent region of this area is the centrally located Western Morava valley which is oriented roughly from northwestern to southeastern. The floor of the valley is flat and very narrow, especially in the middle. The southern valley sides are higher with peak values over 1.5 km above the valley floor. The Zlatibor plateau in the western part of the valley is an important source of air mass hailstorms (Ćurić, 1982).

We analyzed the seeded air mass and frontal hailstorms moving over analyzed area from NE, SE, SW and NW directions. The air mass hail clouds that move from NW are of the special interest due to the formation of the hailstreaks along the major axis of the Western Morava valley. A hailstreak has the surface ranged in the interval between 100 and 500 km^2. For each hailstorm, they are observed at the approximately same locations. Spatial distribution of hail point frequencies for air mass hailstorms from NW is shown in Fig. 4. As noted, the alternate change of hail-point frequency maxima and minima may be observed along the major axis of the Western Morava valley

The locations of local maxima are correlated well with the forced lifting of the environmental warm air above the gust-front head (Ćurić,1982). This process lead to a cell regeneration in front of the mother cloud.

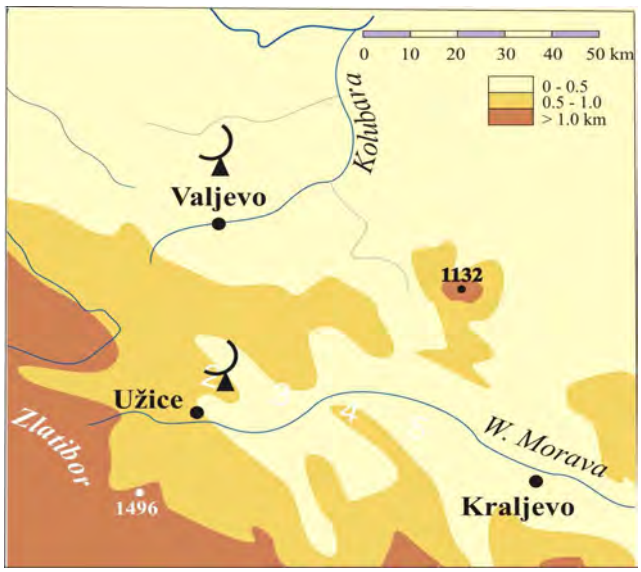


Fig. 3. The analyzed area.

We select 28 air mass hailstorms in the treated period. If the circular form of seeded hail cell is used that obtained from the radar data (Branolas et al., 2010) we estimated that the deposited silver iodide amount exceeds the given threshold in the six cases with the maximum per seeding event of 1.6 μg/m^2. This is affected by the fact that air-mass hailstorms recover only small part of the target area.

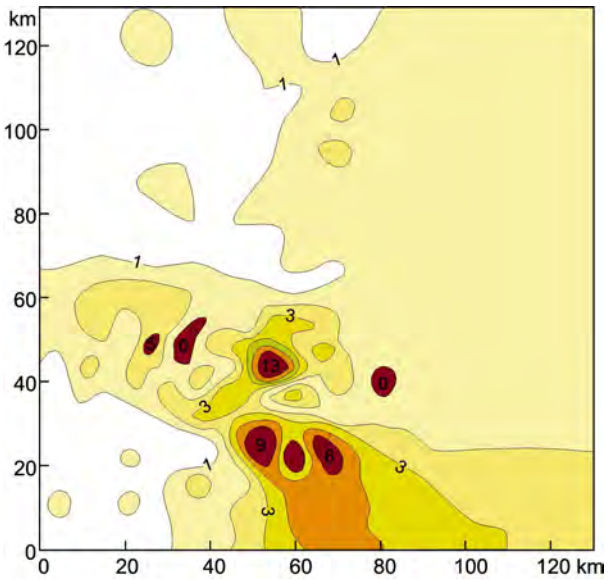


Fig. 4. Point frequency of soft, moderate or heavy shower of hail for 1981-86 period from air mass Cb clouds which move from NW direction.

Hailstorms associated with approaching frontal systems are characteristically more severe and more frequent than air mass hailstorms. Hail point frequencies for frontal Cb clouds from NW are presented in Fig. 5. As expected, the maxima locations are more or less uniform in the along-line direction of a front. Frontal hailstorms spread over larger area and produce more uniform pattern of hail

point frequencies. We analyzed 41 storms from this period. In this case, our methodology always give the the deposited silver-iodide amount below the given threshold with the maximum of 0.4 μg/m^2.

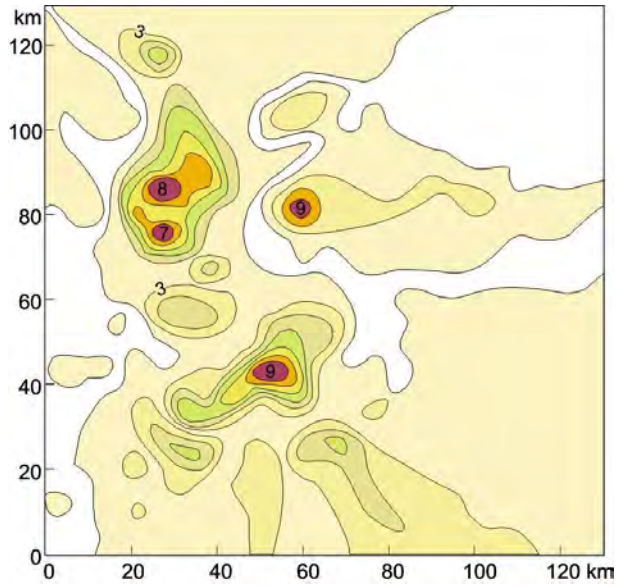


Fig. 5. Point frequency of hail for 1981-86 period from frontal Cb clouds which move from NW direction.

Fig. 6 presents the hail point frequency for frontal and air mass hailstorms from SW. As noted there is only one local maximum (35) associated with orographic effects. We select 42 hailstorms (29 frontal and 13 air mass) for our analysis. We found that the two air mass hailstorms produce the deposited silver iodide amount over the threshold with the maximum value of 1.35 μg/m^2.

Our calculations show that the amounts of the deposited silver iodide in average are below the proposed threshold value in most cases, especially for frontal hailstorms. The analysis, however, shows that these amounts may exceed the threshold in the eight analyzed cases of the seeded air mass storms with significant consumption of the silver iodide agent. The deposited silver iodide amounts are underestimated because the silver iodide particles are not uniformly distributed in the accumulated precipitation area as well as they do not fall down suddenly via precipitation after seeding performed. However, the seeding agent tends to move towards the target cloud if we perform seeding following the criterion of the “Hail Suppression Project” in Serbia. This is illustrated by Figs. 7 and 8 as obtained by the cloud-resolving model simulation.

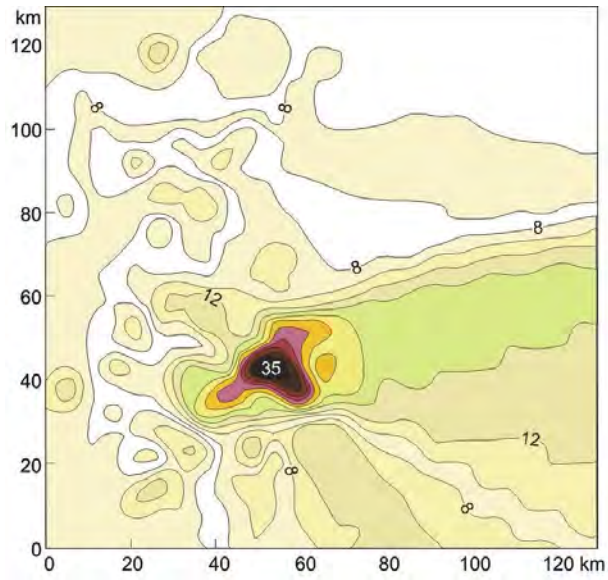


Fig. 6. Point frequency of all types of hail for Cb clouds which move from SW direction.

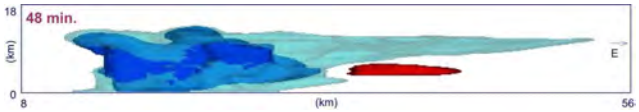


Fig.7. Visual appearance of reflectivity (green-coloured area), hail field (blue-coloured area) and the seeding agent field (red-coloured area) from west if the seeding was performed between - 8℃ and -12℃.

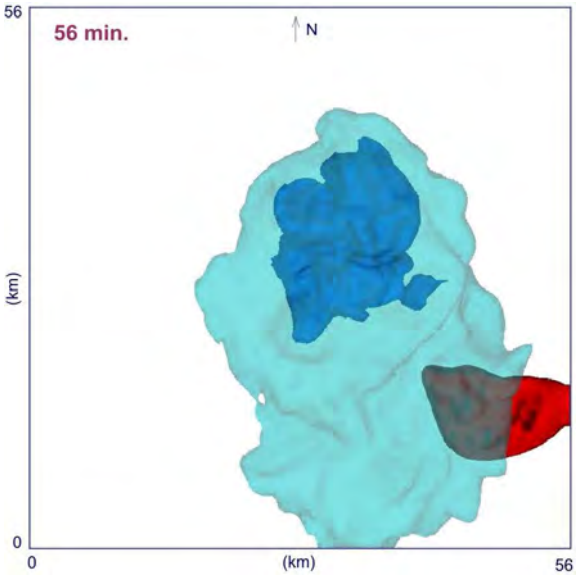


Fig.8. Visual appearance of reflectivity (green-coloured area), hail field (blue-coloured area) and the seeding agent field (red-coloured area) from above if the seeding was performed between - 8℃ and -12℃.

3. Conclusions

The proposed method for the estimation of the deposited seeding agent amounts and their spatial distribution may give the basis for further investigation. For the smaller total seeding agent consumption, the critical threshold for the deposited silver iodide amount also may be attained in some areas after one seeding event. The estimation of the averaged deposited seeding agent amounts based on the total agent consumption and the corresponding target area significantly underestimates the real seeding effects. Our method gives an scientific-based idea how to estimate the real deposited agent amounts during the seeding events. Seeding scenarios with considerable amounts of the deposited silver iodide are the warnings for scientists of different profiles to organize the special observations after seeding events with the large agent consumption. We do believe that the amounts of silver iodide may be decreased by the improvement of hail suppression methodology based on additional investigations.

Acknowledgements

This research was supported by the Ministry of Science of Serbia. We gratefully acknowledge Mr. Dragomir Bulatović for technical preparation of the figures.

References

Bigg E.K., Tests for persistent effects of cloud seeding in a recent Australian experiment. *J. Appl. Meteor.*,**34**, 2406-2411, 1995.

Bigg E.K. and E. Turton, Persistent effects of cloud seeding with silver iodide. *J. Appl. Meteor.*, **27**, 505-514, 1988.

Barnolas, M., Rigo, T., and Llasat, M.C.: Characteristics of 2-D convective structures in Catalonia (NE Spain): an analysis using radar data and GIS. Hydrol. Eart Syst. Sci.,14, 129-139, 2010.

Cooper, C. F. and W.C. Jolly, Ecological effects of silver iodide and other weather modification agents: a review. *Water Resources Research*, **6 (1)**, 88-98, 1970.

Ćurić, M., The development of the cumulonimbus clouds which moves along a valley. In: Cloud Dynamics (eds. Agee,E.M., Asai,T.). Dordrecht: D. Reidel, 259-272, 1982.

Ćurić M., One evidence of the hail suppression efficiency derived from the radar measurements. *J. Wea. Mod.*, **22**, 79-81, 1990.

Ćurić, M., D. Janc, D. and V. Vučković, Precipitation change from a Cumulonimbus cloud downwind of a seeded target area. *J. Geophys. Res*., **113**, D11215, doi: 10.1029/2007JD009483, 2008.

Dessens J., A physical evaluation of a hail suppression project with silver iodide ground burners in southwestern France. *J. Appl. Meteor.* , **37**, 1588-1599, 1998.

Goettl, J. P. and P.H. Davies, Water Pollution Studies. *Colorado Job Progress Report*, Colorado Division of Wildlife, Department of Natural Resources, Boulder, Colorado, 1978.

Mather G.K., E.K. Bigg and S. Renton, Apparent persistence effects in the Nelspruit area from silver iodide seeding for hail suppression. *J. Appl. Meteor.*, **29**, 806-811, 1990.

Integral radar parameters of hailstorms used on hail suppression projects.

Viktor Makitov, Weather Modification Inc., 3802 20th St N, Fargo, ND 58102, USA, vsmakitov@hotmail.com

1. Introduction.

One of the most important questions in radar maintenance of hail suppression projects is the exact indication of hail and potential hail clouds, detection of hail zones in the clouds and the areas of hailfalls on the ground. The correct decision of these problems in many respects defines success of realizing the seeding technology and operative estimation of its efficiency. In carrying out hail suppression projects with the use of the Russian rocket technology (Makitov, 1999), the basic characteristics for the parameterization of intensity fields of hailfalls are the hail kinetic energy flux Ė (J/m^{2}s) and total kinetic energy per unit of area E (J/m^2). Reception of formulae for radar measurement methods of these parameters is not considered difficult and is well described in the scientific literature (Ulbrich, 1978; Waldvogel et al., 1978; Abshaev et al., 1985). Both parameters are measured by modern radar methods. The kinetic energy flux Ė is calculated from radar reflectivity Z (dBZ) on one or two wavelengths. The Z– Ė relations obtained by various theoretical and experimental methods are usually used. The special algorithm for discriminating hail zone from rain zone is necessary to use in practice. The total kinetic energy per unit area E is determined as a result of time integral.

Various computerized systems of collecting, processing and analyzing of radar information are widely used at present (Dixon and Wiener, 1993; Abshaev et al., 1994). Modern computerized systems allow to execute more complex calculations and to improve the measurements of quantitative radar parameters. In this connection the purpose of this work is the development of radar echo zone determination method for calculating the kinetic energy of hailfalls and the specification of the used formulae for a hail–rain mixture zone.

2. Theoretical and semi-empirical Z–Ė relations.

The basis of all known methods of calculating the hail kinetic energy flux is the assumption of an empirical relation between hailstone fallspeed in still air and its diameter, and choice of the concrete function of hailstone size distribution. The general type of the theoretical formulae for Ė of various authors not strongly differs. The most full expression for Ė accounting the correlation between upflow and downflow air velocity in a zone of the hailfall is presented by Iniuchin and Makitov (1987):

$$\dot{E} = \frac{\pi\rho}{12}\int_{d\,\min}^{d\,\max} n(d)d^3\left[v(d) \pm u\right]^3 dd\,, \qquad (1)$$

where ρ and d are the density and diameter of hailstone, respectively; v(d) is hailstone velocity in a still air; u is the velocity of vertical air flow in the hailfall zone (with the “sign” plus for downflow and with the “sign” minus for upflow); n(d) is the function of the hailstone size distribution. As a function of hailstone size distribution, the three-parameter Γ-function, which is optimal for heavy rain and hail, is used here. The detailed analysis of the correlation between hailstone diameter and its fall speed (Iniuchin and Makitov, 1987) shows that the coefficient γ most often used in empirical dependency v(d) = γd$^{0.5}$ is variable within the broad limits. However, γ =13.96 m/(cm$^{0.5}$ s) is used in many experimental works (Ulbrich, 1978; Waldvogel et al., 1978; Abshaev et al., 1985). According to the author's opinion, this value well reproduces the spectra of the velocities for the big statistics. As a result, expression (1) can be written in the following form when Γ-functions with parameter μ=2 is used:

$$\dot{E} = 1.14\ N\ \bar{d}_3^{4.5}, \qquad (2)$$

where N and $\bar{d}_3$ are the concentration and medium-cubic diameter of hailstones, respectively.

This is the main formula for converting from *N* and $\bar{d}_3$ to radar reflectivity. In the most correct way, it is possible when the dual-wavelength radar measurements are used. Herewith it is necessary to take into account that the radar features of the hailstones depend on the phase condition of their surfaces. The water coat thickness h on the surfaces of hailstones growing in wet mode or melting strongly influences on the radar reflectivity and attenuation factor. In the assumption of the constant for water coat thickness h=0.05 cm, the following formula for calculating Ė from radar reflectivity on two wavelengths is received by Abshaev et al., (1985):

$$\dot{E} = 1{,}53\cdot 10^7 \eta_{10}^{0{,}73}\eta_{3{,}2}^{0{,}27}, \qquad (3)$$

where η_{10} and $\eta_{3,2}$ (cm^{-1}) are radar reflectivity on the wavelength 10 cm (S-band) and 3,2 cm (X-band), respectively.

The conversion from dual-wavelength formula for calculation Ė to one-wavelength in Abshaev, et all, (1985) is executed with the assumption of the constant for hailstones concentration N = 5 m^{-3}. As a result dual-wavelength formula (3) is converted to one-wavelength:

$$\dot{E} = 2{,}61\cdot 10^6 \eta_{10}^{0{,}83}, \qquad (4)$$

However, assumption of the constant for hailstones concentration is roughly enough. That is why, the approach, used in Iniuchin and Makitov (1987), where similar formula is obtained as a result of numerical simulation of the relations between Ė and η_{10} for large number of hail spectrums with various $\bar{d}_3$, N and μ, looks more correct. In this case, dependence

between $\dot{E}$ and η_{10} is approximated by following expression:

$$\dot{E} = 3.34 \cdot 10^{7} \eta_{10}^{1.018} \quad (5)$$

When the radar reflectivity is used in Z (dBZ), expressions (4) and (5) can be written as:

$$\dot{E} = 1.47 \cdot 10^{-5} 10^{0,083Z} \quad (6)$$

$$\dot{E} = 5.35 \cdot 10^{-7} 10^{0,1018Z} \quad (7)$$

The set of one-wavelength formulae for the calculation $\dot{E}$ was obtained by Ulbrich (1978) for four wavelengths and five different thicknesses of the water coat on the surfaces of the hailstones. In this work, the assumption about exponential distribution of hailstones was used. For S-band reflectivity and water coat thickness h=0.05 cm, Z–$\dot{E}$ relation is given as:

$$\dot{E} = 7.02 \cdot 10^{-6} 10^{0,086Z} \quad (8)$$

The special interest presents Z–$\dot{E}$ relation obtained on the base of the analysis of experimental data of the hail spectrum on surface (Waldvogel et al., 1978). The dense hailpad network in the region of the radar observations and some mobile hail spectrometers have allowed the authors to get 175 hail spectrums. As a result of spectrums analysis, the following Z–$\dot{E}$ relation was obtained:

$$\dot{E} = 5.00 \cdot 10^{-6} 10^{0,084Z} \quad (9)$$

The expressions (6)–(9) are presented on Fig. 1 in the form of dependencies between $\dot{E}$ and radar reflectivity Z (dBZ).

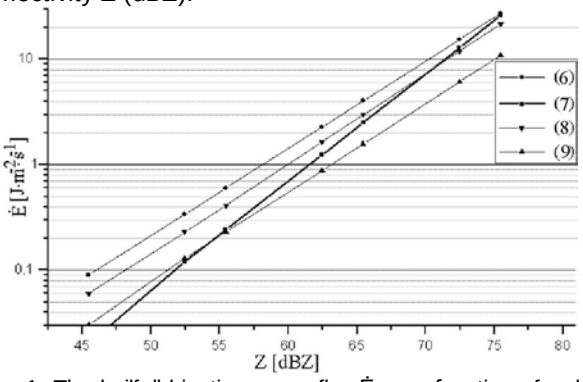


Fig. 1. The hailfall kinetic energy flux $\dot{E}$ as a function of radar reflectivity Z for various Z-$\dot{E}$ relations. The lines numbers correspond to numbers of expressions in the text.

As it can be seen from this figure, all lines are situated in the local area, independently of the way each line was obtained. However, even a small difference between these line positions can cause a significant difference of the calculation of total kinetic energy per unit area E. So the choice of the formula for calculating $\dot{E}$ in an ideal event must be based on the results of the compared ground network data and radar measurements, as in Waldvogel et al. (1978, 1979) and Schmid et al. (1992). In these works, such comparison is executed for expressions (8) and (9). The authors show for sure that the use of these formulae for calculating $\dot{E}$ and E provokes significant increase of E for small and average hail. So expression (7) is more preferred because for small and average hail values of $\dot{E}$ are lower than values obtained according of expressions (8) and (9).

3. Radar echo zone determination method for calculation of kinetic energy of hailfalls and its application in a hail–rain mixture zone.

However the choice of the optimum Z–$\dot{E}$ relation does not solve completely the question of calculating E with maximum accuracy. It is necessary to use the special algorithm for discriminating hail zone from rain zone of radar echo. It is obvious that dual-wavelength relations like (3) can be used automatically only for radar echo zones, where ratio $\eta_{3.2}/\eta_{10}$ is less than concrete constant ("rain constant"). However, in the majority of operative hail suppression projects, only conventional radar and one-wavelength reflectivity measurements alone are usually used. In this case, impossible to use various polarization, doppler or multiwavelength measurements where the physical properties of the hail can be used to advantage for it detection. So in various projects for one-wavelength measurements, the special algorithms for separating hailfalls and rainfalls are used.

In the given work, the new algorithm for determining the radar echo zone for calculating the kinetic energy flux is presented. This algorithm is based on empirical dependence between the probability of hail Ph and the height of radar echo zone with reflectivity Z_{45} above the level of zero isotherm ΔH_{45}.

According the new algorithm $\dot{E}$ is computed only for an area for which two conditions are met: Z>55 dBZ at the surface and ΔH_{45}>2 km. These two conditions limit the hailfall zone for which the calculation of $\dot{E}$ makes sense. The radar echo zone that does not satisfy these conditions is considered as the rainfall of different intensity. However, such separation of the hail and rain zones does not solve completely the problem because, in many cases, hail and rain precipitate simultaneously from the same volume. That is why the special algorithm for calculating $\dot{E}$ in the hail–rain mixture zone is necessary.

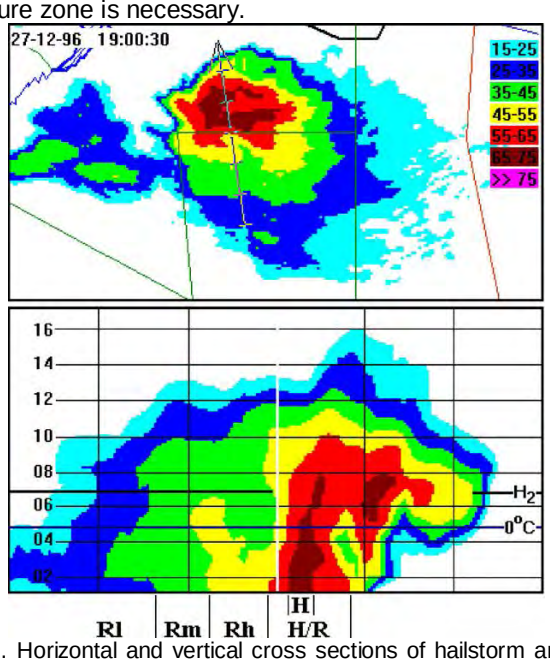


Fig.2. Horizontal and vertical cross sections of hailstorm and general scheme of precipitation zone: H is hail, H/R is hail-rain mixture, Rh is heavy rain, Rm is moderate rain, Rl is light rain.

In Fig. 2, horizontal and vertical cross-sections of hailstorm and a general scheme of the precipitation zone are shown. The kinetic energy flux for hail-rain mixture zone Ė is computed using:

$$\dot{E} = 5.35 \cdot 10^{-7} \cdot P_h \cdot 10^{0.1018 Z_{10}} \qquad (10)$$

where $P_h = \begin{cases} 0 \rightarrow \Delta H_{45} < 2.0km \\ P_h(\Delta H_{45}) \rightarrow 2.0km \le \Delta H_{45} \le 5.8km \\ 1 \rightarrow \Delta H_{45} > 5.8km \end{cases}$

and $P_h(\Delta H_{45}) = -1.20231 + 1.00184 \Delta H_{45} - 0.17018 \Delta H_{45}^2 + 0.01086 \Delta H_{45}^3$ (11)

Expression (11) is a result of the polynomial approximation of the experimental data from Witt et al. (1998).

Obviously, realization of such algorithm in computerized systems does not present any difficulties. In Fig. 3, as an example of the restoration of fields of total kinetic energy E per unit area using this algorithm, two variants of radar information maps for 27.11.98 are presented. These data are obtained on hail suppression project in the Mendoza province (Argentina) using the Russian rocket technology (Makitov, 1999) and computerized system described in Abshaev et al. (1994).

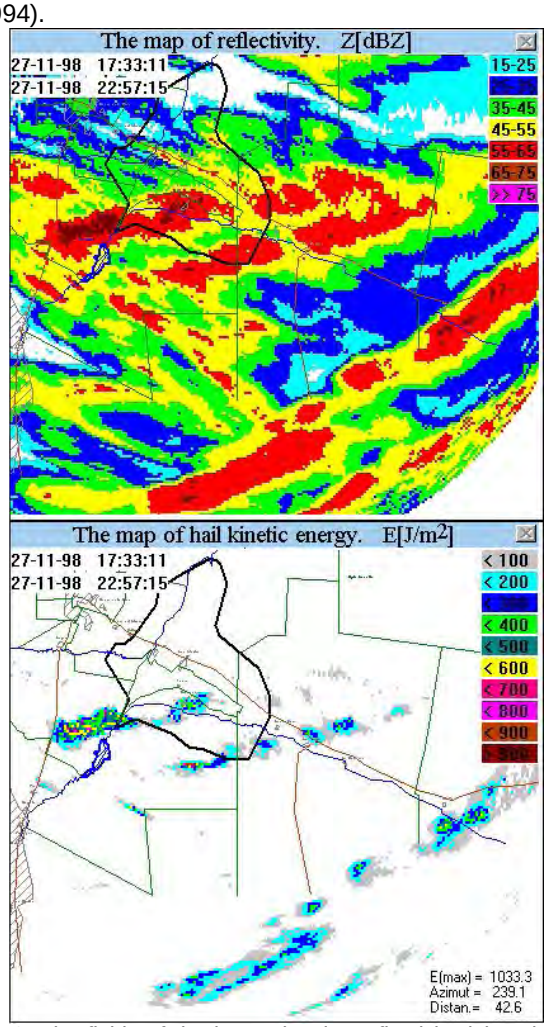


Fig. 3. The fields of the integral radar reflectivity (above) and total kinetic energy E per unit area (below) of 27 Nov 1998 in Mendoza province (Argentina).

In Fig. 3 the fields of the integral radar reflectivity (above) and total kinetic energy E per unit area (below) are shown. As can be seen on this figure, the major part of the increased reflectivity area does not correspond to the fields of the hail kinetic energy. The comparison of the fields of total kinetic energy E with the real crop hail damage (Makitov, 1999; Foote et al., 2005) shows the good correspondence as to localization of the damage area, as to the damage rate. Other example of the application of the presented algorithm for obtaining the fields of the total hail kinetic energy is shown in Fig. 4.

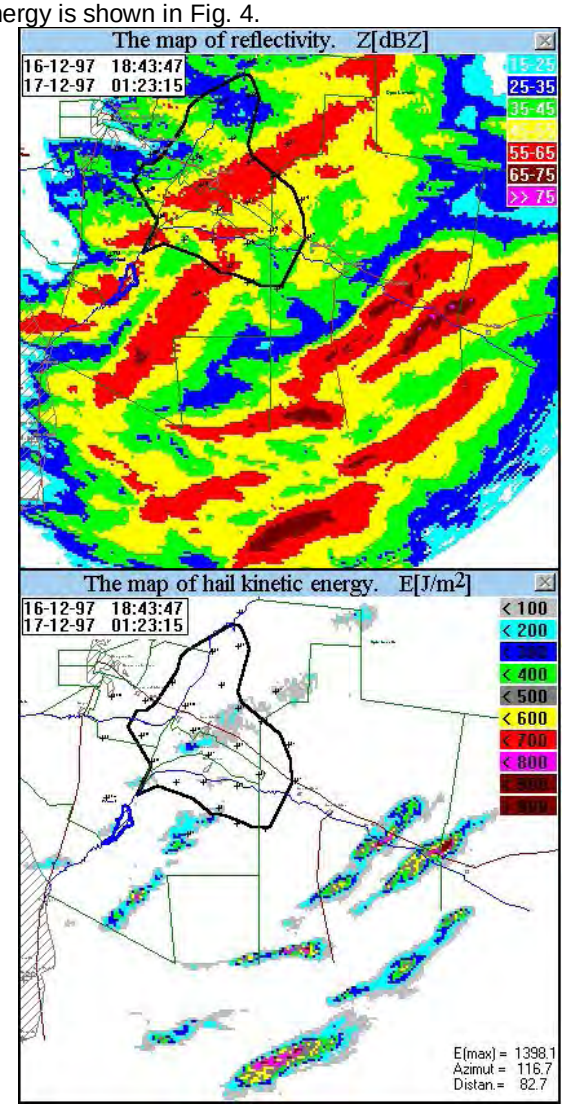


Fig. 4. The fields of the integral radar reflectivity (above) and total kinetic energy E per unit area (below) of 16 -17 Dec 1997 in Mendoza province (Argentina).

Obviously, a more appropriate control of the offered method is possible only when the radar measurements are realized directly over ground hailpad network.

4. Summary and conclusions.

The exact quantitative estimation of hailstorm precipitation intensity, allowing determining successfully the crop hail damage, is extremely necessary while carrying out of programs of experimental researches of the hail clouds as well as at realization of operative

projects on hail suppression. On the other hand, the possibility of obtaining trustworthy information about changes of hailfall intensity during cloud seeding operations enables to judge more objectively about seeding effect and to make a decision about its beginning and termination. Just because of such a parameter, the kinetic energy of hailfalls presents a great interest for the researchers. As it is known, measuring the kinetic energy of hailfalls is carried out both directly by ground network of hailpads, and by radar methods. The accuracy of the radar methods of the hail kinetic energy measurement strongly depends not only on the choice of an optimum formula for calculation but also on the algorithm used for separating hail and rain parts of radar echo and on the way it was used in the hail–rain mixture zone of precipitation.

The possibility of the radar measurement methods of kinetic energy flux Ė and calculating the total kinetic energy E fields on this base depends on the choice of optimum Z– Ė relation and reliability of the used algorithm for discriminating the hail part from the rain part of radar echo. Such algorithm offered in this work is based on the empirical dependence between the hail probability Ph and the height of the radar echo zone with reflectivity of 45 dBZ above level zero isotherm ΔH_{45}. Its realization in any computerized system does not present any difficulties. On the other hand, such approach imposes the raised requirements to the accuracy of the radar and computerized systems calibration because instrumental errors in this case can be more significant than methodical. This method of getting of the total kinetic energy fields allows to correct Z– Ė relations using data of the ground hailpad network on any stage of the calculation. It is a good possibility to increase the accuracy of the radar measurements.

5. References.

Abshaev M.T., V.S. Makitov, M.D. Atabiev, Radar measurements of kinetic energy of hailfalls. *Trans. High Mountain Geophysical Institute,* **59**, 60–77, 1985 (in Russian).

Abshaev M.T., V.O. Tapaskhanov, V.S. Iniukhin, Computerized system of hail suppression. Sixth WMO Scientific Conferenceon Weather Modification, Paestum, Italy, vol. I, 99–100, 1994.

Dixon, M., Wiener, G., TITAN: thunderstorm identification, tracking, analysis, and nowcasting – a radar-based methodology. *J. Atmos. Ocean. Technol.* **10 (6),** 785–797, 1993.

Foote, Brant G., Krauss, Terrence W., Makitov, Viktor, Hail metrics using conventional radar. *85th AMS Annual Meeting*, 9–13 January, San Diego, CA, 2005.

Iniuchin, V.S., V.S. Makitov, An experimental and theoretical study of methods of radar measurements of kinetic energy of hailfalls. *Trans. High Mountain Geophysical Institute,* **69**, 62–69 1987,(in Russian).

Iniuchin, V.S., V.S Makitov, H.M. Djakamikhov, Radar reflectivity of melting hail. *Trans. High Mountain Geophysical Institute,* **82,** 40–52, 1989 (in Russian).

Kessinger, C.J., Brandes, E.A., A Comparison of Hail Detection Algorithms. *Summary Project Report.* National Center for Atmospheric Research, Boulder. 52 pp. 1995.

Makitov, V., Organization and main results of the hail suppression program in the northern area of the province of Mendoza, Argentina. *J. Weather Modif*. **31**, 76–86, 1999.

Makitov V., V. Stasenko, An automated rocket hail suppression system, *7-th WMO Scientific Conference on Weather Modification,* Chiang Mai, Thailand, 17-22 February, 1999.

Makitov V., Radar measurements of integral parameters of hailstorms used on hail suppression projects, *Atmospheric Research*, **83**, 380-388, 2007.

Schmid,W., Schiesser, H.,Waldvogel, A., The kinetic energy of hailfalls: Part IV. Patterns of hailpad and radar data. *J. Appl. Meteorol.* **31 (10),** 1165–1178, 1992.

Ulbrich,W., Relationships of equivalent reflectivity factor to the vertical fluxes of mass and kinetic energy of hail. *J. Appl. Meteorol.* **17 (12),** 1802–1808, 1978.

Waldvogel, A., Schmid, W., Federer, B., The kinetic energy of hailfalls: Part I. Hailstone spectra. *J. Appl. Meteorol.* **17 (11),** 515–520, 1978.

Waldvogel, A., Schmid,W., Grimm, P., Criteria for the detection of hail cells. *J. Appl. Meteorol.* **18**, 1521–1525, 1979.

Witt, A., Filts, D., Stumpf, J., et al., An enhanced hail detection algorithm for the WSR-88D. *Weather and Forecasting*, **13**, 286–302, 1998.

Cloud Seeding Techniques in Eastern Region of Thailand

Prapaporn Srisathidtham[1], and Wassana Wongrat[2]
[1] Scientist, Research and Development Group, Bureau of Royal Rainmaking and Agricultural, Thailand
[2] Scientist, Eastern Region Operation Center, Bureau of Royal Rainmaking and Agricultural, Thailand

1. Abstract

Thailand has affected by drought disaster more frequently and tend to be more severe than in the past. By the disaster statistics (1900 – 2010), drought has been affected about 10 million people and more than 400 million USD. It is a matter of great concern of His Majesty King Bhumibol Adulyadej devoted himself to studying and researching artificial rainmaking techniques and donates his private funds to launch the Royal Rainmaking Project in Thailand. The technology of rainmaking science of weather modification emphasizing enhancement and/or redistribution of rain in order to prevent or alleviate drought disaster resulting from less rainfall than normal or delayed rains. Since the early phase of Royal Rainmaking, His Majesty the King has closely monitored the planning, experiments, and reporting most of the time. In 1999, His Majesty discovered a new technique and named "Super Sandwich", this technique is the step of the Royal Rain operation that combines the techniques of warm clouds (7,000 – 10,000 feet) and cold clouds (up to 20,000 feet) simultaneously to increase the amount and extent of rainfall. Today, the Bureau of Royal Rainmaking and Agricultural Aviation has been involved with the design and implementation of a series of experiments and set up five Royal Rainmaking operations center in every region of the country.

Eastern Region of Thailand is characterized by short mountain ranges alternating with small basins of short rivers which drain into the Gulf of Thailand. A major factor economy of this region is fruit, which is well-known export, for example, Durian, Mangosteen, and Rambuton. Cloud seeding operation in Eastern region is unique and different from the other region. The operation flight pattern, type and quantity of chemical substances, duration of operation were examined based on typical climate data. The results of operation would increase the natural rainfall indicated by weather radar evaluation and local people network's report.

Acknowledgements

The authors are grateful to the Bureau of Royal Rainmaking and Agricultural Aviation (BRRAA) and Eastern Region Operation Center for supporting data.

References

Bureau of Royal Rainmaking and Agricultural Aviation,1998, *Our King and Royal Rainmaking* ,Bangkok : Ministry of Agricultural and Cooperatives.

Bureau of Royal Rainmaking and Agricultural Aviation,2001, *Father of Royal Rainmaking* ,Bangkok : Ministry of Agricultural and Cooperatives. (written in Thai)

Bureau of Royal Rainmaking and Agricultural Aviation,2004, *Royal Rainmaking from Our King Bhumibol* , Bangkok : Ministry of Agricultural and Cooperatives. (written in Thai)

Eastern Region Operation Center, 2010, *The Operational Plan of Eastern Region Operation 2010*, Bureau of Royal Rainmaking and Agricultural Aviation. (written in Thai)

Eastern Region Operation Center, 2010, *The Operational Report of Eastern Region Operation 2010*, Bureau of Royal Rainmaking and Agricultural Aviation. (written in Thai)

Weather Modification Program using Powder at West Java, Indonesia

Sutrisno 1), Tri Handoko Seto 2), Samsul Bahri 3), Tukiyat, Heru Widodo, Sunu Tikno, Budi Harsoyo, Djazim Syaifullah, Halda Aditya, Mimin Karmini and Krisna Aditya, Dini Harsanti

Weather Modification Center, Agency for the Asessment nd Application of Technology, Indonesia

BPPT 1st building 19th floor, Jl. M. H. Thamrin no. 8 Jakarta, Indonesia

sutris83@yahoo.com. 1):, thseto@yahoo.com, 2) sbahripan@yahoo.com 3)

1. Introduction

The Citarum Catchment Area (CCA) is the largest and longest CA in West Java, Indonesia (geographically it spans from 106° 51'36" - 107℃ 5 1' E and 7° 19' - 6° 24' S). The area width is 718.268,53 Ac. Its length is 269 Km (main river) and 14.346,24 Km if tributaries are included. The presence of Citarum CA has an important significance due to its water resources potential utilized for various needs by the surrounding downstream area including for communities living in The Greater Jakarta Area.

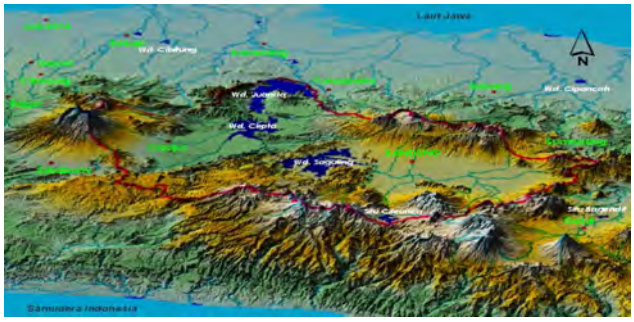


Figure X.1. A 3D View of The Citarum Catchment Area

The history of Weather Modification Center in Indonesia begun in 1977 with The Citarum CA as a testing ground for the 1977 artificial rain application. At the time, artificial rain operations are assessed and tested for the first time under the initiative of the then Indonesian President, President Soeharto facilitated by Prof.Dr.Ing. BJ Habibie through Advance Technologies Division (Pertamina) as an embrio of The Agency of Assessment and Application of Technology, under the assistance of Prof. Devakul from Thailand's Royal Rainmaking.

Water flow from The Citarum River irrigates a farming area as large as 305.000 hectar acres in West Java's northern coast areas (including The Districts of Karawang, Bekasi, Subang and Indramayu) which are national rice production centers. Water from this river (largest in West Java) also supplied drinking water needs for The Drinking Water District Company (PDAM) for several districts in West Java and Jakarta and also drinking water for industrial belts present in Jakarta and the surrounding area. Besides that, The citarum river flow is also utilized for Hydroelectric Plant capable of producing an average electrical energy of 1000 million kwh per year.

In order to anticipate and overcome water-deficiency conditions during draught season on the three Citarum cascade dams, The Citarum CA Dam management required the service of Weather Modification Technology Center, Agency of Assesment and Application of Technology (WMTC-BPPT) to conduct weather modification activity in order to increase rainfall in The Citarum CA. Since 1980 up to the present Weather Modification activities in The Citarum has been conducted more than 20 times, either for research or service purposes.

2. Climatology

In general, The Citarum CA rainfall pattern follwos a monsoonal pattern with the highest maximum rainfall occuring in January and the lowest in July.

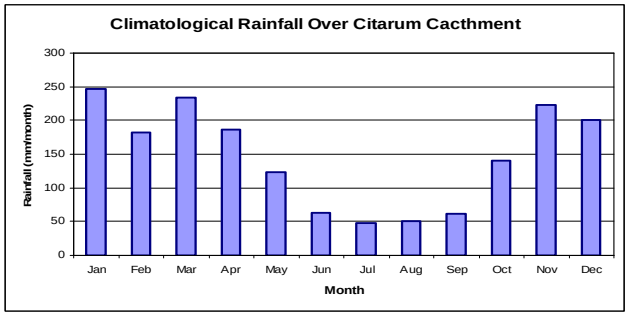


Figure X.2. The Citarum CA Rainfall Pattern

From figure 2, we could see that historically, Citarum CA had a maximum rainfall of 247 mm occuring in January. Whilst the minimum rainfall, occuring in July, was 47 mm Therefore, in general, The Citarum CA had entered drought from May to October.

The Citarum CA rainfall periodicity could be seen from spectral anaylisis. Spectral Analysis was performed to observe clearly the periodicity of The Citarum CA rainfall data time series. With this analysis, iterations which are not clear on time domain will be straightforward on frequency domain. Depicted below is The Citarum CA rainfall power density.[1)]

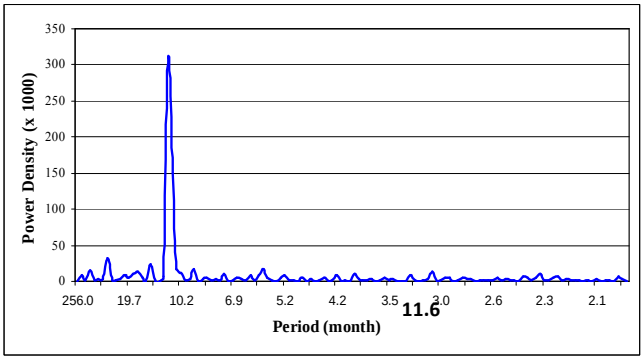


Figure X2. Power density with respect to The Citarum CA Monthly Rainfall during The Last 19 Years.

From Figure it could be seen that periodicity peak occured on 11.6 months value (around 12 months) and 32 months. This shows that the dominant period is an annual followed by an approximately three year period.

Variability analysis showed that The Citarum CA rainfall has a high variability of about 70% [2)] This indicates that the rainfall variability is influenced by global phenomenon such as The Central Indian Precipitation (CIP), Global Temperature (GT), Dipole Mode Index (DMI), Pacific Warm Pool (PWP) and Precipitable Water (PW).

The Citarum CA rainfall variability is strongly connected with The Central Indian Precipitation (CIP). Rainfall in The Citarum CA is also haevily influenced by Indian monsoon variability. Ruminta ,et. Al showed a significant correlation (around -0.52) between rainfall with CIP which is one of Indian monsoon indicator.

The Citarum CA rainfall is also influenced by local factors / orographics, Western CA boundary in the form of Mount Pangrango with a height of 12 ribu feet and southern CA boundary in the form of Malabar Mountains with a height of 9000 feet causes intense orographic process so much so that orographic process occurs heavily in downstream area.

3. Facilities and Instrumentation

Operations Center

Operations Center (Command Post) serves as a center of all cloud seeding program activity, for the discussions, briefings, and as the central data analysis. In the Operation Center all of incoming data is analyzed by the Flight Scientist Team. Bandung Husein Sastranegara air base was chosen as the Operation Center after considering various aspects; there are airport facilities included fuel, hangar space, seeding material storing facilities, and office space. Sufficient and reliable electrical power and communications were also available. Communications with the aircraft were conducted from this location, and relative position of this air base is in the middle of the Citarum river basin so that the distance and travel time flights to all corners/location of the target area relatively the same.

Meteorology Observation Station

To support cloud seeding program/activities in Citarum CA, meteorologycal observation station was made inside citarum CA. This stations report weather and cloud condition in target area hourly to the operation center using radio communication. Weather parameters that reported to the operation center were pressure, temperature, relative humidity, wind speed and direction, also cloud type, height and position, etc.

Mobile Weather Radar

Since 2007, BPPT use 1 (one) unit Mobile X-Band Radar type Doppler system (Fig. 2.), that use to monitor the growth of cloud in the target area to a radius of 100-150 km distance. X-Band radar is able to monitor the movement of clouds and water content in the cloud. Placement of mobile radar located near the Operation Center, with consideration that it can cover presence of the cloud in all over of Citarum CA and further facilitates the coordination and delivery of information to the Command Post.



Figure 2. Mobile Weather Radar *Aircraft*

Since the first cloud seeding program in the Citarum CA back in 1978, the type of aircraft used very diverse, like Hercules, twin otter, Dakota, casa, etc. But in 1993, BPPT had five planes casa NC 212-200 rain maker version for use in cloud seeding operations. So from 1993, BPPT use CASA NC 212-200 aircraft rain making version (Fig. 3.) to deliver seeding agent to the clouds in the Citarum CA. This Aircraft was modified that seeding agents would go into clouds directly. Modifications include making holes with a diameter of 18 cm on the floor. In this hole then inserted a large funnel with a mouth diameter about 60 cm. The funnel line extended until it reaches the stomach on the exterior of the aircraft. In the area around the mouth of the funnel, that 2 (two) officers releases the seeding material to the mouth of the funnel was covered with plastic to form a compartment that prevents salt dust flying out. This is done to prevent damage at aircraft instrument panel in the cockpit caused by salt dust. Aircraft were equipped by a GPS so that track of the cloud seeding activities can be tracked.



Figure 3. CASA NC 212-200 rain maker version

4. Seeding Activities

Latest program on Cloud seeding in Citarum CA was conducted early this year. Seeding activities always start with a briefing in the morning. Briefing aimed to evaluate yesterday cloud seeding flight and to discuss today condition, is it potential enough to conduct cloud seeding flight. The data came from meteorogical office representative, report from meteorology observation station and also image from mobile weather radar. After briefing, field coordinator made a decision about what time does flight start based on report from officer in meteorology observation station and from mobile weather radar perhour. After that, then seeding material loaded to the aircraft. Seeding material used was NaCl shaped in "super-fine powder" (which is amazingly fine powder) in the order of microns (μ). Seeding material in the form of fine powder obtained through a long process that takes time, i.e. from the beginning stages of processing at the plant (combustion at high temperatures, milling, and packaging), until the stage of shipment from the factory to the site.

This cloud seeding program result was total 340 million m^3 water in 3 reservoirs, using 74.42 ton NaCL as seeding material, delivered with 91 flight sortie as long as 101 hours and 36 minutes flight hour

5. Evaluation

Evaluation of WMTC activities is performed through quantitative and qualitative approach. Quantitative approach is performed in order to investigate the additional sum of water volume as a result of WMTC activities, whilst qualitative evaluation is performed in order to find out the environmental effects especially quality effects as a result of WMTC on the target area.

Quantitative rainfall addition evaluation could be done with the target only methods, double ratio method and flow method. Mathematically, The Target Only Model could be described as follows:

$$R = \frac{CH_a - Ch_s}{Ch_s} x100\%$$

Where,
R = Rain addition level (%)
Cha = Actual area rainfall in the target area (mm)
Chs = Average historical rainfall of the target area (mm)

This model analyzes the presence of seeding influences and that the size of rainfall addition could be calculated by comparing rainfall at a certain time in the target area during seeding period with historical rainfall at the same time in that target area.

Based on the results of evaluation using the target only model, we obtained the result that during WMTC seeding activities at the time of the observational period, there exist additional rainfall with an average of 11,5%. Empirically, this is shown on the table below:

Table the Citarum CA rainfall addition calculation result using The Target Only Method

No.	Period	Days	CHa (mm)	CHs (mm)	R (%)
1	1 - 21 Mar 1988	21	149	201	-26,1
2	1 - 24 Mar 1989	24	104	203	-48,8
3	25 Mar - 23 Apr 1995	30	278	209	32,9
4	17 Feb - 18 Mar 1998	30	390	203	92,1
5	12 Mar - 10 Apr 2001	30	318	195	63,3
6	14 Feb - 15 Mar 2011	30	117	210	-44,3
				Mean R (%)	***11,5***

The double ratio method is an evaluation method which compares the ratio of target area rainfall relative to the control area on cloud seeding periods, with the ratio of target area rainfall relative to the control area on periods without cloud seeding. Mathematically this model is represented as follows:

$$R = \frac{T / C_s}{T / C_{us}}$$

Where,

R = "Double Ratio" Value
$(T/C)_a$ = Comparison between actual rainfall in the target area during cloud seeding intervals with the control area rainfall at the same intervals.
$(T/C)_{us}$ = Comparison between target area rainfall and the control area rainfall during periods without cloud seeding activities.

Rainfall increase due to seeding could be calculated by the below equation:

$$R\ \% = (DR - 1) \times 100\ \%$$

Double ratio model evaluation results shows that seeding activities could increase average rainfall as much as 85,3%. Empirical results for each operational periods is shown in the table below:

Table the Citarum CA rainfall addition calculation result using The Double Ratio Method

No.	Period	Days	Ts	Cs	Tus	Cus	DR	R (%)
1	1 - 21 Mar 1988	21	149	201	172	347	1,5	49,4
2	1 - 24 Mar 1989	24	104	203	230	347	0,8	-22,8
3	25 Mar - 23 Apr 1995	30	278	209	221	347	2,1	108,9
4	17 Feb - 18 Mar 1998	30	390	203	191	300	3,0	202,0
5	12 Mar - 10 Apr 2001	30	318	195	189	331	2,9	185,9
6	14 Feb - 15 Mar 2011	30	117	210	214	340	0,9	-11,5
							Mean R (%)	***85,3***

Operational results evaluation by way of flow method is perfomed by observing inflow data in the target area during WMTC activities. The underlying principle behind this method is to compare inflow value during WMTC activities with the inflow value without WMTC activities. Suspect Inflow value without WMTC operations could be obtained from historical data by utilizing the Weibull method or via hydrological model. Flow increase level is described through the equation below:

$$R = Q_{HB} - Q_A$$

R = Addition flow volume (m^3)
Q_{HB} = Inflow during WMTC activities (m^3)
Q_A = Inflow without WMTC activitie (m^3).

From evaluation results by way of flow method, WMTC activities in 1990 results in an R of 264 million m3, in 1991 as much as 263,7 million m3, in 1992 as much as 138 million m3, in 1995 as much as 122,82 million m3, in 1997 as much as 174,31 million m3, in 1998 as much as 366,95 million m3, in 2001 as much as 214 million m3, in 2003 as much as 523,7 million m3 and in 2004 as much as 744,2 million m^3

Qualitative evaluation is mean to monitored the environment and discover:
a. Rainfall or dam water quality
b. Environmental Morphology by taking photographies of dominant commodity plants in the target area.

This evaluation activity is directed to water quality condition observation of either rain drops or body of water such as: dams and rivers. Water quality monitoring with regards to the seeding material was performed by laboratory testing by observing the chemical elements associated with the seeding material, such as NaCl (Sodium Chloride); $CaCl_2$ (Calcium Chloride); CaO (Calcium Oxyde); $Ca(OH)_2$ (Calcium Hydroxide) and Urea.

Environmental observation activities are divided to 3 stages; i.e.: (1) pre-activity stage; (2) stage during activity; (3) post-activity stage. Environmental observation and monitoring results on rain drops and dam water qualities shows that there are no significant difference in water qualities before, during and after WMTC activities in The Citarum CA.

6. Summary

Based on the target only method, water addition level due to WMTC is as much 11.5% and with the double ratio it is 85.3%. Rainfall quality during WMTC do not differ significantly with the water quality before and after WMTC. From the monitoring of plant commodity conditions in the target area, WMTC does not shown negative influences.

Acknowledgements

The Authors would like to thank Indonesia Power and Jasa Tirta II Public Company who have given the chance to WMTC to conduct weather modifications in The Citarum CA. We would also like to thank Mr. Suyatno, Mr. Ade Jahidin and Mrs. Erni which supports us through their invaluable data in the writing of this paper.

References

1. Syaifullah, D., Analisis suhu muka laut selatan Jawa dan pengaruhnya terhadap curah hujan DAS Citarum,
2. Ruminta et al. Persistensi dan Variabilitas Hidrometeorologi Daerah Aliran Sungai Citarum, *Jurnal Matematika dan Sains, September 2006, Vol. 11 No. 3*
3. Harsoyo, B., Evaluation of Weather Modification in West Java, IndonesiaUsing Rainfall Data Analysis

A SYNTHESIS OF PHYSICAL AND STATISTICAL ANALYSES FROM THE QUEENSLAND CLOUD SEEDING RESEARCH PROGRAM

Sarah A. Tessendorf[*1], Roelof Bruintjes[1], Courtney Weeks[1], James W. Wilson[1], Charles A. Knight[1], Rita D. Roberts[1], Michael Dixon[1], Matt Pocernich[1], Peter R. Buseck[2], Evelyn Freney[2], and Duncan Axisa[1]*

[1]*National Center for Atmospheric Research, Boulder, CO*
[2]*Arizona State University, Tempe, AZ*

1 INTRODUCTION

An extreme drought in Southeast Queensland (SEQ), Australia (prior to 2010) prompted the Queensland government to seek ways to create more water resources. As a response, the Queensland Cloud Seeding Research Program (QCSRP) was conducted to investigate the feasibility of precipitation enhancement via cloud seeding. Scientists from the United States, South Africa, and Australia conducted the feasibility study for rainfall enhancement via cloud seeding during the summer rainfall regime. The QCSRP feasibility study included a variety of measurement systems, some using novel technologies.

The QCSRP program design, including a detailed description of the facilities and research objectives, is provided in Tessendorf et al. (2010). A brief summary of the aerosol and in situ microphysical analyses is provided in Section 2 herein. Section 3 describes some of the dual-polarization radar analysis results, and a brief summary of the hygroscopic seeding evaluation is presented in Section 4, and includes some preliminary results from the aircraft measurements and statistical analysis. Conclusions and future work are summarized in Section 5.

2 AEROSOL ANALYSIS

Regular measurements just below cloud base were collected by a research aircraft in the QCSRP domain and from these measurements a summary of the cloud base aerosol conditions has been compiled. To characterize the aerosol conditions, 120-hr back trajectories were calculated from each cloud base aerosol measurement using the Hybrid Single-Particle Lagrangian Integrated Trajectory (HYSPLIT) model (Draxler and Hess 1998). The trajectories were then grouped into regimes with similar paths based on the time each trajectory spent over land below 2 km (proxy for the boundary layer). As shown in Fig. 1, two regimes were identified: a regime with a maritime influence and one with a continental influence on the observed aerosol. Measured aerosol and cloud condensation nuclei (CCN) concentrations were significantly different between these two regimes as well, with those measurements being higher in the continental regime (Fig. 2). The continental aerosol measurements tended to be more variable than the maritime regime measurements, and additional factors such as fires occurring along a trajectory or close proximity of the trajectory to the city of Brisbane also were found to correspond with the higher aerosol measurements observed in a given regime. To assess the composition of the aerosol, a three-stage particle impact sampler (MPS-3, California Measurements, Inc.) was used to collect aerosol particles during the QCSRP and then a transmission electron microscope (TEM) was used to determine the properties of the individual aerosol particles (Freney et al. 2009, Posfai and Buseck 2010). Major particle types observed were mineral dust, ammonium sulfate, sodium chloride, and magnesium-bearing organic particles (Fig. 3). Particles in the coarse fraction were almost exclusively mineral dust, whereas the fine-mode particle compositions were more variable in composition, depending on air mass origin. Days containing the highest number of sulfur-bearing particles in the fine fraction also had the highest CCN concentrations and had back trajectories indicative of continental or urban-influenced air masses (Jan 22 and 24 in Fig. 3). The more maritime-influenced cases, like Jan 26 and Feb 14, had the highest number of salt-bearing fine-mode particles, while having the lowest aerosol and CCN concentrations overall (Fig. 3).

The initial drop size distribution (DSD) measured within 300-600 m of cloud base has been characterized for each aerosol regime as well using various calculation methods (see Section 4.2 for one example; otherwise see Tessendorf et al. 2011).

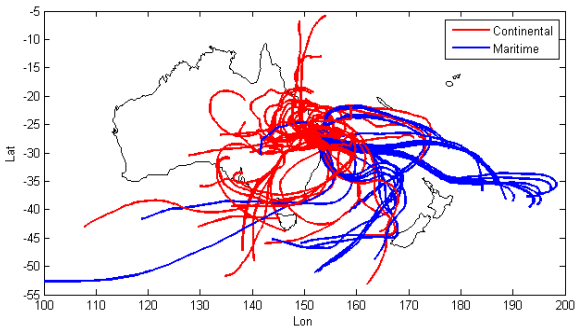
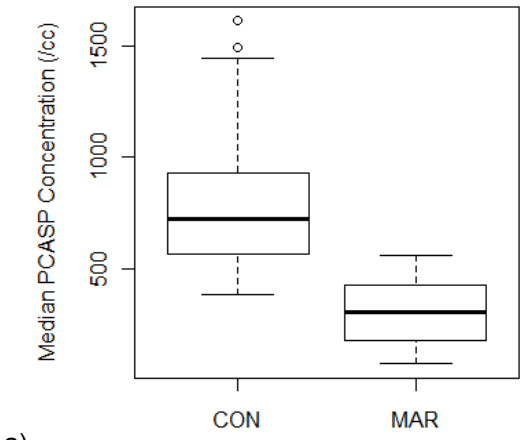
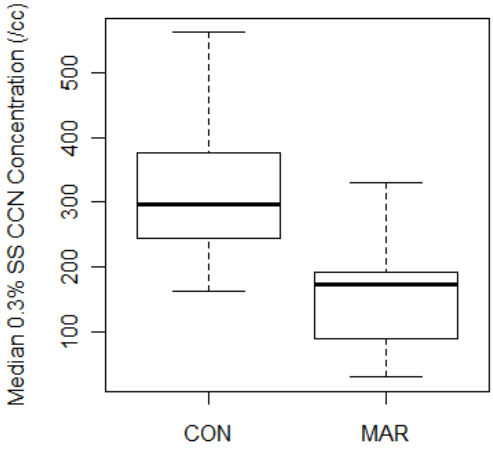


Figure 1. All cloud base aerosol back trajectories colored by maritime (red) or continental (blue) aerosol regimes.

**Corresponding Author*: Sarah A. Tessendorf, Research Applications Laboratory, National Center for Atmospheric Research, P.O. Box 3000, Boulder, CO 80307. saraht@ucar.edu



a)



b)

Figure 2. Box and whiskers plots of measured (a) PCASP aerosol and (b) 0.3% supersaturation CCN concentrations by each aerosol regime.

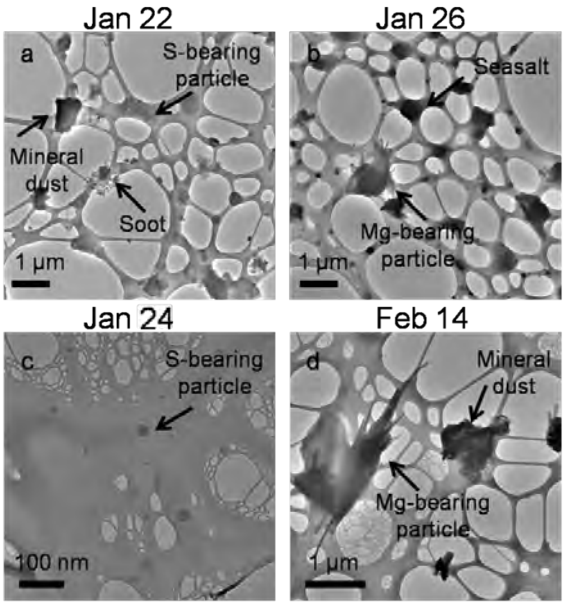
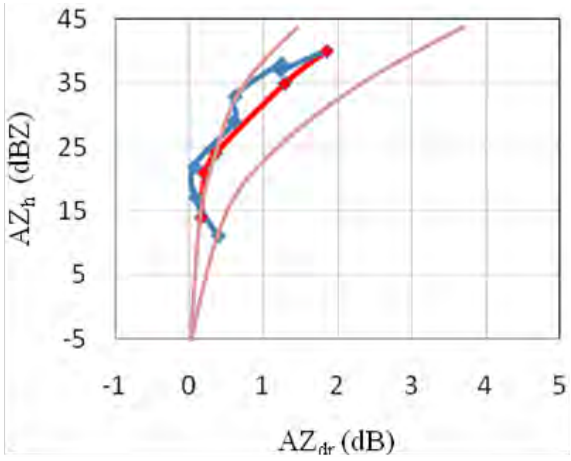


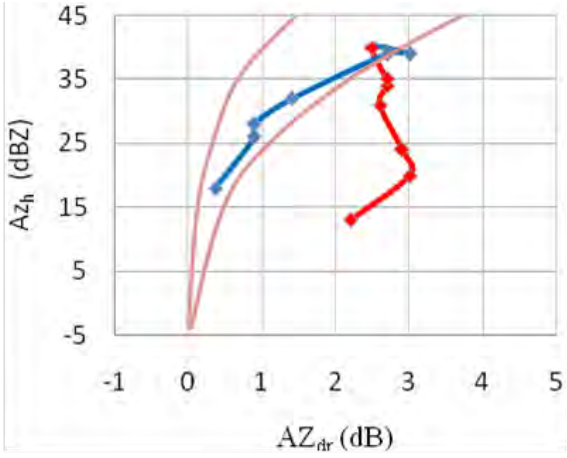
Figure 3. Examples of particles collected during selected research flights. "S-bearing" particles are sulfur bearing, and "Mg-bearing" are magnesium-bearing particles. The fibrous, spider-web-like material is the lacy-carbon substrate on which the particles were collected. The date on which particles were sampled is shown above each image, all of which occurred in 2009. Note the different scale for the Jan 24 image.

3 DUAL-POLARIZATION RADAR ANALYSIS

Dual-polarization radar measurements from the CP2 radar can offer unique insight into the microphysical properties of seeded and unseeded clouds. For example, the differential radar reflectivity (Z_{DR}) is a polarimetric variable related to the size of raindrops (Bringi et al. 1986, Wakimoto and Bringi 1988, Brandes et al. 2004). Wilson et al. (2011) studied the evolution between radar reflectivity and Z_{DR} (referred to as raindrop size evolution) over the lifetimes of 45 isolated cells observed by the CP2 radar in SEQ. They found that two general types of raindrop size evolution occurred in the region, and that they tended to be most related to the air mass influence as determined by back trajectories presented in Section 2. Type 1 clouds often had a more maritime aerosol influence and the raindrop evolution seemed to follow a more Marshall-Palmer distribution during both growing and dissipating stages, however, the Type 2 clouds were more continentally influenced and during the growth stage exhibited very large raindrops in low concentrations (see Fig. 4).



a)



b)

Figure 4. Two examples of the types of raindrop size evolution presented in Wilson et al. (2011): (a) a maritime-influenced "Type 1" case and (b) a continentally-influenced "Type 2" case (right). Red (blue) lines connect points during the growth (dissipating) stage.

4 HYGROSCOPIC SEEDING EVALUATION

4.1 Randomized Seeding Statistical Analysis

A total of 127 randomized cases were declared over two seasons of field research operations. Based on the statistical analysis criteria (set to match that used for the South African and Mexican experiments; see Tessendorf et al. 2010), 39 (19 seeded and 20 unseeded) of the 127 total randomized cases were included in the statistical analysis. One of the major obstacles in the statistical analysis of rainfall enhancement experiments, such as the QCSRP, has always been the effect of initial biases and outliers (large storms) that could easily overwhelm and dominate the statistical results. In addition, the effects of merging or splitting storms can influence and complicate the analysis substantially. Several such cases of storm mergers into large outliers were observed in the QCSRP data set. To remove the effects of such large storms on the analysis, and consistent with the findings of Mather et al. (1997), we concluded that the statistical analysis and interpretation should focus on the storms that are less than 750 km^3 in volume because they exclude large merged complexes and line storms. This threshold also yielded the most equal representation of seeded and unseeded cases (see Fig. 5).

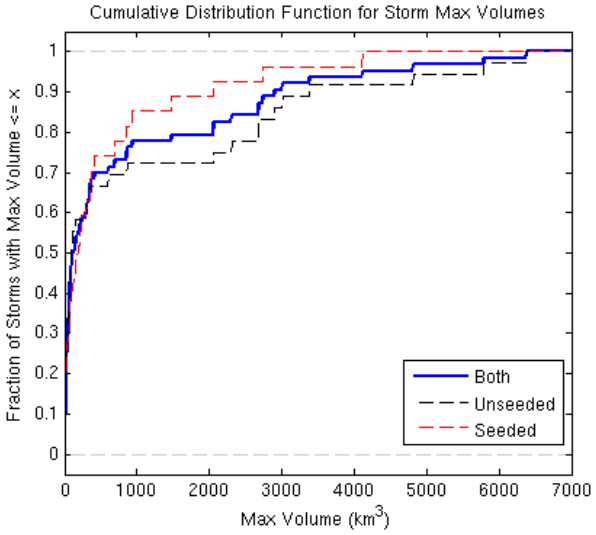
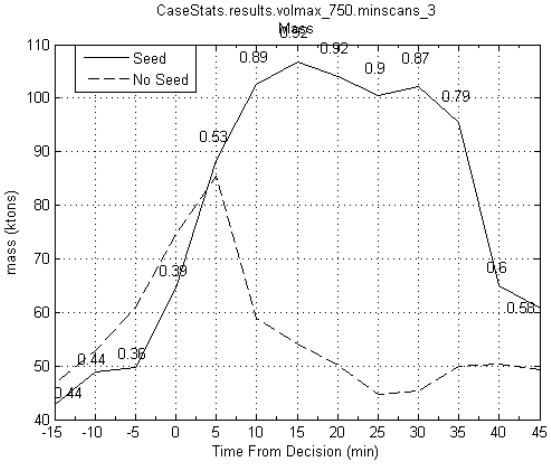
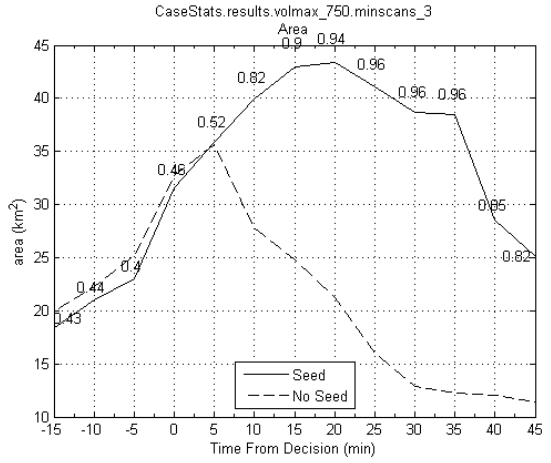


Figure 5. Normalized frequency distribution of seeded (red), unseeded (black) and total (blue) storm tracks as a function of maximum volume of tracks.

The initial results for the 39 cases that satisfied the statistical analysis criteria seem to indicate similar tendencies (although not statistically significant) for the radar-derived rain mass, area, precipitation flux, and integrated precipitation mass (see Fig. 6) to what was found in the South African and Mexican experiments (see Mather et al. 1997, Foote and Bruintjes 2000, and Tessendorf et al. 2010). The only significant difference between the seeded and unseeded clouds, as determined in re-randomization tests, was for the duration of the clouds after seeding, with the seeded clouds living significantly longer than the unseeded clouds (p-value of 0.04; not shown). This is also a similar result as to what was found in the South African and Mexican results.



a)



b)

Figure 6. Radar-derived (a) rain mass and (b) area of the 35-dBZ echo as a function of time from 15 minutes prior to seeding decision time to 45 minutes after decision time for seeded (solid) and unseeded (dashed) cases. These results were not significant above the 95% confidence level.

4.2 Randomized Seeding Physical Analysis

To complement the traditional statistical analysis of the randomized experiment, we also have analyzed our physical measurements in seeded and unseeded clouds. That said, without having a tracer released with the hygroscopic flares it is nearly impossible to know when in situ measurements were impacted by seeding material. Thus, here we take a more statistical approach by comparing the initial DSD just above (within 300-600 m) cloud base for seeded and unseeded clouds from our randomized experiment. To do this, we first separate them by aerosol regime (maritime or continental influence as described in section 2), and we assume that the natural background (unseeded) DSD would be similar within a given aerosol regime and thus any deviations from that background DSD may be attributed to seeding. Results for one DSD calculation method are shown in Fig. 7. The mean diameter and concentration of drops greater than 20 μm was significantly greater (at the

95% confidence level) for the seeded clouds in the continental regime. The maritime regime was more variable and the seeded DSDs did not exhibit a significant difference. This could be suggesting that the first step in the hygroscopic seeding conceptual model (broadening of narrow DSDs) is occurring from hygroscopic flare seeding in the continental regime. Based on the conceptual model, one might expect more of a seeding response in the continental regime, which typically has a more narrow background DSD to begin with and would presumably have a lower warm rain efficiency as a result.

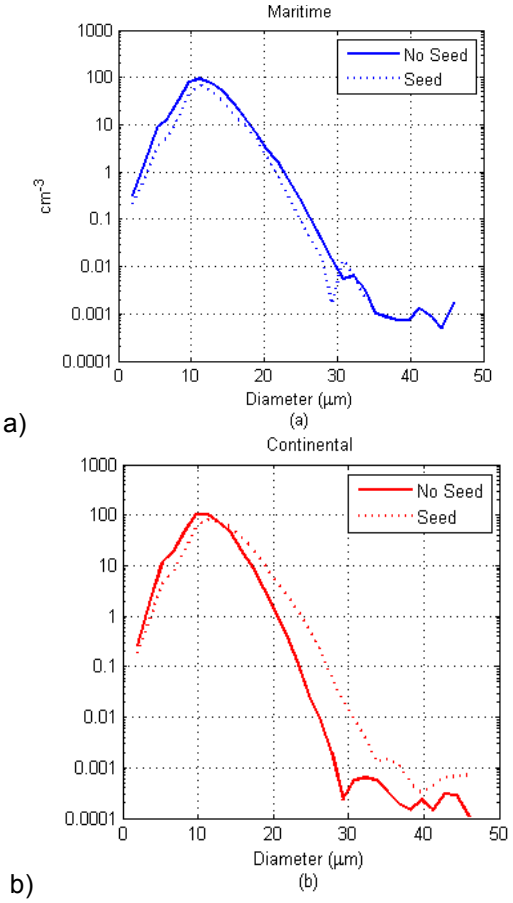


Figure 7. Mean DSDs for seeded and unseeded clouds in (a) the maritime regime and (b) the continental regime. Solid (dotted) lines indicate unseeded (seeded) mean DSDs.

5 CONCLUSIONS

The randomized seeding statistical results seem to show the same tendencies that were observed in previous experiments in South Africa and Mexico, which used the same hygroscopic seeding techniques. Nonetheless, the sample size is still too small to make any meaningful conclusions. Efforts are being made to use physical analysis techniques utilizing in situ and dual-polarization radar data to interpret and understand the results. We have observed that the QCSRP region has alternating aerosol influences, from more maritime to more continental, which can affect cloud microphysical processes as is evidenced by their potential influence on the initial DSD and raindrop size evolution. We also found some evidence that the first step in the hygroscopic seeding conceptual model may be occurring in the more continentally-influenced clouds.

5.1 Future Work

Given the vast amount of data collected in the two seasons of the QCSRP, there is a lot of analysis that can still be done. Efforts to utilize the dual-Doppler radar data for assessing the effects of cloud seeding are one key area for future work. Furthermore, we plan to incorporate cloud resolving and parcel modeling into the analyses in order to corroborate and help explain the physical observations.

Acknowledgements

The Queensland Cloud Seeding Research Program was sponsored by the Queensland Government Department of Environment and Resource Management through the Queensland Climate Change Centre of Excellence.

REFERENCES

Brandes, E. A., G. Zhang and J. Vivekanandan, 2004: Drop size distribution retrieval with polarimetric radar: Model and application. *J. Appl. Meteor.*, **43**, 461–475.

Bringi, V. N., R. M. Rasmussen and J. Vivekanandan, 1986: Multiparameter radar measurements in Colorado convective storms, Part I: Graupel melting studies. *J. Atmos. Sci.*, **43**, 2545–2562.

Draxler, R.R., and G.D. Hess, 1998: An overview of the HYSPLIT_4 modeling system for trajectories, dispersion, and deposition. *Aust. Meteor. Mag.*, **47**, 295–308.

Foote, G.B., and R.T. Bruintjes (eds.), 2000: WMO International Workshop on Hygroscopic Seeding: Experimental Results, Physical Processes, and Research Needs (1999 : Mazatlán, México). World Meteorological Organization, WMP Report No. 35, WMO/TD No. 1006, Geneva, 68 pp.

Freney, E., S. Martin, and P. Buseck, 2009: Deliquesecence and efflorescence of potassium salts relevant to biomass-burning aerosol particles. *Aerosol Sci. Tech.,* **43**, 799-807.

Mather, G. K., D. E. Terblanche, f. e. Steffens and L. Fletcher, 1997: Results of the South African cloud-seeding experiments using hygroscopic flares, *J. Appl. Meteor.*, **36**, 1433–1447.

Pósfai, M., and P.R. Buseck, 2010: Nature and climate effects of individual tropospheric aerosol particles. *Ann. Rev. Earth Planet Sci.,* **38**, 17-43.

Tessendorf, S.A., and co-authors, 2010: Overview of the Queensland Cloud Seeding Research Program. *J. Wea. Modification*, **42**, 33-48.

Tessendorf, S.A., C.E. Weeks, R.T. Bruintjes, and D. Axisa, 2011: Cloud base aerosol characteristics and implications for cloud microphysics in Southeast Queensland. Preprints, *18th Conf. Planned and Inadvertent Weather Modification,* Amer. Meteor. Soc., Seattle, WA.

Wakimoto, R. M. and V. N. Bringi, 1988: Dual-polarization observations of microbursts associated with intense convection: The 20 July storm during the MIST Project. *Mon. Wea Rev.*, **116**, 1521–1539.

Wilson, J.W., C.A. Knight, S.A. Tessendorf, and C. Weeks, 2011: Polarimetric radar analysis of rain drop size variability in maritime and continental clouds. *J. Appl. Meteor. Clim.,* in press.

‘Do no harm’ geoengineering of climate and hurricanes

Roland List,
Dept. of Physics, University of Toronto, Toronto, Canada

1. Introduction

There is a lot of excitement in the scientific and engineering worlds about geo-engineering, GeoE, and the expectation to provide quick fixes for vital, climate-related problems of mankind. Big efforts are presently being made – without really knowing what the non-scientific boundary conditions are. One is reminded about the early days of weather modification, WM, with its unregulated turmoil. Thus, a comparison may be in order. To do that the questions surrounding WM and its relevance to GeoE will be discussed. Suggestions will then be made about how GeoE can be made safe and robust for political, scientific and engineering aspects. The ‘Do no harm” principle, introduced to medicine by Hypocrates, will then be applied to GeoE with the help of a sequence of “reversible” steps. Examples will clarify possible solutions by characterizing present shortcomings and how they can be remedied.

This ‘Do no harm’ safety net is necessary for the protection of the scientists and engineers involved in GeoE operations.

Before delving into the above aspects, the GeoE issues will be restricted to large weather systems (hurricanes, Hu, and climate, Cl). Thus, the methods will involve the injection into the atmosphere of gases and/or particles as well as the placing of devices in space, such as mechanical radiation shields. The discussion will not encompass the chemistry of the oceans. An interesting quick summary of all such issues is to be found in R. Hauser and N. Gordon (2010).

2. Tackling WM issues by WMO

The SAHEL drought in the sixties and seventies exposed the wild situation in WM, as practiced by many commercial companies. Several tried to outbid each other in Dakar. Bids to increase precipitation (personal communi-cation by Dr. Seck, Director of the Meteorological Service of Senegal, 1973) varied from 20 to 90%. This prompted the Executive Committee of the World Meteorological Organization in 1972 to establish a WM Panel with the purpose of bringing order into the field. This Panel consisted of Gagin, Warner, Goldsmith, Cunningham, Alusa, Sedunov, Krastanov, Borivikov, Bojkov, etc. with List as chair. This Panel started to produce a ‘Statement of the Art of Weather Modification’, set-up of ‘Guidelines for WM Experiments’, and a world registry of WM projects, organized topical quadrennial WMO Scientific Conferences on WM, and produced 50+ reports on all aspects of WM. It also initiated the ‘Precipitation Enhancement Project, PEP’ in Spain. PEP, while not having the financial support to go into the seeding phase, nevertheless, was a textbook example about how to setup and evaluate WM experiments.

The criteria for acceptable WM Experiments were established as follows:

(i) The experiment had to be randomized and evaluated statistically;
(ii) The effectiveness had to be judged on the rain increase *at the ground*.
(iii) The statistical success required *support by physical insight and understanding*.
(iv) The methods had to be transferable to other parts of the world.

The papers by List (2003, 2004) give an overview of these issues.

3. Application to large systems, Hu + Cl

3.1. General aspects

The scale of WM and GeoE projects is different. GeoE involves operations across the jurisdiction of many countries to world-scale projects, while WM is basically a national issue and governed by local authorities. In GeoE the legal frame setting is international. The consequence is that: *all countries affected by a GeoE project have to agree with the planned interference*. On first sight this seems to make actual GeoE nearly impossible. However, examining the issue leads to a solution: the guiding principle of ***“Do no Harm”*** has to be incorporated into all GeoE projects.

Another issue is the evaluation of success. Contrary to WM projects, GeoE will not be statistically evaluated because every single interference has to have a positive

outcome. No negative results are acceptable. This can be achieved by choosing a "*reversible*" approach, i.e. careful testing of the science and engineering has to be done in a *step-by-step* approach. Only advances are to be made when a phase has been completed with the postulated progress. The issues can be separated into two categories: engineering and science. Engineering aspects: Can gases or particulates be produced in desirable form, and be delivered into the atmosphere (troposphere or stratosphere) with the right dosage, at the right time and where intended. What is the residence time of these substances and how are they diluted or concentrated, and redistributed? Can devices such as mechanical radiation screens (small at first) be deployed in space and how effective are they, etc.

As in WM the main question mark in GeoE is scientific: Physical understanding. Are the processes to be interfered with fully understood? This is only a rhetorical question since the answer is definitely "NO". Hurricanes, for example, are only described by general features, and no details about the interplay of the convective entities are known. That asks for major *measuring programs* involving numerous satellites and radars and swarms of aircraft and cloud physics equipped drones . Where is the equipment, where is the manpower? Then there are the *models*. The most sophisticated ones are prone to hand-waving and are generally without sufficient and credible predictive power. The understanding of climate and climate change is still in its infancy. The ignorance of the precipitation processes is appalling, and the suggested linking of precipitation to temperature is incomprehensible.

Besides an elaboration of these comments, detailed reversible steps will be described.

3.2. Engineering issues, the delivery system

If an approach requires the injection of gases or particulate matter into the lower or upper atmosphere, then methods of delivery of the seed material have to be developed that disperses the substances into a known volume with a known concentration distribution. It is not sufficient that such information is available right after injection, it is also necessary to know how the injected material disperses and if it is in part washed up in certain corners of the atmosphere. Is it altered with time, does it stay effective?

In WM launching of rockets and burning of flares from aircraft are standard. Anti-aircraft guns have also been used to deliver shells with seeding agents. Targeting is normally based on Doppler radar information. Rockets can be set to release seeding materials at the right elevations and for a desirable burn-time. Shelling also produces good results if the reach of the guns is adequate. Seeding has also been done by ground devices (AgI burners). Targeting, however, is difficult in that situation – which may not be an issue in GeoE as long as the seeding material reaches the intended zones. The cost of methods generally applied in WM, however, would be prohibitive for GeoE over areas of 10^6 km^2 and up.

3.3 The 'Do no harm' principle

The 'Do no harm' principle should guide any modification test or application, be it of engineering or scientific nature. An inert "placebo" approach may be chosen first to study aspects of materials' delivery, dispersion and residence time. Once the physics of the process is understood and quantified, active seeding agents may be used with the restriction that the target area be small at first and the test be short in duration, but be stepwise increased if the gain in insight and the outcome justify it. Should the physics be different from expectation, the theoretical understanding should be developed and deepened to fully explain the experimental results. Afterwards testing can resume. By proceeding in this fashion the maximum damage should be short-lived and reversible, particularly if the operational area is not large enough to induce measurable effects on climate and hurricanes. The stepping up of scale could then be resumed. The conditions in a test area, initially of size of o.100 km^2, are not expected to be of consequence to large scale climate. That may start at 1000 km^2 and up.

Not only should the science be tested, so should be the engineering, its apparatus and procedures.

3.5 Mechanical radiation shields in space

The step by step approach is also necessary for the case of space shields to redirect the sun's radiation. It is suggested that, from the science point of view, the initial maximum shield area should not exceed 10^3 km. It would have to be calculated on the basis that a full blocking of the sun's radiation would be possible in the center of

its shadow on the earth. From the engineering point of view the matter of shield deployment may start at smaller sizes. Is it possible to float the shields at geostationary fashion over the equator or would they "roam" in non-stationary fashion according to known physical laws. Could freely floating shields of limited dimension produce a reduction in solar radiation sufficient for limited but sufficient cooling. A back of the envelope calculation gives total shield dimensions of 10^6 km^2 for an overall radiation reduction of 1%, if centered in line sun/earth.

3.6. The Peter-robbing-Paul Principle

The second requirement of WM in Section 2 was required because ~ 50% of precipitation never reaches the ground. There is not equivalent need in climate modification – climate is addressing the atmosphere near the ground.

But the Peter-robbing-Paul effect, which is of importance in WM, will also be important to GeoE. [In rainmaking there is a possibility that inducing more precipitation in one area may diminish rain in an adjacent area.]

Radiation modification may well have larger effects on certain areas than others, even by design. This may be easier to assess if mechanical shields are used, and not methods based on gases or particulates

4. Hurricane modification

In 1974 WMO organized a Typhoon Modification Conference in Manila (chaired by R. List) at a time when the Philippines and the US considered launching a typhoon seeding project. At that time this area experienced ~16 typhoons per annum. The recommendation was not to seed within 1 h before landfall. China, being not in the UN at that time, let it be known that they were against such modification, and that they rather had the damage and the rain, than no damage and no rain. This is a legitimate concern also in the Caribbean where 40+ % of the annual precipitation comes from hurricane systems. The climate of some of the islands is fragile and less rain could easily transform some of them into deserts. Scientists have been very nonchalant and claimed that their assessments did not reveal any such problems.

5. Physics and numerical models

Physical understanding is often transformed into numerical models. Unfortunately, the availability of lavish climate change research funds has syphoned off most of the cloud modelers. Thus, nearly no progress has been made in the past decades about the formation of precipitation in clouds. As a consequence, no basis exists for reliable and predictive models. The present models are insufficient and the attempt to replace cloud physics by stochastic statistics, as it is being done at ECMWF ["such models give better results"!], is abominable. It is *never* stated by the IPCC that present climate change models have basically no skills when it comes to precipitation. Climate models are based on balance equations equating solar input in the equatorial regions to the pole-ward transport of heat, and speculations have been made about a possible correlation between *precipitation and temperature*. Horrible! Luckily for some climate modelers, there are the ensemble models which can be abused to prove anything.

6. Actions to be taken

Geoengineering with its hurricane and climate modification requires a UN agreement, like the Law of the Sea, stating that no GeoE activities are allowed to interfere within the jurisdiction of individual countries unless they explicitly approve. Obviously, a 'Law of the Atmosphere', similar to the 'Law of the Sea', has no chance to get approved before another 200 years have passed. However, a 'Protocol', like the 'Montreal Protocol' on freons, should be politically feasible.

- This Protocol should be laying out the rational and contain frames and mechanisms, stating how climate and hurricane modification can be can be carried out.
- The Protocol should outline how a guiding and controlling body, the Intergovernmental Panel for Geo-Engineering, IPGE, be set up and what its main functions are.
- It is suggested that the IPGE be responsible for formulating its tasks which are culminating in the execution and evaluation of a modification operation. The IPGE could be composed of heads of large research institutions (related to atmospheric physics), top scientists and engineers, two specialists in international law, and the head of one of the world's biggest Re-Insurance companies.

- The IPGE would not operate like a regular panel, it would use hybrid modes. For some issues, the heads of the large institutions would also make the expertise of their specialists available.

[*The function of the IPGE should not be assumed by the ICCP, which is considered incompetent in matters relating to proper consideration of precipitation processes as integral parts of the climate issue*.]

- The main initial functions of the IPGE would be
  - o To setup Guidelines for reversible step-by-step climate change projects recognizing the 'do no harm' approach. Such Guidelines would also contain assessment and selection criteria.
  - o To start a collection of proposed projects and select 2-3 for further in-depth study.
  - o Preliminary first assessment of the scientific and technical feasibility and the required financial resources.
  - o Project selection and securement of resources.
  - o Overseeing project.

It has to be understood that a climate change operation would be the biggest project man has ever undertaken.

Other Requirements

- Measuring capabilities need to be dramatically improved, thereby remembering that the scales and resolutions and data volume are beyond past operations.
- Physical understanding needs to be substantially improved and models have to be developed, capable of producing reliable and realistic representations which approach the limit of predictability. The UN should be encouraged to agree on a Protocol declaring that every country has to agree to GeoE if they affect their country. The UN should endorse a 'Do no harm' concept for GeoE;
- A highest-level scientific-technical-legal UN committee, the IPGE, has to be in overall charge of acceptable GeoE projects.

7. Summary

- The WMO criteria for weather modification are of value for geoengineering. - Physical under-standing is a common requirement and is the top priority in both fields. - The Peter-robbing-Paul principle is of even more importance in geoengineering than in weather modification, considering that uneven climate changes may be a much bigger issue. – It is obvious that statistical evaluation is not an issue in climate modification because every attempt has to be on target. - The elaborate seeding technology and strategy of rain making has direct application to both climate and hurricane modification.
- A 'Do no harm' approach makes it possible to embark on GeoE of hurricanes and climate because it creates safe conditions for the citizens of the world. Not the least benefit is the legal protection for the scientists and engineers involved in GeoE.
- A UN Protocol has been suggested to establish that right to 'no harm' underlining the right of people to have a safe environment.
- A body has been suggested similar to the ICCP but addressing the issues of GeoE. Working guidelines have been listed to achieve the goals of climate modification.
- It is recognized that tremendous progress is required in science and engineering to enable safe GeoE projects. Present physical insight into the systems to be modified is totally insufficient to even think of geoengineering hurricanes and climate. It is easy to realize that a 'Do no harm' approach is not cheap as some of the proponents of GeoE envisage. GeoE is not a quick fix considering that the price tag could easily be $ 100 billion just to get started. Producing measurement platforms and instruments, a firm scientific basis, and the training and education of the necessary manpower is everything but cheap.

Geoengineering of hurricanes and climate is a tremendous challenge - it may even be as big as to wean mankind from the energy addiction and use of fossil fuel.

References

Hauser, R., and N. Gordon, 2010: Getting serious about geo-engineering, Fall 2010, *UCAR Magazine* (with contributions by J. Latham, K. Lackner, D. Keith, K. Caldeira, A. Robock, and P. Rasch).

List, R., 2004: Weather Modification – A scen-ario for the future. *Bull. Amer. Met. Soc*., **85**, 51-63.

List, Roland, 2003: WMO weather modification activities, a fifty year history and outlook. 8th WMO Scientific Weather Modification Conference, Casablanca, Marocco, 7-17 April, *WMP Report* No 39, 1-10 (invited paper).

WMO, 1974: Typhoon modification. Proceedings WMO Technical Conference, Manila, 15-18 Oct., *WMO – No. 408.*

REINVENTING WEATHER MODIFICATION

Roland List

Department of Physics, University of Toronto, Toronto, Canada

1. The state of weather modification

Over the past 2-3 decades the science of Weather Modification, WM, has barely moved forward. Very few new randomized experiments,designed for statistical evaluation, have been started. No consolidation of testing of several similar operations into one project has been consideredwithin individual countries or internationally. This despite the economic and scientific gains they could produce. Each WM experiment has been and still is small in scale, and often meteorological data collection is minimal and no records are being kept for later extended evaluation. Further, there is little advance in knowledge of the physics of precipitation. Mostly case studies are being presented at the WMO Scientific WM conferences, often with a content which would not let them pass a reviewing process. Further, noscientific synthesis of the results of in-country achievements is being done.

The biggest disappointment is the lack of application of statistical methods as developed by Prof. Ruben Gabriel (2002) whoproposed, among many other things, an assessment of multiple experiments or of Dr. Bernie Silverman's successful statistical assessment of long-duration *operations*. He made statistical processing of operations after 50+ years possible,but opportunities in WM operations are beingsquandered by not leavingsingle areas unseeded for comparison. Further, List(2004) proposed away of assessing the effect of seeding in every seeding unit (day) rightafter execution by a bootstrap procedure which would require a relaxation of the "blindness" rule or its modification. There has been no follow up discussion.

Of note is also the lack of infusion of new ideas and efforts into cloud modeling. Why not discard "mathematical" turbulence and simulate "wake turbulence" with its flow of organized vortices (similar to the global circulation). Turbulent flow is not a continuum of singularities!It follows the Navier-Stokes equations.

The Working Group on Cloud Physics and WM (formerly an EC panel) has not developednew ideas and concepts. It seems to have used its sessions to "*word-smithing"* the WMO Statement on WM and the connected guidelines. It has provided little leadership, if any. Thus, its demotion from the status of Panel of the WMO Executive Council was to be expected. Becoming an entity under the Commission of Atmospheric Sciences, controlled by dynamicists and climate affichionados (don't forget the atmospheric chemists and radiation specialists which are closely attached to climate change), could be suffocating.

Positive achievements are: the application of remote sensing by satellite, the improvement of the delivery systems for seeding agents, and the development/improvement and testing of very effective new seeding materials.WM statistics has reached a very high level -unfortunately, none of the new concepts has been applied.Further, the successful operationaldispersal of warm and cold fog at airports has lost most of its glamor because aircraft landing systems are working now at zero visibility.

In summary, Weather Modification, after some significant successes in its earlier decades (List, 2003), is barely surviving and may not even qualify for palliative care. The scientific community has not spent much effort to understanding the underlying physics, and past progress is being disregarded or has never been understood.

In defence of this situation it has to be stated that the seeding of convective clouds is

very difficult because many details of how clouds work are unknown and very difficult to assess.

Among the specific reasons for the debacle are:

(i) Piece-meal individual experiments;

(ii) Difficulties in getting proper statistical advice;

(iii) Lack of funding to provide adequate scientific and technical infrastructure;

(iv) Lack of funding due to lack of convincing results or proposals with insufficient scientific merit;

(v) Lack of multi-national experiments and/or coordinated and co-evaluated modification experiments;

(vi) Forgotten past achievements;

(vii) The general trend in Meteorology towards larger scales;

(viii) Loss of specialists in cloud dynamics, seeing greener fields in climate change;

(ix) Field not made attractive enough for bright students.

It has become obvious that the *scientific* objective of WM has been forgotten, it has also not been recognized as the main driver of an appropriate program and activity: **UNDERSTANDING THE PHYSICS OF PRECIPITATION IN ALL ITS FORMS**. In this context WM is used to test newly developed science and to see if modification of clouds induces reactions and new processes as predicted.

2. The precipitation treatment in climate change models

The lack of scientific understanding is the reason for the stalled WM. But it is much more than that and also applies to Climate Change Modeling! Precipitation forecasting of convective systems has always been difficult and is not particularly successful – as any forecaster knows. Thus, it was no surprise that (~ 10 years ago) the administrator of NOAA, General Kelly, chided the climate modeling community at a town hall meeting during an AMS annual assembly for the lack of credibility of predicting precipitation in climate forecasts. This has not changed since. There is some basic concept, linking solar input, concentrated mostly in the equatorial regions, to the pole-ward transport of energy involving H_2O. How this is partitioned into longitude and then broken down into 30x30 km pixels is murky, to say the least. Now, climate change modelers are preparing for 10x10 km grids. That also will involve higher resolutions of precipitation climate forecasts. What a travesty!

I have observed that climate modelers are at great pain to explain the basis of precipitation modeling during climate change. One leader told me that it is linked to temperature!?

The secret to proving absurd research results is simple. It is by incorrectly applyingensemble models. Scenario: a group of modelers from the world's top centers is getting together and discusses the issue. One makes a suggestion. In lack of anything better they all agree, go home and run their models based on similar assumptions. Let us now assume that another one, who did not attend the "crucial" meeting, makes the right assumptions. After a while, the model results are then compared in an ensemble model. Guess what: The ones modeling with the agreed upon assumption turn out to be "correct", while the one with the correct model produces outlayer points – and thus, his model has to be rejected. QED.

The *measurement of precipitation* has always been a sore point in Meteorology, considering that ~ 170 different rain gauges have been used all over the world. Precipitation is not only an issue in meteorology but also in agriculture, forestry and other services and institutions. In other words, precipitation data could not easily be assembled and compared on a national, continental or world scale. The algorithm

for this gigantic problem was put together by the DeutscherWetterdienst in Offenbach, which operates the *Global Precipitation Climatology Centre, GPCC*. It *"analyses the monthly precipitation on earth's landsurface based on raingauge station data. It supports global and regional climate monitoring and research and is a German contribution to the World Climate Research Programme (WCRP) and to the Global Climate Observing System (GCOS)"* [from the DWD Webpage].No climate modeler I have met was familiar with this operation and the available datasets.

Precipitation is a factor in climate that is as important as temperature. To me "no rain is desert, rain is life". Thus, it requires respect and not avoidance and circumvention. A group at ECMWF is using statistics to replace cloud physics. "It produces better and reproducible results and does not have the same complexity". Statistics has its place in physics, but not this one. Unfortunately, this approach is getting common in science and engineering – where it becomes detached from and insensitive to science.*We will not, we cannot find a solution to the climate/precipitation question unless we concentrate on the physics.* This takes manpower and time. Example: In 1963 I published a new theory on hail growth including the growth "spongy ice". Within a few month I will submit a new theory based on four *new* variables (instead of the old six), with new insights and simplifications. It is based on 60 years of numerous laboratory and theoretical studies as well as Doppler radar investigations, all condensed into > 130 scientific papers and 29 PhD and 39 MSc theses. Imagine what could be done with 10 dedicated groups?

3. The goal of "Experimental Meteorology, EM"

This title implies that the name "Weather Modification" should be upgraded to "Experimental Meteorology" (or similar), not just because of the witchcraft connotations associated with WM, but also to express the much wider range of the issues. ["Experimental Meteorology" was the title of what is now recognized as the first international conference of both "Cloud Physics" and "Weather Modification", held in Zurich in 1954 (List, 2003). It could also include "Geoengineering", the large scale modification of climate (and hurricanes)[not including the oceans].

Going back to the basics reveals the double purpose of the "old" WM. (i) WM is the test bed for the science we develop in Cloud Physics. All the combined research from the laboratory, observations and measurements in nature, results of models, mathematical assessment procedures, etc. need to be tested in order to establish how nature really works. This requires field experiments for the verification of concepts and theory, through testing of how the clouds react to specific interferences. This is "scientific" WM. (ii) the second step is to apply the established modification to achieve our needs, be they rain enhancement, hail suppression, fog dispersal orsevere storm moderation, etc. These two remain as major objectives.

The purpose of "Experimental Meteorology"could be described as follows:

(i) Development of the physics and dynamics of the formation of clouds and precipitation.

(ii) Development of testing concepts by designing appropriate modification strategies, technologies and evaluation criteria;

(iii) Interference "in the field" with cloud processes to validate newly developed insights and theories of how precipitation is formed in nature;

(iv) Application to changing precipitation in all its forms and at any scale for economic benefits;

(v) *Creation ofa proper basis for the modeling of the precipitation climate*.

This list is to be expanded should geoengineering become part of the new initiative. The private sector should be involved at all times, considering its substantial contributions to our knowledge in WM and its valuable skills and experience.

We should not restrict our activities to day-to-day WM. We must consider the larger issue and concentrate on precipitation in general. Rain

is more than a local phenomenon, it is also a key component of the climate system.

4. Strategy of approach

What is needed is a plan detailing the scientific and technical components and setting specific large and small-scale goals of complex experiments. That may involve new measuring platforms such as fully equipped drones for small scale measurements in large systems, mobile ground Doppler radars to measure particle size distribution and updrafts aloft, Navier-Stokes-based models of turbulence in updrafts, etc.Planning for different research phases is preferable because the financial resources to be asked for are easier to obtain after demonstrating success in a step-by-step program. If no official committee can be setup due to lack of financial resources, then a group of individuals could lay out a scientific plan and find associates to contribute parts. Meetings, if necessary, can always be arranged at the time of conferences where expenses are covered by other bodies.

Remember, the key issue is the science, funding will come later. However, it is advisable to be prepared for a big fight should a piece of the lavish funding of climate change research (at the tune of several billion $/annum) be part of our desires. This would also be the main reason for the climate modelers to defend the validity of their questionable treatment of precipitation – unless a compromise can be reached. It is expected that the Intergovernmental Panel on Climate Change, IPCC, will defend its position up to the last stand.

There are two possibilities: (i) Go through the UN with a proposal to “regulate” and “closely monitor” Geoengineering, GE, with the scientific goals relating to precipitation attached; (ii) to go through WMO Congress or its Executive Committee, EC. I may approach the UN SG about the regulatory issues concerning GE. I know that his advice might be to go through a UN Member (country). This is also the way to proceed with WMO. However, within WMO, there is only one chance for survival: to become a Panel of EC again by a scientifically sound, important and large-scale proposal, independent of CAS. (WMO EC and Congress in particular have a great interest in WM (rainmaking) due to the “overheating” and drying out of many countries.

Should Geoengineering be the goal, then the steering body, the Intergovernmental Panel on Precipitation or IPP would have to be a UN body because it has to deal automatically with economic, legal and re-insurance issues. This would not prevent WMO from becoming the host of IPP, as it is now for IPCC.

In principle, precipitation issues should really be part of IPCC. However,IPCC has not husbanded its scientific resources well by *not*recognizing the need for improving the knowledge of the Physics of Precipitation. It is partner in the suppressing and misjudging of a key component of climate: precipitation. The IPCC would only become acceptable after a total turnover of its leaders, a revamping of its goals and a fair distribution of resources. Further, those resources need substantial expansion. [In my estimation the price tag of testing of a single climate modification concept, including the assessment of its technical feasibility may well be >$100 billion.]

Some of us may know WMO EC members or a WMO Permanent (country) Representative. They could be the conduits for getting Meteorological Experimentation on the meeting agenda. Afterwards, only the quality of the proposal counts. Note that there will be no funding for research alone, direct applications have to be included.

One small example:As the representative of IUGG with WMO I had successfully launched the IAPSAG initiative toassess the impact of manmade aerosols on precipitation at theWMO Congress XIV (2003). The study itself was first led by Prof. Hobbs and, after his death, by Profs. Z. Levin and W.R. Cotton. This study waspublished in book form by WMO and IAMAS, the International Association for Atmospheric Research (Levin and Cotton, 2008). It serves as an example of what can be done by committed top scientists.

5. Final comment

It is up to the Cloud Physics and Weather Modification Community to work out a proposal for Experimental Meteorology. Do we have the leaders, the dreamers, the visionaries and the hard workers to put an exciting scientific plan together to study the Physics of Precipitation with the purpose of establishing how sufficient precipitation can be obtained and maintained in a

changing climate. A further purpose is the substantial improvement of the credibility, quality and predictive power of climate change models. Better understanding of the mechanics of damaging weather systems can and will further lead to their successful modification. This is not easy to achieve, but it is also not pie in the sky.

A footnote: When talking to climate modelers always ask for an explanation of how precipitation is included.

References

Gabriel, R., Confidence regions and pooling – some statistics for weather experimentation. J. Appl., Meteor., 41, 505-518, 2002.

Levin, Z., and W. R. Cotton, Aerosol pollution impact on precipitation: a scientific review. Springer Verlag, Berlin, pp. 407, 2008.

List, R., WMO weather modification activities, a fifty year history and outlook. 8th WMO Scientific Weather Modification Conference, Casablanca, Morocco, 7 April, WMP Report No 39, 1-10, 2003.

List, R., The 1954 International conference on experimental meteorology in Zurich, Switzerland (A historical note), Proceedings 14th Intern. Conf. Cloudsand Precipitation, Bologna, Italy, 19-23 July, Vol. 2, 858-860, 2004.

List, R., Weather modification - A scenario for the future.*Bull. Amer. Met.*Soc., 51-63, January. 2004.

World Weather Research Programme (WWRP)
Report Series

Sixth WMO International Workshop on Tropical Cyclones (IWTC-VI), San Jose, Costa Rica, 21-30 November 2006 (WMO TD No. 1383**) (WWRP 2007 - 1).**

Third WMO International Verification Workshop Emphasizing Training Aspects, ECMWF, Reading, UK, 29 January - 2 February 2007) (WMO TD No. 1391) **(WWRP 2007 - 2).**

WMO International Training Workshop on Tropical Cyclone Disaster Reduction (Guangzhou, China, 26 - 31 March 2007) (WMO TD No. 1392) **(WWRP 2007 - 3)**.

Report of the WMO/CAS Working Group on Tropical Meteorology Research (Guangzhou, China, 22-24 March 2007) (WMO TD No. 1393) **(WWRP 2007 - 4).**

Report of the First Session of the Joint Scientific Committee (JSC) for the World Weather Research Programme (WWRP), (Geneva, Switzerland, 23-25 April 2007) (WMO TD No. 1412) **(WWRP 2007 – 5).**

Report of the CAS Working Group on Tropical Meteorology Research (Shenzhen, China, 12-16 December 2005) (WMO TD No. 1414) **(WWRP 2007 – 6).**

Preprints of Abstracts of Papers for the Fourth WMO International Workshop on Monsoons (IWM-IV) (Beijing, China, 20-25 October 2008) (WMO TD No. 1446) **(WWRP 2008 – 1).**

Proceedings of the Fourth WMO International Workshop on Monsoons (IWM-IV) (Beijing, China, 20-25 October 2008) (WMO TD No. 1447) **(WWRP 2008 – 2).**

WMO Training Workshop on Operational Monsoon Research and Forecast Issues – Lecture Notes, Beijing, China, 24-25 October 2008 (WMO TD No. 1453**) (WWRP 2008 – 3).**

Expert Meeting to Evaluate Skill of Tropical Cyclone Seasonal Forecasts (Boulder, Colorado, USA, 24-25 April 2008) (WMO TD No. 1455) **(WWRP 2008 – 4).**

Recommendations for the Verification and Intercomparison of QPFS and PQPFS from Operational NWP Models – Revision 2 - October 2008 (WMO TD No. 1485) **(WWRP 2009 - 1).**

Strategic Plan for the Implementation of WMO's World Weather Research Programme (WWRP): 2009-2017 (WMO TD No. 1505) **(WWRP 2009 – 2).**

4th WMO International Verification Methods Workshop, Helsinki, Finland, 8-10 June 2009 (WMO TD No. 1540) **(WWRP 2010 - 1).**

1st WMO International Conference on Indian Ocean Tropical Cyclones and Climate Change, Muscat, Sultanate of Oman, 8-11 March 2009 (WMO TD No. 1541) **(WWRP 2010 - 2).**

Training Workshop on Tropical Cyclone Forecasting WMO Typhoon Landfall Forecast Demonstration Project, Shanghai, China, 24-28 May 2010 (WMO TD No. 1547) **(WWRP 2010 - 3)** (CD only).

2nd WMO International Workshop on Tropical Cyclone Landfall Processes (IWTCLP-II), Shanghai, China, 19-23 October 2009 (WMO TD No. 1548) **(WWRP 2010 - 4).**

5th WMO Symposium on Data Assimilation, Melbourne, Australia, 5-9 October 2009 (WMO TD No. 1549) **(WWRP 2010 - 5).**

7th International Workshop on Tropical Cyclones (IWTC-VII), Saint-Gilles-Les-Bains, La Réunion, France, 15-20 November 2010 **(WMO TD No. 1561) (WWRP 2011 – 1).**

Report of the Fourth Session of the Joint Scientific Committee (JSC) for the World Weather Research Programme (WWRP), Geneva, Switzerland, 21-24 February 2011, **(WWRP 2011 - 2).**

WWRP/ETRP Workshop on Operational Monsoon Research and Forecast Issues – Lecture Notes, Beijing, China, 24-25 October 2008, **(WWRP 2011 - 3).**

Recommended Methods for Evaluating Cloud and Related Parameters **(WWRP 2012-1).**

Proceedings of the 10th WMO Scientific Conference on Weather Modification, Bali, Indonesia, 4-7 October 2011 **(WWRP 2012-2).**